Loughborough University

This item is held in Loughborough University's Institutional Repository (https://dspace.lboro.ac.uk/) and was harvested from the British Library's EThOS service (http://www.ethos.bl.uk/). It is made available under the following Creative Commons Licence conditions.

creative commons

COMMONS DEED

Attribution-NonCommercial-NoDerivs 2.5

You are free:

- to copy, distribute, display, and perform the work

Under the following conditions:

Attribution. You must attribute the work in the manner specified by the author or licensor.

Noncommercial. You may not use this work for commercial purposes.

No Derivative Works. You may not alter, transform, or build upon this work.

- For any reuse or distribution, you must make clear to others the license terms of this work.
- Any of these conditions can be waived if you get permission from the copyright holder.

Your fair use and other rights are in no way affected by the above.

This is a human-readable summary of the Legal Code (the full license).

Disclaimer

For the full text of this licence, please go to:
http://creativecommons.org/licenses/by-nc-nd/2.5/

Ion Current Sensing For Controlled Auto Ignition in Internal Combustion Engines

By

Dimosthenis Panousakis

A Doctoral Thesis

Submitted in partial fulfillment of the requirements for the award of

Doctor of Philosophy of Loughborough University

May 2009

© Dimosthenis Panousakis, 2009

List of publications

- **"Analysis of SI Combustion Diagnostics Methods Using Ion-current Sensing Techniques", SAE 2006-01-1345**

  By D. Panousakis (Loughborough Univ.), A. Gazis (Loughborough Univ.), J. Patterson (Loughborough Univ.) R. Chen (Loughborough Univ.).

- **"Computationally Inexpensive Methods of Ion Current Signal Manipulation for Predicting the Characteristics of Engine In-Cylinder Pressure", International Journal of Engine Research, EU_CA_143, 2006**

  By A. Gazis (Loughborough Univ.), D. Panousakis (Loughborough Univ.), R.Chen, W-H Chen (Loughborough Univ.).

- **"Using Ion-current Sensing to Interpret Gasoline HCCI Combustion Processes", SAE 2006-01-0024**

  By D. Panousakis (Loughborough Univ.), A. Gazis (Loughborough Univ.), J. Patterson (Loughborough Univ.), R. Chen (Loughborough Univ.), J.W. Turner (Lotus Engineering, Norwich, Gbr), N. Milovanovic (Lotus Engineering, Norwich, Gbr), D. Blundel (Lotus Engineering, Norwich, Gbr).

- **"Ion Current Signal Interpretation via Artificial Neural Networks for Gasoline HCCI control", SAE 2006-01-1345**

  By A. Gazis (Loughborough Univ.), D. Panousakis (Loughborough Univ.), R.Chen (Loughborough Univ.), J.W. Turner (Lotus Engineering, Norwich, Gbr), N. Milovanovic (Lotus Engineering, Norwich, Gbr), D. Blundel (Lotus Engineering, Norwich, Gbr).

- **"The Advance Combustion Control in a Hybrid SI/HCCI Engine by Using Ion Current Sensing" JSAE 20065415**

  By N. Milovanovic (Lotus Engineering, Norwich, Gbr), D. Blundel (Lotus Engineering, Norwich, Gbr), J.W. Turner (Lotus Engineering, Norwich, Gbr), D. Panousakis (Loughborough Univ.), A. Gazis (Loughborough Univ.), J. Patterson (Loughborough Univ.), R.Chen (Loughborough Univ.).

- **"Using In-Cylinder Gas Internal Energy Balance to Calibrate Cylinder Pressure Data and Estimate Residual Gas Amount in Gasoline Homogeneous Charge Compression Ignition Combustion" Experimental Heat Transfer 1521-0480, Volume 21, Issue 4, 2008**

  By A. Gazis (Loughborough Univ.), D. Panousakis (Loughborough Univ.), R.Chen (Loughborough Univ.), (J.W. Turner (Lotus Engineering, Norwich, Gbr).

Abstract

Environmental pollution is a subject that needs urgent addressing. Since the internal combustion engine has its fair share of accountability on this, research on techniques for increasing engine efficiency and emissions is necessary. Controlled Auto Ignition is a promising combustion mode, which increases fuel efficiency while also reducing NOx emissions to negligible levels.

This Thesis concentrates on the implementation of this mode through experimental research, on an engine equipped with a fully variable valvetrain. Investigation of the operational window, emissions, fuel consumption, thermodynamic efficiency is carried out and ways to improve on these are discussed.

The governing consideration, however, is the control method for this rather intricate combustion mode. As such, experimental data acquisition and analysis of ion current under the whole operating spectrum, from spark ignition to full autoignition is made.

It is found that the expected gains in fuel consumption and emissions are realized. In addition, ion current proves to be a very powerful and cost effective tool for engine monitoring, diagnosis and control.

The author concludes that Controlled Auto Ignition is a viable proposition for mass production engine designs and that ion current, although not absolutely vital for engine control, considerably increases engine control thus allowing for greater operating window under autoignition, without compromising reliability or cost.

Loughborough University
Pilkington Library
Date 03/10
Class
Acc. 0402699122

Acknowledgements

First and foremost I would like to thank my supervisor Dr. Rui Chen for giving me guidance and coordinating the collaboration between Loughborough University and Lotus, while also allowing me all the freedom needed in tackling such a complex subject.

I would also like to thank Lotus Engineering Ltd for giving me access to their experimental engine where all Controlled Autoignition data was collected. A special thank should go to my friend and research colleague Andreas Gazis for developing the algorithms needed to post process all this data.

Last but not least my girlfriend, my family and my friends (they know who they are) deserve my expression of gratitude for making things a lot less hard. And believe me, they were very hard at times.

TABLE OF CONTENTS

LIST OF PUBLICATIONS **1**

ABSTRACT **2**

ACKNOWLEDGEMENTS **3**

1. INTRODUCTION **7**

2. LITERATURE REVIEW **8**

2.1.1 Air resources pollution *8*
2.1.2 Main engine technology trends *10*
2.2 INTERNAL COMBUSTION ENGINES AT PRESENT 13
2.2.1 Spark Ignition (SI) Engines *13*
2.2.2 Compression Ignition Engines (CI) *15*
2.3 FUNDAMENTALS OF HOMOGENEOUS CHARGE COMPRESSION IGNITION (HCCI) 16
2.3.1 Advantages *18*
2.3.2 Historic outline *22*
2.3.3 Challenges of HCCI *25*
2.3.3.1 HC and CO Emissions 26
2.3.3.2 Ignition Timing Control 27
2.3.3.3 Methods 28
2.3.3.4 Extending HCCI Operation to Wider Range of Speeds/Loads 35
2.3.3.5 Low Load 35
2.3.3.6 Thermal Barrier Coatings 36
2.4 ALTERNATIVE HCCI USES 39
2.4.1 Free piston engines *39*
2.4.2 Reduced-size HCCI Combustion System *45*
2.4.3 Micro HCCI *45*
2.4.3.1 Free piston micro-engines 46
2.4.3.2 MEMS Rotary Engine 46
2.4.3.3 Remote Control Model Engines 48
2.5 CHEMICAL KINETICS - HYDROCARBON OXIDATION CHEMISTRY 53
2.6 GASOLINE HCCI DETAILED ANALYSIS 55
2.7 ION CURRENT THEORY 64
2.7.1 Ion Current Formation Models *69*
2.7.2 Saitzkoff-Reinmann model *69*
2.7.3 Calcote model *71*
2.7.4 Yoshiyama-Tomita model *72*
2.7.5 General Ion Current Technique Remarks *73*
2.7.6 Effects of EGR on ion current *74*

3. AIM **76**

4. METHODOLOGY **77**

4.1 HCCI IMPLEMENTATION CONSIDERATIONS 77
4.2 RENAULT ENGINE AND TEST RIG 78
4.3 LOTUS ENGINE AND TEST RIG 80
4.3.1 Valve strategies *82*
4.4 CYLINDER PRESSURE SIGNAL MANIPULATION FOR COMBUSTION ANALYSIS 86
4.4.1 Theory of Heat Exchange Calculation *87*
4.4.2 Implementation *91*
4.4.3 Pressure Trace Pegging *91*
4.4.3.1 Averaged Signal TRG Estimation 93
4.4.3.2 Evidence of Pressure Trace Imbalance 94
4.4.3.3 TRG Estimation via Corrected Pressure Trace 95
4.4.4 Cycle-to-Cycle Analysis *97*
4.4.5 Post-Processing Utilization *99*
4.4.5.1 TRG Representation 99
4.4.5.2 In Depth Cycle-to-Cycle Investigation 101
4.4.6 Conclusion *102*

5. EXPERIMENTAL INVESTIGATION OF GENERAL CAI PERFORMANCE **104**

5.1 EMISSIONS AND FUEL CONSUMPTION 104

5.2 THERMODYNAMIC CYCLE CONSIDERATIONS 109
5.2.1 Theoretical vs. Experimental Combustion Analysis 112
5.2.2 MFB50 Location 118
5.2.3 Gas Exchange Losses 119
5.2.3.1 Gas Exchange Theory 120
5.2.3.2 Experimental Investigation 122
5.2.3.3 Pumping Cycle Analysis Discussion 124
5.2.3.4 Correction factors implemented in CAI 130
5.2.3.5 Conclusion 135

6. SI ION CURRENT 136

6.1 ANALYSIS OF SI COMBUSTION DIAGNOSTICS METHODS USING ION CURRENT SENSING TECHNIQUES 136
6.1.1 Misfire 138
6.1.2 Ignition timing 139
6.1.3 Air to fuel ratio 139
6.1.4 Compression ratio 142
6.1.5 Load/Speed 142
6.1.6 Knock 143
6.1.7 Transient operation performance 144
6.2 COMPUTATIONALLY INEXPENSIVE METHODS OF ION CURRENT SIGNAL MANIPULATION FOR PREDICTING THE CHARACTERISTICS OF ENGINE IN-CYLINDER PRESSURE 146
6.2.1 Signal Interpretation 147
6.2.2 Feature Relations 150
6.2.3 Artificial Neural Networks 152
6.2.4 Measurant Predicting Network 155
6.2.5 Curve Predicting Network 158
6.2.6 Knock 160
6.2.7 Discussion 161
6.3 CONCLUSION 165

7. CAI ION CURRENT 167

7.1 USING ION CURRENT SENSING TO INTERPRET GASOLINE CAI COMBUSTION PROCESSES 168
7.1.1 CAI Combustion 168
7.1.2 Ion Current Signal and its treatment 169
7.1.3 The Ion Current Measurant Extraction Procedure 171
7.1.4 Dynamic Trigger Estimation of Signal Start 174
7.1.5 TRG Levels and Ion Current Signal 176
7.1.6 Combustion Performance and Ion Current Signal 178
7.1.7 ITA Effect on Ion Current Signal 182
7.2 ION CURRENT SIGNAL INTERPRETATION VIA ARTIFICIAL NEURAL NETWORKS FOR GASOLINE CAI CONTROL 185
7.2.1 Wavelet Based Estimation of Signal Start 185
7.2.2 The Wavelet Decomposition of the Ion Current signal procedure 188
7.3 ARTIFICIAL NEURAL NETWORK BASED PREDICTIONS 189
7.3.1 Types of Input 189
7.3.2 ANN Testing within Different Speed Sites 191
7.3.3 ANN Testing Across Different Speed Sites 194
7.4 USE OF ION CURRENT IN SWITCHING TRG LEVELS 197
7.4.1 Switching among different TRG levels in CAI operation 198
7.5 CONCLUSION 201

8. AUTOIGNITION TIMING INVESTIGATION AND ION CURRENT AS A MEASURE AVOIDANCE TOOL OF INSTABILITY 205

8.1 INTRODUCTION 205
8.2 OBSERVED BEHAVIOR OF EXPERIMENTAL DATA 205
8.3 DATA ANALYSIS 208
8.3.1 Autoignition mechanism 211
8.3.1.1 Potential mechanisms involved 211
8.3.1.2 Noteworthy Engine Characteristics 212
8.3.1.3 Proposed mechanism 212
8.3.1.4 Instability 215
8.3.2 Ignition Coil Ion Sensing 224

8.3.3 Conclusion *227*

9. ENDING CONCLUSION & FUTURE ISSUES 228

9.1 FUTURE WORK 229

APPENDIX 1 - INFORMATION ON CERAMIC THERMAL BARRIER COATINGS 231

APPENDIX 2 - PHOTOGRAPHS OF ENGINES FOR REMOTE CONTROLLED VEHICLES ... 233

APPENDIX 3 – CHEMICAL KINETICS 234

10. REFERENCES 238

1. Introduction

Starting by portraying the current strain imposed on air resources by modern combustion reciprocating engines, namely the gasoline and diesel engines, this thesis goes on to explain their pros and cons. It then compares these technologies to the possibilities that become available through the use of Homogeneous Charge Compression Ignition, to quote the more common term. Focus is given specifically to gasoline HCCI implementations or, more correctly, Controlled Auto Ignition.

Up to this point the reader becomes familiar with the literature surrounding this technology, in order to get a fuller understanding of the experimental design decisions and the necessity for the data acquisition that arose from its implementation. Next, after a description of the engine test rig and the in-cylinder pressure signal manipulation that was used throughout the experiments, preliminary tests of emissions, thermodynamic cycles and gas exchange losses under varying operating conditions are shown.

By confirming that the engine performance mostly complies with other researchers' findings, the challenging behaviour of Controlled Auto Ignition also becomes apparent. Despite its name, it displays oversensitivity to operating conditions, making it difficult to control.

Since a control method appears necessary, ion current, a cost effective diagnostic technology, is assessed firstly in a conventionally ignited gasoline engine and then transferred to a hybrid Spark Ignition and Controlled Auto Ignition engine. The signal's effectiveness is compared with the in-cylinder pressure signal, both in "raw" form and also after detailed post processing with various mathematical approaches, including Artificial Neural Networks. Finally, an autoignition mechanism specific to this engine is discussed.

2. Literature review

The question that needs to be answered before someone decides whether to read this PhD thesis is why HCCI is a technology that is worth wasting time on.

2.1.1 Air resources pollution

The majority of energy expenditure is covered by fossil fuels, in today's world. Fossil fuels possess tremendous energy density with diesel and gasoline providing around 45 MJ/kg. In comparison, a top of the range battery holds only 1.5 MJ/kg. In addition, when the cost of the life cycle of a battery is compared with that of fossil fuels, the latter become an even more tempting proposition. Unfortunately fossil fuels do not come without their drawbacks, emissions being the major one. In fact, one of the major city pollution sources, Figure 1, is road transport. In addition, the major health and environmental implications of this, affect the globe in its entirety not only the developed countries.

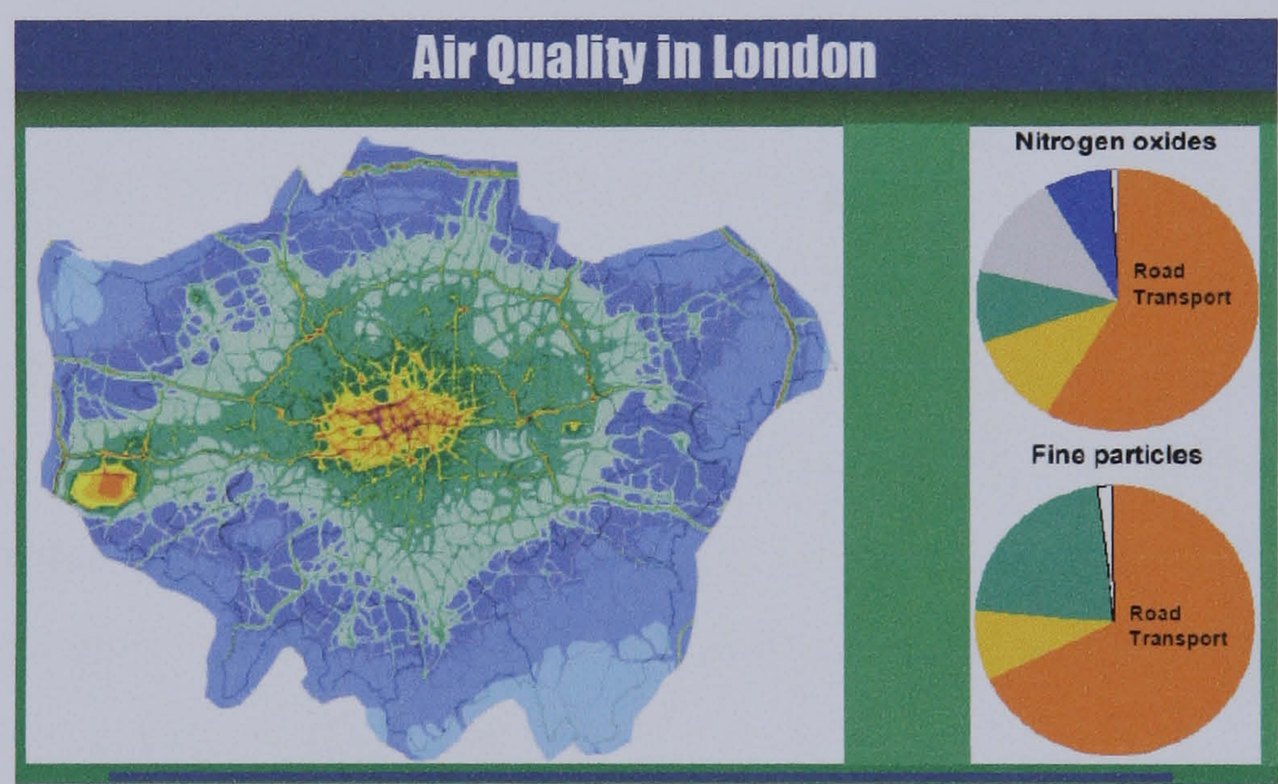

Figure 1: Air Quality in London. [1]

According to the latest United Nations estimates, by 2020 the earth's population could approach seven-and a-half billion people. If 15 percent of those people own automobiles (which is only slightly more than today), the total number of vehicles in the world, could top one billion. Taking into account that the population increases will be greatest in developing countries, future industry growth will be concentrated in markets in Asia Pacific, Central Europe, Latin America, Africa, and the Middle East. The greatest growth is noticed in the following eight markets: Brazil, China, India, Korea, Mexico, Poland, Russia, and Thailand.

Vehicle sales in these markets will be fueled by a growing middle class, increased urbanization, and rising per capita income, which correlate almost directly with vehicle ownership. These demographics are driving the global car manufacturing business today. The development of new vehicle technologies and alternative fuels must ultimately remove the automobile from the environmental equation. Clearly, a breakthrough in energy efficiency and continued emissions reductions are needed to meet future vehicle demands in a sustainable, high-quality environment [1].

A historical look reveals that cars emissions have dropped considerably in the past 40 years. Compared to the unregulated 1960s,

Hydrocarbons are down 98%

Carbon monoxide is down 96%

Oxides of nitrogen are down 90% [2]

There is no significant reason, other than cost, why this trend can't continue.

To estimate the number of internal combustion engines produced worldwide, it is necessary to consider the number of motorcycles produced in addition to the number of cars and trucks. Preliminary research estimates the approximate total number of internal combustion engines produced for the motor vehicle and motorbike industry per year, in the US, as being over 62,425,563 units. A broader estimate of the total number of internal combustion engines produced in the world may be made adding the total number of motorcycles and motor vehicles. This sum represents over 90 million internal combustion engines produced worldwide each year [3].

The Automotive Industry is a major player on the internal combustion engines industry, accounting for an important share of its demand and production. It is also the driving force on technology advancements and innovation. In this instance, the most important technological trends for internal combustion engines derive from automotive use. The automotive industry has been, in the past years, investing in research and development of more advanced vehicle and fuel technologies in order to comply with government emissions regulations and achieve the demand for more efficient, environmentally-friendly fuels.

This trend will play an important role in the performance of the automotive industry in coming years, with the adoption of tougher emissions regulations by different countries, greater awareness of consumers to environment issues and competition between

manufacturer companies for better technologies and market opportunities. One example of tougher emission policy is the California Air Resources Board that has implemented a "zero-emission vehicle program" that requires the motor companies to provide a certain number of "zero-emission" vehicles per year.

2.1.2 Main engine technology trends

Until now, the main trends in terms of technologies and fuels used by the automotive industry in "production" vehicles are the following:

Diesel Engines

Alternative Fuel IC Engines

Hybrid Cars

Fuel Cell Technology

Diesel engines account for more than 40% of all cars sold in Europe and the European market is presenting a growing demand for the cleaner, more efficient diesel engines. This encouraged automotive companies like PSA Peugeot Citroen, Ford and Honda to invest in the development and manufacture of this kind of engine for that specific market. PSA Peugeot Citroen invested US$ 1.08 billion to make new 1.6 liter and 2.0 liter diesel engines, expecting to produce 1.6 million engines a year from 2005 onwards. The Japanese company Honda developed and is about the launch its 2.2 liter i-CTDi diesel engine that fully complies with Euro 4 emission standards to compete in the European market. Also in the launch stage is the 6.0L Power Stroke Diesel developed by Ford to be used in full-size pickups and the SUV Excursion. Hybrid cars combine improved petrol performance and low emissions, and may represent the next step in the evolution of the internal combustion engine. Automotive companies have been increasingly interested in this technology with Honda and Toyota already offering hybrid cars, with Toyota's hybrid Prius selling over 150,000 between its launch in 2000 and the start of 2008. Following the trend, by the end of 2005 Ford and Lexus intend to have launched hybrid SUVs, Chrysler announced the launch of a hybrid pick-up and GM announced that it would soon offer hybrid-powered cars, all within the year [3].

Throughout the world, over one billion people are suffering from severe air pollution. Scientists estimate, that in the U.S. alone the number of deaths associated with air

pollution range from 50,000 to 100,000 per year. For comparison, the total number of American combat dead and missing in the Vietnam War is estimated at 55,000.

Smoke from diesel engines is considered a possible carcinogen. Diesel trucks, without particular filters, emit three times more soot and smog forming pollutants than a coal-fired power plant, for every unit of energy they convert.

More than 94 % of the vehicles available in the 2002 model year achieve less than 30 miles to a gallon of gas. According to the Environmental Protection Agency (EPA), today's motor vehicles in the U.S. account for: 65% of U.S. oil consumption, 78% of all carbon monoxide emissions, 45% of nitrogen oxide emissions and 37% of volatile organic compounds. In addition, for every liter of gasoline manufactured, distributed and then consumed in a vehicle, roughly 4 kilograms of carbon dioxide are released. Similar trends are apparent all over the world [4].

A closer look at emissions legislation reveals that the governments around the world have realized the need for change towards cleaner burning engines (Figure 2).

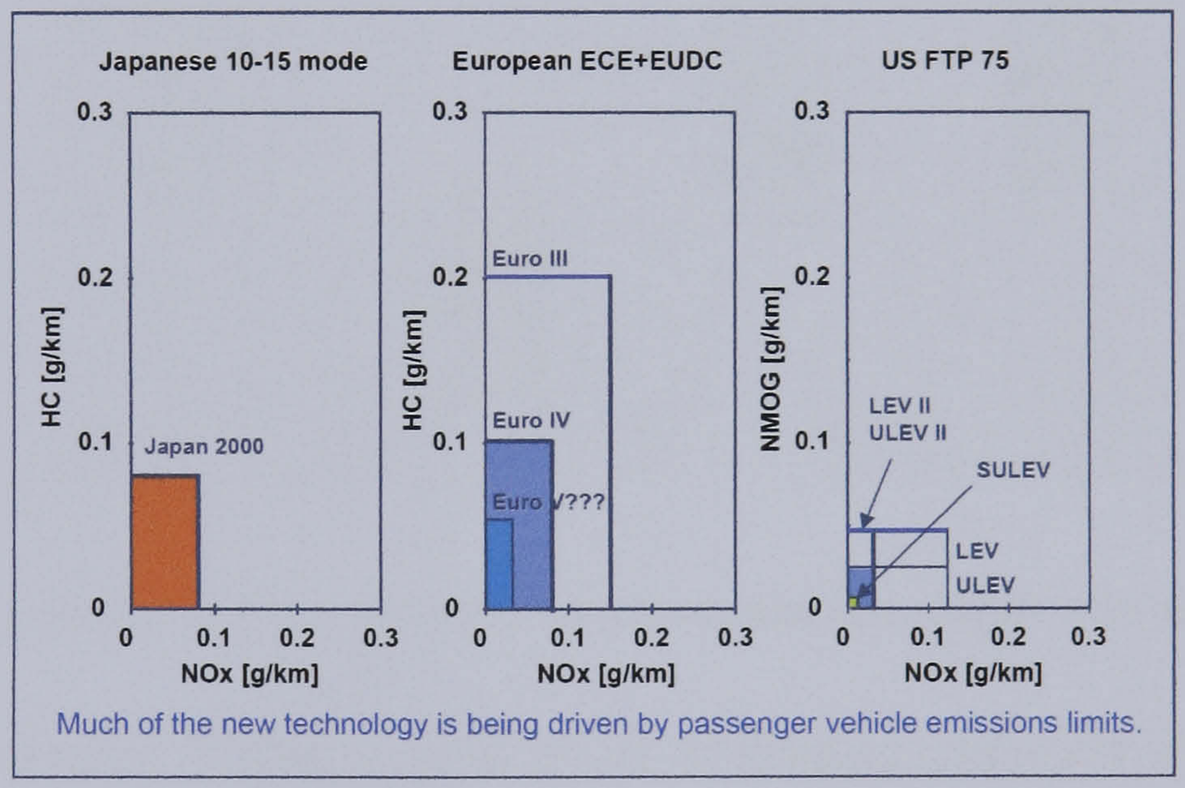

Figure 2: Comparison of Worldwide Gasoline Vehicle Emissions Registration. [5]

Although slightly different approaches are taken, the same trend is exhibited throughout. A more analytic graph of European legislation, for petrol cars is shown in Figure 3.

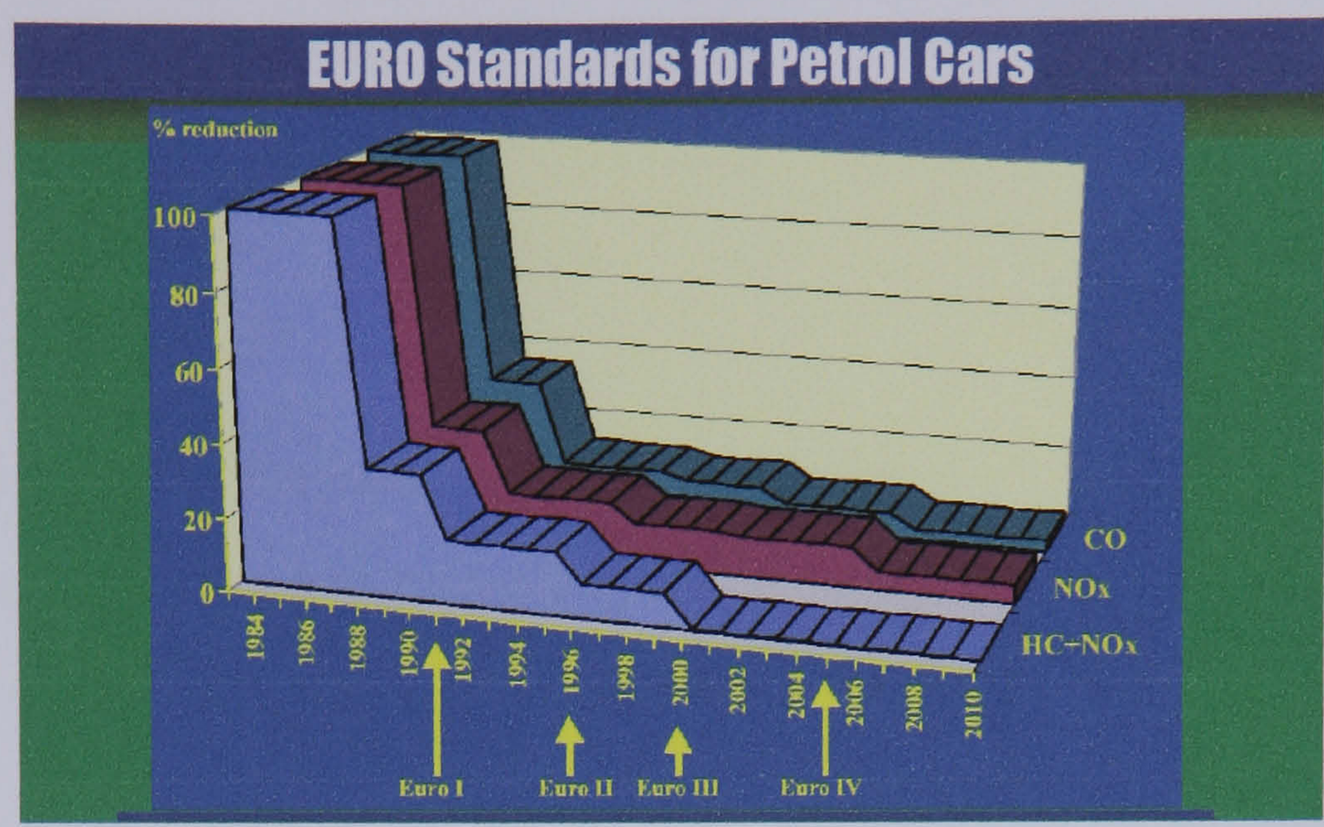

Figure 3: EURO Standards for Petrol Cars. [6]

Despite stringent legislation, because of the global increase in transportation needs, the related fuel consumption does not appear to be dropping (Figure 4).

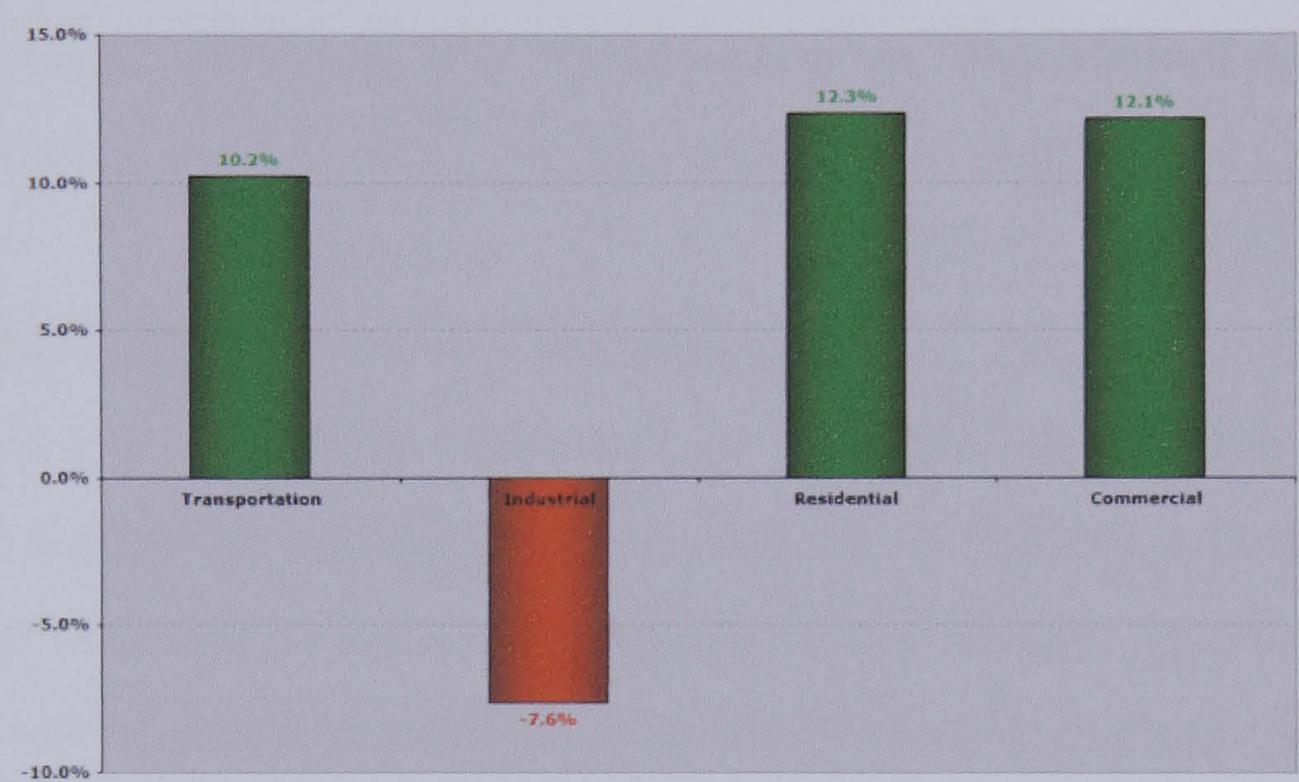

Figure 4: Percentage change in CO_2 emissions, from fossil fuel consumption, by sector 1997-2004 [4].

Although, as mentioned before, a number of alternative chemical energy conversion "engines" are being developed, it seems like the internal combustion engine will be with us for a long time to come. This is both because of industrial inertia, but also due to its proven service record. The industrial inertia can be split into mental inertia of the entrepreneurs involved that dislike high risk investments, but also due to the capital expenditure already invested in the current scheme.

As far as the internal combustion engine's service record is concerned, it has to be said that in terms of performance, economy, durability, driveability and cost, no real rival is in sight. Besides, it becomes apparent that the research and development of this sector will keep on attracting a lot of investing and scientific attention accounting for the already laid

out supporting infrastructure for this type of energy conversion and also the successful history of its evolution.

2.2 Internal Combustion Engines at Present

Looking at internal combustion piston engines which are the norm in road transport, two main categories can be defined: The spark ignition (SI) and the compression ignition (CI) engines.

In general, before looking at each individual engine type, it can be said that there are limited areas where improvements can be made. These are reduction in pumping losses, improvement in the compression and expansion work (Atkinson – Miller cycles), improvement in combustion duration (more efficient Otto cycle), improvement in chemical conversion efficiency (i.e. completeness of combustion) and reduction in mechanical friction.

2.2.1 Spark Ignition (SI) Engines

SI engines inhale a homogeneous mixture of air and fuel. A spark plug is used to ignite this mixture. It then relies on the flame propagation to achieve a good completion of combustion thus converting chemical energy to kinetic energy. In order for this flame propagation to occur, stoichiometric or near stoichiometric mixtures have to be used. Stoichiometric mixtures also provide a means of using three-way catalysts (TWC) as an exhaust after-treatment method. The SI engines at the moment achieve quite low emissions, however their efficiency is low, mainly due to pumping losses and long combustion duration as analyzed below, thus a large amount of CO_2 is produced. This could be tackled by the use of bio-fuels which are carbon neutral (i.e. bio-fuels don't contribute to a net CO_2 increase in the atmosphere when looking at their complete life cycle).

The limitation for the SI engines comes from two main sources. One is that throttling is needed in order to control the load, thus imposing pumping losses during the gas exchange process. In addition the resulting effective compression ratio is low thus decreasing thermodynamic efficiency. The second drawback comes from the reliance on flame propagation itself. Flame propagation, even at the pressure reached after the compression of the air-fuel mixture, attains speeds of around 30-40 m/s. In order to

follow the Otto cycle more closely higher flame speeds are needed. However, the use of higher compression ratios (CR) which would promote higher flame speeds cannot be realized since knocking would occur. Knocking is when the mixture outside the "flame ball" propagating inside the combustion chamber, autoignites due to the higher ambient pressures and temperatures. When autoignition occurs flame propagation reaches supersonic speeds (in the order of 2000 m/sec) and instead of achieving deflagration, detonation ensues.

When both of these limitations are present, i.e. an engine design with compression ratios that will allow operation over the entire speed and load range, and also high amounts of throttling, part-load efficiency drops considerably. This implies that any modern spark ignition engine idling at the traffic lights, exhibits very low flame propagation speeds and very high pumping losses.

An exception to this are the gasoline direct injection (GDI) SI engines (more formally designated spark ignition direct injection (SIDI) engines – hereafter, the term GDI will be used to describe SIDI engines collectively, although the fuel does not necessarily need to be gasoline). These, in general, induce tumble through wall or piston guided air streams, achieving the presentation of an ignitable mixture around the spark plug, despite an overall excess of air in the cylinder. They thus negate the need for homogeneity throughout the entire combustion chamber, by confining combustion in a smaller volume in the vicinity of the spark plug. GDI engines increase their effective compression ratio and reduce their pumping losses by being able to operate throttleless at low engine loads, owing to stratified combustion.

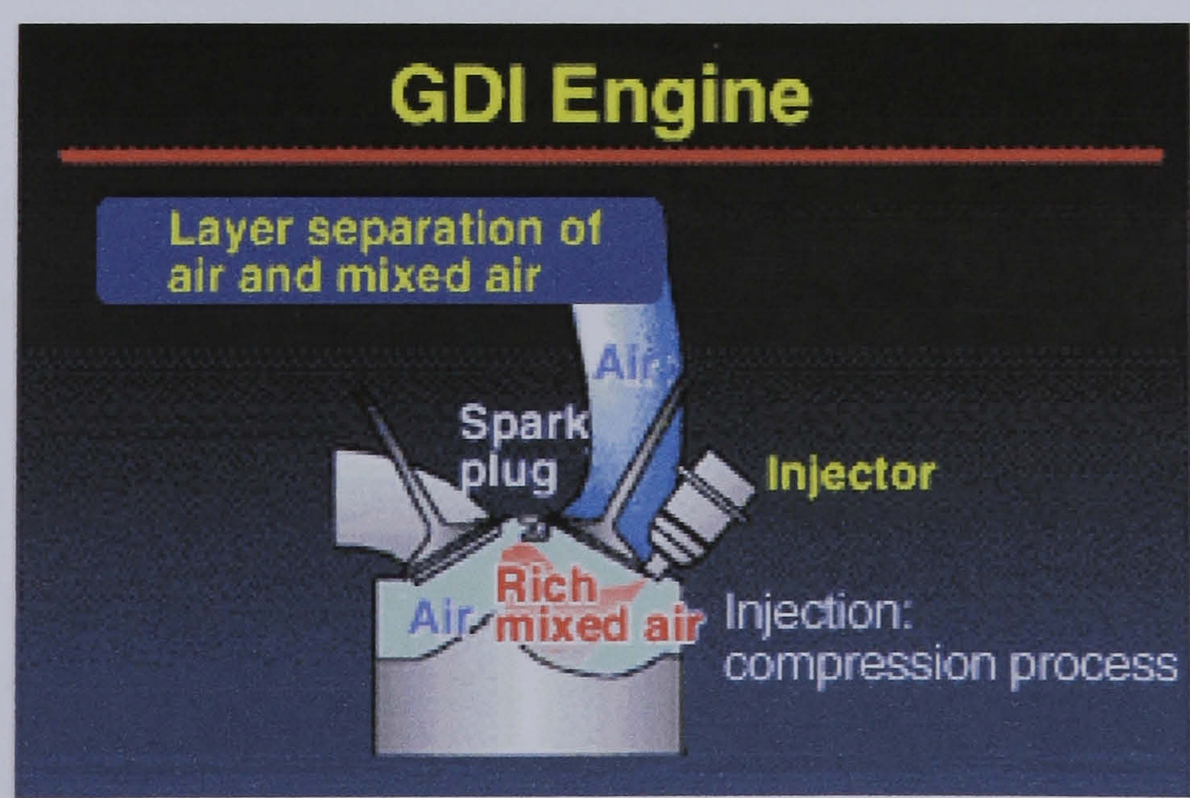

Figure 5: Mitsubishi GDI combustion chamber. [7]

Another exception is the lean burn spark ignition engines. These sometimes utilize special ignition systems and inlet/combustion chamber designs that encourage tumble and/or swirl so that flame propagation is promoted. However, both of these technologies, at the moment, can't be thoroughly used, with Three Way Catalysts (TWCs) as the only after-treatment method. The use of NOx traps is essential as an exhaust after-treatment method. Moreover, and considering that NOx traps generally need to be cold while TWCs need to be warm to operate efficiently, and that very low sulfur fuel is required for the traps to operate, commercial application of this technology has been limited. Nevertheless, in the US this fuel is available and this technology is more widely used than in Europe. This goes to show that improvements can be made when infrastructure is developed in conjunction with engine technology.

Cylinder deactivation is also a serious proposal for increasing efficiency and decreasing emissions. As part load efficiency of the SI engine is low, using fewer cylinders subjected to higher loads makes sense. It needs quite a complicated valvetrain, however, although a basic implementation of the system is already in production, whereby one bank of V8 engines is deactivated. The same can be easily done on V6 engine, too, although NVH might be an issue with the odd-firing of a three cylinder bank.

2.2.2 Compression Ignition Engines (CI)

CI engines can use very high compression ratios and also operate unthrottled throughout the operating range. This means that very high part-load efficiencies are achievable. This is because these engines operate on the principle of compressing the inhaled air to the point at which fuel, which is directly injected in the combustion chamber, ignites.

This principle of operation gives high efficiency potential. But again it comes with its own disadvantages, namely limitations on emissions' reduction. Since the fuel is ignited as it's injected inside the combustion chamber it is consumed through diffusion flame. This means that on the outside boundaries of the fuel jet very lean combustion occurs, and also the jet core very rich combustion occurs. Although this inadequate mixing is tackled through the use of swirl imposed on the intake air-steams by swirl pots or specially shaped inlet tracts the results can't match the emission levels of SI engines. As a general comment it can be said here that NOx and smoke are high in diesels, but UHC and CO tend to be lower. In addition, due to the necessarily low air utilization, as stoichiometric mixtures would result in very high particulate emissions (smoke limit), specific power outputs of normally aspirated diesels is low.

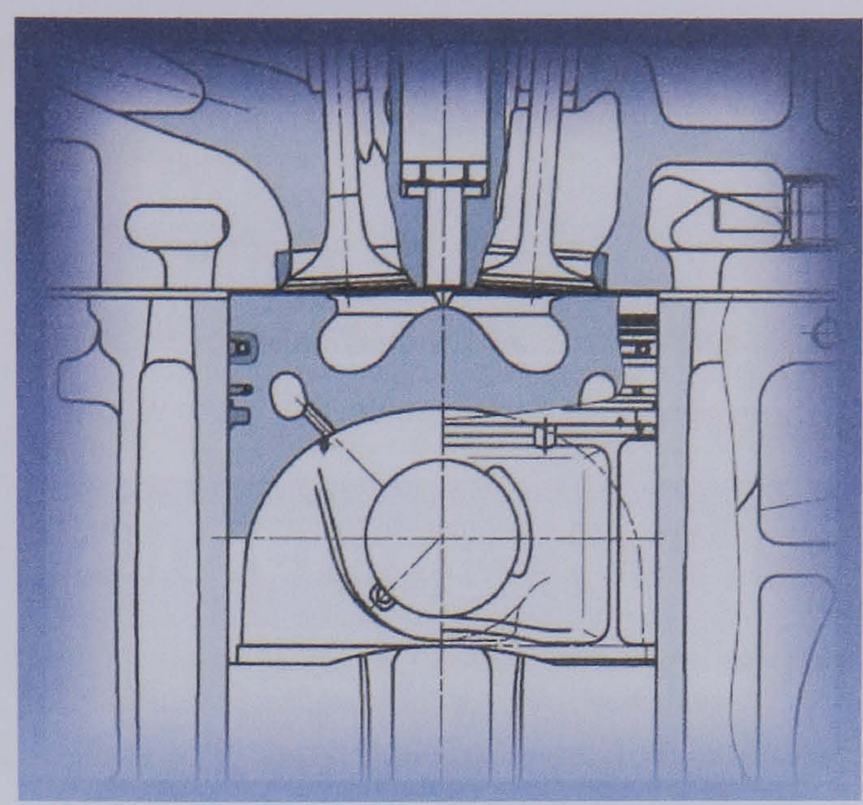

Figure 6: Typical CIDI combustion chamber. [8]

However, CI engines can be perfectly complemented with turbochargers that further increase their efficiency and (recently in combination with common rail systems) put their power density on a par with SI engines. Most importantly, turbocharging can be used without the compression ratio reduction requirement which is necessary for turbocharged SI engines. Again this comes as a direct result of the knock free (in the "end gas knocking" sense) operation of diffusion flame combustion.

2.3 Fundamentals of Homogeneous Charge Compression Ignition (HCCI)

Given the differences of the SI and CI engines it is not surprising that trying to combine the advantages of both processes while at the same time eliminating their disadvantages, is an idea that has persisted in time. HCCI or more accurately described as Controlled Auto-Ignition (CAI) combustion, is an aspiring proposition given its suggested potential for being a highly efficient combustion method.

HCCI combustion is an alternative, to the traditional spark ignition (SI) or compression ignition (CI). It allows unthrottled operation at light load, like CI, but also allows CI or SI full load operation, depending on engine origin. Thus, this combustion process can provide part-load efficiencies as high as compression ignition direct injection (CIDI) engines and energy densities as high as SI engines, if an SI engine is used as a basis. It can do this without producing high levels of nitrogen oxides (NOx) or particulate matter (PM) hydrocarbon emissions, like CIDI engines do. The principle of operation involves reaching the thermal oxidization barrier of a homogeneous air-fuel mixture, by diluting it

with re-circulated or trapped exhaust gases in a premixed charge manner and compressing it all together. Thus it incorporates the best of both SI and CI worlds. By being homogeneous, in contrast to stratified, the charge is well mixed avoiding particulate emissions, and by using exhaust gases for load regulation it does without the need for throttled operation thus reducing gas exchange losses, allowing the realization of high efficiencies.

The "trick" which permits this new combustion practice is the use of uncommonly high amounts of exhaust gas recirculation and/or highly diluted mixtures thus keeping combustion temperatures down. Introduction of exhaust gases in the mixture can be made either as external exhaust gas re-circulation (EGR) or by using early exhaust valve close (EVC) timing (or re-breathing by using late EVC) to retain trapped residual gases (TRG) within the cylinder. Note here that sometimes the terms EGR, internal EGR or trapped EGR are used instead of TRG.

Reducing combustion temperature through these methods reduces NOx production to ultra low levels, while compression ignition asserts combustion throughout the volume of the premixed charge almost simultaneously. Figure 7 [9], shows the different timescales and attributes between SI and HCCI. This technique triumphs over the problem of flame travelling through such a highly diluted, with exhaust gases and/or air, mixture. As such, very lean AFRs can be used even with further dilution through exhaust gas recirculation or trapping.

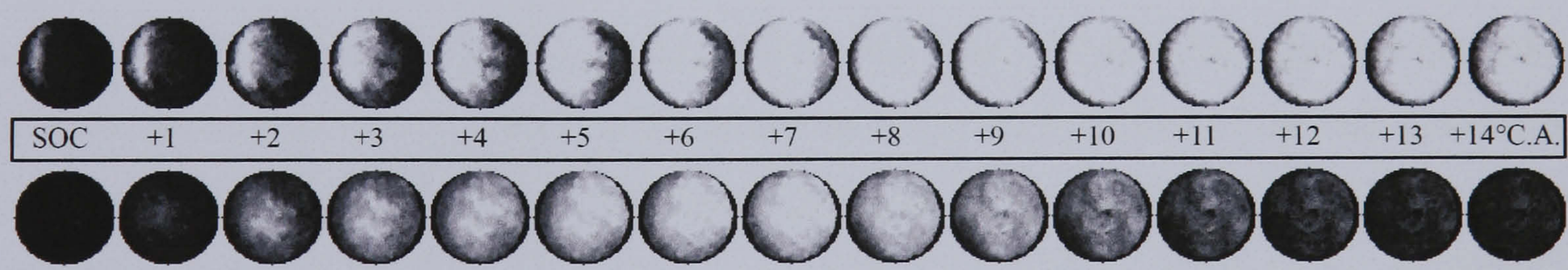

Figure 7: Comparison of SI combustion (upper row) and HCCI combustion (lower row) at 1500rpm, IMEP = 2.5bar.

Over the years a variety of names have been attributed to this process (although there are slight differences in their implementation).

Some examples are:

Active Thermo Atmosphere Combustion (ATAC)

Activated Radicals Combustion (AR, Honda)

Toyota Soken Combustion (TS, Toyota)

Premixed-Charge Compression Ignition (PCCI)

Homogeneous Charge Compression Ignition (HCCI)

Controlled Auto-Ignition (CAI, Lotus, Ford)

The first four names are mostly used in Japan, while the term HCCI is mostly used in the USA. CAI appears to be the preferred name in the UK.

In the opinion of the author HCCI is an accurate description of what is happening in a homogeneous diesel engine. But in a gasoline engine the mixture isn't necessarily ignited due to compression alone, as in most of the operating region of this type of combustion, the spark is still used to position the heat release in the desirable time window.

As commented in [10] PCCI implies fuel and air mixture formation in the inlet manifold, which is not necessarily the case, especially with GDI and diesel engines. More importantly, this combustion can be achieved not only by compression but also by intake charge heating. It is thus proposed, in the same paper, that CAI describes more closely the generic features of this new combustion process. Firstly, because this combustion process is initiated by autoignition of the combustible charge and, secondly, the autoignition combustion process needs to be controlled in order to avoid violent knocking combustion. It is also noted, that the term CAI is compatible with the conventional classification of internal combustion engines into spark ignition (SI) and compression ignition (CI) combustion engines. The author would like to add, that CAI also includes the operation window mentioned above, where spark is still used, but autoignition of the end gas occurs under controlled conditions. In this thesis, however, the term HCCI will be used as a collective term to describe all approaches while CAI will be used when specifically referring to gasoline engines.

2.3.1 Advantages

A more comprehensive understanding can be gained by again comparing HCCI with SI and CI engines.

Compared to SI engines one of the main advantages is higher efficiency. This owes to three sources:

a) Throttleless operation – reduced pumping losses

b) Higher compression ratios (sometimes as high as DI diesel engines) – increased combustion efficiency

c) Shorter combustion duration – minimized thermal losses to the cylinder walls, due to lower peak combustion temperature and closer resemblance to the Otto cycle.

Another advantage is lower NOx emissions. Especially when compared to GDI engines, the drop in NOx emissions is massive (up to a 98%), but even compared to normal SI engines the reduction may be enough (up to a 90%), to eliminate the need for a NOx reducing catalyst.

Compared to CIDI engines, both PM and NOx emissions of HCCI engines are lower. This is the result of the homogeneous diluted mixture which reduces PM by avoiding rich AFR regions and NOx due to dilution by avoiding high combustion temperatures. Ignition temperatures for HCCI are in the region of 800 to 1100K (depending on fuel type) and peak combustion temperatures are typically less than 1500K while, in comparison, CI ignition temperatures are around 500K but flame temperatures reach at least 1900 to 2100K. It is thus understandable that the levels of NOx produced from these two methods would be of entirely different orders.

The shorter combustion duration of HCCI, gives an efficiency advantage over CI engines too. Diesel engines are limited by the rate of fuel-air mixing thus fast combustion is an impossibility even with very high fuel injection pressures.

An additional major advantage of HCCI combustion, which is often overlooked, is fuel flexibility. HCCI operation has been shown possible for a wide range of fuels [11]. Multi-fuel capabilities can be exploited by converting to alternative fuel use, bio-diesel in particular. Bio-diesels exhibit two significant advantages [12], first very lean mixtures ($\varphi \leq 0.2$) become possible and second, variations in ignition timing with changes in the equivalence ratio and engine speed were shown considerably less than with n-heptane and DME.

On top of fuel flexibility, the range of possible air fuel ratios can also be increased. The range, especially towards lean operation is, theoretically, unlimited since flame propagation is not required for combustion (i.e. no flammability limits). It is thus possible to burn extremely lean, global or local, mixtures (in the order of AFR~90) in a homogeneous manner. Practically, this is limited by the exhaust gas temperatures becoming very low, in the case of TRG use for autoignition, or the actual amount of work

that is required for intake heating, becoming larger than the work that can be taken from the engine.

Coming back to emissions, HCCI is a very promising solution. CIDI or GDI engines at the moment seem to have reached their development limit. Even with the introduction of exhaust after-treatment devices, which it has to be said, are as of yet unproven and expensive, there is very little hope of them meeting future Federal or European emission standards. The main problem is that usually NOx and PM emissions after-treatment controls counteract each other. They, also, require the use of ultra low sulphur fuels (<15ppm) which are expensive and not available, particularly in Europe. In addition, the fuel injection systems that need to be used are highly expensive, accounting for 1/3 of total engine costs. There is also an associated fuel consumption increase with after-treatment, but the use of HCCI, for at least a significant portion of the driving cycle, looks as if it can seriously reduce the economic burden of lowering emissions.

GDI engines, on the other hand, need to operate lean to produce lower emissions. Consequently the common three way catalyst cannot be used, and NOx traps have to be employed. These, like in the CIDI case, require ultra-low-sulphur fuels. Even with the sulphur content specified by the EPA Tier 2 light-duty vehicle emissions standards in mind, an average of 30ppm and a maximum of 80ppm, much lower of that being used in Europe, these devices are unlikely to meet the necessary durability requirements [13].

For numerical comparison purposes the pumping losses, NOx emissions and fuel consumption of HCCI compared to GDI engine strategies is show in the following tables [14].

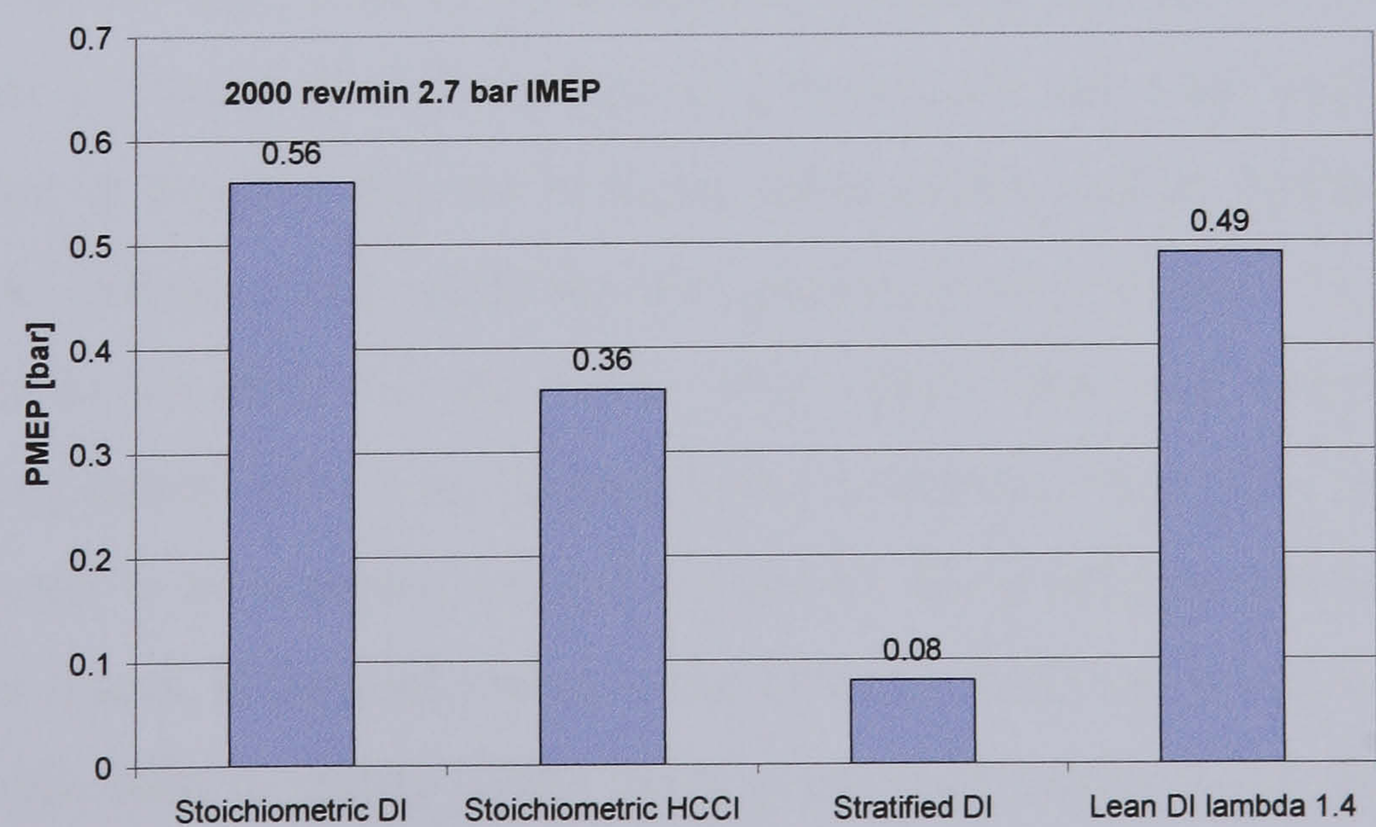

Figure 8: Pumping Losses Comparison.

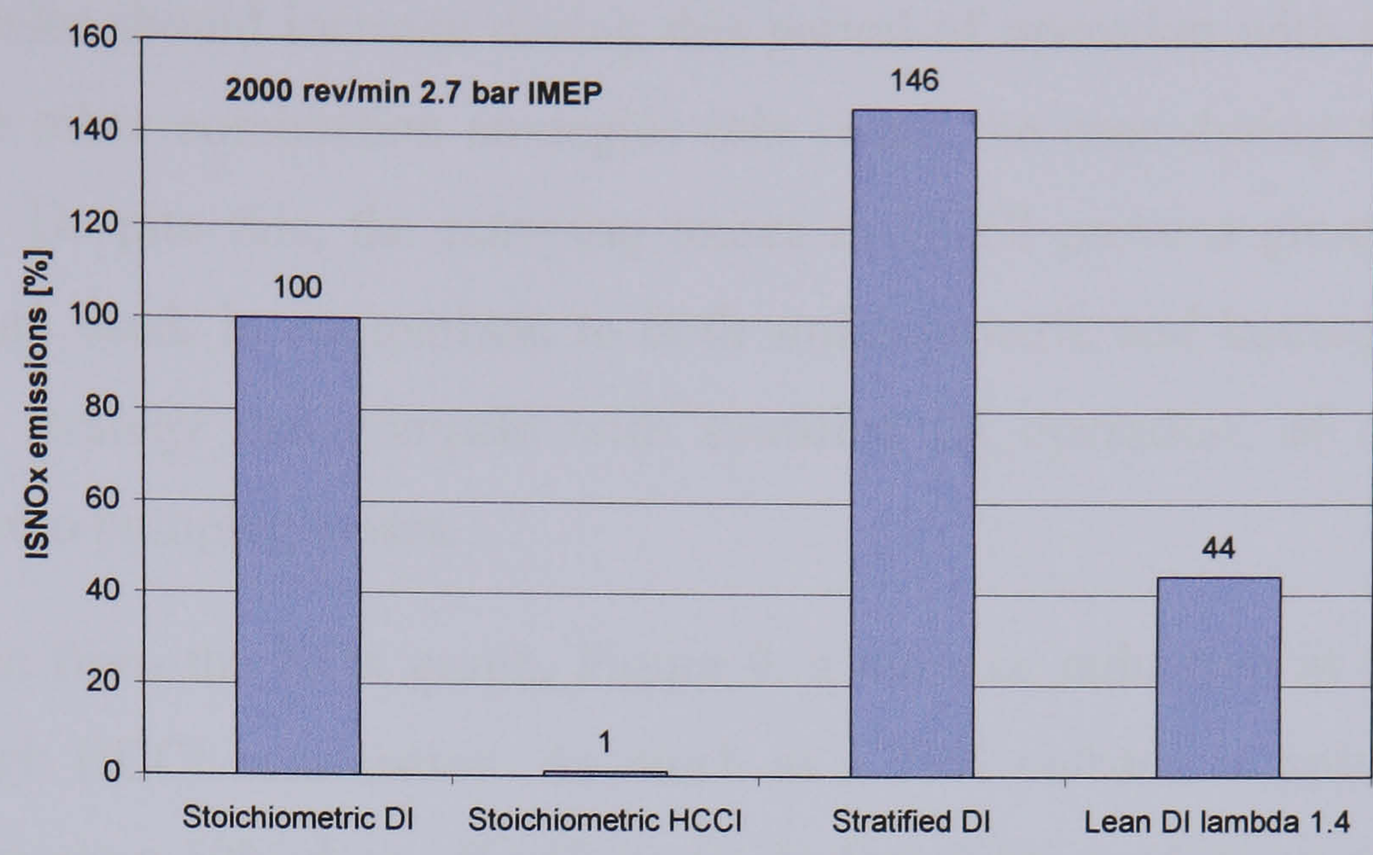

Figure 9: NOx Emissions Comparison.

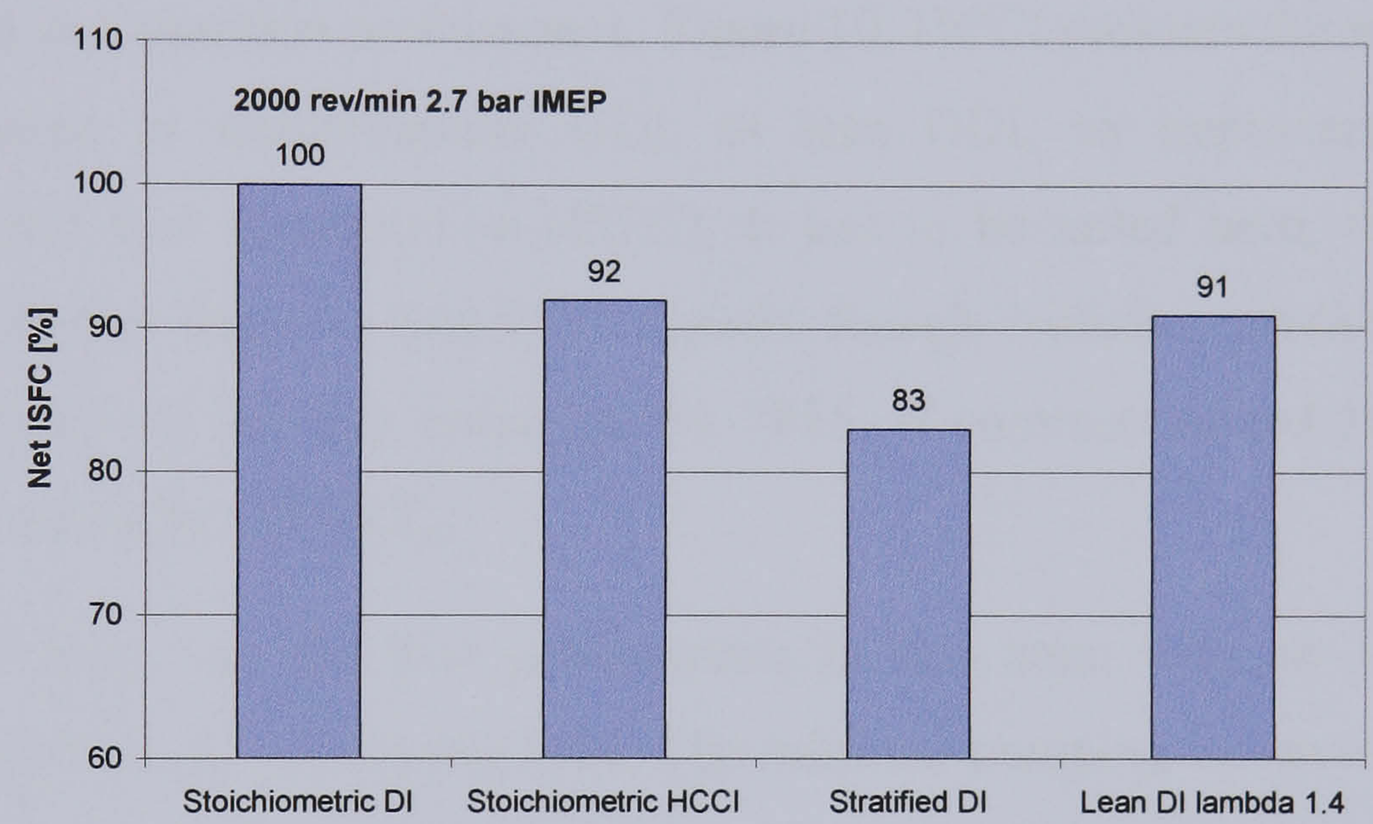

Figure 10: ISFC Comparison.

Pumping losses are a major issue of investigation, currently, in HCCI. Preliminary studies demonstrated, as in Figure 8, that the pumping losses are less than with stoichiometric GDI. This is due to the fact that the exhaust valve closes earlier, trapping combustion gases within the cylinder, and requiring less pumping work during the exhaust cycle. Also, compared to throttled SI, the inlet valve opens later and closes earlier again reducing pumping losses. However, thermal losses come into play now, since the trapped residual gases need to be compressed and expanded. Theoretically this part of the cycle would have zero losses, if thermal losses to the cylinder walls are not accounted for. This is of course not the case in reality so the work given back to the piston during expansion is not quite what the piston gave to the gases to compress them. Thus, a less than ideal pneumatic spring effect occurs. In addition, the frictional losses between piston/piston

rings and cylinder should increase during this period of operation with a loaded piston, while with the other combustion strategies this is not the case during the exhaust and intake strokes. Despite this, the pumping losses in HCCI prove a gross gain from the negative overlap used, in comparison to both stoichiometric and homogeneous lean SI operation. No strategy can compete with stratified DI operation, of course, since it presents near zero pumping losses.

As can be seen from the NOx graph, Figure 9, a massive reduction in this pollutant is realized through HCCI combustion. As much as a 99% cutback is possible and in the worst case scenario a 50% drop off will occur. In fact, NOx production negates the need of catalyst treatment, for this pollutant. The graph also shows that stratified DI strategies produce the most NOx, in contrast to HCCI.

Coming to fuel consumption performance, Figure 10, HCCI presents the same percentage benefit, compared to stoichiometric GDI, as lean GDI, an improvement of 8% in indicated specific fuel consumption (ISFC). It has to be noted here, than lean HCCI operation can further improve this ISFC benefit. Rough estimates predict a half million barrels of primary oil per day reduction by 2015, if commercialized HCCI passenger vehicles are released by 2010[15].

Stratified GDI bears out the best performance in this area, with an 18% difference, compared to baseline stoichiometric GDI. The minimal pumping losses of stratified GDI are also a major contributor to this lead.

In view of the above, HCCI offers a bundle of advantages that no other strategy does. In addition, there is room for further improvement in all the aforementioned areas, keeping in mind that serious development and research work has only started a few years now.

2.3.2 Historic outline

HCCI operation is unconventional, but is not new. As early as 1957 experiments with premixed charges of hexane and air, and n-heptane and air in a Diesel engine were being done [16]. They found that under certain operating conditions their single cylinder engine would run quite well in a premixed mode with no direct fuel injection whatsoever.

Some years later in 1979, HCCI combustion, a result of unscavenged exhaust gases from the previous cycle, was recorded [17], in two stroke engines. It was termed "Active Thermo-Atmospheric Combustion" (ATAC). It was the tendency of the engine for run-on, after turning the ignition off, that gave away the fact that some form of autoignition

was taking place. It was found out that this was the result of the high levels of residuals at part load, in two stroke engines. By exploiting this unique feature, i.e. high initial charge temperatures due to high levels of residuals, the engine operation, fuel efficiency and refinement were drastically improved. This came as a result of the cycle-to-cycle variability almost being eliminated in the "ATAC" combustion mode.

It has to be noted here, that a fact that is often overlooked when comparing normal two stroke operation to HCCI operation, is the very low compression ratio used on these engines. Especially when considering the effective compression at part load, it is obvious that it is greatly improved when the load is controlled by the amount of residuals present, instead of reducing the cylinder pressure by some form of throttling.

Observations in their optical engine showed a fine pattern of density variations and gradual combustion reactions throughout the entire chamber during combustion, instead of the normal flame front propagation.

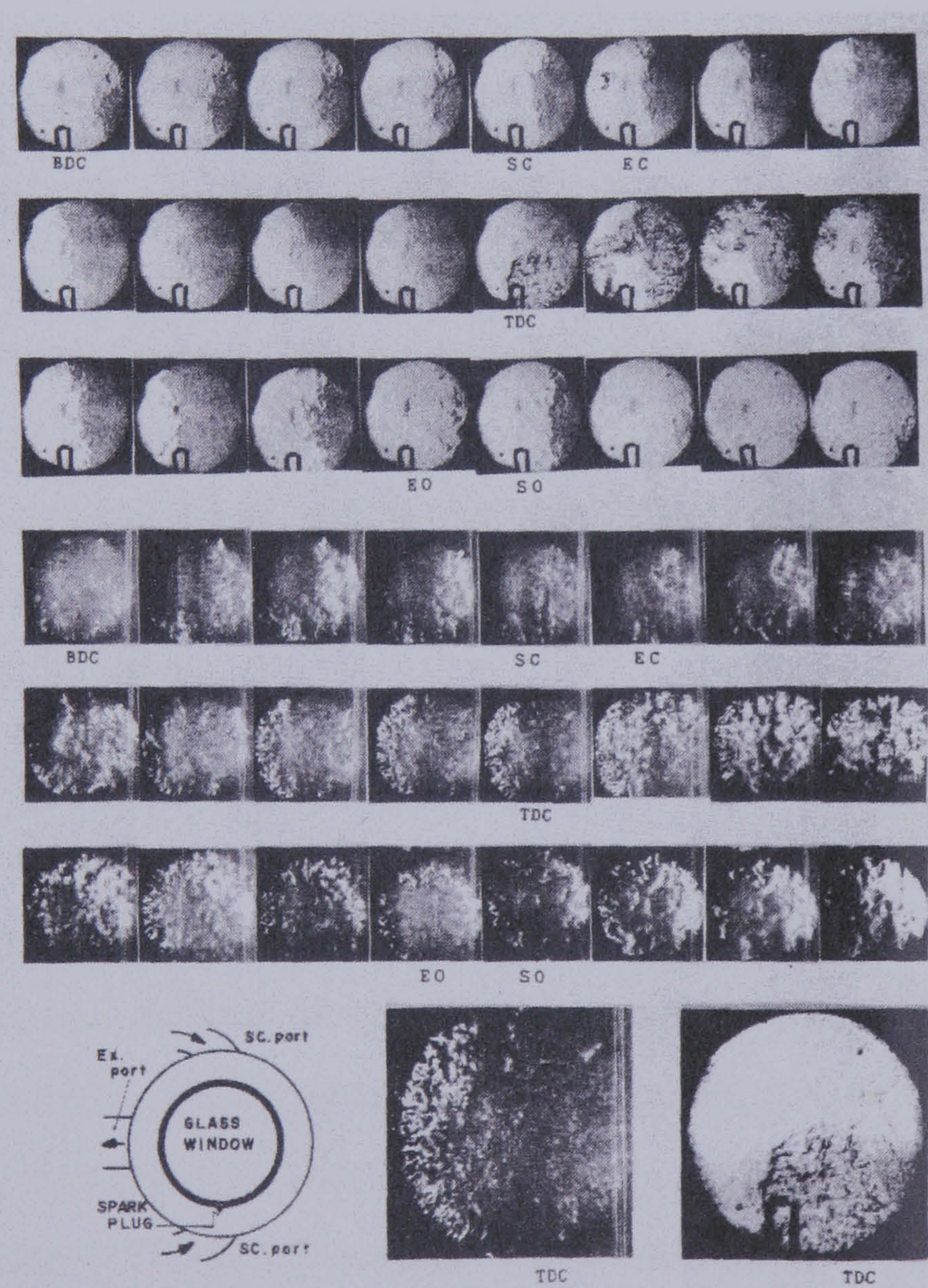

Figure 11: Schlieren photography of SI (top three rows–flame propagation) and HCCI (bottom three rows – autoignition) and close ups. [17]

The critical parameters of HCCI combustion were identified as 1) high levels of dilution to obtain high enough temperatures for autoignition, 2) uniform mixing between residual and fresh charge, 3) repeatable cycle-to-cycle scavenging [17].

At the same time, experimental work performed by Toyota and Nippon Soken Inc. [18] revealed similar behavior again on two stroke engines. The authors concluded that HCCI combustion is very well suited for part load two stroke engine operation and that while the overall burn rates were very fast, combustion was smooth and fuel consumption and emissions were vastly improved.

However, keeping in mind how inefficient two stroke engines were at part load, one understands that there was huge scope for improvement. By throttling the exhaust, or the transfer port, greatly improved gas exchange manipulation can be managed. In contrast to just leaving it to the exhaust and intake, tuning that only work efficiently in a very narrow operating band, usually close to maximum engine torque.

From optical investigations during this research at Toyota, multiple sites of ignition and no discernable flame front propagation were evident. Spectroscopic analysis revealed high levels of CH_2O, HO_2, and O radicals well before autoignition. These species are characteristic of low-temperature autoignition chemistry of larger paraffinic hydrocarbon fuels. During combustion, high concentrations of CH, H and OH radicals were recorded, indicative of high-temperature chemistry during the bulk-burn. These measurements resembled concentrations found in end-gas autoignition and knock, thus confirming the similarities between HCCI and combustion and knock while also justifying the use of the term Controlled Auto-Ignition.

Work in four-stroke engines, has also been done using blends of paraffinic and aromatic fuels over different engine speeds and loads (dilution), simulated internal residuals by heating the intake air [19]. Chemical kinetic modelling and heat release analysis of experimental data showed that two semi-independent processes of ignition and bulk fuel combustion were present. HCCI autoignition is governed by the low-temperature chemistry (>1000K) that leads to knock in SI engines. The bulk energy release comes from high temperature (>1000K) CO oxidation. Based on chemical kinetics alone, a correlation for the energy release that simulated the experimental results was developed that explained HCCI behavior to changes in compression ratio, equivalence ratio, dilution level, engine speed and fuel type. These results and the previous work on two-strokes concluded that HCCI is a chemical kinetic combustion process controlled by the

temperature, pressure and composition (which can be time dependent) of the charge. This work, [19] concluded that HCCI is not a mixing-controlled process, but rather resembles a compression-ignited, stirred chemical reactor. Further work [20] examined HCCI operation of a single-cylinder engine using fully blended gasoline. Again, air to fuel ratio and external EGR rates were varied in an attempt to find the limits of this operating regime.

Much of our knowledge of knock chemistry has been based on experiments in shock tubes, constant pressure flow reactors, rapid compression machines and motored engine layouts. These experiments have highlighted the importance of low and intermediate temperature chemistry in knock processes [21,22]. The data have also been used to develop and validate detailed reaction mechanisms for higher-carbon-number fuels such as n-heptane and iso-octane [23,24].

As with all of the above researchers, the limitations of speeds and loads that an HCCI engine can cover is always observed. A hybrid engine operating strategy was first suggested in 1989 [20], where part of the operation would be conventional SI, while HCCI could cover the more favourable, for this type of combustion, regions.

From all of the above, it can be concluded that HCCI is a process where mechanical means are used to control what is basically a chemically controlled process. By having an understanding of the underlying chemistry it becomes easier to explain experimental observations and to devise methods for its control.

Still, the implementation of HCCI engines is not straightforward. With current technology status, HCCI can only be used for hybrid electric powertrain applications. This is because electric power generation does not require operation over a wide range of speed/load conditions, which is where HCCI engines currently struggle. It is the control issues of HCCI engines over wide windows of operation that are holding them back presently and it is this area that this research is going to be concentrating on.

2.3.3 Challenges of HCCI

HCCI control is achieved by management of the factors that affect fuel autoignition. These are mainly pressure, temperature, fuel composition and mixture strength. On top of these, secondary parameters that influence autoignition like ambient humidity, fuel temperature history and others exist, but these are even more difficult to measure and

manipulate. It is this chemical nature and interdependence of these parameters that imposes a great challenge over real life implementation of such engines.

In addition, despite the very promising integration of the CI and SI engine concepts in HCCI engines, new and unique problems of this mode of combustion arise. These are high hydrocarbon and CO emissions, a comparatively narrow operating range and ignition timing and heat release rate control. As such, they constitute the principal areas that need resolving and are the focus of current research.

2.3.3.1 HC and CO Emissions

HC and CO emissions in homogeneous charge engines mainly arise from the crevices in the combustion chamber. This is due to the fact that the portion of the mixture that gets trapped in these, fails to combust completely. The cooling of this mixture is a lot more pronounced due to the greater surface to volume ratio in the crevices. Also, more importantly, the difficulty of the flame to propagate into these, contribute to this phenomenon. However, in SI engines the temperatures in the cylinder are high enough to support the conversion of the hydrocarbons as the piston moves down and the trapped gases are mostly released. This is not the case in HCCI engines were peak combustion temperatures are typically less than 1500K. At these temperatures, even the autoigniting mixture that lies in the heart of the combustion chamber fails to complete the CO to CO_2 oxidation and the combustion efficiency deteriorates precipitously at lower loads were the lowest temperatures occur. High combustion temperatures in stoichiometric SI engines allow post combustion oxidation processes to continue into the expansion stroke and blowdown process [25]. In HCCI this post combustion CO oxidation becomes inefficient due to the low temperatures. Freezing of CO in the cylinder when fuel and intermediate species cannot react into ultimate products and some hydrocarbons emitted from combustion chamber crevices only partially oxidize to CO [26].

In addition, if one considers the near-wall region where flame extinction occurs due to heat transfer and the crevice volumes, it becomes apparent that HC emissions may increase. One more issue is the resulting low exhaust gases temperature that can then result in reduced after-treatment efficiency, further adding to the problem. However, studies have proven that the exhaust temperature when air to fuel ratios are close to stoichiometric ($0.95<\lambda<1.15$) and a standard SI compression ratio the temperature level remains between 450 and 560°C which is sufficient for after-treatment with an oxidation catalyst [9].

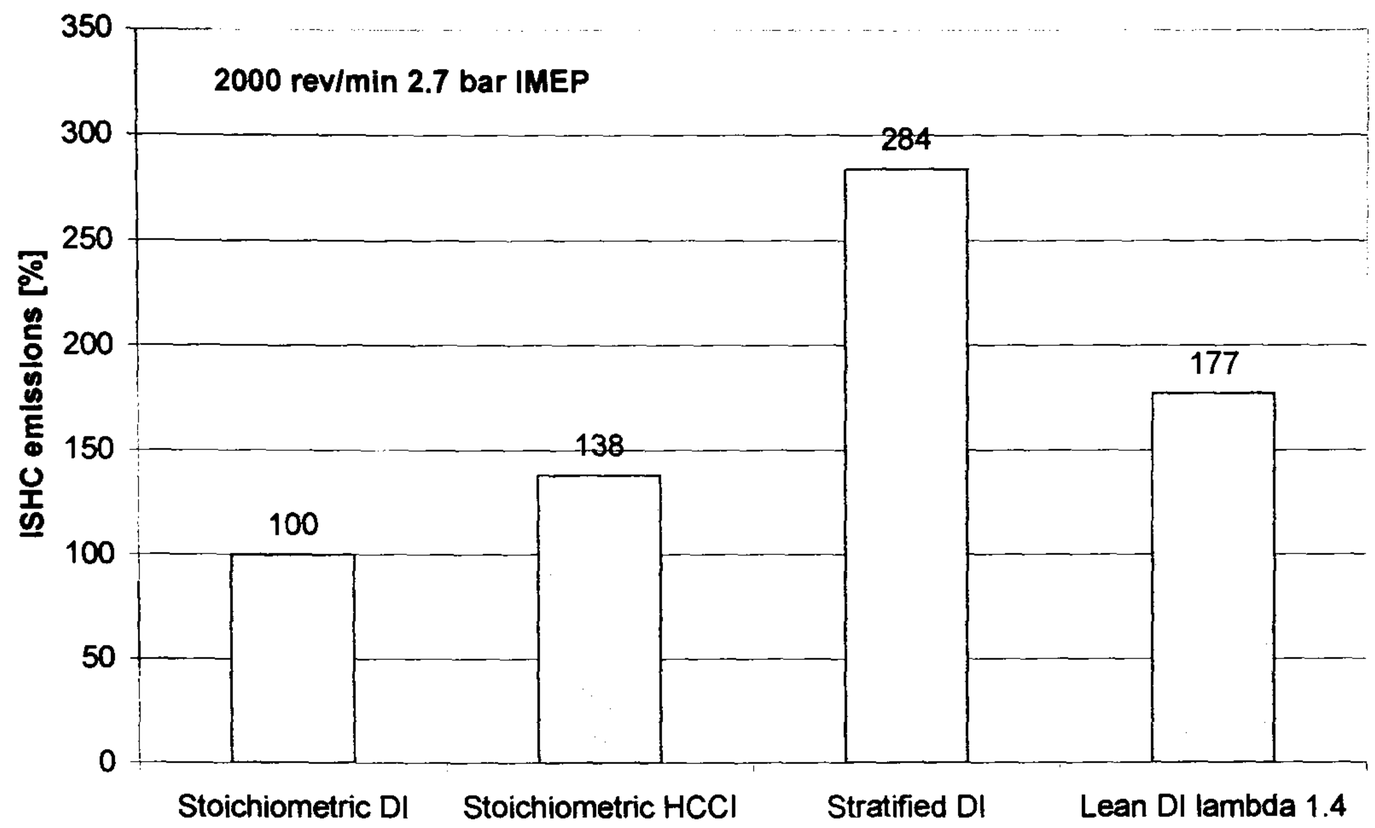

Figure 12: HC Emissions Comparison.

The results of HC emissions can be observed in Figure 12 above. A small increase in HC pollutants is visible when HCCI is compared to standard stoichiometric direct injection SI. However, this will not necessarily pose a problem since with the lean exhaust gas possible with HCCI, very good conversion rates are possible with standard catalyst technology [27]. In addition, zero smoke emissions are expected in HCCI combustion due the homogeneous mixture.

By having the low load operation limited due to the combustion inefficiencies that arise as a result of the low combustion temperatures, it immediately transpires that a multi-mode, or hybrid, engine is needed to serve the complete operating range.

When one also considers that the high loads, in "diesel" implementations of HCCI, are also limited by the large heat release rates that occur due to the low mixture dilution and enriched mixtures, the seamless transition between the modes of combustion appears as a fundamental issue for the implementation of such an engine. Transient behaviour of HCCI engines, be it within the autoignition operating region, or where mode switching is necessitated, is still an unresolved issue at the centre of research attention.

2.3.3.2 Ignition Timing Control

Ignition timing control is the most important control parameter. It is governed by the chemical kinetic reaction rates of the mixture, which are in turn governed by time, temperature, pressure and mixture composition. Temperature is the leading factor here, but its interdependence to mixture pressure and composition cannot be neglected. More

fuel means higher heat capacity, which implies that everything else kept the same (EGR levels, air temp, inlet manifold pressure, compression ratio etc) higher AFR values than stoichiometric retard ignition timing. In addition, lower than stoichiometric AFR also retards ignition timing since less low-temperature reactions lead to delayed temperature increase. However, AFR also affects exhaust gas temperature thus complicating matters even more. In addition speed can also have a major effect on ignition timing. Furthermore, if transients are considered, matters become considerably more complex.

It goes without saying that, if full flexibility over engine operation is desired, a simple engine map like the ones currently used for spark ignition timing in SI engines, or injection timing in CI engines is not adequate for ignition control. Some sort of closed-loop control must be employed, avoiding driveability problems and (more importantly) engine damage.

The elements of this control system will depend on the engine configuration and control strategy. One more consideration is the source of feedback that will be employed. These issues will be discussed in more detail later, and are some of the core issues of this research.

Depending on fuel type used, the strategies will vary. One-stage-ignition fuels (e.g. gasoline) need different handling compared to two-stage-ignition fuels (e.g. diesel fuel).

In essence, all of the various methods employed to control HCCI, employ some controlling variables in order to achieve autoignition near TDC. These methods are described below.

2.3.3.3 Methods

A closer look of the methods for provoking autoignition reveals that this can be divided into two main categories.

The first one is usually termed "Thermal Control". This method uses as controlling parameters the temperature, pressure and composition of the mixture at the beginning of the compression stroke i.e. at IVC. It includes intake air heating, variable compression ratio (VCI) or residual gas trapping. One more controlling parameter that can be used in conjunction with this method is direct injection during compression and expansion of the trapped exhaust gases allowing "fuel reformation". It basically gives time to the fuel to break up making it more prone to autoignition. The second method is to use dual fuels. This is more of a "Chemical Control" technique that can manage autoignition timing.

In conjunction mostly with the first method, use of an advanced ignition system is also thought as a way of "nudging" the mixture further into HCCI. These ideas include the rotating ark spark plug (RASP) [28], Figure 13, pulsed flame jet (PFJ) [29], Figure 14, and capillary force vaporizer (CFV) [30]. All of these essentially increase the possibility of ignition at the desired point by introducing energy into the system, usually in the order of 100+ times that of a spark plug.

Figure 13: The Rotating Arc Spark Plug (RASP).

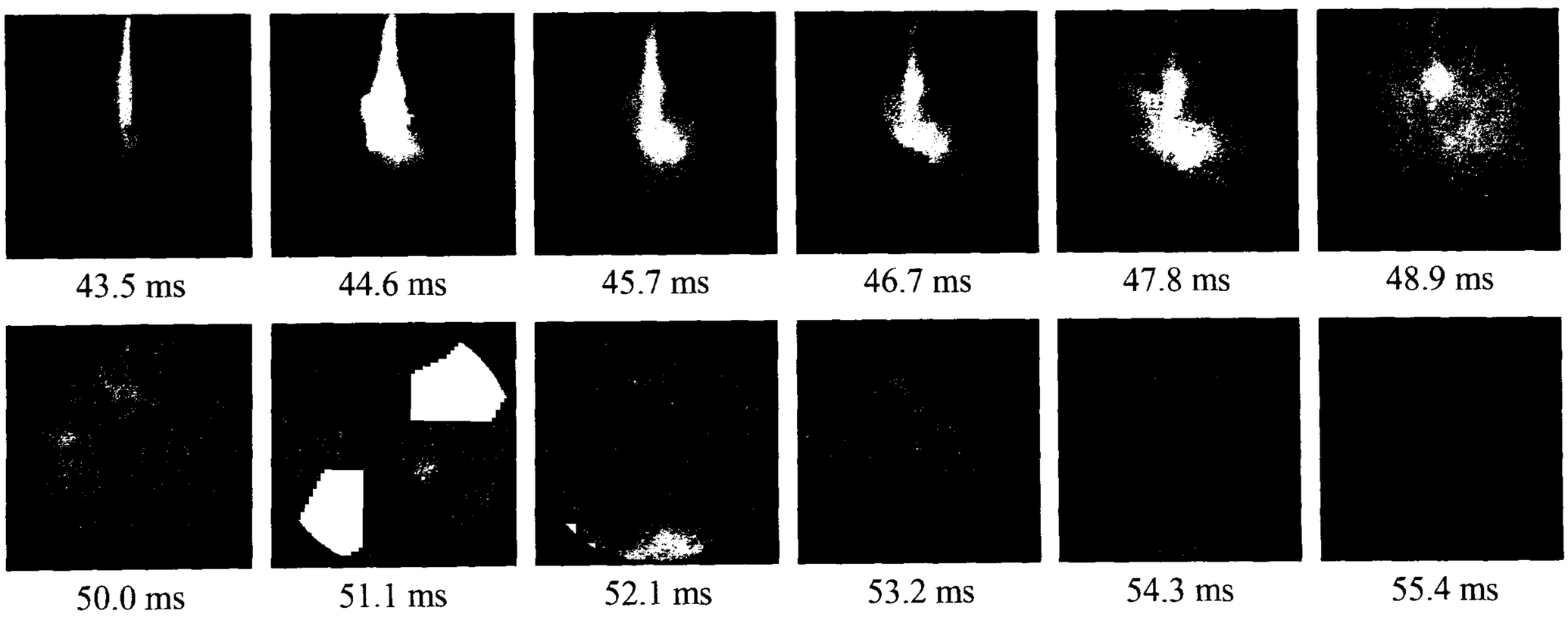

Figure 14: PFJ initiated HCCI combustion.

Heating the intake air

The necessary temperature for promoting autoignition at the required crank angle can be achieved through intake air heating. This can be done using electric heaters or, more efficiently, by using heat exchangers that take advantage of the high temperature exhaust gases. With charge heating, the operational area is limited. Since the mixture is not

diluted with exhaust gases the only way to avoid too fast a rate of heat release is to operate very lean. A very lean mixture will lower the flame temperature and this temperature decrease will slow down the reaction rate [31]. The lambda usually used is in the order of 2.5 – 4. Start of combustion can be trimmed through varying the charge temperature or lambda.

It needs to be considered here that, for example, when a cylinder with a displacement volume of 0.5l is operated at 2000rpm at a load of 2.8bar NMEP, unthrottled, the power delivery by the engine is 1.2kW. The power required to heat up the inlet air with an electric heater is 1.13kW [32], so the overall engine efficiency is very low.

Another disadvantage of this method is the very slow transient response of the inlet charge temperature. It would be difficult to practically control this temperature during transient demands by the driver, in real life applications. In addition, when the engine will need to switch between SI and HCCI operation a problematic operation area occurs. This is because the volumetric efficiency of the engine is greatly reduced when hot air is used. The density of air at 25°C is 1.2kg/m^3 while at a temperature of 180°C, typical for HCCI operation, it is only 0.779kg/m^3. Unless two separate intake air systems are used, the time requirement for heating or cooling the intake air to transition from SI to HCCI and back, would certainly cause driveability issues.

A possibility is to increase the temperature of the intake air by passing it through a compressor i.e. a super- or turbo-charger. Although this would be a much more efficient way, it introduces further degrees of freedom to the system thus increasing complexity and control demands even more.

Variable Compression Ratio

Varying the compression ratio is a method that mechanically controls mixture temperature at the end of the compression stroke. In theory the thermal efficiency of an internal combustion engine is directly proportional to the compression ratio, as shown in the equation below.

$$\eta_{therm.} = 1 - \frac{1}{CR^{k-1}}$$

This means that fuel consumption can be reduced when a higher compression ratio is used. However, compression ratios are limited due to a number of different reasons. In gasoline engines it is limited mainly due to knock. Knock propensity increases with

increasing compression ratio, since higher pressures and temperatures are reached at the end of the compression stroke. This increases the fuel octane requirement. With modern day fuels the compression ratio is limited to about 12:1 on a naturally aspirated engine and even less on super or turbo charge engines. The compression ratio could be increased more if ignition timing was retarded but this would sacrifice overall efficiency.

In diesel engines compression ratios are higher, typically in the order of 20:1. But this higher compression ratio also increases friction due to the higher cylinder pressures. Also the unfavourable shape that the combustion chamber needs to have to achieve such high compression (flat deck cylinder head) increases energy losses due to heat transfer because of the greater surface-to-volume ratio. Furthermore, this shape slows down combustion introducing "time losses". An "ideal" compression ratio according to Heywood [33] is between 14 – 16:1.

A variable compression ratio would be very beneficial, even in SI engines. This is because high compression ratios can be used at low loads while lower ratios can be used at high loads. This would allow for maximum efficiency during throttling and maximum power density at wide open throttle (WOT).

For HCCI applications the variable compression ratio can influence the temperature level at the end of the compression stroke, thus affecting autoignition timing. However, typical compression ratios do not lead to a temperature that is high enough for autoignition at the end of the compression stroke. Thus this technique is usually used in conjunction with a heater or variable valve timing [11,34,35,36].

There are a number of engine examples and companies working on VCR systems [37,38,39]. Most notable are the SAAB developed system that is based on a hinged, tilting cylinder arrangement [40] and a project that varied the compression ratio by varying the position of a plunger mounted in the cylinder head [11]. The variable position plunger is the only method that has already been proved to work in HCCI method. It was shown that this method can control combustion phasing over a wide variety of intake temperatures and fuel types of different octane numbers.

Dual Fuel

Ignition enhancing additives are yet another way of going about autoignition engines. If, for instance, two fuels with different octane numbers (or methane numbers) are used, the low octane fuel can be used to control combustion timing (trigger fuel) while the high

octane one can be used as the main fuel (base fuel). The cool flame produced by the low octane fuel at low temperatures is basically used to elevate the temperature, thus leading the high octane fuel to autoignition.

Systems presented include dimethyl ether (DME) [41] in combination with methane, natural gas and naphtha fuel (gas and liquid) [42], ethanol and n-heptane [43], iso-octane and n-heptane [44] and also propane and ozone [45]. This last enhancer, ozone, has the added advantage of requiring only very small amounts of it to be added and also does not require a second fuel tank, since it is claimed that ozone can be produced on-board with a relatively inexpensive and fast response system. One more possibility is the use of natural gas and hydrogen, using hydrogen as the ignition improver. Again, hydrogen can be produced on board using a natural gas reformer [46].

Exhaust Gas Trapping

Trapping exhaust gases performs a dual function in the autoignition process. This method is a combination of thermal and chemical control. Firstly, it introduces energy in the system thus bringing the mixture to the required temperature near the end of compression. Secondly, it dilutes the mixture with inert gas so that the rate of heat release after autoignition is brought down to an acceptable level. Chemical effects are an ongoing debate mainly concerning the inertness of the gases. Many researchers claim that these freshly trapped exhaust gases contain radicals that help break up the fuel molecules, thus aiding autoignition in a way other than just increasing the temperature. This is based upon the observation that the autoignition temperature, when trapped residual gases (TRG) are used, are lower than with intake air heating. It is said that the importance of active species was confirmed by experiments where preheated air or nitrogen, in similar quantities and temperatures to real EGR (TRG) were used to dilute the charge and where autoignition was possible with EGR it was not with the other inert substitutes [25]. The opinion of the author is that apart from the fact that it is very difficult to accurately estimate TRG content in the final mixture, it is also very hard to estimate the heat addition that this TRG provides. This is mainly because, it is almost impossible to guarantee that there is no remaining traces of fuel, or partially combusted fuel in these exhaust gases which will react at an early stage during compression, further helping autoignition. This claim is based on the fact that it is very usual to observe combustion during the TRG compression and expansion stroke i.e. the gas exchange cycle, during the negative valve overlap

period. Incandescent particulate matter of partially oxidized fuel can provide hot spots that will promote autoignition in the next cycle.

In the case where a combination of SI and HCCI combustion modes is used, a conventional compression ratio in the order of 10 – 12:1 must be used. To calculate the temperature at the beginning of the compression stroke so that a temperature of 1100K would be reached at the end of it, a rough calculation can be performed as follows:

$$T_{BDC} = \frac{T_{TDC}}{CR^{k-1}}$$

Assuming a specific heat ratio k of 1.33 and adiabatic compression, the equation becomes:

$$T_{BDC} = \frac{1100}{11^{1.33-1}} = 499K$$

i.e. very close to 500K.

If the residual mass temperature is known, the mass required to promote autoignition can be calculated. However, this temperature will depend on the residual mass used during combustion. The temperature of TRG drops when a lot of TRG is used during combustion. So adding more of it, will not necessarily advance ignition timing. It is this dependence of the combustion cycle on the previous gas exchange cycle that complicates control on HCCI engines. On the other hand, as can be seen, TRG has a self stabilizing effect, since increasing its fraction will also reduce its temperature. Cyclic behaviour can be seen owing to this effect. Especially during transients, where TRG temperatures from the previous cycles might be very different to that required for steady state of the new operating condition, this effect can have drastic consequences. Thus it is this behaviour that should be closely monitored and resolved, for transient operation to be made practically possible.

Two techniques are used for trapping the exhaust gases. One is by early exhaust valve closing and late inlet valve opening [47], while the other is keeping the exhaust valve open during the intake stroke so that the exhaust gases can be re-breathed [48]. The first technique introduces thermal losses and possibly additional frictional losses, during compression and expansion of the gases, i.e. during the negative valve overlap. The second technique might result in better mixing but will introduce additional pumping losses and reduce the charge temperature, at the start of compression.

There exist various ways for varying the valve timing. The simplest form of implementation is mechanical VVT systems, variable valve lift (VVL) systems and cam profile switching (CPS) systems. There is a notable cost penalty for implementation of VVT, VVL, CPS and/or phasers on production engines, but many forms of these systems are already in production in upmarket models.

However, fully variable valve actuation (FVVA) systems provide the much greater flexibility needed for a complete realisation of the potential of HCCI. This later category consists mainly of electro-mechanic and electro-hydraulic valve actuators. Electro-mechanic (or electromagnetic as they are otherwise known) systems are, usually, fixed valve lift devices. Electro-hydraulic systems offer the most flexibility, with cam profiles being able to change readily, on a cycle-to-cycle basis at the press of a button on the controlling PC.

Trapping exhaust gases, offers exceptional control and transient possibilities. It is thus being used more and more by various researchers [49,50,48,51,36]. It is argued that TRG has multiple effects on combustion. Apart from the obvious thermal effect, four others can be identified [12]. These are:

Heat Capacity

TRG increases the specific heat capacity of the mixture (air-fuel-TRG) due to the presence of large percentage of CO_2 and H_2O, resulting in significantly lower peak temperatures, when compared to SI combustion, using the same amount of fresh charge.

Dilution

TRG introduction dilutes the air/fuel charge with "inert" (arguably) gases. Since dilution may be up to 80% the oxygen dilution that the fuel will "see" has a pronounced slowing down effect on combustion rate.

Exhaust Gas Species Concentration Increase

Since CO_2 and H_2O concentrations are high, even before combustion starts, their net production rate during combustion tends to decrease.

Radical Production and Destruction Influence

It is claimed that, "some exhaust gas species, particularly residual (active) radicals (such as H, OH, HO_2), may influence the production and destruction reactions of some radicals.

Also, water vapour as an effective third body may affect reactions where a third body plays an important role, such as in termination reactions".

2.3.3.4 Extending HCCI Operation to Wider Range of Speeds/Loads

Extending the operating range of HCCI engines is another challenge that needs to be won on the road to production. There are two considerations here, one is load the other is speed. In general HCCI operation is suitable for loads between 15% and 40% IMEP, whilst typical speeds covered in automotive engines are between 1250 and 3500 rpm.

2.3.3.5 Low Load

The lower load limit is due to what is termed the misfire limit. As load is decreased the TRG is increased leaving less room for fresh charge, allowing throttleless operation. However, with less and less fresh charge, the heat release becomes inadequate for heating up the exhaust gases to the point of making them suitable for autoigniting the next cycle's fresh charge. Thus misfire occurs. HCCI combustion was first observed in two-stroke engines and it has to be noted here that a major difference of those engines to four-strokes are the very different heat losses involved. TRG in two-strokes is fresh from combustion, thus more can be tolerated and also idle operation is possible.

Heat management is a way of improving low load performance in four-strokes. Heat losses must be decreased so that the sensible energy carried by TRG will suffice for autoignition. One method of reducing heat losses is heat insulation of the combustion chamber. Heat-insulated engines constructed with ceramics around the combustion chamber and without water cooling exhibit very high wall temperatures, exceeding 900K [52]. This causes the intake charge temperature to increase more than that of a conventional water-cooled engine by approximately 250K at the end of the compression stroke [52] (note: compression ratio used for their experiments was 15-16:1). They used sintered silicon nitride (Si_3N_4) and air gaps or gaskets having low thermal conductivities. They also claim that the use of ceramics alone, with water cooling, are not adequate for the drastic heat insulation required.

Extending to low load operation is very important for HCCI. This is because it if it was made possible for autoignition to occur during idle, a great fuel saving, especially during real-life use, would be possible. Efficient idle operation in gasoline engines is at the

moment a GDI stronghold. Diesels are also very efficient during idle for the same reasons, that are lean, overall, combustion and low throttling losses.

As far as meeting emissions standards is concerned, HCCI would be particularly difficult to realize during cold start idle, which is a very important area for emission reduction during both the European and Federal driving cycles. During this time which is before catalyst light-off a large percentage of the total pollutants of the driving cycle are produced. With a cold engine autoignition will be very difficult to achieve. If it was made possible however, it would be a real breakthrough in emissions production (around 17% of time spend at idle during the drive cycles, as seen in the following pictures).

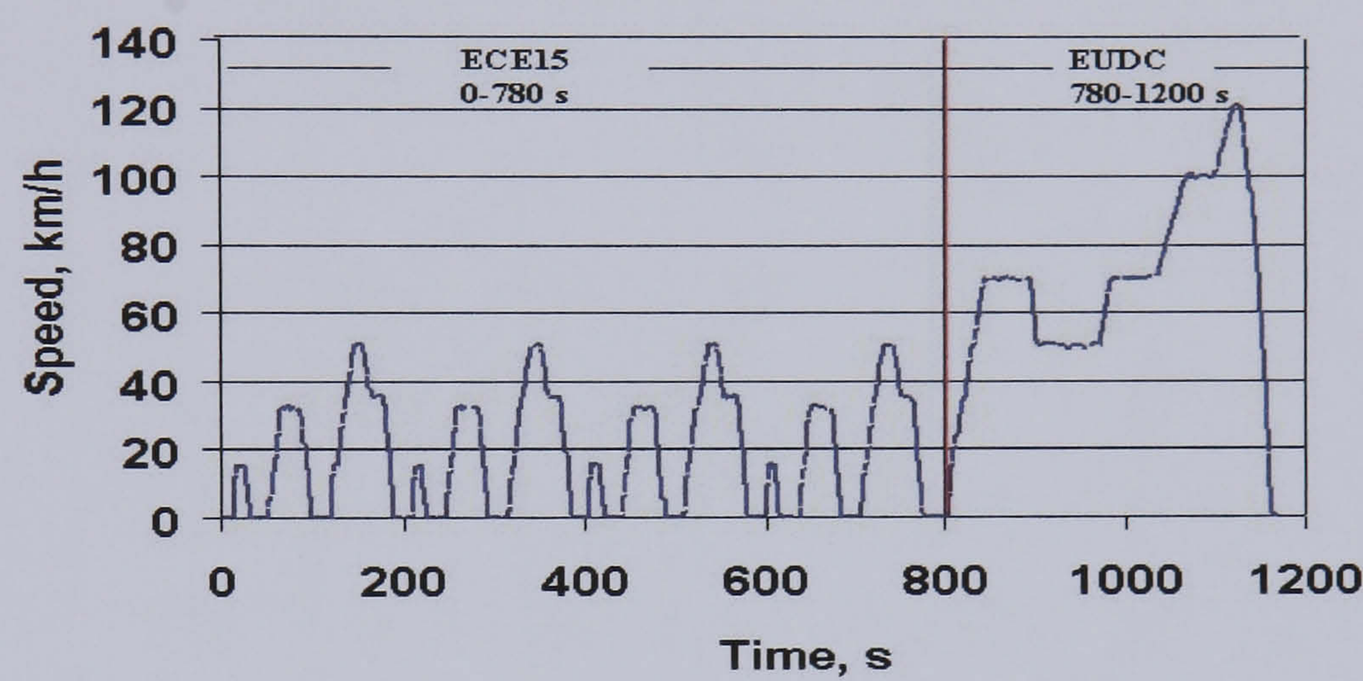

Figure 15: European Test Cycle (EC2000) [53].

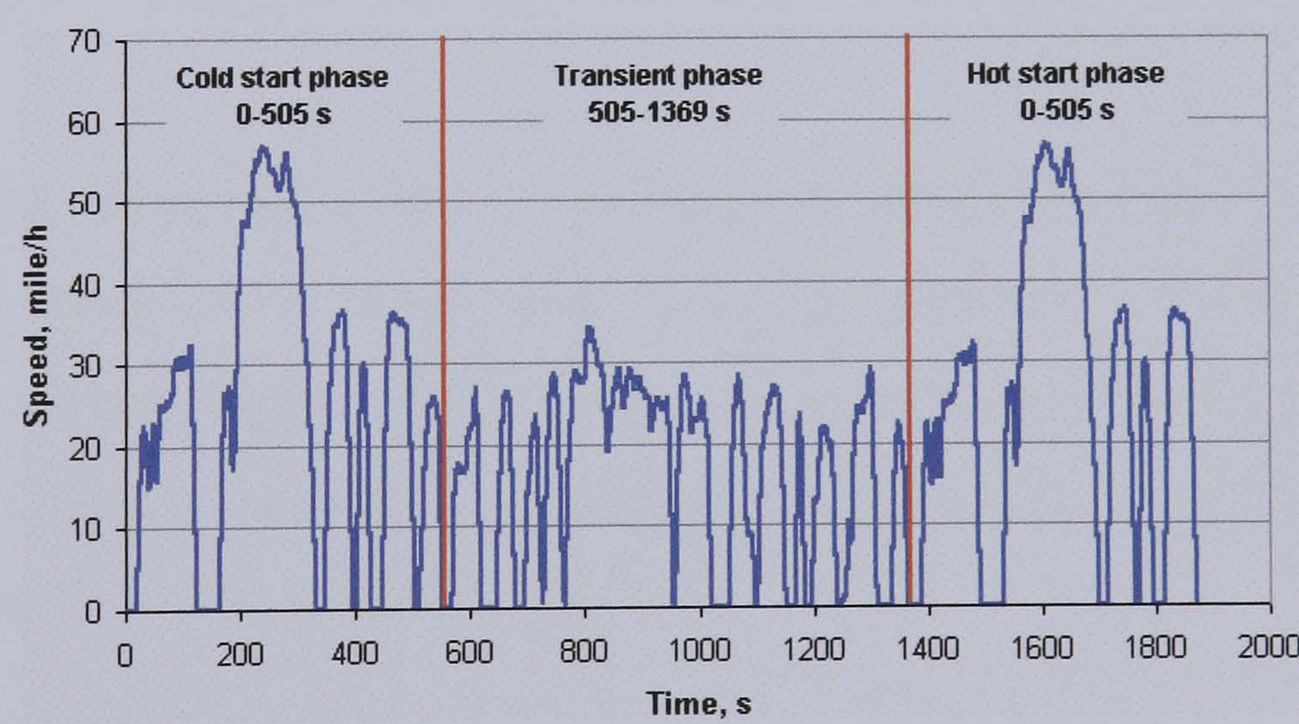

Figure 16: Federal Test Cycle (FTP-75) [53].

2.3.3.6 Thermal Barrier Coatings

Since low load operation is considered vital for HCCI and thermal barrier coatings are felt to be a good suggestion for its implementation, an extract from [54] will be quoted here.

Thermal barrier coatings are becoming increasingly important in providing thermal insulation for low heat rejection (LHR) engine components. For such an engine the insulating material must possess low thermal conductivity, low specific heat, high strength, high fracture toughness, high thermal shock resistance, low friction and wear resistance, high temperature capability, high expansion coefficient and chemical inertness for high resistance to erosion and corrosion. More information on thermal barrier coatings can be found in Appendix 1.

Material	Ultimate flexure strength MPa	Den g/cc	Young's modulus at 1260°C GPa	Coeff.of therm Exp. 300-1260°k 10^{-6}/°k	Coeff.of therm Cond W/m°k
Si_3N_4	300	3.1	300	3.2	12
SiC	450	3.15	400	4.5	40
AMS	20	2.2	12	0.6	1
ZrO_2	300	5.7	200	9.8	2.5
Al_20_3 TiO_2	20	3.2	23	3.0	2

Figure 17: Typical ceramic insulation materials and their properties [55].

A more subtle way of reducing heat-losses could be coolant water management. This is not difficult to achieve during steady state operation. However, the transient response of the coolant management system will probably not be such that whenever the engine idles for short periods, engine temperature management would be possible, due to the heat capacity of the water located in the engine block.

It has been argued that the major difference in two and four-stroke engines cannot be solely attributed to the different heat losses. Active species are theorised to play an important role [25], which will readily survive into the next combustion cycle in a two-stroke engine. These active species result in a triggering of low temperature reactions prior to autoignition. This can be backed by the fact that a two-stroke exhibits different emissions with reduced HC and CO, under HCCI operation. In the same paper the mechanism of autoignition is said to be based on low temperature oxygen addition reactions:

$$R\bullet + O_2 \Leftrightarrow RO_2\bullet$$

that take over and are strongly biased in the forward direction, because $E^+=0.0$ and $E^-=27.4$ kcal/mole so:

$$RO_2\bullet + RO_2\bullet \Rightarrow RO\bullet + RO\bullet + O_2$$

will be underway because it too has a small activation energy, E=5.09 kcal/mole. Further RO• is unstable and tends to decompose quite readily into small stable oxygenate species, primarily aldehydes or ketones, in addition to small alkyl species. Since aldehydes are also reactive and the small alkyl species lead to a smaller alkyl species following similar reaction paths, the decomposition of RO• accelerates the process [56]. The reaction of any alkyl radical with O_2 are strongly exothermic, therefore the extent of these reactions was proposed to be large enough to form many small reactive species, which are the cause for either autoignition (or spark ignition) of highly diluted mixtures or late cycle autoignition, where, again, temperatures are low.

Development of methods to slow down combustion in HCCI at high loads is needed. This is to prevent excessive noise and more importantly engine damage. Also methods for providing positive ignition of the charge at low loads are needed, since the basic current strategies do not function satisfactorily at this condition.

The limits exist mainly for the following reasons. The lower load limit occurs because after a point, exhaust temperature decreases to a point where misfire starts occurring. As the load lowers the mixture of air/fuel needed to produce the torque required also reduces. This produces lower temperature exhaust gases which in turn return colder TRG. In every engine there is a specific speed/load curve beyond which autoignition will fail. Increasing the compression ratio or reducing heat losses can extend the low load limit.

The upper load limit is a by-product of not being able to trap enough TRG to initiate combustion, since a high quantity of fuel/air mixture is required to grant the torque demand. As more of the cylinder displacement needs to be filled with combustible mixture, less room for TRG is left. A way to overcome this problem is to use higher than atmospheric intake pressures by super/turbo charging it. This boost in pressure will allow more mixture to be squeezed into the cylinder despite of the high amount of trapped TRG. However, even this method won't allow us to realize operation over the entire range of a typical SI engine, since the maximum rate of pressure rise will then become the limiting factor, above a certain load level. If spark assisted operation is introduced to initiate

combustion at high loads and lower TRG levels, instead of boost, then this HCCI-SI hybrid combustion may continue again up to where the rate of pressure rise will rule it out and then fully spark ignited operation should be instituted. A last resort is to use reaction suppressors, water, methanol, ethanol, 1-propano, methane etc, which will decrease oxidization rates, thus allowing excursions into higher load areas. However, their use in production cars can't be easily implemented, so this method must not be considered as a viable proposition, at least not with the current customer perception and fuel infrastructure.

One last method of extending the operating range to lower usable loads/speeds and also extending the lean limit of HCCI is called "fuel-reformation". This is a completely different approach since it uses a novel double injection sequence. In addition this method can only be used by direct injection (DI) engines, but there is no need for separate fuel tanks. In essence what this method does, is injecting some fuel before the TDC of the exhaust stroke, allowing a much bigger than normal time interval to reform under the influence of the high temperature, due to TRG, and the further increase in pressure, inflicted by the compression of the trapped exhaust gases, going towards TDC. This reformed amount, thus prepared for easier combustion, will then push the rest of the fuel, which is injected normally during the intake stroke, to ignition. Consequently combustion can take place at much lower average exhaust manifold temperatures than it would, without the help of the elongated temperature fuel history. The amount of fuel that should be injected towards the end of the exhaust stroke is a research subject at the time of writing. What is clear, as of yet, is that not all of the fuel needed to produce the torque required, should be injected then. A small amount (in the order of 1/3 to 1/2) of the fuel should only be injected. More will lead to lower fuel efficiencies, since quite a lot of it will be burned at the time of injection, especially with lean mixtures. Less will not produce enough reformed fuel to readily ignite the rest that will be injected on the second pulse. Please note that the overall fuel efficiency of this method is not proven yet.

2.4 Alternative HCCI Uses

2.4.1 Free piston engines

HCCI combustion has the unique feature, for internal combustion engines, of not needing an ignition circuit or an in-cylinder injector (direct injection) and the associated high

pressure fuelling system. In its simplest form, the homogeneous mixture, prepared by either a carburetor or low pressure port fuel injection just needs to be compressed to its autoignition point. This reduces both cost and complexity. It is thus a combustion method that lends it self nicely to free piston engines and especially micro-internal-combustion-engines.

One very well known proposition is that of a free piston linear alternator [57]. They argued that electrical generators capable of high conversion efficiencies and extremely low exhaust emissions will no doubt be a good proposition for powering advanced hybrid vehicles and stationary power systems. In comparison to fuel cells, the existing infrastructure for the maintenance of internal combustion engines, gives such an idea a very competitive advantage.

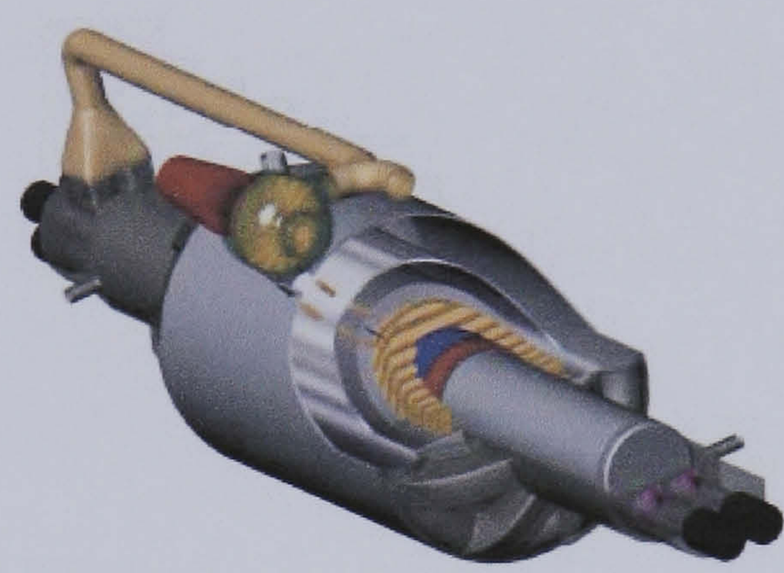

Figure 18: Free Piston Linear Alternator.

Homogeneous charge compression ignition (HCCI) combustion could be used to solve the problems of burn duration and allow ideal Otto cycle operation to be more closely approached. Weak mixtures can be used and further, the useful compression ratio can be increased, as higher temperatures are required to autoignite weak mixtures [58].

Most of the HCCI studies to date however, have concentrated on achieving smooth releases of energy under conventional compression ratios, with crankshaft driven pistons. Because of these operating parameters, successful HCCI operation has required extensive EGR and/or intake air preheating.

The same paper claims that in order to maximize the efficiency potential of HCCI operation much higher compression ratios must be used and a very rapid combustion event must be achieved.

The free piston linear alternator illustrated in Figure 18 has been designed in hopes of approaching ideal Otto cycle performance through HCCI operation. In this configuration, high compression ratios can be used and rapid combustion can be achieved.

The linear alternator is designed such that electricity is generated directly from the piston's oscillating motion, as rare earth permanent magnets fixed to the piston are driven back and forth through the alternator's coils. Combustion occurs alternately at each end of the piston and a two-stroke cycle scavenging process is used. The alternator component controls the piston's motion, and thus the extent of cylinder gas compression, by managing the piston's kinetic energy through each stroke. Compression of the fuel/air mixture is achieved inertially and as a result, a mechanically simple, variable compression ratio design is possible, although very sophisticated electronic control will be required.

The use of free pistons in internal combustion engines has been investigated for quite some time. In the 1950's, experiments were conducted with free piston engines in automotive applications. In these early designs, the engine was used as a gasifier for a single stage turbine [59,60]. Thus the materials that had to be used in the turbine were less critical, since the gases had already expanded in the free-pistons combustion chamber.

More recent developments have integrated hydraulic pumps into the engine's design [61].

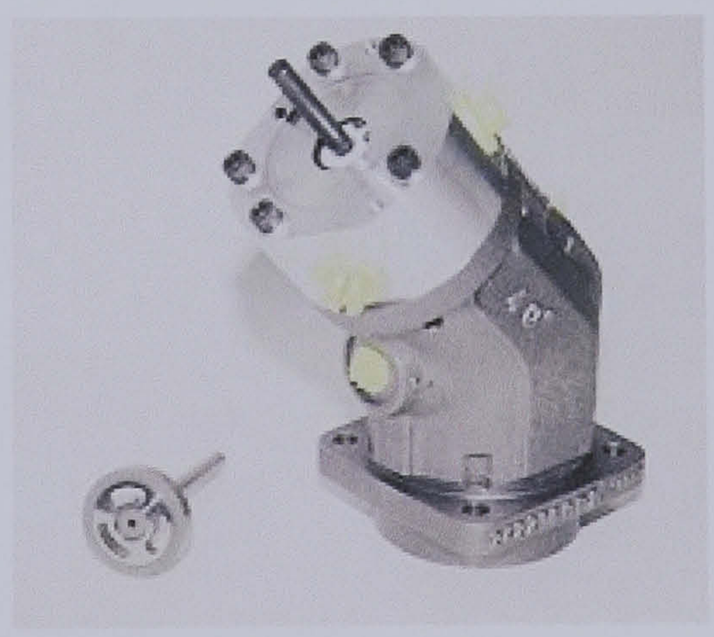

Figure 19: Innas' CPR system, which integrates a Centaur free-piston engine and hydraulic transformers. [62]

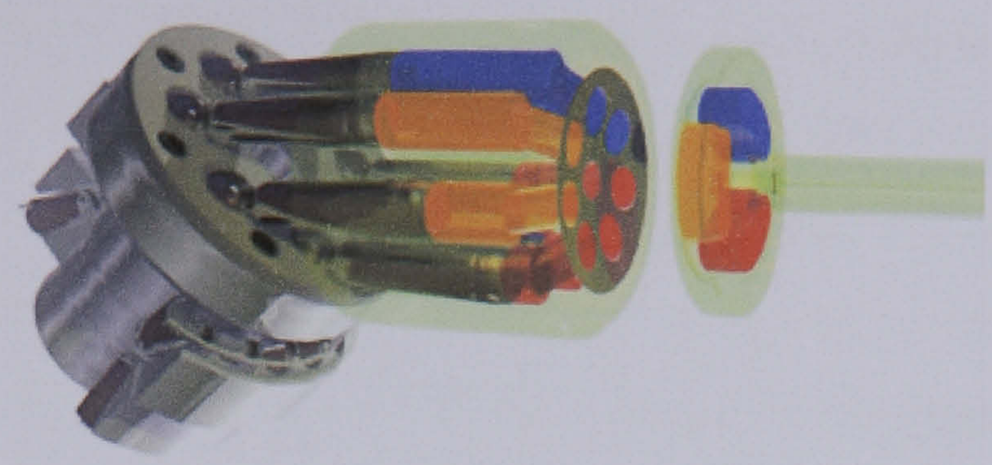

Figure 20: The hydraulic pump of the Innas system.

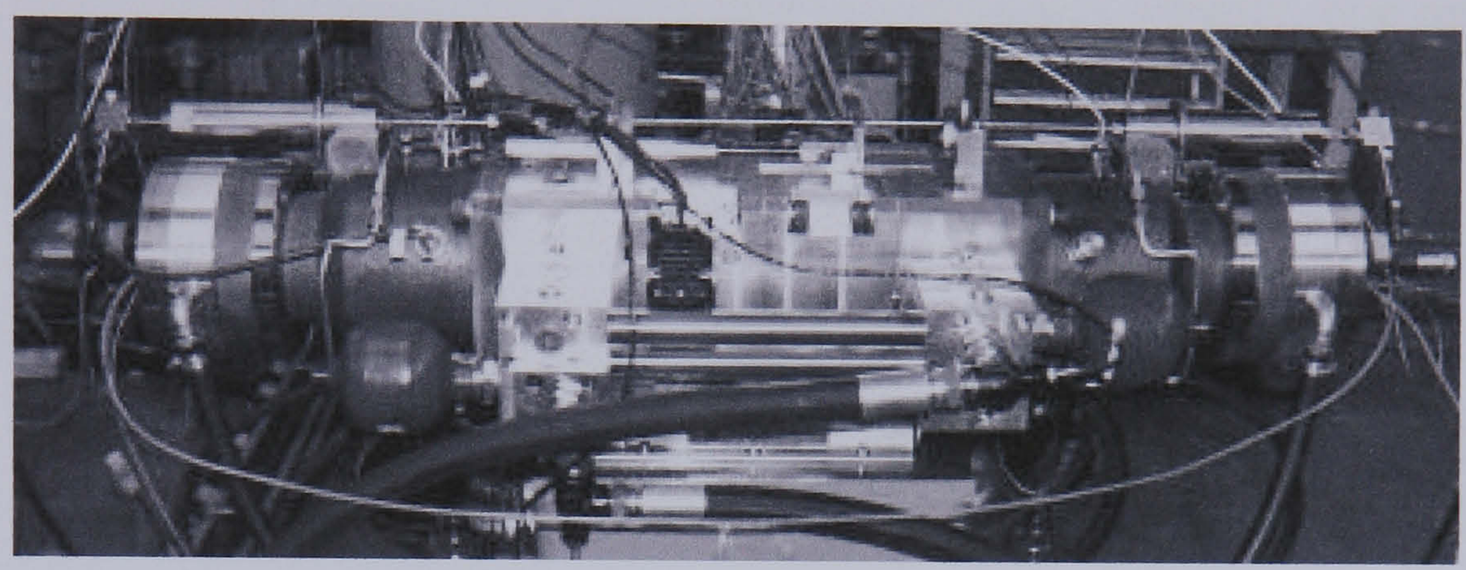

Figure 21: Free piston engine with hydraulic transformer. [63]

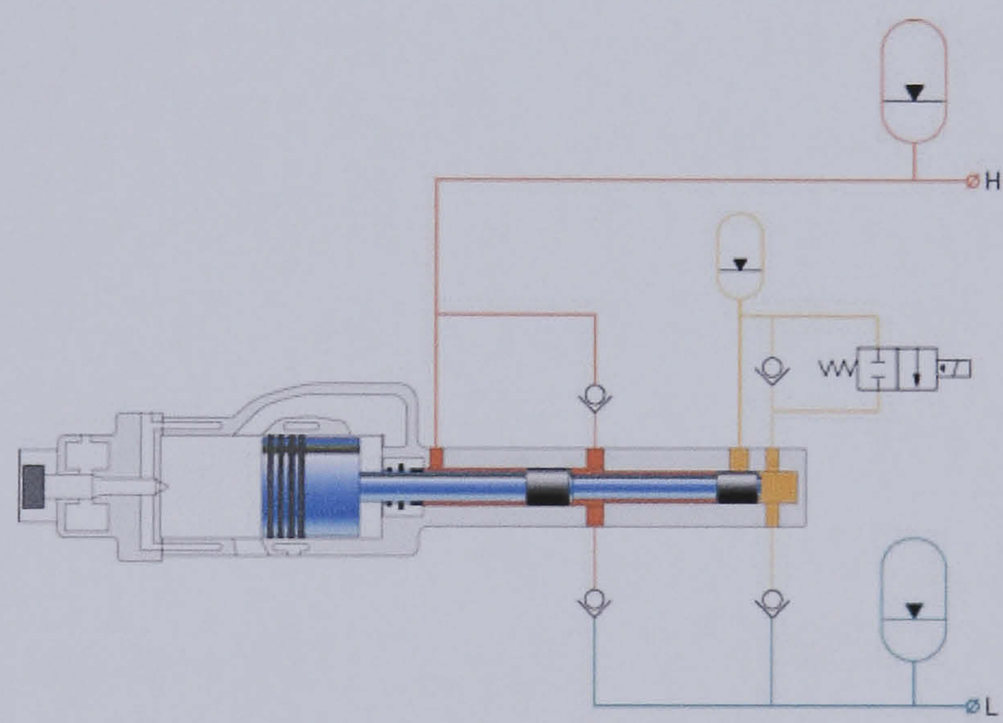

Figure 22: Working principle of hydraulic transformer.

The working principle is really quite simple. Be it a single, or double (or double-faced) piston, a connecting rod is used to couple it to a piston pump and from there a few one-way valves ensure that oil is pumped from the reservoir and pushed towards the control valves.

Several advantages have been noted for free piston IC engines. First, the compression ratio of the engine is variable; this is dependent mainly on the engine's operating conditions (e.g., fuel type, equivalence ratio, temperature, etc.). As a result, the desired compression ratio can be achieved through modification of the operating parameters, as opposed to changes in the engine's hardware.

An additional benefit is that the mechanical friction can be reduced relative to crankshaft driven geometries since there is only one moving engine part and no piston side loads. It is also claimed that combustion seems to be faster than in conventional slider-crank configurations (this might be the case if higher compression ratios are used, which is plausible with free piston engines). Further, the unique piston dynamics (characteristically non-sinusoidal) seem to improve the engine's fuel economy and NO_x emissions by limiting the time that the combustion gases spend at top dead center (TDC) (thereby reducing engine heat transfer and limiting the NO_x kinetics). Finally, one researcher [64] reports that the cylinder/piston/ring wear characteristics are superior to slider/crank configurations by a factor of 4.

Thus, although at a mostly theoretical stage at the moment, the combination of the HCCI combustion process and the free piston geometry is expected to result in significant improvements in the engine's thermal efficiency and its exhaust emissions. The claim by the same paper is that the following advantages should be found:

1. For a given maximum piston velocity, the free piston arrangement is capable of achieving a desired compression ratio more quickly than a crankshaft driven piston configuration. This point is illustrated in Figure 23 where the piston position profiles of both configurations are plotted. The reduced compression time should result in higher compression of the premixed charge before the onset of autoignition.

2. High compression ratio operation is better suited to the free piston engine since the piston develops compression inertially, and as such there are no bearings or kinematic constraints that must survive high cylinder pressures or the high rates of pressure increase (shock). The use of low equivalence ratios in the HCCI application should further reduce the possibility of combustion chamber surface destruction.

3. The free piston design is more capable of supporting the low IMEP levels inherent in low equivalence ratio operation due to the reduction in mechanical friction.

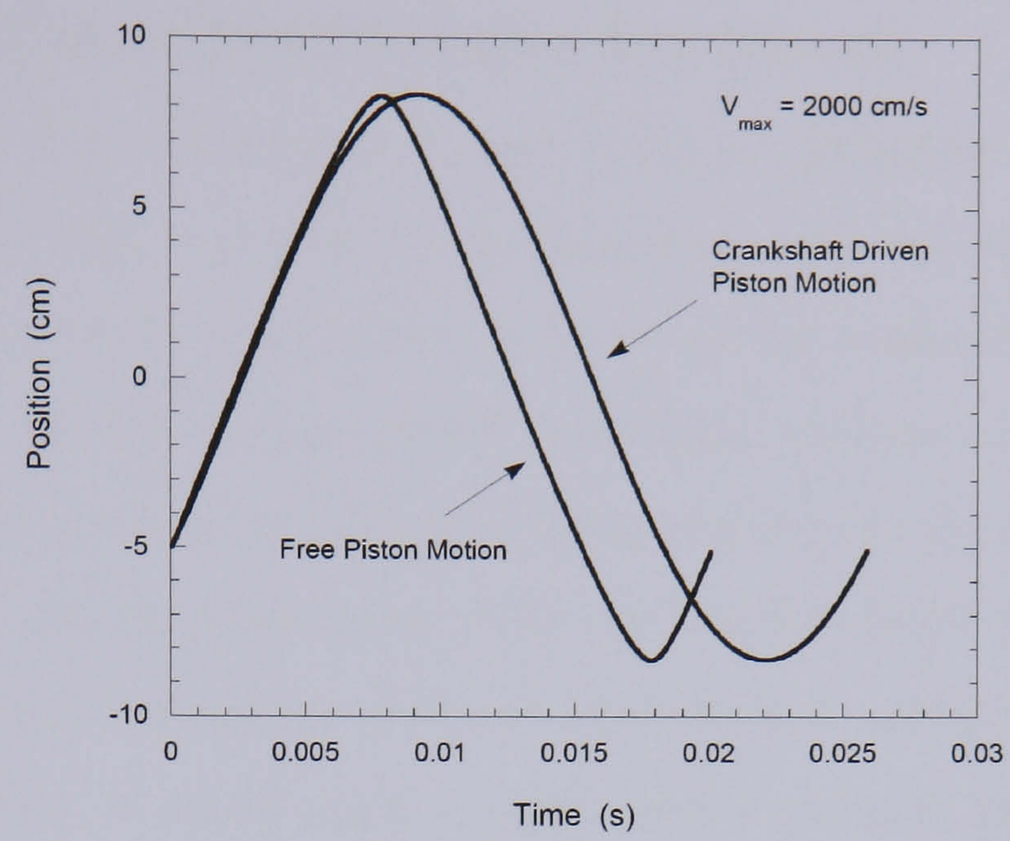

Figure 23: Free and crankshaft driven piston motion comparison.

The linear electric alternator they use is based on technology developed for brushless DC motors. This class of motors is characterized by high efficiency and high power density, typically 96% efficiency and 1 hp per pound density. An easy way to conceptualize this alternator is to imagine that the rotary configuration is unrolled until flat, then rolled back up, perpendicular to the first unrolling, to arrive at the linear configuration. Relative to the rotary geometry the linear device is approximately 30% heavier since not all the coils are driven at the same time. Efficiency however, is claimed to be comparable.

Inherent in double-faced configurations is the need to scavenge the exhaust gases out of the cylinder and replace them with fresh fuel/air charge while the piston is down at the bottom of the cylinder. This is because trapped gases are needed in the cylinder to act as a spring, as well as to provide the next combustion event.

Since this engine is only needed to run at a very narrow operating speed, the free piston oscillation is essentially fixed, and power is varied by decreasing the equivalence ratio, or by adding some level of boost. Power density is said not to be a driving requirement.

In general pumping losses (η_{pm}~0.7) ensue for sufficiently high scavenged operation (η_{sc}~0.8). This is because of the relatively high 2:1 compression stroke to bore ratio used (for adequate clearance at TDC). Additionally, either high pumping losses, or low power output will ensue in order to achieve adequate cylinder charging.

2.4.2 Reduced-size HCCI Combustion System

Another area of focus from the same program is the investigation of a greatly reduced-power output device. The key area of investigation was to determine if high fuel conversion efficiencies (56% seen previously) could be maintained at a 2 kW size. Problems anticipated related to the greatly increased surface to volume area of the combustion chamber at ignition, and the reduced time available for combustion due to the higher oscillation rate. On the other hand, if the combustion event is fast enough then the increased oscillation rate will reduce the time for heat loss, compensating for the larger surface to volume ratio. A small rapid compression expansion machine (RCEM) was fabricated with a bore of 1.2 cm, compared to the larger RCEM dimension of 7.6 centimeters.

It is claimed that the performance of this small scale variant was comparable to the large scale one. The equivalence ratio had to be increased, however, by a factor of almost two. This may lead to NOx emissions problems, but it was not possible to measure these with the small quantity of gas produced. The intended applications for a generator of this size, though, do not consider NOx emissions as a primary design goal. As such this may not be a significant issue.

2.4.3 Micro HCCI

Electronic devices have greatly benefited because of miniaturization. Reduced size brings reduced cost. As such, Micro Electro-Mechanical Systems (MEMS) are being used vastly in sensors and actuators. It makes sense then to develop micro-scale internal combustion engines, so that reduced costs and power density can be had. Considering once again the vastly different power densities of fossil fuels and batteries it is easy to calculate that fuel conversion efficiencies of just 2.5% are enough to outperform any battery. Thus micro-engines could prove a valuable power plant. It is thus not surprising that various micro-engines programmes are run today. The Massachusetts Institute of Technology with the Micro-Gas Turbine Engine, the University of California Berkeley with the MEMS Rotary Engine, Honeywell International with the Free-Piston Knock Engine and the Georgia Institute of Technology with the MEMS Free-Piston Engine Generator are all aiming to develop an engine generator that will deliver 10-20W of electricity from a package volume of around $1cm^3$.

However, just scaling down the engine dimensions would not work, because phenomena differ in small scales [65,66].

This is mostly because of the different heat losses associated with small scales that present a much higher surface to volume ratio. These increased heat losses result in reduced combustion efficiencies and reduced flammability limits. Flame quenching becomes a crucial limitation and thus spark ignition (gasoline) or diffusion flames (diesel) become almost impossible.

In addition, "parasitic heat transfer" also becomes an issue. Parasitic heat transfer is when the hot and cold thermal reservoirs of an engine are not well-isolated and thus thermal energy can bypass the engine reducing net work [66].

Other problems include reduced residence times if the combustion chamber is not suitably resized, but even with resizing fuel-air mixing will be difficult in such a short time.

Hydrogen use is considered a very good proposition since it possesses short reaction times, large diffusion velocities and wide flammability limits [67].

2.4.3.1 Free piston micro-engines

Several propositions for free piston micro engines have been made, but most closely resemble the aforementioned full scale free piston engine. In general it is found that flame-wall interaction tends to quench deflagrations before the charge can be consumed [68]. This in turn, reduces peak pressures and greatly curtails performance.

To characterize these phenomena, spark-ignition combustion experiments were conducted in a transparent fixed-volume chamber 50mm long and 13mm wide [68]. The chamber height was adjustable from 3.175mm to 12.7mm. The charge is ignited with spark plugs electroplated on the combustion chamber walls and the spark gaps are approximately 2mm. They subsequently found that peak pressures are inversely proportional to the surface area to volume ratio. Three different igniter locations were tried and also firing all of them together. It was noted that similar results were obtained from using any of the three igniters separately but when all three were used the pressure was maximized. They also note that the pressure rise is less sensitive to igniter configuration when the surface-area-to-volume ratio decreases.

2.4.3.2 MEMS Rotary Engine

A MEMS Rotary Engine is under development at the University of California, Berkeley [69]. Two prototypes are depicted in Figure 24 and Figure 25. A rotary (Wankel) configuration was chosen [69] because the part geometries are essentially planar and

valves are not required. Flame quenching and poor rotor-housing sealing however, are well-known problems of conventional rotary engines and one can expect them to be exacerbated by small scales. The MEMS Rotary Engine employs thermal management to circumvent flame quenching. That is, the engine body is heated and low thermal conductivity materials e.g., silicon carbide, are used [70]. Millimeter-scale prototypes of this engine have delivered 2.7W at 9300rpm.

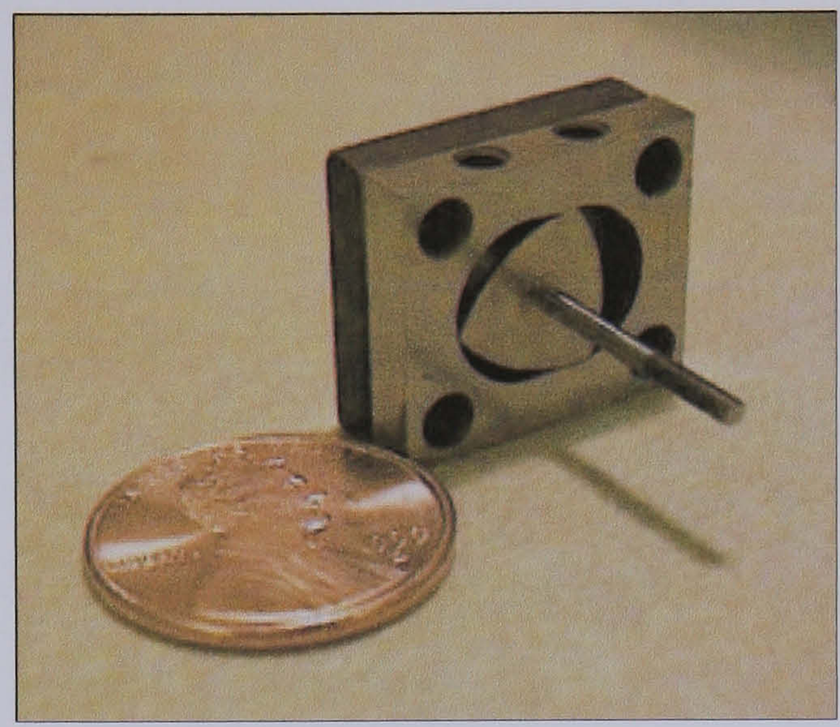

Figure 24: Millimeter-scale rotary MEMS (3mm rotor –seen next to a penny).

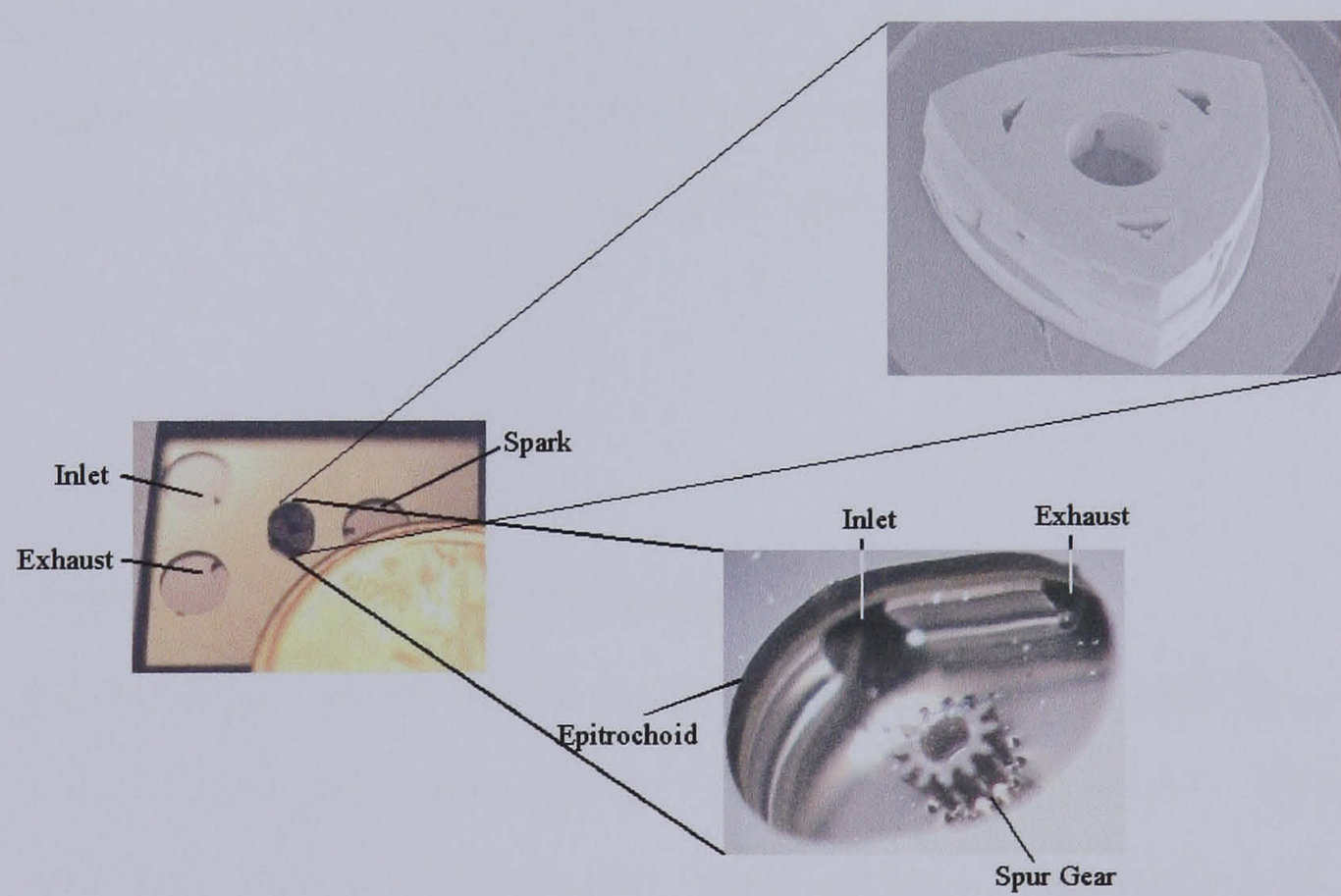

Figure 25: Micro-scale rotary MEMS.

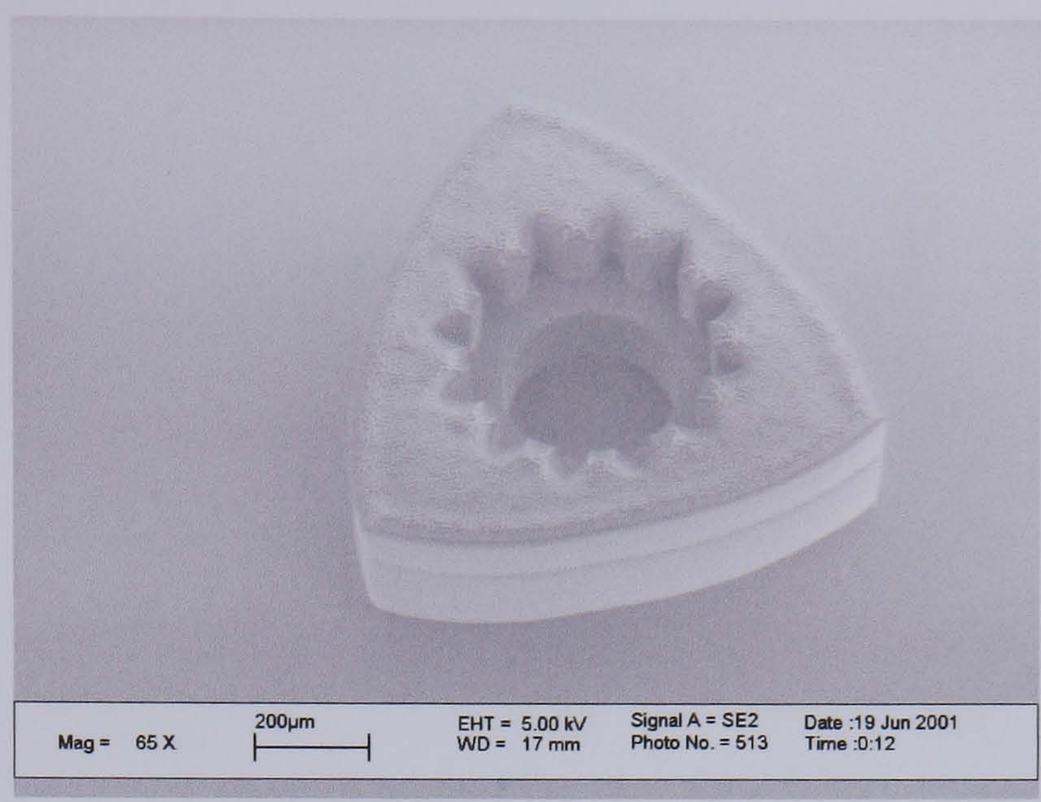

Figure 26: 1mm rotor.

By considering that flame-quenching is a prevalent problem and that multiple ignition sites seem to improve the situation, HCCI springs to mind. By creating multiple autoignition sites within the combustion chamber, it triumphs over the problems at hand.

In addition, extended flammability limits, increased combustion rates, fuel flexibility and the lack of need for energy thirsty ignition systems add up to suggest that HCCI is the most efficient and practical way of implementing micro-engines. Even more fascinating is the fact that mini-scale HCCI engines have been around more than 25 years before any HCCI publications surfaced.

2.4.3.3 Remote Control Model Engines

Perhaps the most striking use of HCCI mini-engines is that in modelling. For decades now, engines with capacities of 0.16cm^3 (0.010in^3) to 15+ cm^3 have been mass manufactured and used for propelling car, boat, airplane and helicopter models. The smallest mass produced engine the "Cox - Tee Dee .010" is reported to have an efficiency of 4%, thus outperforming a battery by having almost double the power density. It produces 0.028hp (20.88W) at 32.000rpm (533Hz) [71]. Bigger engines of the same type (around 15cm^3) produce around 5hp at 8000rpm and weigh up to 4.5kg [72].

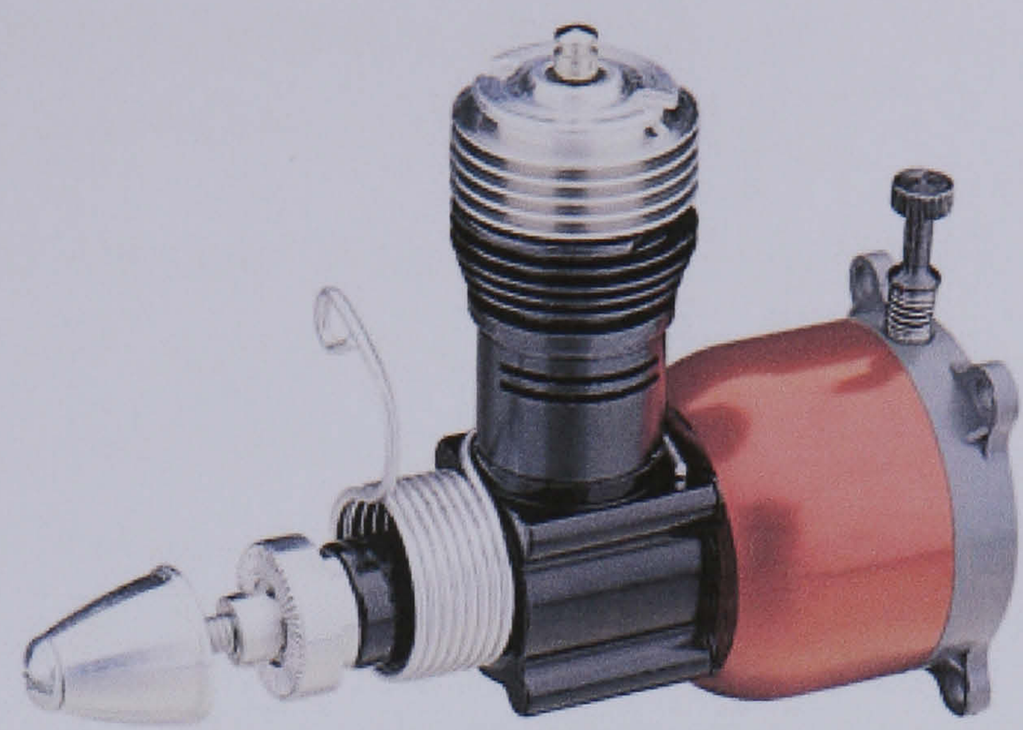

Figure 27: The Cox Engine (2-stroke).

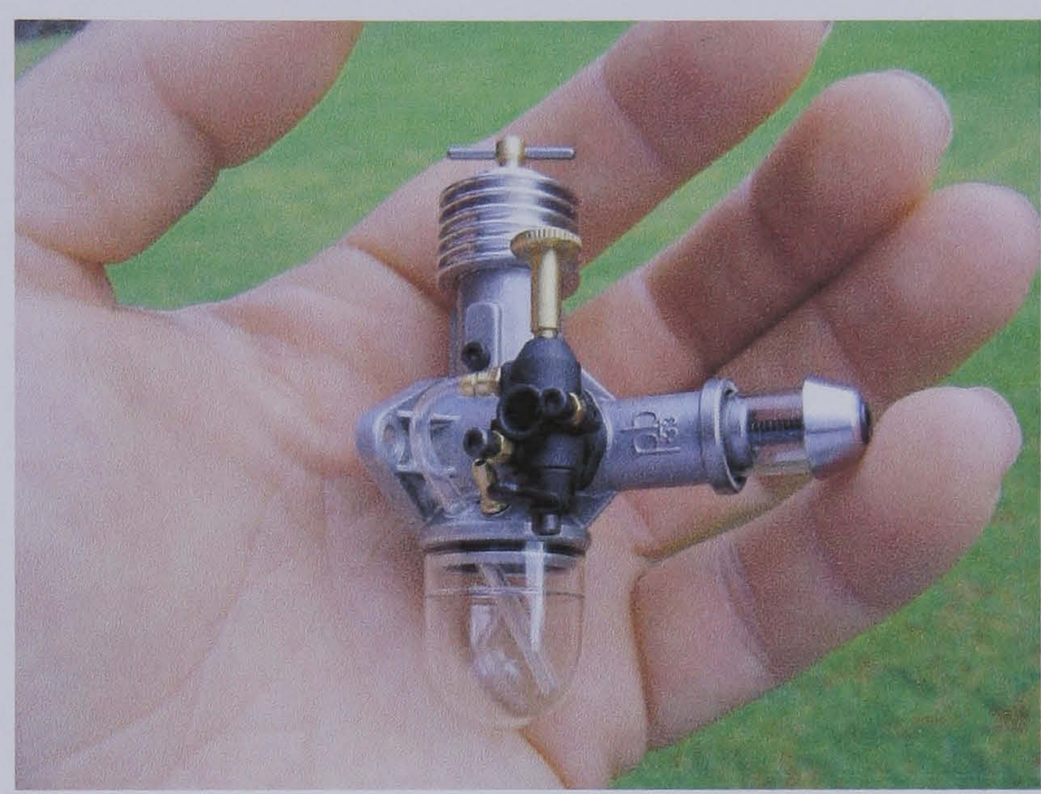

Figure 28: A 2-stroke medium sized "diesel" engine. The compression ratio adjusting screw can be seen at the top of the cylinder head.

More pictures can be found in Appendix 2.

The first model engines, which were manufactured pre-1940, (mainly airplane engines then) were SI engines. However, the advent of the other two types, in the late 1940s revolutionized the modelling world by getting rid of the, then, unreliable ignition system [73].

In the glow plug engines, ignition is initiated by a hot platinum wire, located inside the central cavity of the glow plug body. Consequently, fuel flexibility (common feature of other HCCI forms) is not, readily, possible. Fuels are limited to mixtures of methanol, nitromethane (typically 5 – 15%) and castor oil (for lubrication) (typically 15 – 30%). The glow plug is heated up by passing a current at start up, but when the engine fires up the heat of the combustion is enough to keep it "glowing" so the current is disconnected. It is

not uncommon for glow plug engines to start unexpectedly, if the crankshaft is rotated a short while after the engine has stopped, i.e. when it still hot.

Actually this is not the only type of engine were this might pose a problem. Very similar behavior of radial aircraft engines (full size, not model) has caused accidents in the past. In common with other radial engines, a hydraulic lock can occur when the aircraft has been standing and oil/fuel has seeped into the lower cylinders. If the engine is started in this condition, serious damage can occur. To guard against this it is the usual practice to turn, or 'pull through' the propeller blades by hand; '10 to 16 blades' is normal. During this process the front cockpit magneto switches should be OFF. If the aircraft is being flown solo, it is common practice for the switches in the rear cockpit to be left ON. If the engine has been recently run and the cylinder head temperature (CHT) is high, the propeller should not be turned by hand as the engine may start due to compression alone. This is most likely to happen through pre-ignition caused by hot spots (normally incandescent carbon deposits); the most critical time is within a few minutes after engine shutdown. All of the above is described in a UK aviation safety report of an accident involving a Yak 52 during engine start up procedure, although it was not concluded that this was the necessarily the cause of the accident in that instance [74] . It is also not unknown, for automotive engines to develop hot spots in the combustion chamber and continue to work after the ignition has been turned off, in carbureted engines. It is also possible for the engine to revolve in the opposite, to normal, direction for a short time, if pre-ignition happens early and powerfully enough to reverse engine direction.

One might argue that this is not true HCCI combustion, since it lacks the basic characteristic of multiple ignition points. The combustion, although most likely a detonation, starts from a single point of ignition. The same is the case in pulse detonation engines (PDE) a very interesting jet engine, which although not new, is still in the research phase, like HCCI. PDEs are very similar to pulse jets, with the only difference being that the combustion is detonation instead of deflagration. The propagation of the detonation wave is complex consisting of waves travelling in regular, but uncommon for deflagrations, shapes. It is plausible that the propagation of the detonation waves between the autoignition sites in HCCI portray a similar structure.

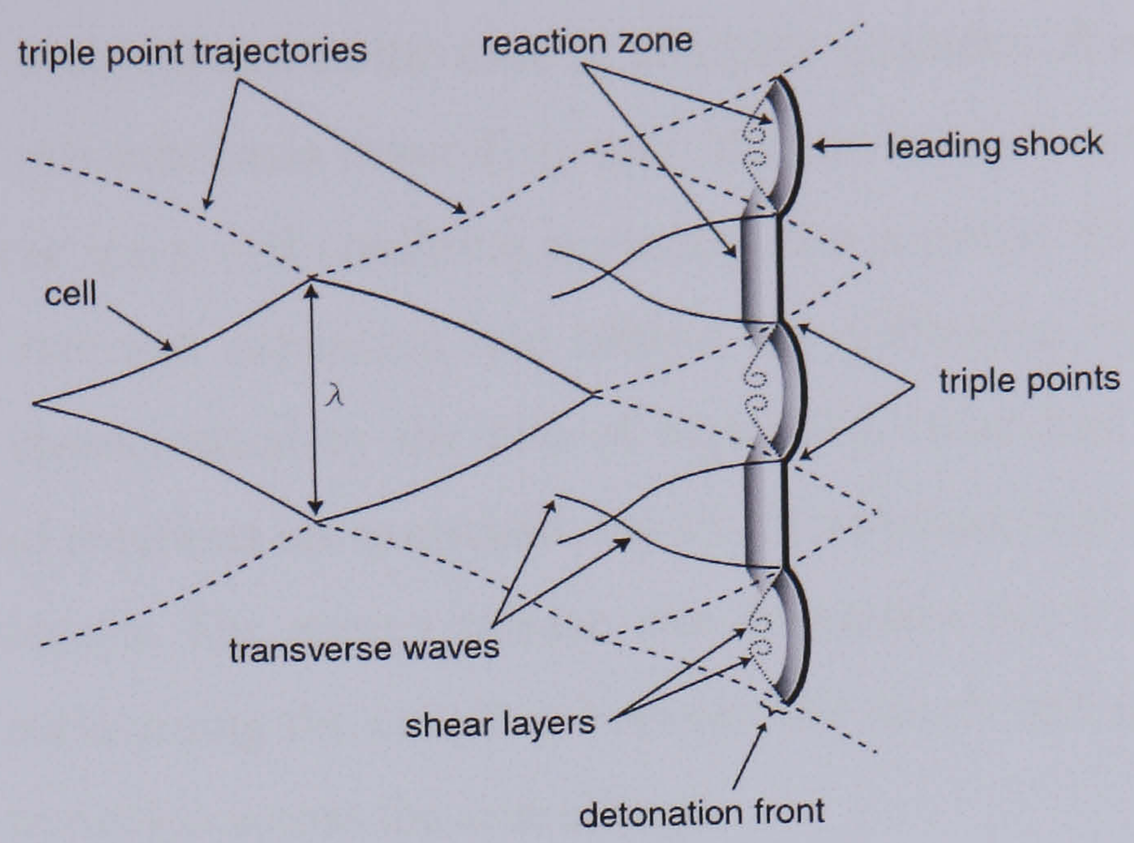

Figure 29: Detonation waves have a multidimensional cellular structure exhibiting transverse waves and cellular pattern. [75]

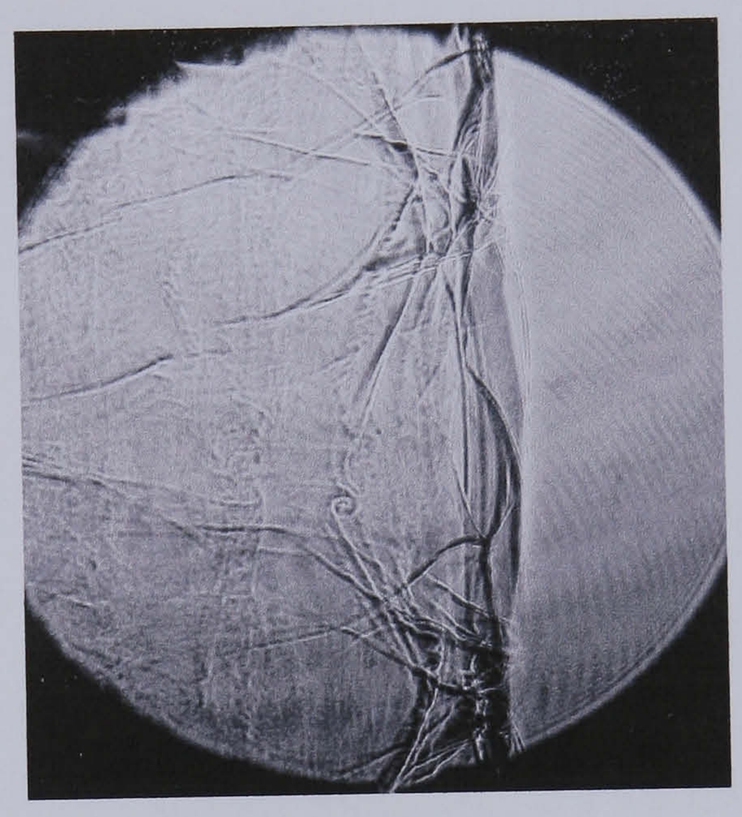

Figure 30: Photograph of the detonation structure 2H2+O2+20Ar, 20 kPa, 295 K. [75]

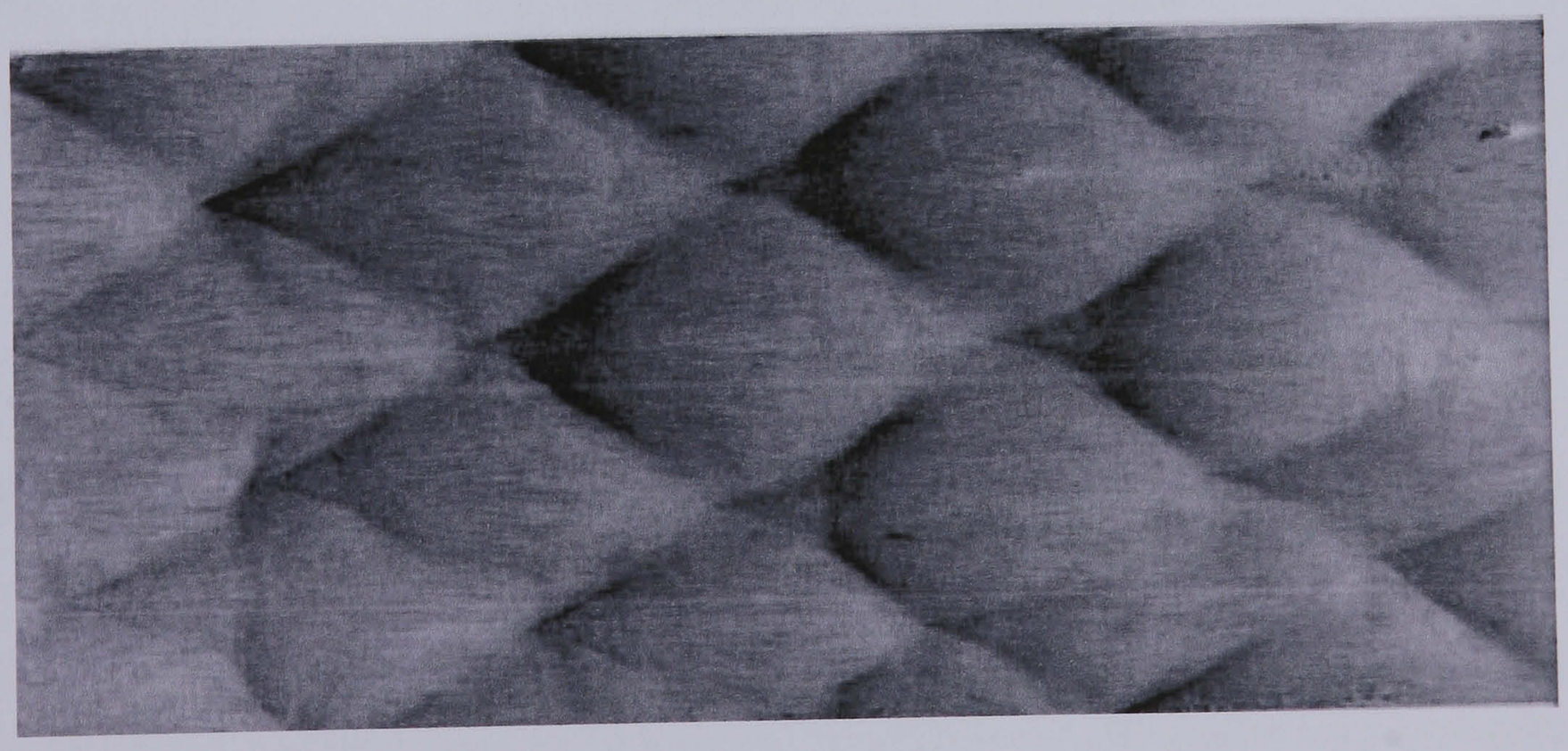

Figure 31: Detail of the cell structure (2H2+O2+17Ar, 20 kPa, 295 K). [75]

The same authors commend that in the case of complex geometry changes in the path of the detonating gas, two outcomes depending upon the combustible mixture composition, initial thermodynamic state, and confining geometry, are possible. Competition between the energy release rate and expansion rate behind the diffracting wave is crucial. The subcritical case is characterized by the rate of expansion exceeding the energy release rate. As the chemical reactions are quenched, the shock wave decouples from the reaction zone and rapidly decays. The energy release rate dominates the expansion rate in the supercritical case, maintaining the coupling between the shock and reaction zone which permits successful transition across the area change.

Clearly, detonation propagation is not an easy subject, but it appears that it is always the most efficient way to combust the fuel available. It is also clear that not all fuels will react in the same way, further complicating matters.

The closest relative of HCCI in model engines is the "diesel" type. These are pure compression ignition engines and no heat source, other than compression, is provided. The adjusting parameters are the air-fuel ratio and the compression ratio. Usually, there is no throttle plate, so the only AFR adjustment is the amount of fuel; this is accomplished by a needle-jet arrangement. The compression ratio is adjusted through a screw located at the top of the cylinder head, Figure 28, which moves an opposing piston (contra-piston). Thus by adjusting the height of this piston in the cylinder, fine adjustment of ignition timing is achieved. Recommended fuel mixtures are consisted of kerosene, ether and castor oil. The ether is essentially an initiator. Typical concentrations of ether are 30% to 50% increasing the concentration with decreasing engine size [76].

The same reference also suggests 2-4% amyl nitrate, amyl nitrite, isopropyl nitrate or methyl ethyl ketone peroxide. These compounds are said to permit lower compression ratios to be used (ignition enhancers) and also to promote smoother operation.

It is also recommended that during the start up procedure of such engines, the compression ratio needs to be increased until the engine fires up, but after the engine starts it should be reduced to the closest possible to the misfire limit. This is probably because as the engine is warming up, heat losses will be reducing and SoC will be advancing. If the compression is not lowered preemptively the engine will pre-ignite and stop or self-destruct. It is also common practice to use higher compression ratios with lean mixtures and vice versa.

"Diesel" engines predate their glow plug equivalents, however engine starting difficulties from cold and objectionable exhaust odor have prevented then from being very popular [73].

Kits for glow plug to "diesel" conversion exist [77]. Essentially the kits consist of a cylinder head with an opposing piston that replaces the original glow plug head. The power increases following such a conversion are substantial. As an example an O.S. 0.40 glow engine developed 0.55hp (410W) before and 0.80hp (597W) after the modification, whilst fuel economy is increased [78].

Model HCCI engines prove that it is possible to cover the whole operating range of such an engine (typical 2000rpm – 30000rpm+) with this type of combustion. However, one has to remember that the structural strength of these small engines is incomparable to their full-sized automotive relatives. They can thus combust almost undiluted mixtures of fuel and air, producing unbelievable power outputs for their size.

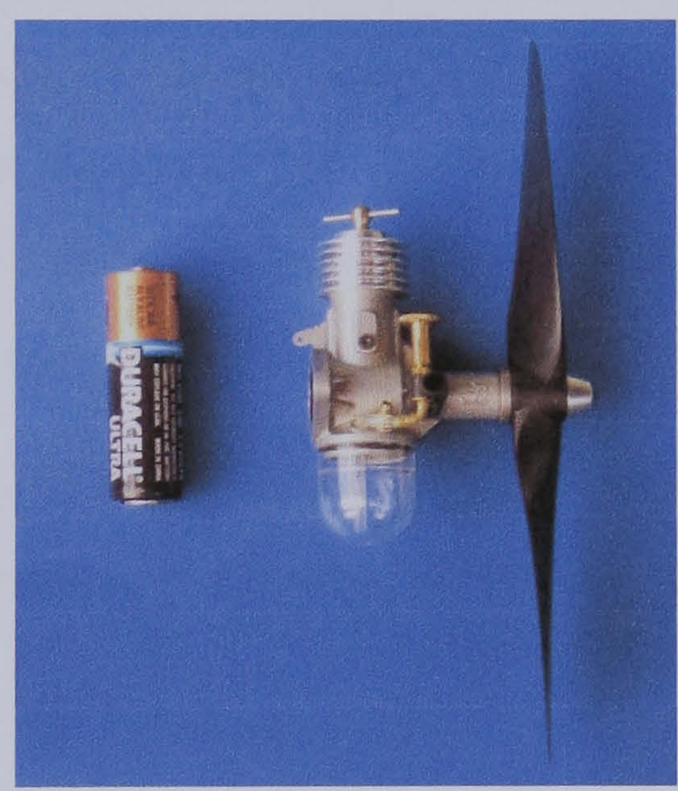

Figure 32: Battery vs. Micro IC engine (diesel type shown). No contest (At least for the moment).

2.5 Chemical Kinetics - Hydrocarbon Oxidation Chemistry

Vastly different experimental results have been published over the years showing sometimes irrational autoignition behaviors like easier autoignition of isooctane (100 ON) compared to 95 ON gasoline. Although this thesis is not focusing on the underlying chemistry of the HCCI process, a closer look is taken here in order to gain a fundamental insight.

An industry average gasoline is composed roughly of 60% paraffins, 10% olefins and 30% aromatics [79]. The oxidation mechanisms of hydrocarbon fuels change substantially

over the ranges of pressure and temperature encountered during a compression stroke. These mechanisms can be divided into three categories i.e. low temperature, intermediate temperature and high temperature oxidations. In low-temperature oxidation, reaction rates increase with increasing temperature. The dominant reactions at this stage are oxygen addition to form alkylperoxy radicals and olefins followed by radical isomerization and decomposition. As the temperature is increased further, the alkyperoxy radicals decompose back into initial reactants, the production of olefins and hydroperoxyl radicals is favoured and the overall reaction rate decreases with increasing temperature. This is the classical "negative temperature coefficient" (NTC) behavior observed in low-temperature oxidation of paraffinic fuels. Olefins, show a less pronounced, or non existent region of negative temperature coefficient [80].

At atmospheric pressure low-temperature oxidation is considered to take place below 600K and the transition to intermediate temperature between 650-700K. At 10 atmospheres the onset of the NTC chemistry does not occur until 750-800K. As the temperature is increased further the reaction rate again increases as more olefinic hydrocarbons and hydrogen peroxide are produced. Eventually, the temperature is increased high enough so that hydrogen-oxygen branching reactions control the reaction rate in the high-temperature regime.

Although thousands of chemical reactions are included in detail chemical kinetics models and analyses, only a very basic understanding of the chemistry involved is sought after here.

Studies have indicated that autoignition in HCCI is mostly governed by hydrogen peroxide (H_2O_2) decomposition [81,82,83]. Hydrogen peroxide decomposes into two OH radicals, which are very efficient at attacking the fuel molecules and releasing energy, increasing the temperature of the reacting mixture and setting in motion a chain branching sequence. Hydrogen peroxide decomposition occurs at a temperature range between 1050 and 1100 K. With high octane fuels such as natural gas, little heat is released prior to this main ignition event at 1050-1100 K; however, with low octane fuels, significant heat producing reactions begin at temperatures of about 800 K [83, 84].

Since paraffins contribute highly to hydrogen peroxide radical production, a more detailed analysis of their chemical kinetics with increasing temperature is given in Appendix 3.

2.6 Gasoline HCCI Detailed Analysis

HCCI combustion depends on various details that differ vastly depending on the exact method used for its implementation. Thus, in this chapter a more in-depth analysis is attempted, with the focus primarily being on pointing out usual misunderstandings and things that are taken for granted, but which, in reality are quite more complicated.

A very common misconception is that HCCI is actually a homogeneous mixture. As already stated, in HCCI the fuel is premixed to create a near homogeneous charge. Numerous studies have been examining exactly how homogeneous this charge is. In the figures on the following pages, a typical in-cylinder fuel and OH distribution can be shown [85,86]. It can be seen that the distribution is far form homogeneous.

This study involved PLIF and LIF imaging of a truck-sized Volvo TD-100 diesel engine that has a lowered compression ratio of 10:1. The engine was also converted to be able to use both standard port fuel injection and a heated 20 liter premix tank. With no direct injection, a pancake combustion chamber and such a low compression ratio the engine resembles closely a gasoline HCCI engine, although the fuel used was a low octane one.

These researches found that even for the heated premix tank fueling method, where the tank was located more than 1.5 meters before the inlet valves, the distribution was very inhomogeneous. It is worth noting that this engine used preheated intake air to induce autoignition and not trapped residual gas. If this is the case when taking every precaution to homogenize the mixture, it can be inferred that using TRG, thus reducing mixing times considerably, can only add further inhomogeneity.

The images show fuel and OH distributions. Fuel distribution is a major parameter in the autoignition process since local air-fuel ratios will dictate the local reactivity and temperature. It can thus be inferred that autoignition will not occur simultaneously in the whole of the combustion chamber. OH distribution is also important, because OH is only present in the reaction zone and is thus a clear indicator between burned and unburned mixture. Again, its distribution verifies that combustion happens locally, although at more than one locations at a time. Also, kernels of earlier activity were not found to be more frequent in the central part of the combustion chamber, thus indicating that heat transfer to the cylinder walls was not the main controlling factor. However, this charge inhomogeneity has only a modest effect on the special variations of the combustion process. Earlier studies [86] using direct imaging techniques did not reveal these inhomogeneities, since the exposure time needed, around 200μs, was large enough to

allow local variations to smooth out. In contrast LIF imaging has an equivalent exposure time closer to 10ns, thus freezing the process.

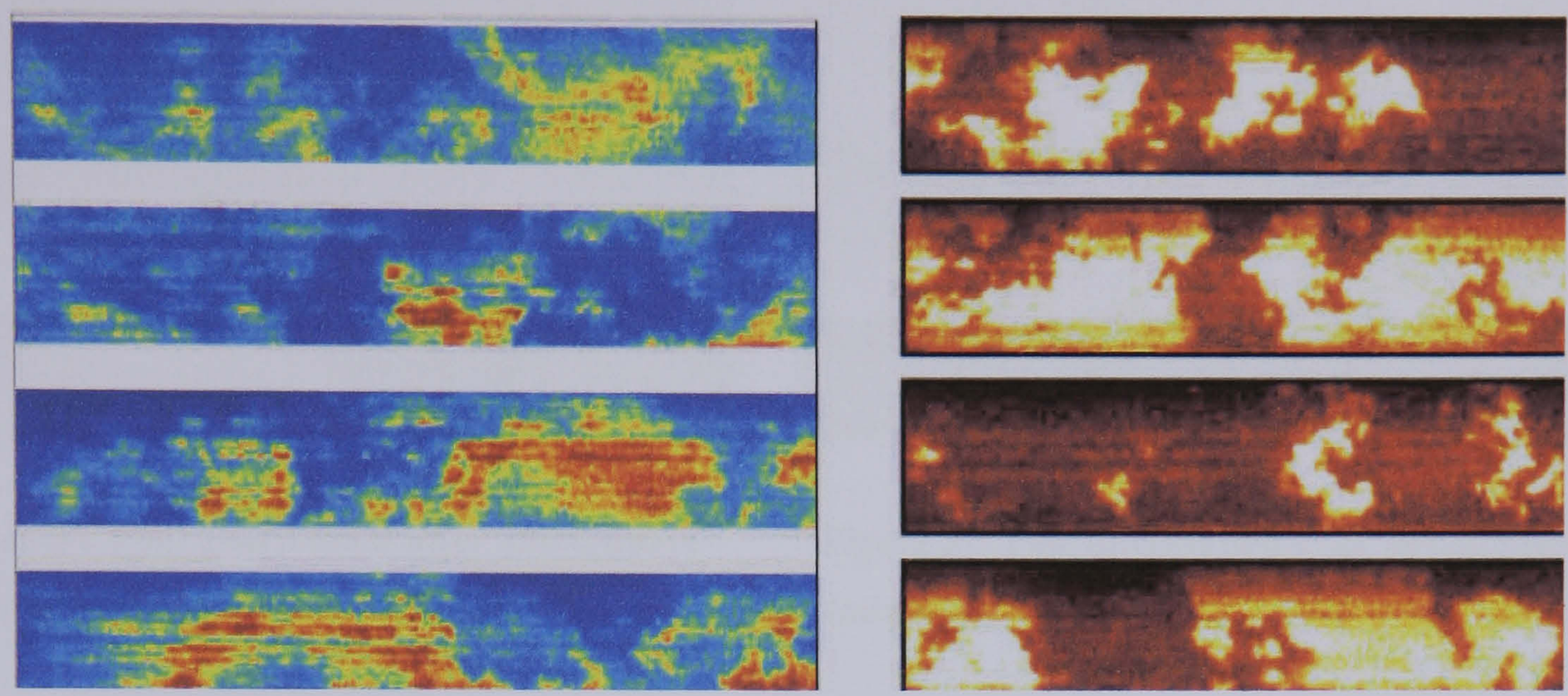

Figure 33: Fuel (left) and OH (right) distribution in an HCCI engine. [86]

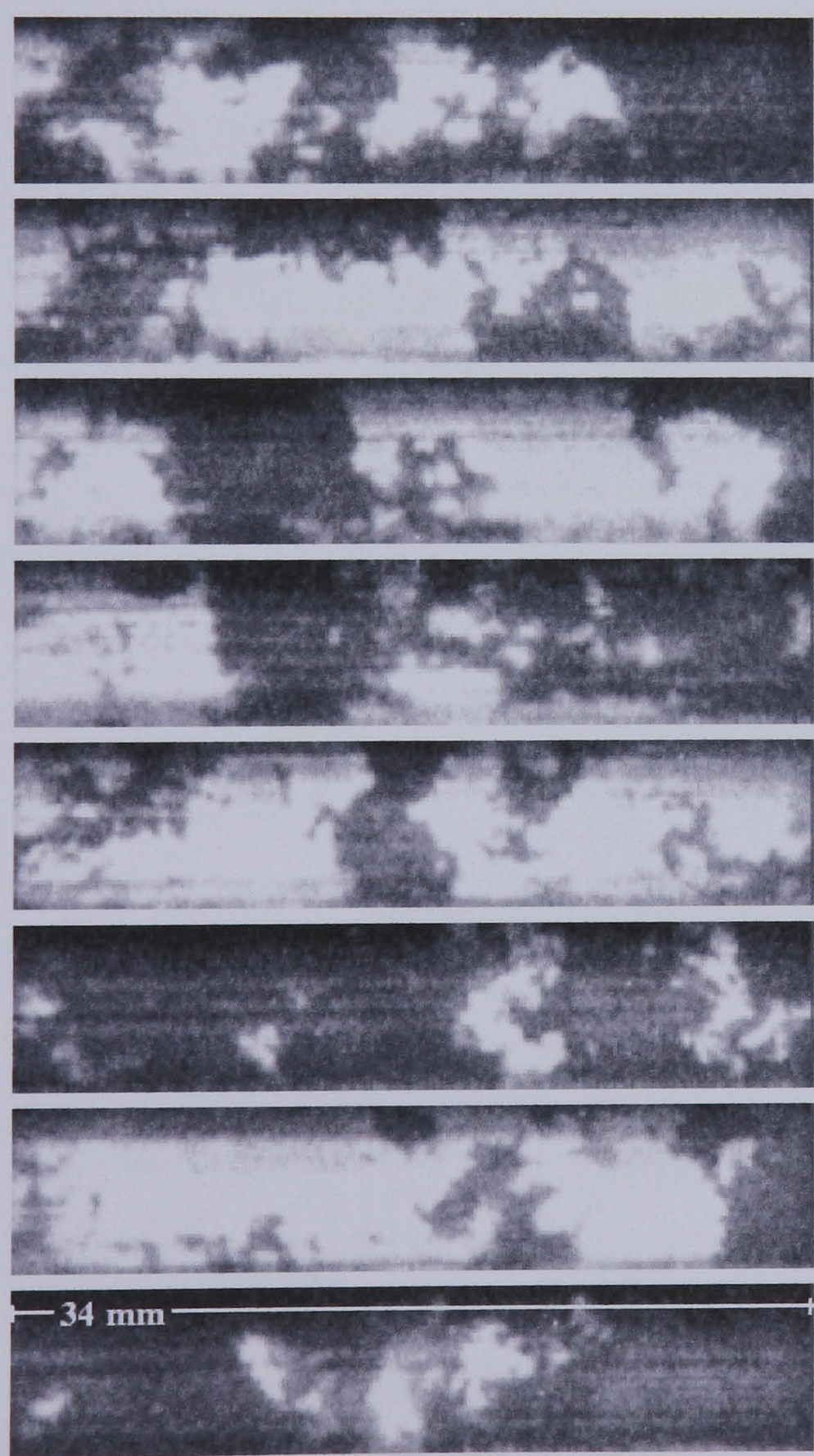

Figure 34: Examples of OH-distribution after autoignition (port-injection, 1 CAD PTDC). [85]

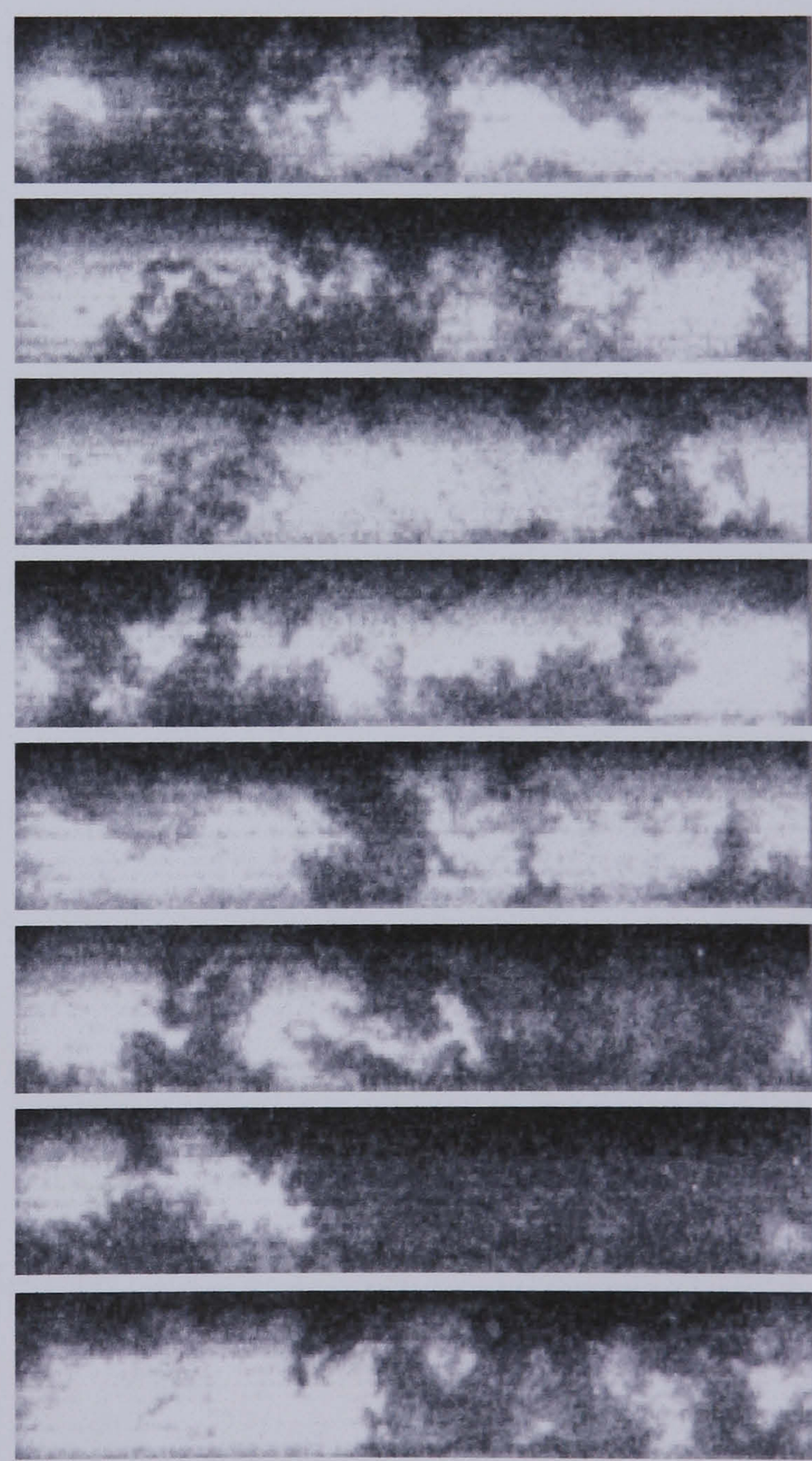

Figure 35: Examples of OH-distribution after autoignition (mix tank, 0 CAD PTDC). [85]

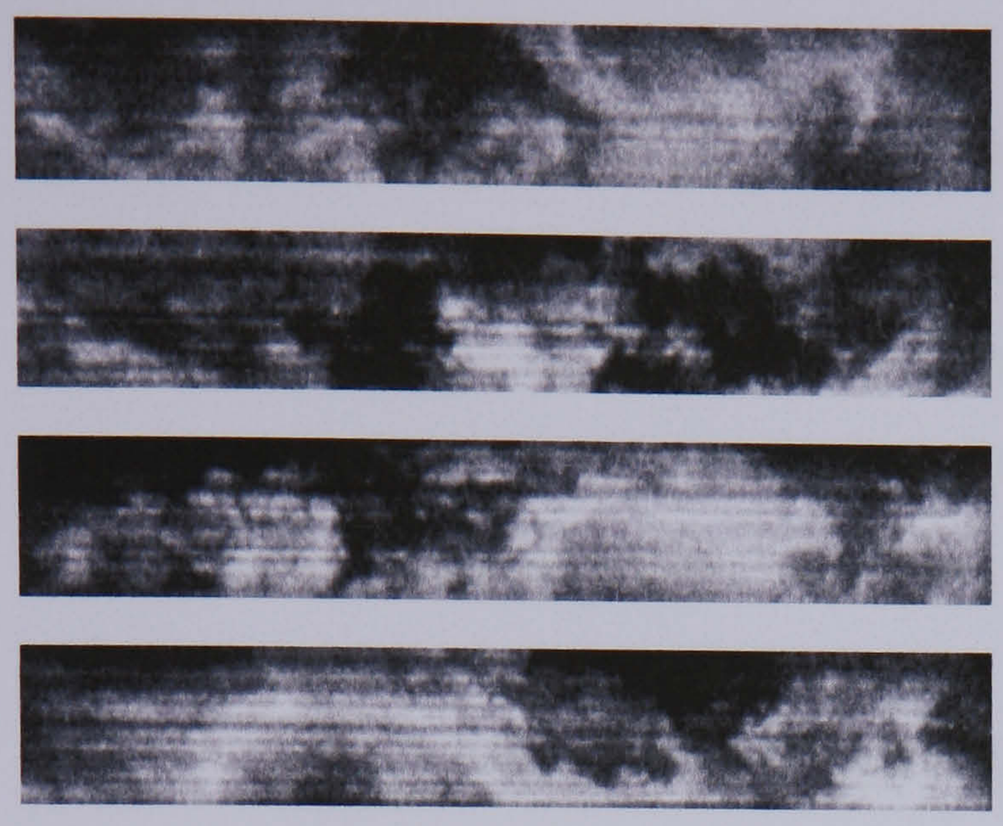

Figure 36: Fuel distribution after autoignition (port-injection, 2 CAD PTDC). [85]

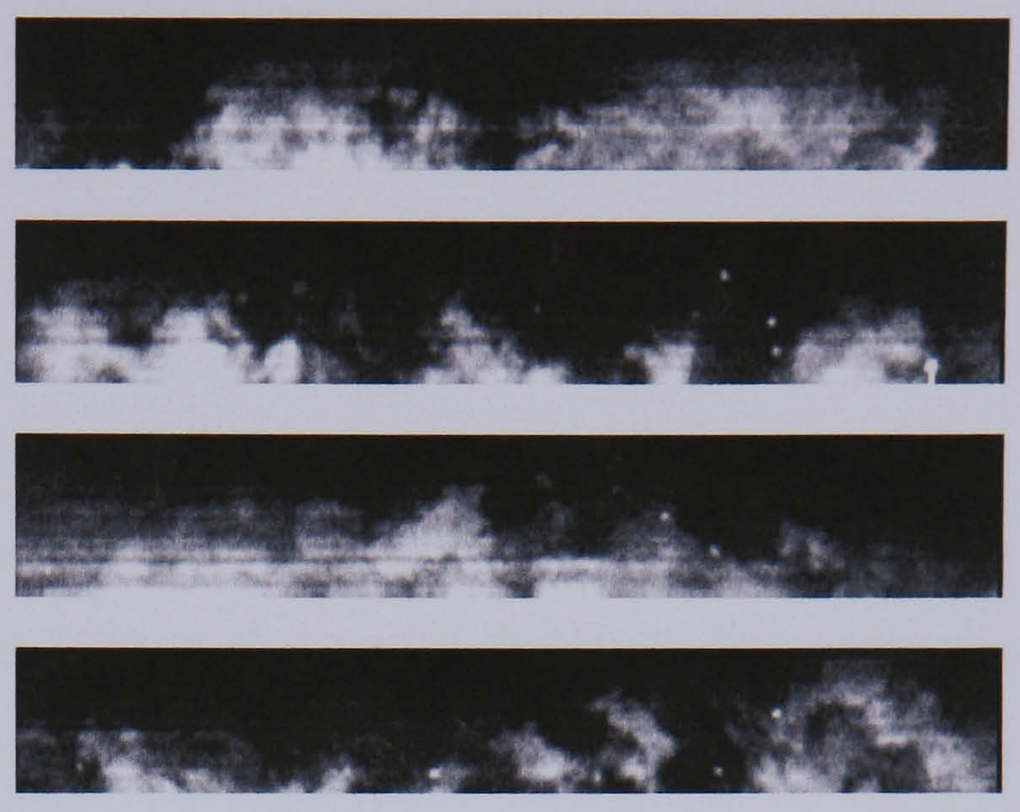

Figure 37: Fuel distribution after autoignition (mix tank, 5 CAD PTDC). [85]

Results obtained from the CFD research group of our university are shown below. These are for engine geometry very similar to the one used for the experiments in this thesis and also for both valve strategies used. These indicated temperature and mixture inhomogeneity, as expected. Note that this CFD modelling involved residual gas trapping techniques (in contrast to the diesel engine above).

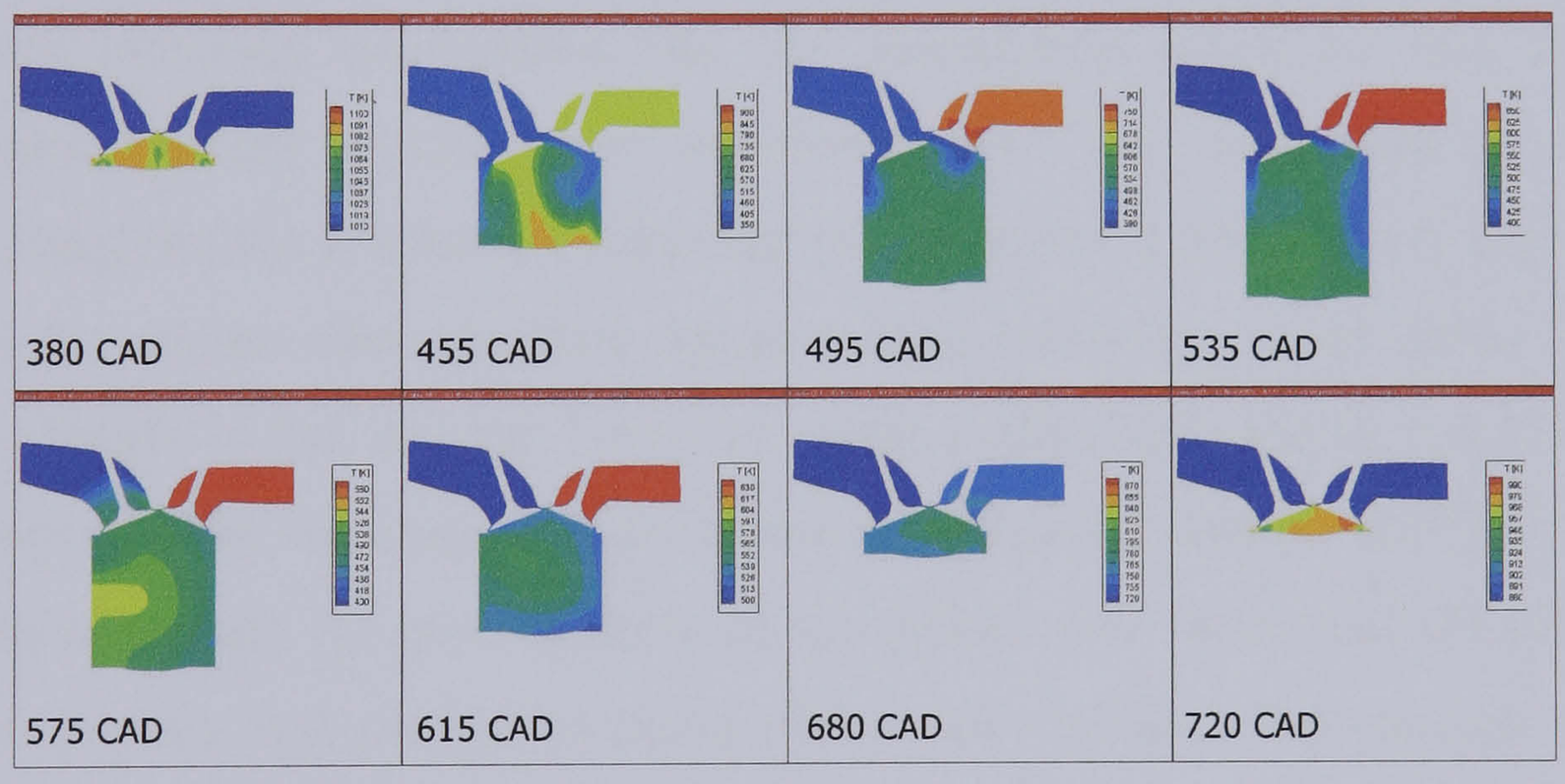

Figure 38: Temperature distribution @ 50%TRG, 2000rpm, λ=1, WOT.

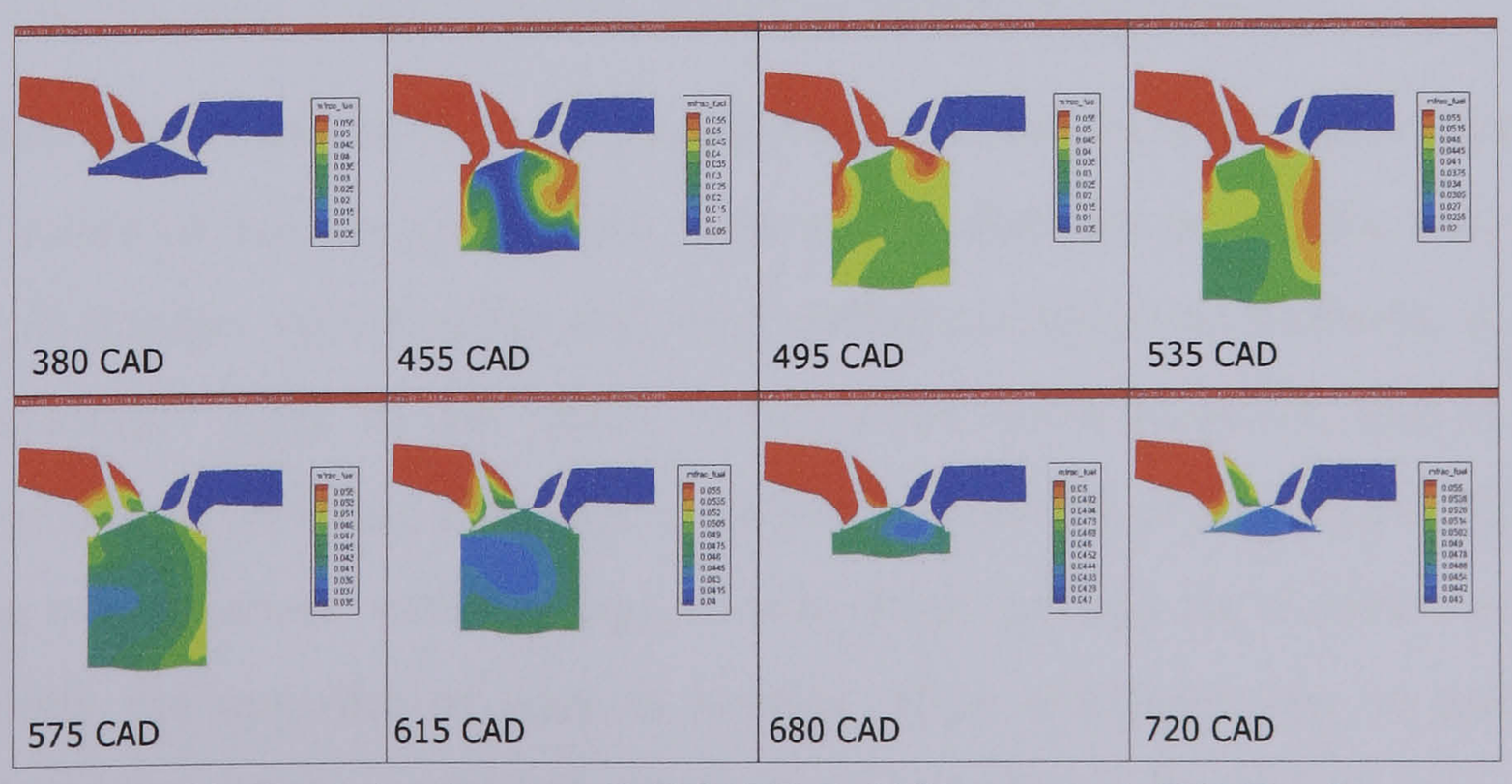

Figure 39: Fuel distribution @ 50%TRG, 2000rpm, λ=1, WOT reference.

A simplistic mixing model proposed by [87], again describes that stratification is to be expected with a top zone mainly comprised of fresh charge, close to the valves, and a bottom zone mainly consisted of hot residuals. Lying between these two zones would be a mixing zone where autoignition is expected to occur first. In an investigation with an optical engine [88] and PLIF it was noted that the earliest hot combustion occurs neither in the central area (where the charge has the highest temperature) nor in the perimeter area (where the charge had the highest fuel concentration) (the locations of the high concentrations of residual gases and fresh charge where engine specific in that the engine used had a non-typical layout, which used side valves to promote mixture stratification). Nevertheless, autoignition occurred somewhere in between these two extremes, in the mixing zone. Different mixtures of n-heptane and isooctane were used, and although the timing changed the locations where formaldehyde started to burn were similar for the three fuels used.

Although little can be done to produce a more homogeneous mixture, inhomogeneity is not necessarily a phenomenon that introduces negative effects. It is not yet clear if homogeneity increases combustion rate. An assumption might be that an absolute homogeneous mixture would ignite simultaneously. The instantaneous combustion reaction throughout the combustion chamber would certainly impose very high structural loading on the engine internals, thus compromising reliability. Combustion duration of appropriate length is thus needed. However, some studies have shown that homogeneity increases combustion duration [89]. In contrast to all of the above, in [90] experiments were conducted where the heterogeneity of the charge was varied and the effect on the combustion process was monitored using planar laser induced fluorescence (PLIF) for crank-angle resolved imaging of fuel and OH. Their conclusion was that charge inhomogeneity has only a modest effect on the combustion process.

The important conclusion is if homogeneity has an effect on combustion duration, then this can be tuned to suit the application. This can be done by tuning the mixture mixing through swirl, tumble, squish zones and other turbulence inducing methods, thus tailoring the thermodynamic cycle to our needs. It has to be noted however, that if turbulence reduces combustion duration, then this, in effect, means that at low speeds (low mixing) the duration will be short, while at high speeds (high mixing) the duration will be long. This is exactly the opposite of what is needed. Short durations can be useful at high engine speeds, where piston velocities are high. High piston velocities can compensate for

high combustion rates, reducing rates of pressure rise and also at these conditions high combustion rates are needed to closely follow the Otto cycle.

Another common assumption for HCCI combustion is that cyclic variation is minimal. Very low cycle-to-cycle covariance was first noted in 1979, concerning two-stroke engines [17,18]. Obviously, low covariance translates to increased thermodynamic efficiency since combustion doesn't have to be tuned for the worst case cyclic scenario. This cyclic repeatability can be attributed to two main factors. The first one is that when a two-stroke or a four-stroke SI engine operates throttled the effective compression ratio is so low that combustion becomes unstable. On the contrary, when high amounts of TRG are used for engine throttling the effective compression ratio is as high as it would be at full load (for a normally aspirated engine) thus increasing stability. The second factor is that when true sparkless autoignition occurs combustion starts from multiple sites within the combustion chamber simultaneously, as noted by the aforementioned reference and a host of other researchers till today, and combustion duration is short. This diminishes the effect of flame front travel uncertainties and heat is released quickly through a self-induced positive feedback process.

However, this description is only accurate for a very short operating region, where true, sparkless, HCCI combustion occurs. In gasoline HCCI engines, spark assistance is used to ensure combustion takes place and also to avoid cascading misfires. This expands the operating range of the engine from very low TRG, SI operation, up to very high TRG concentrations. However, where combustion is spark dominated, at low TRG levels, part of the mixture is consumed through conventional flame front propagation. Also, where TRG concentrations exceed the optimum value, combustion becomes unstable. It is common for the bottom end BMEP to be limited by this combustion instability introduced through excessive, relatively cool, TRG levels. In both cases, effectively the area surrounding true sparkless operation, cyclic variations occur, potentially of very high covariance when no spark assistance is used.

It is also worth discussing what happens during the negative valve overlap (NVO) period of the cycle. It is usually considered as a phase of the cycle where nothing noteworthy happens. Apart from the pumping losses, that mainly arise due to thermal losses occurring at this high temperature period in a cycle, an issue which will be discussed in great detail in the pumping losses chapter of this thesis, unexpected combustion might also occur. This usually happens when incomplete combustion has taken place during expansion and

thus the unburned mixture reignites during NVO. Usually incomplete combustion happens when ultra lean mixtures are used. Ultra lean mixtures display slow reaction rates that are even more impeded by the relatively cold TRG that the previous ultra lean combustion produced. An issue arising by combustion taking place during NVO is that if it happens late during expansion of the TRG the resulting mixture temperature at the start of compression (IVC) of the next cycle is high. This leads to early SoC which then produces cold TRG. This cyclic effect can continue indefinitely and is a frequent occurrence under unstable HCCI combustion. It is one more phenomenon leading to cycle-to-cycle variability in HCCI engines [91].

A technique sometimes used to control SoC is by direct fuel injection during NVO [92]. This allows control over the available time for the fuel to reform. It is argued that autoignition timing can be controlled in this way. However, as shown in Figure 40, temperatures during NVO are so high that will consume, at least part of the fuel, immediately after injection, when TRG contains oxygen, i.e. lean mixtures are used. Again, inhomogeneous combustion takes place (during the main combustion), although the fuel was injected early during the NVO compression.

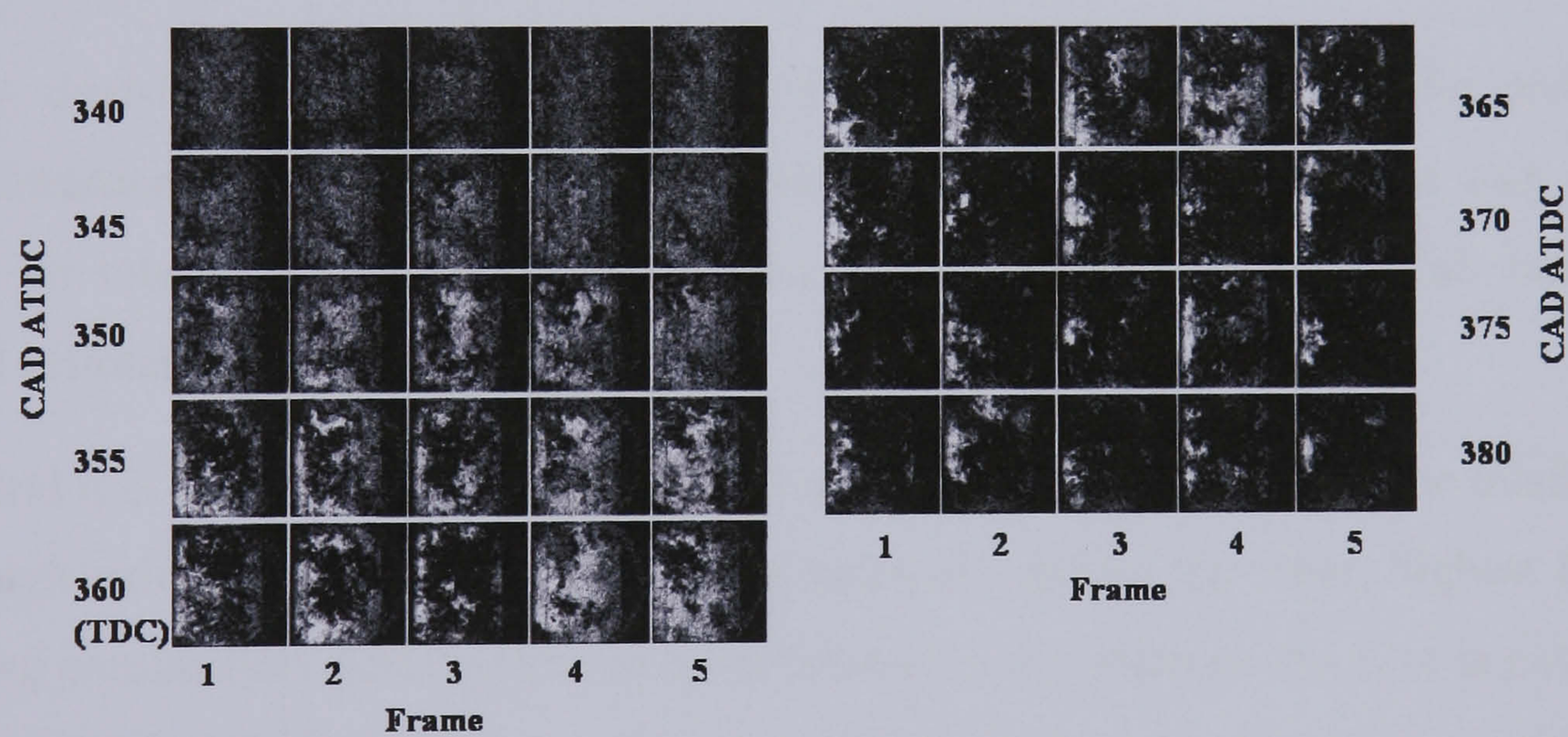

Figure 40: PLIF images of the formation and reaction of formaldehyde measured during the negative valve overlap and with the laser sheet located 2 mm below the sparkplug. [93]

Even with the pilot injection disengaged, a small amount of formaldehyde (HCHO) was present due to unburned hydrocarbons left from the preceding main combustion.

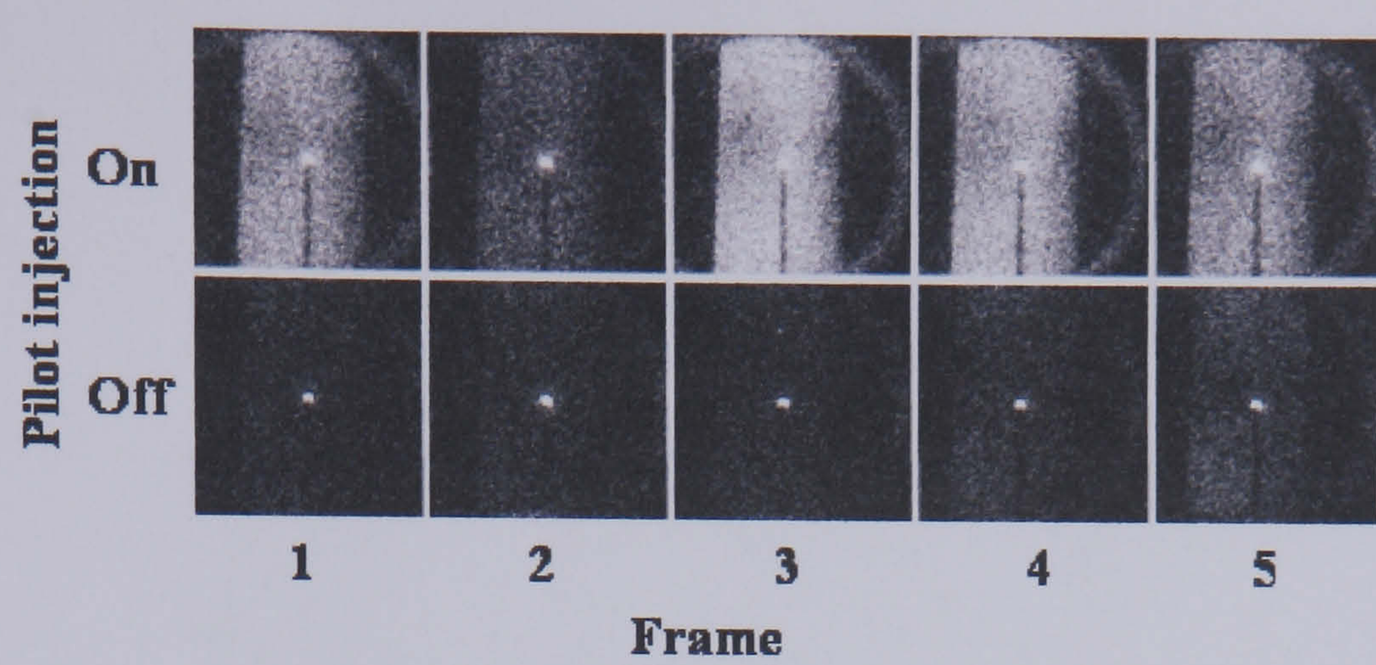

Figure 41: PLIF images of formaldehyde taken -30 CAD (BTDC $_{main\ comb}$) and before injection of the main fuel amount for the cases with and without pilot fuel injection. The laser sheet is touching the sparkplug. Each frame indicates an individual engine cycle. [93]

Figure 41 shows that with the pilot injection turned off not a lot is happening in the cylinder at -30 CAD BTDC $_{main\ comb}$. This is because combustion is phased later with it turned off, since less fuel break up occurred during NVO.

But what is of more interest is that even with the pilot fuel injected at the start of NVO, its distribution is heterogeneous throughout the combustion chamber, even more than 360 CAD after fuel injection. Cyclic variation is also evident.

Leaving dual-fuel and variable compression ratio out, as not practical for production implementation, three main approaches are used for HCCI combustion and control. Heated air intake, external exhaust gas recirculation (EGR) with heated air intake and trapped residual gas (TRG).

In general it is believed that HCCI is limited on one side, lowest load, by the misfire limit (very high exhaust recirculation, internal or external) and on the other, highest load, by knocking combustion. Although the misfire limit is always present, the case is not always there for knock. Misfires will occur because either the temperature is too low or the AFR is too lean. However, in the experience of the author, knock does not occur in gasoline – here meaning engines with compression ratio low enough to be unable to promote autoignition with no other source of energy present – HCCI engines, under "normal" operating conditions.

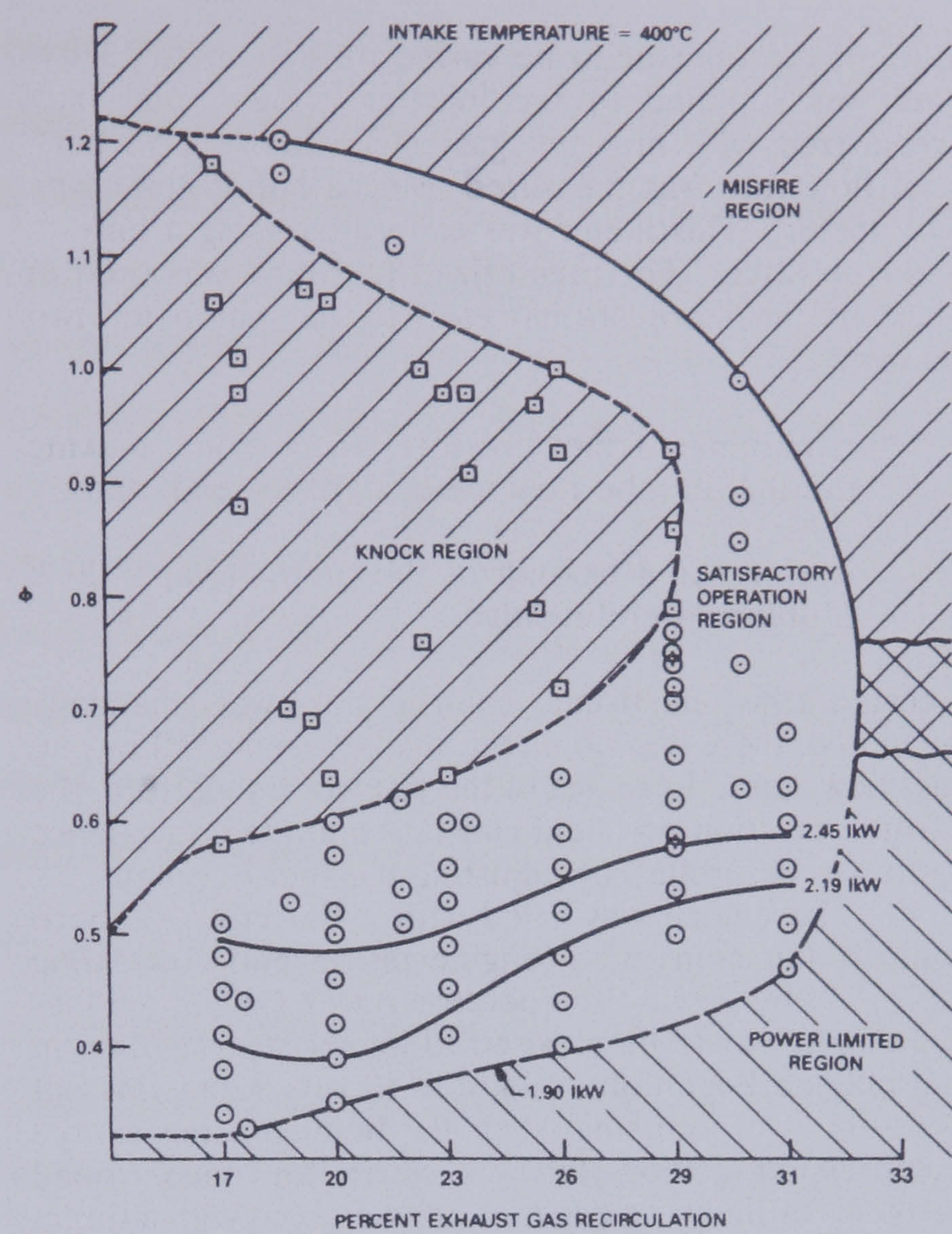

Figure 42: HCCI Operation Map - Engine Speed: 1500 rpm, Fuel: Gasoline, Throttle Position: Standard, Intake Temperature: 400 °C. [20]

In engines using heated air intake as in Figure 42, regardless of diesel or gasoline being used as fuel, controlling the load is mainly achieved through AFR regulation. Mixtures very far from stoichiometric are used, to improve fuel efficiency since autoignition lends itself to ultra lean combustion, but also to avoid engine damage. This is because, in the presence of so much excess oxygen, reaction rates tend to be extremely fast. The only way to increase AFR, without compromising engine reliability, is to dilute the mixture with EGR. EGR dilution tends to increase combustion duration by basically lowering the percentage of oxygen present in the combustion chamber. However, if more power is required from the engine, the onset of knock will commence as soon as the dilution is lowered to increase the room available for fresh charge. The actual temperature of the intake air, and EGR if used, can be regulated to control the SoC but regulating the heat release rate is not as easy. This is especially so, when high compression ratios are used.

However, when typical gasoline engine compression ratios are used and especially when high octane fuels are consumed in conjunction with TRG as the energy addition method, knock does not occur, at the high load side. This is because, on one hand high octane fuels are knock resilient but also the low compression ratio does not promote autoignition

unless TRG is present. Now, when TRG is present autoignition will occur, but the dilution of the mixture will suppress knock. As TRG is reduced to increase the power output, autoignition delays and starts to fail so a spark is needed to start the combustion process. This gives good control over the phasing of the process. The, somewhat diluted, end gas will tend to autoignite in the later stages of the combustion, since the already warm by the TRG mixture will reach its "thermal barrier" as the flame ball enlarges adding heat to the system. But this autoignition is controllable and knock levels are kept within minimum limits, As less and less TRG is used, the combustion resembles more and more conventional SI operation, up to the point where the overlap can be changed gradually from negative to positive, with no problems occurring. As mentioned before, that is why this process can be quite accurately described as Controlled Auto-Ignition (or Spark Assisted Controlled Auto-Ignition – SACAI).

Knock can occur, of course, when the ignition timing is advanced beyond optimum, as is the case in SI. It can also occur when modes (SI – HCCI) are switched abruptly or when great variations in TRG amounts happen between two consecutive cycles (due to imposed large changes in overlap). Hot TRG from a moderately diluted cycle can provoke early autoignition and consequently knock if it is used to highly dilute the next cycle. But during steady state, or gradual transition, knock is not an issue in gasoline CAI.

2.7 Ion Current Theory

Ion current has long been investigated as a combustion diagnostic tool [94,95,96,97,98,99]. It has been mainly researched as a method to control SI engines [100,101]. It has also been used for CI engine control, for injection timing optimization and even for some more extreme applications like pulse jets or pulse detonation engines. It is the only in-cylinder sensor in production and at this time the most cost efficient solution. It is also quite a robust sensor since, it can be the spark plug itself or it can be solely constituted of an electrode and an insulation sleeve, of some sort. Some low cost pressure transducer designs have been proposed, however, their use in mass production vehicles has been extremely limited. Being located within the combustion chamber it can record various information concerning flame properties that would otherwise be estimated by indirect measurements. Ion current is a measure of the conductivity of the ionized combustion gases. This conductivity can be measured by applying a voltage, DC or AC, in the order of 200V between two electrodes and measuring the current flow between them [99,102]. In most cases the combustion chamber serves as one of these. Currently, it is only used for simple tasks like misfire detection, in mass production.

It is common practice to measure the ion current signal by using the central firing spark plug, as the ionization sensor. A typical trace of data acquired through this method is shown in Figure 43. [103]

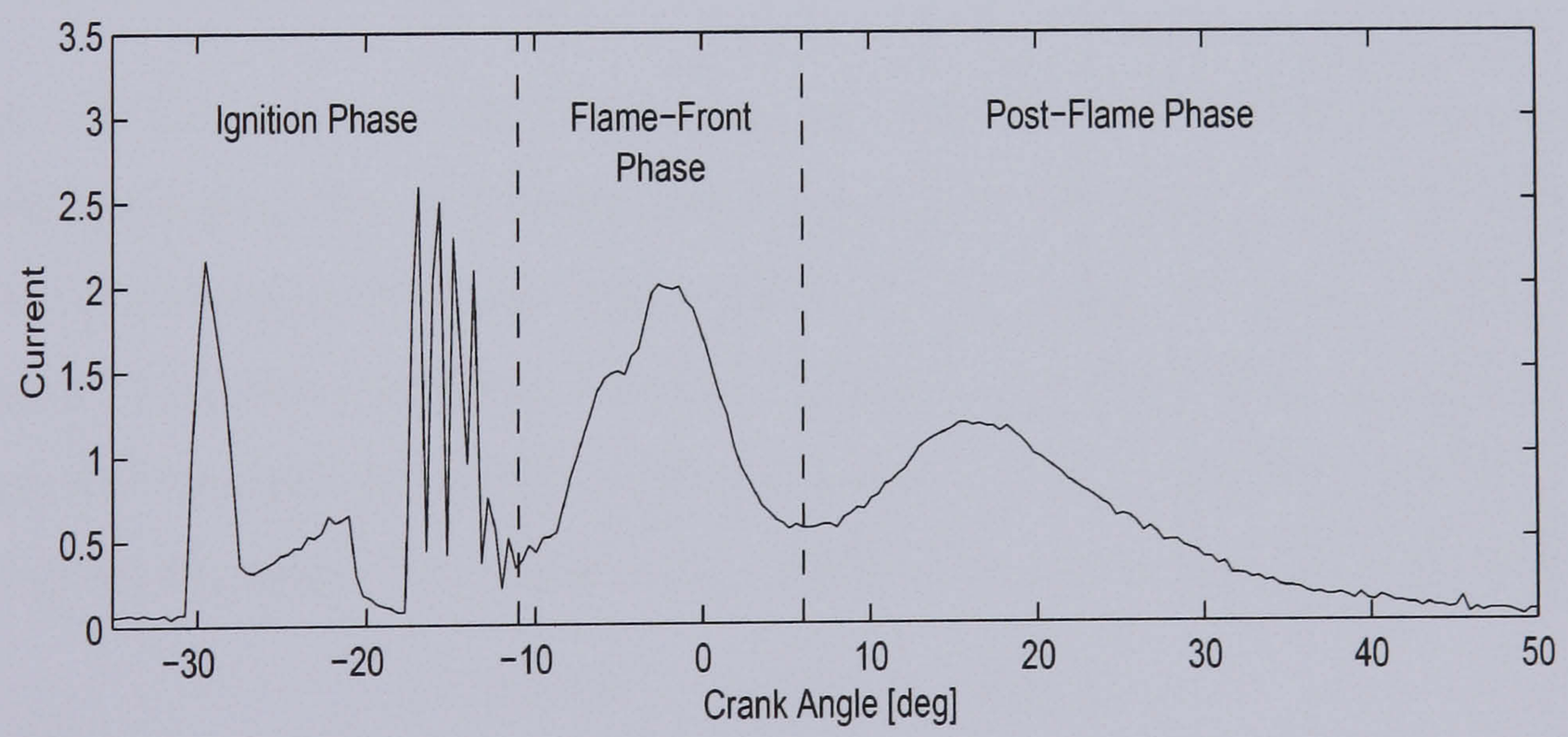

Figure 43: Typical ion trace from SI engine, measuring from igniting spark plug.

A typical averaged trace of data acquired by this method is shown in Figure 44 [104], where the signal has been averaged over a number of engine cycles that were acquired with the firing plug.

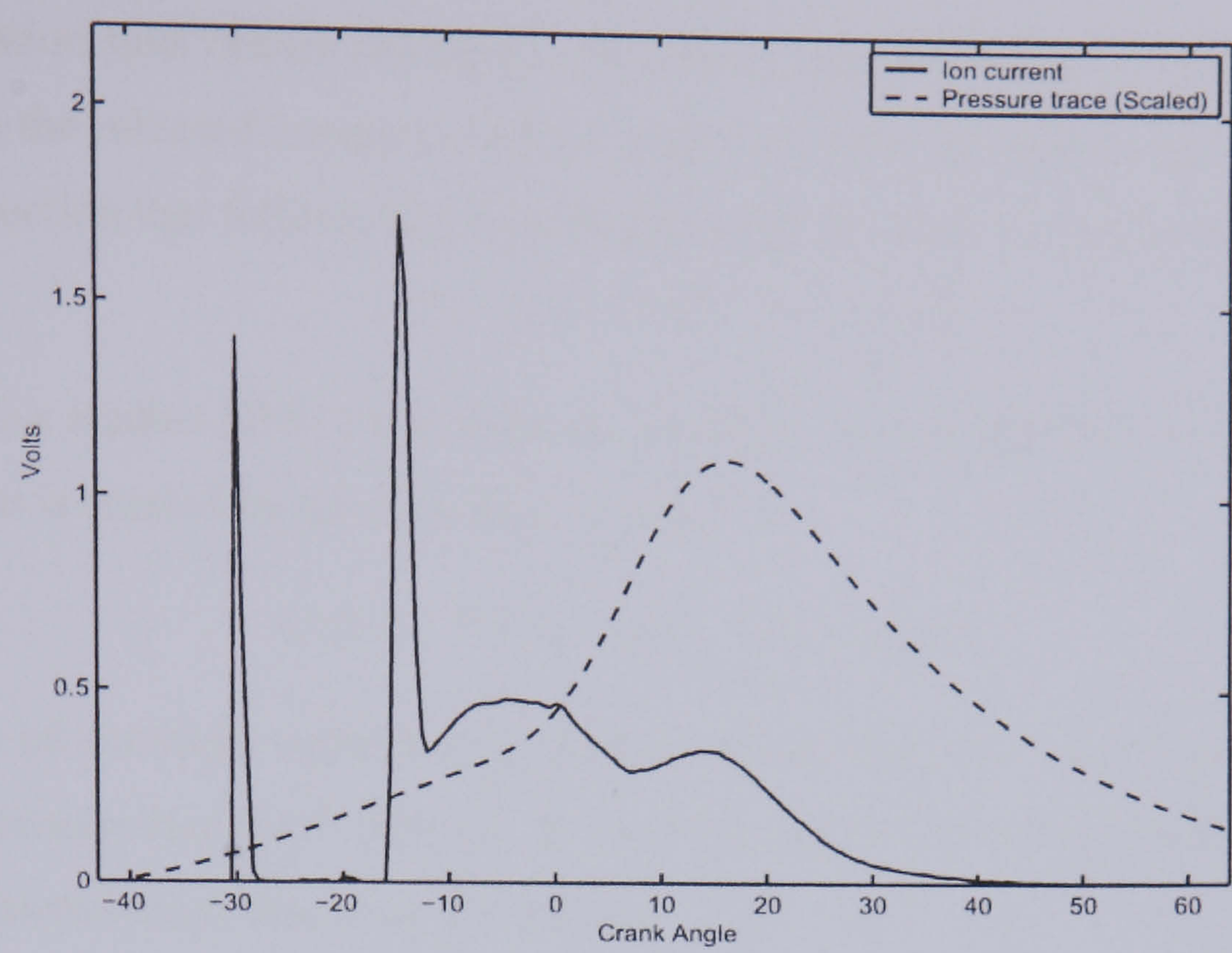

Figure 44: Typical ion current signal (and pressure signal) recorded by a central plug.

As can be seen, the signal can be divided into three phases. The first region of sharp spikes (between 35, 10 CAD BTDC) are due to the ignition and measuring circuit ringing where the ion current is measured most commonly from the low voltage side of the coil, and the emf interference causes some spikes to appear in the ion current signal. This problem also occurs even when the less common practice of measuring from the high voltage side of the coil is employed.

At about –10 CA deg the first hump starts as a result of the flame kernel developing around the spark plug tips. All of the above happens as the flame-front travels though the electrodes. The flame front phase is dependent on the amount of ions in the reaction zone of the flame. This was studied in detail by Calcote in the late fifties, who found that the ionization was strongly dependent on the chemistry of the combustion process [105,106] so it was given the name Chemi-ionization. The process can be generally described by:

$$A + B \rightarrow C + D^{+} + e^{-} \quad \text{Eq.(1)}$$

The energy that is available for the ionization is the energy of the reaction ΔH and the activation energy E. The activation energy is the energy that is necessary for the reaction $A+B \rightarrow C+D$ to take place. During this reaction the energy ΔH is released. The energy required for the ionization to take place is V_i. For the reaction to end up in the ionized state the following requirement must then be met:

$$V_i \leq \Delta H + E$$

Chemi-ionization thus occurs during an elementary reaction when the activation energy together with the released energy is large enough to ionize one of the reactants. The most significant reaction that follows this requirement has been claimed [94] to be:

$$CH + O \rightarrow CHO^{+} + e^{-} \quad \text{Eq.(2)}$$

However, other studies [106] have claimed that H_3O^+ is the dominant ion in the reaction zone. This ion is created by the following reaction:

$$CHO^{+} + H_2O \rightarrow H_3O^{+} + CO \quad \text{Eq.(3)}$$

The reaction of chemical equation (2) is much faster than the reaction of equation (1) which is the reason that H_3O^+ -ions are much more common than the CHO^+ -ions as these ions are destructed faster than they are created.

The removal of the H_3O^+ ion is obtained by the dissociative recombination with an electron to form water and a hydrogen atom.

$$H_3O^{+} + e^{-} \rightarrow H_2O + H$$

After the establishment of the combustion kernel, flame propagation towards the rest of the mixture starts. The intensified heat energy release from the burning "flame ball" growing in the cylinder warms the burned gas inside it and further increases their temperature. As a result, the internal energy of the burned gas increases and the ion formation rate becomes strong in comparison to the ion recombination rate [104,107]. The burned gas near the spark plug is compressed by the moving flame-front and folds back on itself, which results in a higher gas temperature. So, after a period of decline the ion signal starts to rise again since the ion formation rate becomes stronger than the ion recombination rate due to the energy provided by the increased pressure and temperature, giving the second hump in the signal. This is effectively a side effect of the increase in the in-cylinder pressure, which compacts the gases back towards the plug gap, called thermal-ionization. Most researchers relate this second peak in the ion curve, called the post-flame or thermal-ionization phase, to peak pressure [108].

Thermal ionization can be regarded as a chemical reaction including only one reactant according to:

$$M \leftrightarrow M^{+} + e^{-}$$

The energy needed for this reaction is taken from the burned gas. Studies have claimed that NO is responsible for a very large part of the ions in the post-flame phase [98]. This is due to the low ionization energy of that species, as can be seen in Table 1. The table also shows the ionization energies for the other major species present in the post-flame zone.

Table 1: Ionization energy for the most important species found in the post-flame zone. [103]

Species	Ionization energy (eV)
NO	9.26405
H_2O_2	10.54
CO	14.0139
CO_2	13.777
H_2O	12.6188
N_2	15.5808
H_2	15.42589

The shape of the ion current signal in the post-flame phase is also affected by the formation of negative ions. These ions are formed when species that have a certain affinity for electrons, called electronegative species, get electrons attached to them. The effect on the ion current is that it is lowered due to the lower mobility of the negative ions compared to the electrons. Table 2 shows the major electronegative species present in the post-flame zone. In the table it can be seen that oxygen atoms have a high affinity for electrons. The value for water is uncertain [103].

Table 2: The most important electronegative species in the post-flame zone, the value for water is uncertain. [103]

Species	Electron Affinity (eV)
O	1.4611103
O_2	0.451
N	0.05
H	0.754209
OH	1.82767
H_2O	0.9?
HO_2	1.078

As the piston moves away further from TDC, the volume of the combustion chamber increases and in-cylinder pressure and temperature of the burned gases decline. The ion recombination rate increases, and the measured ion current signal starts to decline. This third phase of the ion-current signal is a post-flame or thermal ionization induced signal [109,110,108,111,101,112], and it has been claimed to be proportional to the cylinder pressure produced by combustion.

The combustion gas' conductivity is also affected by the negative ions that are present. Species that have an affinity towards electrons are called electronegative. These, usually radicals, can attach to electrons and form negative ions. Since the mobility of an ion is

much smaller than that of an electron, the effect will be that the current will be lower than if no negative ions were present [113]. Thus, the air to fuel ratio can affect the signal.

However, this second hump is not always present. It disappears at low to medium engine load. Since this phase is dependant on the in-cylinder pressure, when the pressure is low, as would be the case when the load is low, this phase vanishes. This has caused quite a debate between researches and some have deemed algorithms that are based on this phase inadequate for low load operating conditions.

In addition, although it might seem that the most obvious way to apply a voltage inside a cylinder is to use two already existing electrodes, the spark plug tips, this approach has some inherent problems. In most engines there is one plug per cylinder which has to generate a spark as well as measure ion current. Because the spark generating voltage is substantially higher than the typical voltages applied in the ion current measuring circuit, the latter has to be protected somehow. This has been accomplished for example by either measuring from the low voltage side of the ignition circuit or by switching the measuring circuit in and out of the high voltage side. Both these approaches complicate matters, the former because of increased noise and bandwidth filtering by the coils, the latter because of the intricacy of such a dedicated circuit. Furthermore, all approaches that measure ion current signals from the ignition spark plug suffer from the fact that no meaningful information can be gathered until the ignition circuit has been fully discharged. As a result, the initial stage of the combustion, which corresponds to the chemical phase of the ion current signal, cannot be recorded [114,115]. This is particular evident at high speeds [115].

Another significant problem of measuring ion current through the firing spark plug is that, since the initial stage of the combustion cannot be well measured, the best signal is derived from the ion current signal's thermal phase. This, however, becomes less pronounced with reduced load and can disappear for load settings less than 75%, thus severely limiting the usefulness of the ion current signal.

In order to address these issues, ion current sensing from dedicated sensors can be employed (remote sensing), introducing significant advantages. On the technical side, signal quality is greatly improved since data acquisition does not need to be interrupted. This continuous measurement allows for acquisition of ion current data throughout the combustion process. This allows for a much a greater volume of information to be extracted from the signal at higher signal to noise ratios. To extract as much information

as possible from this signal, sophisticated signal processing strategies need to be employed.

On the cost side, this approach offers the opportunity for simpler, more robust therefore more cost efficient designs for the measuring circuit, since there is no consideration of coupling with the ignition circuit to be taken into account. On the down side, locating a probe inside the combustion chamber introduces the need for extra machining and potentially packaging and sealing problems, as well.

On the upside, signal quality is greatly improved using remote sensing, thus permitting true cycle-to-cycle engine diagnosis and control. Thus, the need for averaging is eliminated, which reduces computational and time requirements.

It might, at first, appear as a significant complication to introduce dedicated ion sensors on mass production engines. However, companies that already offer head gaskets with multiple ion collectors exist. This makes modifications to the cylinder head and engine block unnecessary. [116,117]. Although, the signal shape from such an application will be quite different to the one collected from somewhere in the flame path, in contrast to the flame terminal.

This research focuses on the examination of the potential of ion current based mainly on the benefits of better signal quality, cheaper electronics and use of computationally inexpensive signal processing algorithms that are made possible through remote sensing.

2.7.1 Ion Current Formation Models

It is common to assume that the measured ion current signal is due to the aforementioned processes. These processes are quite complicated and although the ion current correlates very nicely with the pressure increase due to combustion, as will be shown extensively later, there is no definitive description as to how exactly this phenomenon is generated. A description of three popular formation models is given by [118] as presented below.

2.7.2 Saitzkoff-Reinmann model

This model was presented in 1996 by Saitzkoff [119] and describes the thermal-ionization phase of the ion current, which is the most important phase in SI. It basically concentrates

the analysis on the volume of space between the spark plug electrodes (control volume). Free electrons from the thermal-ionization of NO and thus can be described by Saha's equation:

$$\frac{n_1 n_e}{n_0} = 2\left(\frac{2\pi m_e kT}{h^2}\right)^{\frac{3}{2}} \frac{B_1}{B_0} \exp\left[-\frac{E_1}{kT}\right]$$

This equation describes the equilibrium balance of ions and electrons for a first order ionization. Combined with models for electron drift velocity and electric field another expression can be obtained:

$$I = U\frac{\pi r^2}{d}\frac{e^2}{\sigma m_e\sqrt{\frac{8kT}{\pi m_e}}}\sqrt{\phi_s}\sqrt{\frac{2\left(\frac{2\pi m_e kT}{h^2}\right)^{\frac{3}{2}}\frac{B_1}{B_0}\exp\left[-\frac{E_1}{kT}\right]}{n_{tot}}}$$

Where:

Table 3: Saitzkoff model parameters.

n_1	Number density of ions
n_e	Number density of free electrons
n_0	Number density of neutral particles
U	Measurement voltage
R	Radius of ion sensor center electrode (probe)
D	Distance between ion sensor's electrode tips
Σ	Collision cross section
T	Gas temperature
φ_s	NO ratio in gas mixture
m_e	Electron mass
B_i	Internal partition function
E_i	Ionization energy
n_{tot}	Total particle number density
k	Boltzmann's constant
h	Planck's constant
e	Unit charge constant

The volume between the sensors electrodes is treated as a free charge space affected by the electrical field generated by the voltage applied to the sensor. Charge movement within this volume does not change the rest of the field inside the combustion chamber,

since this volume is relatively small; however the change if the electric field within this volume is measurable by the circuit. The limitation on the ion signal magnitude is imposed by the number of free electrons in that volume space.

A similar model but with more detailed electric field and chemical calculations has been also described by Wilstermann [120]. The main difference is that the chemical reactions in the flame front are considered a source of free charge, which Saitzkoff does not disregard.

2.7.3 Calcote model

Calcote is one of the most cited authors in the ions in flames field. Calcote's analysis, dating back to 1963, considers the electrode physics when electrons enter or leave the sensors tips. This model has also been used by Wilstermann [120] to explain the occurrence of measurable current.

The ion sensor is modeled as a Langmuir probe with the central electrode having an electric potential U_s relative to ground (i.e. combustion chamber wall). The combustion chamber volume is thought to be consisted of a distribution of partly ionized gases where there are positive and negative ions and free electrons. The movement of particles is dominated by temperature when U_s is low.

If U_s is negative enough no electrons will reach the center electrode surface, since they will be repelled. Positive ions will be attracted to the electrode and produce some current, although these ions are heavy, as has already been mentioned, and the current will not be as high as if it was electrons that were being attracted. When U_s is increased towards positive the fastest electrons will start reaching the electrode. At some point, when U_s is still negative, the current contribution from the electrons and the positive ions will be equal, so the net current will be zero. This point is called the Floating Potential. At U_s=0 the electron current will dominate over the positive ion current due to the higher mobility and the higher temperature.

The electrical field around the center electrode is thought to cause a redistribution of the charge in the combustion chamber. Charge with opposite sign to U_s will gather around the electrode and eliminate the field in the rest of the combustion chamber. For positive U_s the electron concentration n_e around the electrode will increase as U_s increases. The current is then limited by the surface process of the electrode. The electrode surface process is described as:

$$I_e = n_e e A_s \sqrt{\frac{kT_e}{2\pi m_e}\left[1+\frac{3ld}{16\lambda_e B_e}\ln\left(\frac{X_e+B_e}{X_e-B_e}\right)\right]^{-1}}$$

$$I_i = n_i e A_s \sqrt{\frac{kT_i}{2\pi m_i}\left[1+\frac{3ld}{16\lambda_i B_i}\ln\left(\frac{X_i+B_i}{X_i-B_i}\right)\right]^{-1}}$$

The first equation describes electrons at a positive electrode and the second positive ions at a negative electrode.

Table 4: Calcote model parameters.

n_e	Electron concentration
m_e	Electron mass
T_e	Electron temperature
λ_e	Electron mean free path
E	Unit charge
L	Probe length
D	Probe diameter
A_s	Probe surface area
X_e	$=l+2\lambda_e$
B_e	$=\sqrt{(X_e^2-(d+2\lambda_e)^2}$
n_i	Ion concentration
m_i	Ion mass
T_i	Ion temperature
λ_i	Ion mean free path
X_i	$=l+2\lambda_i$
B_i	$=\sqrt{(X_i^2-(d+2\lambda_i)^2}$

As the measurement voltage U_s increases the electron concentration around the electrode will increase and thus the measured current. No direct relationship between U_s and n_e is given. In practice, a "saturation" voltage value exists, over which no further current increase is possible with further voltage increase [122].

2.7.4 Yoshiyama-Tomita model

Yoshiyama [99] bases his theory on flame front ionization. Combustion bomb experiments were performed. The electrodes could be either completely isolated form the combustion chamber wall or any one of the electrodes could be connected to it. Optical analysis was also performed by correlating the ion current measured to the images taken with a camera. The traces taken resemble the typical ion current trace, as previously

shown in Figure 43, only when the negative electrode was connected to the wall. That is, the first ion current peak was always present independent of the configuration of electrode connection to the wall, but the second only appeared if the wall was grounded, as is typically the case with engine experiments. Its timing coincided with the flame front reaching the wall. So from these experiments the main two conclusions that can be drawn are:

- The shape of the ion current trace is dependant upon the flame position and electrode polarity.
- Ions and electrons are generated in the flame front by chemical reaction and thermal ionization is negligible.

In the theory presented in that paper the experimental results are explained. It has to be noted, however, that the start pressure of 4bar and start temperature of 290K, may lead to the disappearance of the thermal ionization, due to the low temperature. Formation of NO, the main source of thermal-ionization, as claimed by Saitzkoff, will be very weak under these conditions.

2.7.5 General Ion Current Technique Remarks

Several general remarks about ion current measurement techniques can be made.

Firstly, the larger the electrode, the higher the signal amplitude all formation theories support this.

Secondly, larger ground electrode increases flame-peak amplitude. This is supported by both Calcote and Yoshiyama-Tomita models. The Saitzkopff-Reinmann model does not account for the flame front phase.

Thirdly, the shape of the flame front peak depends on the shape of the ground electrode. This is also supported by both Calcote and Yoshiyama-Tomita models.

And lastly, the shape of the thermal peak depends on the supply of electrons from the ionized species (thought to be NOx and alkali metals). This fact can be explained directly by the Saitzkopff-Reinmann model, but, in addition, does not contradict the other two models.

2.7.6 Effects of EGR on ion current

Here, comments made here by [121] concerning ion current in GDI engine (i.e. SIDI) at increasing amount of EGR are outlined. Although in our case the engine is port fuel injected and not stratified, the effects of increasing amount of dilution, is a common concern. Note that external gas recirculation is used here, not residual gas trapping.

In a GDI engine working in stratified mode there is a high amount of excess air. The oxygen in the air will then attach a lot of electrons to it reducing the ion current. This in combination with the lower temperature are the reasons that the post-flame phase of the ion current signal for the stratified mode lacks the typical second maximum that can be seen in the signal from engines with a homogeneous mixture.

The introduction of non-reactive gas, in this case exhaust gas (especially external EGR), into the cylinder affects combustion and thus ion current. In Figure 45, the effect that different EGR rates have on the ion current signal can be seen. In the figure there are two lines for each EGR rate between 0% and 25% in steps of 5%. Each line is the average of 120 cycles. The 0% EGR has the highest amplitude and the earliest position of the first maximum.

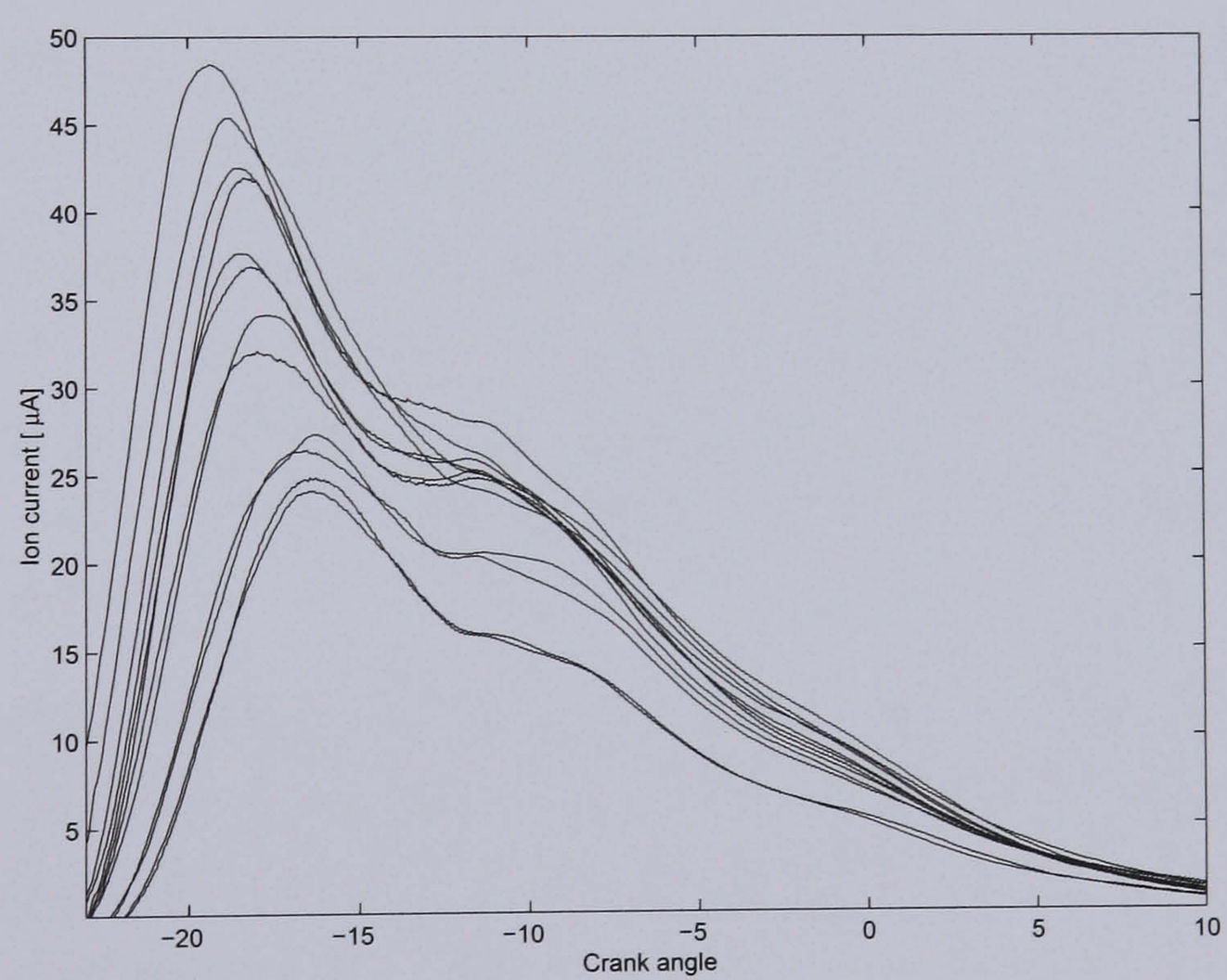

Figure 45: Ion current signal with increasing EGR rates.

As has been stated earlier the main reason to use the EGR system is that it reduces the formation of NOx in the engine. This is due to exhaust gas lowering the peak temperature in the cylinder. The lower temperature is because the exhaust gas increases the heat capacity ratio γ which means that more energy is needed to raise the temperature of the gas.

The same author argues, with reference to Figure 45 that:

- High EGR rates lower combustion temperatures which lead to lower amounts of NO that also lower post-flame zone ion current amplitude.
- However, introduction of exhaust gases also lowers the amount of excess air in the cylinder which lead to less O atoms that can attach electrons and lower the ion current. So the lower amount of positive ions are balanced, up to a point, by the lower amount of negative ions.

The same paper goes on to say that at very high EGR rates the expected effect on the signal can be seen and that the conclusion is that the last part of the ion current signal can not be used to get any information about the amount of exhaust gas in the cylinder. He also comments that the only possibility left for estimating the EGR rate from the ion current signal is by looking at the flame-front phase of the signal. In Figure 45 it can be seen that the effect of EGR in this phase is a lower amplitude and a later positioning of the first maximum and also a diminishing post-flame signal.

The total amount of created ions is also lowered as can be seen by studying the area under the maximum. The lower amplitude and lower amount of ions is expected mainly due to the decreased temperature which reduces the available energy ΔH. This means that fewer reactions will fulfil the requirements for formation of ions leading to that less ions are formed. Another reason for the lowered amplitude is that the rates of recombination of the ions aren't affected as much as the production of the ions.

The positioning is affected by the time it takes for the flame to leave the vicinity of the spark plug where the measurement is made. As can be seen in Figure 45 the first maximum occurs later for higher EGR rates. This effect is also due to the lowered temperature as it leads to a lower burning speed of the flame which in turn gives a slower flame kernel formation.

Keeping in mind that in the case of CAI the excess air is not affected by the amount of EGR (or TRG) when the engine is operating at stoichiometry and also that the amount of residual gas dilution used in CAI are a lot higher than in possible in GDI engines (leading to minute NOx emissions), it can be concluded that the thermal-zone ion current amplitude will be almost completely absent. This is, in fact, the case in the experimental data collected, as is described in the CAI ion current chapter later in the thesis.

In the rest of this thesis experimental results will be presented and discussed. These cover the entire CAI operation spectrum of the engine used, from positive to negative overlap, up to the misfire limit. It will be seen that no knocking or unstable combustion occurs within this spectrum i.e. from SI operation up to the misfire limit and that ion current provides useful feedback throughout.

3. Aim

The possibility of improvement of the reciprocating internal combustion engine is an inspiration to any engineer. Consequently, HCCI combustion is a very exciting research area since it promises substantial improvements in both efficiency and emissions. To this end, the preliminary aim of the author was to better understand the mechanics surrounding this combustion method. Thus its advantages, implementation possibilities and challenges had to be analyzed first. Then concentration was given on arriving to decisions upon the research methodology and apparatus that would be suited for analytical and evaluative work on the most promising configuration, keeping in mind direct mass production potential.

An experimental study is thought to be the best approach in delivering fast and verifiable results. Since information on controlled gasoline autoignition is limited and holds great potential for power density and ease of control, especially in combination with a Fully Variable Valve Timing system, this configuration was chosen as a research platform. More specifically, the presence of the spark plug in the combustion chamber ensures combustion even when moving out the pure autoignition window while a Fully Variable Valve System allows precise and instantaneous control over the amount of Trapped Residual Gas.

Investigation of emissions and fuel consumption, thermodynamic cycle and combustion behaviour considerations under varying operating conditions in CAI have to be performed in order to better quantify its potential. Due to the harsh conditions presented by the auto igniting nature of this combustion, cylinder pressure signal manipulation is also required for suitable analysis.

Control swiftly proves to be the most significant issue in an engine where ignition is only indirectly managed. So, focus on identifying feedback control signal candidates and associated manipulation techniques yielding best performance is necessary. The typical feedback signal is that of an in-cylinder piezoelectric pressure transducer, however, cost considerations point to ion current as a viable alternative for mass production purposes. Their corresponding signals have to be studied and compared so that a realistic and informed judgment can materialize.

Based on the above, it becomes clear that the aim of this thesis is to develop an engine taking advantage of the benefits of CAI, in an operating window as large as possible and suitable for real life mass production implementation.

4. Methodology

4.1 HCCI Implementation Considerations

From the literature review so far, it becomes obvious that there are various ways of HCCI implementation. It thus needs to be decided upon which way is thought "best". The solution should allow for an implementation that would be both cost efficient and also practically achievable in the shortest possible time frame. Since HCCI cannot cover the whole operating spectrum needed for an automotive application, an engine being capable of working in dual mode is required. This engine would start and warm up in SI or CI mode and would switch in HCCI mode where and when possible.

This presents us with the first choice that needs to be made, i.e. between SI or CI for conventional operation. It was decided that SI should be used since it allows the residual gases amount to be increased gradually. In addition the spark plug can be used to control the ignition timing when lower or higher residual gas percentages, than would be required for pure autoignition, are present. This possibility for smooth transitions from SI to CAI and also the additional control on ignition timing where thought to be adequate reasons to justify this choice.

Since there are more than one way to instigate CAI combustion, more detailed decisions also had to be made, namely which way of residual gases presentation was to be used. Since a fast response system was sought after in order to have better control, a variable valve timing (VVT) system offered a good solution. This should give cycle- to-cycle response thus giving ultimate control over each combustion event.

The next step is to decide on a valve timing strategy. The variables that can be changed are timing, duration and lift. The answer to this had to come from a back to back experimental comparison between two different strategies. One was a fixed duration, fixed lift, variable timing strategy and the other was a fixed inlet valve close (IVC), fixed exhaust valve open (EVO) and variable inlet valve open (IVO) and variable exhaust valve close (EVC), at fixed lift. Answers on the issues of control, gas exchange losses and emissions of the respective strategies need to be given.

With control being the most demanding aspect of CAI combustion a feedback signal becomes imperative. Consequently, the in-cylinder pressure signal will be used for in-depth analysis of combustion properties. However, a more cost effective suggestion for an in-cylinder feedback signal needs to be made, since in-cylinder pressure transducers and their amplifiers are prohibitively expensive for mass production. Ion current appears to be

a promising solution to this problem. To experimentally test its potential an in-cylinder ion probe can be added with the addition of an external voltage source. Having decided on the experimental apparatus that needs to be used for extensive SI-CAI investigation, the question of ion current being a valid proposition for real life CAI viability remains to be answered.

4.2 Renault Engine and Test Rig

A single cylinder 4-stroke Renault research engine was used for preliminary SI investigation. The Lotus engine described fully in section 5.3 "Lotus Engine and Test Rig" was used for more detailed and CAI, ion current data acquisition. Full specification, of the Renault engine, is presented in Table 5. The engine featured variable compression ratio, variable ignition timing, variable air to fuel ratio and four access points in the cylinder head.

Table 5: Engine Specification.

Bore	80 mm
Stoke	100 mm
Inlet Valve Opening	12degCA BTDC
Inlet Valve Closing	64degCA ABDC
Exhaust Valve Opening	64degCA BBDC
Exhaust Valve Closing	12degCA ATDC
Compression Ratio	4.5:1 - 13:1
Ignition Timing	55degCA BTDC – 20degCA ATDC

Figure 46 and Figure 47 show the arrangement of the cylinder head and the spark plug locations. The firing plug, which is located next to the inlet valve, was used as the ignition source and one or both of the two remote sensing plugs were used as the ion current sensing units. One was fitted on the other side of the inlet valve opposite to the firing plug (sensing plug (1) in the diagram) whilst the other, (sensing plug (2)), was fitted next to the engine exhaust valve. The distance between sensing plug (1) and the firing plug was 42mm, and the distance between the sensing plug (2) and the firing plug was 55mm.

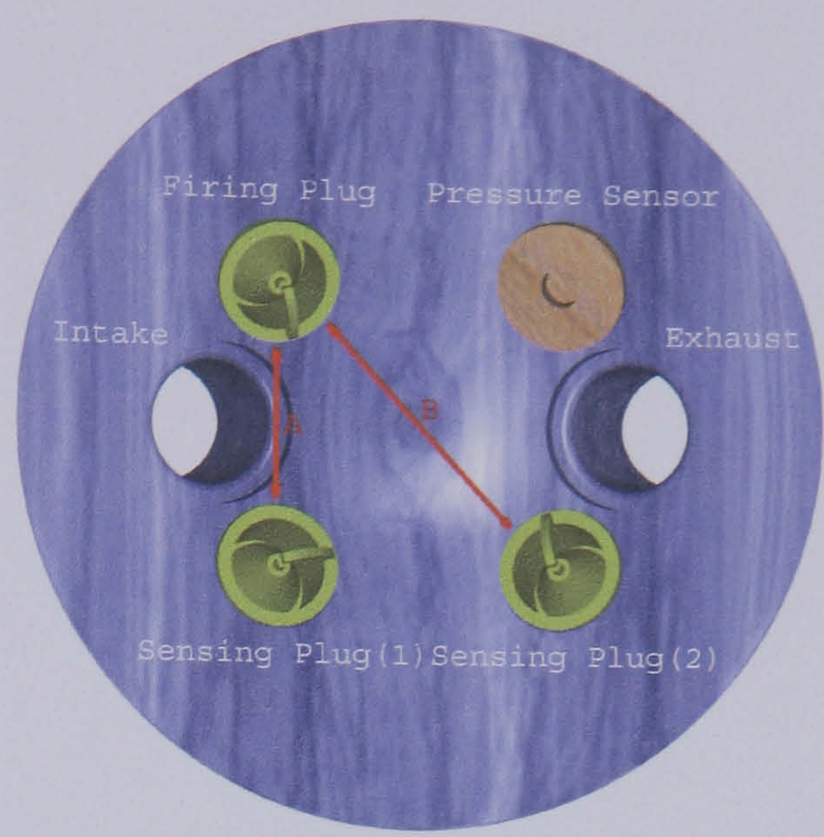

Figure 46: Cylinder head 2D view. Distances between firing and measuring plugs indicated.

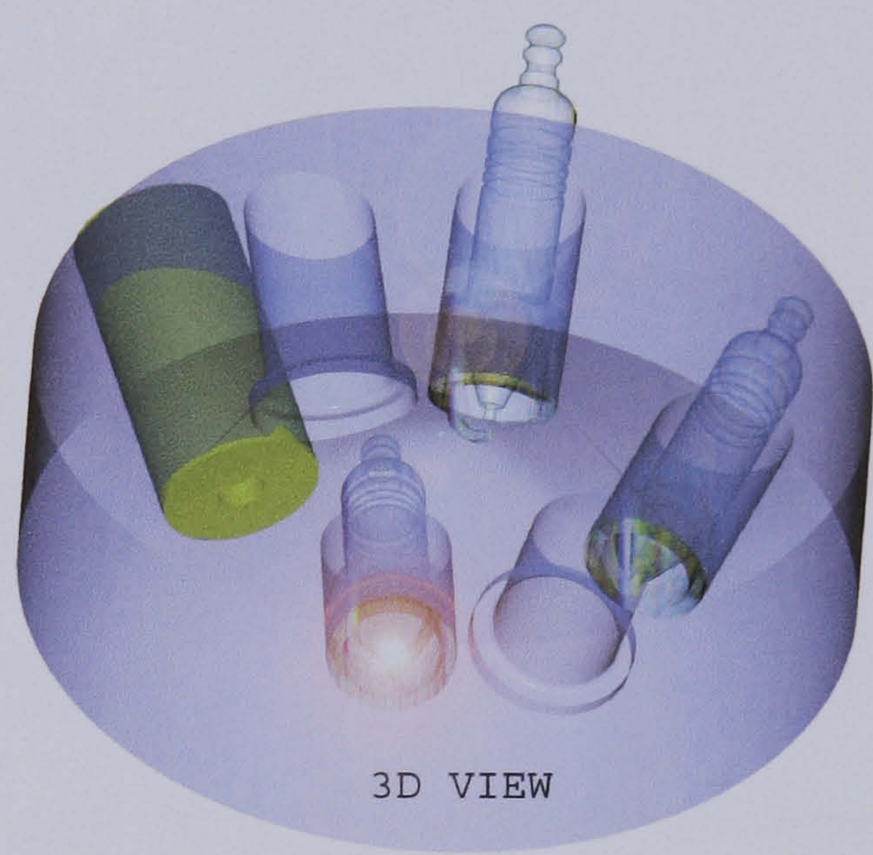

Figure 47: Cylinder head 3D view. The firing spark plug, two sensing plugs and pressure sensor.

The voltage polarity at the gap of sensing spark plugs was, as already stated, selected so that the small area spark plug electrode, the centre electrode, was positive, and the large area electrode and the rest of the combustion chamber were negative.

A purpose built DC voltage source, very similar to the one used in the Lotus engine, was put together to power the measuring plugs. The main difference was that this could be connected in parallel with multiple ion sensors, as can be seen in Figure 48. The output of the voltage divider was passed to a data acquisition (DAQ) board as the ion current signal. The voltage divider would produce a voltage that was inversely proportional to the sensed ion current (i.e. 5V for zero ion current and 0V for infinite) to avoid the possibility of damage caused due to excessive voltage. The signal was inverted during the post processing phase.

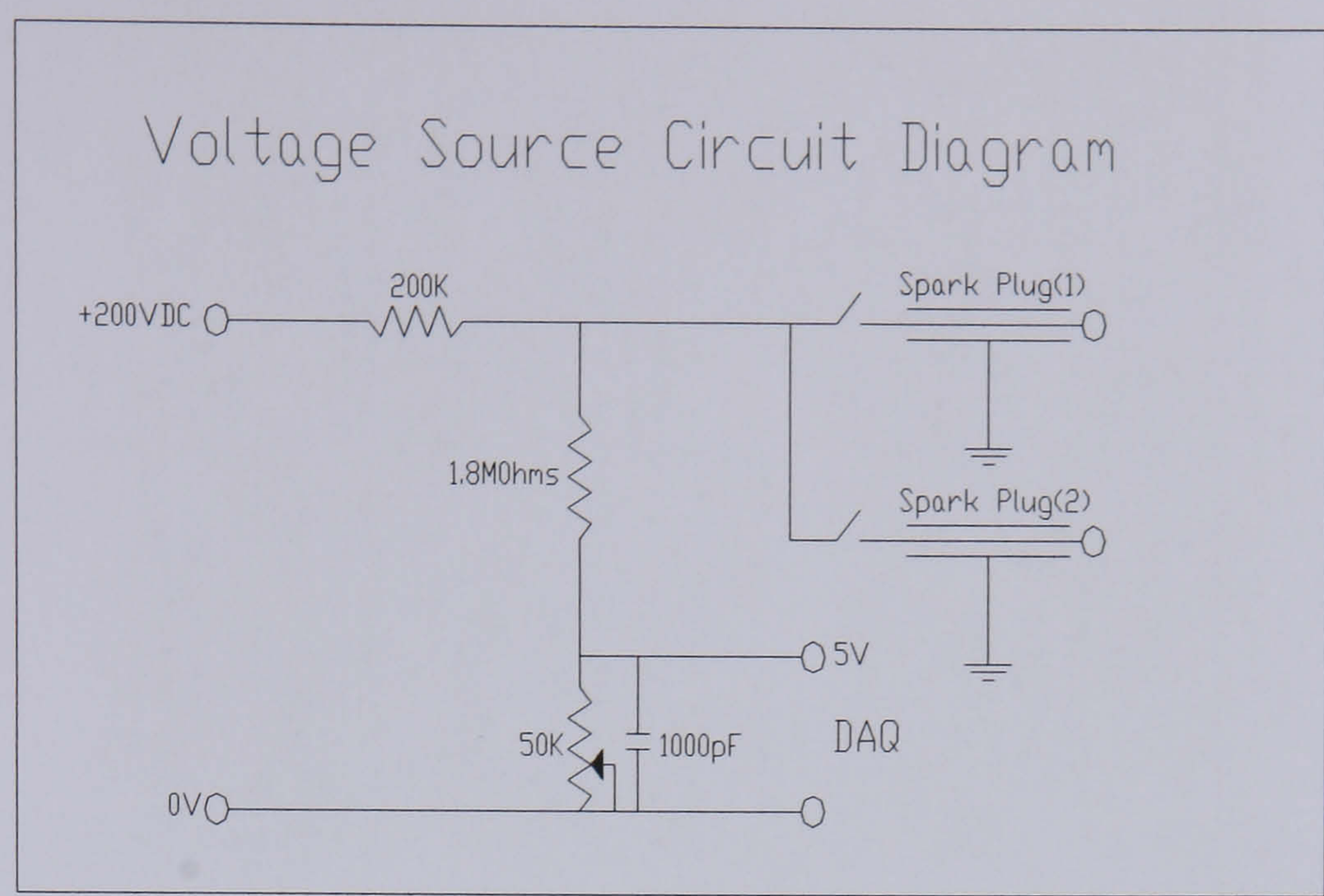

Figure 48: Circuit Diagram of DC Source.

The DAQ sampling rate was one sample per 2 degCA. Data were acquired using either only sensing plug (1) or both. When using both sensing plugs, these were connected in parallel, as shown in Figure 48, which essentially results in the addition of the two ion current signals. All experiments were conducted using the single ion current sensor, and then both sensors to assess the extent by which additional sensors improve the quality of ion-current data.

When the flame front passes the sensing plug, the gas around the plug is burned. The balance between the ionization and recombination of the burned gas constituents is then a function of temperature and pressure. This leads to a post-flame hump similar to that recorded when the firing plug is used for measurement.

4.3 Lotus Engine and Test Rig

As mentioned before an engine capable of operating in CAI as well as SI is needed. Thus, the engine employed was a single cylinder, gasoline port fuel injected, 4-stroke research engine; based on a GM Family One, 1.8L series architecture, shown by Figure 49.

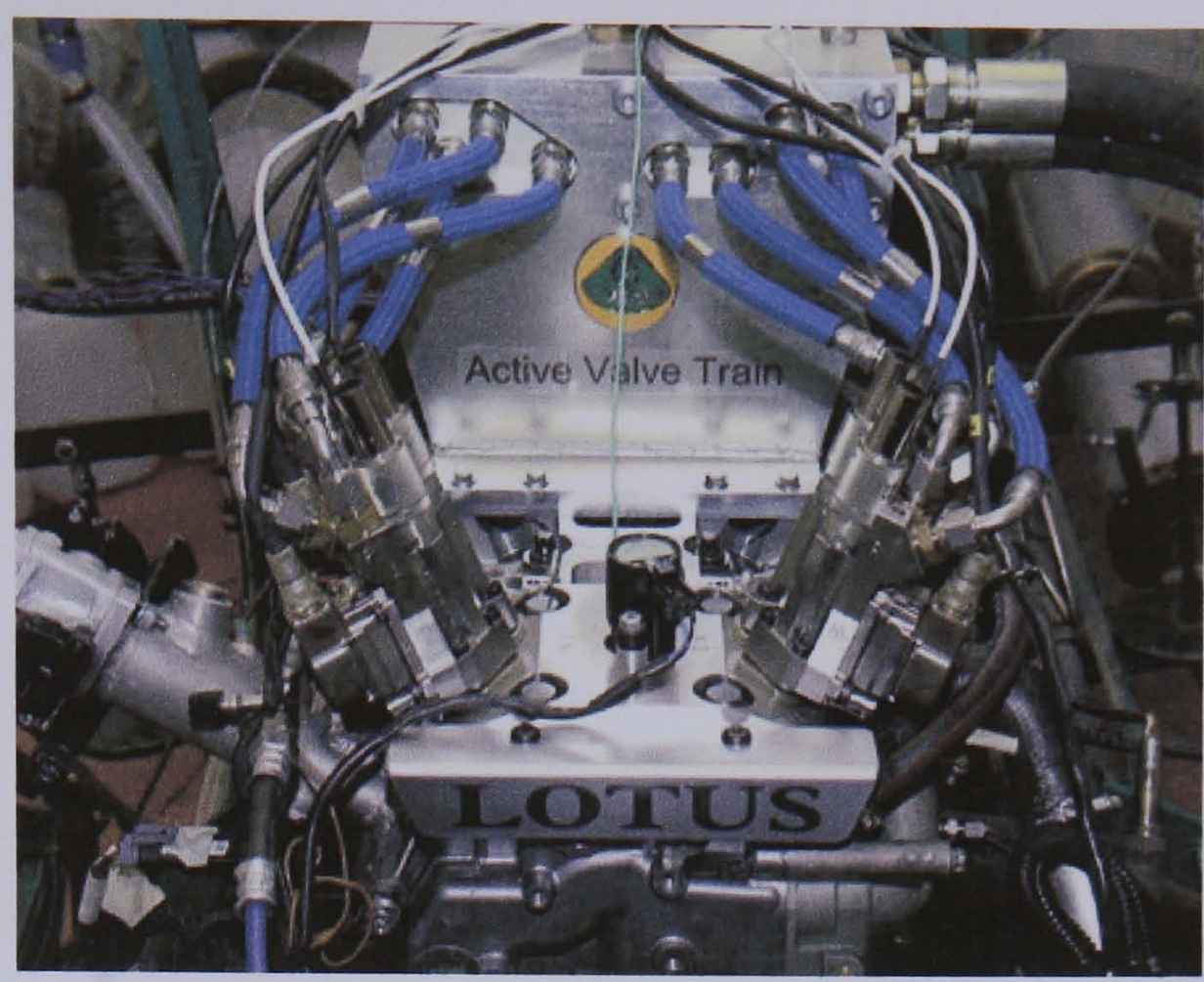

Figure 49: Single-cylinder research engine with AVT system.

A standard 4-cylinder head is mounted on top of a water cooled barrel, with a custom made bottom end. Only the front cylinder (first cylinder) of the head is operational. A fully variable valve timing (FVVT) system named Active Valve Train (AVT), manufactured by Lotus Engineering, was fitted to allow a variable valve timing strategy, details which are shown in Figure 50, Figure 51, Figure 52. This is a high pressure hydraulic valvetrain system that uses high speed digital valves to control the oil pressure in a hydraulic piston driving the valve stem.

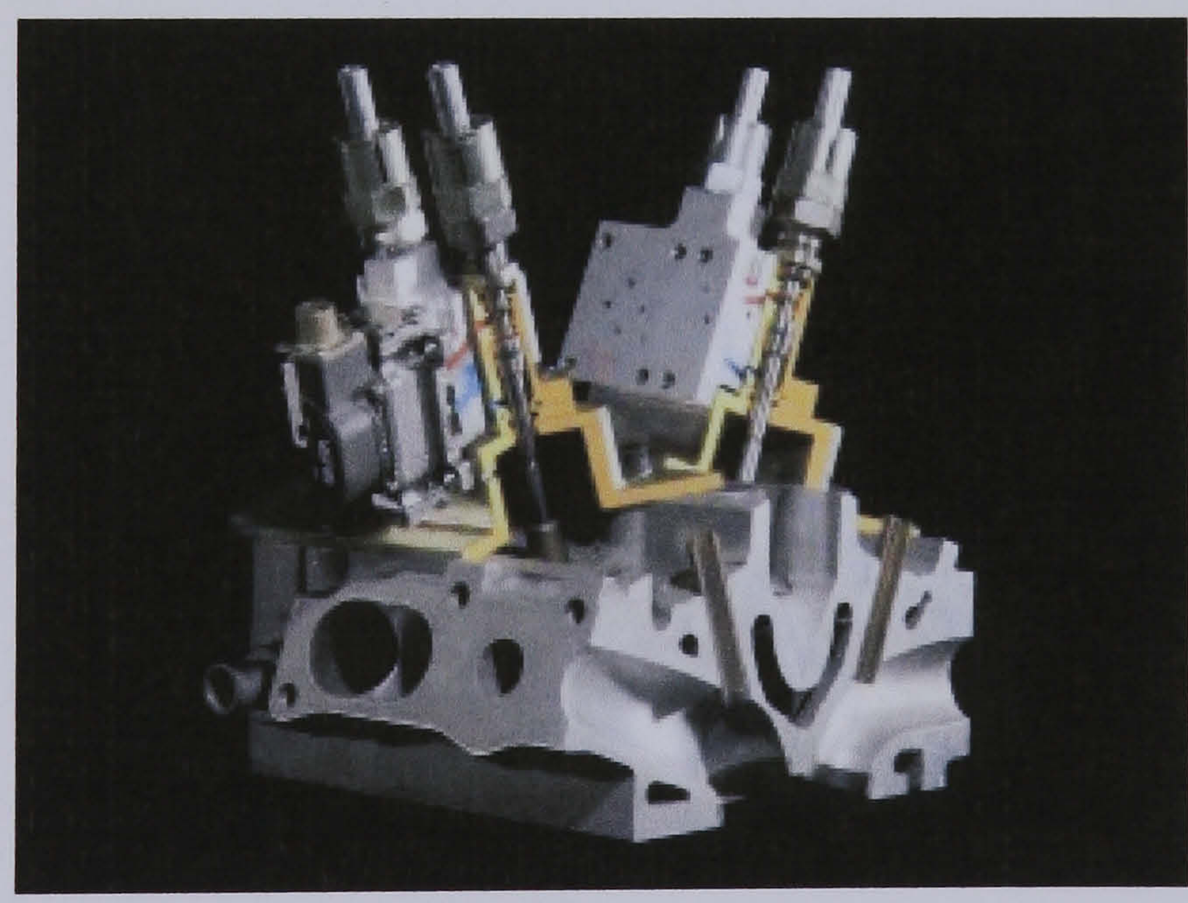

Figure 50: Hydraulic valvetrain cutaway.

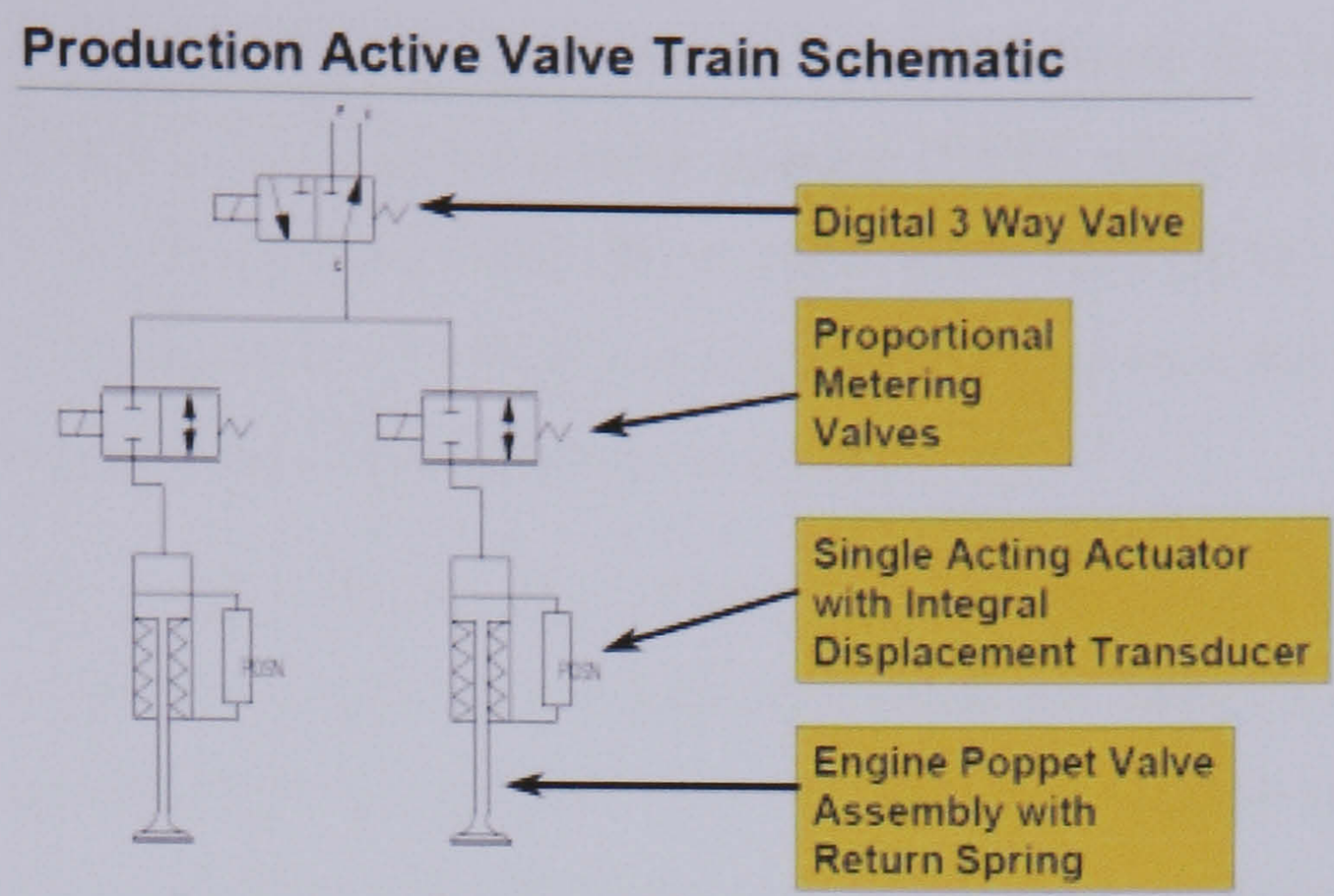

Figure 51: Hydraulic circuit of AVT.

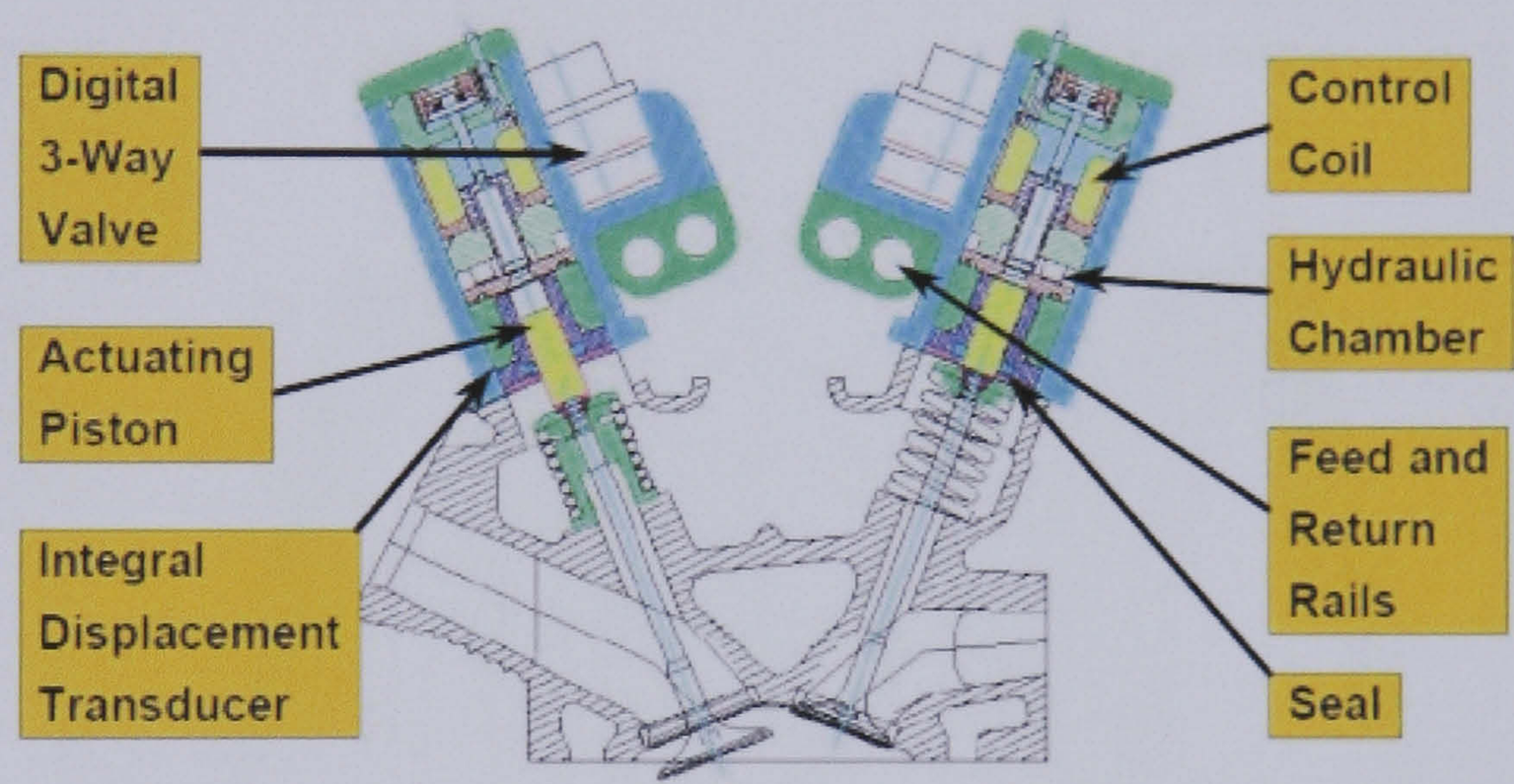

Figure 52: Schematic of hydraulic valvetrain.

The AVT system is computer controlled and can change valve profiles whilst the engine is running and within an engine cycle. Variable quantities of trapped residual gas (TRG) can be captured in this way. In addition, TRG amount can be changed on a cycle-to-cycle basis and SI to CAI and back switches can also be performed.

4.3.1 Valve strategies

Although any valve profile can be used, the strategies that were the main focus of the research here were as follows:

For SI operation the standard profile used in the production engine equivalent was used which involves positive overlap, high lift (8-9mm) and a fixed duration and phasing. CAI operation was realized in two distinct ways. In both strategies, TRG is retained, rather

than recirculated, by early closing of the exhaust valve. However, in one valve strategy, the inlet valve close (IVC) and exhaust valve opening (EVO) were kept constant sharing their timing with the SI profiles, while the exhaust valve close (EVC) and inlet valve opening point (IVO) shift away from the gas exchange TDC to increase TRG amount, or towards it to reduce it. Also, a high lift of 6mm is used.

In the second valve strategy, the duration of the valve opening always remains constant, hence shifting of the EVC, which is necessary to regulate the TRG amount, also moves EVO along. Since the inlet valve, whose opening timing is roughly symmetrical with EVC around the gas exchange TDC will change, the IVC timing will change with it. The lift used in this latter strategy was low (2.5mm). The valve profiles of these two strategies can be seen in Figure 53 and Figure 54.

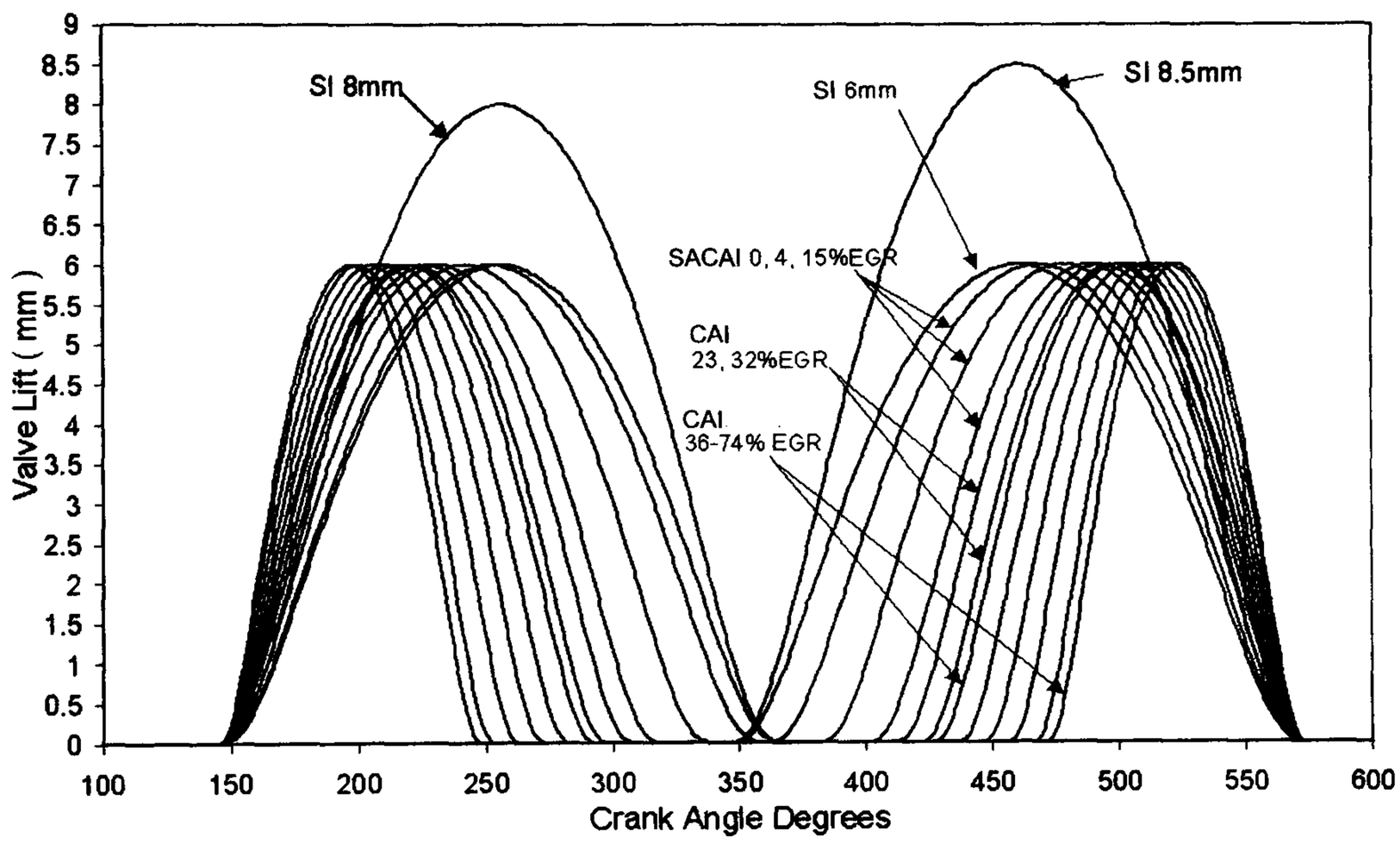

Figure 53: Constant IVC, EVO valve profiles. Lifts, Duration and corresponding volumetric EGR% are shown.

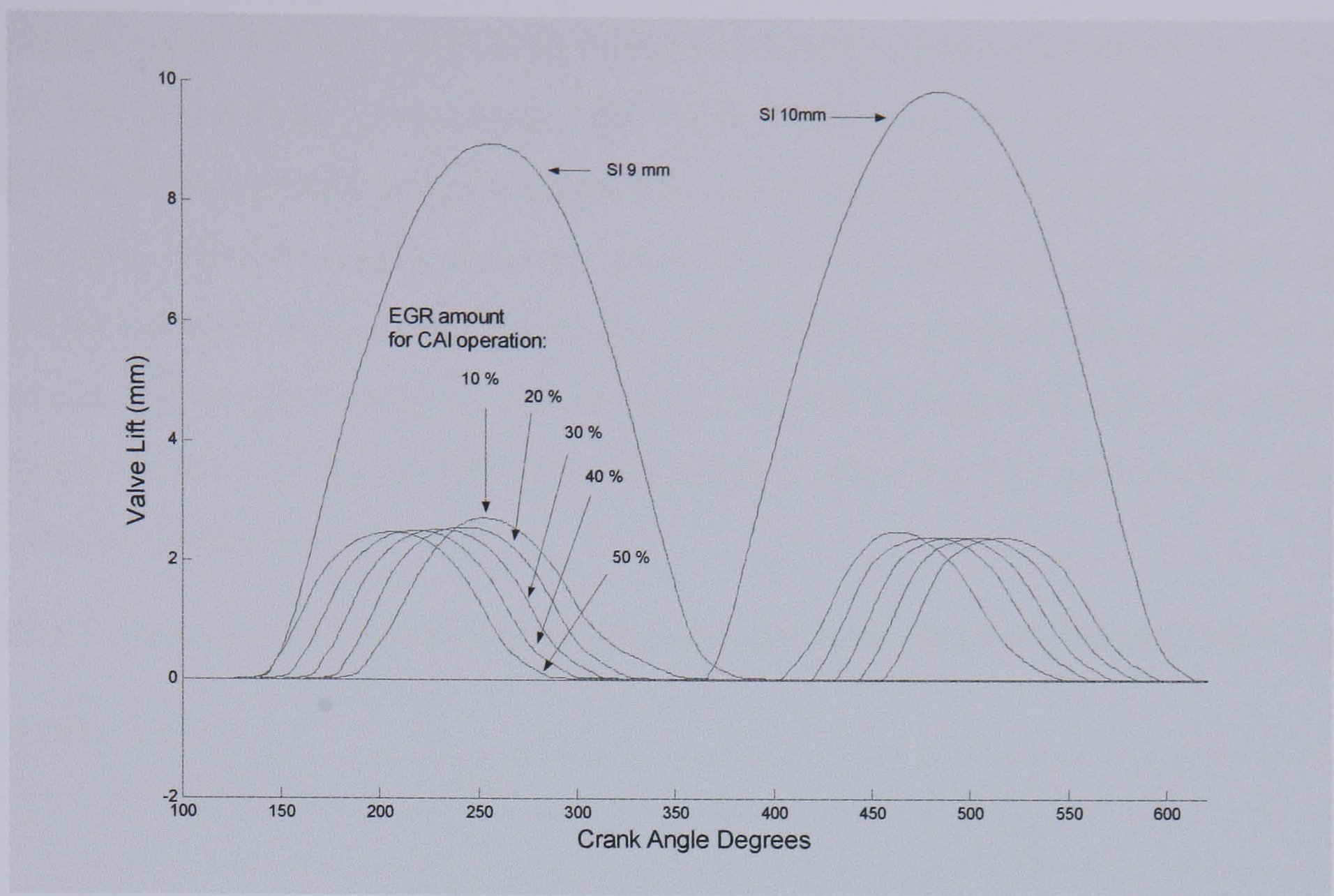

Figure 54: Constant duration valve profiles. Lifts, Duration and corresponding volumetric EGR% are shown.

Of these two strategies, the latter reduces the effective compression ratio as TRG level increases, since high TRG requires early EVC leading to late IVO and hence late IVC, since a high level of TRG is normally needed for pure CAI operation.

The engine was equipped with an electronic throttle, on top of a standard mechanical one, that was used for load control, especially keeping the load constant whilst switching from SI to CAI and back.

The use of conventional parts in the combustion system, wherever possible, ensures that the cost of rebuild is low in case of any component failures (because of uncontrolled detonation, for example). The Compression Ratio (CR) can easily be changed in this engine, both because of the separate barrel and, more importantly, because of the AVT system negating the need to consider modifications to belt runs. Any change in CR is achieved by means of the deck height being moved up and down by spacers or special short liners, or a combination of the two. The bottom end can accept various strokes up to and including 100mm, and is capable of running to 7000rpm (depending on stroke). For all investigations carried out here, the compression ratio was set to 10.5 and the fuel used was commercial gasoline 95 RON.

The engine was connected to a Froude AG30 30kW eddy-current dynamometer. A redline ACAP data acquisition system from DSP Technologies Inc. was used, together with a Kistler 6123 piezoelectric pressure transducer. This transducer is not water cooled since only a 6mm diameter sensor could be fitted, due to the confined cylinder head space. Special mention has to be made here of the susceptibility to thermal shock and base drift, due to this. More specifically, as can be seen in Table 6, underestimation of IMEP and maximum pressure of up to 10% and 3% respectively. The full sensor Data Sheet is available in Appendix 4.

Table 6: Pressure Sensor Data (Difference from reference sensor 7061B at 1500rpm, IMEP=9 bar).

Thermal Shock		
Δp (short-time drift)	Bar	< -1.5
ΔIMEP up to	%	< -10
Δpmax up to	%	< -3

A Horiba MEXA 7100 DEGR analyzer was used for emissions measurement. Port fuel injection was employed, managed by a conventional Lotus V8 engine controller.

The experiments also involved ion current signal acquisition. This was done by locating an ionization probe in the four-valve cylinder head between one of the inlet and one of the exhaust valves as shown in Figure 55. The probe was electrically isolated from the cylinder head by means of a ceramic sleeve. The diameter of the sensing element was slightly less than 1mm and the tip protrusion into the combustion chamber was approximately 3.5 mm.

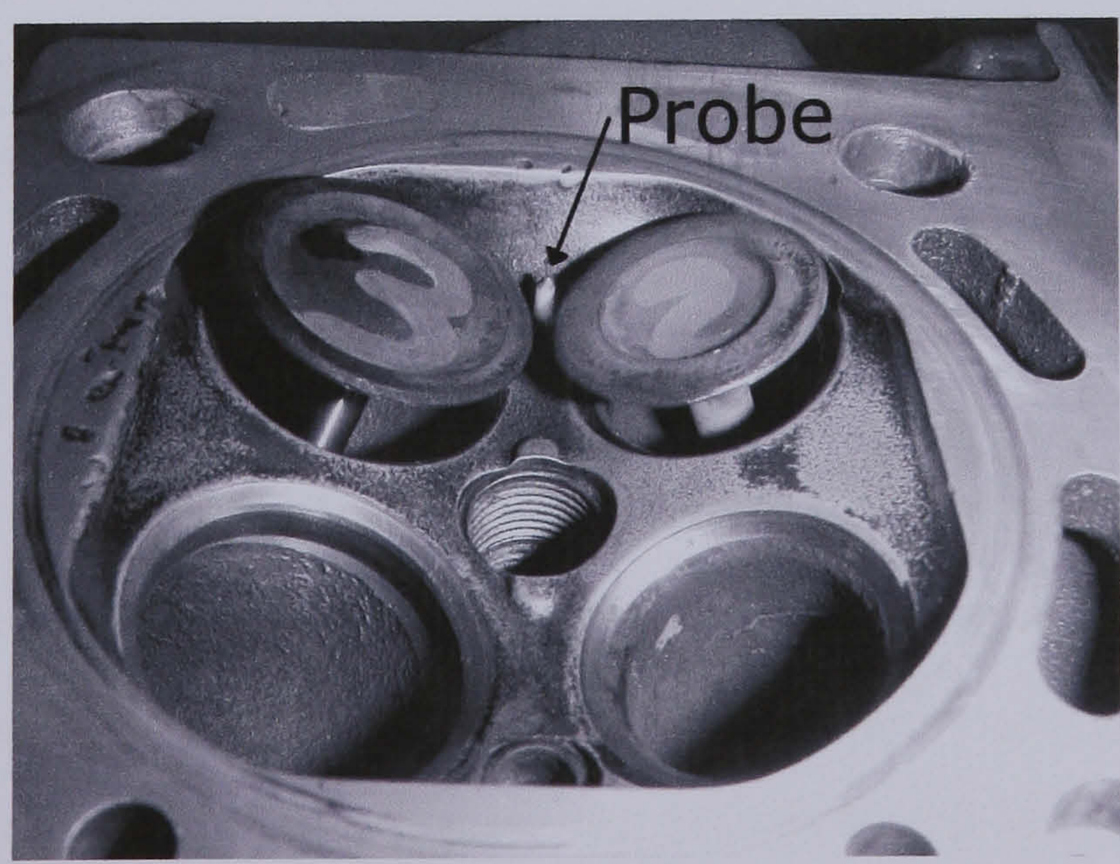

Figure 55: Photograph of cylinder head showing the location of the ionization probe.

Since the mass of positive ions, such as H3O+, is approximately 30,000 times larger than that of an electron (negative charge), the light electrons can be accelerated much more easily towards the positive electrode than the heavy ions [122], when driven by an applied electromagnetic field. The voltage polarity at the gap of sensing spark plugs was therefore selected such that the small area centre electrode was positive and the rest of the combustion chamber was negative. This coincides conveniently with the original engine polarity where the engine block is negative, earth.

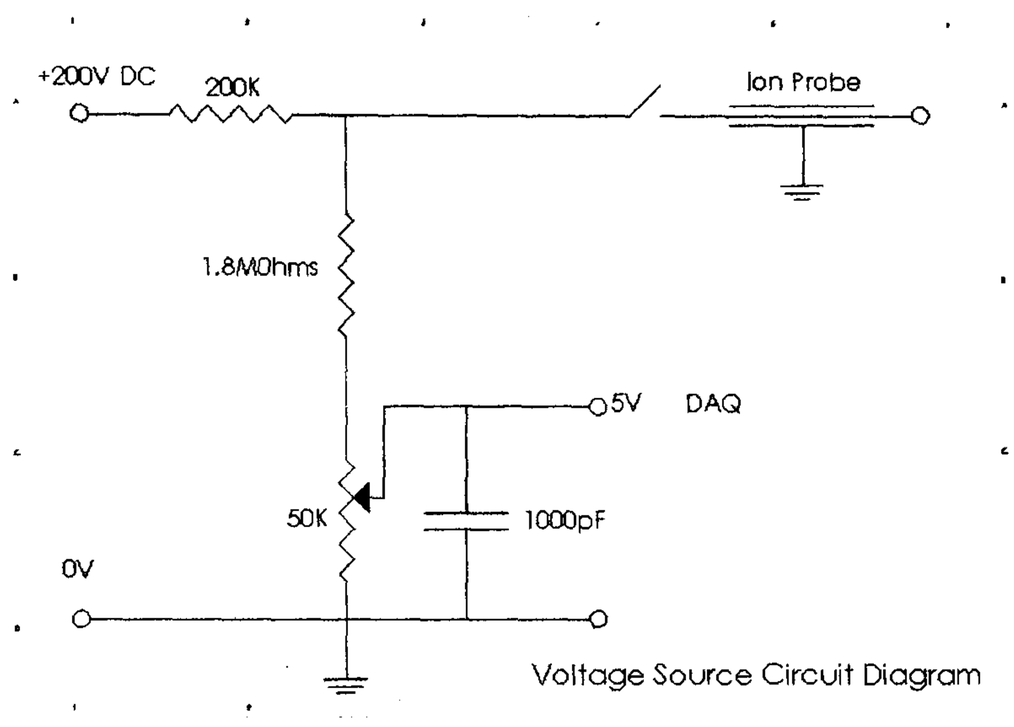

Figure 56: Voltage source circuit diagram.

A one-off DC voltage source, as shown in Figure 56, was used to power the measuring probe. The DAQ board was fed the output of the voltage divider as the ion current signal, which was inversely proportional to the sensed ion current (i.e. 5V for zero ion current and 0V for infinite) to avoid the possibility of damage caused due to excessive voltage. The signal was then inverted during the post processing phase. The RC filter that can be seen in the Voltage Source circuit has negligible effects on the signal since only frequencies below 20kHz are of interest. The sample rate for the acquisition of all signals including the pressure and the ion current signals was set to 1 sample/degCA, unless specifically stated otherwise.

4.4 Cylinder pressure signal manipulation for combustion analysis

Since in-cylinder pressure is of capital importance in understanding and analyzing the combustion mechanics, it becomes obvious that its signal needs to be trustworthy. Manipulation techniques can help in improving its quality by diminishing the effects of short and long time drift thus allowing for better cycle-to-cycle analysis. For instance, in

order to investigate the combustion parameters of a CAI gasoline engine, heat release analysis of the in-cylinder pressure time history [123] is a powerful combustion diagnostic tool. Heat release analysis[1] involves the application of the first law of thermodynamics to the cylinder contents to reveal information relating to chemical reaction rate processes occurring in the combustion chamber, whilst retaining the advantage of simplicity and hence computational efficiency. This advantage is particularly important in light of the complexity of a CAI engine. Thus, for many CAI diagnosis and control problems, it is beneficial to have information that can be derived from the cylinder pressure data directly [124], or related to cylinder pressure via another method, e.g. ion current [125]. This type of information has particular application in CAI engines for control of Trapped Residual Gas (TRG) levels, valve timing, misfire and knock detection [126].

Accurate heat release rate analysis relies on having obtained an accurate in-cylinder pressure trace, and then applying a number of assumptions to the data, such as at what point to peg an absolute value of pressure to the relative data, how much residual gas has been trapped, what is the composition and number of moles of the charge and so on. While techniques to establish these parameters have been well established for conventional SI combustion [127], they do not apply so well to CAI conditions, as the performance of one engine cycle is highly dependent on the events occurring in the previous cycle, rendering averaging techniques inadequate.

A brief analysis of techniques used in heat release rate analysis paying specific attention to calibration techniques is performed in this chapter. It was found that some opportunities for refinement could be made in relation to cylinder pressure pegging, TRG estimation, estimation of polytropic index and cycle-to-cycle analysis. These refined techniques were implemented in MATLAB and a method to analyze and evaluate the engine data is provided. A more detailed analysis can be found in [128].

4.4.1 Theory of Heat Exchange Calculation

The well known zero dimensional treatment of the gases inside the cylinder approximated as ideal gases is used.

The equation of state for an ideal gas can be written as:

[1] Heat Release Rate and Chemical Reaction Rate are considered synonyms by the author. However, the former is generally used in this Thesis, since it complies with Heywood's terminology.

$$PV = NRT \quad \text{Eq.(1)}$$

The volume of the cylinder is known as a function of Crank Angle Degrees (CAD) through the use of the crank slider with pin offset equation, which yields cylinder volume as a function of CAD:

$$V = V_C + \pi \times \frac{b^2}{4} \times \left\{ l + \frac{s}{2} - \frac{s}{2} \times \cos(\vartheta) - l \times \cos\left(\arcsin\left(\frac{\frac{s}{2} \times \sin(\vartheta) + PinOffset}{l} \right) \right) \right\} \quad \text{Eq.(2)}$$

One of the most powerful uses of equation (1) is to connect the pressure to the temperature. However, this is not always easy, as the total amount of moles in the cylinder has to be estimated first. Assuming, correct estimation of the total number of moles inside the cylinder, the first law of thermodynamics can be invoked for further analysis. The first law can be written in differential form as:

$$\frac{dQ}{d\vartheta} - \frac{PdV}{d\vartheta} = mc_V \frac{dT}{d\vartheta} \quad \text{Eq.(3)}$$

where Q stands for heat, m stands for mass and c_v stands for specific heat capacity at constant volume. The expressions are differentiated for CAD, dθ. Thus by using pre-calculated variables P, V and T, changes in energy can be tracked. The expression for dV/dθ is easy to calculate differentiating the standard equations describing cylinder volume as a function of CAD. P and m are known from experiment, although m is only correct assuming precise estimation of the cylinder gases. c_v is dependent on the species present in the gases and the temperature can be calculated by making use of the JANAF Thermochemical tables [129]. Finally, dT/dθ can be evaluated at every point since by making use of equation (1), the temperature profile is derived. The evaluated expression, dQ/dθ, represents heat flow with respect to CAD. Since these correspond almost linearly to time within each engine cycle, they can be thought of as heat flow with respect to time, in effect Joules per second i.e. Watts.

Figure 57, shows a typical pressure trace, accompanied by the relevant heat flow trace. The energy term has been labelled Heat Exchange Flow because it represents the net heat flow between the gases and the environment, including heat generated chemically from within the gases. Even though it would be tempting to assume that it represents the chemical heat release trace this is not true as it is interlinked with the energy lost to the

cylinder walls. Some further manipulation is needed in order to extract the apparent net heat release rate.

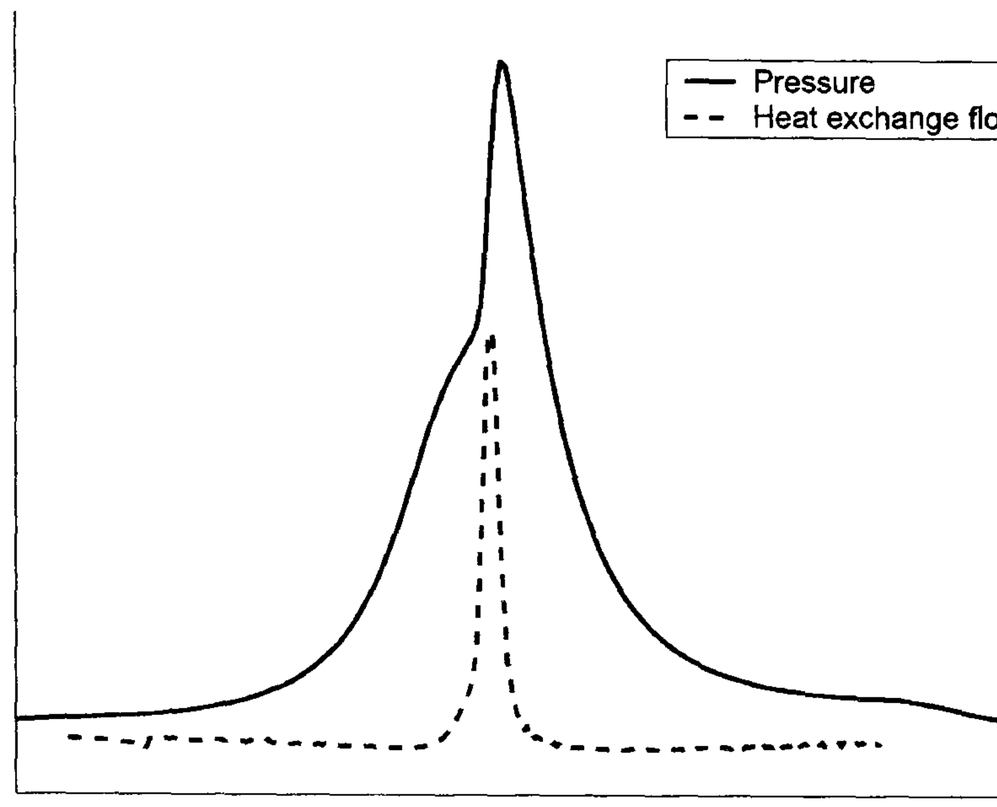

Figure 57 : Typical Pressure and Heat Exchange Flow traces.

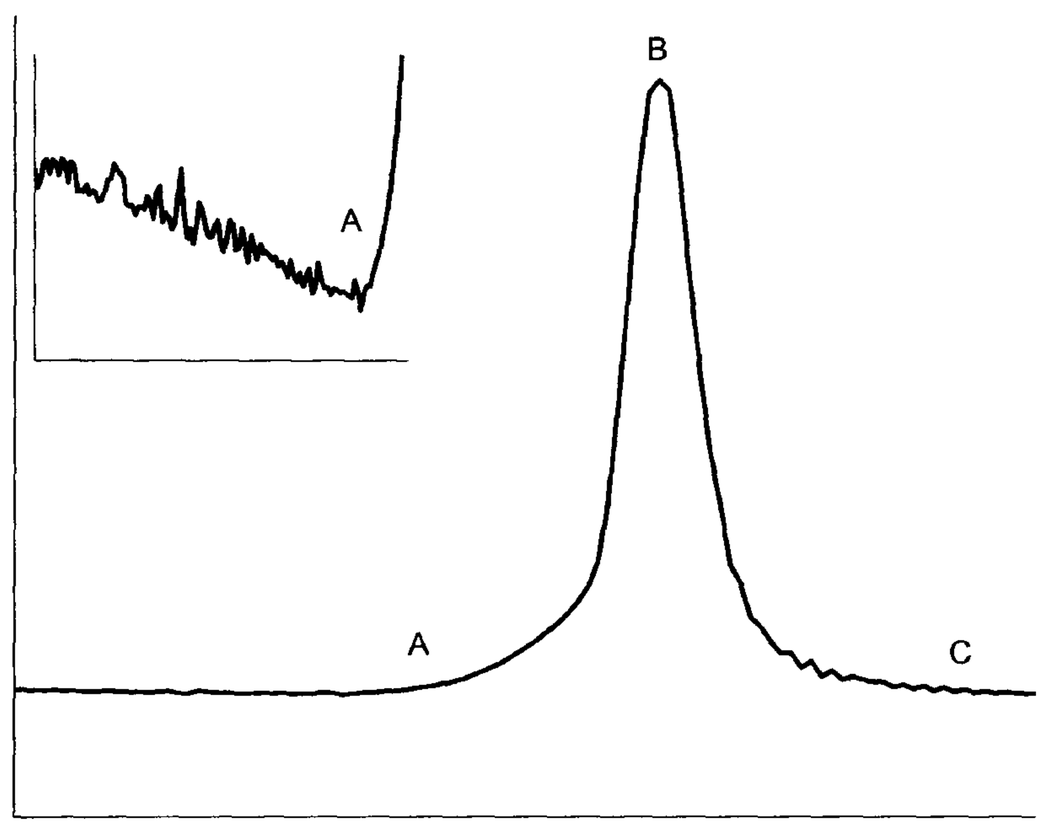

Figure 58: Breakdown of Heat Exchange Flow trace.

The analysis of the heat exchange lies in identifying points A and C as shown in Figure 58. A typical trace will strongly resemble a bell shaped curve. The important characteristics are the start and end of the bell, points A and C on the figure. These correspond to the start and end of the chemical heat release into the gases (and their subsequent chemical transformation), in other words, the limits of combustion. The curve to the left of A is not, in fact a straight line. A zoom of this area is shown in the inset of the figure. The reason the curve drops is because it indicates an increasing loss of energy to the cylinder walls as the gases temperature increases due to compression by the moving

piston. If no combustion occurs, this trend should continue as long as the temperature rises, that is, until TDC. However, any energy injection into the gases will reverse this trend. Thus, A is defined as the point where there is a turning point in this descending curve. By finding A, a very precise estimate of the start of combustion can be made [130]. Treating the curve similarly for C, the limits of combustion can be derived.

Once the limits of combustion have been established, further analysis is possible. The curve considered so far is dQ/dθ thus the area under it corresponds to energy. At any point, this new integrated curve gives the total of the heat exchanged by the gases since the start of the integration. The exchange implies also the heat injection by the chemical heat release. This is shown in Figure 59.

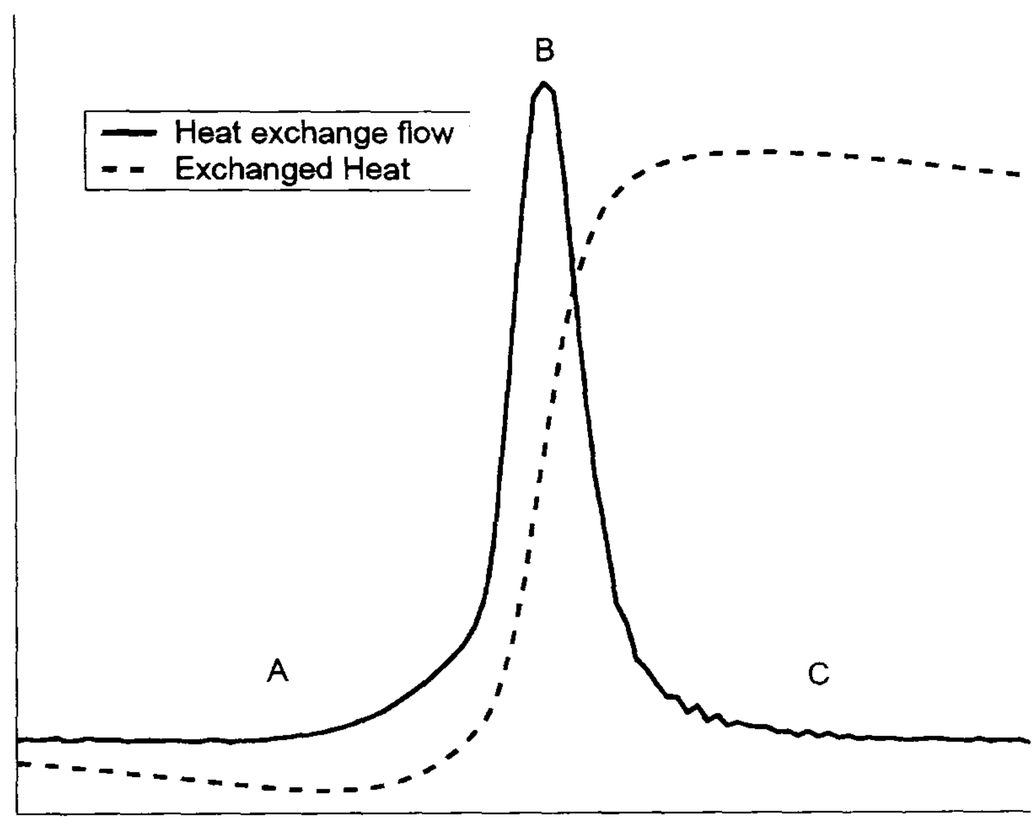

Figure 59: Heat exchange flow curve and its integral (MFB).

This heat curve is the fingerprint of combustion. If we assume that heat release and mixture species transformation are linearly related, then it follows that, scaled between 0 and 1 between the A and C points, the curve corresponds to the Mass Fraction Burnt (MFB) trace. Note also that point B is traditionally taken to be a good indication of the Location of 50% Mass Fraction Burnt (MFB50) point, where half the charge has been converted.

Extraction of the MFB curve concludes the combustion analysis of a pressure trace. By using this curve as a reference, as well as the pre-calculated curves of P, V and T, a detailed investigation of the combustion event can be performed. However, the steps outlined in this chapter are by no means straightforward when it comes to implementation. An analysis of how these were carried out in this research follows.

4.4.2 Implementation

First, a differentiation between averaged and cycle-to-cycle data should be made. In general, it is much easier to treat averaged traces, as averaging removes pressure signal noise and the presence of cyclic variation. Also, most other engine sensors are not fast enough to track changes on a cycle-to-cycle basis. Techniques that treat cycles on an individual basis need to be established, since this is necessary in a CAI engine due to each engine cycle's dependence on its previous cycle.

Three fundamental measurements are needed to give accurate results:

1. The pressure trace is tracked by the pressure transducer. The resulting trace suffers from at least two factors, base drift, which affects a single cycle as a whole and thermal shock which results in inconsistencies within a given cycle.

2. The cylinder gases are not tracked directly whilst the valves are open. The appropriate measurements in this case are the air and fuel flow, which give the average flows throughout a given data set and are hence only useable in treating the averaged pressure trace.

3. The final measurement needed for the treatment of the data is the exhaust gas temperature. Like the air and fuel flows, this is also an average measurement for a given operating condition.

Starting by analysing how the pressure signal was treated, an analysis of averaged signal cycles is given and finally a cycle-to-cycle analysis technique is described.

4.4.3 Pressure Trace Pegging

The first problem of the pressure trace is drift. This drift shifts any given cycle by an unknown, constant amount. To counter this, this amount has to be established so the cycle can be repositioned at the right values. There are two techniques for doing this, described in [131].

The first method assumes knowledge of a pressure value from an independent sensor, typically Manifold Air Pressure (MAP). Pegging then becomes a matter of matching the two signals at some appropriate position, e.g. when the inlet valve is open, while taking into account, engine speed and other effects on volumetric efficiency.

The second method uses the polytropic process equation:

$$P \cdot V^{\kappa} = C \quad \text{Eq. (4)}$$

where C is a constant, to model the theoretical pressure trace of the cylinder gases. If the exponent, κ, is known, and the measured pressure, Pm, has an unknown shift ΔP from the actual value of P, the equation becomes:

$$(P_m - \Delta P) \cdot V^{\kappa} = C \quad \text{Eq.(5)}$$

where P = Pm-ΔP. Given any two points, a system of two equations with two unknowns ΔP and C is derived.

In the more advanced form of this method, the equation is rewritten as:

$$P_m = CV^{-\kappa} + \Delta P \quad \text{Eq.(6)}$$

which can be written in matrix form as:

$$P_m = (1 \quad V^{-\kappa}) \cdot \begin{pmatrix} \Delta P \\ C \end{pmatrix} \quad \text{Eq.(7)}$$

For multiple P_m and V values, the equation is generalized as:

$$\begin{pmatrix} P_{m1} \\ \cdot \\ \cdot \\ P_{mn} \end{pmatrix} = \begin{pmatrix} 1 & V_1^{-\kappa} \\ \cdot & \cdot \\ \cdot & \cdot \\ 1 & V_n^{-\kappa} \end{pmatrix} \cdot \begin{pmatrix} \Delta P \\ C \end{pmatrix} \quad \text{Eq.(8)}$$

This form can be solved using matrix algebra to yield values for ΔP and C.

In this research, this second method has been used. Even though, MAP data was available, the presence of what is, in effect, an unknown amount of TRG, greatly complicates matters as far as volumetric efficiency is concerned.

However, the second method is not without problems of its own. The greatest issue is the choice of the exponent κ. Traditionally, this can be established by estimating the slope of the compression part of a log(P) vs. log(V) plot. However, this requires a previously pegged pressure trace so it cannot be used in this context.

Another course of action takes into account the fact that in an ideal process, κ=γ, where $\gamma = c_p/c_v$ and c_p, c_v can be calculated through use of the JANAF Thermochemical tables and knowledge of the mixture composition. Experimental data deviates from an ideal process but it gives a starting estimate which is close to the real value since the compression part

is very close to an adiabatic process. The question then to be asked is how much deviation there is between the estimated γ and the actual value of κ.

A starting value of κ=1.4 was assumed and then in order to get a more accurate value for κ, iterative methods have been used. The pressure trace is pegged with any reasonable initial value. This trace is then analyzed and values for the mass and temperature of the mixture at IVC are extracted. Using these in conjunction with the JANAF Thermochemical tables, new values can be worked out for c_p, c_v and γ. This new value of γ is then used as a polytropic exponent to peg the trace to a new value and the procedure is repeated until γ stabilizes between iterations. The values converge very fast; typically there is less than 0.004% difference between successive values after only 5 iterations.

4.4.3.1 Averaged Signal TRG Estimation

An application of equation (1) at EVC yields a value for the moles of TRG. Assuming no significant blowby losses during the compression/expansion of TRG, this is the amount of TRG that will be present in the following cycle's combustion stroke. Since we are looking at an averaged trace for steady-state operating conditions, this is one and the same. So, all that is needed is to add to it the amount of charge induced in one cycle (calculated through knowledge of the average intake flows and the engine speed) and the total number of moles and composition of the mixture can then be approximated.

In practice, this number of moles for the mixture yields an unrealistic value for the temperature of the mixture at IVC, as calculated through Equation(1). Certain data sets return a higher value for the temperature of the total mixture at IVC than the temperature of TRG at Inlet Valve Opening time (IVO), which is impossible since a hot gas (TRG) is being mixed with a colder gas (charge). The problem could have been simply erroneous pegging, resulting in a wrong value for TRG amount. However, shifting of the whole curve does not return realistic values at any point. On the other hand, adding negative numbers very quickly leads to negative values during the induction where the pressure is lowest.

The other very suspicious value is the exhaust gas temperature which is assumed to equal the gases temperature at EVC. However, changes to it result in different scaling of the problem but not in its resolution. Thus, a different source of error has to be identified in order for physically meaningful results to be obtained.

4.4.3.2 Evidence of Pressure Trace Imbalance

The problem potentially lies with the response of the pressure transducer to thermal shock. The specifications of the non water cooled transducer used in this research, as mentioned before, allow for a possible -10% error in Indicated Mean Effective Pressure (IMEP) estimation on an SI engine. Furthermore, CAI combustion places a greater strain on the transducer due to the increased rate of pressure rise.

Rai et al [132] mention that cyclic exposure of a piezoelectric pressure transducer to combustion results in the expansion and contraction of its diaphragm due to large temperature variations throughout the cycle. The same paper also states that this causes the force on the quartz crystal to be different to that applied by the cylinder pressure alone and that thermal shock affects all parameters derived from pressure data, but the greatest is IMEP which can be affected more than -10%. Thermal shock was found to be more significant at advanced ignition timings. Rai et al [132] derived an equation to compensate for thermal shock of a Kistler 6125A transducer used on a Ford Zetec engine. This equation is:

$$IMEP_{corr} = IMEP_{meas} + (F \cdot P_{\max}) + Offset \quad \text{Eq.(9)}$$

Where F and Offset are a function of engine speed only. Although this equation cannot be used here directly, since it was tuned for a different engine, what is more important is that the compensation factor derived is only a factor of engine speed and maximum pressure. The greater the maximum pressure and the engine speed, the greater the correction needed. It follows that CAI combustion, with its greater peak in-cylinder pressures, has a greater effect on the IMEP measured by the sensor.

Further evidence in support of this scenario surfaces when investigating unstable combustion. In these cases, a misfiring cycle will produce exhaust gases partly made up of its unburnt charge. When these are recompressed, during the TRG compression phase, they can sometimes ignite. This ignition leads to an underestimation of the descending side of the curve. It is easier to appreciate this in the IVO region because the pressure values are expected to be in the region of 1 bar as is demonstrated in Figure 60.

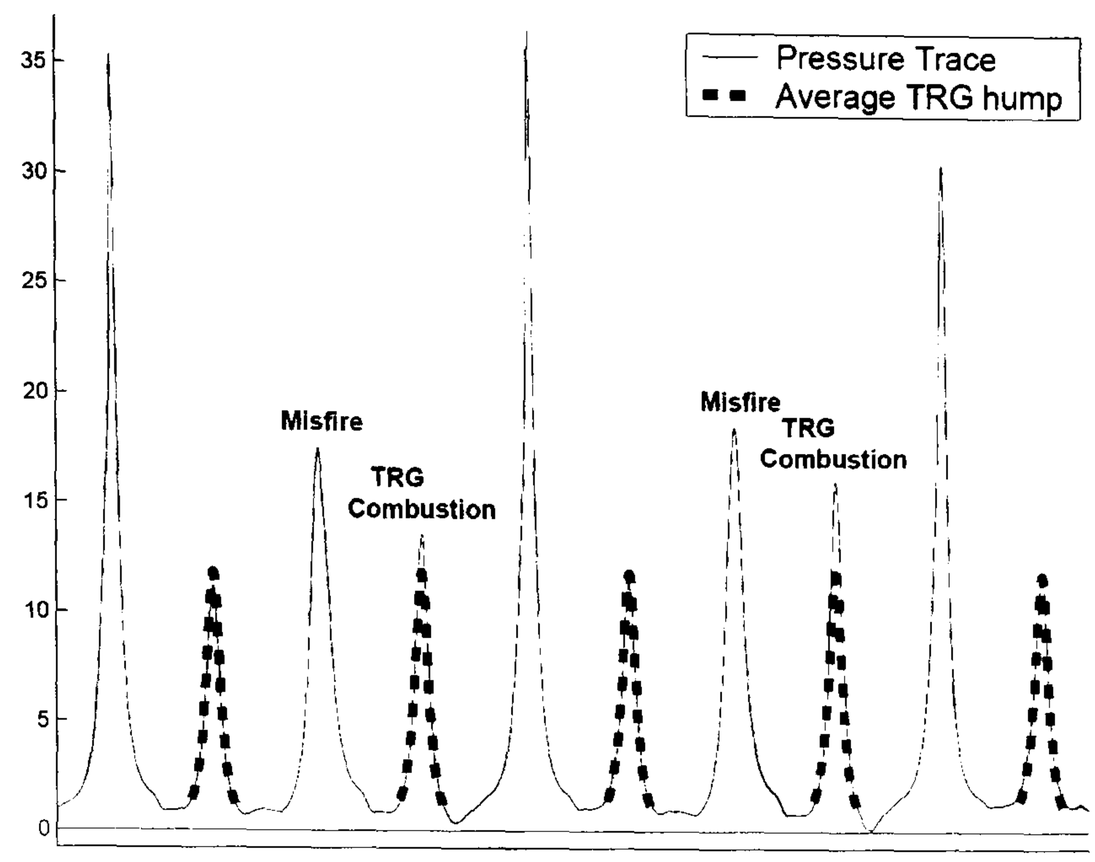

Figure 60: Thermal shock evidence following TRG combustion.

In this figure, the second and fourth cycles misfire. Their respective TRG compression humps are noticeably larger than the average (shown as a thick, dashed line). It is clearly visible that the lowest points of their IVO regions are unrealistically lower than their neighbours, in the case of the fourth cycle almost reaching a pressure of zero.

4.4.3.3 TRG Estimation via Corrected Pressure Trace

The evidence in favour of a measuring imbalance between the `hot' and `cold' parts of a cycle seems convincing. In order to do this, some further equations have to be considered. What happens during the induction is that the hot exhaust gases in the TRG mix with the cold charge.

Assuming negligible heat losses during this process, the sum of the energies of each must equal the energy of the total mixture at IVC, i.e.:

$$(m_{trg} + m_{ch}) \cdot C_{vmixt(Tmixt)} \cdot T_{mixt} = m_{trg} \cdot c_{vtrg(Ttrg)} \cdot T_{trg} + m_{ch} \cdot C_{vch(Tch)} \cdot T_{ch} \quad \text{Eq.(10)}$$

which is a conservation of internal energy equation between charge, TRG and their mixture. m_{trg} and m_{ch} are the masses of TRG and charge respectively. T_{mixt}, T_{trg} and T_{ch} are the temperatures of mixture, TRG and charge respectively. Finally, $c_{vmixt(Tmixt)}$, $c_{vtrg(T_{trg})}$ and $c_{vch(T_{ch})}$ are the specific heats of mixture, TRG and charge at their respective temperatures.

In addition to the above, equation (1) for the case of the total mixture at IVC becomes:

$$P_{ivc} \cdot V_{ivc} = (N_{trg} + N_{ch}) \cdot R \cdot T_{mixt} \quad \text{Eq.(11)}$$

In both equations (10) and (11), there are two unknowns, the amount of TRG, mentioned as mass in equation (10) and moles in equation (11) and the final temperature of the total mixture. Mass and moles are equally valid descriptions as they are connected through a constant, the molecular weight so that mass = moles x molecular weight, which is known for a known composition.

Also, `unknown' is the specific heat of the total mixture (since it is at an unknown temperature). However, specific heat changes slightly with temperature and it can initially be taken as a constant until iterative methods yield a precise value.

The value of the TRG temperature is only dependent on the pressure values and not the moles of TRG as can be deduced from the equation of state. Hence, by estimating specific heat values for the TRG, which has a known composition, and the charge, an initial estimate for the specific heat of the mixture can be made by taking an average. The composition of the TRG is calculated through applying the equations for species' transformation, found in Heywood [33], to the charge, whose composition is known through measurement of the fuel and air flows. Plugging these values into equations (10) and (11) yields values for both the amount of TRG and the total mixture temperature. Recalculating the specific heat of the mixture based on the new temperature value yields more accurate values and so on until all terms in the equation balance.

What has been described above is in effect a statement that reads: calculate the amount of TRG at known temperature that, when mixed with a known amount of charge at a known temperature, will yield a mixture at an unknown temperature, occupying volume V_{ivc} at a pressure P_{ivc}.

However, there is also the initial method of estimation of TRG, based on the equation of state. These two methods should yield the same results. Unsurprisingly, they don't, which is where the pressure trace imbalance comes into play.

Hence, the first step in the analysis is one outer iteration whose aim it is to establish the shift of the `hot' and `cold' regions of the pressure trace. The aim of this iteration is to establish a positioning of the `hot' region that yields a TRG amount and temperature at IVO that agrees with that predicted through the mixing method.

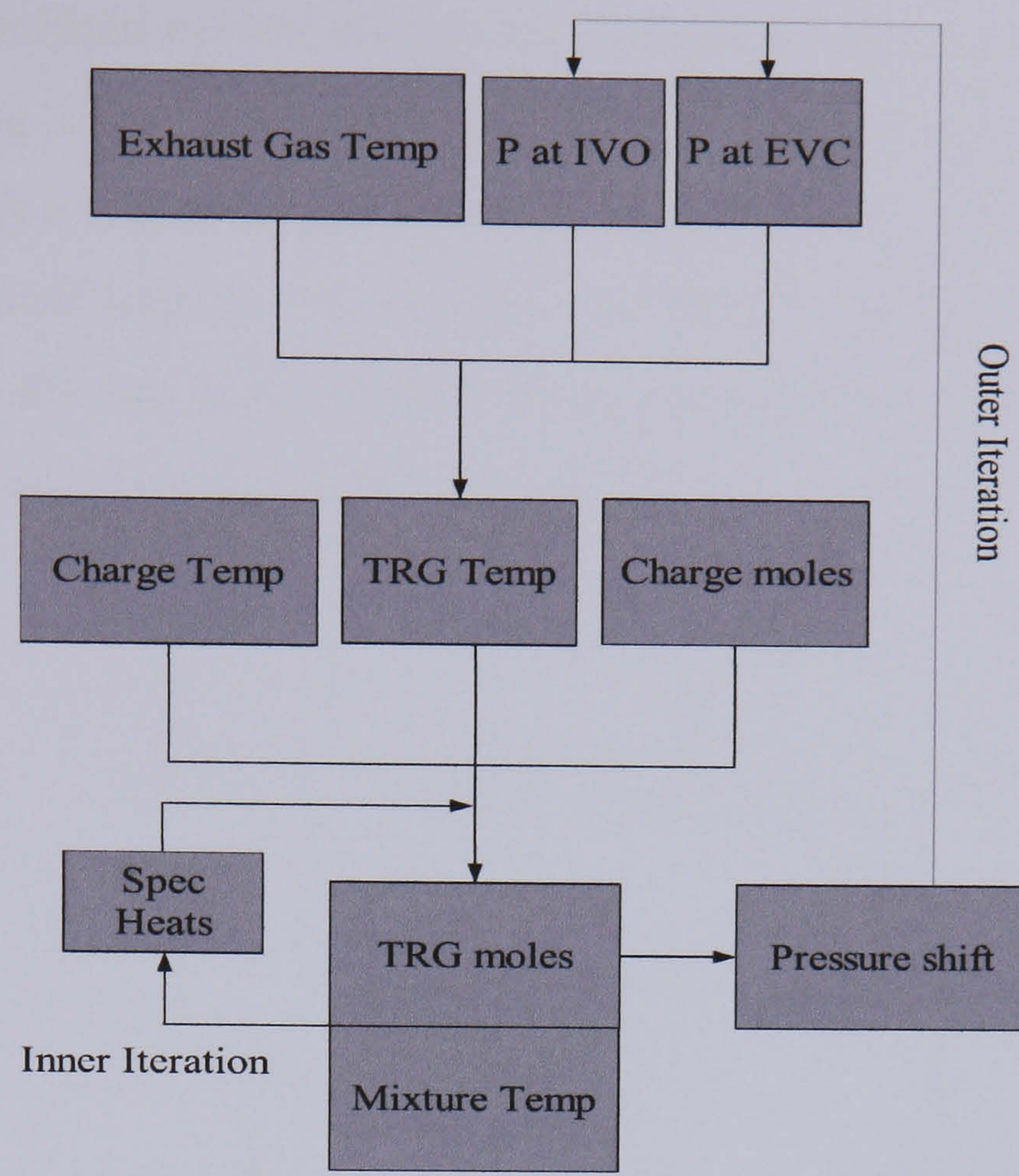

Figure 61: TRG, Mixture Temperature and Pressure Shift calculation process.

Once both these iterative methods have been executed, the values for both TRG amount and hot-cold trace shift are established. The schematic in Figure 61 sums up the procedure.

All the procedures described so far only apply to averaged traces. This is because it is only for these that the vital information supplied by the intake flows and exhaust gas temperature apply. Before treating cycles on an individual basis, as will be discussed in the following section, the averaged trace for the data set in question must be treated.

4.4.4 Cycle-to-Cycle Analysis

Once the combustion analysis for the averaged trace has been carried out, cycle-to-cycle analysis can be performed. This is because those variables which are only valid on average can be reasonably replaced by the results of the averaged trace analysis. To be more specific, the charge moles and exhaust temperature will be close, but not exactly those used during the averaged signal analysis. In the case of unstable combustion, where misfires and other extreme phenomena are common, these can vary greatly. In this section, the procedure used for extending the analysis to individual cycles will be explained.

Given a trace of multiple cycles, each cycle is treated individually, yet 'inherits" data from the preceding cycle, namely TRG amount and temperature. This has been implemented in such a way as to safeguard against cumulative errors leading to runaway results as is described later in this section. The first cycle "inherits" the data of the averaged cycle as a starting point. In the following text, we will consider the treatment of a random cycle, graphically represented in Figure 62.

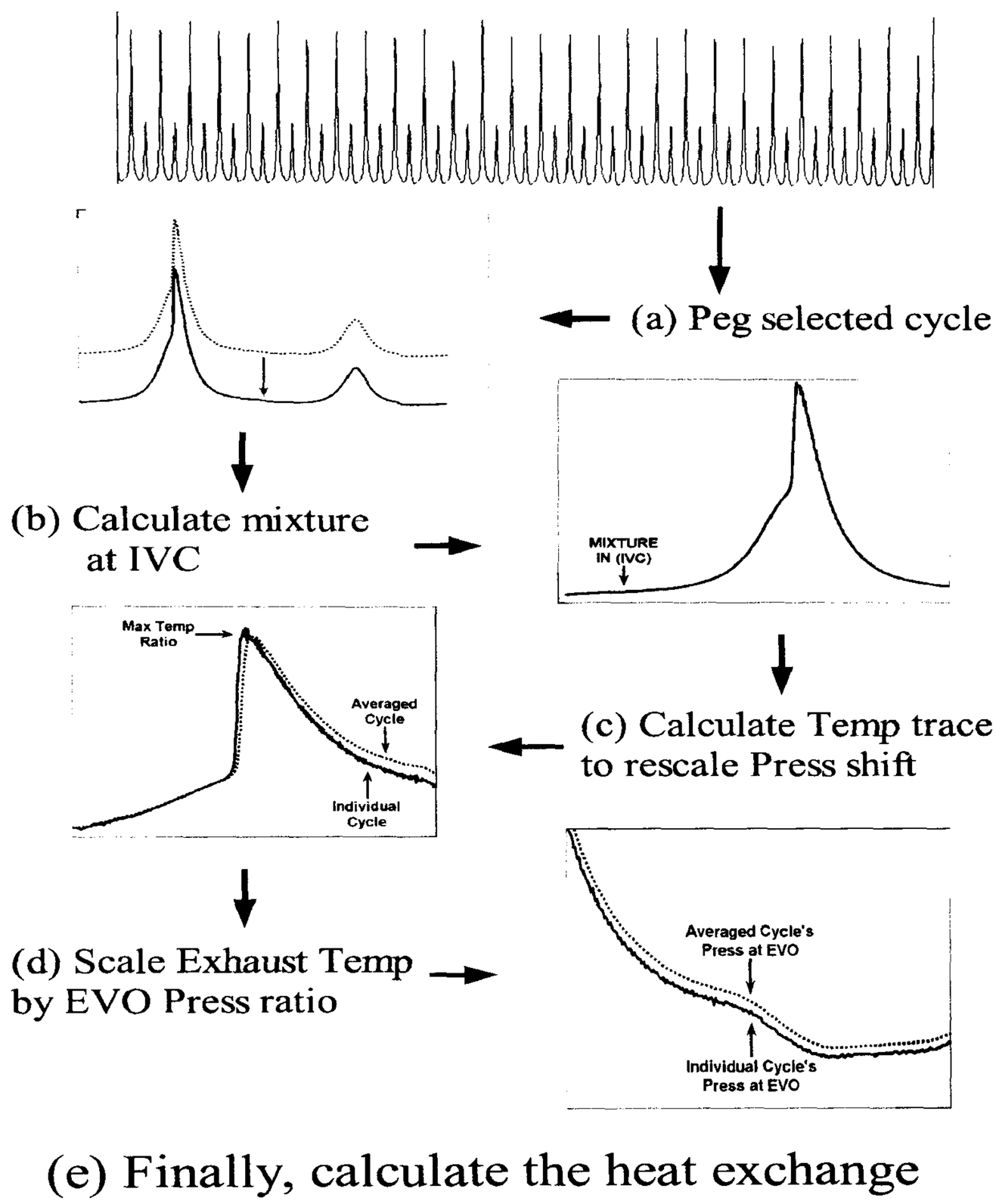

Figure 62: Treatment of individual cycles for cycle-per-cycle calculations.

First, the cycle is pegged, using the value of κ estimated for the averaged cycle for the given data set (Figure 62 (a)). Once the cycle is pegged, the pressure at IVC is known. This, in conjunction with the amount and temperature of TRG passed from the preceding cycle, the temperature and composition of the charge and the volume at IVC, yield the final amount of charge-TRG mixture at IVC.

The pegged pressure trace is still not treated for the hot-cold shift. The shift calculated in the averaged case has been applied as a step change in the region between 20 CAD after TDC and IVO. Since there is no way of estimating how much this shift varies between cycles, a simple technique has been employed. Given that the pressure and volume traces

are known for the individual and averaged cycles, and the total number of moles has been calculated at IVC, a temperature trace can also be worked out for the individual cycle through equation (1). Assuming that the shift is affected mostly by temperature, the shift of the averaged signal is then scaled by the ratio of the maximum temperatures of the two traces before being applied to the individual trace (Figure 62(c)).

One more variable that varies between cycles but whose value can't be directly measured is the exhaust gas temperature. From equation (1), it follows that it is equal to PV/NR. Since V at the valve events during fixed operating conditions is constant and R is also constant, the variation in this can be tracked by the P/N fraction.

However, using the number of moles of mixture, N_{mixt}, into the exhaust temperature calculation, introduces a variable that is inherited directly across cycles. That is, a value which is only known for the averaged cycle must be used for the calculation of N_{mixt} of the first cycle at IVC to the n_{th} cycle. This will lead to runaway results. Thus, the variation in exhaust gas temperature is being scaled by the fraction of pressures only (averaged and individual) at EVC. Pressure is known for every cycle and so no inheritance associated problems exist.

The operations described above yield all the variables needed to convert any given cycle to one treatable as per the average cycle treatment. Knowledge of the number of moles in the closed valve regions, IVC to EVO and EVC to IVO, also allows the calculation of the heat exchange.

4.4.5 Post-Processing Utilization

After analyzing the data as described, a wealth of information presents itself for further investigation. Here focus will be given to two basic categories of results. These correspond to the two major procedures described. The first, corresponding to the treatment of the averaged trace, concerns the calculation of TRG. The second, corresponding to the cycle-to-cycle analysis, exhibits how the cycle's variables can be "read" to build an understanding of CAI combustion dynamics.

4.4.5.1 TRG Representation

Before proceeding, it is worth explaining in more detail the concept of molar TRG estimation. Often, TRG is quoted as a ratio of volume at EVC to total cylinder volume.

This is a good tool for easy classification of data points but fails to take into account the effects of the engine's operating conditions on gas dynamics.

On the contrary, by calculating the amounts of gases present, the ratios of moles or masses can be quoted. In this research, moles rather than masses have been used because, when dealing with gases at the same temperature and pressure, moles directly relate to volumes. Hence, quoting a number for molar TRG of a homogeneous mixture, effectively gives the volume ratio of the gases. This is comparable to the classic "volumetric" method mentioned above, with the added bonus that this number reflects a more accurate ratio of gases, implicitly taking the effects of gas dynamics into account. The obvious drawback is that, in order to calculate it, one has to carry out the procedures described in this chapter.

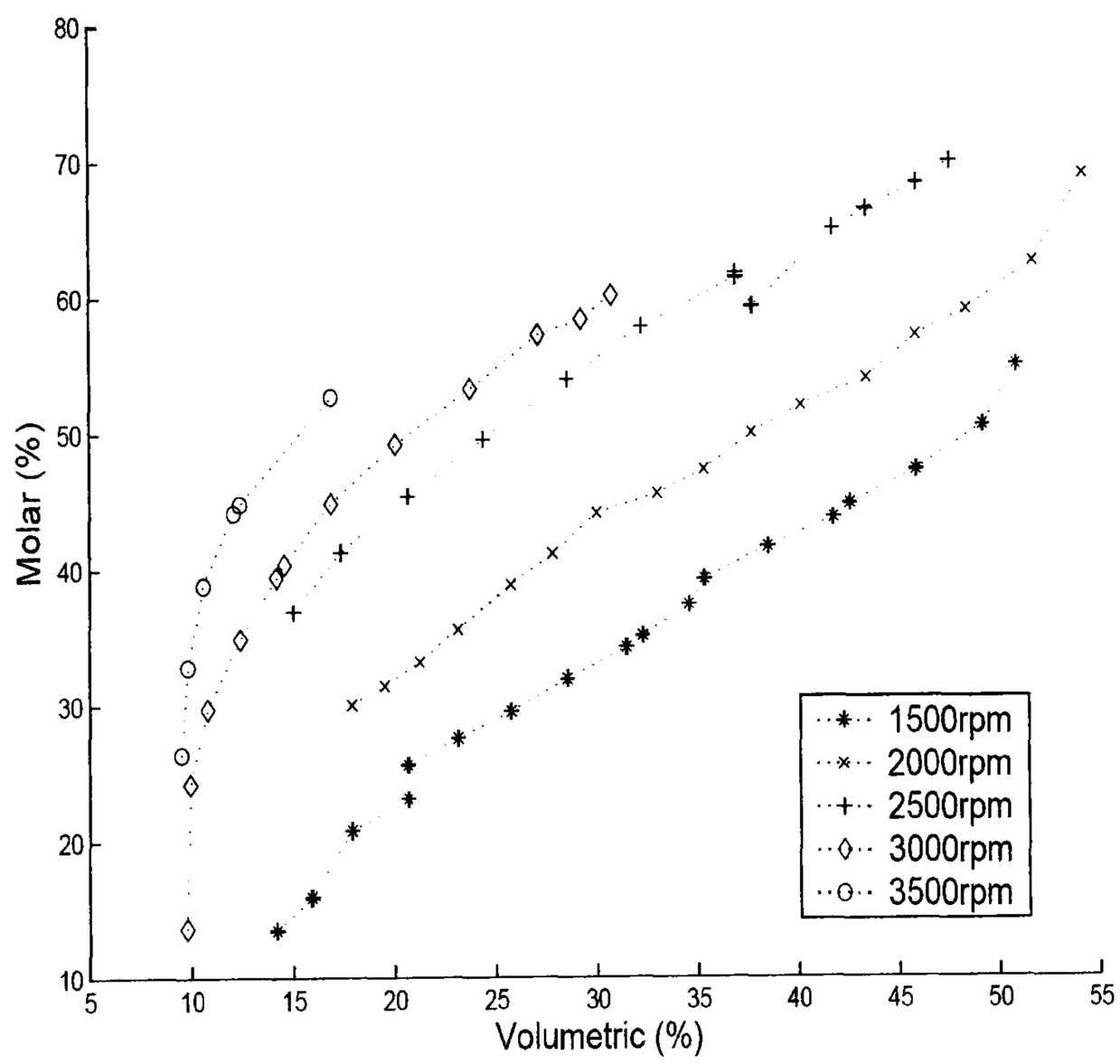

Figure 63: Comparison between TRG measuring methods.

Figure 63 highlights the relation between the two. It is noticeable that, in general, molar TRG is higher than volumetric. This is because the exhaust gases present at EVC are always at a pressure higher than that of the inlet (due to both exhaust back pressure being higher than inlet pressure and the low valve lift of 2.5mm employed in the logging of some of the data). Hence, when the remaining volume fills up with fresh charge with the whole cylinder equating with the inlet pressure, the TRG takes up more volume than it did at EVC. The effect gets more noticeable with increasing RPM.

These results can be calculated from an averaged pressure trace with knowledge of inlet flows and exhaust gas temperature without any need to go into a detailed combustion analysis.

4.4.5.2 In Depth Cycle-to-Cycle Investigation

The full power of the analysis becomes apparent when looking at cycle-to-cycle results. Figure 64 displays cycles from the same region as Figure 60. In order to understand the flow of events, information on the following variables is very useful:

1. Moles of charge
2. Moles of TRG
3. Moles of total mixture
4. TRG temperature (at IVO)
5. Exhaust gas temperature (at EVO)
6. Start of Combustion
7. Duration of Combustion

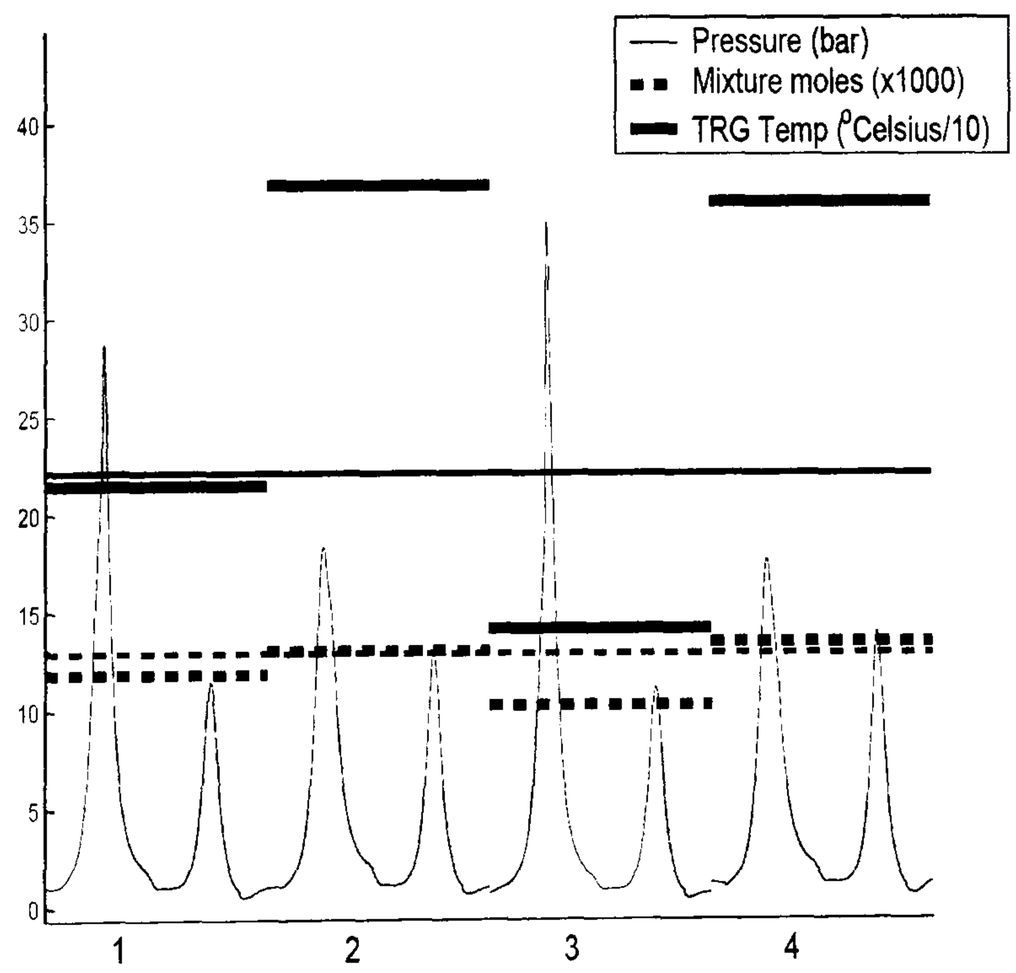

Figure 64: Cycle-to-cycle analysis of unstable combustion.

In order not to overly clutter the figure, only parameters 3 and 4 are displayed. The data set is from unstable combustion at high TRG values (50% volumetric, 55% molar), at 1500 rpm, ITA=34. The values of the moles of total mixture and TRG temperature are displayed as thick bars of different styles over the regions of their respective pressure traces. The thinner bars in the same style mark their respective mean values for the whole

data set and act as reference. The addition of standard deviation bars would lead to cluttering problems so these have been omitted as well. It should, therefore, be noted that the temperature variation on the Y axis is much larger than that of the moles of total mixture.

The average moles are presented with a continuous thin dashed bar and the average temperature is presented with a continuous thin solid bar. Starting with the leftmost cycle, it can be seen that it is slightly less energetic than average, having started with a little lower number of mixture moles (thick dashed bar). It is followed by a normal TRG compression hump, at the end of which, TRG has a temperature very slightly lower than average (thick solid bar).

The slightly low TRG temperature of the first cycle, leads to a good intake at the start of the second cycle (as the fresh charge is not heated too much), ending up with a total mixture just above average. The cycle then misfires, as can be seen by the low peak pressure of this cycle. The misfire leads to TRG, which is rich in unburnt charge, being compressed during the second hump of the cycle. This second compression ignites the unburnt charge, leading to a high peak pressure for the second hump and a TRG temperature far above average.

This very hot TRG now mixes with fresh charge at the start of the third cycle. Due to the high temperature heating up and expanding the incoming charge, the moles of total mixture end up very low. The cycle ignites relatively early, hence the high peak pressure. Then due to the early ignition leading to increased heat losses and low initial charge, bringing in less chemical energy, the final TRG temperature is very low.

This TRG at low temperature mixes with fresh charge in the final cycle, leading to the highest value of total mixture of these four cycles. The cycle then also misfires and ignites during the TRG compression as can be seen from the high peak pressure and TRG temperature.

4.4.6 Conclusion

In this chapter an exploration of techniques of post processing pressure data in order to gain a deeper understanding of events on a cycle-to-cycle basis was performed. The focus was on CAI combustion, which poses certain demands not normally associated with SI

operation. However, the same techniques in a simplified form (no need for TRG estimation, thermal shock not as important an issue) could be adapted for SI data analysis.

The drive for devising such an analysis has been the nature of CAI combustion. Because of the interlinking between cycles, a close look at the conditions dominating each individual cycle is a valuable tool in order to obtain an understanding of how and why certain behaviours are observed. This information cannot always be supplied directly by present-day sensors and must thus be calculated in as computationally efficient a way as possible. By carrying out the presented analysis the following are derived:

1. polytropic of compression
2. pressure trace pegging
3. pressure trace shift between hot and cold region
4. TRG and charge composition
5. temperature trace
6. heat exchange trace
7. MFB trace

Items 4 to 7 are available on a cycle to cycle basis. This information is particularly useful in investigating the behaviour of CAI combustion.

Hereafter all results presented employ this analysis method. Use of the tools described in this chapter will be shown, later in this thesis to be helpful in investigating the feasibility of predicting the behaviour of a cycle in advance. This, potentially, opens the way to sophisticated control algorithms for real time implementation.

5. Experimental Investigation of general CAI performance

5.1 Emissions and Fuel Consumption

In the effort to control the engine the valve timing will be altered almost constantly in a real life automotive application. A basic understanding on the cause and effect between valve timing and emissions should be gained before the control strategy can be decided upon. In this chapter emissions and brake specific fuel consumption (BSFC) data collected during steady state operation at varying amounts of TRG are presented. Data for both valve strategies are shown. In addition, data from an AFR loop and an injection timing loop whilst under the first strategy (constant IVC – EVO) and second strategy (constant duration) respectively are shown and analyzed.

In Figure 65 data collected under the constant IVC – EVO valve strategy at various TRG levels can be seen. The engine was operating at 2000rpm, which is a speed that permits a wide range of TRGs to be used on this engine. With this valve strategy it was possible to reach levels of up to 74% TRG. The engine load was kept constant using throttling at low TRG and the mixture was stoichiometric.

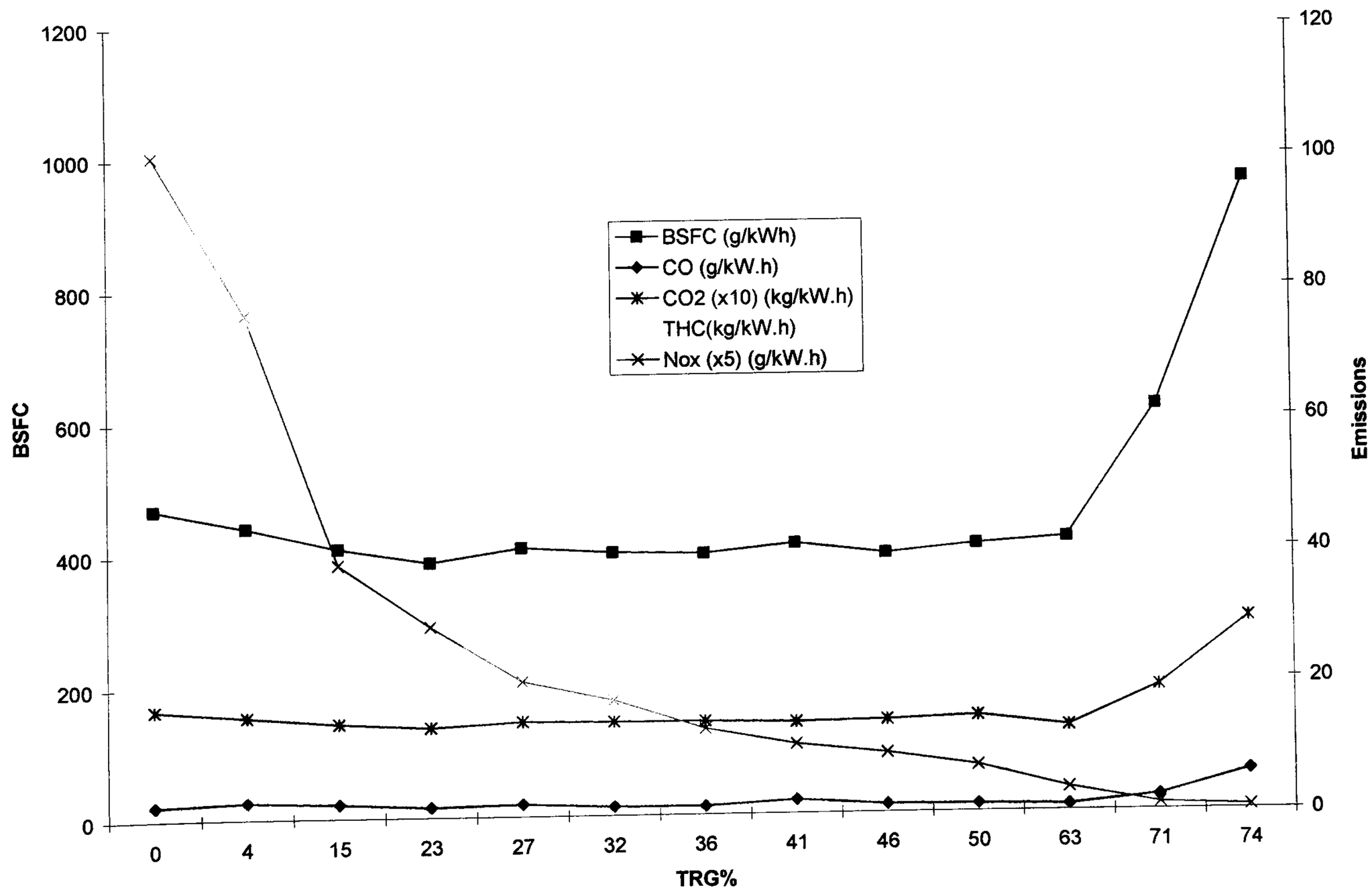

Figure 65: Specific Emissions and BSFC (TRG loop, 2000 rpm, λ=1, constant IVC – EVO).

The behaviour, as expected, is very similar to the one described by other researchers in the literature review. NOx levels diminish considerably as TRG is increased owing to the lower combustion temperatures. CO_2 also reduces with this reduction being reflected in the BSFC as well with an up to 18% BSFC improvement. It has to be noted that up to 7% of this can be attributed to the reduced pumping losses due to the unthrottled operation made possible through TRG use. CO and THC remain almost constant (in fact THC slightly reduces – in contrast to what is usually experienced) up to 63% TRG, but of course increase, along with a major increase in BSFC, after that point. This can be attributed to the very low combustion temperatures experienced at such high TRG levels, with the fuel (chemical) conversion efficiency dropping rapidly.

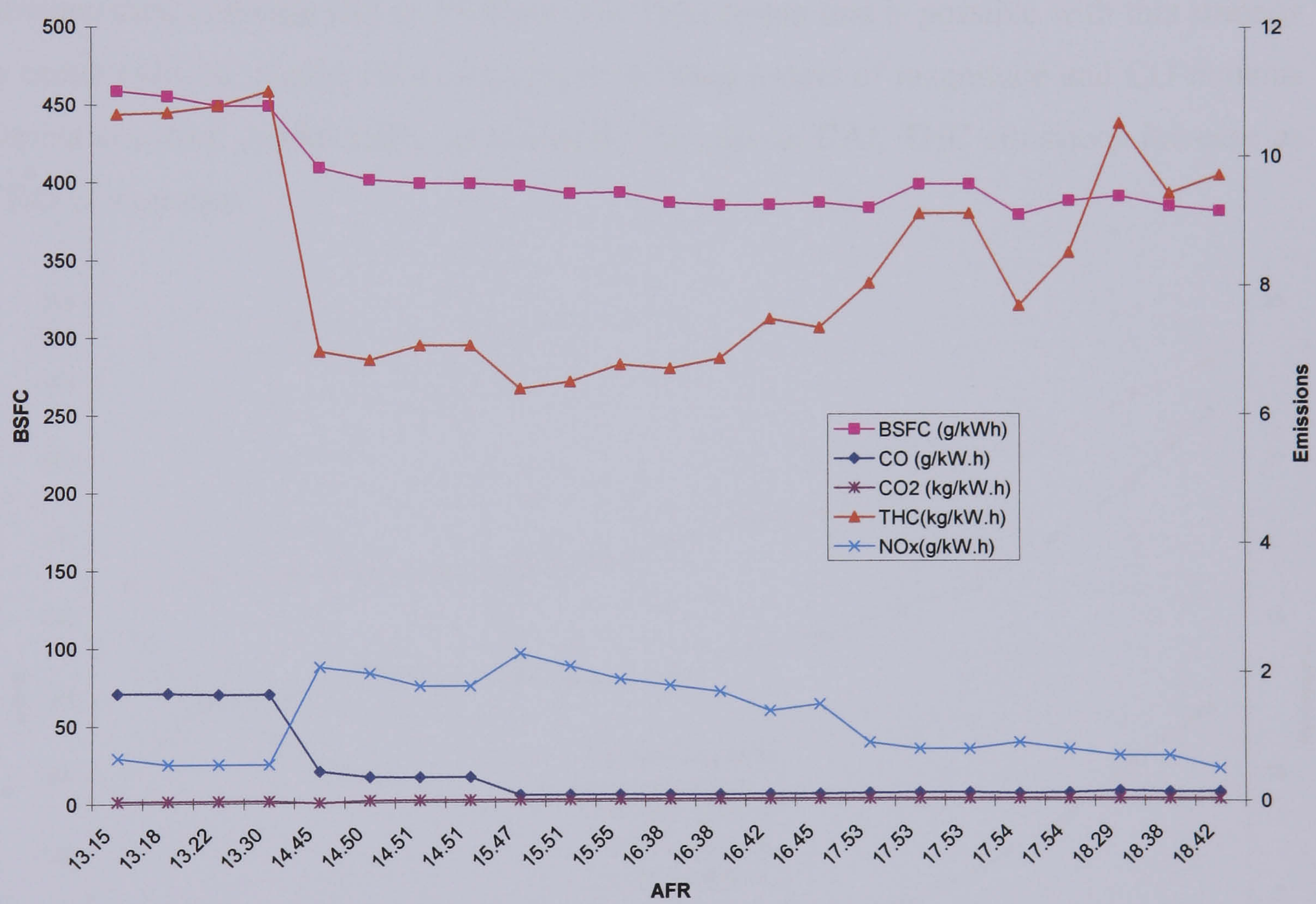

Figure 66: Specific Emissions and BSFC (AFR loop, 2000rpm, 41%TRG, constant IVC – EVO).

In Figure 66 the results of an unthrottled AFR loop at 41% TRG can be seen. BSFC is seen to reduce as the mixture is leaned out. This percentage was chosen since it is at midway TRG, under this strategy, thus making it a representative example. Evidently, operation under very lean mixtures is more unstable, at standard compression ratios, and this is reflected in an increase in THC. Apparent is also the decrease in NOx as the mixture moves away from stoichiometric, in either direction, due to the reduced in-

cylinder temperatures. At 41% TRG slightly lean mixtures do not succeed in increasing combustion temperature, as would be the case in SI operation. CO, as expected, increases as the mixture is richened up and no available oxygen for complete oxidation is left.

Moving on to the constant duration valve strategy, the corresponding data can be seen in Figure 67. Again, a TRG loop is performed, this time unthrottled, so IMEP is not constant. The speed is, as before, 2000rpm and the mixture is stoichiometric. BSFC can be seen to increase, mainly because BMEP drops as TRG is increased. This is because, in this second valve strategy the effective compression ratio is decreased as the valves move to increase the TRG amount, resulting in reduced thermodynamic and chemical conversion efficiency. CO_2 emissions also increase as a result of this. Furthermore, it is obvious that, although still at 2000rpm, the TRG sweep that is possible with this strategy is much reduced. Again, NOx is reduced by many orders of magnitude and CO remains almost constant. Additionally, as is usually the case in CAI, THC emissions increase as TRG is increased.

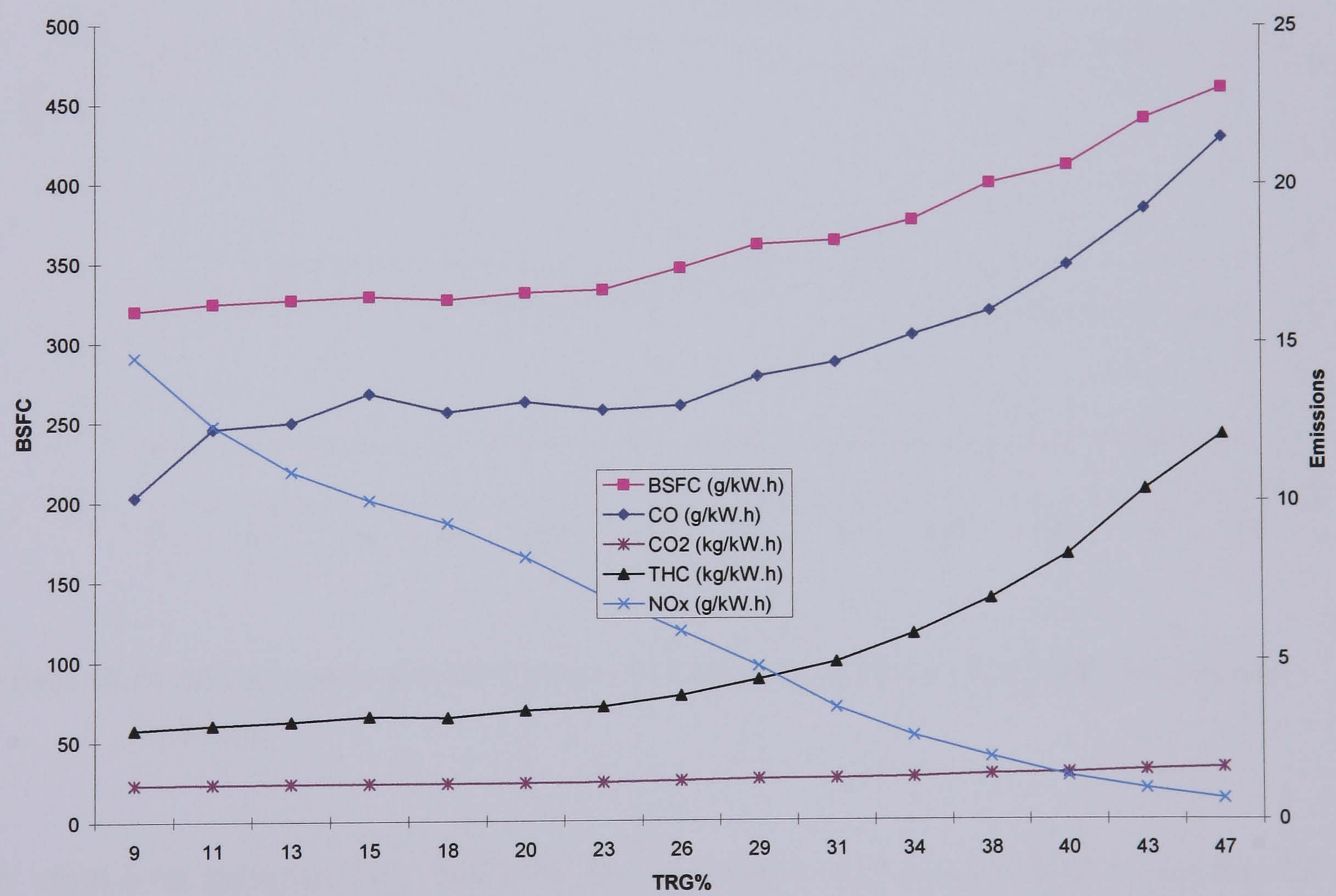

Figure 67: Specific Emissions and BSFC (TRG loop, 2000 rpm, λ=1, constant duration).

It is worth considering here, that keeping the effective compression ratio high or, even better, increasing it as TRG is increased, might keep THC emissions low, although a

slight penalty in NOx production might be paid. Also, injection timing might prove of some importance here, by altering the initial fresh charge temperature.

Another variable that can be altered to manage CAI combustion is port fuel injection timing. To examine the possible effects of this on emissions and BSFC, a test was performed at 2250rpm with the TRG level set to 22% and the mixture being stoichiometric. The injection timing was swept around the 4 stroke cycle. As can be seen in Figure 68 the most interesting behaviour is exhibited around 360 CAD (360 translates to NVO period TDC).

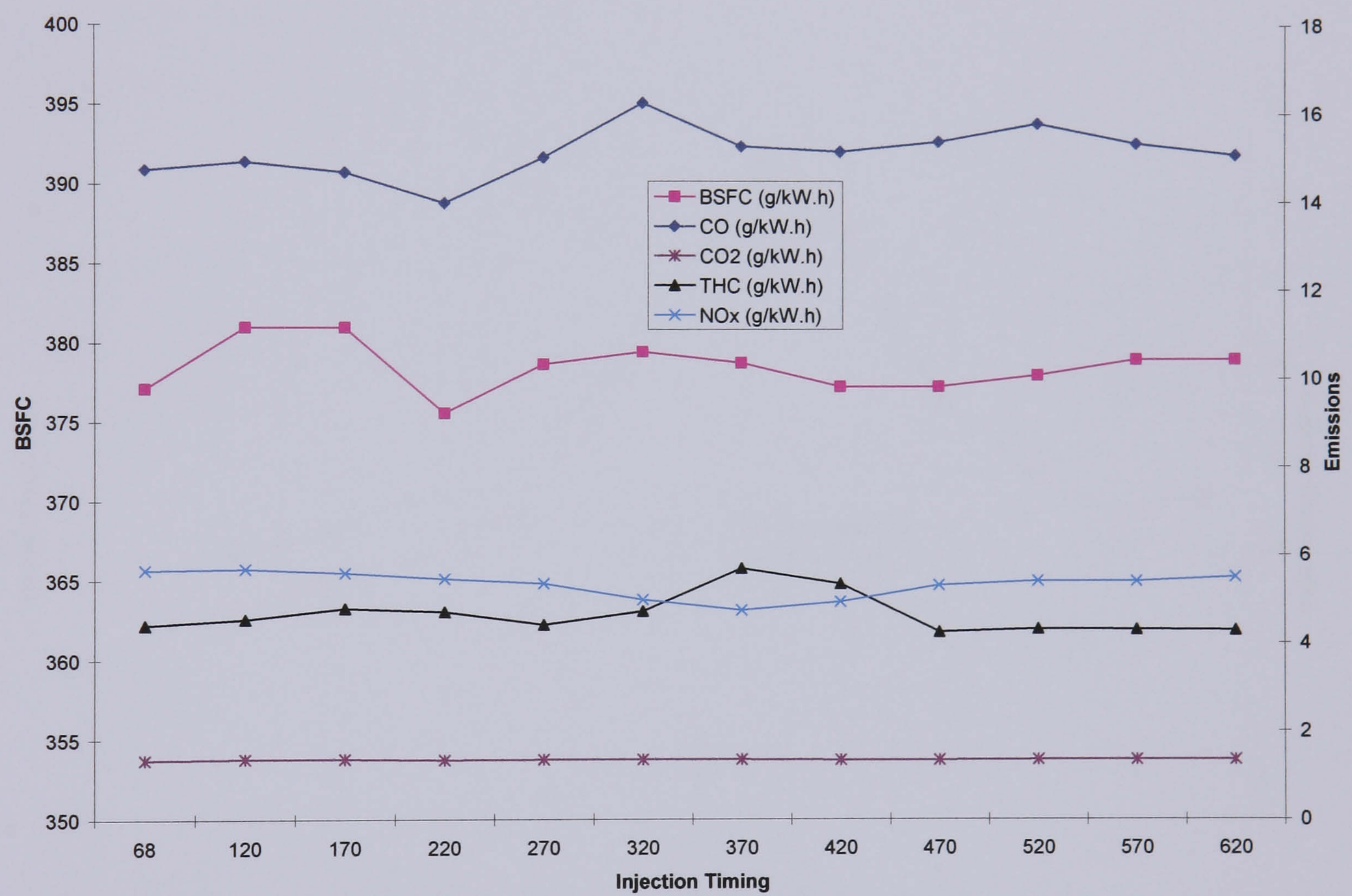

Figure 68: Specific Emissions and BSFC (Injection timing loop, 2250 rpm, 22% TRG, λ=1, constant duration).

A cross over between THC and NOx is experienced at that point. This is because the injection timing is coming close to the inlet valve open period. Bearing in mind that the injection event itself has a pulse width of over 100 CAD and IVO is at 473 CAD, the injector is spraying some amount of fuel directly into the cylinder from 373 CAD to 473. The THC start to increase and NOx starts to decrease at an injection timing around 300 CAD. This is because as less and less time is left for the fuel to vaporize in the inlet (the

injector is located very close to the valve) the fuel entering the cylinder starts to have a cooling effect on the mixture, due to its lower than the in-cylinder gases' temperature and latent heat. Thus NOx emissions decrease and THC emissions increase at the same time. As injection timing moves away from the valve open period, after 473, the fuel inhaled by the cylinder has spent up to 720 CAD in the inlet, thus having more time to evaporate. CO also increases slightly near the crossover point since the non-fully evaporated fuel is more difficult to combust efficiently. The effects on BSFC and CO_2 are negligible. In addition, the effect of injection timing on exhaust manifold temperature, Figure 69, and also on PPP, is worth mentioning (keeping in mind that spark timing is constant at 10 CAD BTDC). As the fuel is not vaporized when it enters the cylinder, combustion is retarded.

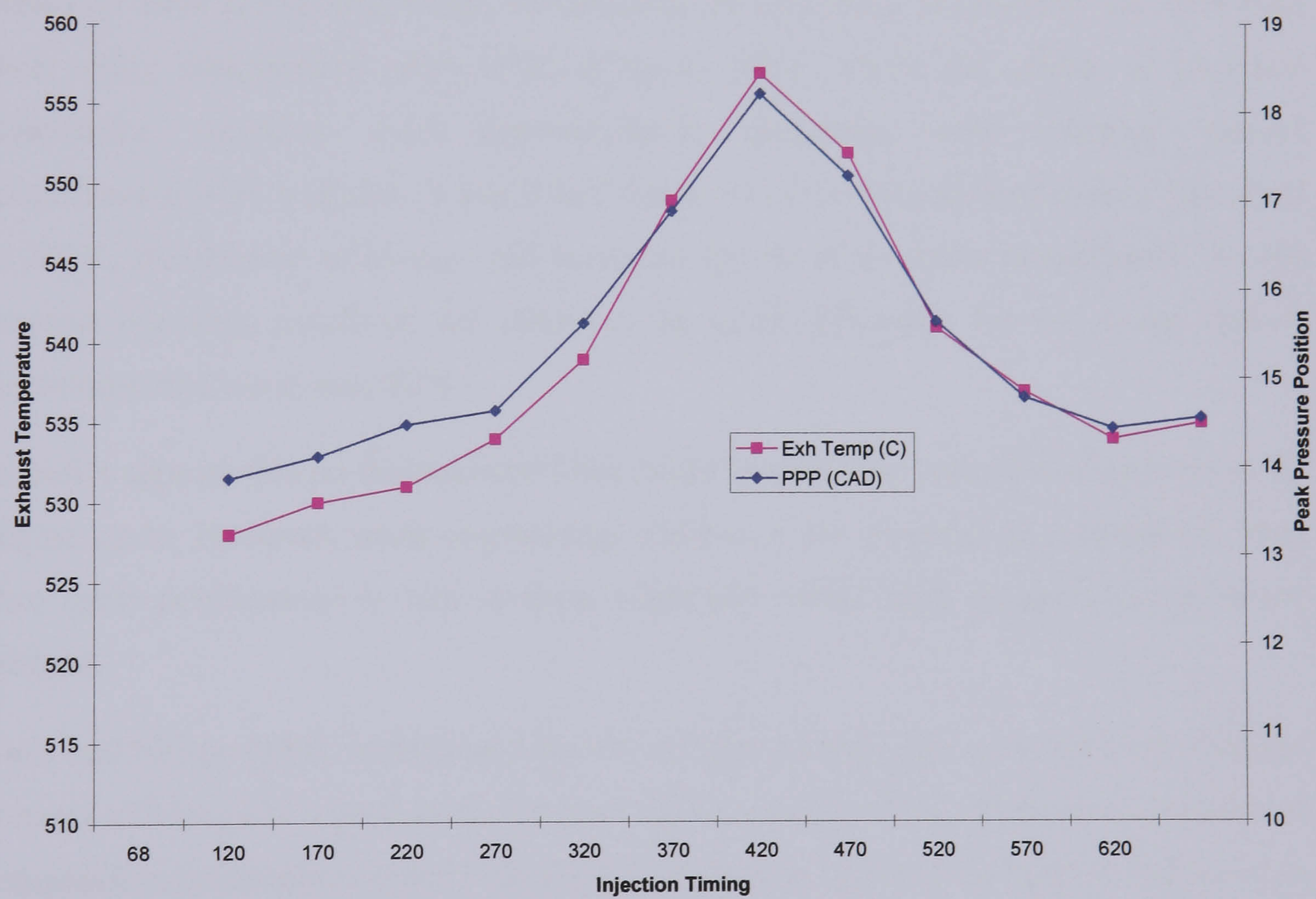

Figure 69: Injection timing effects on exhaust temperature and PPP.

This can be seen on PPP values. In return the exhaust temperature increases as more and more fuel is burned later in the cycle. This behaviour is noteworthy as these effects can be explored at SI to CAI switching for SoC control, in pure autoignition. The effects are obvious, although this data set was collected at medium TRG levels, where combustion timing was primarily controlled through spark advance.

5.2 Thermodynamic Cycle Considerations

A brief analysis on the CAI thermodynamic cycle should be made before delving into more intricate features of its behaviour. This is because an understanding on why CAI can be more efficient will be gained. In addition, the effects of the main combustion control variable, namely, valve timing will be better understood.

In regards to thermodynamic efficiency, the Otto cycle theoretically represents the best option for an IC engine cycle. This is due to the fact that the fuel energy is converted to heat at constant volume when the working fluid is at maximum compression. This combustion condition leads to the highest possible peak temperatures, and thus the highest possible thermal efficiencies.

Edson, in 1964 [133], analytically investigated the efficiency potential of the ideal Otto cycle using compression ratios (CR) at up to 300:1, where the effects of chemical dissociation, working fluid thermodynamic properties, and chemical species concentration were included. It was found that even as the compression ratio is increased to 300:1, the thermal efficiency still increases for all of the fuels investigated. At this extreme operating condition for instance, the cycle efficiency for iso-octane fuel at stoichiometric ratio is over 80%.

Indeed it appears that no fundamental limit exists to achieving high efficiency from an IC engine cycle. However, many engineering challenges are involved in approaching ideal Otto cycle performance in real systems, especially where high compression ratios are utilized.

Caris and Nelson [134], investigated the use of high compression ratios for improving the thermal efficiency of a production V8 spark ignition engine. They found that operation at compression ratios above about 17:1 did not continue to improve the thermal efficiency in their configuration. They concluded that this was due to the problem of non-constant volume combustion, as time is required to propagate the spark-ignited flame.

In addition to the problem of burn duration, other barriers exist. These include the transfer of heat energy from the combustion gases to the cylinder walls, as well as the operating difficulties associated with increased pressure levels for engines configured to compression ratios above 25:1 (Overington and Thring [135], Muranaka and Ishida [136]). Still, finite burn duration remains the fundamental challenge to using high compression ratios.

The goal of emissions compliance further restricts the design possibilities for an optimized IC engine. For example, in order to eliminate the production of nitrogen oxides (NO_x), the fuel/air mixture must be homogeneous and very lean at the time of combustion (Das [137], Van Blarigan [138]). (It is subsequently possible to use oxidation catalyst technologies to sufficiently control other regulated emissions such as HC and CO). Homogeneous operation precludes diesel-type combustion, and spark-ignition operation on premixed charges tends to limit the operating compression ratio due to uncontrolled autoignition, or knock. In addition, very lean fuel/air mixtures are difficult or impossible to spark ignite.

On the other hand, lean charges have more favourable specific heat ratios relative to stoichiometric mixtures, and this leads to improved cycle thermal efficiencies. Equivalence ratio (φ) is no longer required to be precisely controlled, as is required in conventional stoichiometric operation when utilizing three way catalysts. Equivalence ratio is defined here as the ratio of the actual fuel/air ratio to the stoichiometric ratio.

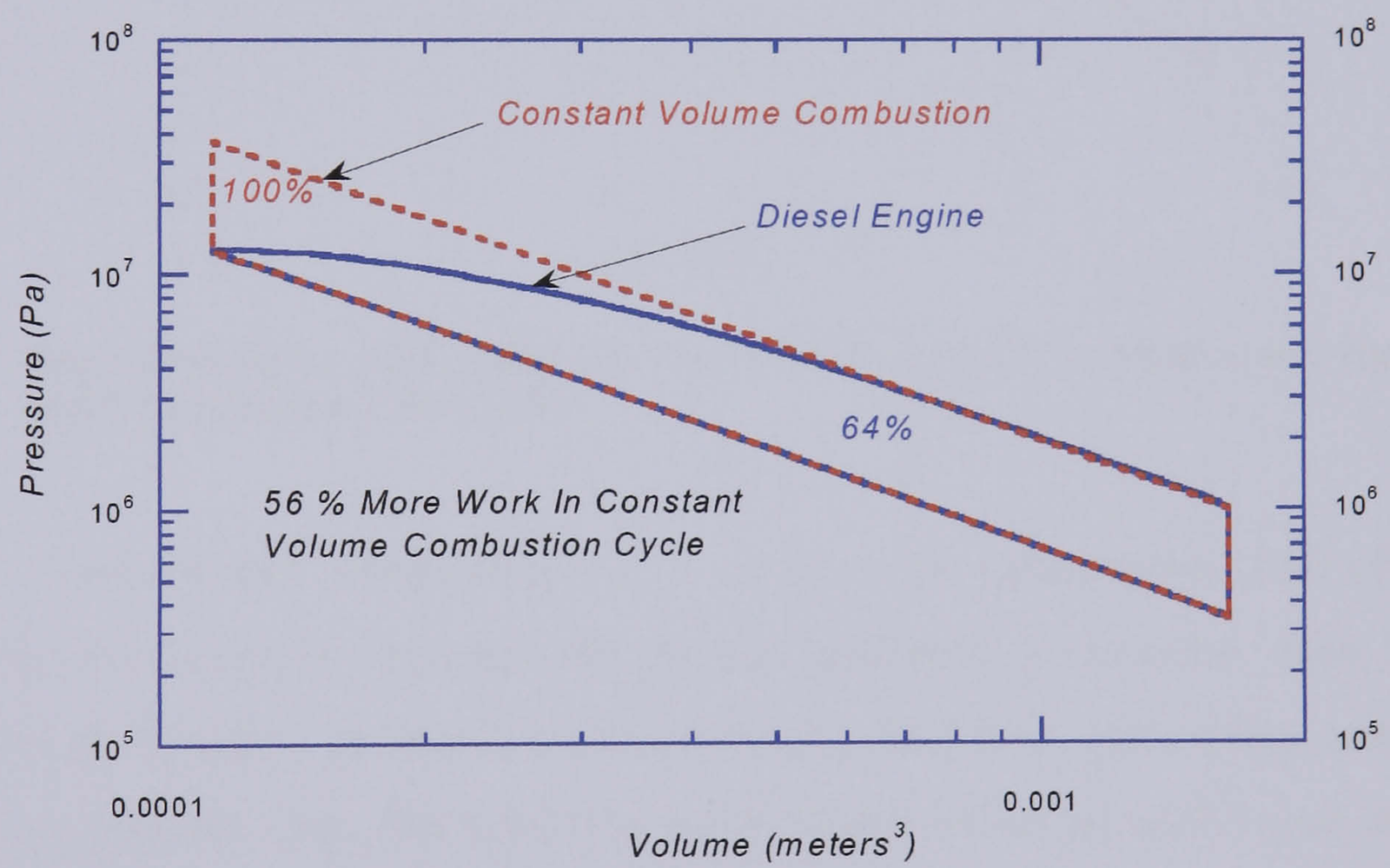

Figure 70: Heavy duty diesel engine thermodynamic performance. [139]

In Figure 70, the amount of work attained from a modern 4-stroke heavy duty diesel engine is shown at CR=16.25:1. The results indicate that under ideal Otto cycle conditions (constant volume combustion), 56% more work is still available. This extreme case of non-ideal Otto cycle behaviour serves to emphasize how much can be gained by approaching constant volume combustion.

Experimental studies by researchers using rapid compression-expansion machines (RCEM) by NASA [139] have approximated the ideal Otto cycle with reasonable success. In the setup of Figure 71 a hydrogen/air mixture has been ignited through compression by a free piston. The combustion of autoigniting hydrogen is very rapid, while the lack of mechanical linkages in the piston avoids potential mechanical damage through the high rates of pressure rise.

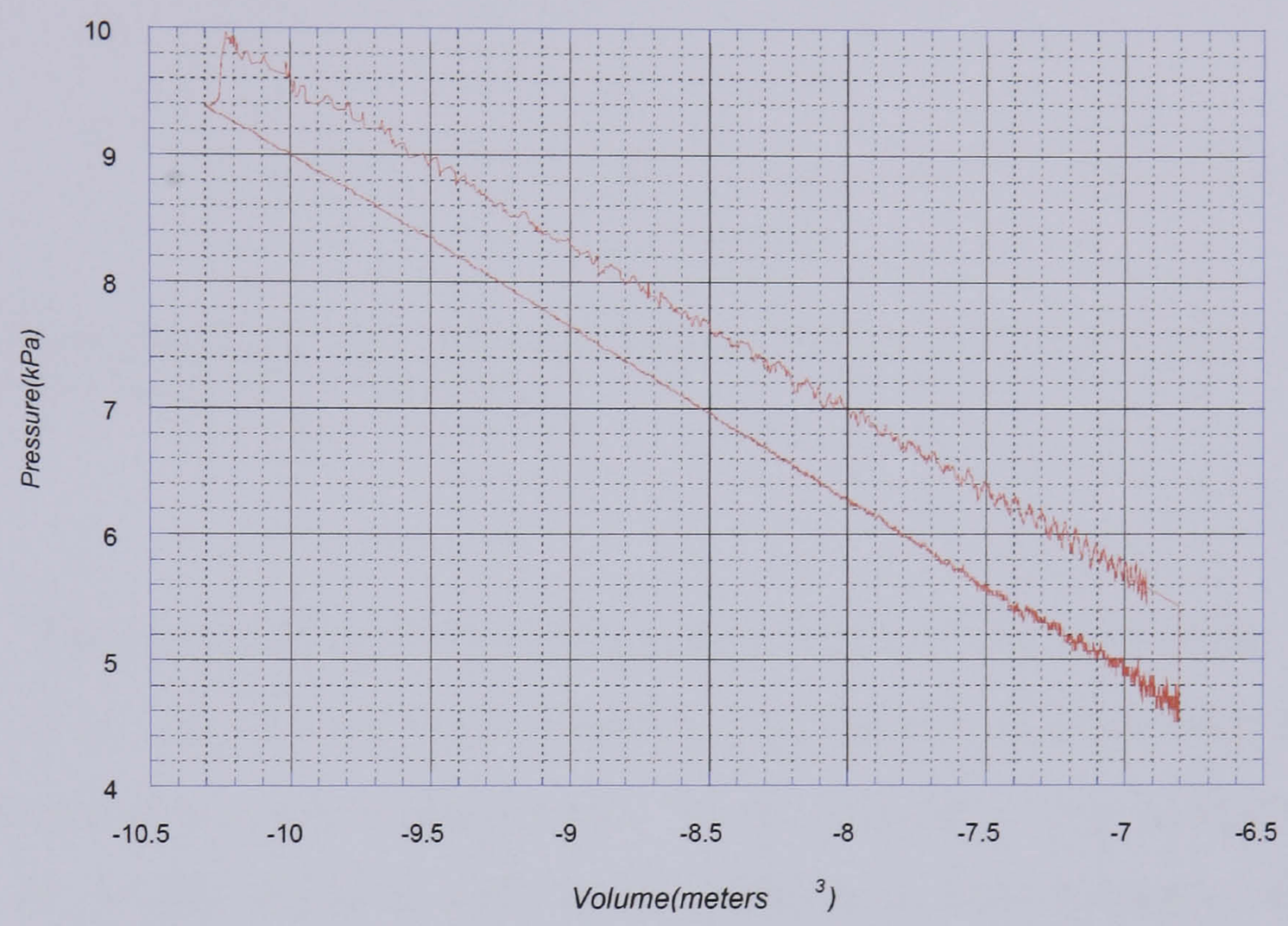

Figure 71: Compression Ratio: 33:1, Indicated Thermal Efficiency: 57%, Equivalence Ratio: 0.319, Initial Temperature: 24C. [139]

Figure 72 demonstrates combustion of a small scale air/propane RCEM. While, compression ratio has been increased, the thermal efficiency is the same. Also, by visual inspection of the graph, a greater deviation from the ideal Otto cycle when compared to Figure 71 is apparent. This illustrates the more drastic effect of heat losses and flame quenching at smaller scale engines as discussed previously in the Micro-HCCI section.

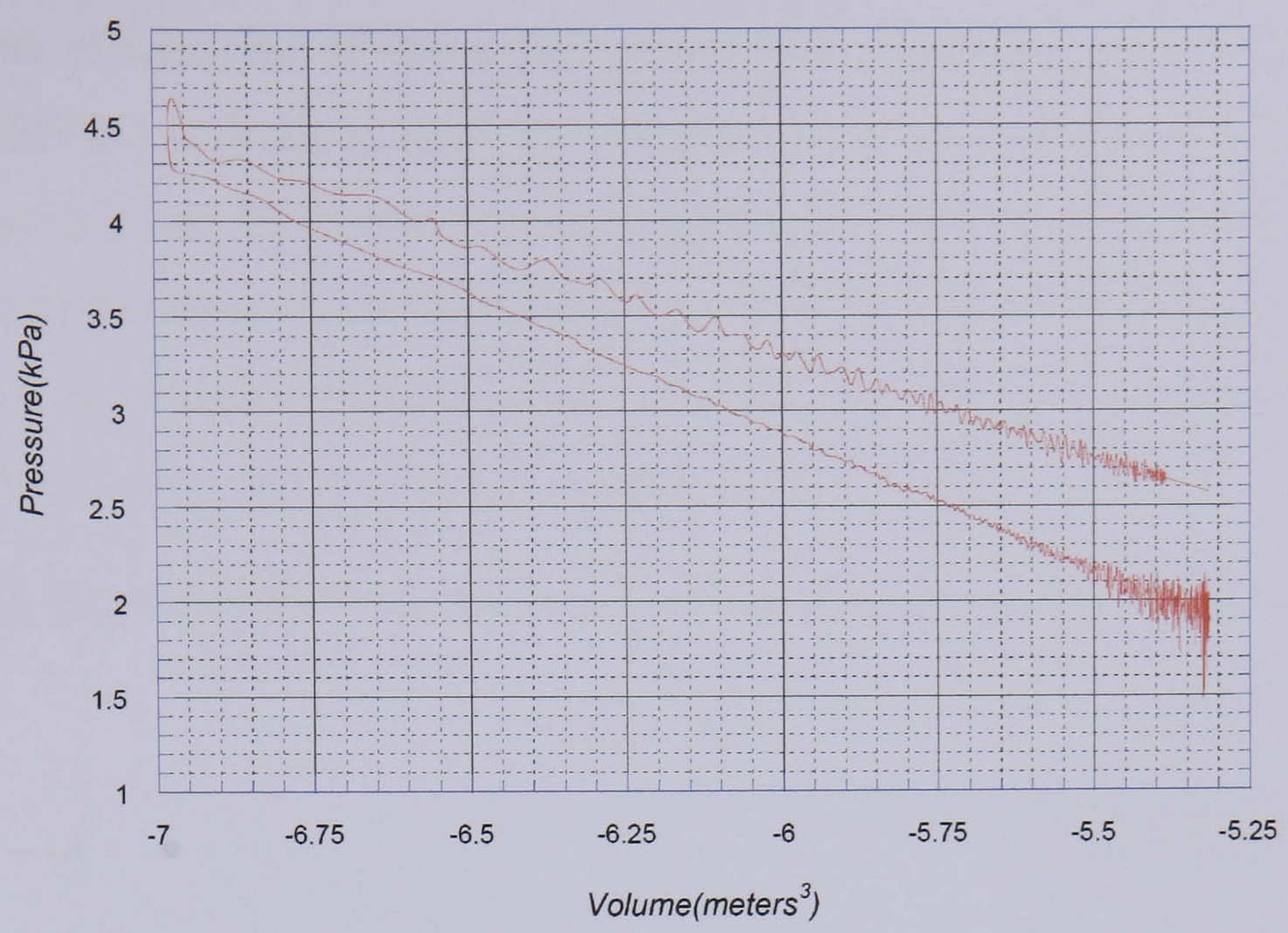

Figure 72: Compression Ratio: 49:1, Indicated Thermal Efficiency: 57%, Equivalence Ratio: 0.679, Initial Temperature: 26C. [139]

5.2.1 Theoretical vs. Experimental Combustion Analysis

In the case of the author's research, recorded experimental data has been compared to their corresponding theoretical ideal cycles. These covered a range stoichiometric CAI combustion at varying TRG, as well as SI combustion. Both constant IVC/EVO and constant duration valve strategies are presented. The ideal cycles have been calculated by assuming zero thermal losses and complete instantaneous conversion of all fuel present (as recorded by experiment) at TDC, as shown on the next pages. The results are summarized in Table 7 and Table 8.

Table 7: Efficiency results for constant IVC/EVO valve strategy.

TRG amount	Ideal Cycle Efficiency	Actual Cycle Efficiency
SI (0%)	42%	34%
4%	44%	34%
32%	45%	34%
36%	46%	35%
50%	47%	36%
71%	48%	33%

In the case of the constant IVC/EVO valve strategy (Table 7), experimental IMEP has been kept constant at approximately 3.5 bar, while engine speed was 2000 rpm, a typical CAI speed site where large TRG sweeps are possible. The trend of the efficiencies of the ideal cycles is for them to monotonically increase with increasing TRG. However,

looking at the efficiencies of the actual cycles, this is not the case. While efficiency increases with TRG, it drops at high TRG (between 50% and 70%). The reason for this is that at low to medium TRG, combustion duration decreases with increasing TRG, thus tending towards the ideal cycles' heat release profiles. At high TRG, combustion duration increases, due to increased dilution, while incomplete oxidation results in less efficient conversion due to very low combustion temperatures.

All of the above can be witnessed on the data presented in Figure 73 to Figure 78.

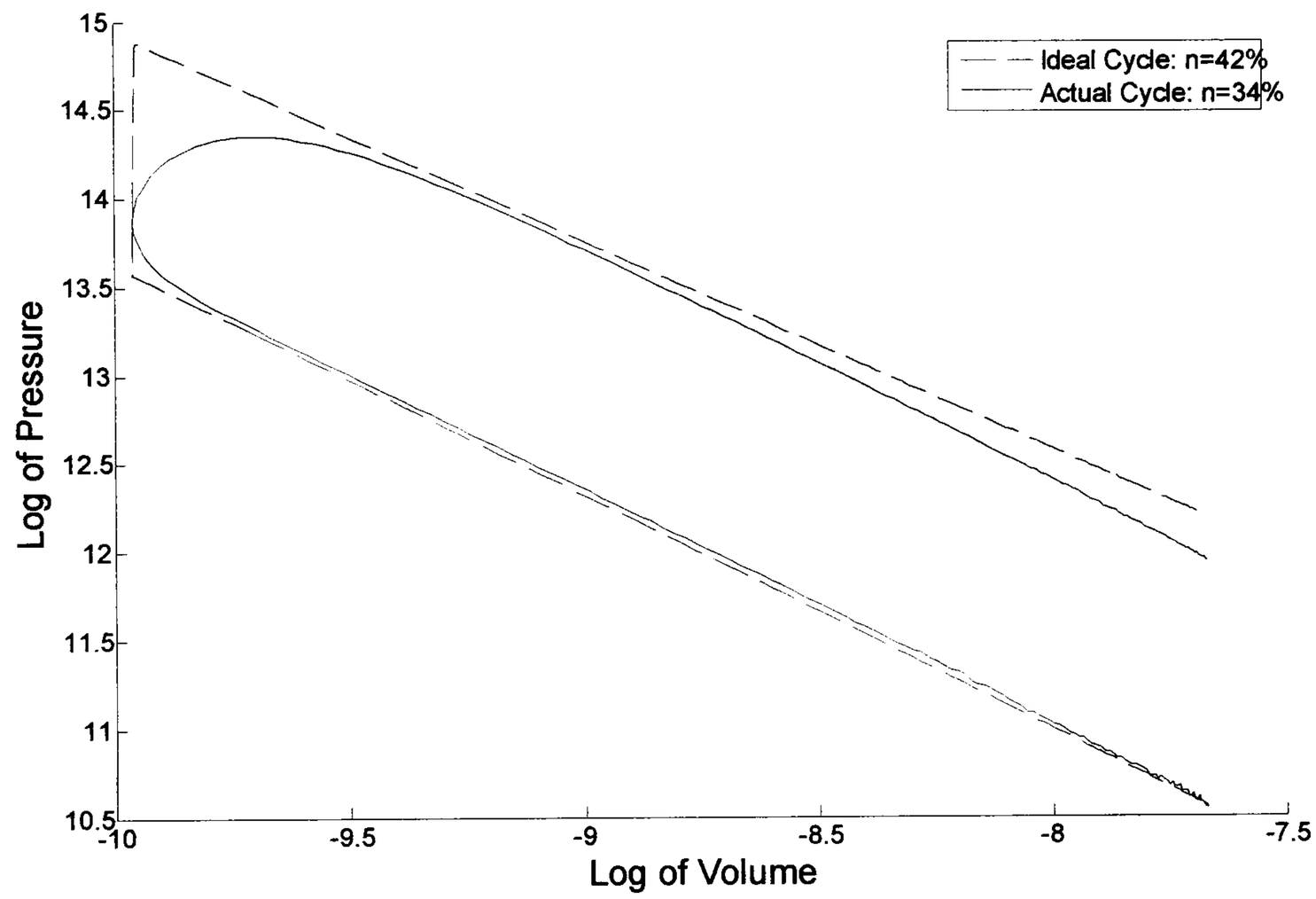

Figure 73: SI ideal and actual cycles in the constant IVC/EVO valve strategy.

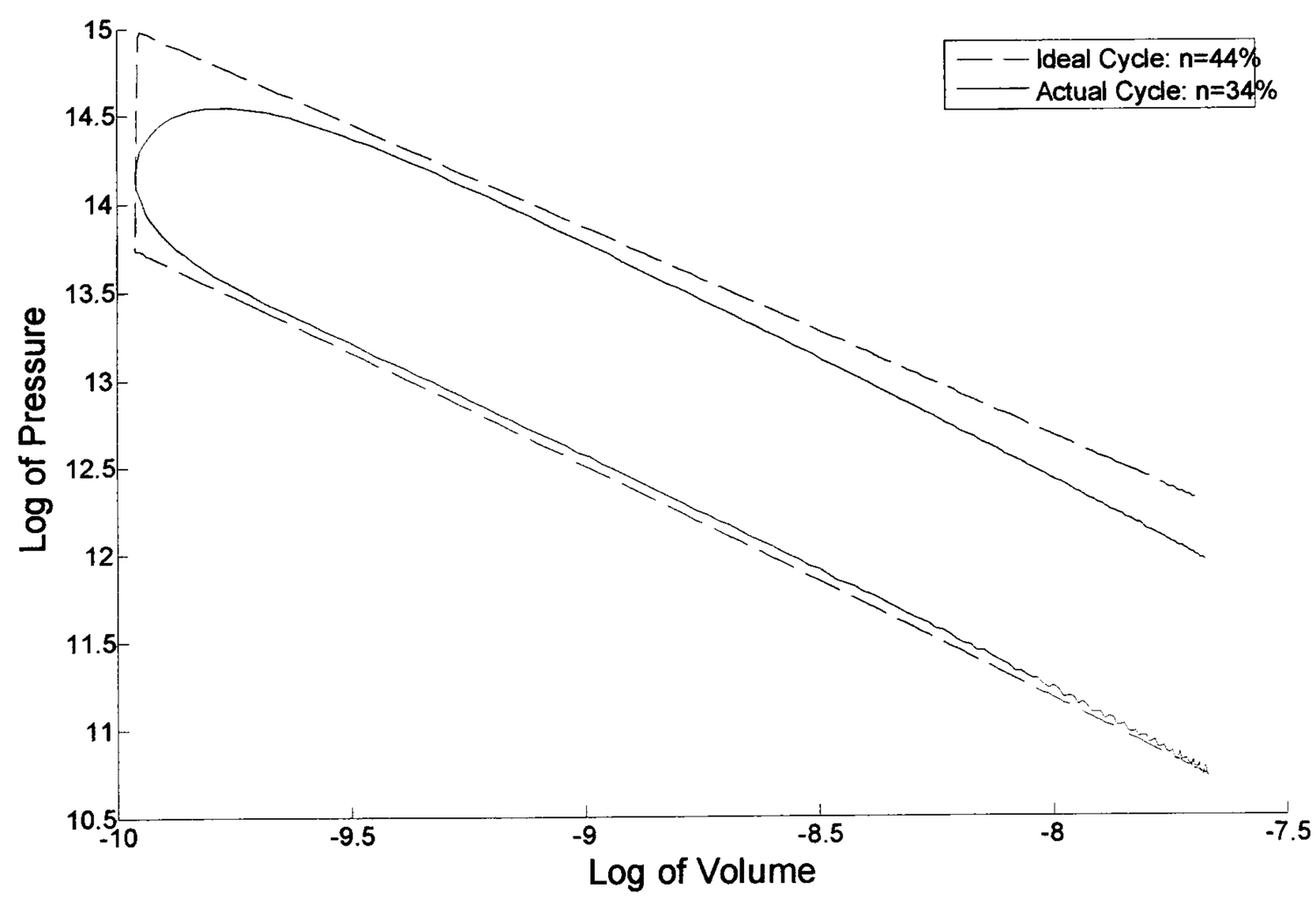

Figure 74: 4% TRG ideal and actual cycles in the constant IVC/EVO valve strategy.

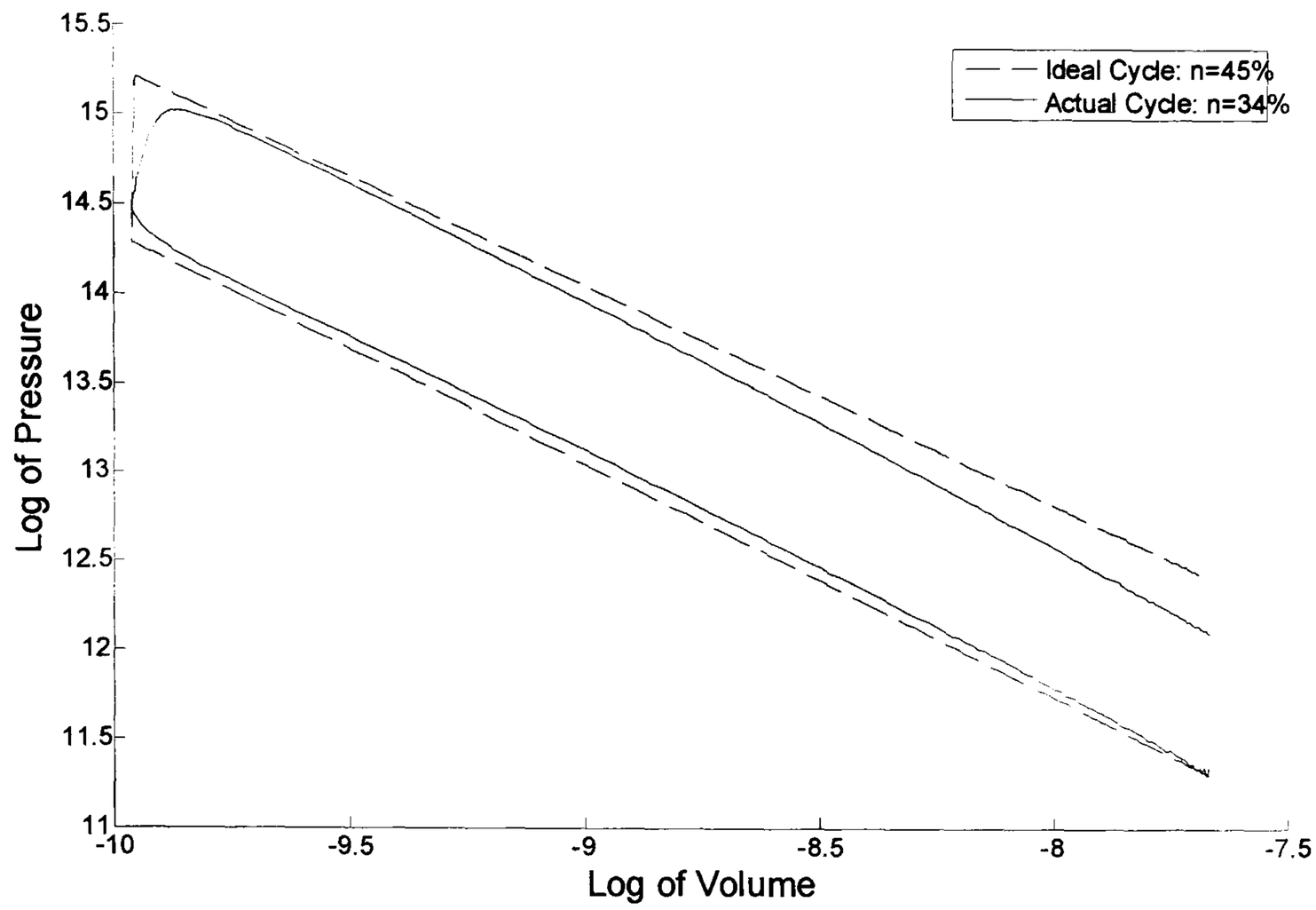

Figure 75: 32% TRG ideal and actual cycles in the constant IVC/EVO valve strategy.

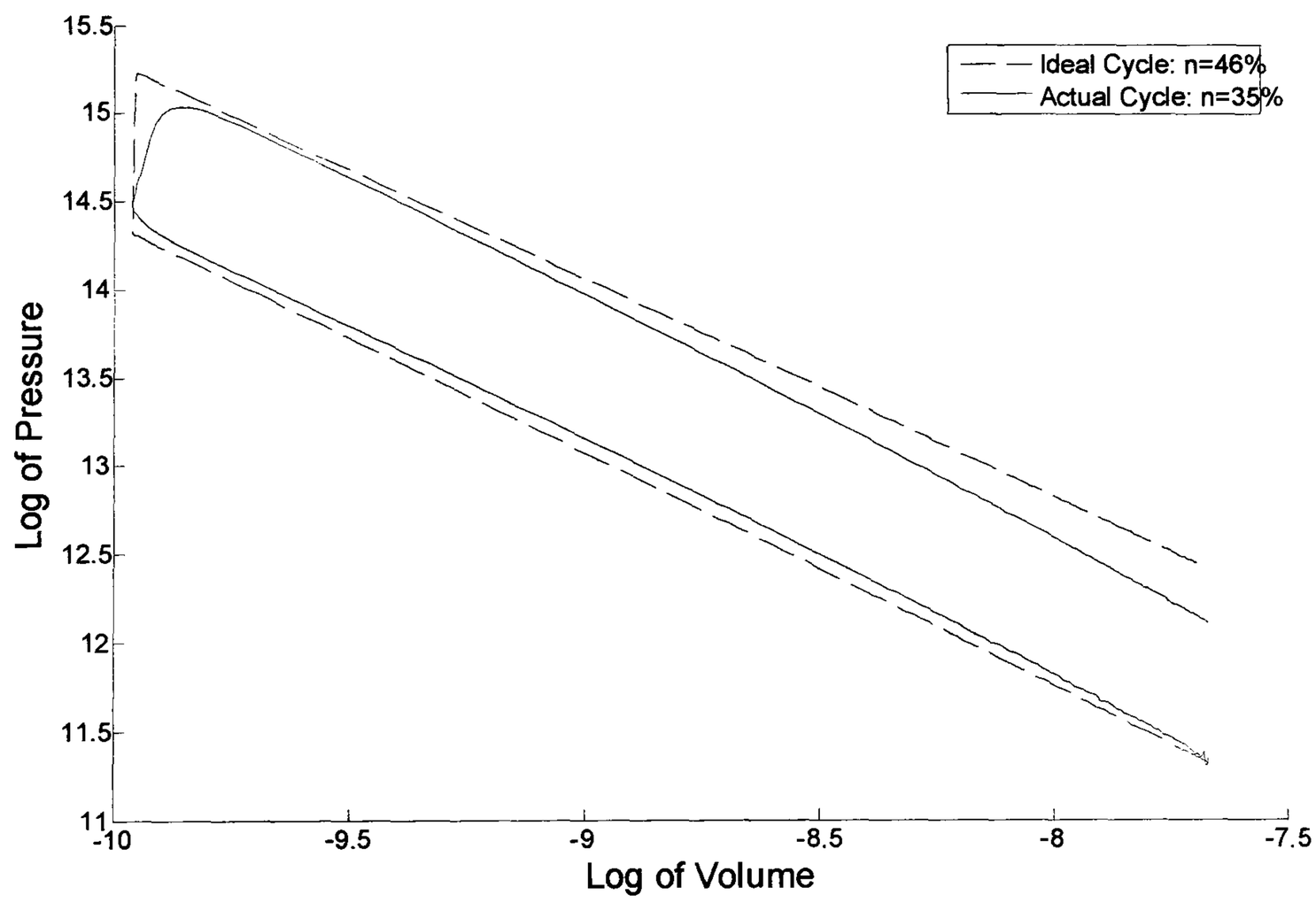

Figure 76: 36% TRG ideal and actual cycles in the constant IVC/EVO valve strategy.

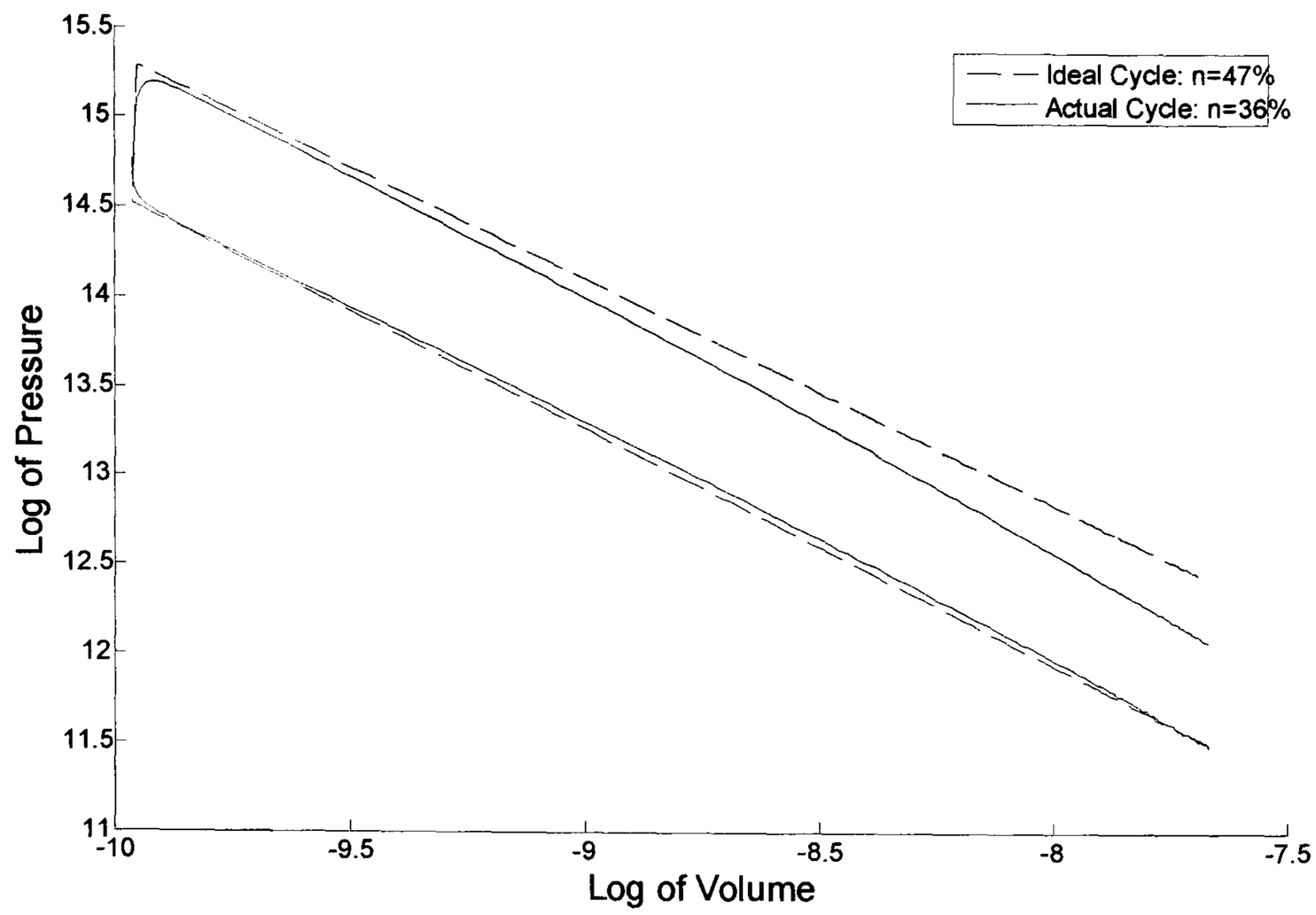

Figure 77: 50% TRG ideal and actual cycles in the constant IVC/EVO valve strategy.

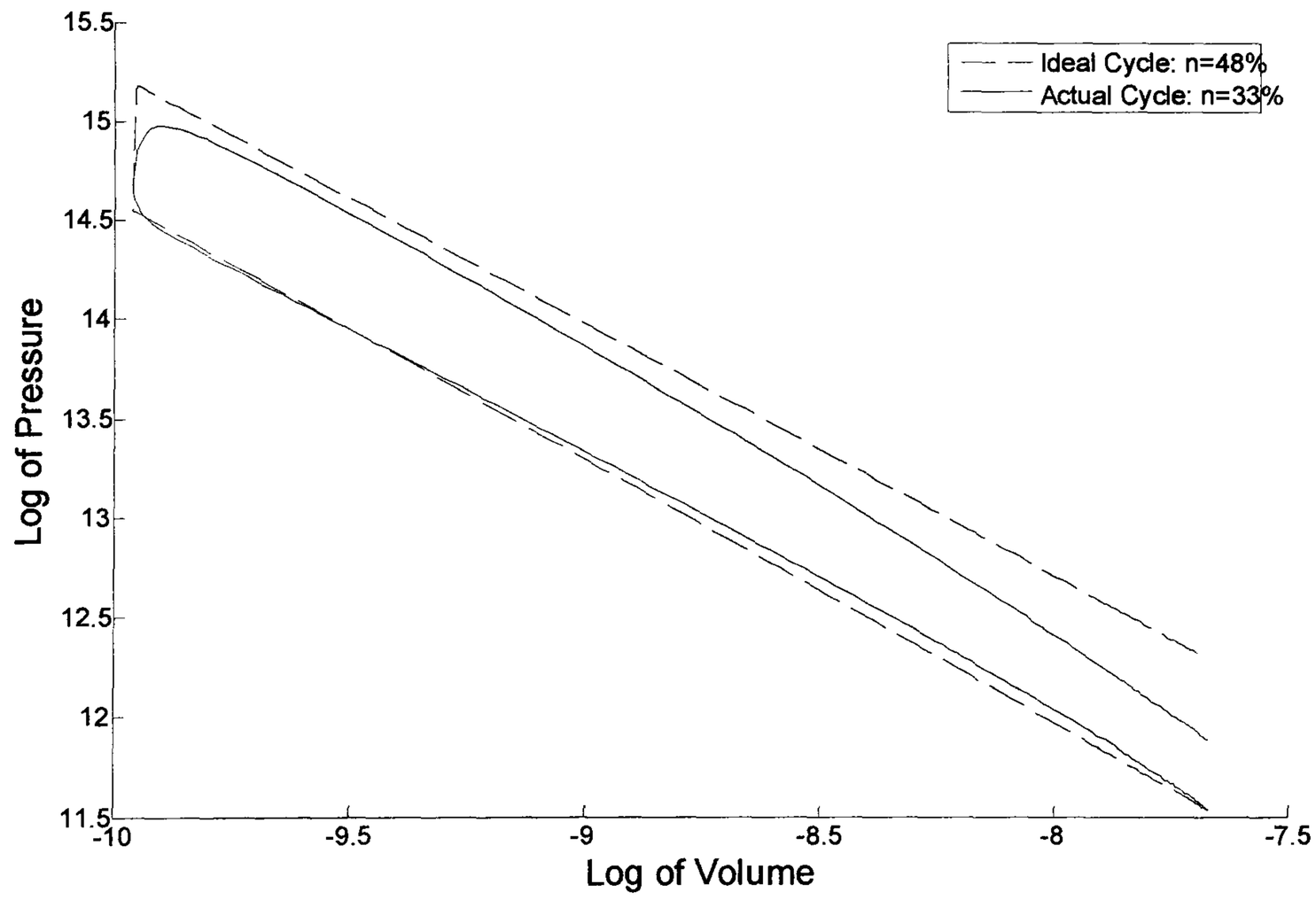

Figure 78: 71% TRG ideal and actual cycles in the constant IVC/EVO valve strategy.

In the case of the constant duration valve strategy (Table 8), the engine was operated at WOT, for the CAI cases, load being controlled by TRG amount, while engine speed was 2000 rpm. The resulting load range for the CAI combustion data is 3 to 7 bar. Two SI files, at the upper and lower edges of this IMEP envelope have also been recorded.

Table 8: Efficiency results for constant duration valve strategy.

TRG amount	Ideal Cycle Efficiency	Actual Cycle Efficiency
SI high load	41%	34%
20%	46%	36%
35%	47%	37%
50%	49%	37%
SI low load	40%	32%

What is seen in this case is that the efficiencies of the ideal CAI cycles increase monotonically with increasing TRG, with both SI cases having the lowest efficiencies. This behaviour is also replicated in the efficiencies of the actual CAI cycles. However, it has to be noted that the efficiency drop at high TRG, witnessed in the case of the constant IVC/EVO valve strategy in Table 7, could not be replicated in this case. This is because, the constant duration valve strategy cannot be operated at the same upper amount of TRG since the late closing of the inlet valve deteriorates the compression ratio, rendering combustion unfeasible. Hence, the effects of severe dilution, negatively affecting combustion in the case of the constant IVC/EVO valve strategy do not come into play in this case.

The traces of these data are presented in Figure 79 to Figure 83.

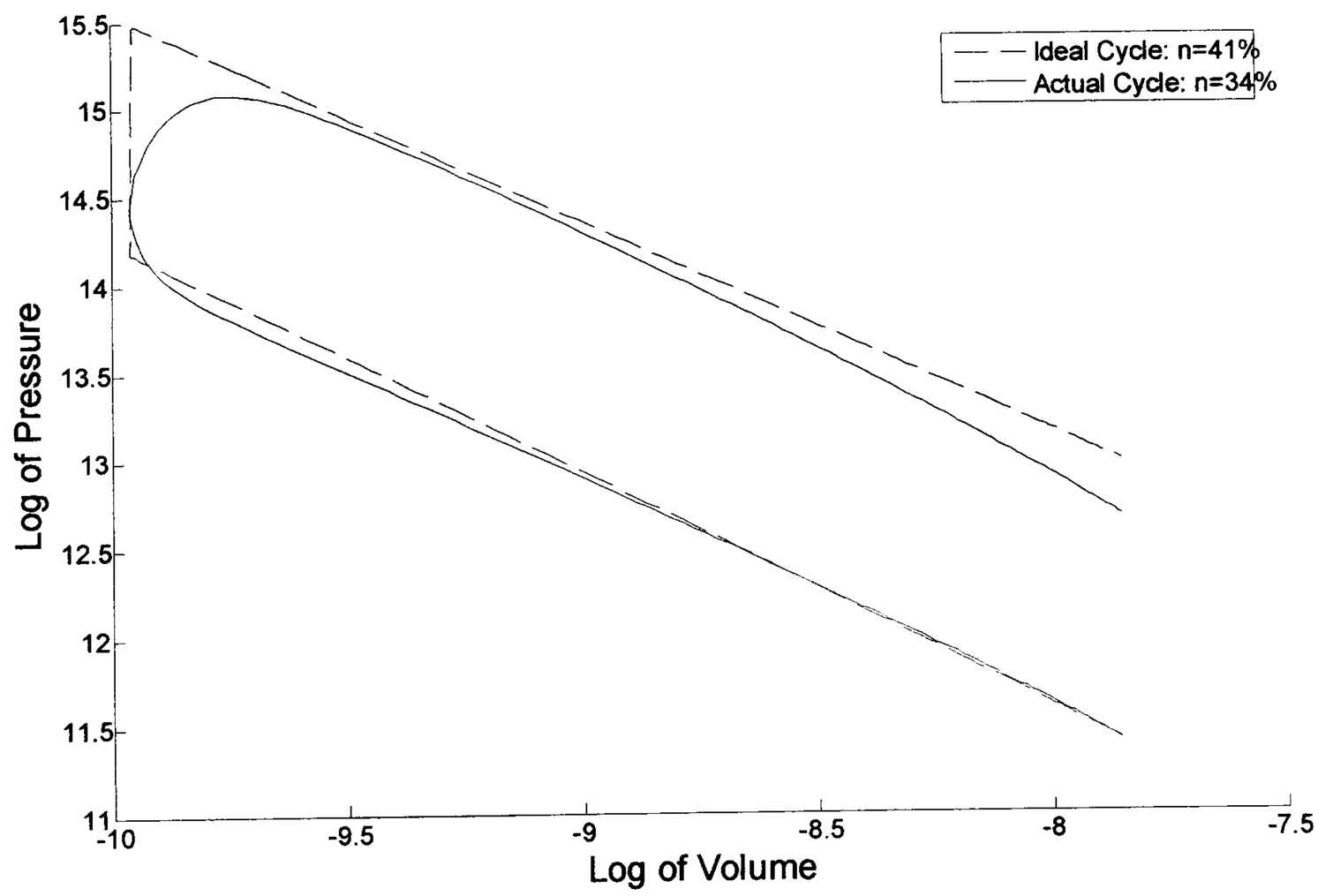

Figure 79: High load SI ideal and actual cycles in the constant duration valve strategy.

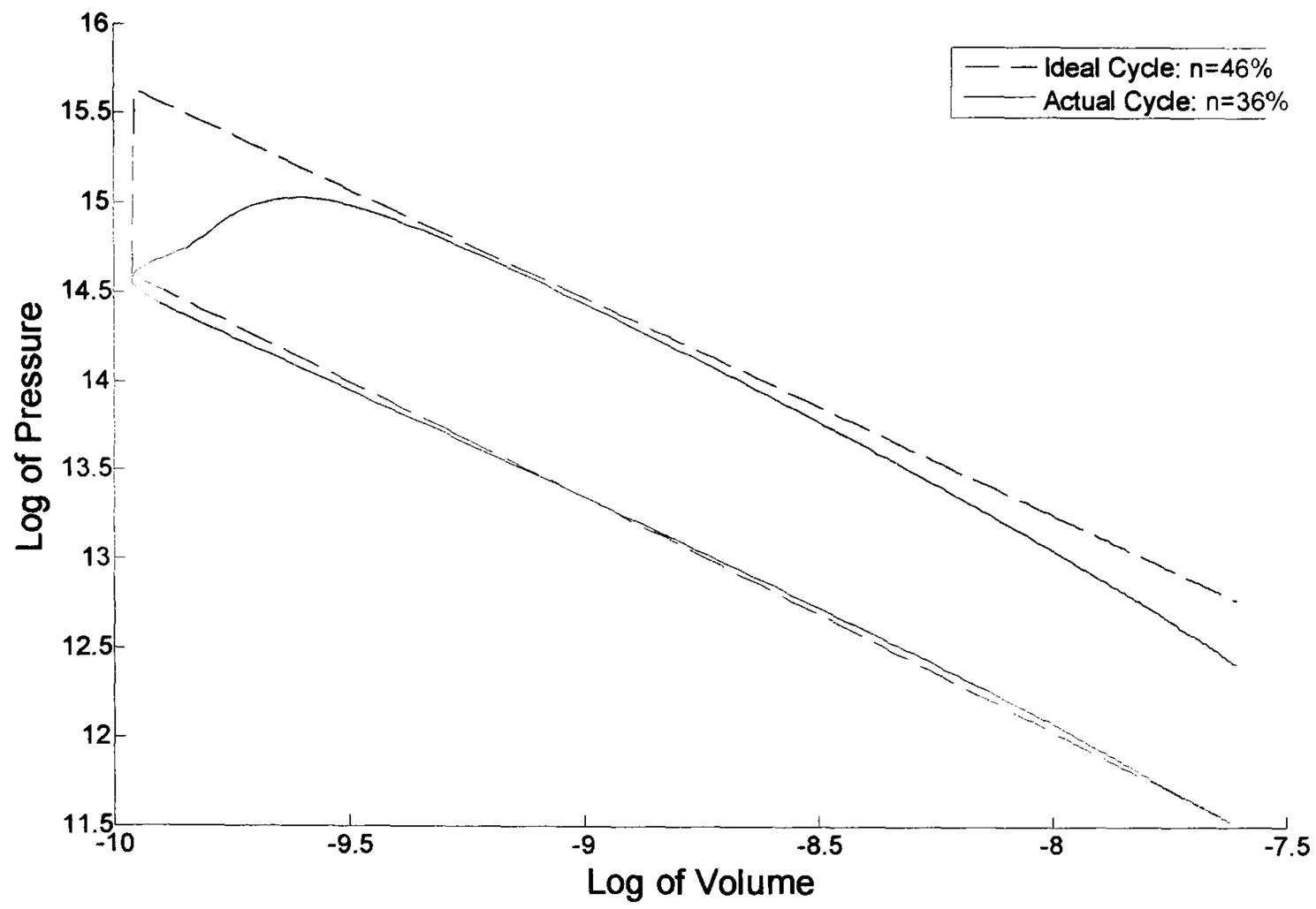

Figure 80: 20% TRG ideal and actual cycles in the constant duration valve strategy.

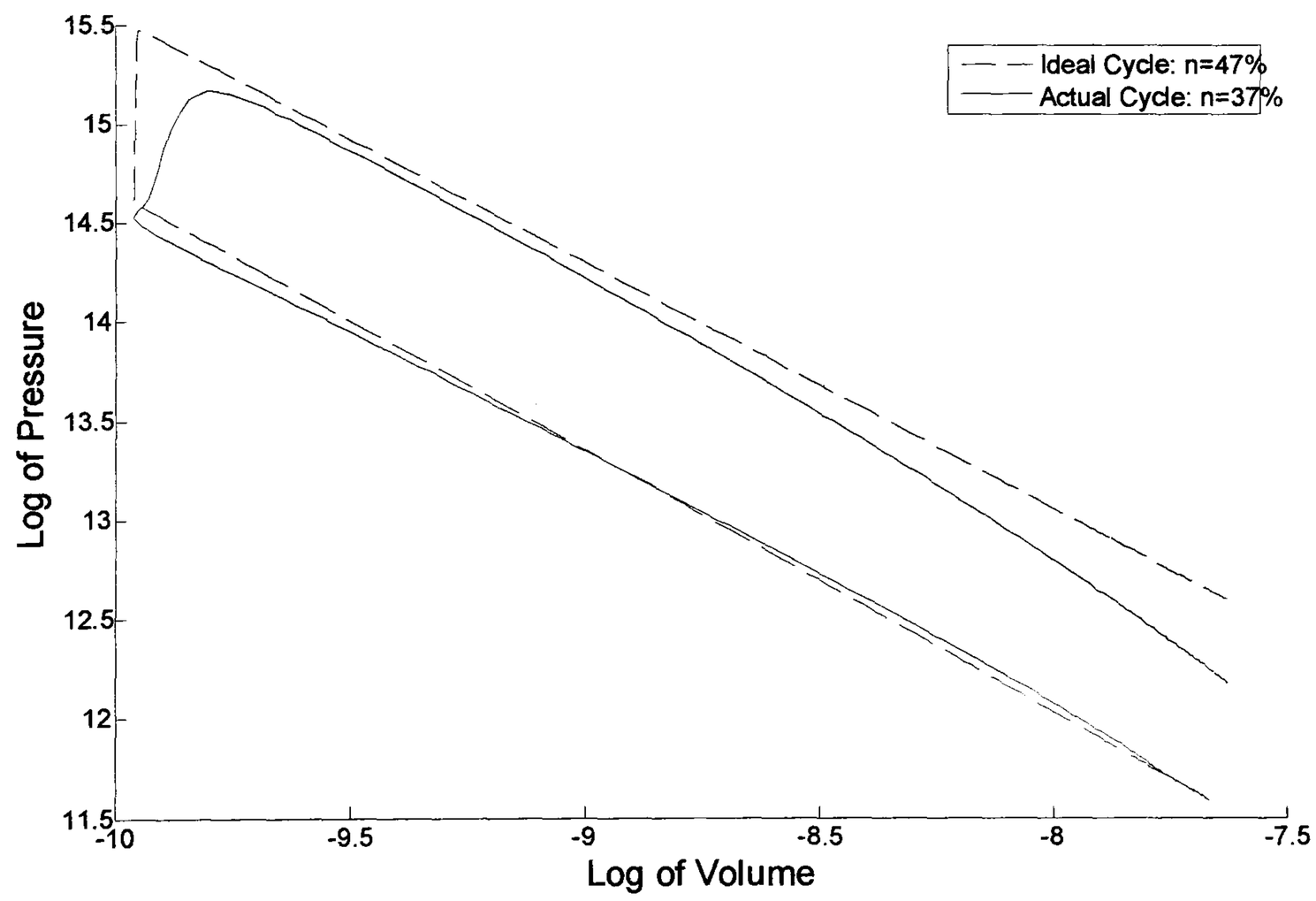

Figure 81: 35% TRG ideal and actual cycles in the constant duration valve strategy.

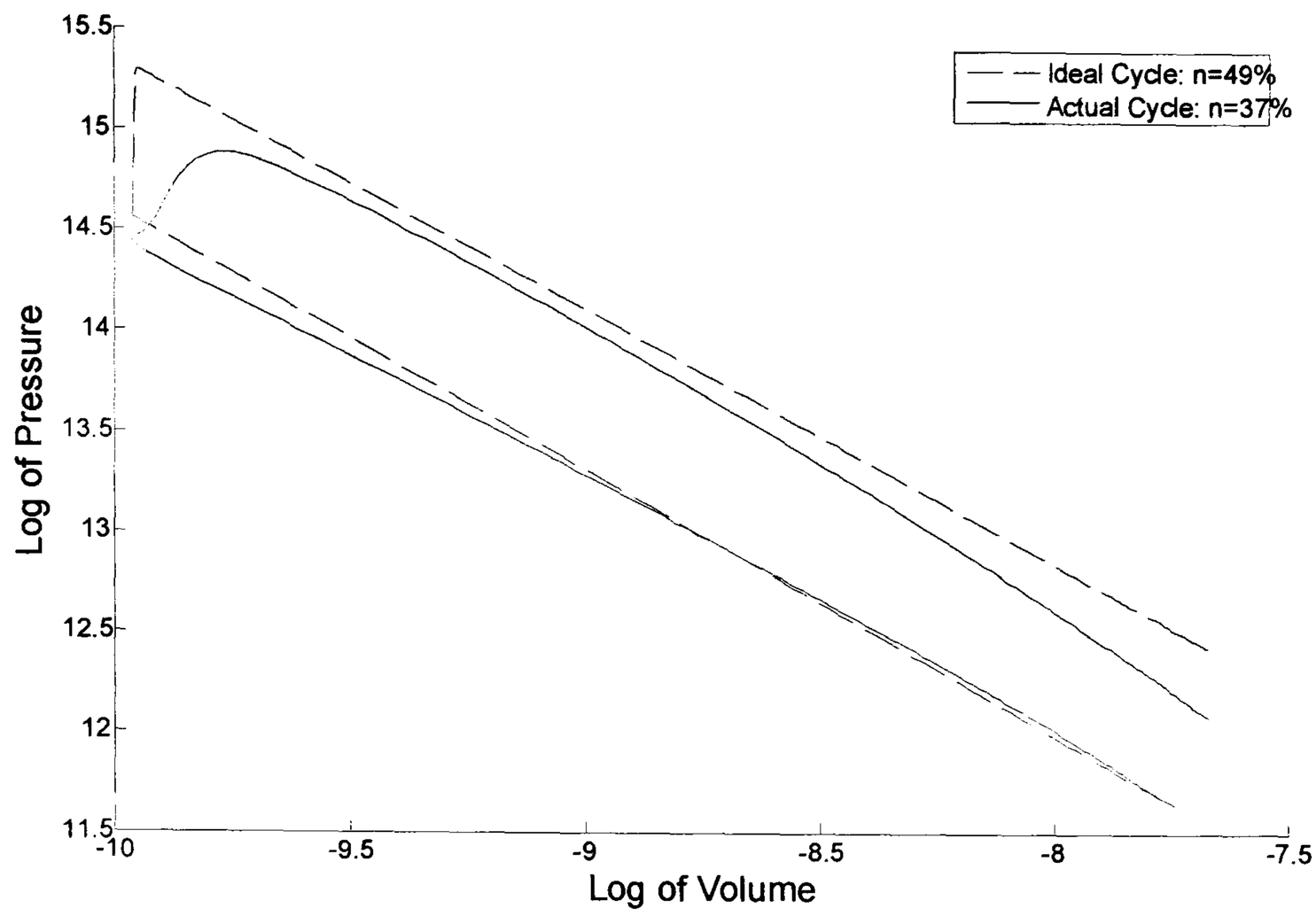

Figure 82: 50% TRG ideal and actual cycles in the constant duration valve strategy.

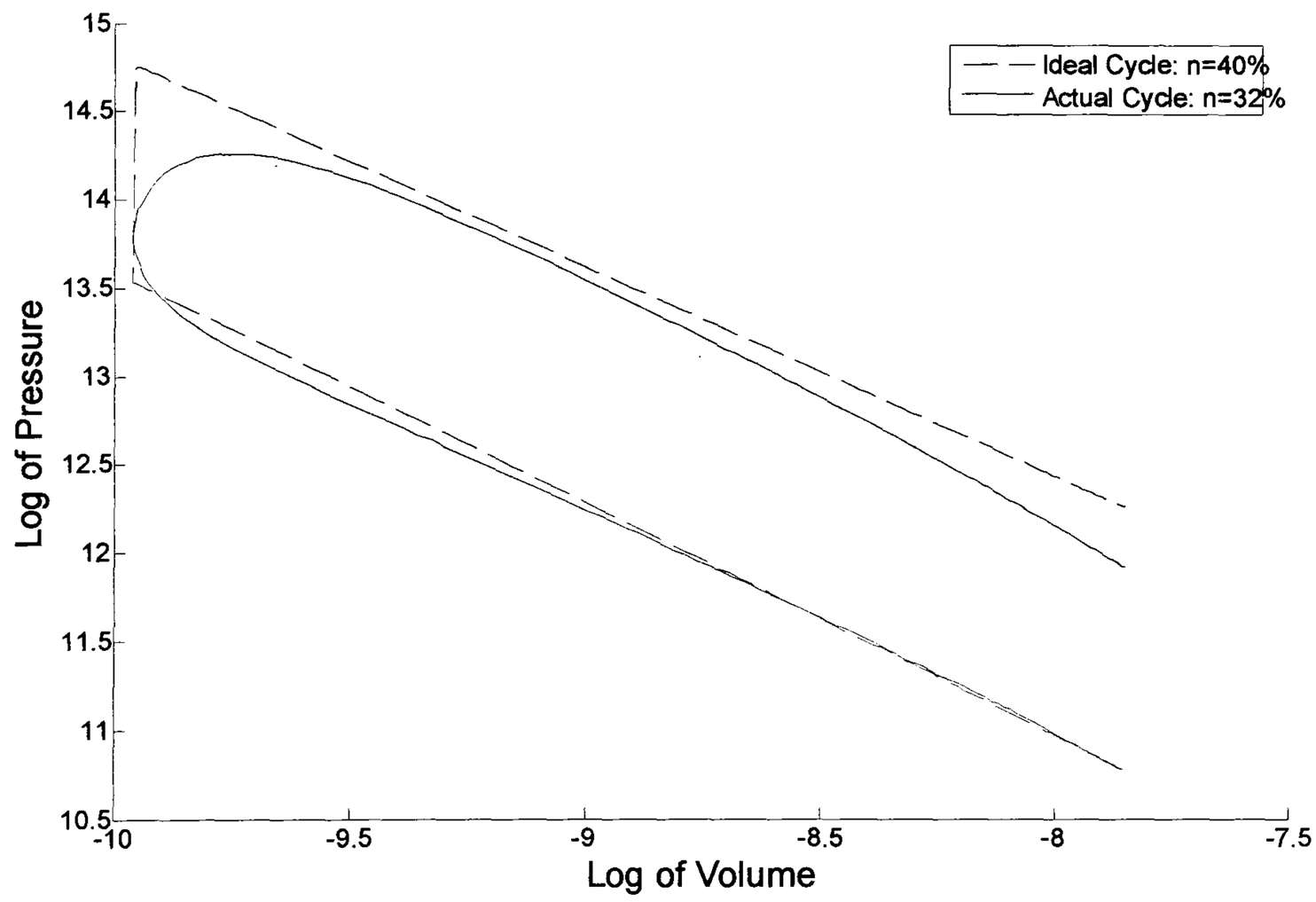

Figure 83: Low load SI ideal and actual cycles in the constant duration valve strategy.

5.2.2 MFB50 Location

One more consideration for optimum thermodynamic efficiency, when not given an instant heat release, is where to locate combustion, in CAD terms, for best results. Here a thermodynamic modelling investigation was done. The model is essentially the same as the one described in the section "Cylinder Pressure Signal Manipulation for Combustion

Analysis". Data were experimentally collected at 2000rpm for a 50% TRG level, to get a baseline reading for combustion duration and flows. These data were then put into this model, whilst the MFB50 location was varied and the corresponding heat transfer calculated through the Woschni equations. These equations had been themselves "calibrated" experimentally to give realistic results. The modelling findings can be seen in Figure 84.

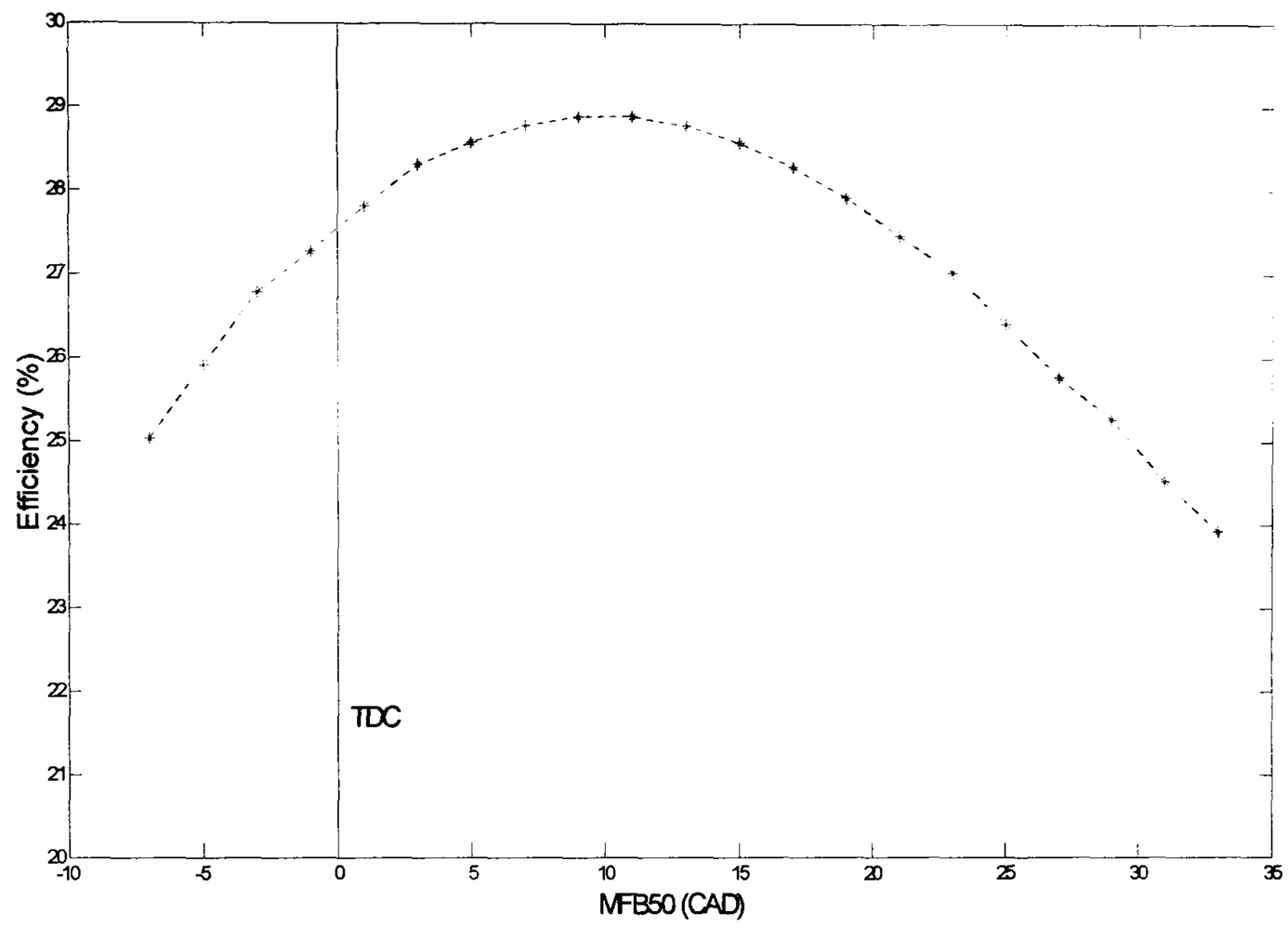

Figure 84: Optimum MFB50.

Brief experimentations on the test rig also confirmed that the optimum efficiency positioning lies in the area of 10 CAD. It can be said that for longer combustion durations this point should be located later and for shorter durations earlier. In this case, the MFB10 to MFB90 combustion duration was in the order of 8 CAD. Making it any shorter would increase maximum rate of pressure rise beyond 8bar/deg (which was how much it was in this case) thus compromising engine reliability. Also, the more the heat losses the later the combustion phasing should be and the inverse. For realistic heat losses though, it was found that MFB10 near TDC (-1 to 1 CAD) gave best results.

5.2.3 Gas Exchange Losses

So far, in the analysis of the thermodynamic cycle during CAI, attention has been paid mainly on the compression and expansion strokes. Analyzing the exhaust and intake strokes, those in CAI also consist of the compression and expansion of TRG, gives a more

informed view on the causes and effects of the valve timing techniques. In this section theory and experimental results obtained by varying the valve timing between SI and pure CAI by increasing the amounts of TRG will be presented.

5.2.3.1 Gas Exchange Theory

Traditionally, pumping work is calculated by the integration of the pressure trace with respect to combustion chamber volume over the period between the expansion Bottom Dead Center (BDC) and the intake BDC as illustrated in Figure 85.

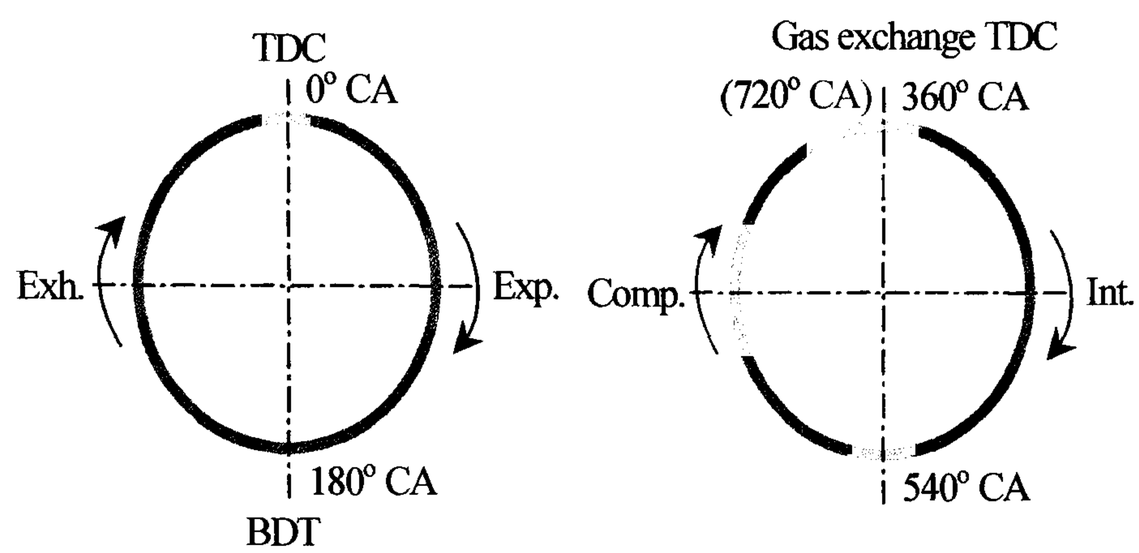

Figure 85: Combustion and gas exchange cycles.

Both Heywood and Tuttle defined the pumping work as the one required to pump charge into and out of the cylinder during the intake and exhaust strokes of the piston

$$W_{pump} = \int_{180^o}^{540^o} P\,dV \quad \text{Eq. (1)}$$

This definition is, also, the conventional definition that most development engineers use. The pumping work equals the energy loss due to gas exchange in an SI four-stroke cycle. The work involved in a typical SI gas exchange process, as shown in Figure 86, is negative in all normally aspirated engines, thus making it a synonym to pumping losses. This is because the exhaust back pressure is always higher than the intake manifold pressure, thus requiring work from the piston to push the gases out during the exhaust stroke and again to draw the gases in during the intake stoke. An exception are highly turbocharged engines [33] where the exhaust back pressure may become lower than the intake pressure near the operating conditions where the turbocharger has its maximum efficiency, but this is not of relevance in this case.

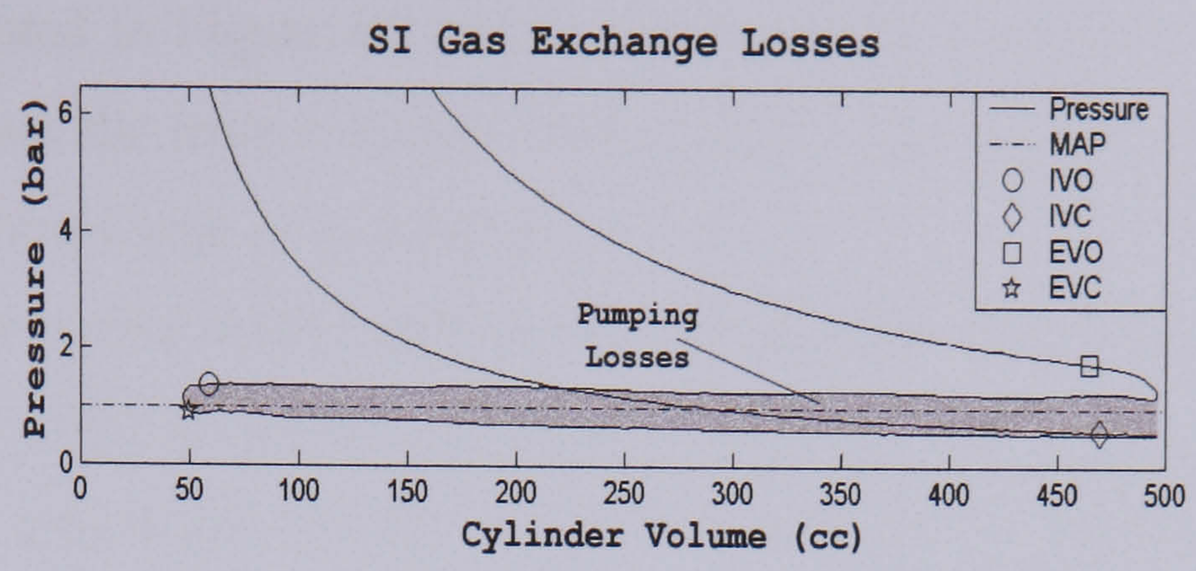

Figure 86: Typical engine gas exchange process.

In the case of CAI combustion the shape of the process in the pressure-volume diagram is significantly different from that of the conventional SI operation mode, shown in Figure 86, due to the high percentage of burned gas that is retained within the cylinder to initiate the next cycle auto ignition, Figure 87.

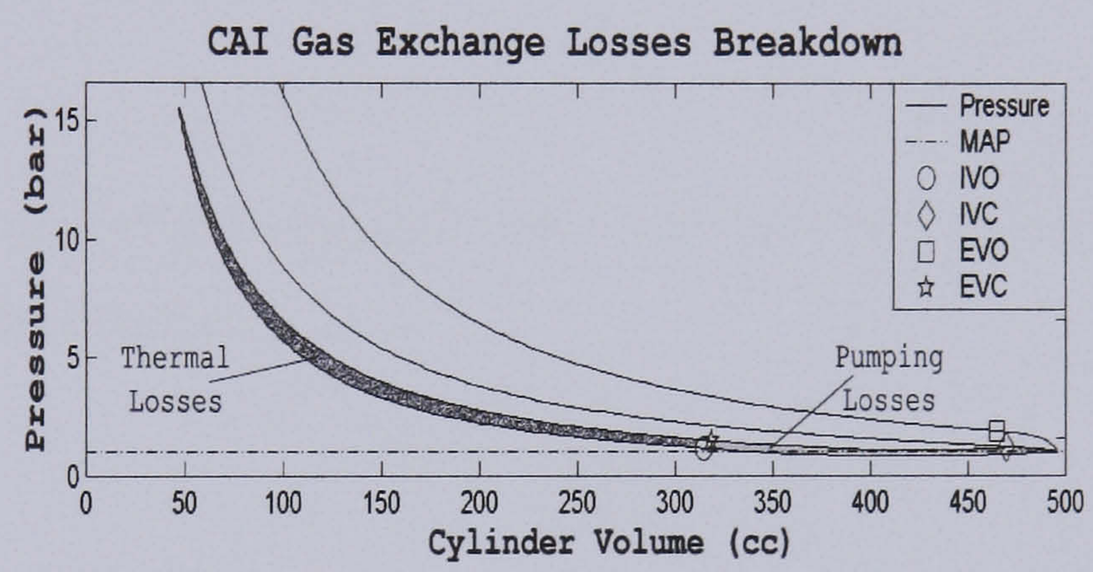

Figure 87: Typical CAI engine gas exchange process

By defining gas exchange work in terms of pumping work only, the part of the pumping cycle between early EVC and late IVO, would appear to have zero losses since no gas exchange occurs. The TRG is compressed between early EVC and gas exchange TDC, and then expanded between the TDC and late IVO. The work given to the TRG by the piston during their compression, will, theoretically, be given back to the piston by the gases during their expansion, since no pumping is involved. Thus a gas exchange work calculation that only takes in account pumping losses, will, by definition, disregard the period of the gas exchange process where the valves are closed. Such a description could be mathematically expressed as:

$$W_{pump} = \int_{180^o}^{EVC} P\,dV + \int_{IVO}^{540^o} P\,dV \quad \text{Eq.(2)}$$

However, as indicated in Figure 87, when a large amount of TRG is trapped inside the combustion chamber, the losses between EVC and IVO are not zero. On the contrary, a significant, but different type of loss occurs.

It has to be noted here that using equation (1) and integrating over the whole exhaust and intake cycles, will yield a correct mathematical result as far as the total gas exchange process losses are concerned. On the other hand, one has to understand that there is a clear distinction between pumping and this new type of loss, which is mainly thermal and blow-by. This loss is only introduced with early EVC and late IVO timing, although equation (1) sums up all losses together.

In order to clarify this new type of losses a series of tests were performed.

5.2.3.2 Experimental Investigation

Two distinct series of tests were performed to investigate the two different valve strategies.

The amount of the deliberately trapped TRG was quantified using a simple geometric model that follows the equation:

$$TRG = \frac{V_{EVC}}{V_{DISP}} \qquad \text{Eq.(3)}$$

where V_{EVC} is the swept volume at EVC and V_{DISP} is the total displacement volume.

Equation (3) implies that the TRG amount is thought of as the percentage of the displacement volume at EVC over the total displacement volume. In other words the clearance volume does not come into the equation. As a result, the values of the amount of TRG quoted are the amount of trapped gases on top of the un-scavenged gases of the clearance volume. The un-scavenged gas should be in the region of 10% by volume on its own, since the CR is 10.5:1.

In the first series of tests, the engine was initially tested under conventional SI operation mode, then gradually shifted to CAI mode by symmetrically reducing the inlet and exhaust valve overlap to increase the amount of trapped TRG, ie the constant EVO and IVC valve strategy (Figure 53).

During the tests, Air to Fuel Ratio (AFR) was kept stoichiometric, the gross Indicated Mean Effective Pressure (IMEPgross) was maintained at a constant level of 3.5bar. At

very high TRG levels, higher than 50%, where the IMEPgross dropped to 3.25 bar for 50%, reaching a minimum of 3.14 bar for 69% of TRG. Therefore the graphs presented only show results of up to 50% TRG, although the trends continue all the way to the highest amounts of TRG.

The engine speed was kept constant at 2000rpm. In order to preserve an IMEPgross of 3.5bar at low levels of TRG, and also in the case of standard SI operation, throttling was applied.

The TRG fractions, calculated using equation (3), used for the experiments were 0, 4, 15, 23, 27, 32, 36, 41, 46, 50, 55, 59.1, 63 and 69%. Zero percentage denotes standard SI operation using a positive overlap.

Figure 88 shows the measured in-cylinder pressure traces logged at different TRG levels. The TRG compression and expansion hump is clearly visible on the traces where trapped TRG exists. Increasing TRG results in a more pronounced hump. Also visible are the combustion humps that change shape depending on the mode of combustion. Again, increasing TRG results in a more pronounced combustion hump. The use of TRG as a throttling method allows greater in-cylinder pressures at IVC and thus the resulting compression of these gases reaches a higher compression pressure. Moreover, as the combustion mode shifts from purely SI to SACAI and, finally, to pure CAI, the combustion duration shortens. It produces a faster heat release which in turn results in higher peak combustion pressures. Keeping in mind that the total energy addition is almost the same, since IMEPgross is kept constant, it follows that the pressure traces will, as they do, coincide at the late phases of the expansion stroke.

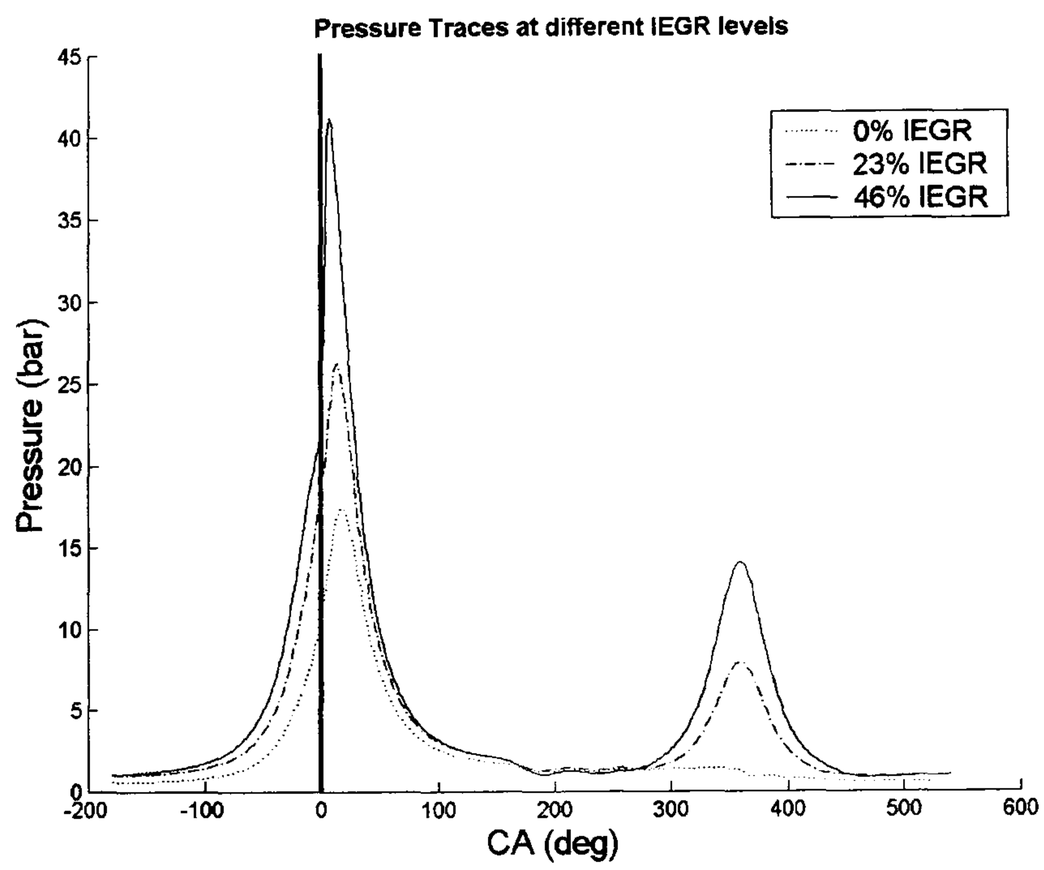

Figure 88: Measured in-cylinder pressure with varying amount of TRG

In the second series of tests, the constant duration valve strategy was employed (Figure 54). Of the two strategies, the latter reduces the effective compression ratio as TRG level increases, since in order to achieve high TRG early EVC is required leading to late IVO and hence late IVC.

Another consideration is the reduced lift (approximately half) in CAI operation, compared to those of the previous valve strategy. Therefore, the maximum amount of TRG that can be used in order to sustain CAI operation is more limited in this latter strategy. The tests in this case, focused on TRG sweeps, from SI to maximum sustainable CAI at different RPM points. In all cases, the mixture was kept stoichiometric and all CAI combustion operated unthrottled, load being controlled by TRG amount. Speed was sampled at 1500, 2000, 2500, 3000 and 3500rpm. TRG ranged from SI to a maximum of 50%, the reason being that in this latter valve strategy, combustion cannot be sustained, due to decreased temperatures, at high values of TRG.

When considering these different valve strategies, EVC and IVO are not of much consequence in that they are both tied to the TRG amount required for an operation setting. In CAI, TRG is dictated by EVC and will necessarily occur sometime before the gas exchange cycle's TDC. The earlier it occurs, the higher the amount of TRG.

Similarly, IVO is dictated by EVC. This is because the inlet must open when the pressure in the cylinder has dropped to levels comparable to those of the inlet. A too early IVO (when in-cylinder pressure is still high above inlet pressure) will allow a large flow of TRG to be established from the cylinder towards the inlet manifold which will then have to be stopped and its direction reversed, all of which incurs energy costs. On the other hand, too late an IVO leaves less time for the valve to be open at close to maximum lift while the piston is before BDC. So, in both valve strategies employed, IVO occurs roughly symmetrically with EVC, mirrored around the gas exchange cycle's TDC.

These two considerations are behind the valve strategies employed in these tests. While the EVC/IVO pair are tied to TRG level, the EVO/IVC pair can be thought of either as entities tied to a specific valve duration, in which case they are “floating” following the timings of their EVC/IVO counterparts, or as fixed points.

5.2.3.3 Pumping Cycle Analysis Discussion

Using the conventional engine pumping loss definition, equation (1), the total Gas Exchange Mean Effective Pressure (GEMEP) can be calculated, as shown in Figure 89

for the data of the valve strategy maintaining constant IMEP. The measured Manifold Absolute Pressure (MAP) is also supplied on the graph to provide an indicator for the throttling applied to keep a steady engine output around 3.5 bar IMEP. It can be seen that the GEMEP decreases as TRG increases up to a level of 20 to 25% of TRG. The reduction in GEMEP in this region is significant, more than 30%, when comparing conventional SI (TRG = 0%) to a CAI modes (23% ≤ TRG ≤ 36%). However, as TRG further increases, the calculated GEMEP starts to increase too. Nonetheless it always remains lower than SI.

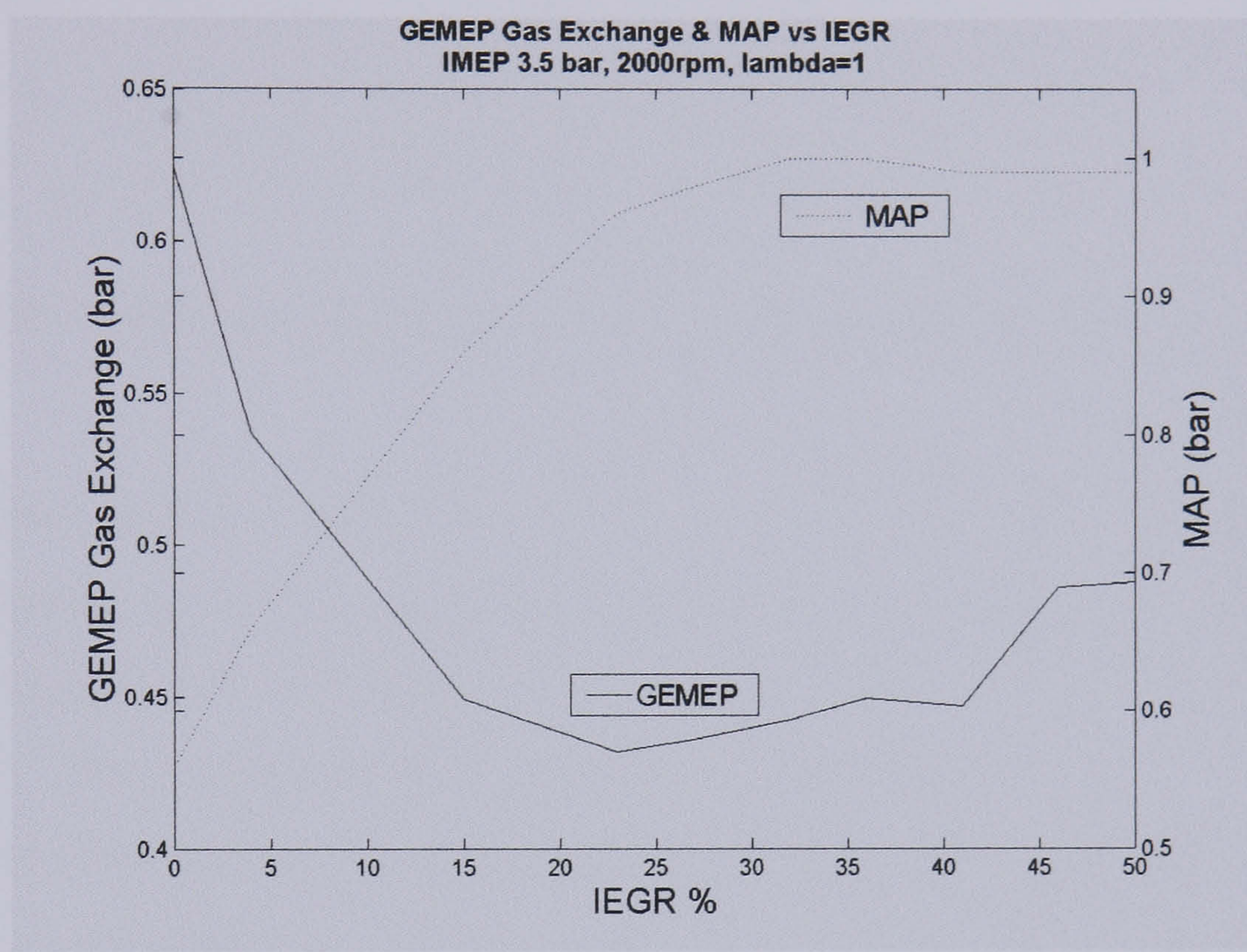

Figure 89: (GEMEP and MAP) The calculated GEMEP using Eq.(1).

As indicated by the measured MAP trace during the test, in order to maintain the consistent IMEPgross of 3.5bar, the engine throttling was gradually decreased as the amount of TRG increased up to a level of about 30%. Decrease in throttling clearly helps to reduce the engine pumping losses. However, if this is the sole parameter affecting GEMEP, then at wide open throttle (WOT) with TRG level higher than about 36%, the GEMEP should remain constant to its lowest level if not further decreased. It is clear that the calculated GEMEP increases as TRG increases when the throttle has been left fully opened. Undoubtedly, some other parameters involved cause the GEMEP to increase.

Figure 90 shows a few typical gas exchange cycle PV diagrams that employ different EVC and IVO timings to vary the amount of TRG.

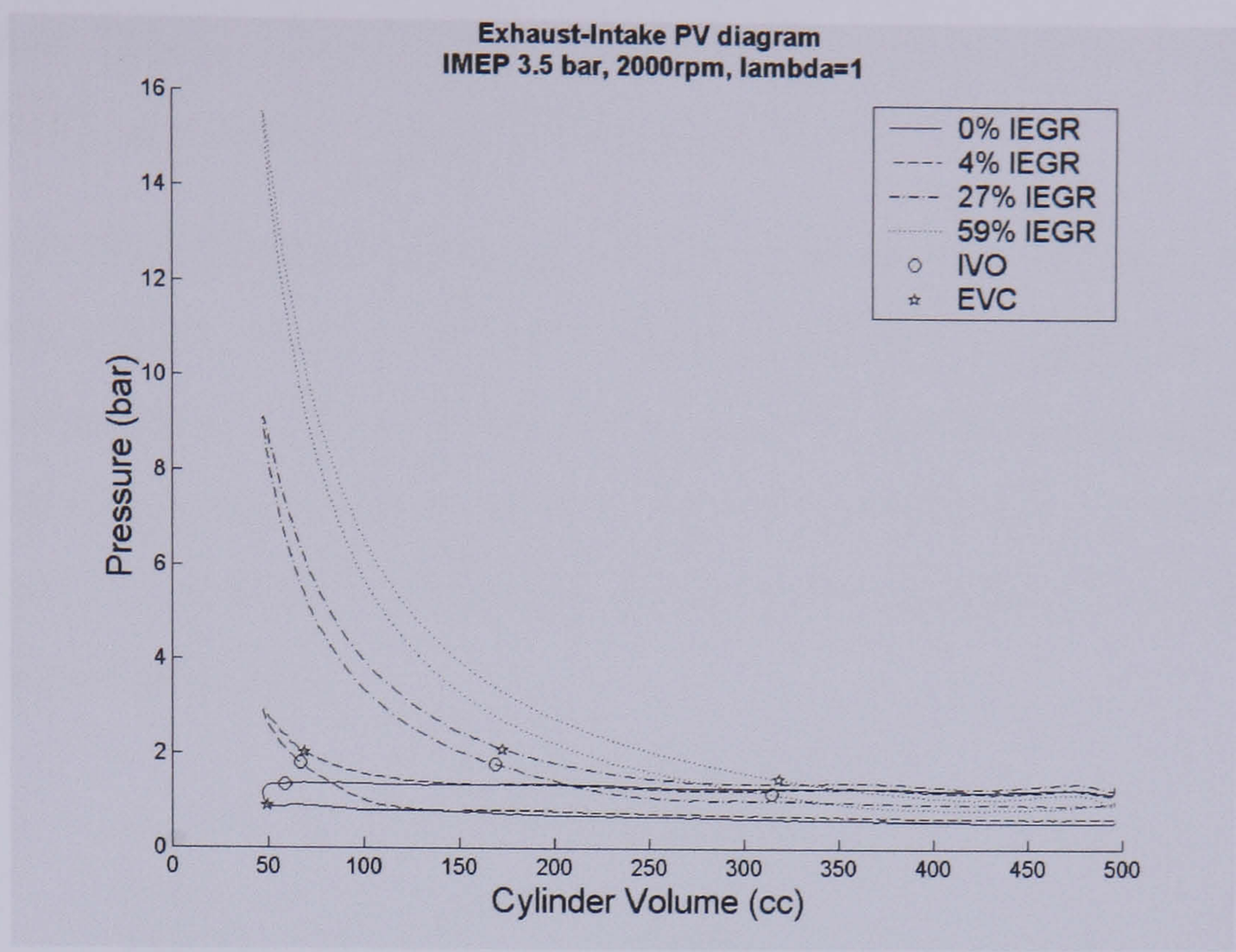

Figure 90: (Pump at varying TRG) Gas exchange process with varying amount of TRG.

By taking a close look at Figure 90, it becomes obvious that the gas exchange process can actually be divided into two parts. The first part is the conventional pumping part which consists of the exhaust process from BDC to EVC and then the intake process from IVO to intake BDC. The second part starts at EVC across to TDC ending at IVO. There is no pumping during this second part. However, the cylinder pressure traces during this period of compression and expansion of the exhaust gases show a considerable loss.

During this period the TRG is at a very high temperature. With the TRG temperature being significantly higher, even at the start of its compression, than that of the engine cylinder walls, a great amount of the gases' energy is lost as thermal losses through the cylinder walls. This loss is further augmented during the compression of the gases that further increases their temperature to values above that of the released exhaust gases. Although, these thermal losses can be calculated in a similar manner to the pumping losses defined in equation (1), they arise from an entirely different source. Integrating over the period, that starts at EVC and ends at IVO, the thermal losses can be calculated in isolation:

$$W_{thermal} = \int_{EVC}^{360^o} P\,dV + \int_{360^o}^{IVO} P\,dV \quad \text{Eq.(4)}$$

If the thermal loss is deducted from the overall gas exchange loss, traditionally described as pumping loss, defined by equation (1), the net pumping losses of CAI combustion can

then be obtained. This is equal to integrating over the period from BDC to EVC and from IVO back to BDC, as previously shown in equation (2).

Figure 91 shows the calculated pumping loss and thermal loss defined by equations (2) and (4), respectively. It can be seen that the pumping loss strictly due to gas swapping reduces as TRG increases. However, the thermal loss due to the heat transfer from the hot trapped TRG to the engine cylinder walls during the period of EVC to IVO, increases as TRG increases. The overall GEMEP calculated from equation (1) is, of course, the combined effect of these two.

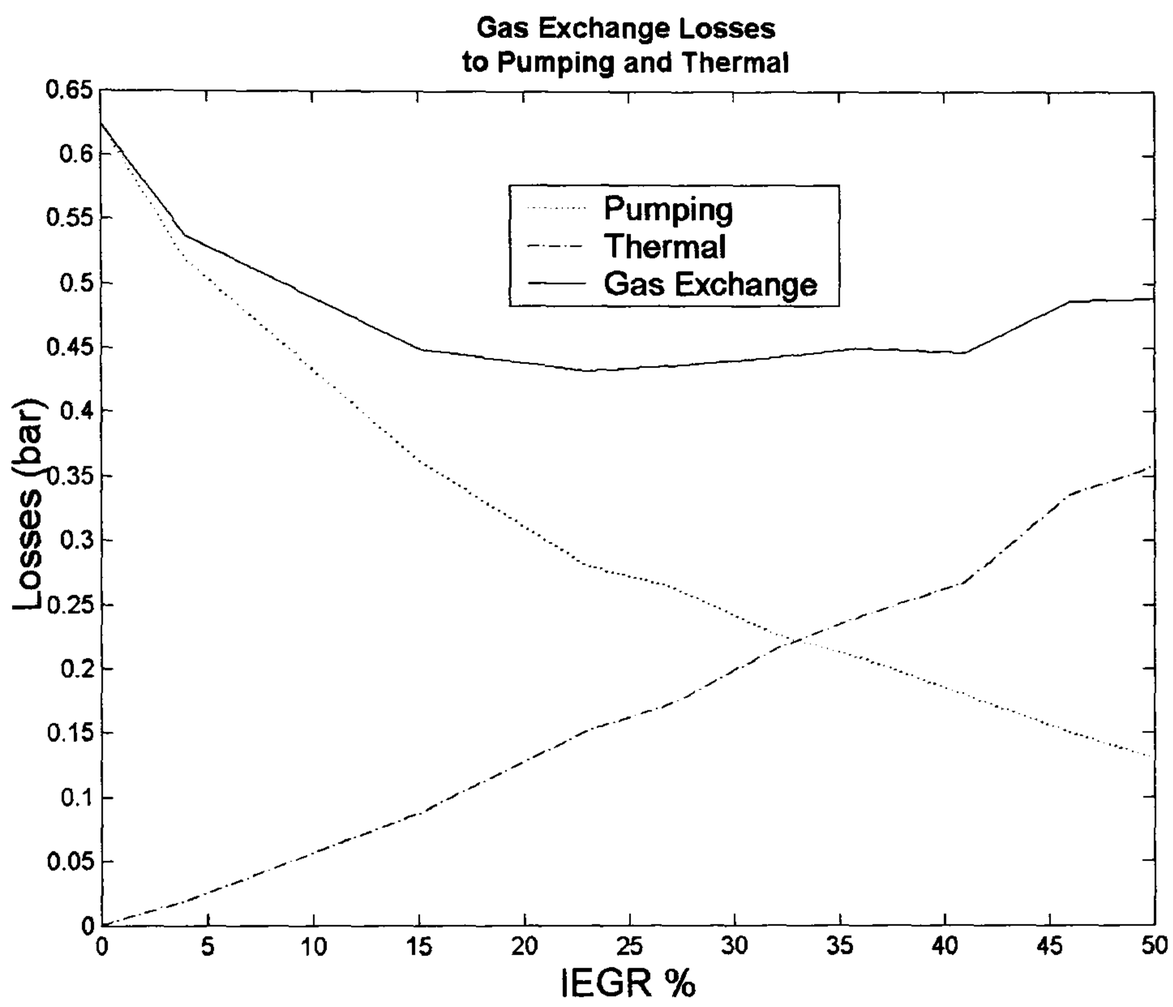

Figure 91: (Pumping and thermal and total loss) Breakdown of the losses to their pumping and thermal components.

Gas Exchange Processes

To look further into the details of the pumping and the thermal losses of CAI combustion, it is necessary to divide the gas exchange cycle into four individual processes: engine exhaust, burned gas compression, burned gas expansion, and intake. To facilitate the calculation of these four individual processes, it is necessary to understand the forces acting on the piston directly and not to simply integrate over the path of the pressure trace on the PV diagram. Since the pressure under the piston, the crankcase pressure, was measured using a pressure transducer its effect could be calculated. By measuring this pressure under the piston and the pressure acting on the piston crown known from the pressure trace the following calculation of the work involved in these processes is possible.

The engine exhaust process can be calculated by adding the work done by the piston on the gas to the work done by the crankcase gas to the piston:

$$W_p = \int_{180^o}^{EVC} P\,dV + \int_{180^o}^{EVC} P_C\,dV_C \quad \text{Eq.(5)}$$

where P_C is the constant crankcase pressure, V is engine swept volume and V_C is the crankcase volume where $dV = -dV_C$.

Similarly, the engine intake process is:

$$W_p = \int_{IVO}^{540^o} P\,dV + \int_{IVO}^{540^o} P_C\,dV_C \quad \text{Eq.(6)}$$

The burned gas compression process:

$$W_t = \int_{EVC}^{360^o} P\,dV + \int_{EVC}^{360^o} P_C\,dV_C \quad \text{Eq.(7)}$$

and the burned gas expansion process:

$$W_t = \int_{360^o}^{IVO} P\,dV + \int_{360^o}^{IVO} P_C\,dV_C \quad \text{Eq. (8)}$$

Figure 92 shows the effect of each single process, represented as percentage against total losses, at varying amounts of TRG.

Firstly, notice the pumping loss during the engine intake process. It drops significantly from contributing approximately 50% of the total losses under SI operation to almost negligible levels at CAI mode. The reason of this reduction is mainly the reduction in throttling losses at high TRG levels.

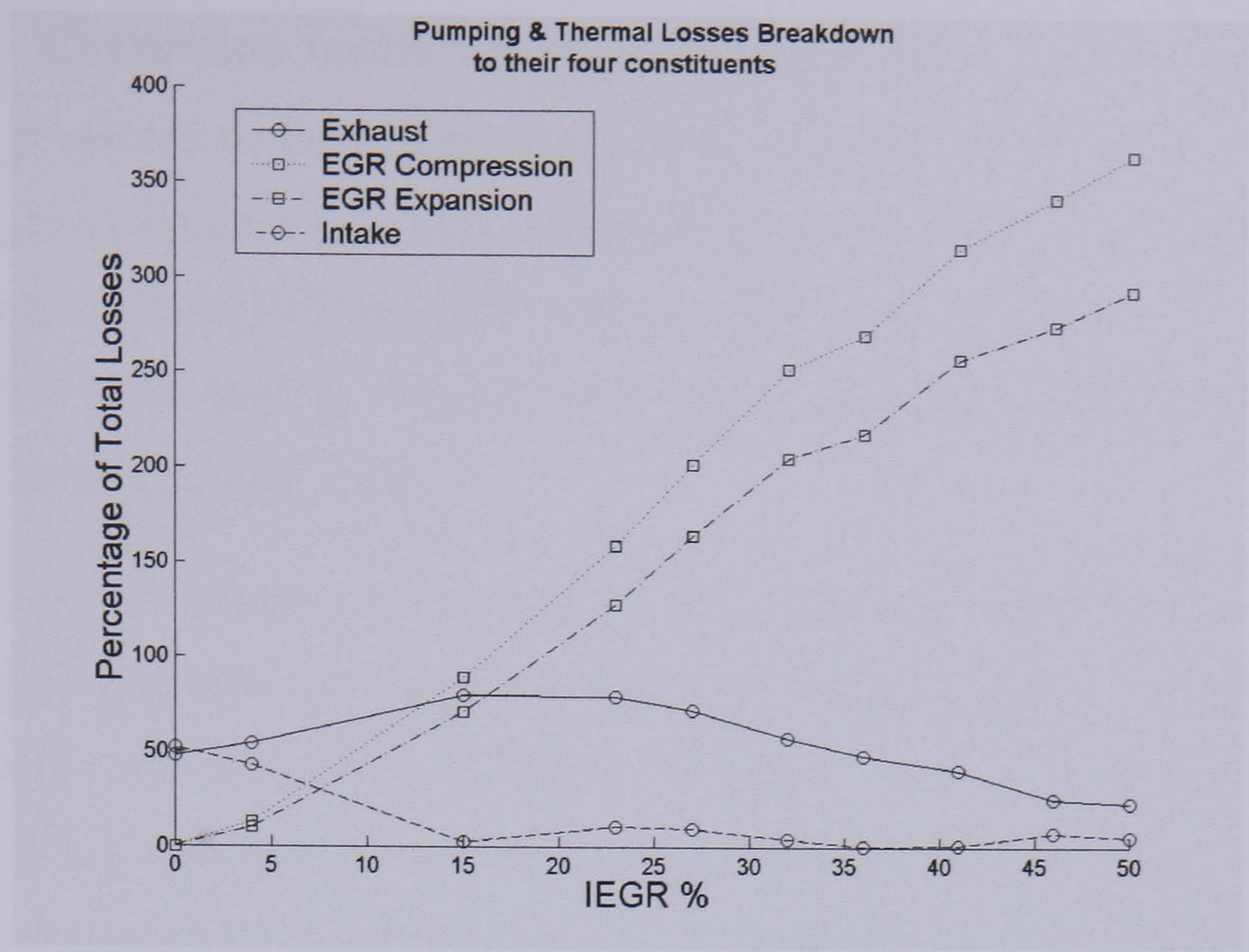

Figure 92: (Four processes of pumping cycle) Four processes of the CAI pumping cycle.

Secondly, interrogating the pumping loss during the engine exhaust process, it is noticeable that it increases as TRG increases up to the amount of 20%. Further increase of the amount of TRG leads to a decline in the pumping loss. This is due to the fact that as TRG is introduced, EVC starts to occur earlier thus the available period of time to expel the exhaust gases, between EVO and EVC, decreases. By decreasing it, the amount of time where maximum lift is present reduces as well. This results in the exhaust gases travelling through a tighter passage for a greater ratio of the time increasing the in-cylinder pressure during the exhaust stroke. However, as TRG is increased by trapping higher and higher amounts of TRG, the actual quantity of combustion gases that has to be expelled by the piston's movement (as opposed to the venting of the higher pressure in-cylinder gases into the exhaust) becomes small enough for the losses to start dropping below their equivalent SI operation value.

Thirdly and fourthly, examination of the thermal losses during compression and expansion of the TRG shows that increased TRG results in higher pressures during its compression. Although increased TRG results in lower temperatures at EVC, higher pressures result in higher "costs" both in terms of thermal losses and blow-by gases. So, despite the fact that expansion pressures increase too, the gap between the two constantly grows. Note here that the percentages, of each of these two processes, exceed 100% because the actual loss is the difference between these two values.

5.2.3.4 Correction factors implemented in CAI

The analysis presented so far is dependent on the assumption that pumping losses occur solely in the gas exchange cycle. This is indeed a reasonable approximation to make when a valve strategy of fixed IVC and EVC is being employed. In the case of these tests, the fixed IVC/EVO valve strategy was such that the volume changed less than 6% between the valve event and the BDC value.

This however is not necessarily the case in all cases, especially when considering the valve strategy of constant valve opening duration. In such a strategy, IVC and EVO can move arbitrarily close to the TDC of the combustion cycle. In the case of late IVC, this reduces the cycle's effective compression ratio. In the case of early EVO, it vents gases that could have provided work. In the case of the fixed duration tests in this research, the latest recorded IVC occurred in such a position that 15% of the total cylinder volume had already been swept.

Shelby et al [140] have proposed a mechanism for accounting for unconventional valve timings. While their work focuses on SI combustion, the concept put forward can be applied equally well to CAI.

Briefly, the technique rests upon the notion of how the measured cycle (of IVC after BDC and EVO before BDC) differs from a theoretical cycle where pressure has been adiabatically extended to a value it would have, had both IVC and EVO been moved to their respective BDC points. Shelby et al, identify two areas on the PV diagram as the EVO expansion loss and Incremental Compression Work, shown in Figure 93, for a typical experimental trace taken from the Lotus engine.

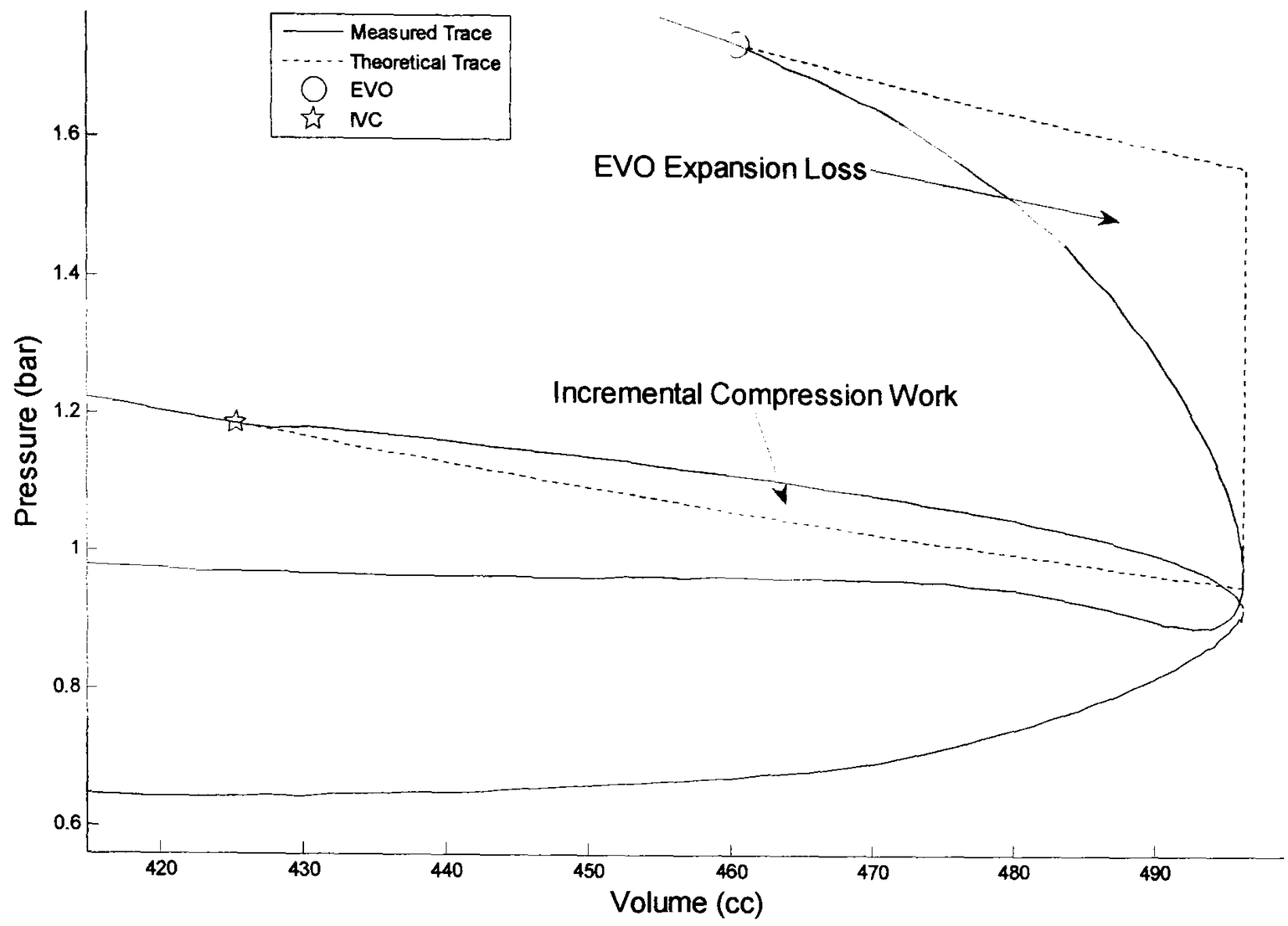

Figure 93: EEL and ICW.

The areas corresponding to EVO expansion loss and Incremental Compression Work are bounded between the measured and the theoretical traces in the EVC-BDC and BDC-IVC regions respectively. By conventional integration of the PV trace to get IMEPgross, these areas are implicitly excluded from the IMEPgross. However, they are both losses, in the sense that, had EVO and IVC occurred at their respective BDC points, IMEPgross would have been greater (theoretically following the dotted trace of Figure 93).

Shelby et al argue that, since these areas should be considered pumping losses, they have to be identified and added to the pumping losses (calculated by conventional integration over the gas exchange cycle), while IMEPgross has to be adjusted. In other words, if both EVO expansion loss and Incremental Compression Work are considered to be positive numbers:

$$IMEP_{adjusted} = IMEP_{conventional} + Incremental\ Compression\ Work + EVO\ expansion\ loss$$

$$PMEP_{adjusted} = PMEP_{conventional} + Incremental\ Compression\ Work + EVO\ expansion\ loss$$

Since these tests employ two different valve strategies, some measure of their respective performance is needed. The fixed IVC/EVO valve strategy by itself would not have needed a correction factor since the fixed timings are located close enough to BDC to make the correction effects negligible. The fixed duration valve strategy however must be

considered with more care, since, at least in principle; the valve timings can be located arbitrarily. To get a measure of the relative performance of the two strategies, the ratio of the adjusted values of GEMEP to IMEPgross will have to be considered. This is because the cycle's efficiency is more dependent upon this ratio than to either of its components considered individually.

This is demonstrated in Figure 94. In the top panel the GEMEP/IMEPgross ratio is displayed in the form of a percentage. This is split further into a solid line and two individual points. The fixed line corresponds to the data from the fixed IVC/EVO strategy and represents all points of constant IMEPgross across the TRG range of that experimental data set. The two points are included in the same graph for comparison and represent the fixed duration strategy. In the case of that experimental data set, IMEP is allowed to vary as TRG sweeps are executed across different RPM settings. These data are all sampled at WOT, load being regulated by TRG alone. For that reason, IMEPgross of 3.5bar requires considerable amounts of TRG and these operating points are close to the edge of stable CAI combustion. For that reason, only two cases of stable CAI combustion were encountered, at 2000 and 2500 rpm.

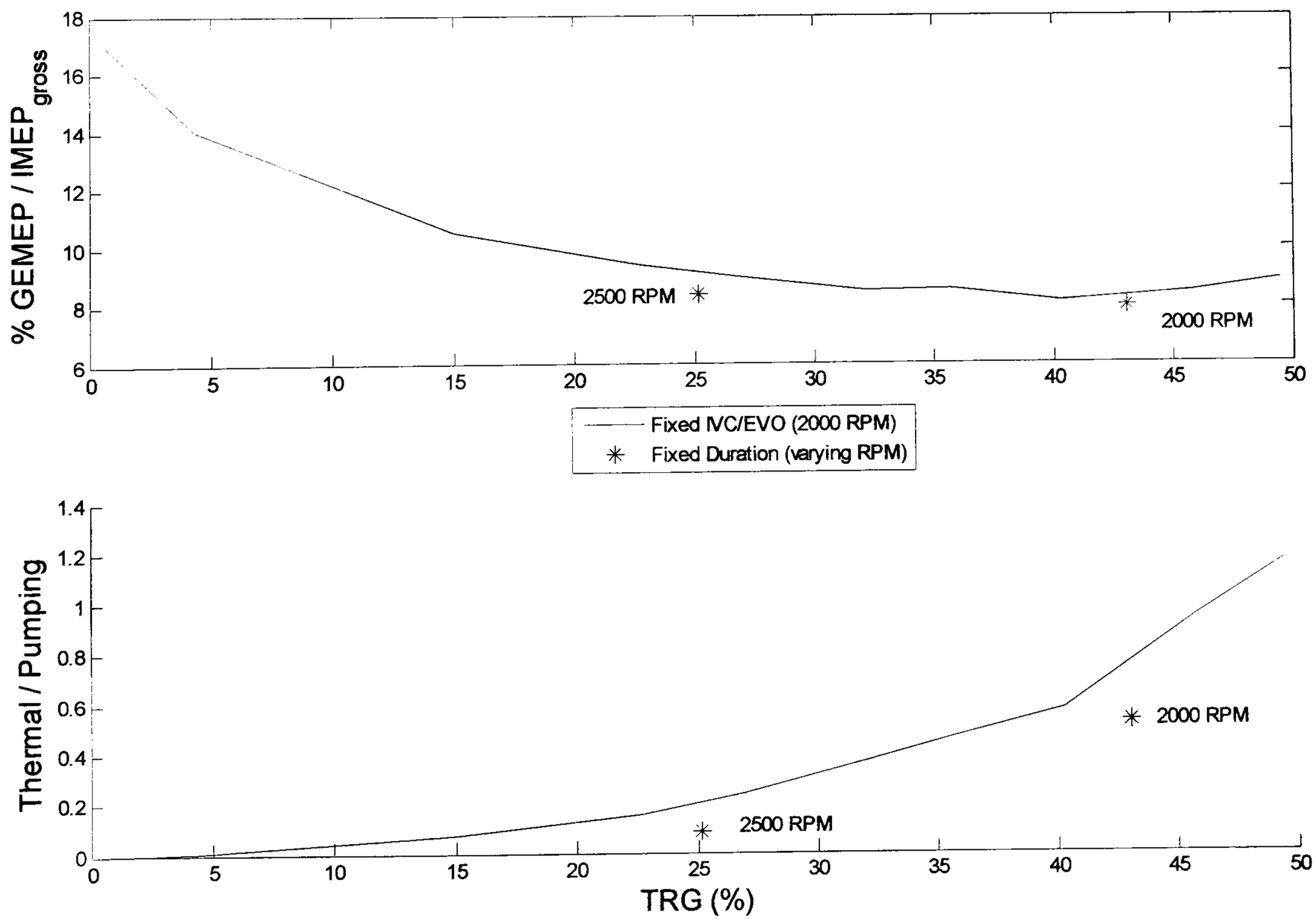

Figure 94: GEMEP/IMEP and Thermal/Pumping.

It is noticeable that, in the case of the fixed IVC/EVO strategy, the GEMEP/IMEPgross ratio decreases until approximately 40% TRG and then rises. This should be compared to Figure 89 which shows the overall trend for GEMEP and the associated MAP, which demonstrates how throttling needs to be applied in order to maintain constant IMEPgross. The same effects are in operation in this case: at low TRG, increased throttling increases the pumping part of GEMEP, reducing overall efficiency. As TRG is increased the pumping part of GEMEP is reduced, while its thermal part increases. Initially, this has no considerable effect but, after a point at approximately 40% TRG, the thermal part becomes significantly large to induce GEMEP efficiency deterioration.

In order to illustrate this effect, the bottom panel of Figure 94 displays the ratio of thermal over pumping losses. In this graph too, there is a marked trend for a sharp increase in the thermal/pumping losses after 40% TRG.

Moving on to the points belonging to the fixed duration valve strategy, the first thing to notice is that they are generally more efficient. This is due to the fact that they operate unthrottled; hence the lower TRG (higher engine speed) point exhibits the biggest efficiency benefit since points at that TRG level have a larger pumping component. Also, the TRG amount needed to keep IMEPgross to 3.5bar varies substantially between the two points, from 43% at 2000 rpm, to 25% at 2500 rpm. This is due to the fact that the volume based TRG value does not capture the gas dynamics which affect the actual TRG mass. When considering data at a single engine speed setting, this is not problematic, as is the case with the data in the fixed IVC/EVO strategy. When however, considering data spanning varying engine speed, then volume based TRG values might prove inadequate. In the case of the fixed duration strategy, where valve lift is also reduced to 3 mm, this is demonstrated by the great difference in TRG required to keep a given value of IMEPgross between engine speed settings differing by only 500 rpm.

The breakdown of the CAI gas exchange cycle into its pumping and thermal components gives the capability to evaluate one additional component of the ideal cycle. That is the one where the TRG compression and expansion performs as an ideal pneumatic spring of zero thermal losses. Since the CAI cycle at high TRG drastically reduces the pumping component, visualising such an ideal process for the TRG compression and expansion yields an upper limit on the performance benefits to be gained by reducing the thermal loss component of the CAI GEMEP. This is shown in Figure 95.

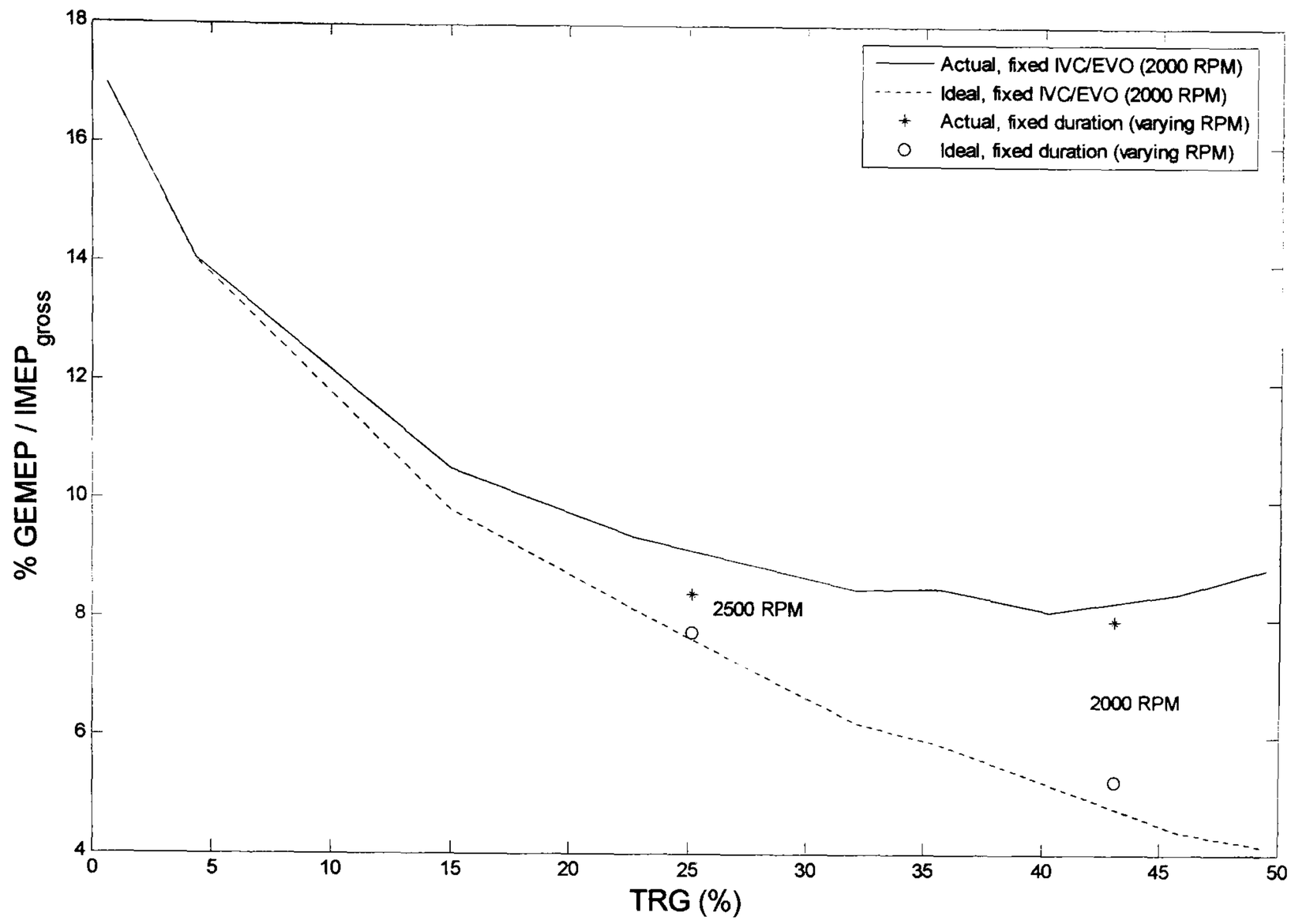

Figure 95: Actual and Ideal GEMEP/IMEP.

The graph shows the GEMEP/IMEPgross percentage ratio as a solid line, which presents the same data as in Figure 94. The dotted line presents this ratio but with GEMEP being represented by its pumping component only.

The worst possible performance occurs at SI operation, where GEMEP is made up of a pumping component only and has a value of 17% of the value of IMEPgross.

Looking at the fixed IVC/EVO strategy, the best actual performance occurs at 40% TRG, where ideal GEMEP is 8% of the value of IMEPgross. Even without considering the ideal performance, this represents a halving of the losses of the SI case, due to the fact that TRG load control allows throttleless operation at that level. The corresponding value of ideal GEMEP at that TRG value is 5%, yielding a performance benefit of 3%. The maximum ideal performance benefit occurs at 50% TRG where ideal GEMEP is 4% of the value of IMEPgross, yielding a performance benefit of 4%.

The fixed duration data exhibit very similar trends. Despite the fact that they are sampled at different engine speeds, TRG level appears to be the more strongly defining feature.

These data have slightly better actual values. As such, the ideal performance benefit for these is slightly less than the alternative valve strategy.

5.2.3.5 Conclusion

The core idea of the analysis is the fact that the gas exchange cycle of CAI only has a limited pumping component, the rest of the cycle being compression and expansion of TRG acting as a pneumatic spring, whose losses are mainly thermal. A methodology for the analysis of gas exchange losses has been put forward, by evaluating the two components separately. Thus, a more detailed understanding of the engine's operation can be gained. The main finding is that the pumping component is reduced by increased TRG levels, while it suffers by application of throttling.

The main difference of the two valve strategies investigated is that, in the case of fixed IVC/EVO, load was controlled by both TRG level and throttling, whereas in the case of fixed duration, load was only controlled by TRG level. Because of this difference, the fixed duration strategy appears slightly more efficient, as far as gas exchange losses are concerned, especially at the low TRG, where the pumping component is more prominent. However, the fixed duration strategy suffers from reduced effective compression ratio as TRG increases, due to the effects of late IVC. The operational range of stable CAI combustion suffers as a result.

It is the author's view that, to reduce the pumping component of the CAI gas exchange cycle, throttleless operation should be sought after by employing TRG for load control over as wide an operational region as possible. Furthermore, to ensure combustion stability, effective compression ratio must not be allowed to suffer, hence IVC must not be delayed beyond a certain point. The thermal component can also be reduced by striving to reduce heat losses when the engine operates at low load. Though the performance benefit from the reduction of the thermal component of the gas exchange cycle might not be considered substantial, the reduced heat losses at low load will benefit the combustion cycle's performance as well, while helping to maintain stability of CAI combustion by not allowing the average engine temperature to drop.

Having a basic understanding on the parameters that affect CAI, its engine speed range capabilities and its control variables, a move can now be made on evaluating real time control strategy possibilities.

6. SI Ion current

Electronic control with closed-loop feedback is a proven and efficient way to optimize the spark ignition engine performance and to control pollutant emissions [122]. Also, it has been shown that ion current signals can be used to estimate the in-cylinder pressure of an SI engine, when using the central firing spark plug as the ionization sensor [104].

In this research, two ion current sensors were used in addition to a spark plug. The spark plug was used only as a combustion initiator, and the ion current sensors were located on the opposite side of the combustion chamber. This configuration allows for the measurement of flame propagation speeds, since the timing of flame arrival at the sensors is possible.

6.1 Analysis of SI Combustion Diagnostics Methods Using Ion Current Sensing Techniques

The ion-current signal was initially measured using a single remote sensor, namely sensing plug (1). Figure 96 shows a typical measured cylinder pressure and a correlated ion current. The data are taken from a random single cycle, rather than from an average of cycles, however, the phase transitions are shown clearly. By comparing Figure 96 with the results obtained from the firing spark plug shown in Figure 44, it can be seen that there is a significant difference in the quality of the two ion current signals. One sharp spike is recorded during the first phase when a remote sensor is used, while no interference from the ignition circuit exist before that. The remote sensing plug detects the flame front as ion-current, caused by ionization within the gap of its electrodes, yielding this single sharp spike. Additionally, as the flame needs a certain time to propagate through the distance between the two plugs, the use of a separate sensor allows for this time to be measured as the delay between spark timing and the ion current spike.

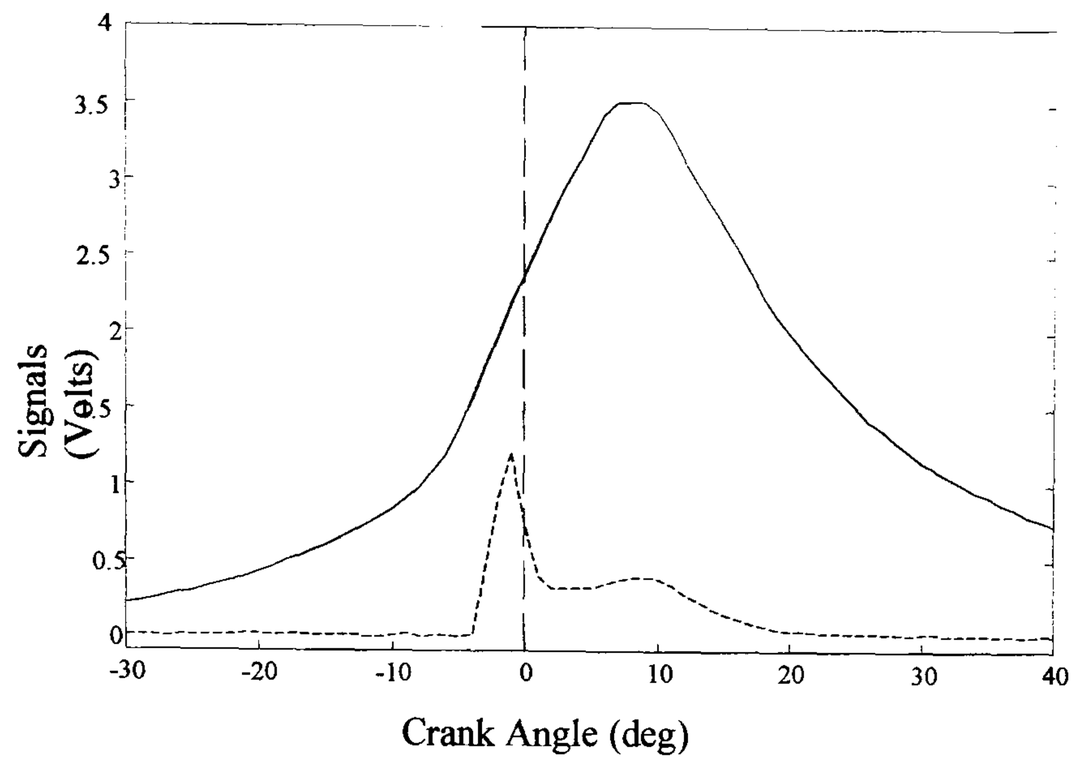

Figure 96: Single Plug Ion Current and Pressure Signals.

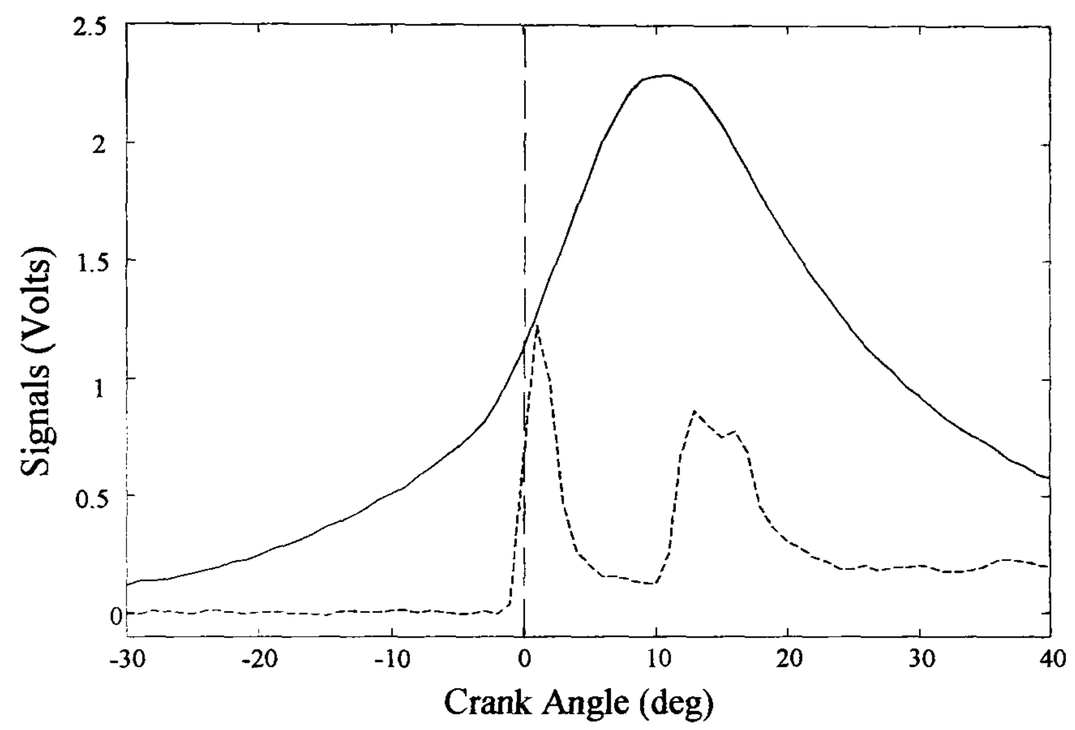

Figure 97: Twin Plug Ion Current and Pressure Signals.

It can be seen in Figure 97 that an additional spike appears between the original spike and hump, when both sensors are used. This is the result of the chemi-ionization ion current signal produced as the flame front hits the second sensor's electrodes. The post flame hump here is the result of the pressure rise after the flame has passed both sensors and thus contains less information.

Comparison of Figure 96 and Figure 97 show that whilst most of the combustion information can be obtained from the spikes, the use of two sensors gives a greater insight into the combustion process, and provides a wider diagnostic window because the signal strength of the second hump is increased. The drawback is that a shorter time window for the post-flame information to be collected is left. The use of a remote sensor provides a

great improvement over using the spark plug as the only sensor where more unstable and inconsistent data are recorded.

The results also show that the location of the remote sensor is important. Assuming that a flame ball is generated by ignition, if the ion current sensor is located at a given radius from the spark plug, the same result will be recorded (in a symmetrical combustion chamber). It is also important to note that the use of a single, or two remote ion-current sensors, presents a marked improvement over the use of sensors embedded in the cylinder head gasket. This is because head gasket sensors might potentially overlay the first ion-current spike and the post flame data. Thus, it is better to locate a sensor in between the ignition site and the flame out site. These effects are described further in the following section.

6.1.1 Misfire

Misfire detection is a major subject of on board diagnostics (OBD). Conventional crankshaft speed fluctuation sensing does not guarantee misfire detection at high engine speeds and low load conditions. This method is particularly poor for multi-cylinder engines where the effect of misfire of a single cylinder on crank shaft speed is masked by the frequent combustion events of the other cylinders. The potential of ion current sensing for misfire detection has already been reported [141,142,143,144,145,146], and this study confirms that when misfire occurs the ion current signal and its integral are zero, while under any other combustion condition they are non-zero. This is demonstrated in Figure 98 where cycles 1 and 3 are misfired. Although, the signal shown here was obtained using one remote sensing plug, identical behaviour was evident with two remote sensing plugs.

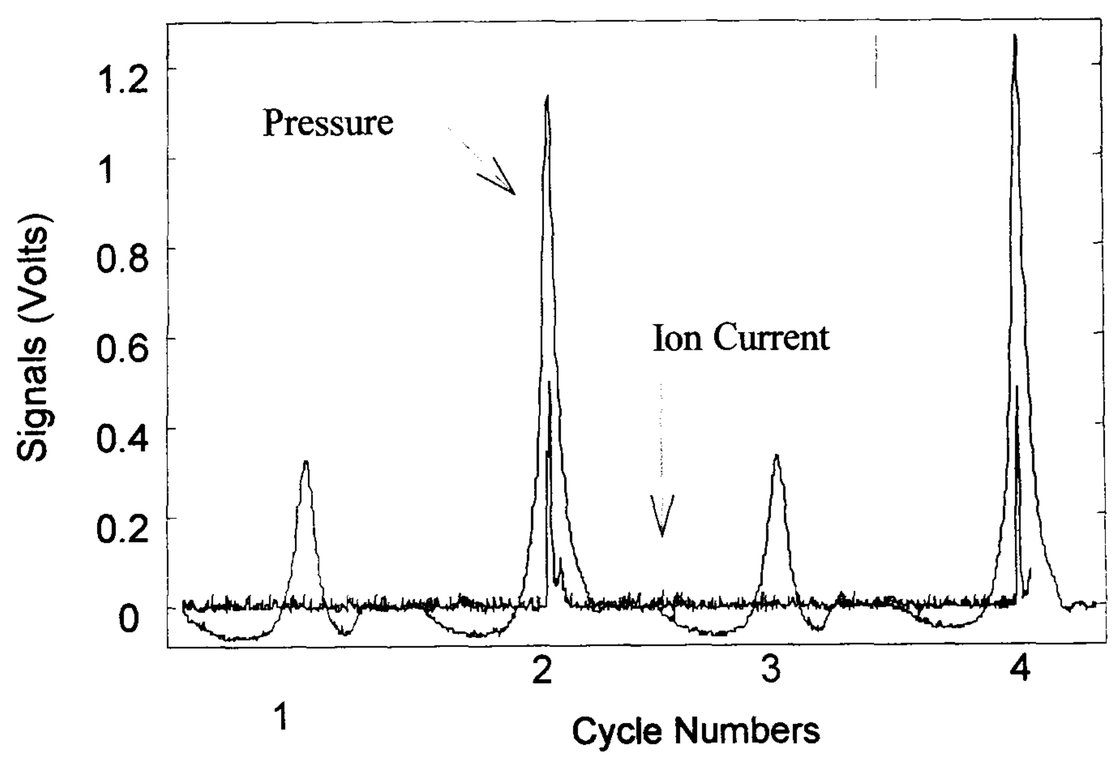

Figure 98: The Misfire Effect on Ion Current.

6.1.2 Ignition timing

The effect of the ignition-timing advance on both pressure and ion current can be seen in Figure 99. Advanced timing results in higher in-cylinder pressures and earlier first spikes of the ion-current signals since the flame propagates earlier. The flame starts earlier but also travels faster due to the increased pressure build-up. Again the number of sensors used is not critical in this application, since most information is given by the location of the starting point of the signal. The only advantage of recording from both sensors is slightly increased precision.

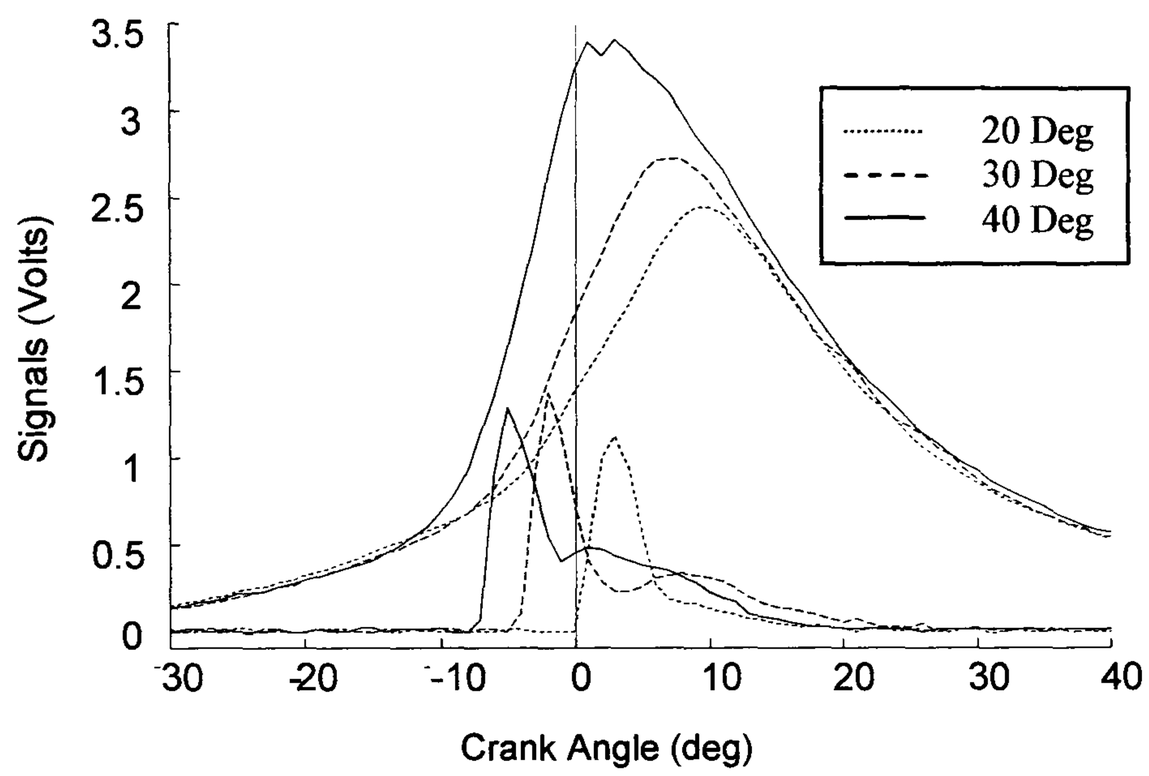

Figure 99: Ignition Timing Advance Effect on Ion Current at 1500 rpm, 50% throttle, 50% load and lambda=0.9.

6.1.3 Air to fuel ratio

Research on air to fuel ratio estimation via ion current has been a hot topic [147,148,149,150,151,152] and closed loop control systems using it as a feedback signal have also been proposed [153,154,155,156]. In the plots shown in Figure 100 and in Figure 101, a comparison between the pressure and the ion current signal under different AFR values is shown using data that was averaged over ten cycles using a single sensing plug. It can be seen that there is a very good correlation between pressure and ion current at each air-fuel ratio.

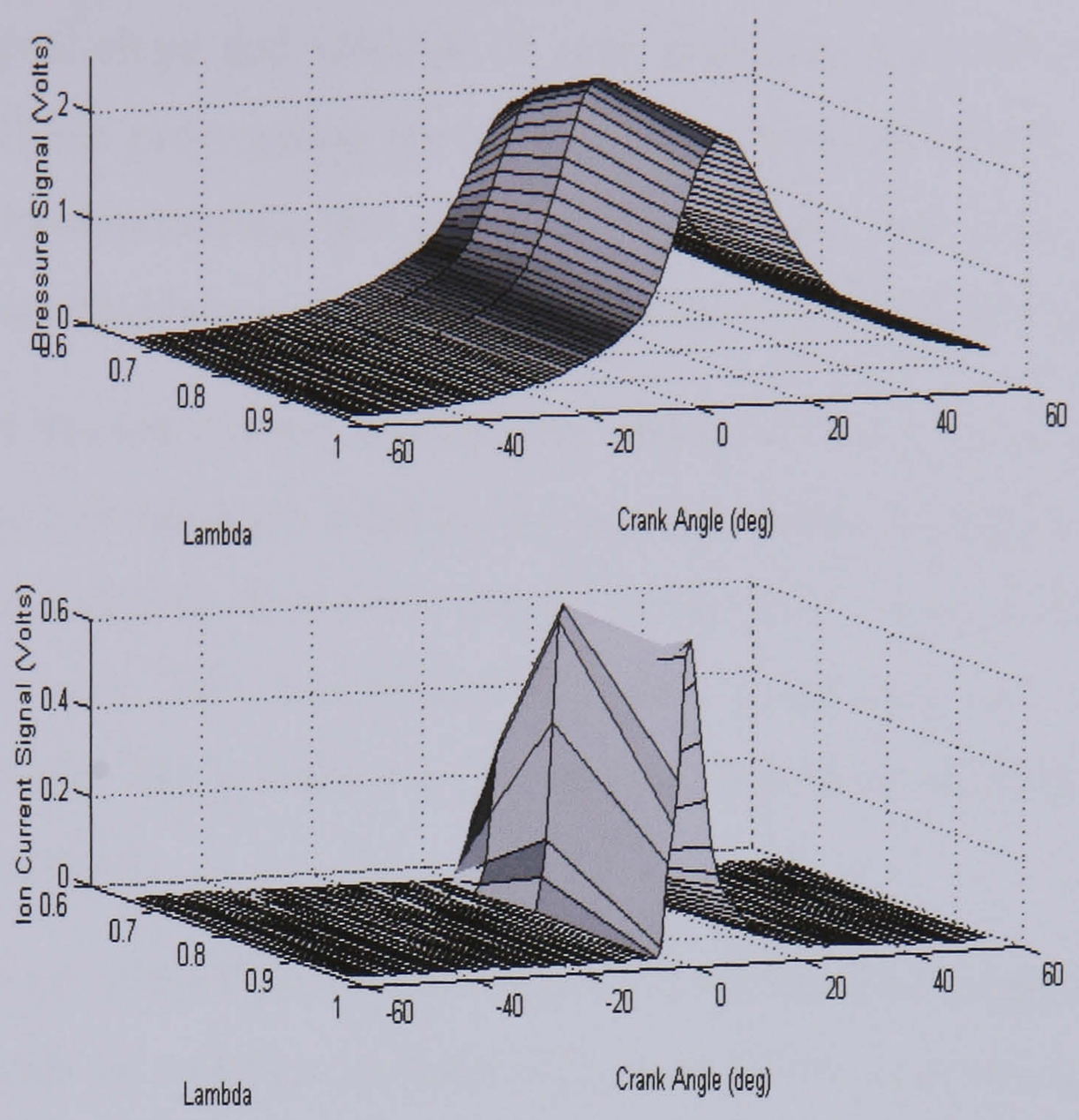

Figure 100: AFR swept from rich to stoichiometric at half load and 1600 rpm.

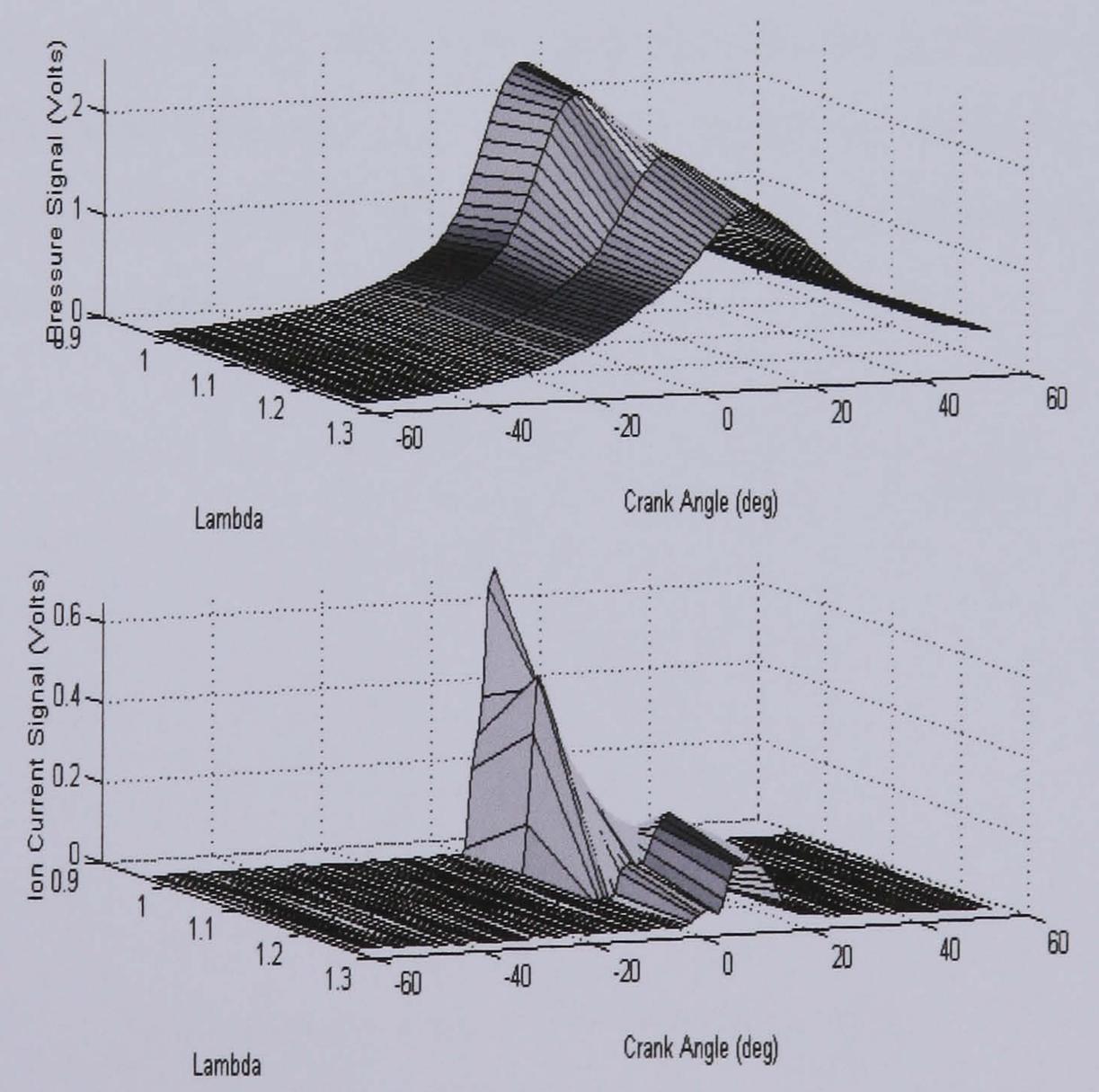

Figure 101: AFR swept from stoichiometric to lean at half load and 1600 rpm.

In Figure 100, the AFR was swept from a value of λ=0.65 to 1 at half load while the engine speed was held constant at 1600 rpm and the ITA was 30 deg. In the second case, (Figure 101), the AFR was swept from λ=1 to 1.26 under the same engine conditions.

The location of start of ion current signal and peak ion current position are interdependent of the pressure signal slope and location of peak pressure, since all of these parameters are a function of flame propagation speed. Where mixtures burn fast (at AFR's that are slightly lean of stoichiometric), the positions of the start and peak ion current occur earlier, but very lean (and hence slow burning) mixtures have the greatest delays.

The magnitudes of the ion current signals also correlate with the magnitudes of pressure signals. The mildly rich mixtures produce the highest values for ion current and pressure signals. The signal strength decreases at both richer and leaner AFR's. For very lean mixtures, as with any low in-cylinder pressure condition, the Post-Flame phase disappears. What looks like a second hump on the signal from the leanest mixtures is in fact very late combustion.

Previous research has identified that the behaviour of the first slope of the ion current signal is an indicator of mixture strength [33], and this is confirmed by the results in Figure 102 where the AFR is plotted against the first ion current slope. Each of the seven slope values is an average over sixty cycles under the same AFR conditions. The trend is for the ion current signal to peak near to a stoichiometric AFR and decrease for richer or leaner mixtures. Further research is required to establish whether the ion current sensor could replace an oxygen sensor, but it is clear that the ion current signal can provide feedback for individual cylinder fuel trims in order to equalize cylinder air/fuel imbalances. The impact that such a strategy will have on the efficiency and emissions of production vehicles is considerable.

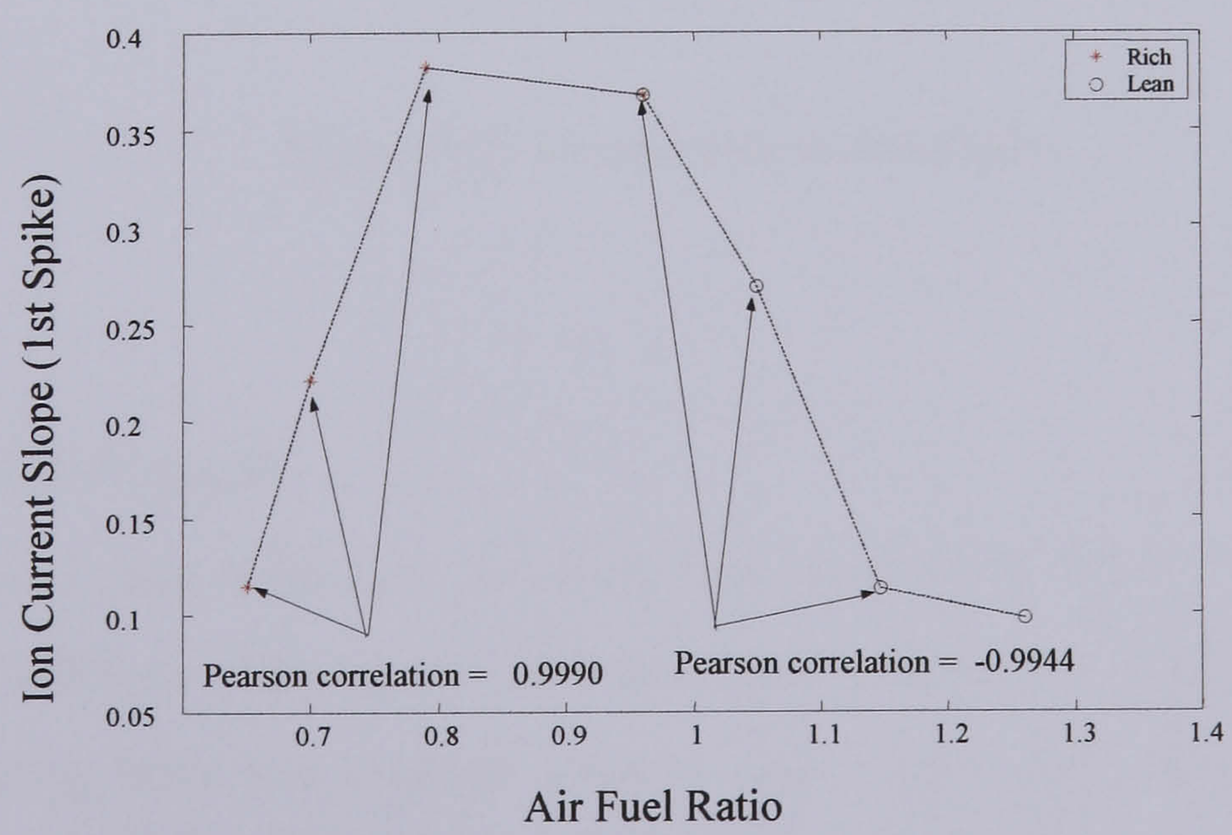

Figure 102: Relationship between the slope of the first Ion Current spike and Air-Fuel Ratio.

6.1.4 Compression ratio

Both sensors were used to acquire the data shown in Figure 103. The engine was run at half load and 1650 rpm, with the ITA at 30 deg BTDC and an air fuel ratio of 0.95. Figure 103 shows plots of the in-cylinder pressure and ion current signal for different compression ratios. As the compression ratio drops reducing the flame propagation speed, the start of the ion current signal is delayed, and the peak pressure is also reduced and retarded.

It is important to note that the engine was rebuilt between each test in order to vary the compression ratio. The reduced compression ratio would have affected the engines thermodynamic efficiency, but this was not compensated for in the experiments.

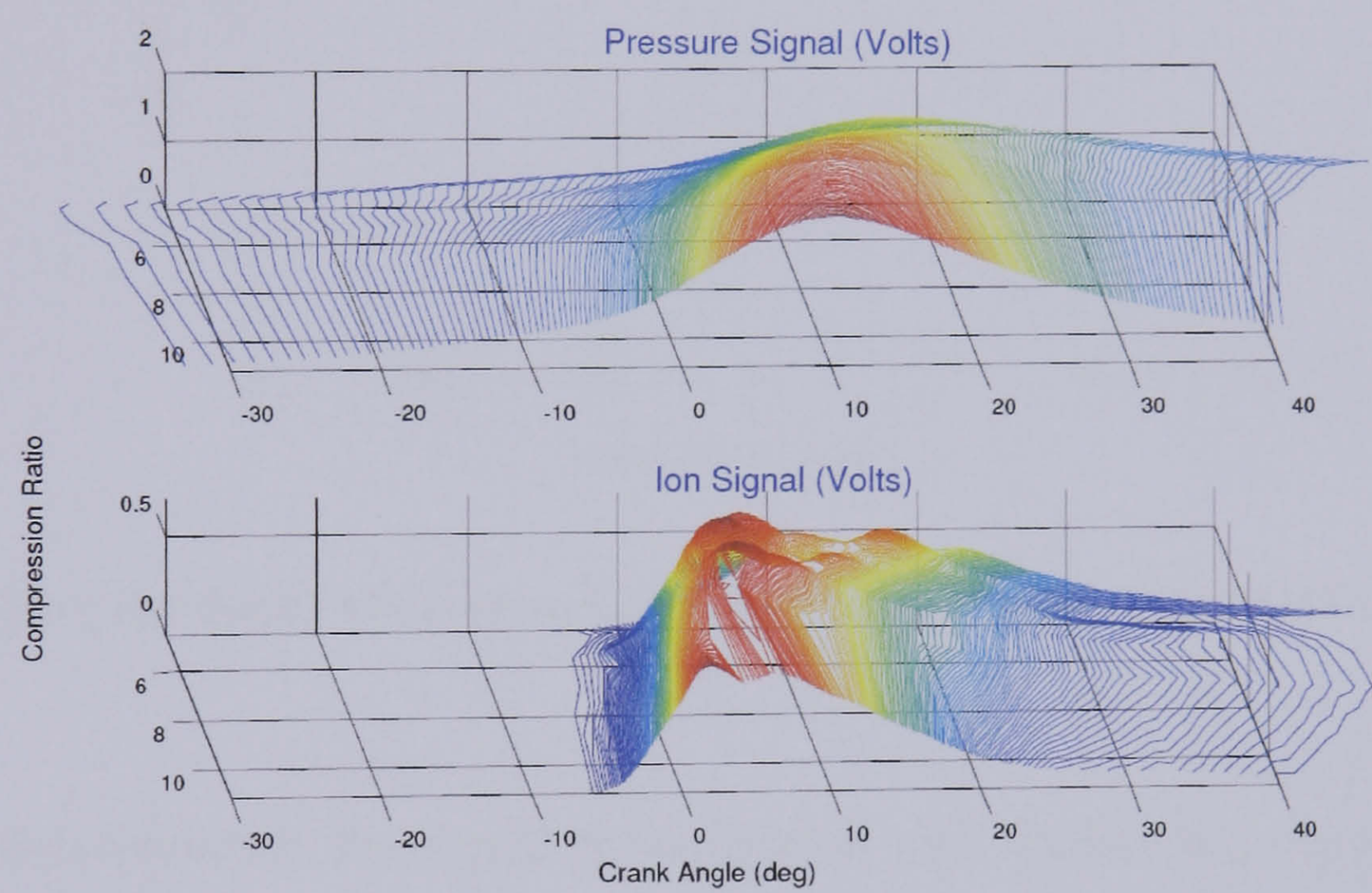

Figure 103: Compression Ratio Effect.

6.1.5 Load/Speed

For the load/speed data collection the load was swept from 0% to 100% and the speed from 1000 to 3000rpm. The air to fuel ratio was held at 0.9 lambda, ion current was recorded by using both ion current sensors and Figure 104 shows that as the load increases the pressure increases and the peak cylinder pressure occurs earlier. The ion current signal also increases and the maximum point appears earlier, but only up to about 75% load. After this point the ion current signal continues to occur earlier but starts to fall in magnitude.

This effect was also observed with a singe ion current sensor, and no easy explanation for this phenomenon is available since the ion formation process is not yet fully understood.

6.1.6 Knock

In order to induce knocking conditions, the engine was operating at 1500rpm, full load, 0.9 lambda and ITA 65 degrees. The effect of knock on the ion current signal can be seen in figure 12, where data is presented from the use of two sensing plugs.

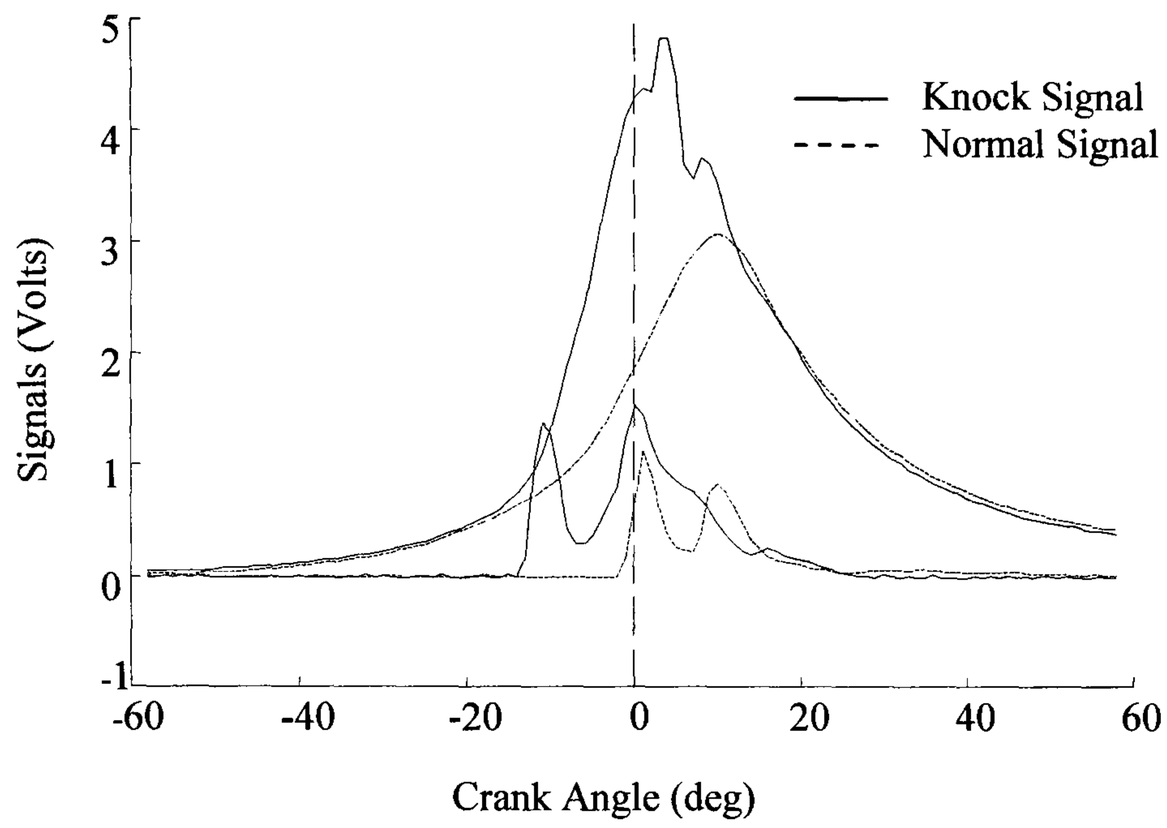

Figure 104: Knock effect on ion Current at 1500rpm, WOT, full load, ITA = 55.

As previously mentioned, the signals were sampled once per two degrees crank angle, but during knock, the oscillations within the cylinder are in the region of 5 to 10 kHz [109]. Nyquist theorem states that when sampling at a given rate, the highest frequency that can appear in the reconstructed signal is half the sampling frequency. So when sampling an analog signal, the sampling rate must have twice the frequency of the measured signal's highest frequency. Sampling at every two degrees our sampling frequency was 4500 kHz, in other words one sample per 2.2×10^{-4} sec. To capture even the lowest frequencies of knock it would have been necessary to have at least a sampling frequency of 10000 kHz, or one sample per 1×10^{-4} sec. Consequently, the typical knock frequency is too high to be accurately represented by our signal and what is recorded here are gross pressure fluctuations.

Nevertheless, the effect of knock on ion current is clear. The starting point of the ion current measurement is greatly advanced, as has already been noted in the ignition timing section. Also visible is that the measurement is higher and that the second ion current

spike is greater than the first. This does not happen in normal combustion, as can be seen on the normal cycle trace (Figure 44). It occurs during knock because the pressure when the flame travels through the second plug's tips under knock is much higher than when going past the first plug. Temperature and pressure are higher during knock, and as the end gas detonates in the later phases of combustion at the same time that the post-flame signal is recorded, the result is superimposed on the second spike, increasing its magnitude. Knock has a measurable effect even at low sampling rates, which implies that the knock sensor can be substituted by an ion current sensor. This has also been put forward by researchers using the firing plug as an ion current sensor [157].

6.1.7 Transient operation performance

The pressure and ion current signals recorded during acceleration are shown in Figure 105, where the engine was accelerated from 1000 rpm to 4000 rpm at full load.

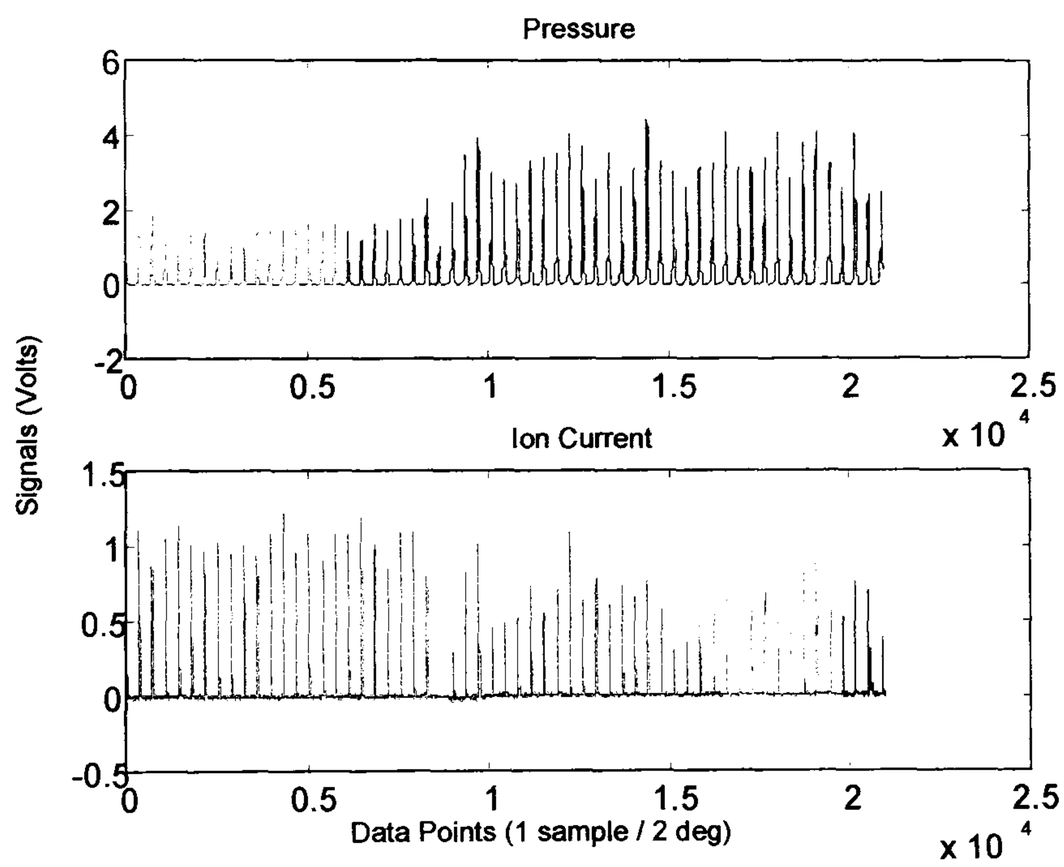

Figure 105: Pressure and Ion Current signals recorded as the engine was accelerated from 1000 rpm to 4000 rpm at full load.

In the data logs of Figure 105, the engine was kept at idle until the 0.8 x 10^4 data point, and then the throttle was suddenly fully opened. It is particularly interesting to note here that although the pressure increases after that point, the ion current drops. This is largely due to the mixture leaning out momentarily at the sudden opening of the throttle, but it may also partly be due to the effect noted in the load/speed section where the magnitude of the ion current signal drops above three quarters load. It can also be seen that misfire occurs at the point where the throttle is opened. This is due to fuel condensation in the inlet manifold and to inability of the carburettor to sustain stoichiometry during transients.

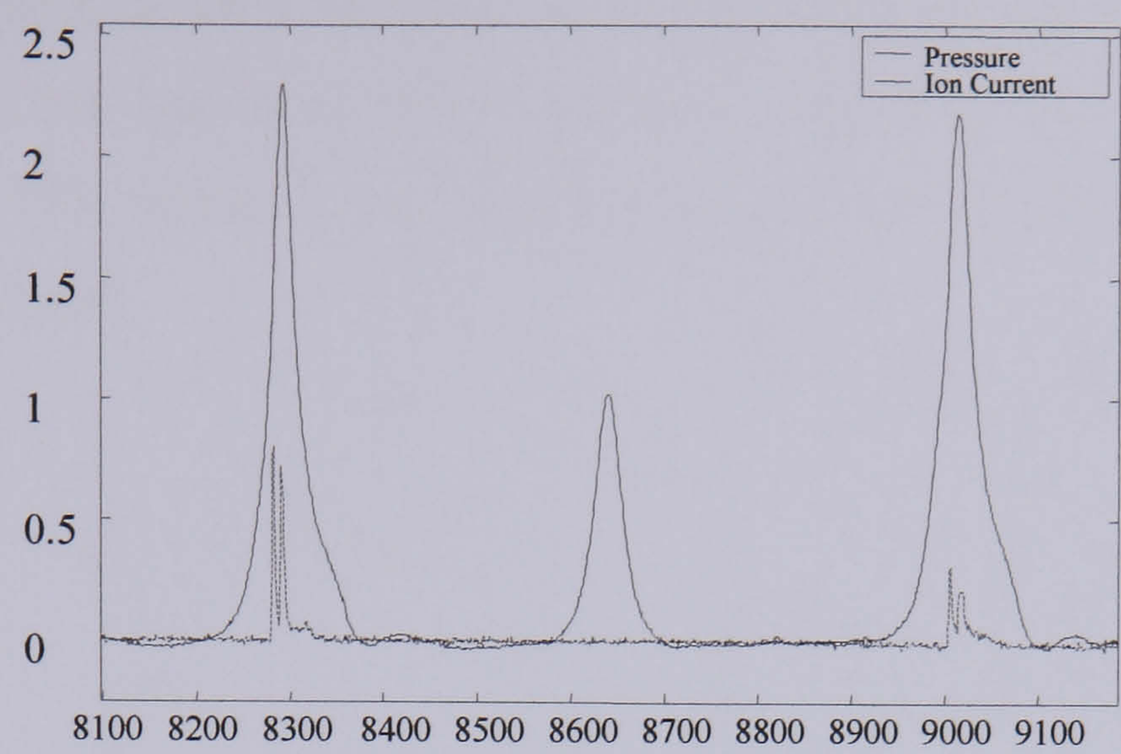

Figure 106: Acceleration Misfire Detail from Figure 105.

Figure 106 is an enlargement of data taken from Figure 105 over the cycles where misfire occurs. It can be seen that the ion current signal is absent on the misfired cycle and weak on the cycle occurring directly after the misfire. A log obtained during deceleration is shown in Figure 107. The engine was decelerated from 4000 rpm to idle speed at three quarters load.

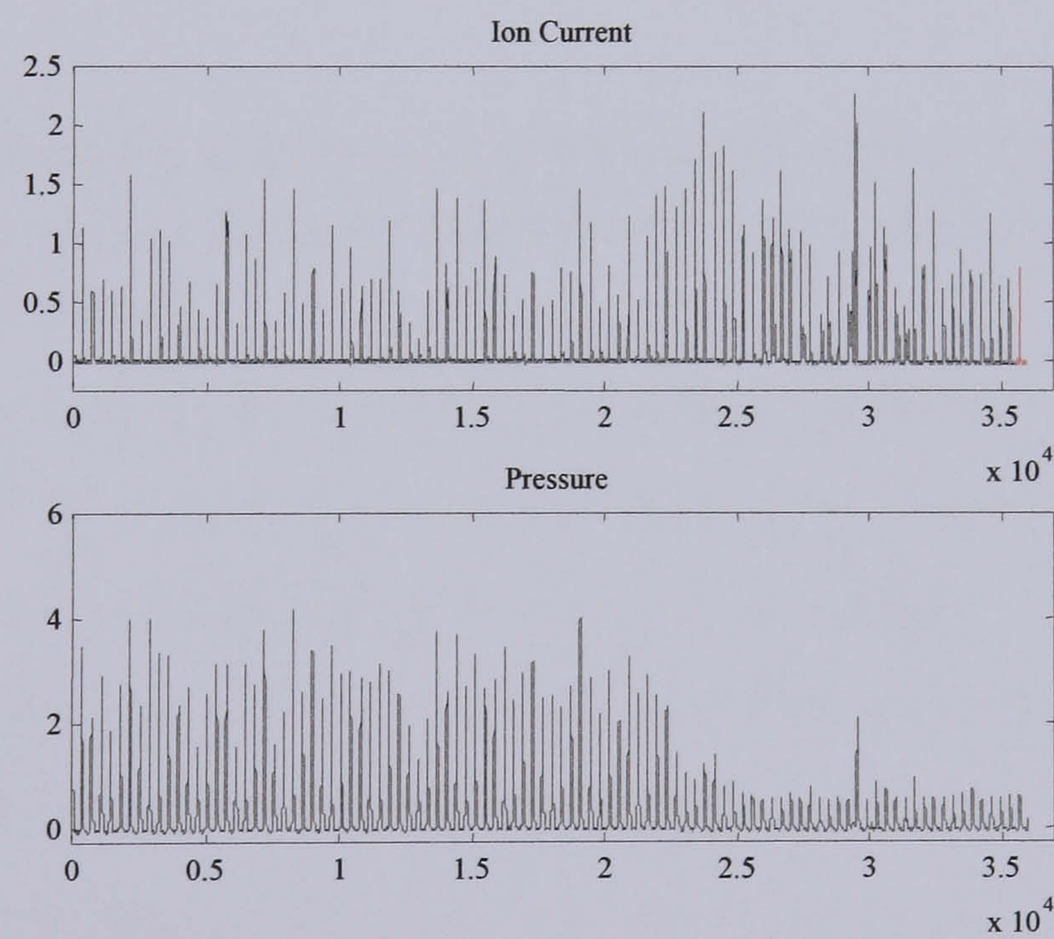

Figure 107: Pressure and Ion Current signals recorded as the engine was decelerated from 4000 rpm to 1000 rpm at three quarters load.

It can be seen that the behaviour of the ion current signal is exactly the opposite of the behaviour shown during acceleration. Again, misfired cycles occur as the throttle is shut off due to momentarily over-leaned air-fuel mixtures. Figure 107 also illustrates that the correlation between ion-current and cylinder pressure is very close in the x direction, but

is much more complex in the y direction as during transient performance, as the cylinder pressure decreases, ion current actually increases. This may be partially understood by examining Figure 108, where it can be seen that the mixture actually ignites after the exhaust valve is opened.

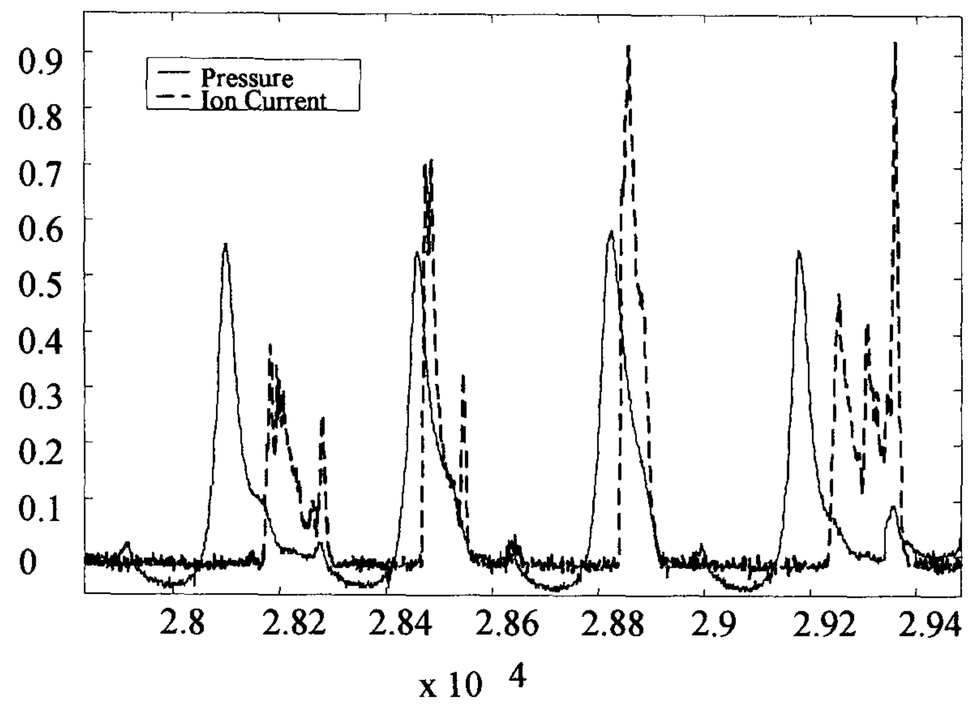

Figure 108: A detail of the deceleration log showing misfired cycles where the mixture ignited at EVO.

6.2 Computationally Inexpensive Methods of Ion Current Signal Manipulation for Predicting the Characteristics of Engine In-cylinder Pressure

Preliminary understanding of the combustion attributes can be achieved by examining the signal characteristics as described above. In order to be able to extract more detailed information, some post-processing of the signal is needed. In this section a brief description of how the signals were analyzed and the portions of the signals (called handles here for convenience) that were used to extract useful information is given.

After examining the relations between the ion current and cylinder pressure and investigating the characteristics of these two signals, Artificial Neural Network (ANN) techniques can be used to deduce the cylinder pressure information from the ion current measurement and knowledge of the operating conditions. To reduce the implementation difficulties, a simple and computationally inexpensive Adaptive Linear Element (ADALINE) type of network is chosen for this purpose. Then the networks are trained with a number of data sets for different operating conditions. The trained networks can deduce the cylinder pressure information required for engine monitoring and cycle-to-

cycle closed-loop engine control from the ion current measurement and the operating conditions such as speed and load. To verify the effectiveness of the proposed techniques, experiments are designed to compare the deduced pressure yielded by the networks using ion current measurement with the actual in-cylinder pressure.

ANNs have been used before to interpret ion current signals [158,159,160,161]. These are most commonly of the Perceptron type, a standard ANN for general usage. ADALINEs are networks widely used in industrial applications too; however their use for ion current interpretation has not been witnessed by the authors in the relevant literature. ANNs offer a promising tool for this type of task, however, for the reasons outlined in section "Artificial Neural Networks", that can be found later in this chapter, ADALINEs are chosen as the best candidate.

6.2.1 Signal Interpretation

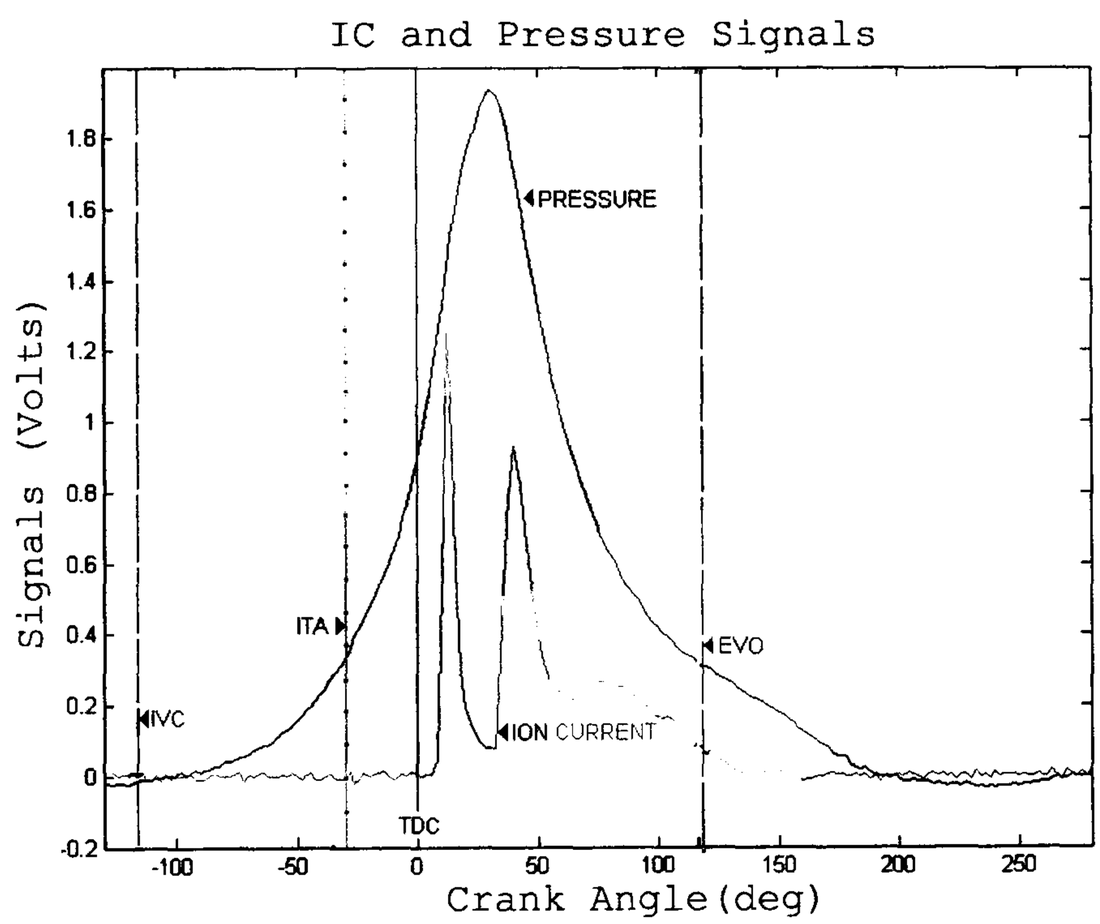

Figure 109: Closer look at pressure and Ion Current signals.

In Figure 109 the leftmost vertical line indicates Inlet Valve Closing (IVC). The next line indicates Ignition Timing Advance (ITA). The line at x-axis zero indicates Top Dead Centre (TDC). The rightmost line indicates Exhaust Valve Opening (EVO).

One point to consider is how signals from two sensing plugs create a single trace. The circuit used simply adds up the two signals so what is seen is the sum of the ion current on both plugs. This would lead one to expect the second spike to be heavily affected by

the post-flame phase, since both measuring plugs are registering at that time (whereas for the first spike, the flame has only reached the first plug), degrading its information content. This, however, is not the case. Figure 110 shows a close up of an ion current trace with only one measuring plug and the engine operating highly throttled so as to minimize the post flame hump. These are the conditions that create the most problems when measuring from the firing plug, as is the usual practice. Hellring et al mention that "the post flame peak essentially vanishes if the load is less than 20% of the maximum load" [109]. It is evident from Figure 108 and Figure 109 that the first spike only lasts for about 10 CA degrees. The post-flame phase is missing completely since ionization due to compression of the gases is low owing to the low load conditions. Employing remote sensing eliminates the dependence on the post flame signal. Employing two remote sensors adds further signal information.

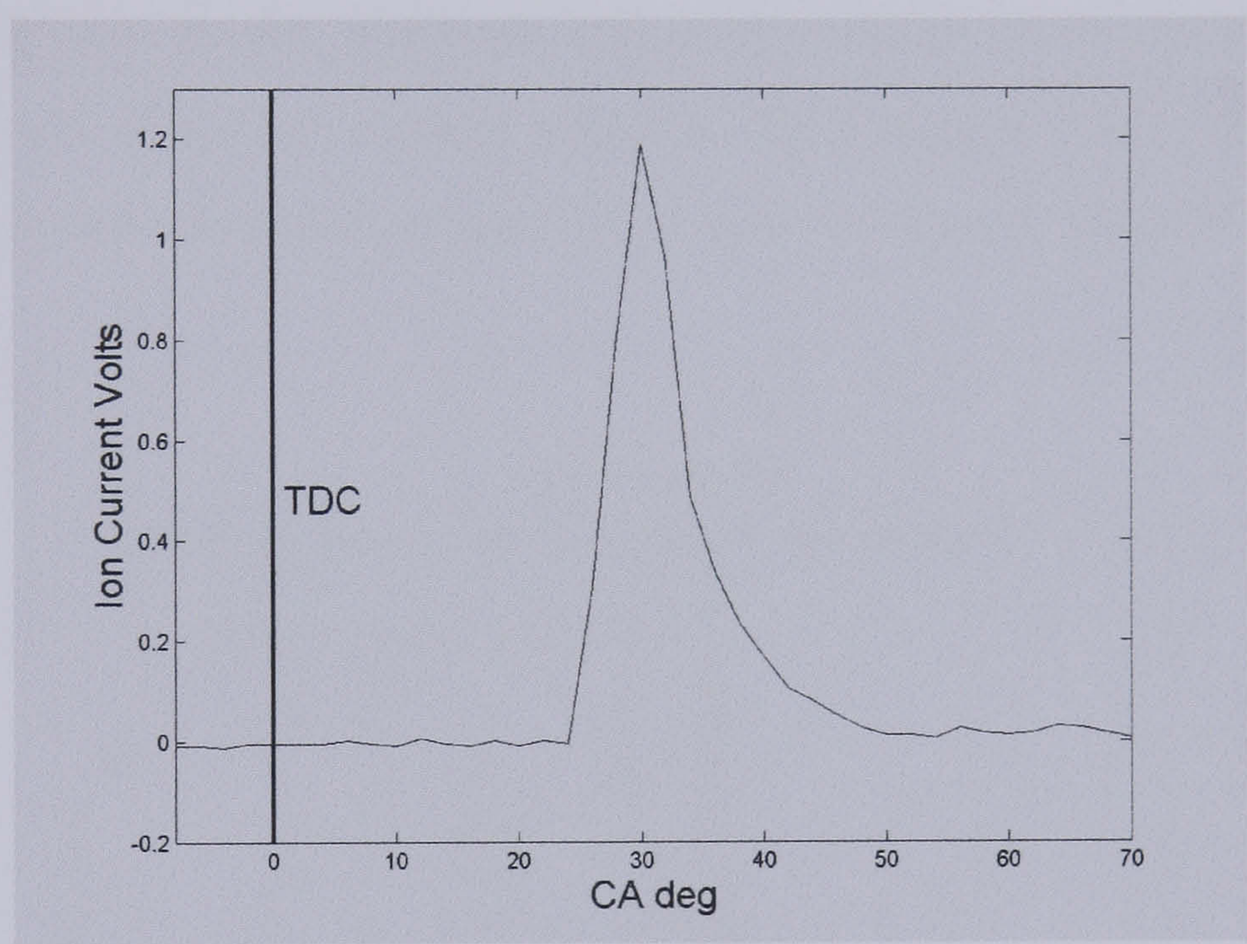

Figure 110: Single plug trace.

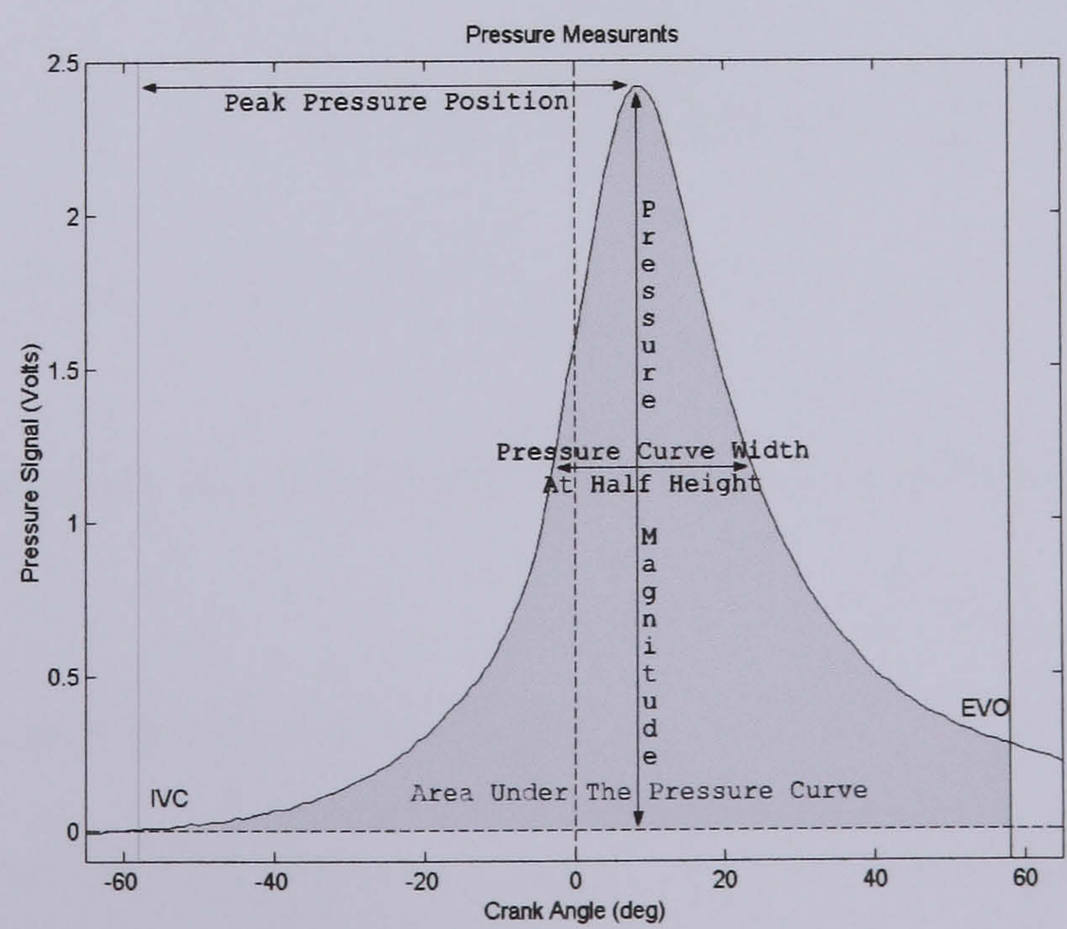

Figure 111: Diagram of relevant pressure signal handles.

For the curve integration, the start and endpoints are taken at the point where the inlet valve closes (IVC) and the exhaust valve opens (EVO) respectively. For the given engine, IVC was 116 degrees before the combustion TDC and EVO 116 degrees after it. Hence, the areas of the pressure curves quoted in this report are all between these two points.

The pressure handles, as shown in Figure 111, with their names and their units are:

1. The position of the signal peak – measured in CA degrees after IVC
2. The magnitude of the signal peak – measured in signal Volts
3. The width of the curve at half its height – measured in CA degrees
4. The area under the curve – measured in CA degrees by signal Volts

For the ion current signal curve integration, the start point is taken as the point where the signal rises above noise levels, while the end point is taken as the point where the signal drops to noise levels. If the ion current signal is still strong at EVO, then this is taken as the end point since any combustion after EVO will not have a considerable effect on the pressure.

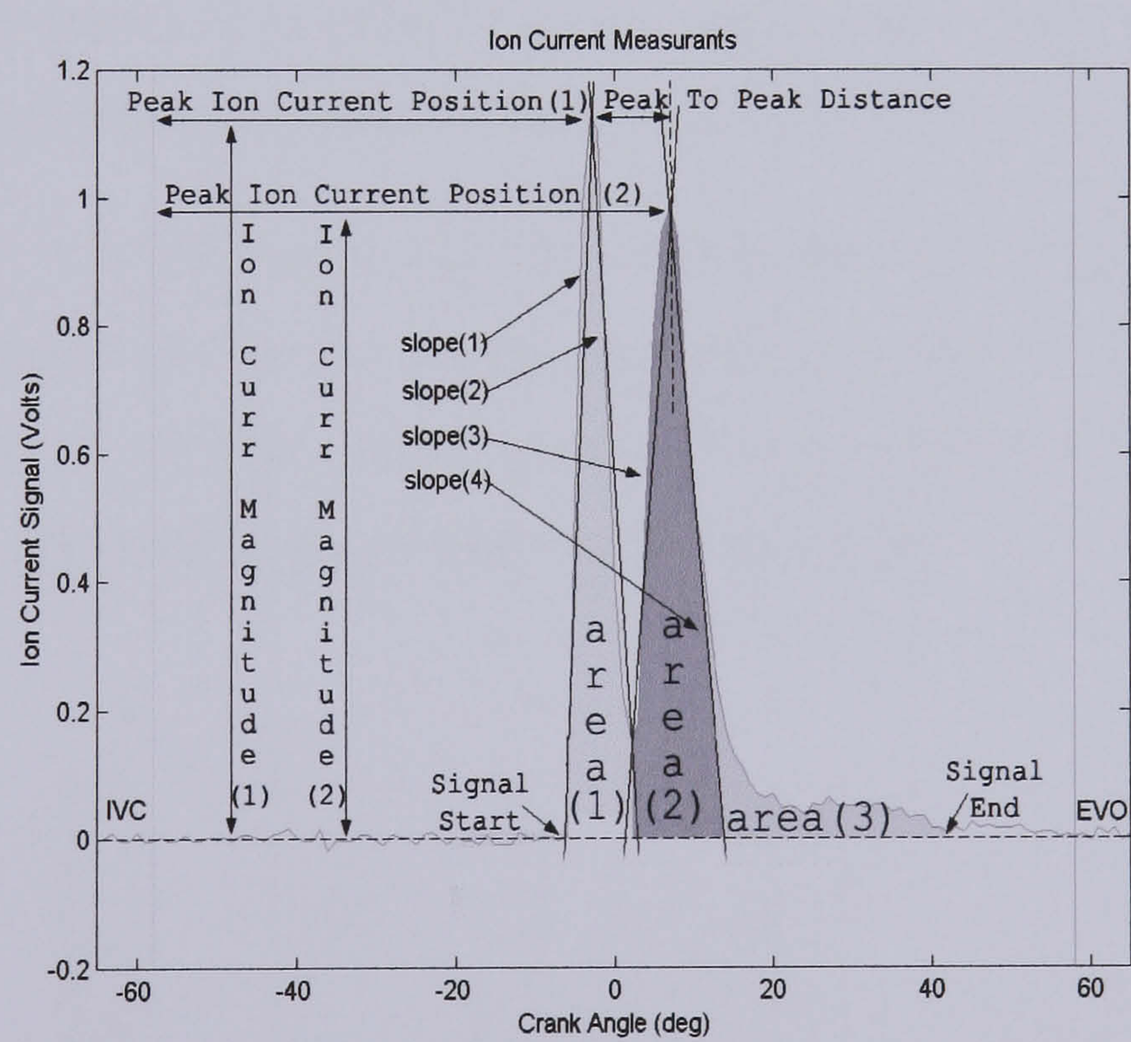

Figure 112: Diagram displaying ion current signal measurants.

The most useful ion current signal handles are:

1 The position of the first point of a signal – measured in CA degrees after IVC, and the difference between the two peaks

2 The positions of the first and second spike peaks – CA degrees after IVC

3 The magnitude of both spikes – Volts

4 The three areas under the different regions of the signal –CA degrees x Volts

5 The four slopes of the spikes – Volts / CA degrees

After comparative tests, these measurants were chosen as carriers of adequate information to describe this signal. Of these, the various x-axis positions proved the most useful, since they are related to flame development. However, all selected measurants contribute in increasing the accuracy of the results.

6.2.2 Feature Relations

Given the measurants extracted, the easiest way to look for relations is to plot them against each other. Ideally, a strong relation between an ion current measurant and one or more pressure measurants will settle the case in favour of ion current. However, things are not that simple. There are conclusions to be drawn by averaging over a number of cycles which is the technique used routinely in treating such signals. These however are not helpful when it comes to developing a tool which should, in practice, be able to help control cycle-to-cycle engine operation which is the aim of this investigation.

Figure 113, Figure 114 and Figure 115 show some cases of strongly related measurants. Ion Current measurants are on the x-axis, pressure measurants are on the y-axis. These data are logged over a varying compression ratio loop, therefore each data point batch corresponds to a compression ratio between 4.5:1 and 11.2:1.

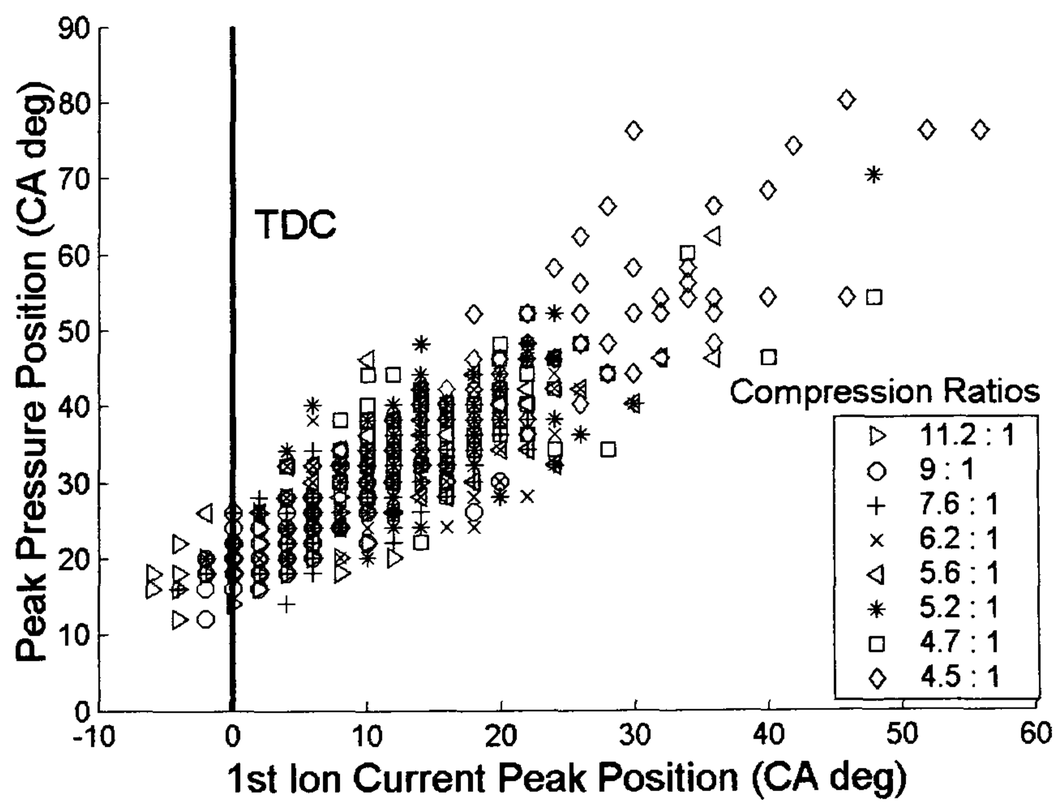

Figure 113: Relationship between 1st ion current peak position and peak cylinder pressure position.

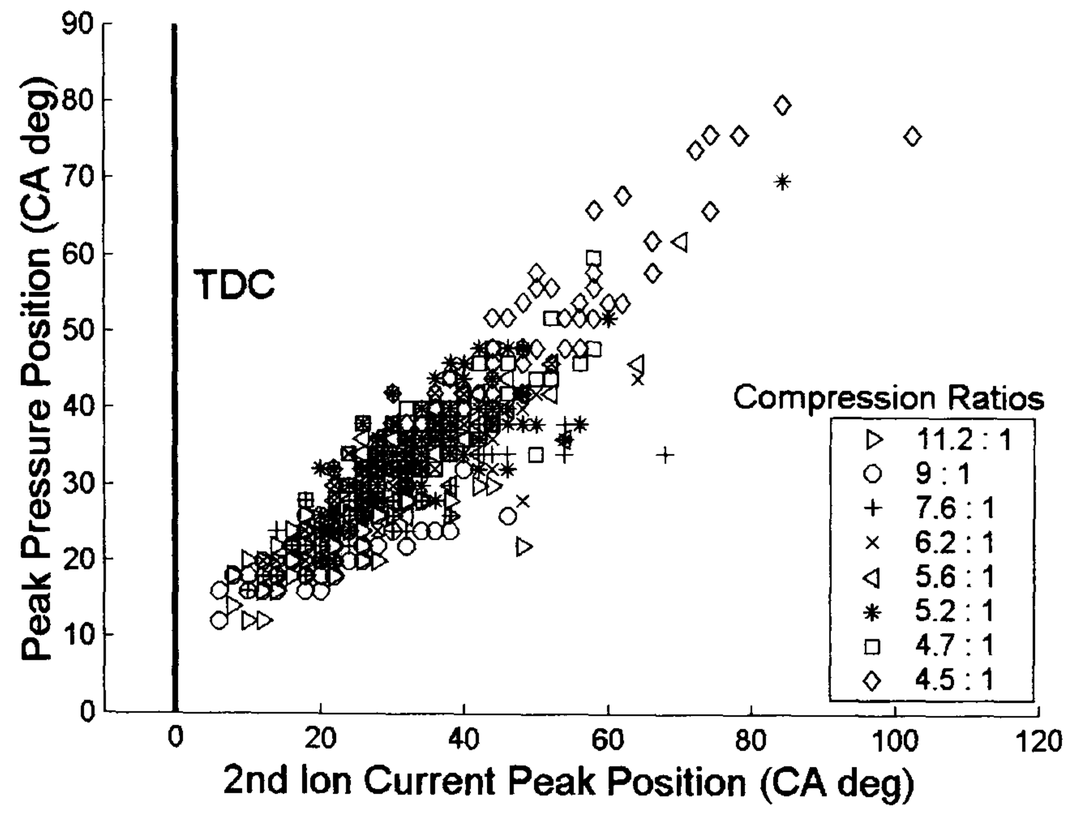

Figure 114: Relationship between 2nd ion current peak position and peak cylinder pressure position.

Figure 113 and Figure 114 are matches for the Peak Pressure Position (PPP) with the positions of the first and second ion current spikes respectively. It shows good correlation with both measurants and that a delayed combustion event results in a late pressure peak position. Another point to notice is that delayed combustion results in a greater uncertainty in PPP. This is due to delayed combustion being more unstable, resulting in higher cycle-to-cycle variation.

Figure 115 is a match between peak pressure magnitude and the position of the second ion current spike. It can be seen that the second peak ion current position has a strong relationship with the peak cylinder pressure magnitude, too. When the second ion current spike occurs late, the flame reaches the second sensing plug late which indicates late combustion. Therefore the peak cylinder pressure magnitude is reduced.

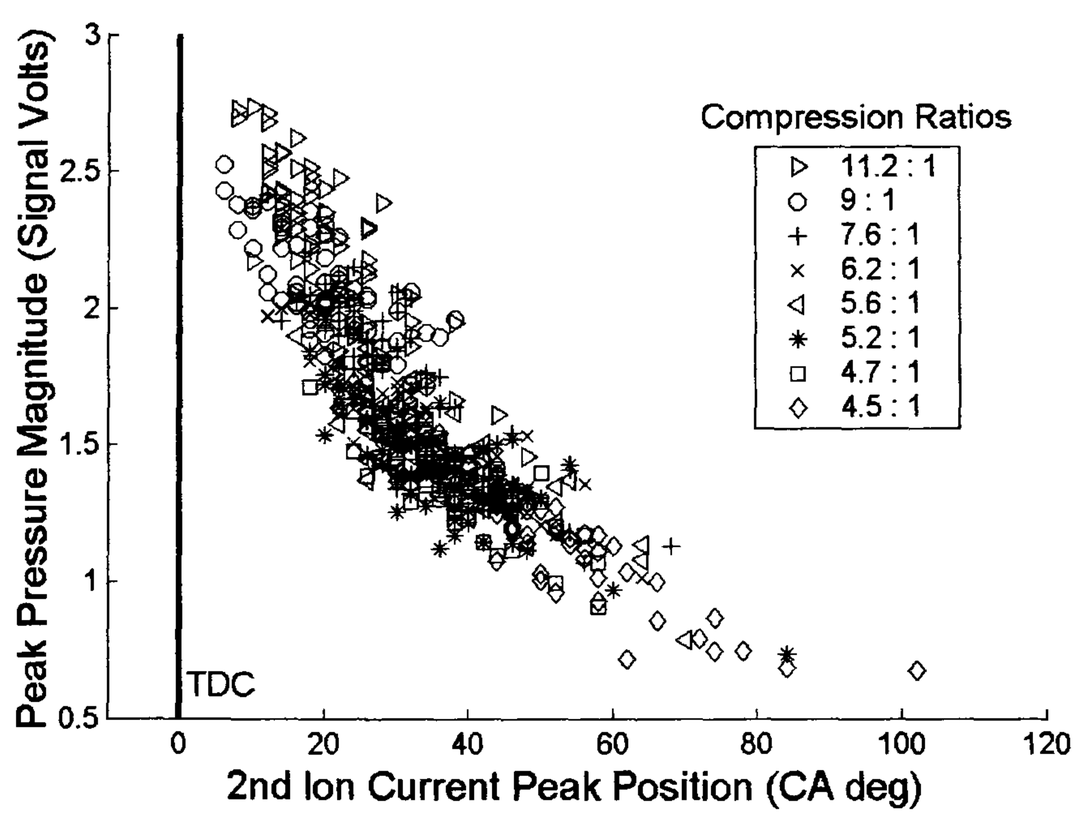

Figure 115: Relationship between 2nd ion current peak position and peak cylinder pressure.

Although the relationships between the first and second ion current spikes with the combustion event are strong, as can be seen in Figure 113, Figure 114 and Figure 115, there is an uncertainty of the order of 10 CA degrees relating to the peak pressure position and of the order of 0.4 Volts relating to the peak pressure magnitude. These uncertainties are not be acceptable for engineering implementation of using iron current as an alternative means of measuring the cylinder pressure. For this reason, a more sophisticated strategy has to be developed and employed for ion current signal interpretation in order to improve its correlation with the pressure signal.

6.2.3 Artificial Neural Networks

Artificial neural networks are a good candidate for tackling this kind of problem [150,110]. These are computational constructs, used in a variety of applications for dealing with complicated inputs. The notion behind them is loosely modelled on real neural networks. Each artificial neuron is a node that takes a number of inputs. These are weighed and then summed as illustrated on the left hand side of Figure 116.

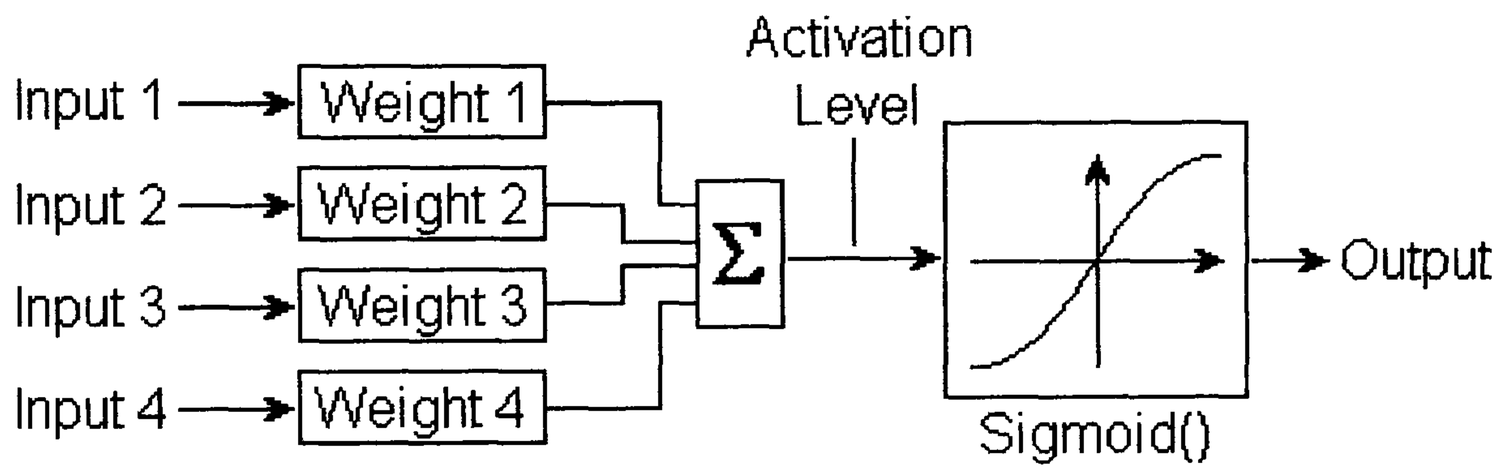

Figure 116: Schematic representation of artificial neuron.

The idea is that, an input with a strong relation to the output will have a relatively big weight associated with it. Thus, fluctuations in important inputs will result in significant changes to the weighted sum.

Finally, the weighed sum is then passed through a transfer function to give the final output. There are various traditionally used transfer functions, some of which are shown in Figure 117.

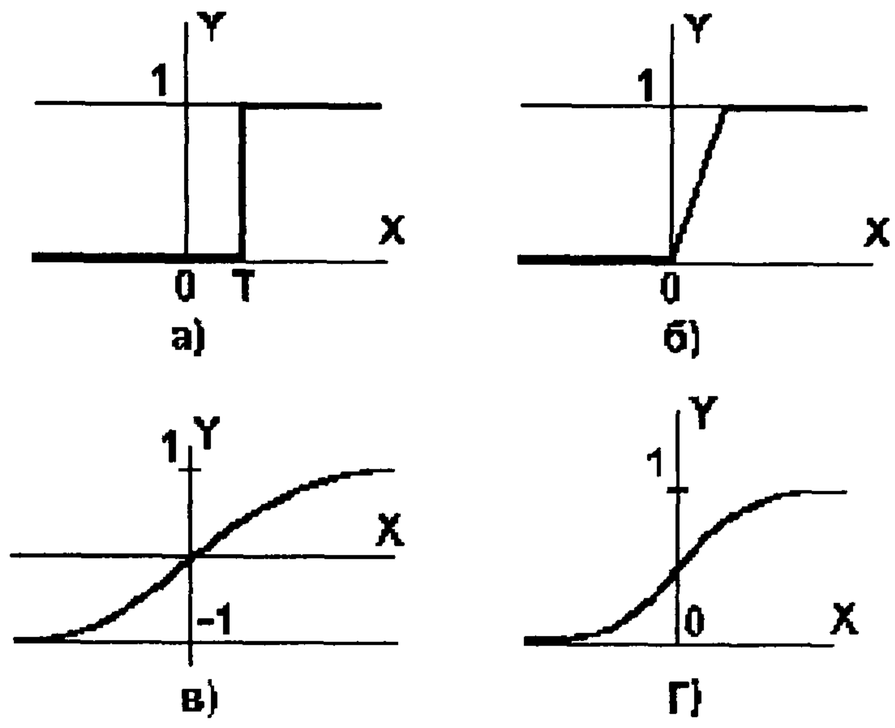

Figure 117: Sample transfer functions.

Their role is to "summarize" the inputs of the neuron into a value. The simple form of the top left is a step function which basically translates to on and off states for the artificial neuron. All the rest are variations on the same theme, making a smoother transition so that information is not lost in the grey area where the weighted sum does not translate clearly into the on or off areas.

A collection of artificial neurons is what is termed the artificial neural network as illustrated in Figure 118. The inputs are taken in by the input layer of artificial neurons. These are then processed through successive layers until they reach the final "output" layer.

The main tasks when designing an artificial neural network is to decide upon the architecture best suited for the task, e.g. number of layers and type of transfer functions and then tune its parameters, e.g. the various weights. There are many different types of training algorithms for this task. Most of them are recursive where a network is presented with successive sets of inputs, small alterations are made each time according to its response compared to the desired values until at some point tuning is decided to be adequate for the task.

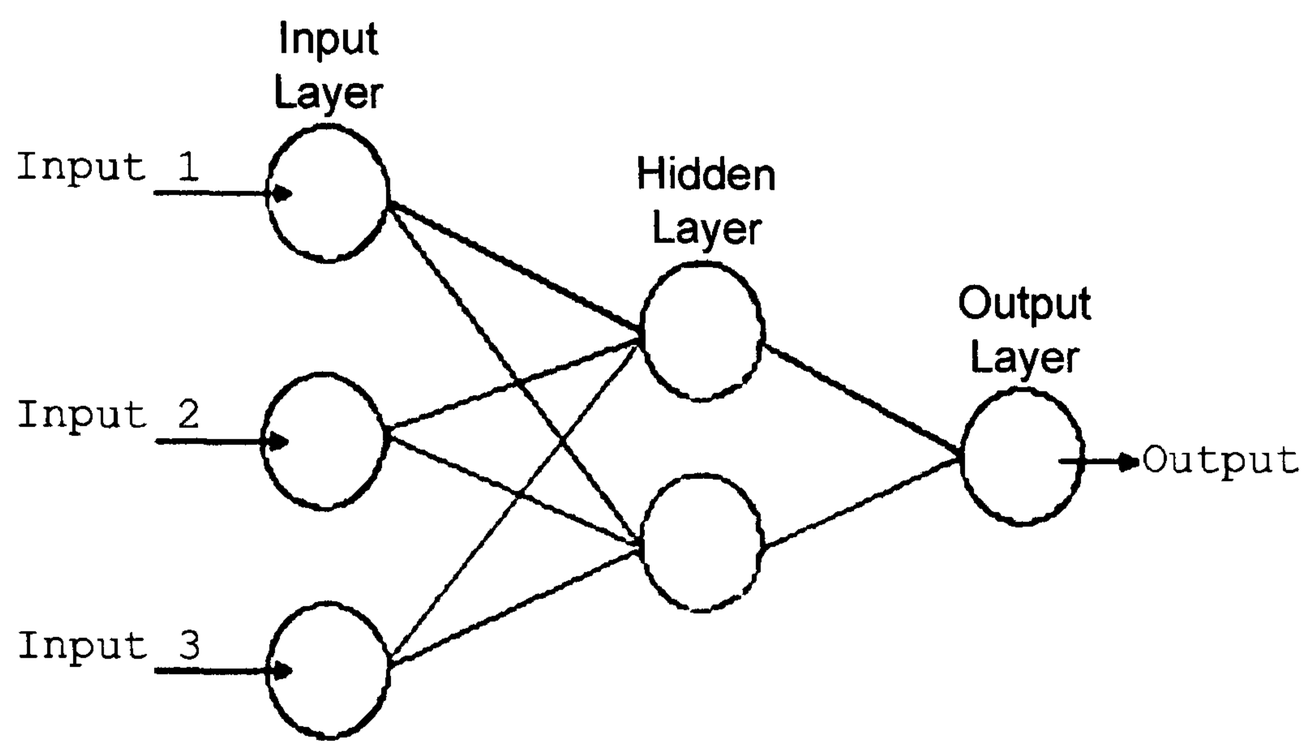

Figure 118: A simple artificial neural network.

In the case of this experiment, the following considerations are taken into account:

First, the network has to be as uncomplicated as possible. If the model is to be usable on a cycle-to-cycle basis by an engine controller, all computations have to be completed fast enough to provide timely results for the next cycle for every cylinder. The simpler the network that does this, the less demand there is on the signal processing electronics that will carry out those computations.

Second, the network or some further algorithm behind it must produce continuous output. This is important as the measurants are numbers that cannot be represented by an on/off state. To code for such using step transfer functions requires a large amount of output artificial neurons for each output.

Third, the network must be easy to train with a reasonably small amount of data. In engineering applications, it is impractical to require a vast amount of data to train a neural network due to the cost and time needed to collect these. The goal was to use as low as 70 combustion events per engine operating condition.

There are several network families to choose from. Keeping the above points in mind, ADALINEs were chosen. These adaptive linear elements are among the classic types of artificial neural network. An ADALINE neuron takes a weighted sum of its inputs but, instead of passing it through a transfer function, sends it straight to its output. This is also helpful for producing continuous output since a single output artificial neuron can produce any real value. The main limitation of ADALINEs is that they will tackle linear relations but will not be very useful beyond these. Looking at the data in Figure 113, Figure 114 and Figure 115, both linear and non linear relationships are indicated.

However, the window of engine operating conditions tested is strongly exaggerated compared with normal operation. Despite this and the fact that linear approximations were used, the obtained results are well within the scope of closed loop engine control implementation. In addition, the range of operating conditions spanned by a production engine is such that the data produced would be in relations even more adequately modeled as linear.

Finally, for training purposes, ADALINEs can be trained using the Least Mean Squares (LMS) algorithm. This is a very important consideration given the low data volume requirement. The strength of the LMS algorithm lies in that it competently handles this case where the data is limited. The way LMS trains the network is as follows: given a set of inputs and a set of desired outputs, the error is defined as the difference between the actual and the desired output. LMS minimizes the average of the sum of the square of these errors. Since this is a quadratic function, it will have at most one minimum. Thus, for a given set of inputs, LMS will tune the network so that their averaged squared errors are minimized. In this research, two sets of networks have been developed and tested. To test these, some data sets were set aside and used afterwards to assess performance under unknown inputs.

6.2.4 Measurant Predicting Network

The first network is the smallest one in terms of artificial neurons. It is a layer of four artificial neurons (ADALINES are single layer networks), each one of which takes the thirteen ion current measurants as inputs and produces one of the predicted pressure measurants as an output. Each input is multiplied by a weight factor and all weighted inputs are then summed up into what becomes the output.

Figure 119 shows the network architecture. The 13 ion current measurants are the set of circles at top left. The set under them, labelled Conditions is a string of numbers (constant for each input file) that describes the operating conditions of the engine at the time. These conditions are: throttle position, engine speed, engine load, air to fuel ratio, ignition timing advance, and compression ratio.

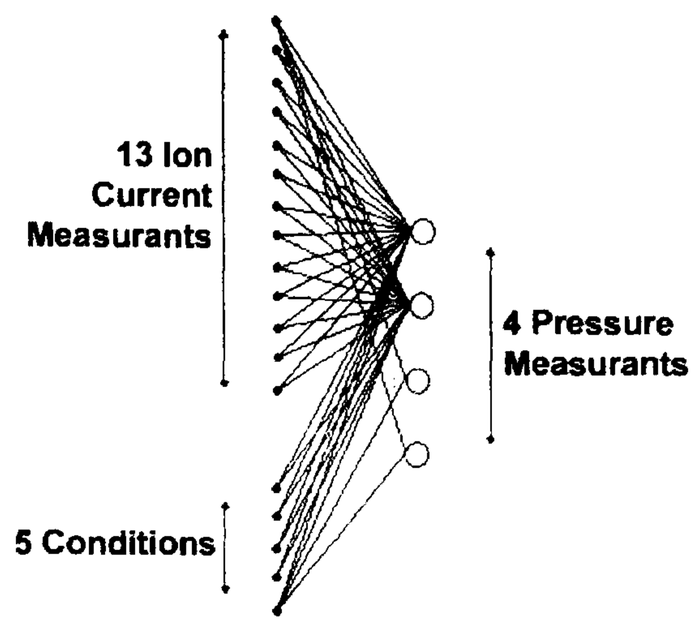

Figure 119: Schematic representation of the network.

Training is done as follows. When data was logged, one of the aforementioned operating conditions was varied and a number of files logged for various values of that condition with everything else kept the same. This created "families" of files, the Compression Ratio family, the Ignition Timing family etc. Of these families, one member is selected to be the "test set", the set of values to be shown to the network after training to test performance. The rest of the family is then used to train the network. Thus, when testing the network, it is given values not encountered during its training. By choosing the test set to be somewhere in the "middle" of the variable condition range, the network arrives at the correct results since these lie within its training window. The results of this process can be seen in Figure 120, Figure 121, Figure 122 and Figure 123.

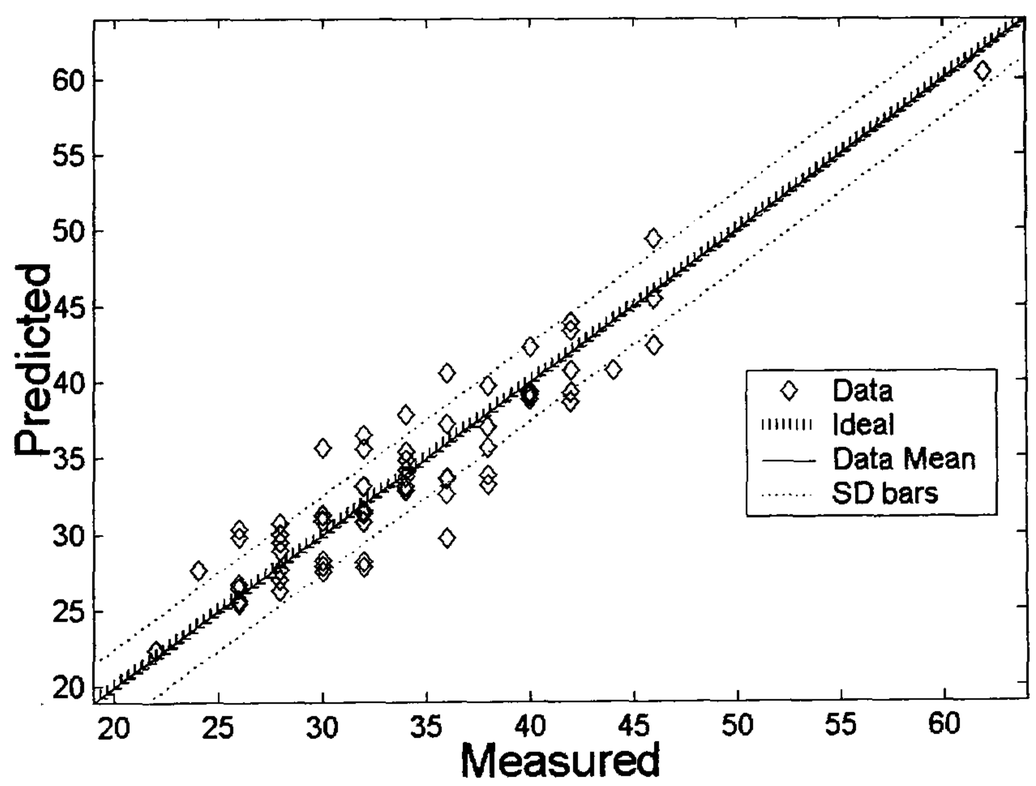

Figure 120: Predictions for Peak Pressure Position.

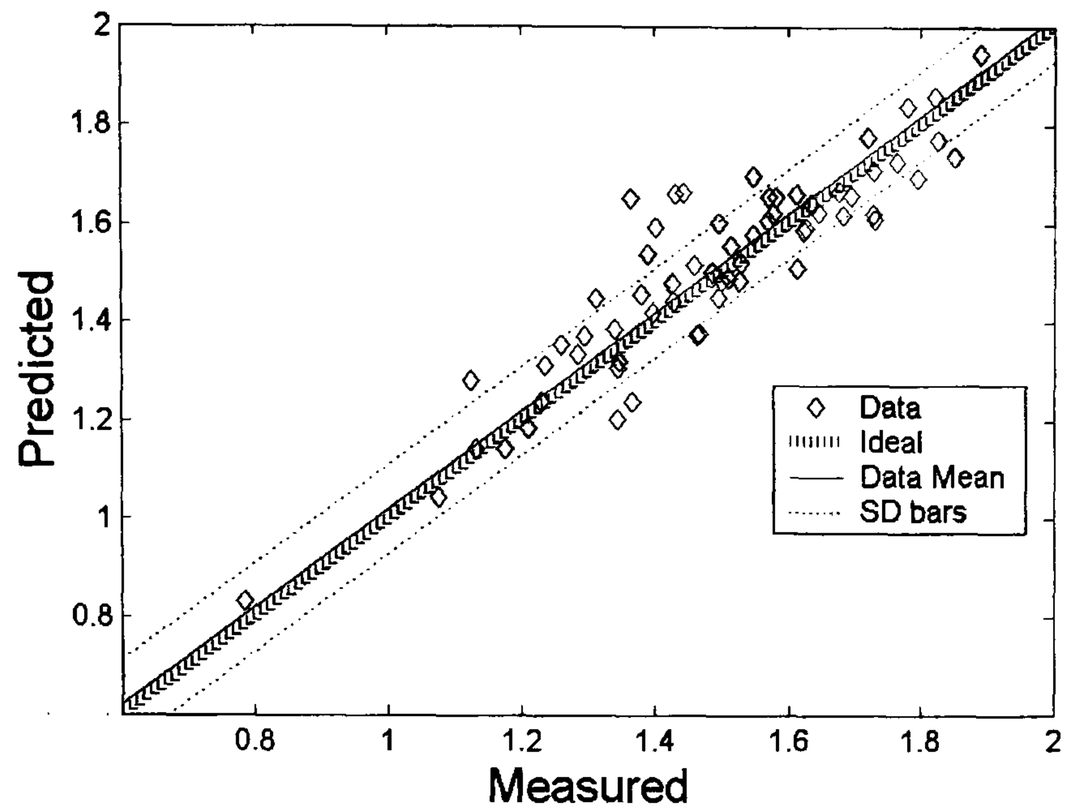

Figure 121: Predictions for Peak Pressure Magnitude.

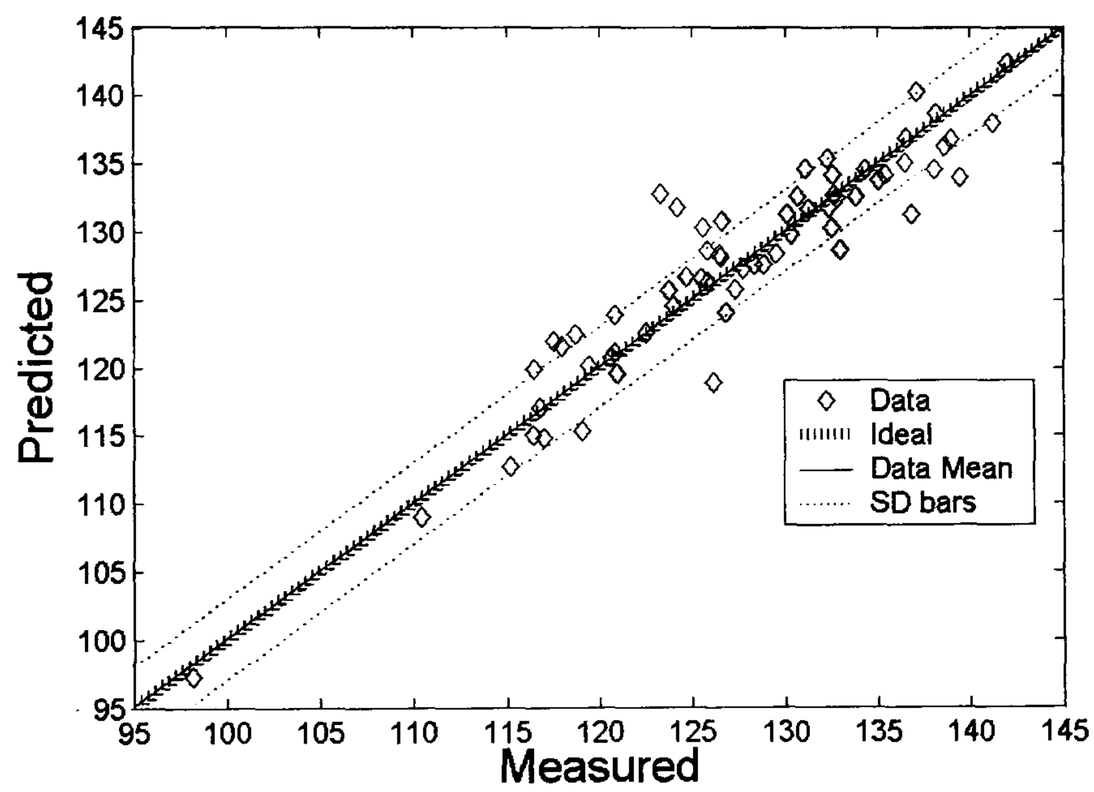

Figure 122: Predictions for Pressure Curve Area.

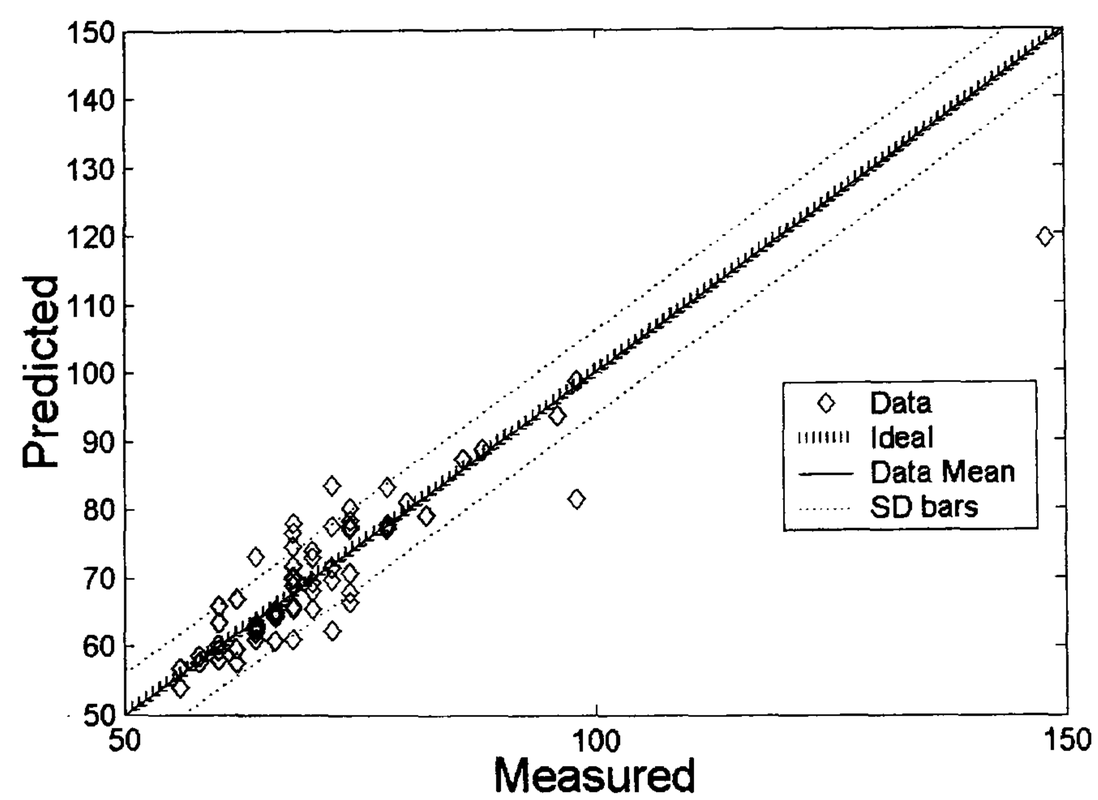

Figure 123: Predictions for Pressure Curve Width.

The entries on the x-axis are the measured values of the measurant, and the entries on the y-axis are the predicted ones. Thus, a perfect prediction would plot a diagonal line. This is the "ideal" line mentioned in the legend and is used for reference. The solid line indicates the data mean. It often coincides to a great extent with the "ideal" line, which indicates a good match between measurements and predictions. The two outer dotted lines indicate the standard deviation of the data. In these four figures, the network performs so well that the mean of the predictions and the diagonal are almost identical. The only figure in which they can be seen separately is Figure 121.

Of the four outputs of the network, the most important are the Peak Pressure Position and Peak Pressure Magnitude which give the x and y coordinates respectively of the pressure curve's peak. Figure 120 shows the predictions for Peak Pressure Position. The mean of the predicted values is shifted by 0.062 degrees from the mean of the actual values and the standard deviation of the predictions is 2.55 degrees. A similar degree of accuracy was obtained for the rest of the in-cylinder pressure measurant predictions. Given that the ion current signal is sampled every two CA degrees, this result is satisfactory.

The predictions in these figures are calculated from a mixed training set. The families used are the Compression Ratio family with varying compression ratios and the Speed and Load family with varying speed and load. The compression ratios for the first family are 11.2:1, 7.6:1, 6.2:1, 5.2:1, 4.7:1 and 4.5:1. The speed/load settings for the second family are 33% at 1400rpm, 75% at 1400rpm, Wide Open Throttle at 1400rpm, 33% at 1750rpm and 75% at 1700 rpm. The test set is a member of the Compression ratio family with a compression ratio of 5.6:1. Ignition timing for these was kept constant at 30 degrees before TDC.

What is worth noticing is that the network gives better results when the families are mixed together than when the training is done on each individual family. This is a satisfactory result, demonstrating how the network can interpolate and select the right predictions for the test set, the operating conditions for which it hasn't encountered at all during training.

6.2.5 Curve Predicting Network

Given the satisfactory performance of the simple ADALINE in tackling the thirteen-input by four-output measurant predictions, a new network was tested predicting the whole pressure curve. Again an ADALINE was used, but this time with the whole ion current

signal as the input and the whole pressure signal as the output. More specifically, each cycle is examined between IVC and EVO. Given the sampling rate and the valve timing, this gives a data string of 117 elements for both ion current and pressure. Thus the network consists of 117 artificial neurons, each of which is connected to all inputs and which produces one output, corresponding to a point on the predicted pressure curve. Figure 124 shows the measured and predicted pressure curves resulting from this network averaged over the whole of the test set. The training set and test set are the same as for the previous network.

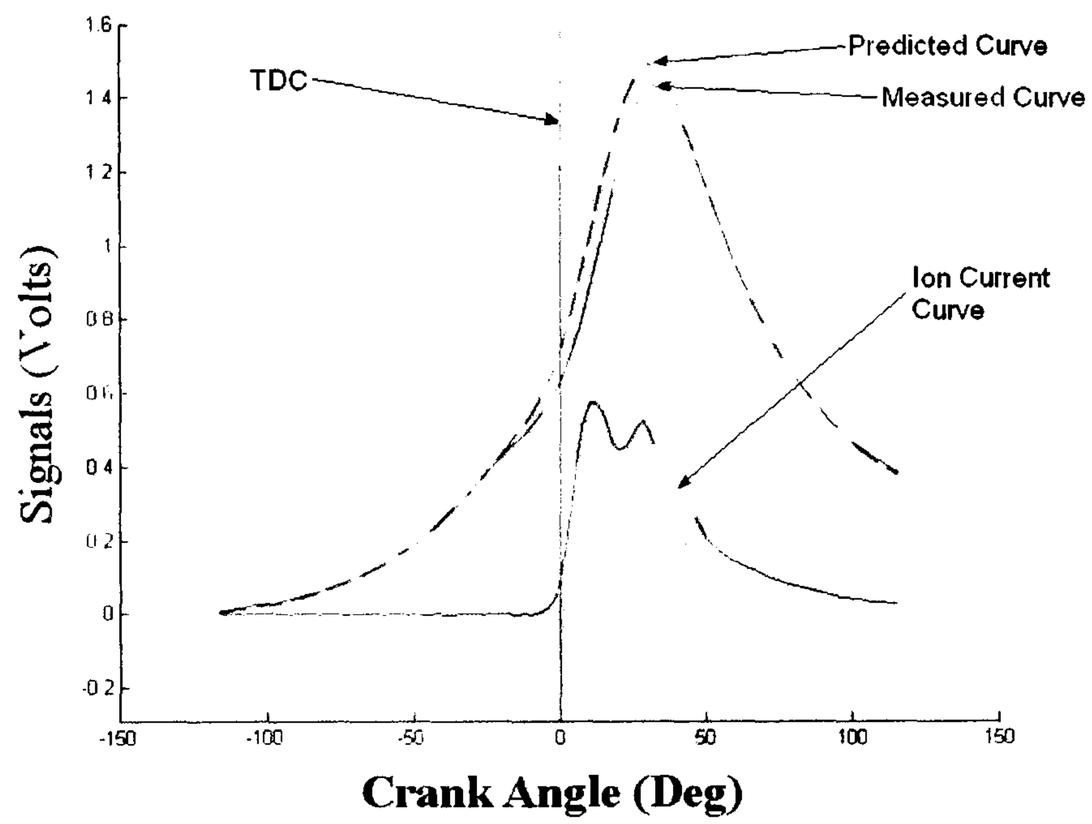

Figure 124: Averaged actual and predicted pressure curves.

Again, the averaged ADALINE follows the target quite closely even though the compression ratio of the test data has never been encountered in its training. However, the measurants extracted from the predicted curves are not as good as for the previous network. Figure 125 shows the actual and predicted values for the Peak Pressure Position. The mean of the predicted values is shifted by 1.69 degrees (compared to 0.062 for the previous network) and the standard deviation is 5.45 degrees (compared to 2.55 for the previous network).

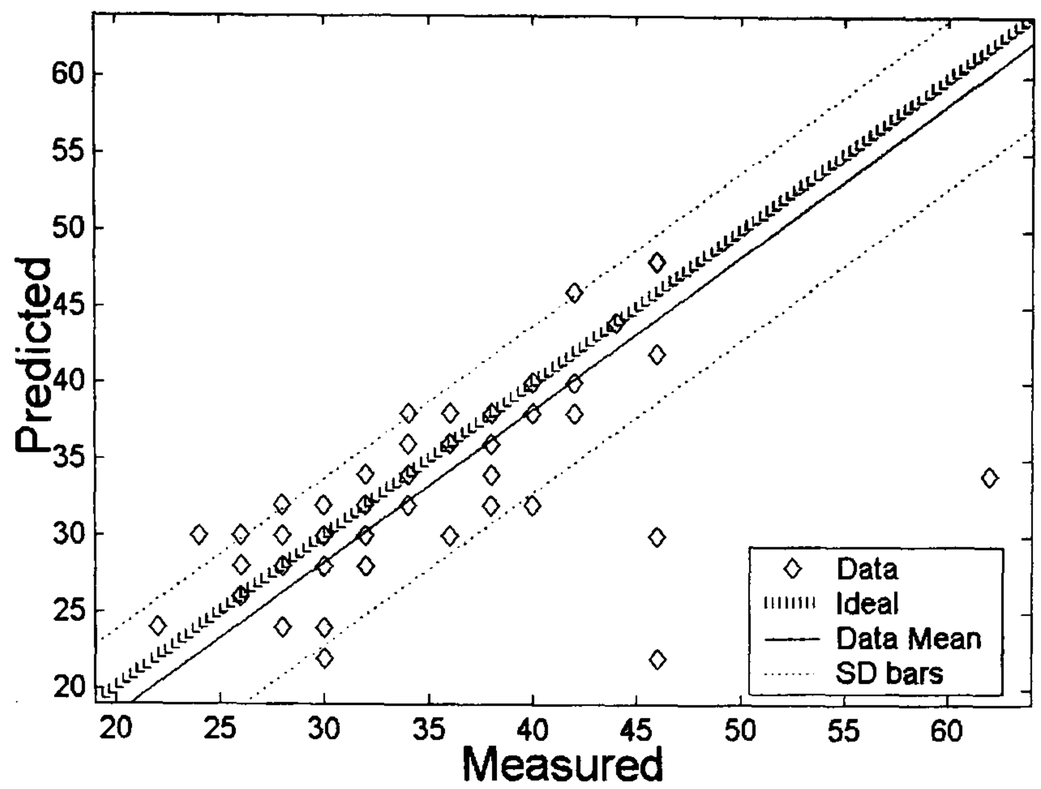

Figure 125: Predictions for Peak Pressure Position.

Similar results are true for the rest of the measurants, with uncertainty increasing roughly twofold compared to the previous network.

This network is created with the task of matching the curve point to point. The objective of training the network is to minimize the average difference between the actual and predicted curves, which may result in that the error between the predicted and actual in-cylinder Pressure Peak Position is not minimum.

6.2.6 Knock

Although, as mentioned earlier, the sampling rate was too low for knocking to be recorded accurately, the ADALINE performs adequately, by "realizing" that there is a combustion abnormality.

The pressure curve prediction output is shown Figure 126 and in Figure 127 for two random knocking cycles. Although the pressure prediction is not very close to the actual pressure, the knocking behaviour is mimicked. The "bad" curve fit may be due to the local nature of knock affecting the sensors readings.

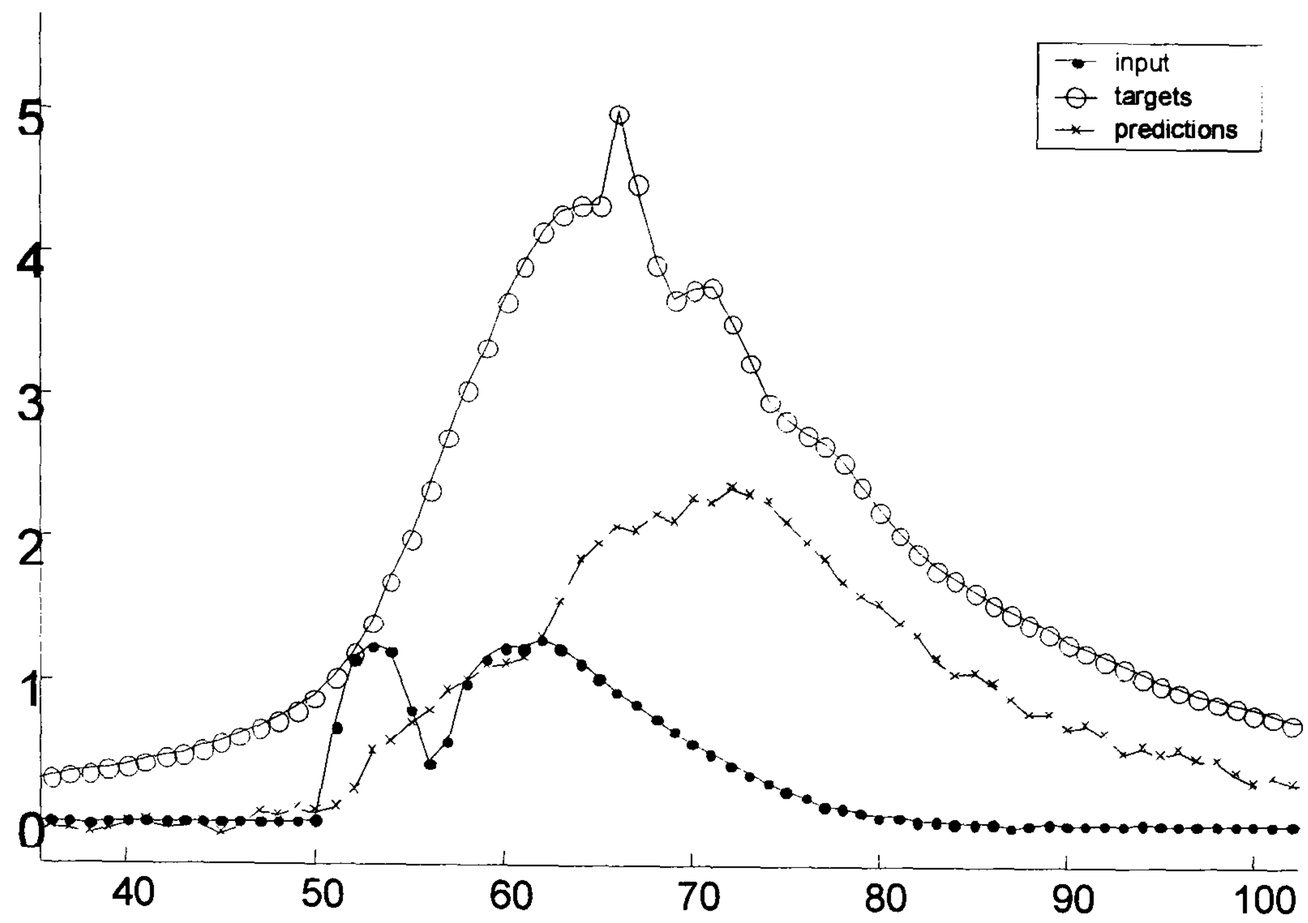

Figure 126: Knock Prediction 1 (X-axis CA deg from IVC).

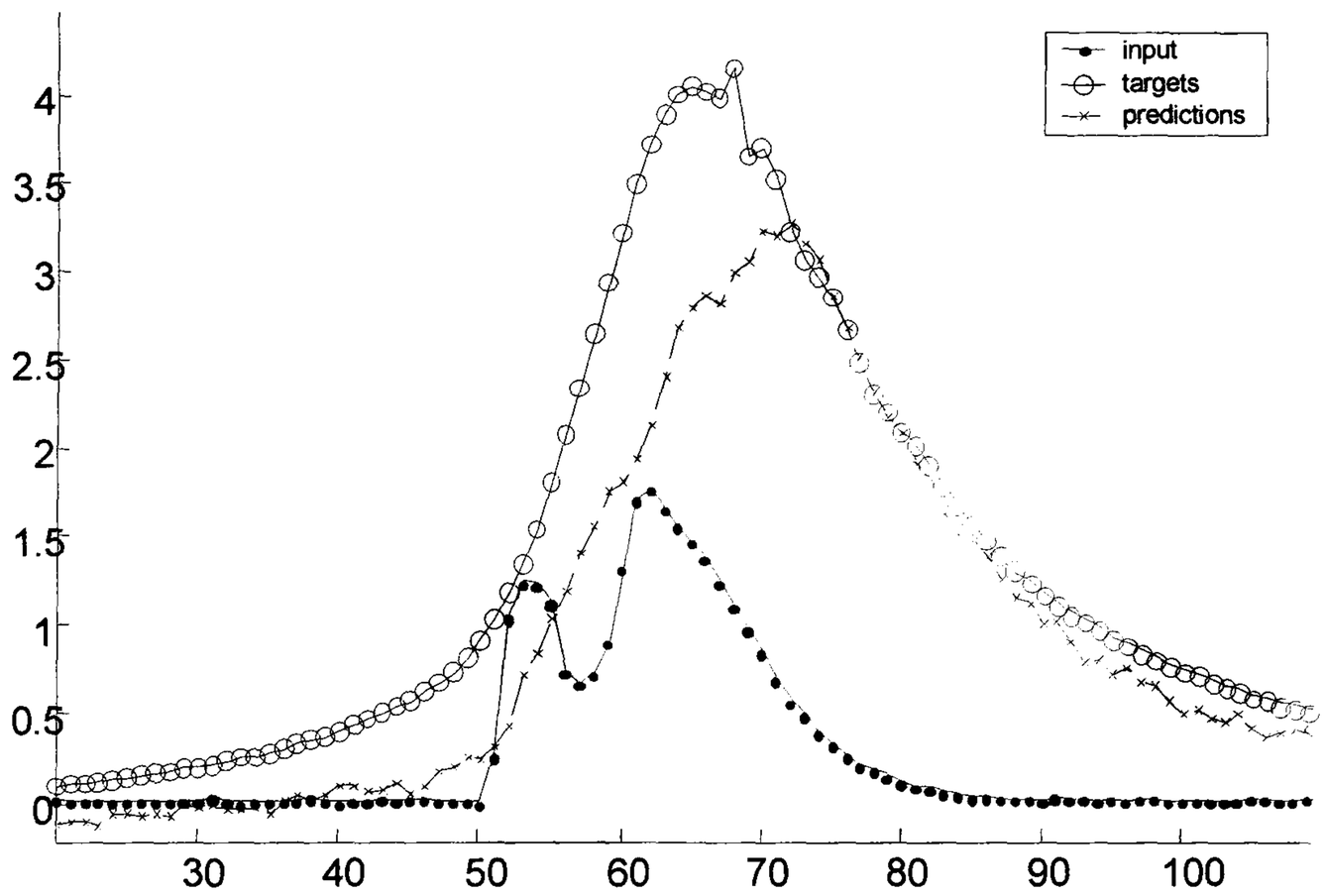

Figure 127: Knock Prediction 2 (X-axis CA deg from IVC).

6.2.7 Discussion

Misfire detection through ion current measurement is a robust and reliable method under all operating conditions, even on a multi cylinder engine because under misfire conditions there is no ion current signal. If the ion current signal were to be incorporated into a closed loop control system, misfire judgment could be made by the time the piston is at

TDC. This would allow the spark to be refired and some of the chemical energy in the charge recovered, and more importantly, the mixture to be burned before it reaches the catalyst. When an ion-current sensor that is separate to the spark plug is used, misfire caused due to electrode tip deposits can also be detected.

Pre-ignition detection is also possible. If an ion current signal is sensed earlier than it is expected, for example because the mixture ignited due to hot surfaces in the chamber, it can be flagged as pre-ignition.

The results indicate that there are some linear relationships between the pressure and ion signals characteristics. An analytical approach might not yield enough accuracy to resolve the feedback problem, but with the help of ANNs the precision of the predicted values, as indicated by the error's RMS and the Pearson coefficient, becomes impressive.

The results reported showed how ion current data can be treated using simple techniques to predict various features of the in-cylinder pressure. Of the two networks presented, the most likely to be suitable for the task of engine control is the first one (measurant prediction). This is by far the cheapest computationally and is specialized in predicting the most important aspect of the pressure curve, the location of its peak. This should be a welcome result for the further development of engine control systems striving to employ fast and simple algorithms for changing engine parameters on cycle-to-cycle time scales. One drawback of this approach is that, even though the network used is itself extremely simple, its inputs are the results of some data processing since the ion current measurants used are themselves the product of various operations. Even though these operations are well within the capabilities of modern electronics, they can be more expensive computationally than the operation of the network itself, something that will have to be taken into account when designing such a system.

Another point to take into account regarding measurants is the y-axis data of the ion current signal. All the measurants strongly affecting the pressure curve results were the ones on the ion current signal x-axis, in other words related to the timing, not the magnitude, of the ion current events. Figure 4 shows an ion current signal. What has to be noticed is the sharp slopes leading up to the two peaks. In some cases, there could be 2-4 data points from bottom to top of the ion current spike. Therefore, the ion current signal might contain frequencies which are too high for our sampling rate. This might be an additional factor in that ion current magnitudes never showed any strong relation to any pressure measurants in the measurant to measurant plots.

The ADALINEs employed in this research manage their predictions based mostly on x-axis ion current measurants. It might be possible that higher sampling rates can improve the results further as the significance of y-axis ion current measurants will be taken into account. However, other researchers [114] have pointed out that large cyclic fluctuations are a typical problem with ion current measurements anyway. Thus, by not relying on ion current magnitude but rather on ion current timing (made easy by measuring from the remote plugs) this problem can be avoided to some extent.

Apart from the most important position of the peak of the pressure curve an ADALINE has been found to be able to tackle quite competently the task of predicting the pressure curve itself. Normally, such tasks are best left to more specialized (and more computationally expensive) tools like radial basis functions. An important point to consider in this second network is that the input is passed to it ``raw" as it were, with no need for pre-processing to extract ion current measurants. There is a cost to pay at the output as pressure measurants are extracted from it but it is a much simpler task as there are only 4 measurants involved in the pressure curve as opposed to 13 in the ion current signal. However, this network is not as effective in locating the peak of the pressure curve.

It might seem to be a logical step to design an ADALINE accepting a "raw" ion current signal and producing pressure curve measurants as output. Variations on this have been tried with poor results. It seems that for this kind of task, simple networks like the ADALINE can no longer keep up.

Finally, not all data are necessarily in linear relations. Figure 115 is an example of two measurants that seem to indicate rather strongly that a non linear relation exists between them. Modified networks have been tried to see if performance can be improved by passing the inputs through a function, thus making the curve resemble a more linear form. The most important measurants, Peak Pressure Position and Magnitude, sometimes improved by as little as 2-3%. This is not a particularly strong case for adding computational cost to the system. It seems that, given the uncertainty in the data and the short segment of curve in question, a linear approximation is best suited for dealing with it.

In real world terms, if the engine parameters are known a PPP prediction is within 2.5^{o} CAD. Also, the pressure magnitude ANN prediction is within 10%. All OBDII vehicles are equipped with the sensors needed to inform the net about the engine operating

conditions, but even if these are not known, the PPP prediction uncertainty only increases to 4° CAD and the pressure magnitude to 11% total errors. These results were attained on a cycle-to-cycle prediction, with a sampling frequency of 1sample/2oC.A., and without averaging nor information about important engine parameters such as coolant temperature, mass air flow, manifold absolute pressure etc and with relatively few "design" cycles. (Upwards of 50,000 cycles are normally used) [109,162,163]. Keeping in mind, that with a linear rpm versus load table interpolation model, like the ones generally used in production vehicles today, the RMS error for PPP estimation is 3.3 C.A. degrees and the Bias error 1 C.A. degrees [109] the net performed adequately.

A further advantage is that table interpolation model performance drops considerably with ageing, whereas the ion current in-cylinder sensor will contain ageing information. This is because the ion current signal will alter as the engine ages and cylinder compression decreases. Although no ageing test was performed, this effect was simulated by varying compression ratio and the results obtained promise good ageing behaviour.

Good estimation capabilities under varying compression ratio were also shown. Altering the compression influences the flame propagation speed. This can be measured with a remote spark plug ion sensor. The main use of this type of information is likely to be for correction of load table interpolation models as the engine ages.

Knock detection through ion current signal measurement was also shown possible. As mentioned earlier, knock detection via ion current is cylinder individual and sensitive, and will not be affected by ambient mechanical noise, engine modifications or ageing. The ion current sensor can replace the knock sensor unit and the associated calibration time thus also lowering engine cost. Also, since one or more cylinders may not knock at all while another may be knocking heavily [125], efficiency and power will increase by retarding only the knocking cylinder(s). Given that low rpm torque output is generally knock-limited, engine performance improvements can be obtained. What is of perhaps higher significance is that knock which leads to cylinder temperature increase can be avoided altogether, thus requiring less drastic ignition timing retardation.

The effect of changing air-fuel ratio was also investigated. It was shown, that in agreement with other researchers' observations, the slope of the first spike of the ion current is indicative of mixture strength. Although the possibility of completely substituting the oxygen sensor is arguable, it is clear that ion current signals can be used for cylinder balancing. It is known that cylinders on a multi cylinder engine can have an

AFR difference of 7% between them, with the oxygen sensor registering a stoichiometric value. If the ion current signal can be used to balance cylinder AFR, the overall emissions will drop, the temperature variance between cylinders will also drop and the output torque of each cylinder will equalize improving engine refinement.

The most commonly used technique for rapid catalyst warm-up is to retard the ignition at start-up. Manufacturing tolerances, equate to differences of AFR, dwell time and airflow between the cylinders and dictate a conservative maximum retard that will not sacrifice drivability, for the worst-case scenario. Ion current sensing will enable the maximum retard to be used, under all conditions.

With regards to the use of the additional ion current sensors, it is noteworthy that since the measuring plug(s) was some distance away from the firing plug, a direct and firm relationship under all conditions of flame propagation speed and the start of the ion current measurements was recorded, as expected. This is a unique characteristic of this investigation that proved worthwhile. When measuring from the firing plug, since the first peak is a result of the flame kernel created by the plug, it does not carry any valuable information. Only the second peak is dependent on the pressure and temperature. The problem with this is that under low load conditions this second peak disappears, since there is not enough pressure in the cylinder to cause post-flame ionization. This was, also, observed in our investigation but had no effect on the results.

The difference in results between one and two sensor usage is small, but more measuring points result in slightly higher accuracy. Sensors are mostly affected by local events, and an averaging strategy through the use of multiple sensors improves the quality of the data.

6.3 Conclusion

In the above sections, an attempt to judge the potential of the ion current measurement as feedback for SI engine control has been made. The sensor's use was tested under different engine operating conditions to obtain an insight on its behaviour when misfire occurs, when the air-fuel ratio changes, when the ignition timing advance or compression ratio are altered and when knock occurs. The results demonstrate the feasibility of bypassing the use of a pressure transducer as a means of in-cylinder data gathering.

The predictive abilities of adaptive linear network designs that take the ion sensor's output as input and calculate PPP, pressure magnitudes, the area under the pressure curve,

the width of the curve and also reconstruct the whole pressure signal were compared. The results prove that there is great potential. Misfire and knock detection is possible. More complicated uses like PPP estimation were also proven accurate enough when the ion current signal is manipulated by computationally inexpensive artificial neural networks. Coupled with the robustness and significantly lower cost of the Ion Current sensing apparatus, this performance is indicative of the importance of Ion Current sensing as a tool in the development of future closed loop controllers needing to acquire fast, cycle-per-cycle combustion information.

Nevertheless, the practical implementation in production vehicles still posses a few challenges, the provision of superior computational power in engine management systems being one of them.

7. CAI Ion current

As mentioned before, a "CAI" production engine for automotive use would have to operate in a hybrid mode, where operation in CAI mode at low and medium loads would switch to spark ignition (SI) mode at a cold start, idle and higher loads. A seamless transition between the two modes of combustion must be attained to achieve acceptable drivability. Therefore considerable control is required to maintain consistent start of combustion (SoC) and heat release rate (dQ), especially during transient performance, and this problem has limited CAI's practical applications thus far.

Ion current seems a promising feedback signal for CAI combustion control. However, experiments have shown that the signal acquired displays only one peak and given the relatively low engine cycle temperature, the ion current from this type of engine is though to come mainly from chemi-ionization [164]. Since in CAI there are low concentrations of NOx, the ion current signal probably results from ions in the reacting gas, i.e. when the electrode gap is in the reaction zone. The reaction zone might be created either due to flame propagation, (low TRG%), due to autoignition, (high TRG%), or a combination of the two in medium TRG%.

It has been identified that provided these problems can be overcome, ion current becomes a suitable and computationally inexpensive means of acquiring data from the CAI combustion process. In this chapter, the potential of using an ion-current sensor in CAI combustion in order to extract and quantify combustion measurants will be investigated, with particular reference to control applications. A presentation of results of ion current sensing for monitoring combustion under steady state operation, over a variety of speeds and trapped residual gas amounts is made. The results show that the ion signal is sufficiently high during CAI under all speeds and loads. Also, estimation of cylinder pressure parameters through the ion signal with promising accuracy is demonstrated. Overall, ion current is proven to be a cost effective and adequately informative feedback signal for both SI and CAI engine control.

7.1 Using Ion Current Sensing to Interpret Gasoline CAI Combustion Processes

7.1.1 CAI Combustion

The Lotus engine was initially tested under conventional SI operation mode. Then TRG quantity was gradually increased, thus moving from pure flame propagation, to spark assisted CAI (SA-CAI), and then to pure CAI as shown in Figure 128.

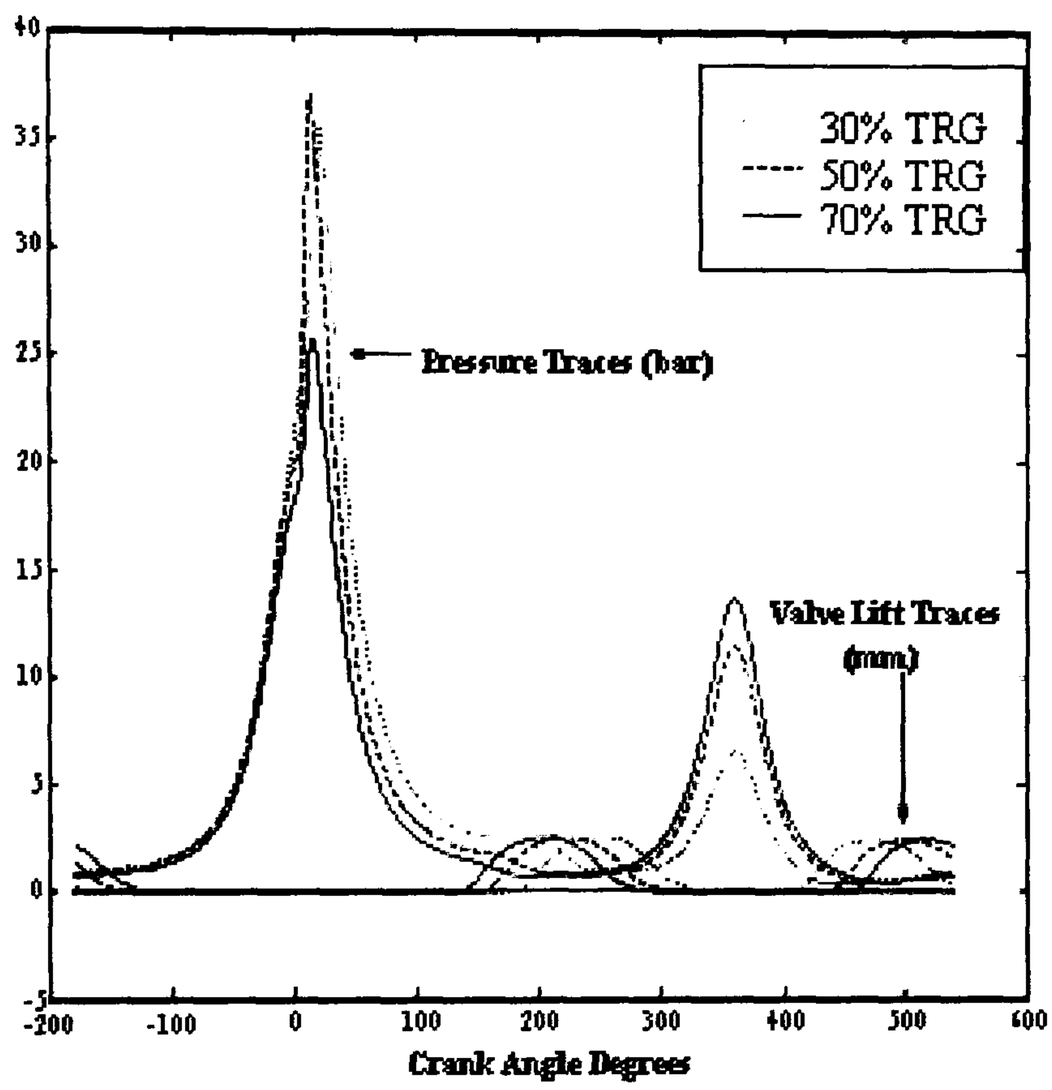

Figure 128: Typical pressure and ion current signals at various TRG levels.

As mentioned before, the amount of TRG noted is the molar ratio of fresh charge to exhaust gases, it was calculated using a zero dimensional thermodynamic model and equation (1).

$$\%TRG = \frac{Charge_Moles}{TRG_Moles} \times 100 \qquad \text{Eq.(1)}$$

The maximum amount of TRG that the engine will accept depends on the engine's speed. Thus, an amount of TRG that is on the edge of CAI at one speed might be in the middle of the operating region, at another. As such, it does not always make sense to speak in absolute terms of TRG%, especially as TRG tolerance is a very engine specific issue. Thus, TRG% will be described as low, medium or high, rather than assigning absolute values that cannot be extrapolated to different engines or research.

The entire CAI and SA-CAI operating range was investigated varying the speed over a range between 1500rpm to 3500rpm. In the area surrounding this range, SI operation was used. Figure 129, shows the speed and load, (in terms of IMEP), and also the corresponding amount of TRG that was used for load control, where zero to misfire limit negative overlap. It can be seen that the negative valve overlap, the controlling parameter of TRG, can't be the same in all speeds, and also that the IMEP possible with CAI can't be the same in all speed.

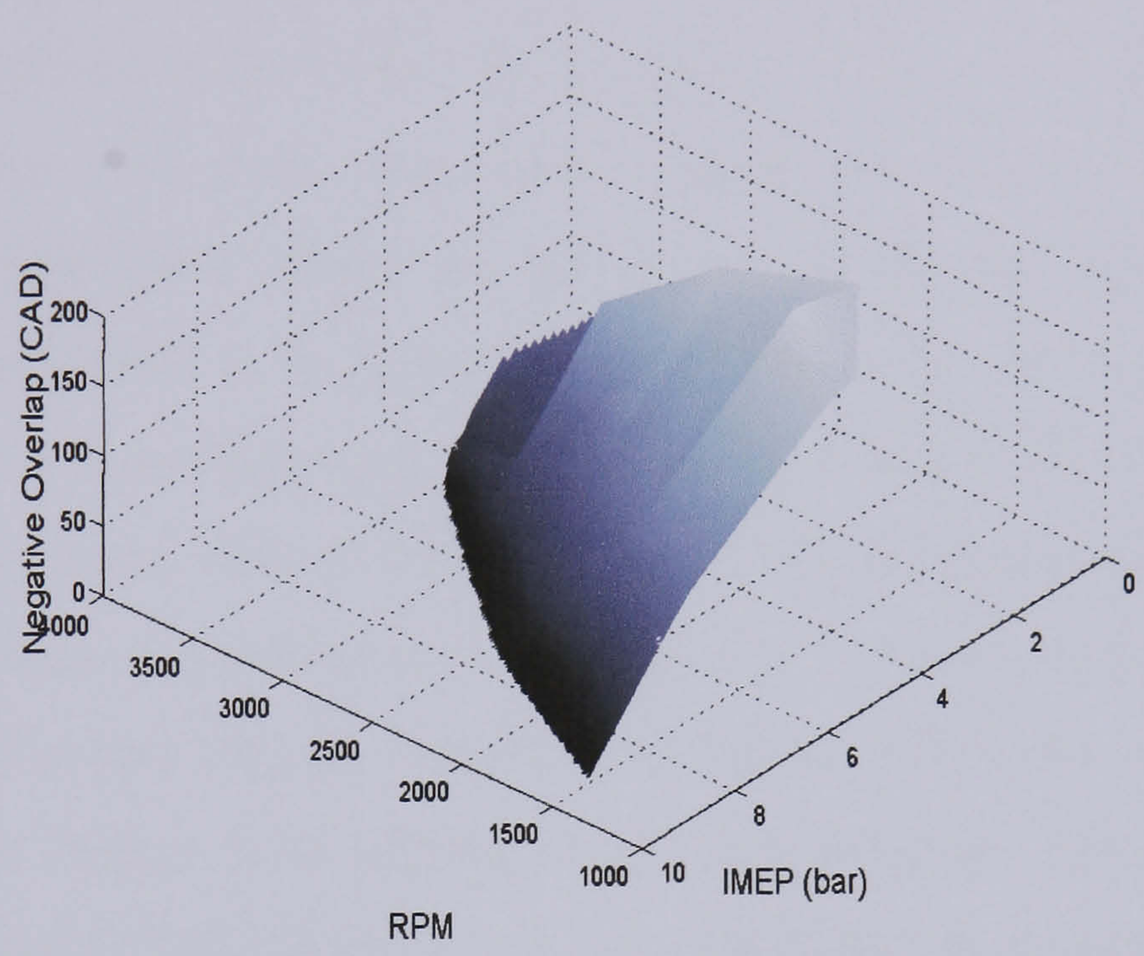

Figure 129: CAI operating range.

7.1.2 Ion Current Signal and its treatment

The ion current signal in CAI is usually in the form of just a sharp spike, as shown in Figure 130.

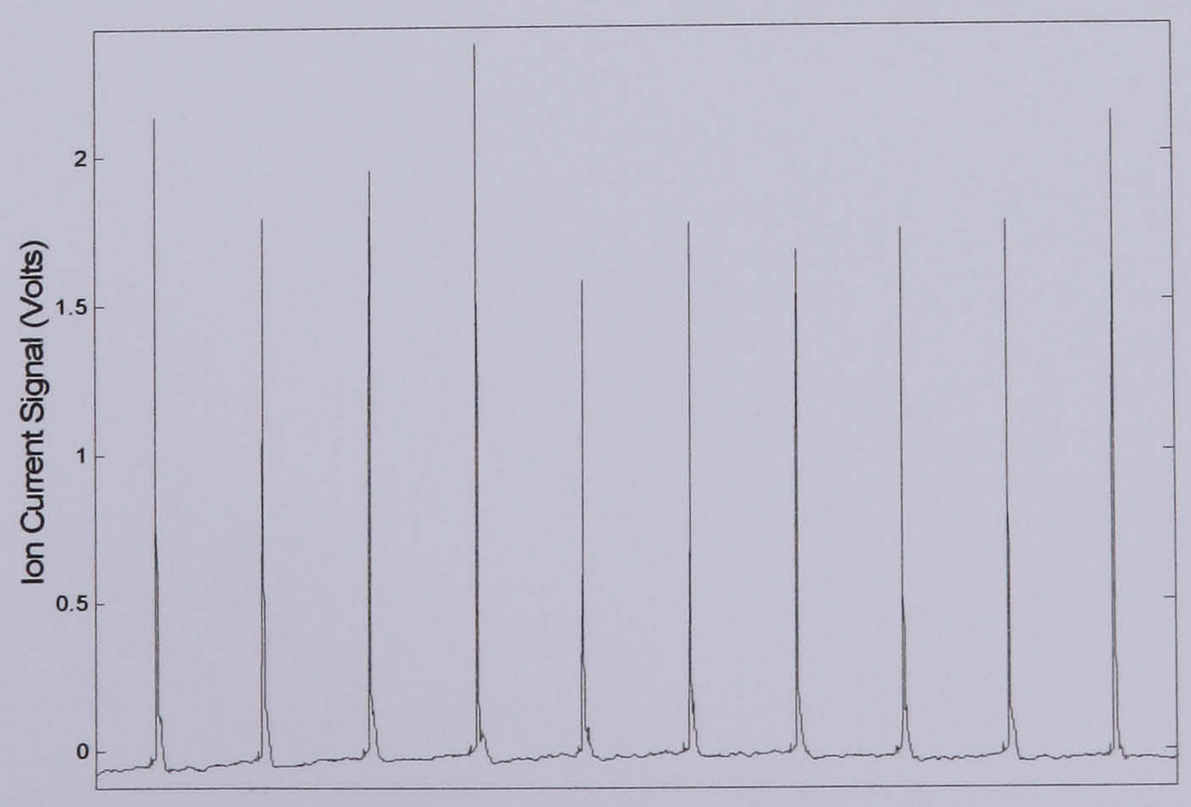

Figure 130: Typical CAI Ion Current Signal.

In a gasoline engine operating in dual mode, four groups of parameters must be known in order to control the combustion process. These are; misfire and preignition detection so that operating conditions leading to unstable combustion can be avoided; Calculation of TRG levels (as load is controlled in CAI mode through TRG); combustion performance parameters so that the engine performance can be monitored; and finally ITA which is used for engine control outside the CAI envelope. Each of these groups will now be examined.

In order to control a gasoline engine operating in CAI mode, a number of features must be monitored on a cycle-by-cycle basis. The simplest of these are misfire and preignition detection. In Figure 131, three consecutive cycles are shown during unstable CAI operation. In the first cycle where the ion current signal starts after TDC, the peak pressure of the combustion is in normal levels and position. In the next cycle a misfire happens and no ion current is present, (thus providing a simple way to monitor the engine for this event). However, during the following TRG compression and expansion, the mixture ignites, which is manifested by the presence of ion current signal during that period. In the third cycle, the ion current starts before TDC since an early combustion occurs resulting in higher than normal in-cylinder pressure and early peak pressure position (PPP). After a TRG compression and expansion that experiences heat release, it is a usual phenomenon for early combustion to occur in the next cycle. This is due to the chemical break-up of the fuel as a result of prolonged contact with the TRG and high pressures and temperatures, which result in early ignition of the fresh charge. It can be added here, that fuel which was near the walls was cooled and not combusted in the combustion compression, but it was then "reshuffled" (basically moved about during expansion and exhaust stroke – or at least the part of the exhaust stroke that the exhaust valve is open) and ignited during TRG compression as it probably was not near the walls anymore.

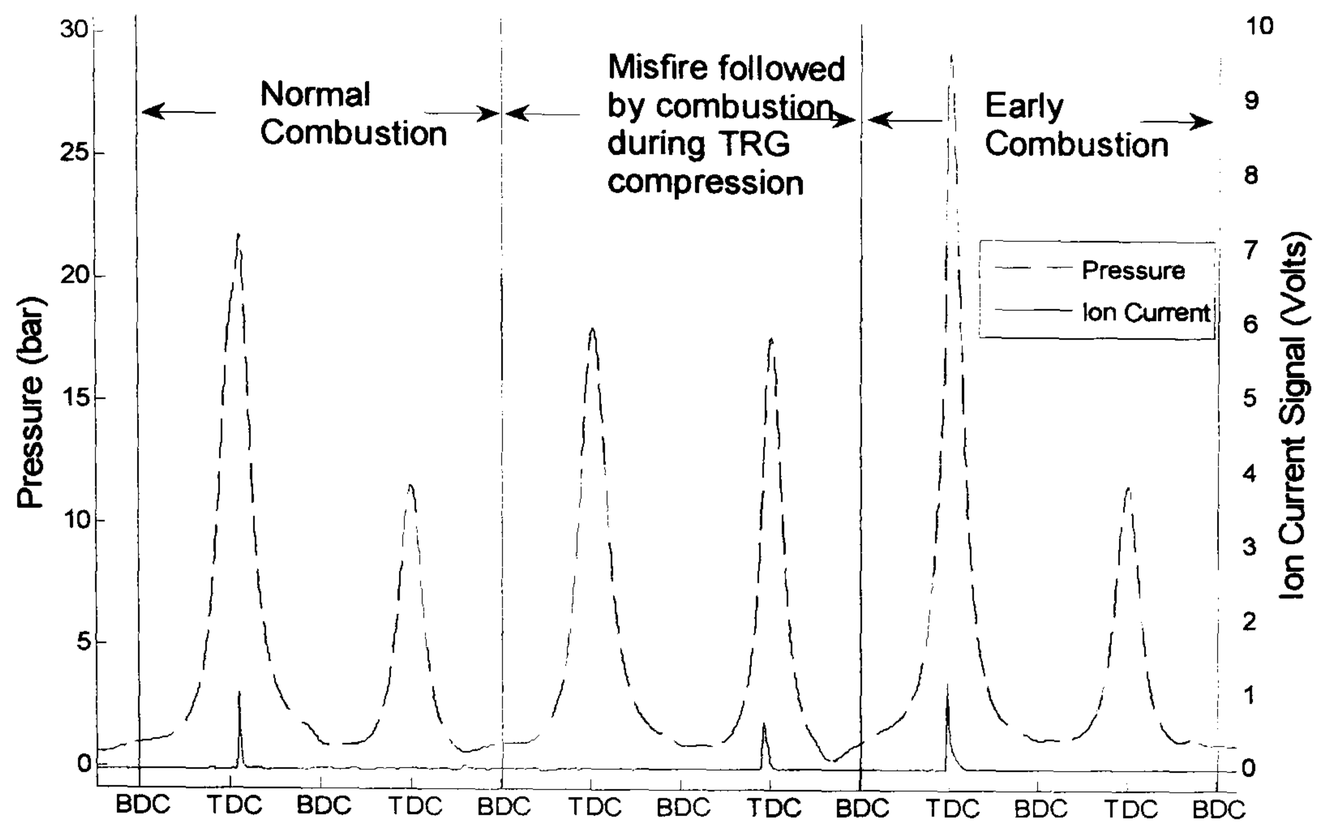

Figure 131: Cylinder pressure trace and corresponding ion-current signal.

Although important conclusions for the combustion can be drawn by simple inspection, and simple diagnostics can be performed directly through the ion current signal; more detailed analysis yields greater insight. In order to do this, the signal needs to be treated in order to extract the most fundamental characteristics of the ion signal curve, so that these can be compared to combustion parameters. This process is, in effect, a compression of the information contained in the signal into a small number of key variables. This has the advantage that, in the first instance, they can be directly investigated for correlation to corresponding measurants of the pressure trace (e.g. peak pressure position) and also that these can be used as a much reduced data source when using further algorithms, e.g. ANNs.

7.1.3 The Ion Current Measurant Extraction Procedure

The breakdown of the measurants extracted from the ion current signal are shown in Figure 132.

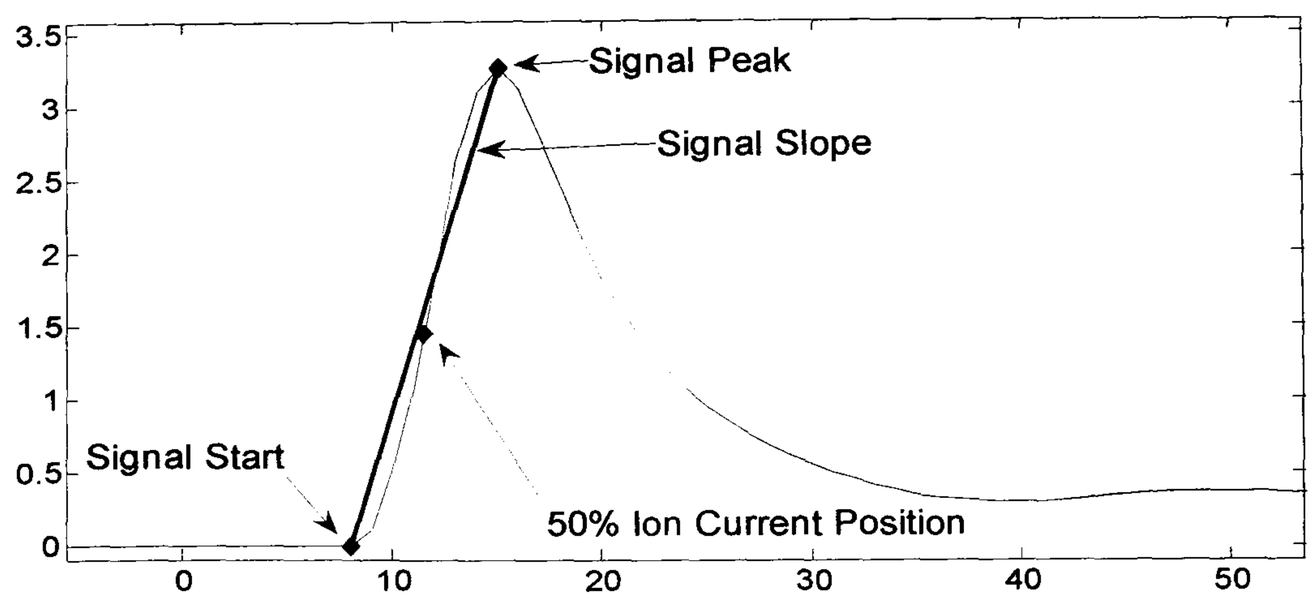

Figure 132: Signal Measurants from ion-current signal.

These are:

1. The start of the signal (X coordinate)
2. The 50% of the signal magnitude (Y coordinate)
3. The position of the 50% point of the signal (X coordinate)
4. The slope of the signal
5. The maximum of the signal (Y coordinate)
6. The position of the maximum of the signal (X coordinate)

The easiest to extract and one of the most information rich is position and magnitude of the spike's peak, which is simply extracted by means of a maximum search. The timing of this has been shown in [125] and in the previous chapter to be a good approximate indicator of combustion timing, having a strong relation with pressure measurants such as PPP.

Another important ion current measurant is the position of the start of the signal. Coupled with the coordinates of the peak, it can lead to an estimation of the slope of the spike. Previous research on SI operation has established a correlation between this slope and Air Fuel Ratio (AFR) [160,165,166]. In CAI, this effect is further complicated by the presence of TRG but still, slope information can be a valuable tool. Thus, in order to acquire it, an estimation of the start of the signal is required.

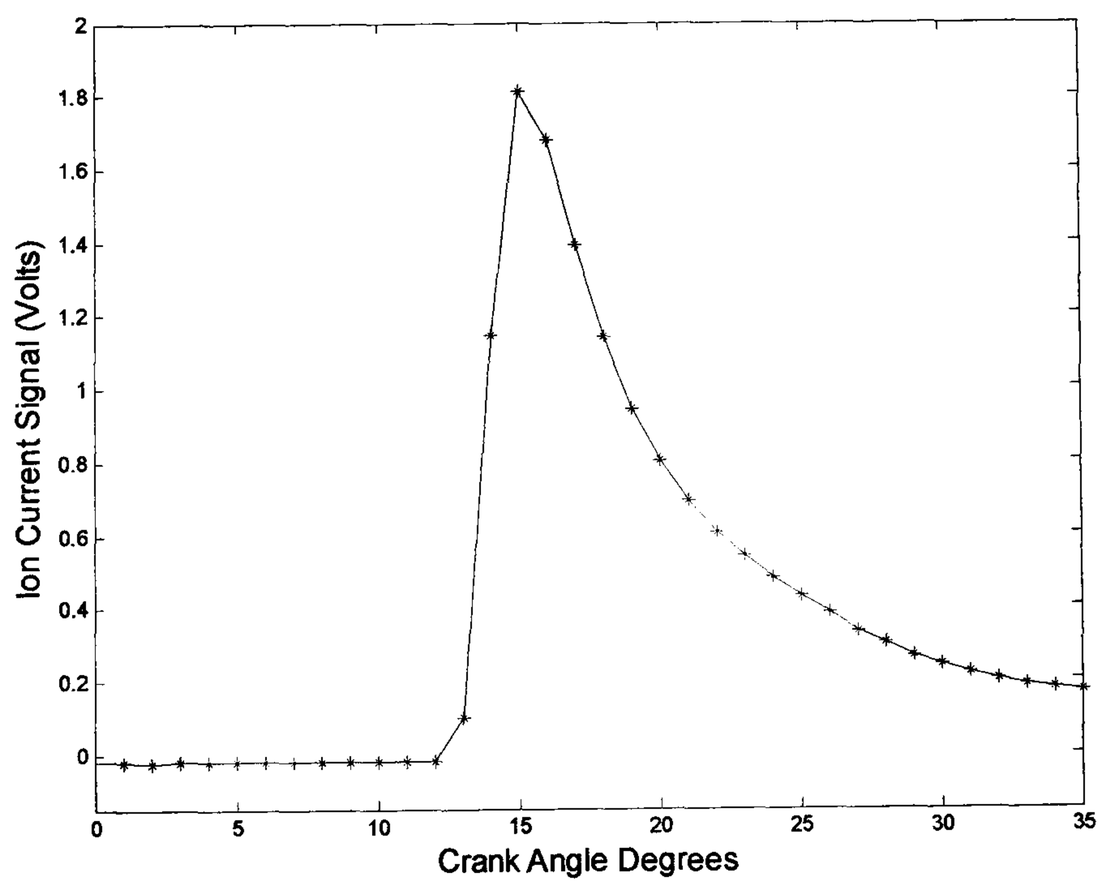

Figure 133: Example of Sudden Spike Rise.

While the spike's peak is very straightforward to extract, its start can be more problematic. This is mainly because the base of the ion current signal can be a very noisy region. Added to that, is the fact that, because CAI combustion is very sudden compared to SI, the spike can rise in a very short time, typical values can be as low as 3 data points (data is sampled every 1 degree CAD) as is demonstrated in

Figure **133**. Hence, an uncertainty of even one or two degrees can have a big effect on the final value for the spike rise duration and hence the slope and the 50% position.

Matters are complicated further by the fact that the start of the signal can be concealed by a noisy region as is shown in

Figure **134**. This should not normally be a problem as the spikes are usually high enough to easily rise above the noise. However, to guarantee a safe detection through a simple technique such as a static trigger level for example, compromises have to be made that will erroneously classify certain cycles.

Another problem is that the ion current signal can suffer from a noticeable base drift (depending on the equipment used), an extreme example of which can be seen in Figure 135. Coupled with the problem of noise and potentially weak spikes, this makes the use of a static trigger inappropriate.

To counter these problems, two different techniques have been tried out. One, designed for maximum speed, is based on classic concepts and employs a dynamic trigger to judge how to classify each candidate point. The other, designed as a more rigorous approach, is based on wavelet analysis and classifies points by processing the high frequency part of the ion current signal. The dynamic trigger technique is outlined in the following section, while wavelets, which were mostly used for ANN implementation, are discussed later.

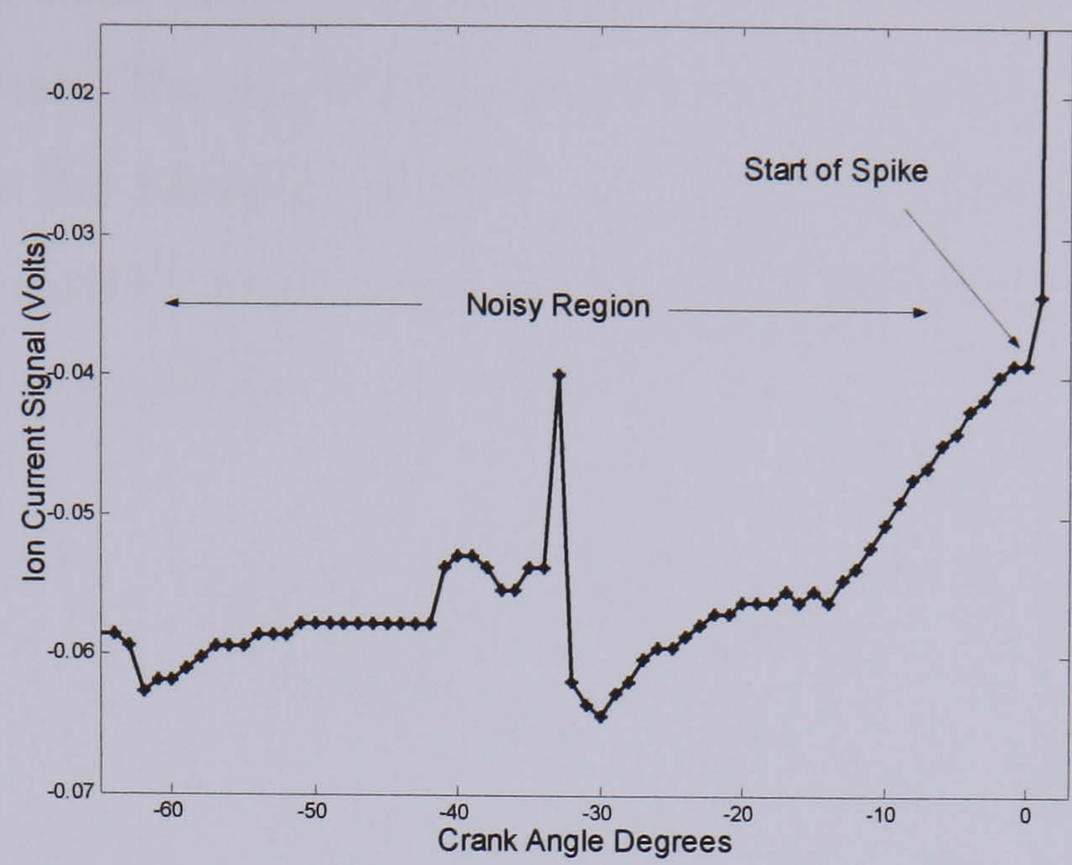

Figure 134: Detail of Noisy Region Before Spike.

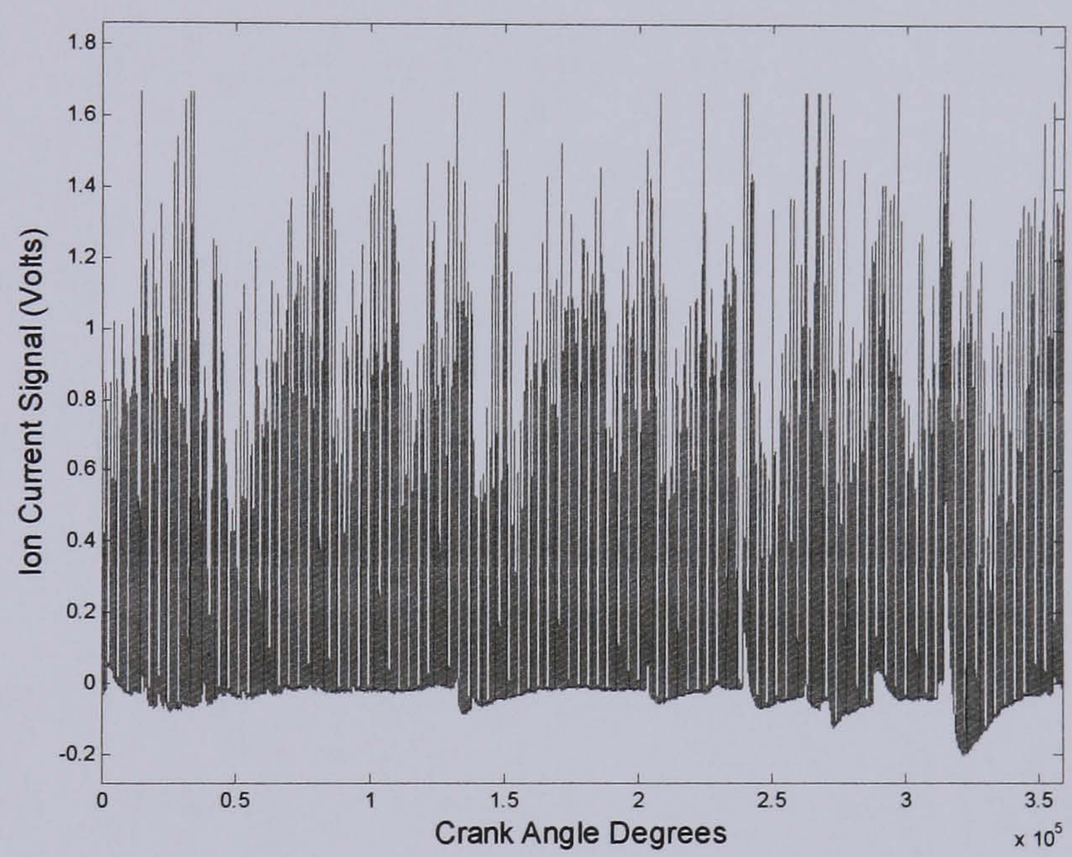

Figure 135: Example of Base Drift.

7.1.4 Dynamic Trigger Estimation of Signal Start

The classic approach is based upon certain assumptions which work well for the type of signal encountered during this research. These are that there is no combustion in the first 100 data points and that the base drift is not fast enough to affect the signal within a cycle. The algorithm employed uses the initial 100 data points of each cycle to work out the value for the base of the signal and to gauge its background noise by taking their standard deviation. A dynamic trigger level can then be established by setting a tolerance window around the base level (in this research and for this signal, set to 10 standard deviations).

The algorithm then starts from the position of the spike's peak and goes backwards towards the cycle's start. The criterion for classifying a point as the spike's start is for it to have dropped within the tolerance window. The value of ten standard deviations quoted might seem as unacceptably high. However, due to the sharpness of the spike, this value has been found to be appropriate.

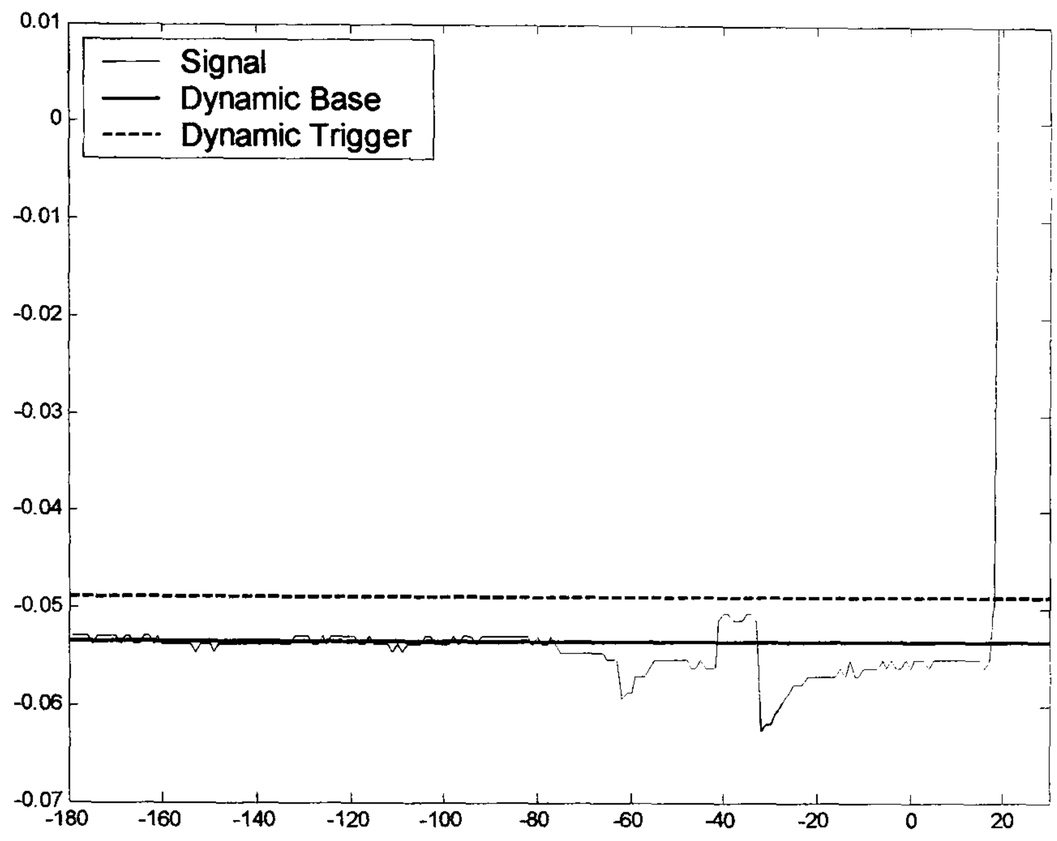

Figure 136: Ion Current Signal Showing Base and Trigger Level.

Another variation of this technique can consider a rolling window instead of single points. This is essentially the same concept, looking at individual points backwards from the spike's maximum. In this scenario however, the average value and standard deviation of all the points previous to the point being considered is being estimated and used as a criterion. This variation also yields good results. However, since, both these variations can be tuned to yield almost identical results, only the first one will be discussed here as it is obviously the faster of the two.

The advantage of this technique is that, because the processing starts at the peak of the signal, it usually terminates after considering very few points, given that the start and peak are normally very close together. It can be further speeded up by considering fewer initial points in order to estimate the dynamic base and trigger level.

The disadvantage is that it needs to be presented with the whole signal since it needs to establish the position of the spike's peak first. This is a problem when considering real time, cycle-to-cycle implementation on a working engine. However, the magnitude of the spike for a non misfiring cycle is normally such that, even a simplistic static trigger

approach should pick it out of the noisy signal (assuming the quality of the signal can remain similar to that encountered in this research, during real time implementation). If that is given, the processing for the estimation of the start of the spike can start immediately after the trigger level has been reached, even if the actual peak has not yet been recorded.

Having finished with the basic treatment of the ion current, further observations on its behaviour with relation to combustion can be made.

7.1.5 TRG Levels and Ion Current Signal

A quite important feature of the ion current signal is that it can be used to determine the TRG%. In practice this is highly important because different intake air temperatures (IAT), manifold absolute pressures (MAP), coolant temperatures (CLT), air humidity and a host of other unknowns such as engine wear, might change the amount of TRG, and this is difficult to express with mathematical models and knowledge of valve timing. By having an in-cylinder sensor, what can be termed as the "effective TRG" can be determined via one of two simple methods.

The first method of finding TRG level is by measuring the ion-current signal strength, shown in Figure 137. Increasing TRG quantity results in a decrease in the measured ion current signal, and a linear correlation is exhibited between the two parameters. It is important to note that in spite of this decrease, the ion current the signal always remains within measurable range. Moreover, higher sensor voltages or signal amplification could be used in applications where signal strength becomes an issue.

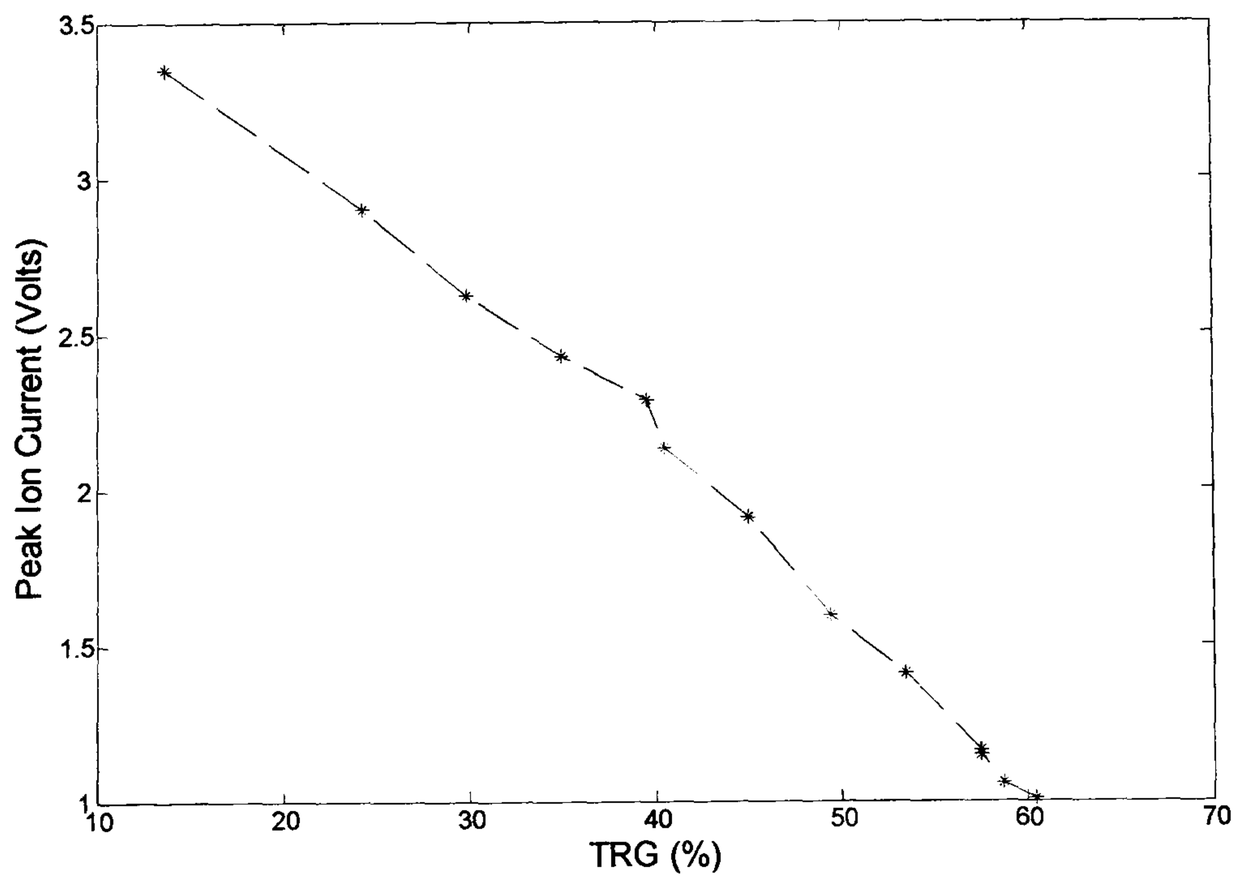

Figure 137: Ion-current signal strength as a function of TRG% at 2000rpm.

The second method of determining the effective TRG levels is through the acquisition of the ion current signal slope. Again, the slope decreases as the TRG amount increases, although not in a linear fashion, as shown in Figure 138. By assuming a simple model that considers the signal start as the point of which the ion current sensor detects any ion activity within a close range of its vicinity and the signal peak as the point of which full activity is apparent, the slope becomes a measure of the time taken between these two events. With this in mind it can be inferred that fast combustion will be presented as a steep slope while slow combustion will give milder slopes. As such, TRG amounts that result in fast combustion will give the steepest slopes. This happens half way between pure SI and pure CAI operation, the exact point depending on factors such as compression ratio and combustion chamber design. Pure SI operation is slow because it is solely deflagration and pure CAI operation is slow because of the high dilution. The region between spark assisted SA-CAI and very early CAI is the region where the exhaust gases have very high temperatures and are of adequate quantity to induce large scale or complete, vigorous detonation.

It has to be noted here that other parameters affecting the speed of combustion, mainly AFR, will also affect the ion current slope, so the AFR should be constant for the ion current slope to be only a function of TRG. In addition, the effect of TRG on the slope of ion current is not as pronounced if the signal is normalized against its maximum value. This implies that the TRG effect on slope is amplified due to the dependency of the signal strength on TRG, before normalization.

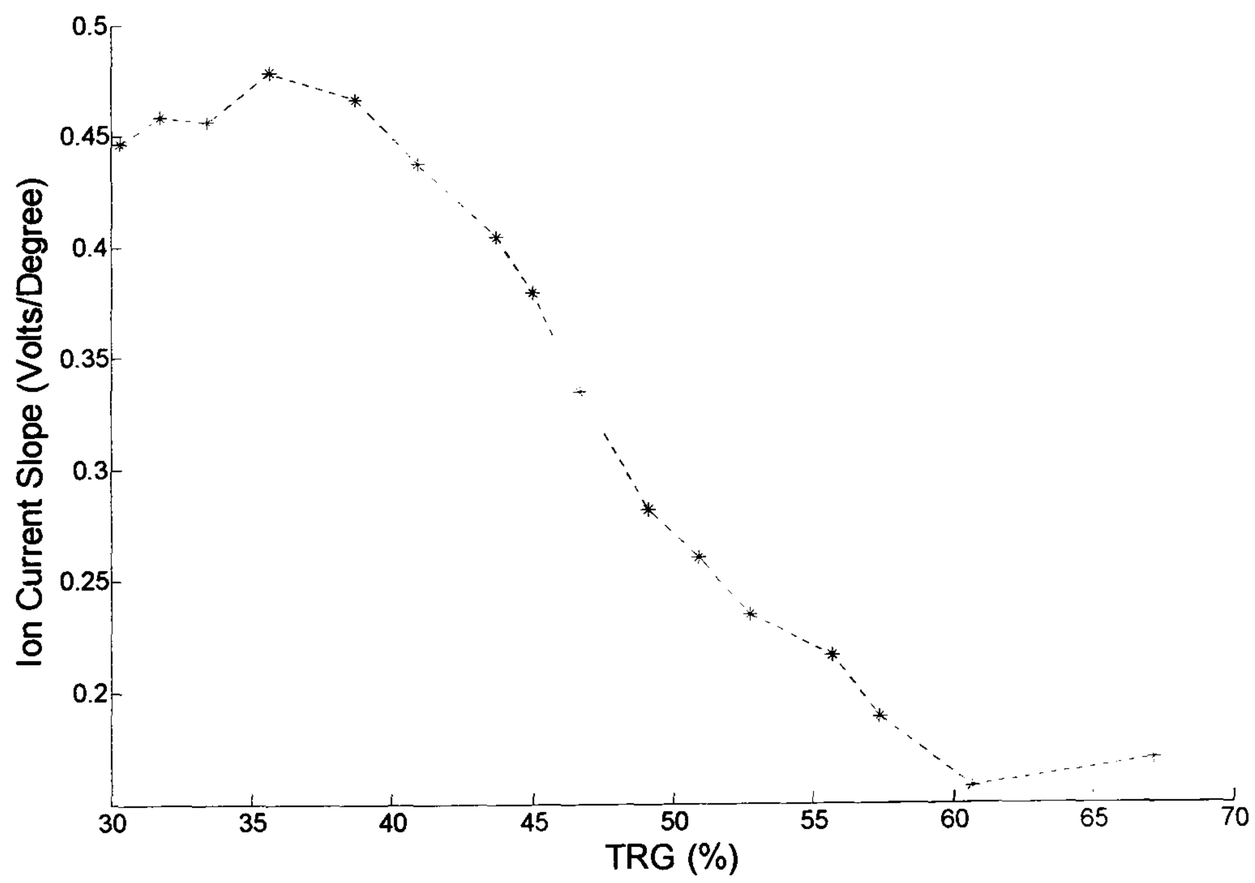

Figure 138: Ion-current signal slope as a function of TRG% at 1500rpm.

7.1.6 Combustion Performance and Ion Current Signal

Ion current can also be used to determine PPP, or similar combustion parameters like MFB50 and maximum rate of heat release (dQ MAX). Determining any of these is important in any engine, however in CAI where control of the SoC and heat release rate are notoriously difficult, it is almost essential. It has to be noted here that in gasoline CAI engines, combustion modes change from flame propagation only (low TRG%) to flame propagation with end-gas autoignition (medium TRG%) and finally bulk autoignition (high TRG%). As these modes change, different relationships occur between PPP, MFB50 and dQ MAX, in contrast to SI engines where their correlation is far simpler.

Three ways of correlating ion current to combustion parameters are shown. The results presented here are for 3000rpm medium TRG%, but similar results are obtained from all operating conditions. The first method is by correlating the start of the ion current, shown in Figure 139. As can be seen correlation coefficients are high and almost identical between the three combustion parameters, and the RMS errors are small and well under 2 crank angle degrees (CAD).

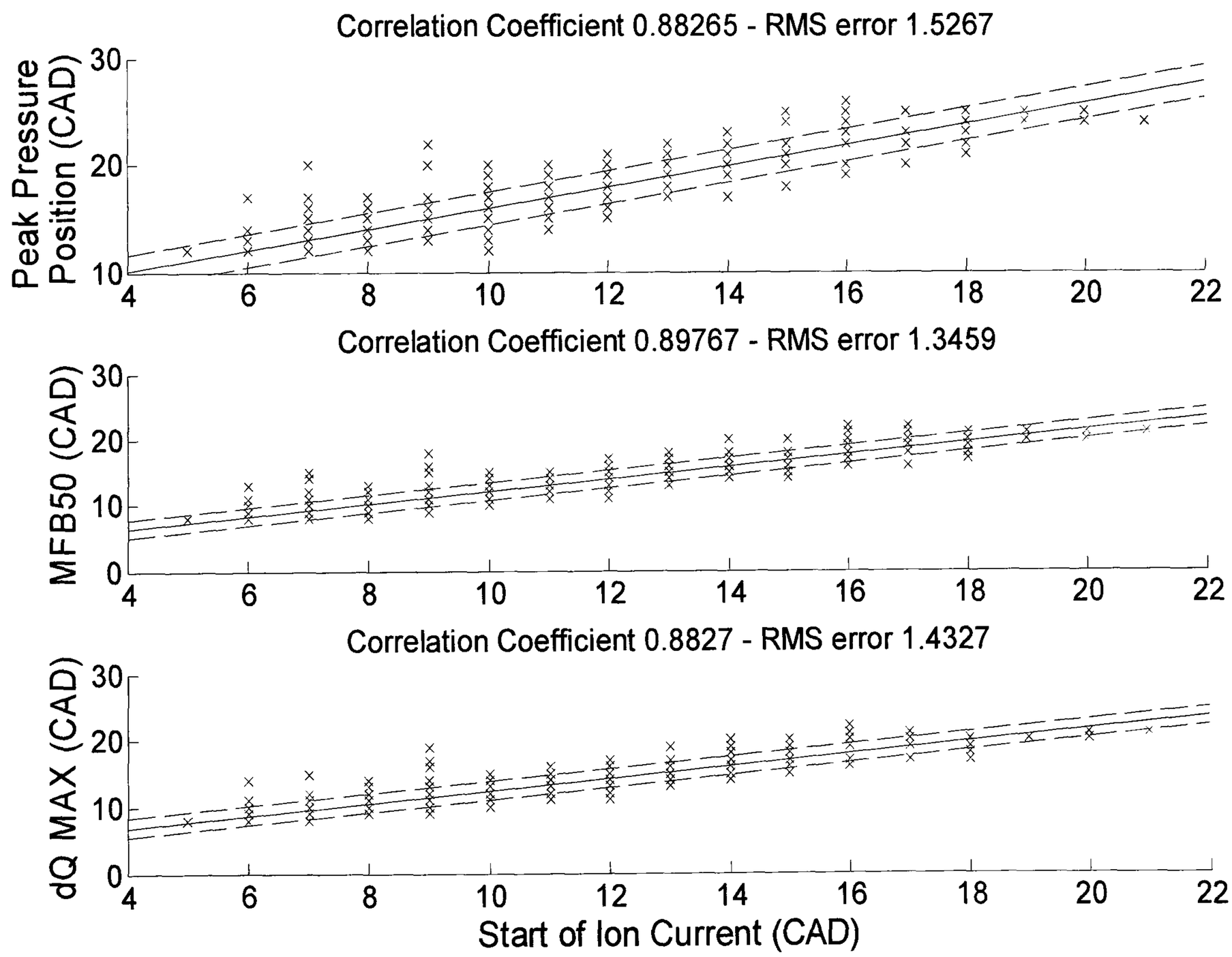

Figure 139: Start of ion current vs. combustion characteristics.

The second method is to correlate the 50% ion current signal as suggested by [167], and the third method is to correlate the position of signal peak. In all three methods, a linear correlation is used and the resulting PPP estimation has an RMS error of less than 2 CAD. However, the estimation is improved when using the peak ion current position as the signal is stronger and thus the signal to noise ratio (SNR) is better. Figure 140 and Figure 141 show the 50% and peak signal correlations with PPP respectively, again at 3000rpm medium TRG%.

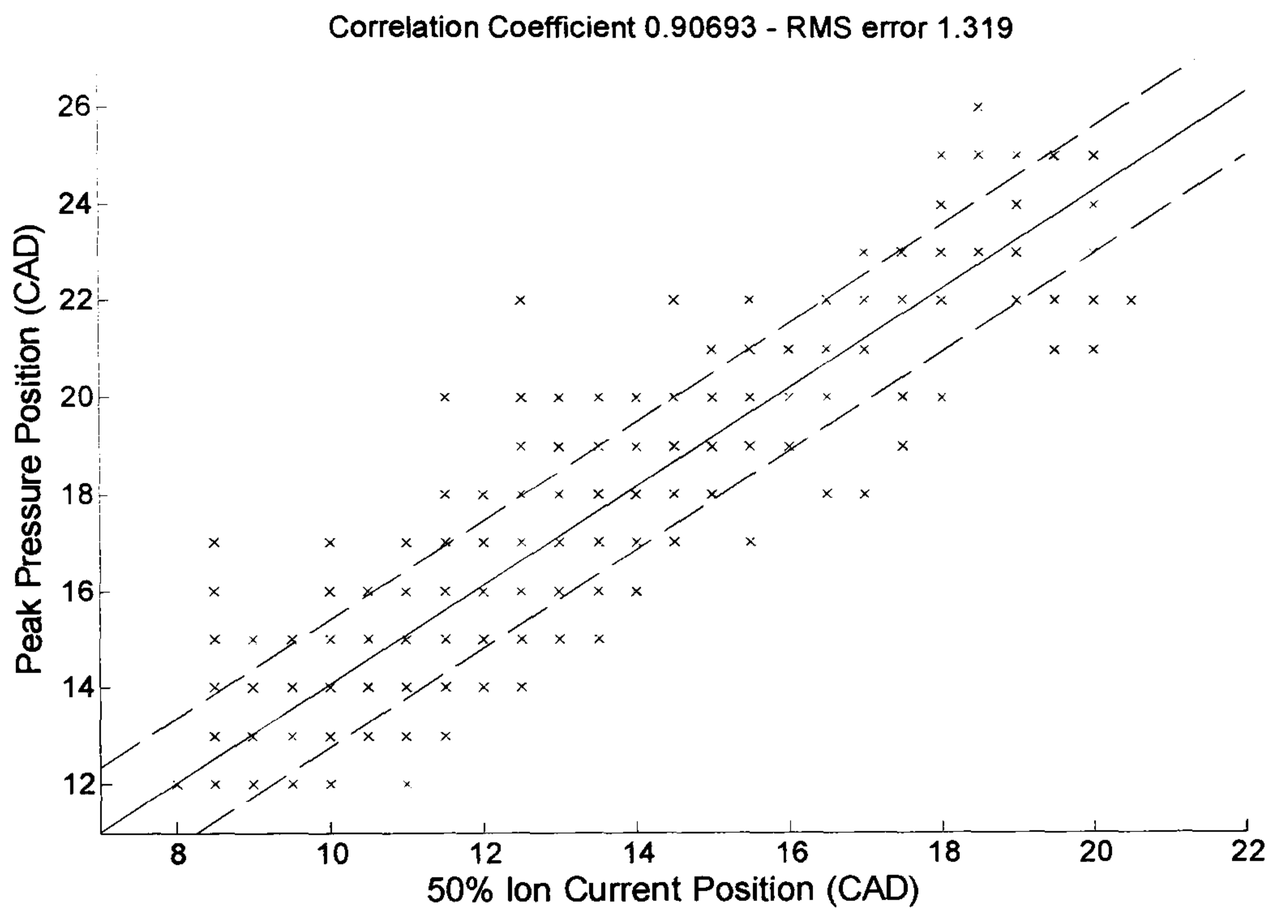

Figure 140: Position of 50% ion current vs. PPP.

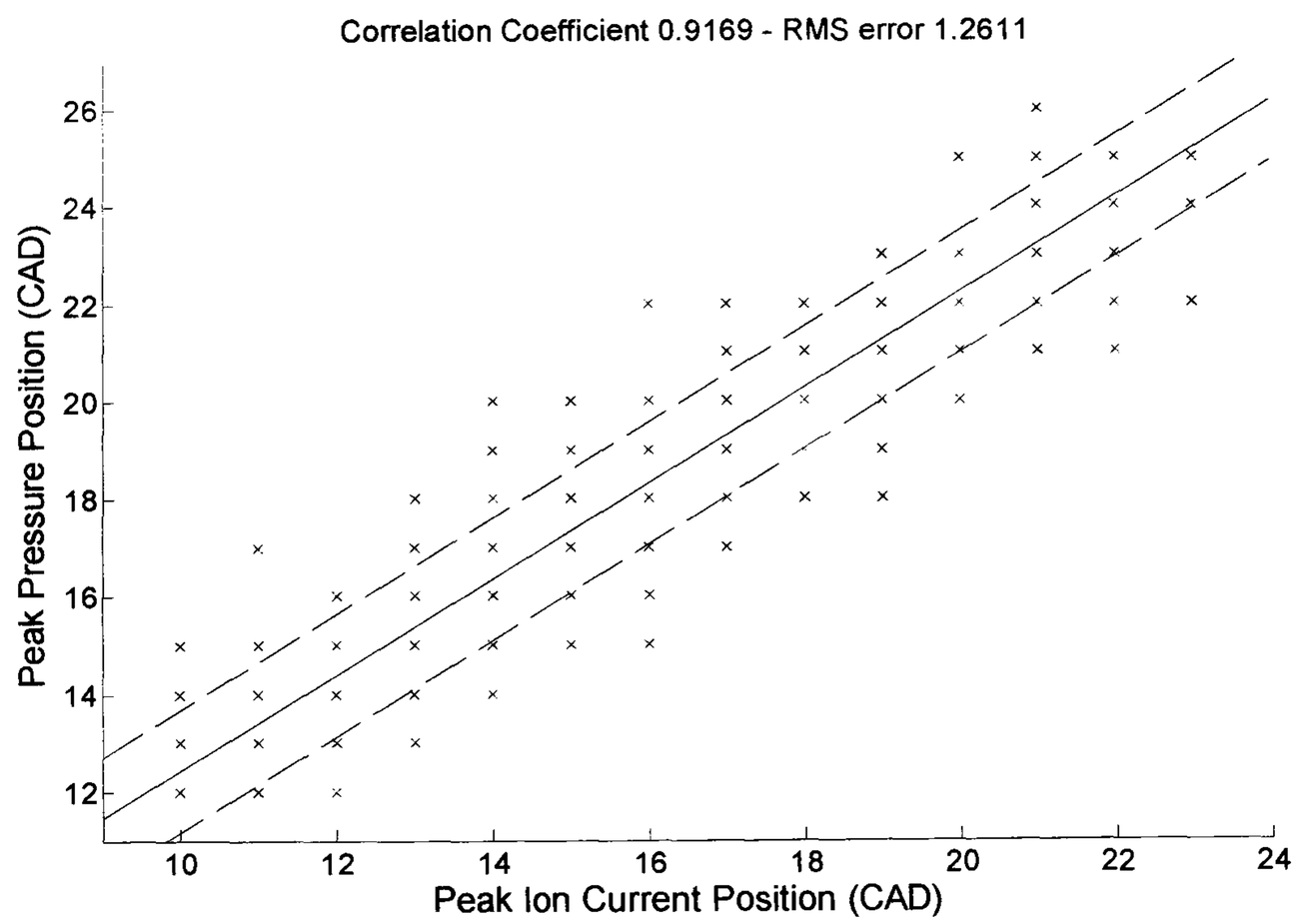

Figure 141: Peak ion current position vs. PPP.

Although a linear estimation is a simple technique and yields acceptable results, it becomes more difficult to implement when a greater range of engine operation is examined, such as varying amounts of TRG. Figure 142 shows the average start of ion current signal and PPP averaged from 500 cycles across the whole CAI operating region between 1500 rpm and 3500 rpm, and from SI to maximum TRG% (misfire limit). The same trends are repeated if 50% ion current or peak ion current were plotted instead of start of ion current.

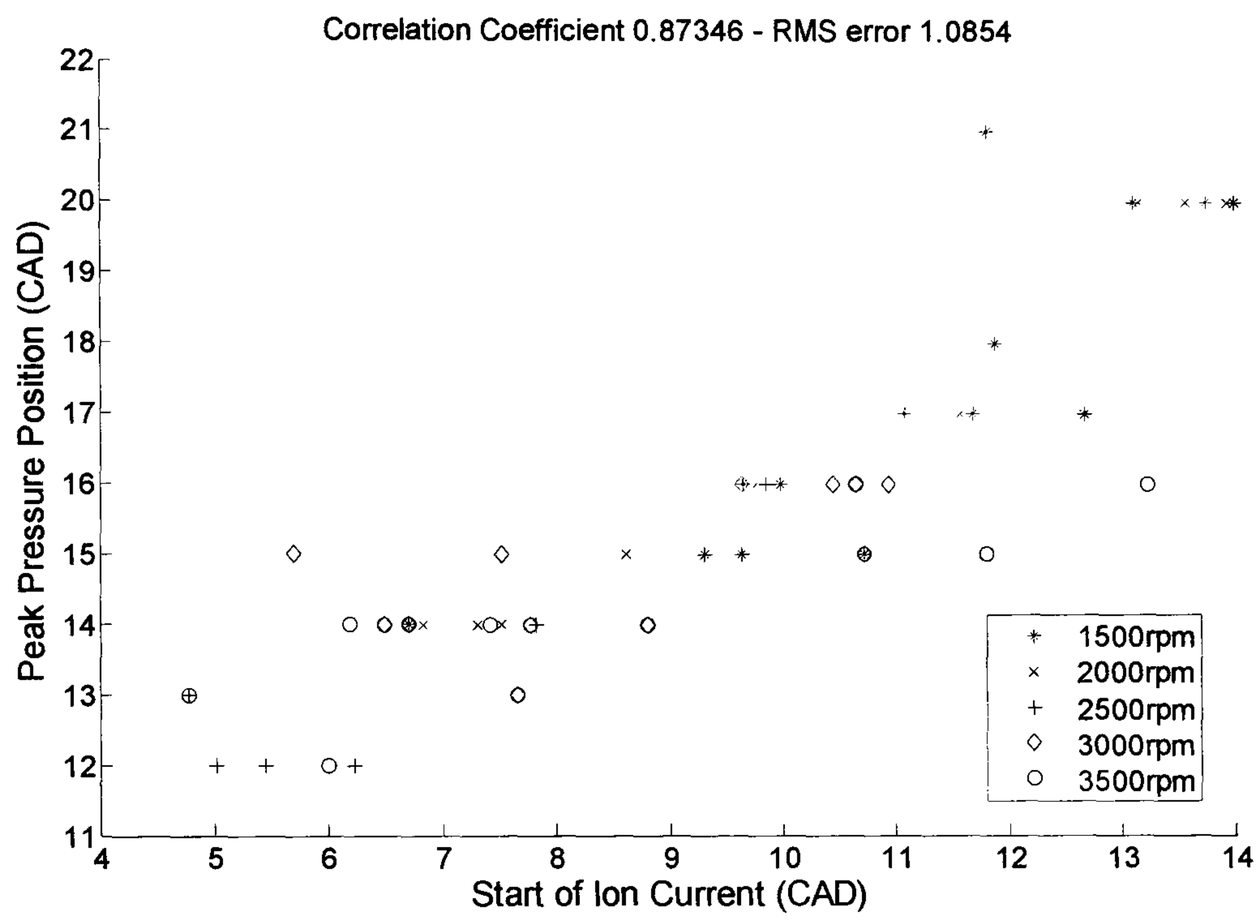

Figure 142: Start of ion current signal and PPP at various speed.

It is obvious that the estimation accuracy reduces if the same linear equation is used for the whole TRG spectrum, regardless of the correlation parameter employed. This is because combustion modes change with varying amounts of TRG thus affecting the signal in more than one ways, so estimation precision could be further increased through the use of more advanced signal interpretation techniques correlating more than one ion current characteristics to PPP, such as ion current slope. Nevertheless; correlation coefficients remain high, even with the simple linear approach. This indicates that ion current could, if computational power is an issue, be directly/linearly correlated for combustion analysis purposes.

On a cycle-to-cycle basis and considering the whole CAI operating envelope, the graphs seem a lot less attractive. Figure 143 and Figure 144 show PPP correlation to peak ion

current position. Despite appearances, the correlation coefficient is still high, and the RMS error is only increased to 2.64 deg CAD.

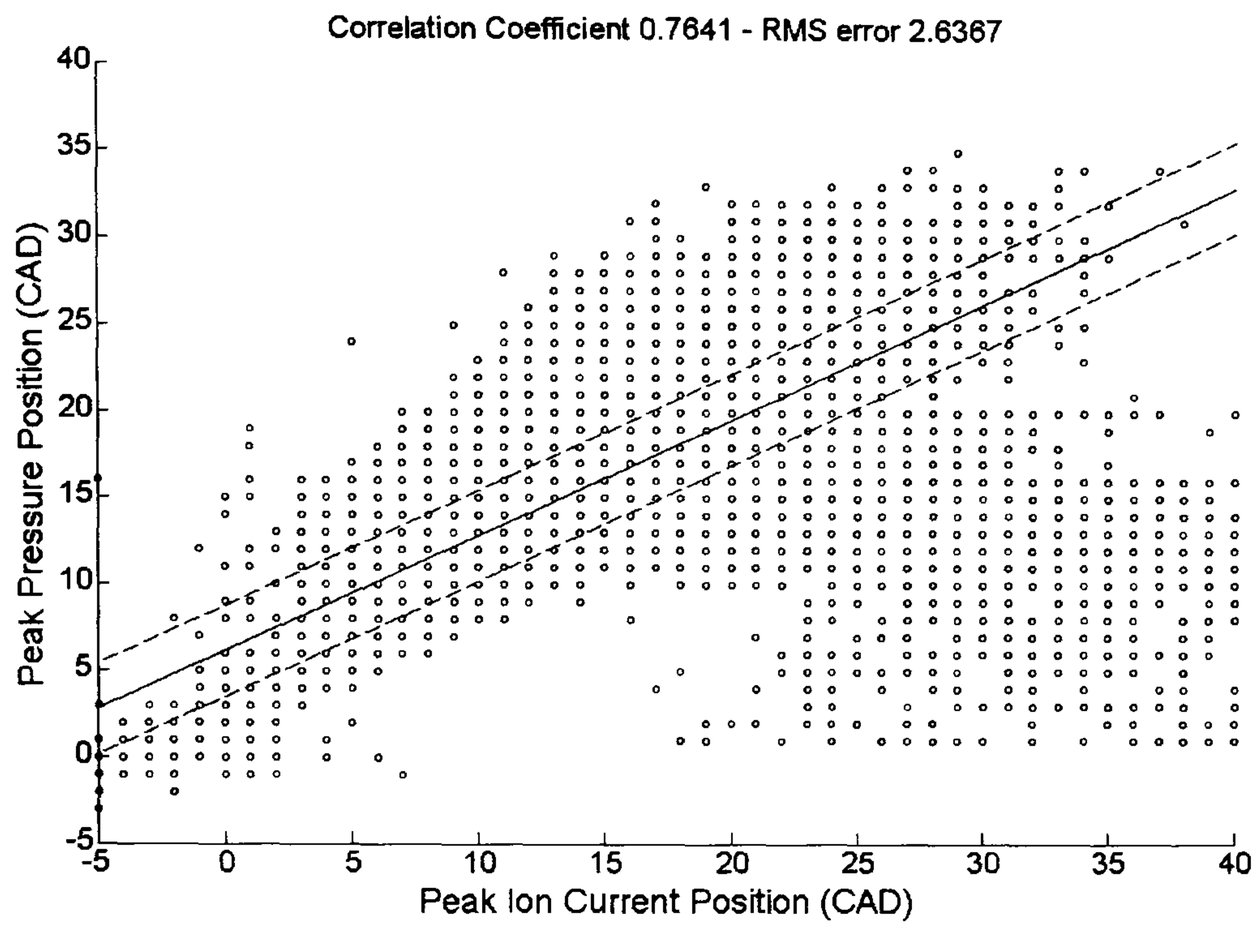

Figure 143: Cycle-to-cycle peak ion current vs. PPP.

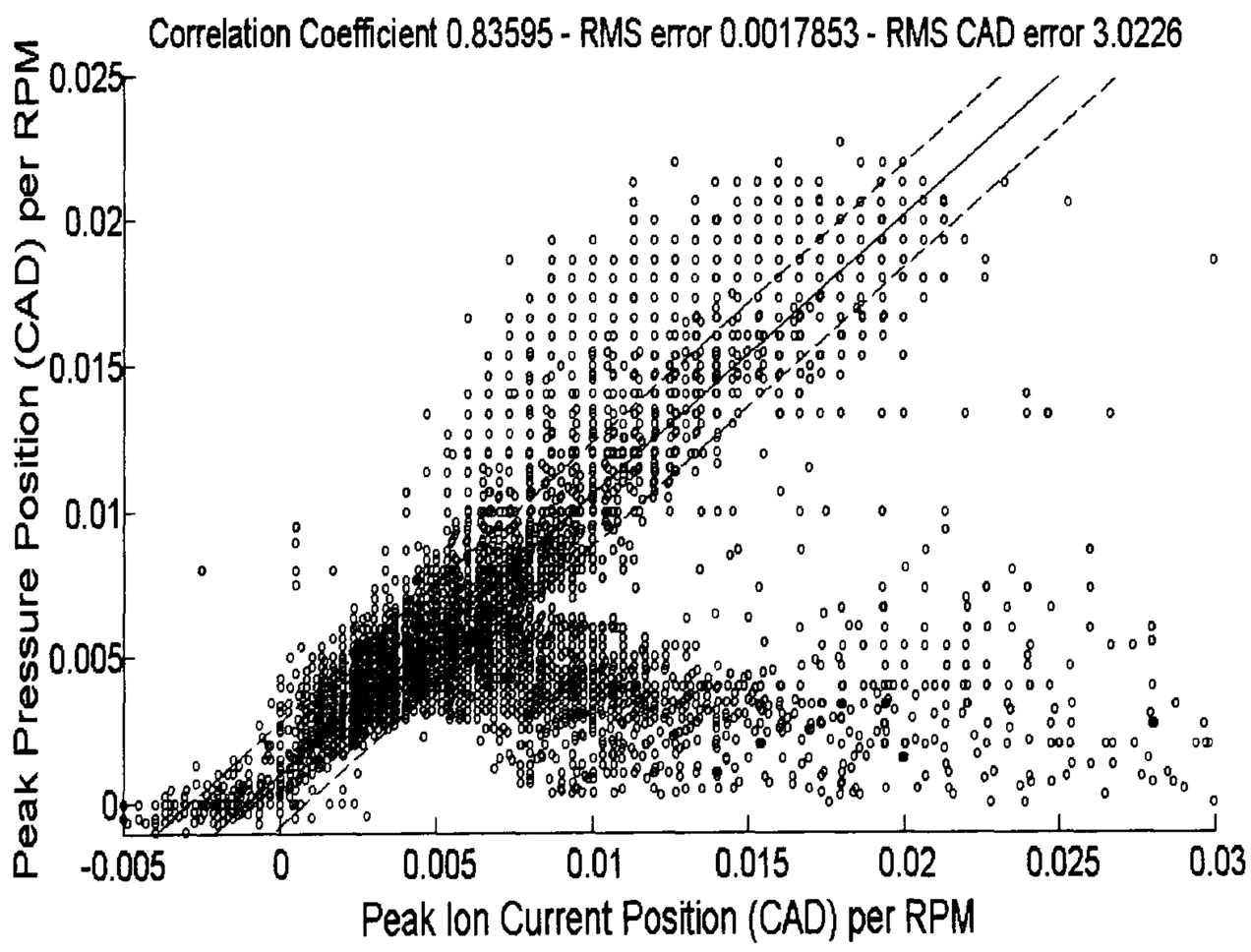

Figure 144: Cycle-to-cycle peak ion current vs. PPP.

Transforming the acquired signals on time domain, (by dividing them by rpm) provides a better insight into this problem as data from different speeds are better separated. As can be seen in both cycle-to-cycle figures however (Figure 143, Figure 144), there is a "leg" of data points that breaks off the main diagonal correlation. In the graph, regardless of the

number of times that a data point occurred, it leaves the same footprint. As such, it is difficult to visually inspect the "weight" of this leg. So, although not easily identifiable on the graph, analysis showed that the percentage of data points on this "leg" are relatively small (<5%), so this is not a major source of error.

A possible explanation for this feature might be that the different knocking modes, that result in different acoustic or oscillation modes, that may occur in a combustion chamber depend on mixture distribution, which can vary, even under the same operating conditions, as suggested in [168]. These modes can vary between circumferential and radial and also have different shapes, within their domain. As mentioned before, more advanced interpretation techniques will improve results by taking in account more than one ion current parameters, i.e. by not looking at Peak Position of Ion Current alone. However, the only way to radically improve accuracy would be to use more than one ion current sensor. This would give a more complete, and less localized, picture of the combustion process.

From the forgoing discussion, it becomes apparent that ion current lends itself to an easy and cost effective solution to combustion diagnostics, during CAI operation. A simple integration of the signal can reveal misfires, while the position of the start, 50% or maximum of the signal can be used to determine more intricate combustion properties like Peak Pressure, MFB50 or DQmax positions. Its strength or slope can determine dilution levels. Irregular positioning of the signal, like very early or very late in the combustion cycle, can reveal preignition or partial late combustion.

Using a simple linear relationship between the ion current measurants and combustion parameters will provide fast and computationally feasible prediction capabilities, of adequate precision, which could be used in a cycle-to-cycle control strategy. Results of less than 3 CAD RMS combustion prediction error where obtained. For comparison, a current map based ignition system for SI engines is capable of controlling PPP to about the same value, on a new engine.

7.1.7 ITA Effect on Ion Current Signal

Since spark assistance is used to control PPP in all but the few pure CAI cases, it is important to determine the effect that the ignition timing advance (ITA) will have on the SoC and thus PPP and ion current signal. SI operation is directly dictated by ITA, while in pure CAI it has a minor effect. It is thus logical to show here a mid-way TRG%

scenario. In Figure 145, the effects of an ignition timing sweep are shown against start of ion current signal at 2200rpm with medium TRG%. Once again, a close correlation of pressure to ion current measurants can be seen. As PPP delays, in crank angle terms, as ITA is retarded, the ion current signal start delays too.

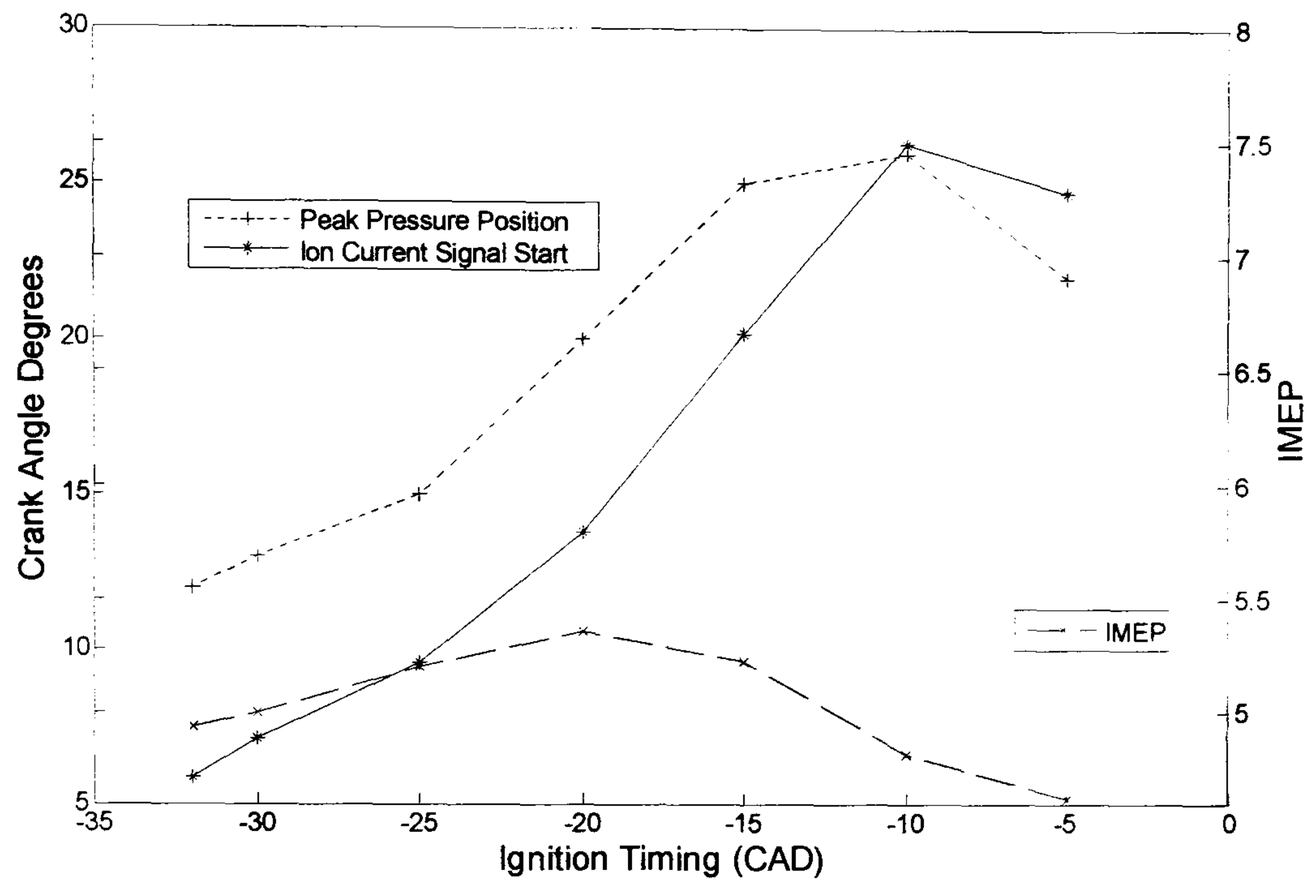

Figure 145: Ignition timing effect on start of ion current.

It is clear that the ITA does have an effect on both PPP and ion current signal. Both are retarded as ITA is retarded in a close correlation.

The cross over point that appears when ITA equals -10 CAD-BTDC (where combustion is delayed beyond the point that would be observed in practical applications). A possible explanation of this phenomenon is that when the spark is delayed enough to allow the fuel time to chemically break up and autoignite, the result is a sharper pressure rise and hence advanced PPP. On the contrary, if the spark is early enough to consume a considerable portion of the combustible mixture, before autoignition pressure rise will be gentler. This explanation is plausible if the mixture is considered as inhomogeneous.

According to the mixing model of [169], referring to a gasoline CAI engine with almost identical valve strategy, the charge around the spark plug is less diluted with EGR, as there is a higher concentration of 'fresh charge' near the top of the combustion chamber, whereas at the bottom where TRG will be mostly concentrated. If this is so, it will be the fresh charge near the spark plug that will combust most vigorously once autoignited. However, if the fresh charge is consumed by SI flame propagation, the heat release will

be slower during both the flame propagation phase and the autoignition phase that will occur at the more diluted end gases.

CAI engines are complicated in that the load has to be controlled by the amount of TRG and with load varying almost continuously; the automotive engine must have the flexibility to adjust TRG whilst also controlling combustion timing. Effectively, when the engine is operating in the CAI region, the throttle pedal angle needs to be interpreted to a torque requirement. This requirement will then command an increased or decreased negative valve overlap, translating to an appropriate TRG%. The ion current measurants during these transients can be used to control combustion in terms of timing, through ignition timing advance (ITA). If SoC is too late, the ignition can be advanced and vice versa. During steady state operation, ITA has enough control over the combustion event to time it appropriately. However, during transients it might be necessary to use other means of control. There exist two possible events when a sudden change in torque demand occurs.

1. In the case where there is a decrease in demanded torque, more TRG will have to be used. This will mean that hot gases from a low or medium TRG combustion will suddenly be used in larger amounts leading to early combustion. Retarding ITA might help: except where early autoignition occurs regardless of ITA. In this case the valve timing transition has to be delaying.

2. Where an increase in torque is required, cold TRG from highly diluted combustion will be required to combust with a lot more fresh charge, since a decrease in TRG will be necessary. Late combustion might be prevented by advancing ITA and lower amounts of TRG equates to higher combustion control through the spark. If this measure proves inadequate, switching to SI operation can rescue the situation.

So, be it transients or steady state operation, the ion current signal can be used by an engine control system to decide on advancing or retarding ITA; or this strategy is inadequate, to adjust valve timing. By using the ion current signal, all this is possible on a cycle-to-cycle basis with no averaging requirements. This is especially helpful during transients, or unstable combustion.

7.2 Ion Current Signal Interpretation via Artificial Neural Networks for Gasoline CAI Control

This chapter intends to expand on the idea of using lightweight ANNs on SI to their application on CAI engines. What is being investigated is the strategy behind the building of a specific algorithm for extracting combustion information from the ion current signal of a CAI engine.

The ideas presented here are based on the following design criteria. On the hardware side, like on the SI implementation the ion current signal is given a dedicated circuit. On the software side, the algorithm must be implemented on a cycle-to-cycle basis with no averaging involved. The rationale is to evaluate the performance of the algorithms at a demanding level.

The next consideration is the algorithms themselves. Since the Adaptive Linear Elements (ADALINEs) type of Artificial Neural Network (ANN) proved to work for SI with good results, it is a candidate. It is a very lightweight and robust ANN type, owing this to its simplicity. Other ion current researchers use [170] Multi-Layer Perceptrons (MLPs). To test other alternatives to MLPs, this research also evaluated Generalised Regression Neural Networks (GRNNs). The advantages of both ADALINEs and GRNNs lie in the relative minimalism of their architecture, which offers little room for ambiguity over the optimum design. GRNNs are very similar to Radial Basis Functions (RBFs). However, for the data used in this research, GRNNs greatly outperformed RBFs so were chosen instead.

The final consideration is the choice of pre-processing techniques. A classic approach is to use signal processing algorithms in order to extract various characteristic measurants from the ion current signal to be used as input to the ANNs. To this end, the use of wavelet algorithms has been evaluated. Wavelets are a signal processing tool that is being used in a variety of applications [171], ion current signal processing being an ideal candidate [172]. An interesting advantage of wavelets is that the treated signal can be reduced in size, thus making the use of the wavelet output directly into the ANN a possibility. This approach is also investigated.

7.2.1 Wavelet Based Estimation of Signal Start

The dynamic trigger that was discussed before as a technique to extract the signal start position produces satisfactory results and would be the weapon of choice for a simple

engine management system. However, when considering ANNs more capable electronics would have to be employed. With this additional computational power at hand, other ways of looking at the problem of signal start estimation can emerge. Thus, a second technique used for estimating the start of the ion current signal that was based on wavelet decomposition, is presented here. Wavelets are a very promising tool for signal analysis which has been implemented in the context of ion current interpretation [172]. Given this particular problem, their strength lies in being able to establish the exact location of various frequency components of a complicated signal. The results described in this research have all been implemented using the Wavelet toolbox in MATLAB.

Traditionally, a wavelet transform works by taking a given waveform (wavelet) scaling it to different wavelengths and comparing it to the signal across the signal's length. This analysis gives a very thorough overview of the signal composition. However, it is unrealistically time consuming for the task at hand. Thus, a faster algorithm can be employed, the discrete wavelet transform Discrete Wavelet Transform (DWT), which in essence works by splitting the signal into a high and low frequency part, where the choice of wavelet acts as the kind of filter to be used. In wavelet analysis, these two low and high frequency components of the signal are often referred to as *approximation* and *details*. Through a process called downsampling, these are reduced to approximately half the length of the original signal.

Although, this process can be repeated to decompose the signal to deeper levels, in this case only the high frequency, *details*, part is of interest and one level of decomposition is adequate.

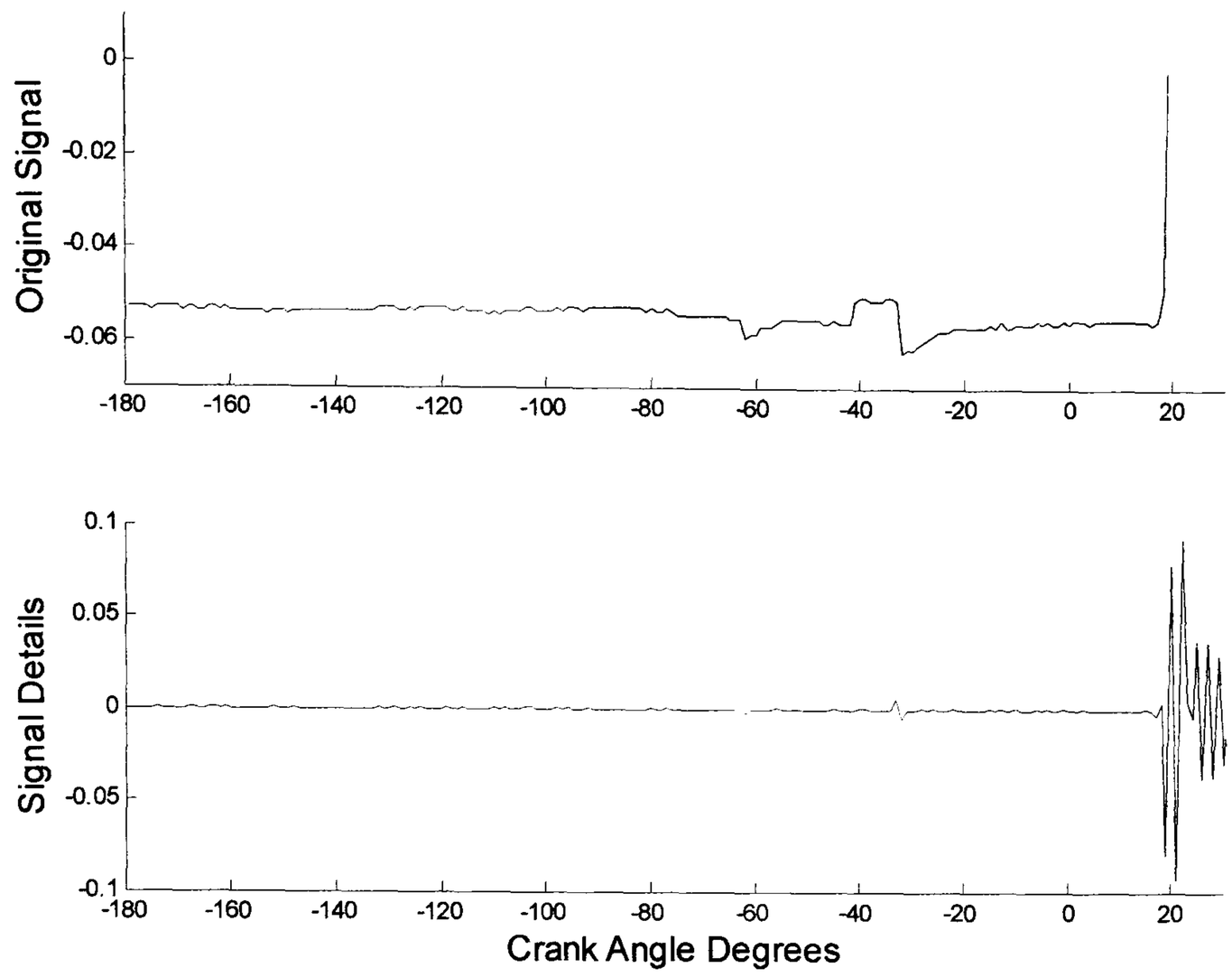

Figure 146: Original Ion Current Signal and DWT Generated Details.

Figure 146 shows the original signal zoomed in before the start of the spike, occurring around 20 CAD, along with its *details* after one decomposition. It is obvious how the *details* easily mark the start of the spike.

This behaviour lends itself to very easy identification of the spike start by simply working backwards from the maximum value of the *details* signal until reaching a "calm" region (implemented by checking that all members of a fixed size window are below a static trigger value) without need for a dynamic trigger. A major advantage, visible in Figure 146 is that the *details* are not affected by the base drift, since the latter has very long wavelength. This is why a static trigger can be successfully implemented in the case of the algorithm employing wavelet decomposition.

Of the available wavelets, the *Daubechies* and *Symlet* families produce results that most readily resemble the results of the classic algorithm. In fact, the best agreement comes from the Daubechies 1 (also Haar) wavelet, where the average error between their results is less than 1 CAD. It has to be pointed out though that the results of the classic algorithm are not necessarily a "correct" target to be met. In most of the ambiguous cases, the precise start of the signal is open to interpretation, even by a human. Having been the first to be developed, the classic algorithm has been the one most closely tuned to return agreeable bulk results. Hence, agreement with it is a good indicator of performance but is

by no means a definitive test since the algorithm can always be tuned to yield even "better" results for a particular wavelet.

This very elegant implementation hides the major processing that is done behind the scenes by the discrete wavelet transform. However, a real time implementation of such a technique can potentially be optimized for the task to an extent much greater than was done in this research where readily available, general purpose functions from the MATLAB wavelet toolbox were used. In addition, the implementation can and indeed must, be narrowed down to a specific window of interest in a real time implementation. In this case, tested as proof of concept on the whole length of the signal, it performed approximately 20 times slower than the classic algorithm, which is a stripped down procedure designed strictly for identifying the signal start. As pointed out however, this is not by any means representative of the relative computational speed a purpose built wavelet based algorithm could achieve. For a real time, cycle-to-cycle implementation, the major concern has to be speed and at this point, this particular implementation of wavelets seems to be at a disadvantage. However, the possibility of treating additional information inherent in the wavelet decomposed signal, coupled with the ability to process the reduced size *approximation* and *details* signals make wavelets a promising tool for analysis of the ion current signal as is described below.

7.2.2 The Wavelet Decomposition of the Ion Current signal procedure

A major strength of the wavelet decomposition lies in the reduction in signal size. The measurant extraction method described previously, explicitly reduces the original signal to a few numbers describing geometrical characteristics. However, decomposing the signal through employing the DWT algorithm reduces the signal while retaining significant information.

Figure 147 shows an ion current signal and the subsequent two levels of decomposition. The figure highlights how varying levels of decomposition reduce the signal length while retaining the main features.

By reducing the signal size in this way, an ANN can be designed whose input layer will be much shorter than would be needed if the whole signal was to be used as an input. Thus, the reduced size ANN will be much faster. However, deeper levels of decomposition take more time on the DWT. Also, deeper decomposition the signal can potentially degrade the ANN output.

Hence, there is a trade-off between time spent on the DWT, time spent on the ANN and the overall performance. All these issues need to be taken into account when designing a system that should, in principle, be able to process cycle-to-cycle information from the ion current signal.

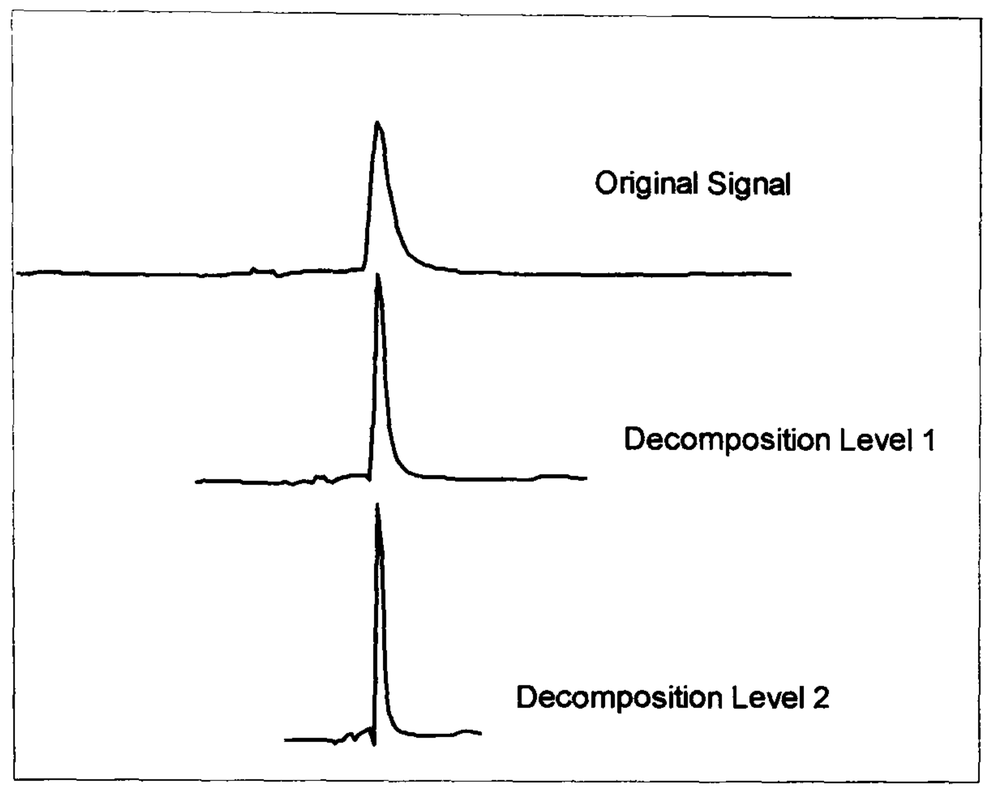

Figure 147: Example of Two Levels of Wavelet Decomposition of Ion Current Signal.

7.3 Artificial Neural Network Based Predictions

7.3.1 Types of Input

In order to test the feasibility of a control system having ion current based information for the pressure measurants, the data extracted by both the dynamic trigger and the wavelet procedures were presented to various different ANNs. The aim is to get the best predictions possible from as uncomplicated ANNs as possible for a great range of operating conditions. The two types of ANNs investigated are ADALINEs, and GRNNs.

ADALINEs are classic single layer ANNs, which use a linear transfer function. Their strength lies in their Least Mean Square training rule, which will always minimise the error of data presented in the training set, thus avoiding the ambiguity over the completeness of training that might be an issue with other ANN training algorithms. Their weakness lies in that they are, in effect, a system of linear equations and are thus not well equipped to respond to non linear relationships. As the sections on the ion current signal use on SI engines indicate, ADALINEs' responses for handling ion current data seem satisfactory for their strengths to compensate for their weaknesses.

GRNNs are two layer ANNs, with a Radial Basis Function (RBF) first layer and a linear second layer. Initial trials demonstrated that GRNNs give promising results. The question is to establish if their increased complexity, which incurs performance penalties, is worth their possible performance benefits.

The ANNs fall into two categories, depending on what kind of inputs they accept. In the first, the inputs consist of the extracted measurants through the use of the dynamic trigger technique. In this case, the ANN input layer size is the 4 extracted ion current measurants that appeared to be the most important ones, plus any additional information on engine operating conditions such as ENGINE SPEED. The 50% signal position and magnitude were not used. In the second, the input consists of the wavelet decomposed signal, normally the *approximation*, plus any engine operating conditions. In this case, the input layer is variable depending on the decomposition level.

In the case of the trigger extracted measurant data, certain additional tests have to be carried out. Before the data is presented to the ANNs, it goes through a final selection process. The data is organized in matrices where a set of inputs and corresponding set of outputs take up a row. Certain rows may represent cycles where one of these numbers has not been established, most likely because of a misfire, in which case ion current information is unavailable. In that case, the whole cycle is removed by deleting the respective row in the matrix. The other part of the selection involves outliers. Again, cycles which are problematic for any reason can either fool the extraction algorithms into returning unrealistic values or the cycles themselves have uncharacteristic values. This is treated by doing a histogram of the data and identifying the left and right edges at which points a certain percentage of the total data is present (set to 1.5% in this research). Data outside the region specified by these edges are discarded.

It has to be noted that none of these techniques have to be employed in a real time implementation. Cycles that return no ion current signal up to a certain point can be quickly classified as misfires anyway. Similarly, predefined triggers based on the operational conditions for the allowable range of values can be employed on the extracted measurants to decide very fast if a cycle is to be considered as normal before proceeding with the processing of its data.

In the case of the ANNs using the whole decomposed signal as an input, no such processing is carried out. This can be considered as a token of added robustness, since

there is no intermediary algorithm, other than the DWT itself, which might complicate the process.

The output of the ANNs is always PPP. In reality, there is a host of pressure related measurants that can be derived from a pressure trace, such as start of combustion, combustion duration etc. However, PPP is preferred because its extraction algorithm, which is simply a maximum point search, is simple to the point of guaranteed perfect accuracy. This is important since there is uncertainty on the input side, especially where the measurant extraction algorithms are concerned. Adding uncertainty on the output side through using a harder to extract measurant, such as start of combustion for example, will yield results that are more unrepresentative. It has to be pointed out, however, that in principle, an ANN can be designed to predict any pressure related measurant.

7.3.2 ANN Testing within Different Speed Sites

The first kind of data to be treated consists of steady state data collected at different engine speeds. TRG sweeps are carried out at each speed. All are WOT, with λ=1. Spark advance varies among members of the same speed site. The revolutions per minute (ENGINE SPEED) range covered is from 1500 to 3500.

To test performance of the algorithms described above, the initial test is done within the members of each speed site. The reasoning is that, at the very least, a control system switching between ANNs, each one trained for a certain ENGINE SPEED region, can be implemented for steady state operation. A question that might arise here is why classify the data according to engine speed and not TRG. The reason is that, unlike RPM, TRG is not directly measurable. For a given valve setting, the engine will trap a different amount of TRG at different RPM. Note that, in this throttleless valve strategy, load is adjusted via TRG, hence the RPM - TRG space is equivalent to the speed and load space.

Each training point corresponds to a cycle. The data points are randomly split into a training and a test group with the training group taking up 80% of the total sample. The ANN is then tested on the test sample. Because of the random nature of the selection of the test sample, no two consecutive tests will give the same result. For that reason, the numbers quoted throughout this research are averages of multiple tests. This scheme has been favored over simpler ones, such as taking the first 20% of data from each data log for example. The reason for this is that, in logs which exhibit areas of localized behavior, such as a series of unstable cycles, these might not be sampled, or not sampled at a

representative fraction. By making the selection random, the test sample is spread evenly over the whole of the data.

The errors quoted throughout are RMS errors of the difference between the ANN prediction and the actual value of the output. The units are always in CAD. The percentage errors quoted in certain cases correspond to the percentage of the error as a fraction of the overall spread of the actual values of the output.

Performance of Measurant Based ANNs

The results presented here correspond to the ANNs taking extracted ion current measurants as inputs. These initial trials do not supply the ANN with information on any other operating conditions. The performance of the ADALINE over the different speed sites is presented below:

Table 9: ADALINE Performance for Each Speed Site, Only Ion Current Measurant Inputs.

RPM	Error Classic (%)	Error Wavelet (%)
1500	2.34 (8)	2.35 (9)
2000	1.46 (6)	1.71 (8)
2500	2.19 (9)	2.23 (9)
3000	2.56 (10)	2.26 (10)
3500	3.08 (13)	3.53 (15)

Table 10: GRNN Performance for Each Speed Site, Only Ion Current Measurant Inputs.

RPM	Error Classic (%)	Error Wavelet (%)
1500	2.31 (9)	2.42 (9)
2000	1.46 (6)	1.40 (6)
2500	2.42 (5)	1.50 (6)
3000	2.14 (9)	1.86 (8)
3500	2.28 (10)	2.57 (11)

Table 9 summarizes the errors for PPP for each engine speed. The “Error Classic" and “Error Wavelet" refer to the CAD error for the speed group, depending on whether classic or wavelet techniques are used to extract the ion current measurants. The number in brackets is the respective percentage error.

The same trials, carried out on GRNNs are displayed on

Table 10.

These trials demonstrate any differences between both the wavelet and classic ion current measurant extraction techniques as well as the relative performance of ADALINEs and GRNNs. The differences between classic and wavelet measurant extraction methods generally appear small enough to be negligible. As far as the ANNs are concerned, the GRNNs seem to offer a slight advantage as well. However, it has to be noted that the GRNN takes approximately 7 times as long to process the same input.

Performance of Decomposed Signal Based ANNs

To get a better understanding of the relative merits of the different ANN designs, the same tests are carried out using the decomposed ion current signal. Table 11 displays the performance of these ANNs.

Table 11: ANN Performance for Each Speed Site, Decomposed Ion Current Signal as Input.

RPM	Error Classic (%)	Error Wavelet (%)
1500	4.04 (14)	4.02 (15)
2000	3.22 (13)	3.24 (15)
2500	3.62 (15)	3.5 (14)
3000	4.04 (16)	4.05 (16)
3500	3.30 (14)	3.33 (14)

These results were produced through ANNs at various decomposition levels. The ion current signal decomposition was carried out using the "db2" wavelet and the levels varied between 1 and 5. The errors quoted are the best results, however, the results did not vary for more than 7% across the decomposition levels in the case of these tests within RPM speed groups. The analysis of the relation between error, computational time and decomposition level is presented in detail in the "Performance of decomposed signal based ANNs" section.

The tests presented here are only carried out to investigate the capabilities of the ANNs on separated sets of data. The most important test, however, is to test performance of a single ANN across the RPM range as well. The feasibility of such an ANN can greatly enhance the performance of a cycle-to-cycle control system.

7.3.3 ANN Testing Across Different Speed Sites

Having tested that the performance of the ANNs seems promising within single engine speed groups, the next step is to test it across the span of RPM. As in the previous section, the results are split between the measurant based and decomposed signal based ANNs.

Performance of Measurant Based ANNs

At this stage, the effect of adding of operation information to the ANNs is assessed. In the first instance an ADALINE and a GRNN are trained and tested on the whole of the RPM range. In the second instance, apart from the ion current measurants, additional information is supplied to the ANNs in the form of the following:

1. RPM

2. Negative overlap

3. Ignition timing

4. Airflow

The negative overlap is one way of measuring amount of TRG. However, it is not directly representative of the actual mass of TRG, as this also depends on volumetric efficiency, a function of engine speed. It is however, an easy way of getting a handle of the TRG. Similarly, the airflow is a rough measure of the each cycle's energy intake. Since all these data are stoichiometric, logged at WOT, the power output is regulated by the TRG amount (which is in turn regulated by the negative overlap), which has a direct impact on the airflow.

Again, to account for statistical error arising from the random nature of the selection of the training and test sets, a series of tests have been performed for each case and the average results quoted. One point worth mentioning here is that care has to be taken when quoting the error across mixed speed groups. There are two factors that can contribute to unequal effects of each group's error on the final value. First, is the fact that not all groups have the same amount of logs in them. This will be reflected in the overall sample, making groups with larger populations dominate the result. Second, is the random selection process of the test points. Despite being superior, the disadvantage is that it adds fuzziness to the amount of cycles taken from each group. To address these concerns, the test points have been labelled according to the speed group they belong to and at the end, errors have been calculated for each individual group. The final error quoted is the mean

of these, thus each group contributes equally to it irrespective of how many of its members make it to the test sample.

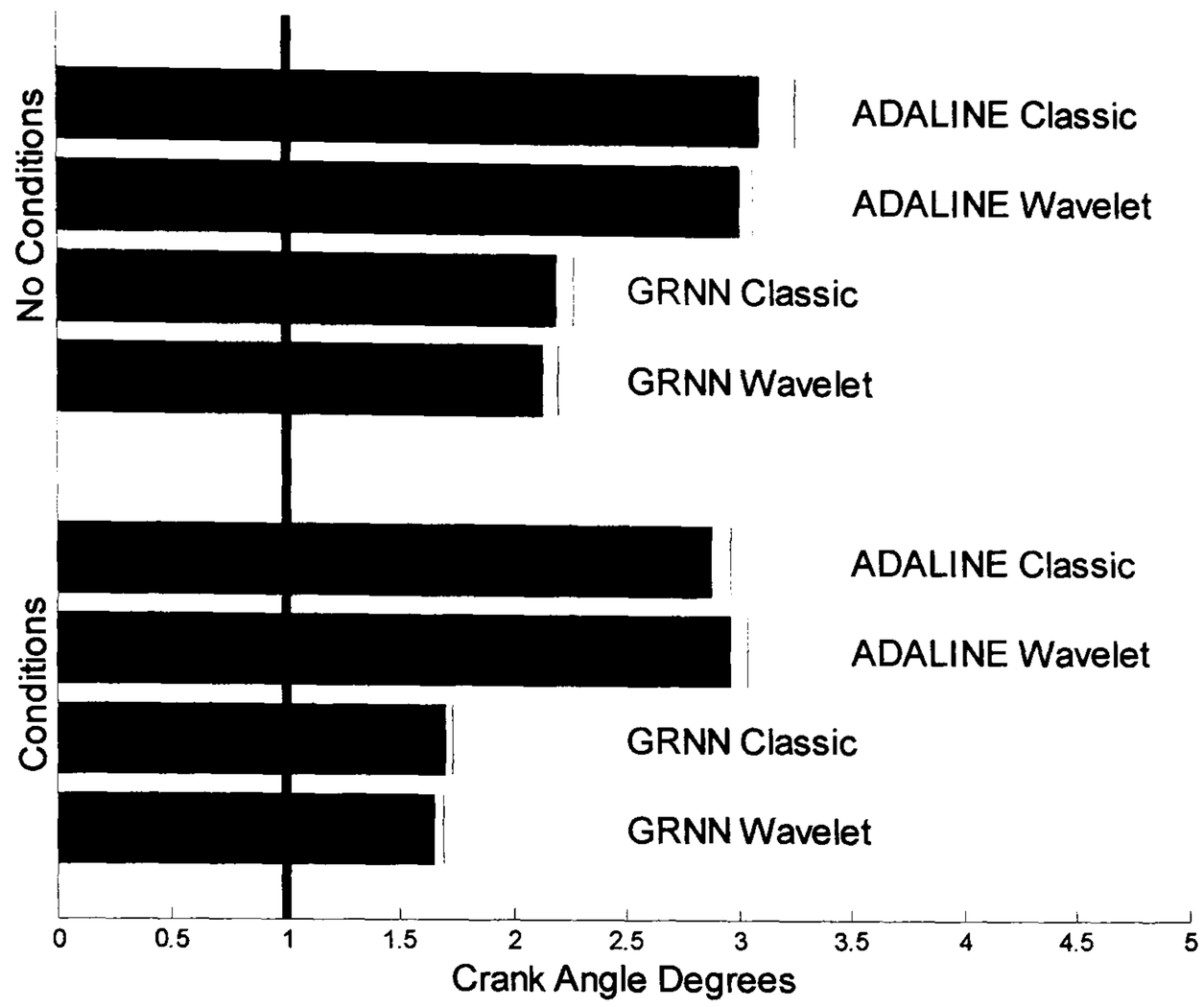

Figure 148: Comparative Results of Different Measurant Based ANNs.

Figure 148 shows the various strategies tested and their associated outcomes. The horizontal bars show the errors for each ANN design. The thin line at the edge of each bar shows the standard deviation encountered between the successive test performed on each design. The thick vertical line at x=1 marks the sampling rate.

The bars are split into two groups, depending on whether the ANNs have operating condition information among their inputs. Within these groups, they are further split into ADALINEs and GRNNs. Finally, each type of ANN is classified depending on whether the measurant extraction procedure employs classic or wavelet methods.

Hence, the top four bars show the cases where no operating condition information is presented to the ANNs. GRNNs outperform ADALINEs, while the type of measurant extraction technique (wavelet or classic) does not have any significant influence on the results.

The bottom four bars show that ADALINEs do not yield any significant improvement by adding operating condition to their inputs. On the contrary, GRNNs respond with a noticeable improvement in performance.

Performance of Decomposed Signal Based ANNs

The second series of tests across speed groups involves the use of the ion current signal decomposed to some level through wavelet decomposition. In this case, certain additional factors need to be taken into account since the decomposition introduces new parameters.

The first parameter is which wavelet to choose for the decomposition. In the case of measurant extraction, the "db1" or "haar" wavelet gave good results. In the case of decomposing the signal, it seems that moving from "db1" to "db2" yields slightly better results. This is possibly due to the fact that the "db1" wavelet, being in essence a step function, generates a less faithful *approximation* signal than the "db2" which is a more sophisticated wavelet. When identifying measurants, the rough results of "db1" are probably best suited for the task. However, when using the decomposed signal as an input, "db2" outperforms "db1".

The other parameter that has to be determined is the level of decomposition. As discussed in section "The Wavelet Decomposition of the Ion Current signal procedure", a deeper level will take more time spent on the decomposition itself but less time on the ANN since the input layer is reduced in size. Clearly, a balance has to be struck. Figure 149 and Figure 150 demonstrate these considerations.

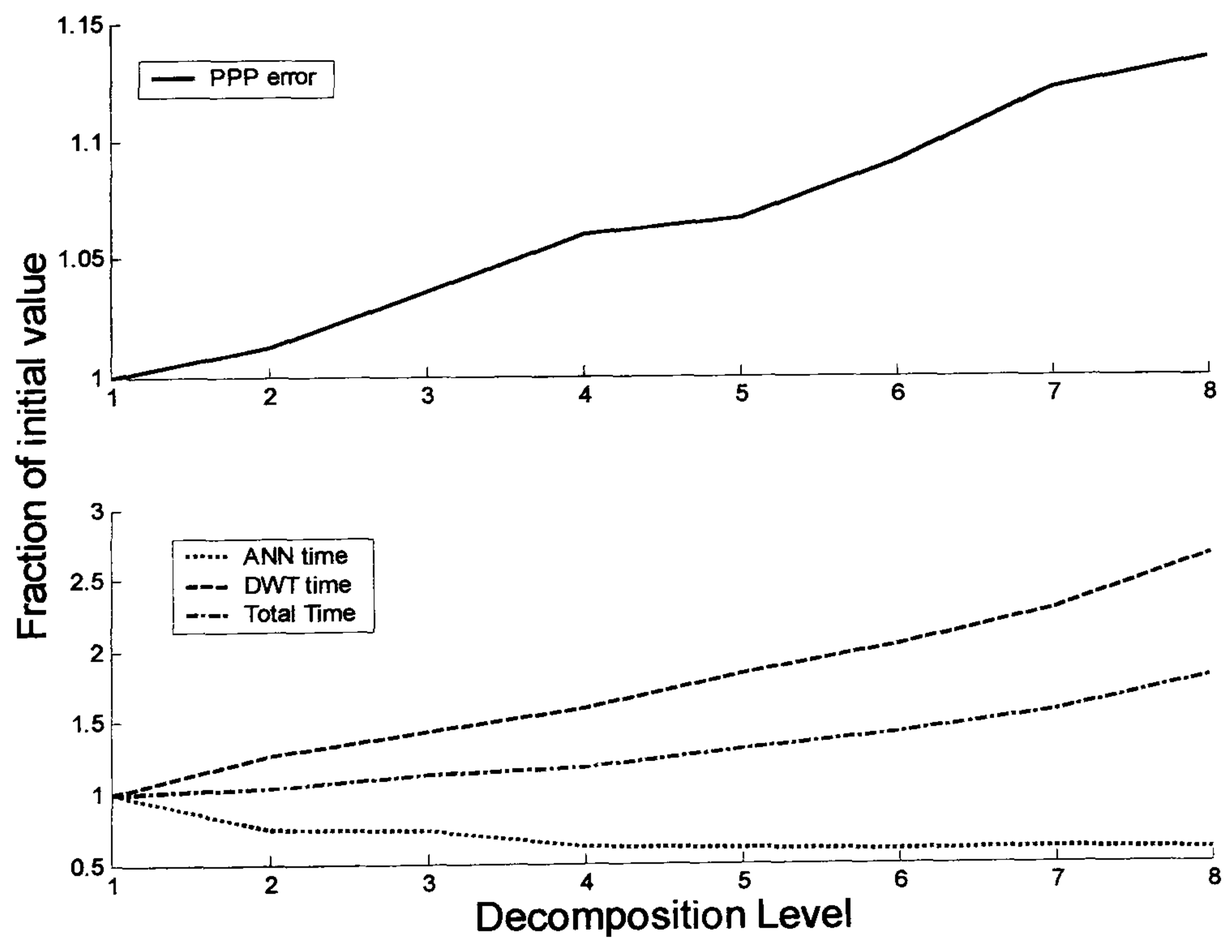

Figure 149: Breakdown of ADALINE Design Parameters.

The x-axis on these figures represents the decomposition level of the ion current signal. The lines represent the error, and the times spent on calculating the DWT and ANN

response to the test input. The y-axis represents these quantities normalized by dividing by their initial (i.e. at decomposition level 1) values.

On Figure 149, which corresponds to the Adaptive Linear Element (ADALINE), the total time spent on both DWT and ANN is clearly dominated by the DWT time. This is because the ADALINE response calculation is a very lightweight process. The error on the other hand shows a clear trend to increase monotonically as the decomposition level increases.

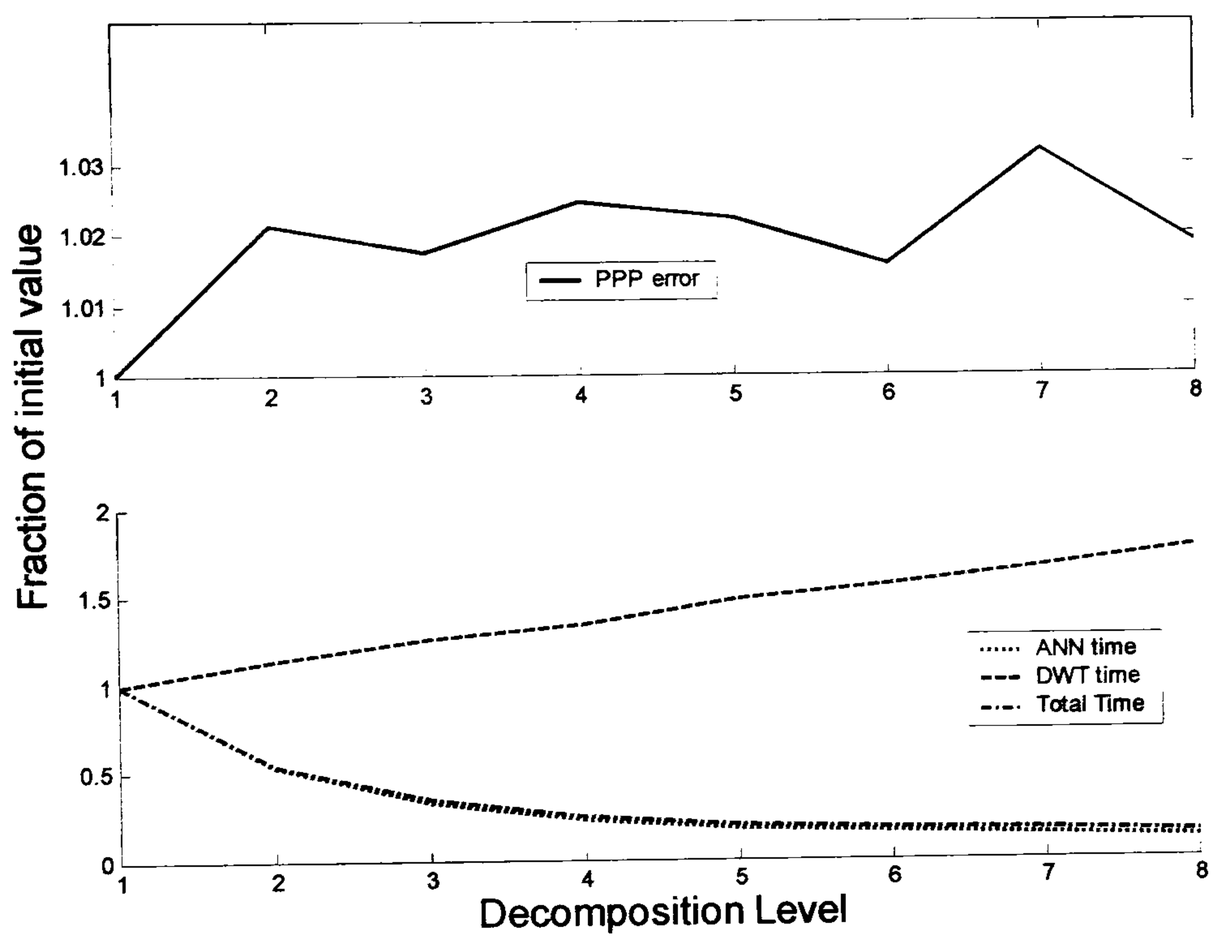

Figure 150: Breakdown of ADALINE Design Parameters.

On the contrary, Figure 150 shows that, in the Generalised Regression Neural Network (GRNN) case, the total computational time is dominated by the ANN response calculation. Meanwhile, the error is not as strongly affected by the depth of the decomposition as it was in the case of the ADALINE.

7.4 Use of Ion Current in Switching TRG levels

Although ion current proved to be of service at steady state operation, estimation and even forecasting (i.e. prediction) of combustion processes during transients is even more important. In order to establish the behaviour of the engine under load transients, a series of tests were performed where valve timings were switched between settings. The engine was switched between different TRG settings of CAI combustion, while everything else was kept unchanged.

7.4.1 Switching among different TRG levels in CAI operation

In the case of CAI combustion, the TRG levels were varied in a series of increasing and decreasing TRG by varying the valves' negative overlap. From the engine control point of view, the variable controlling TRG is the NVO and as such it is used in the subsequent graphs.

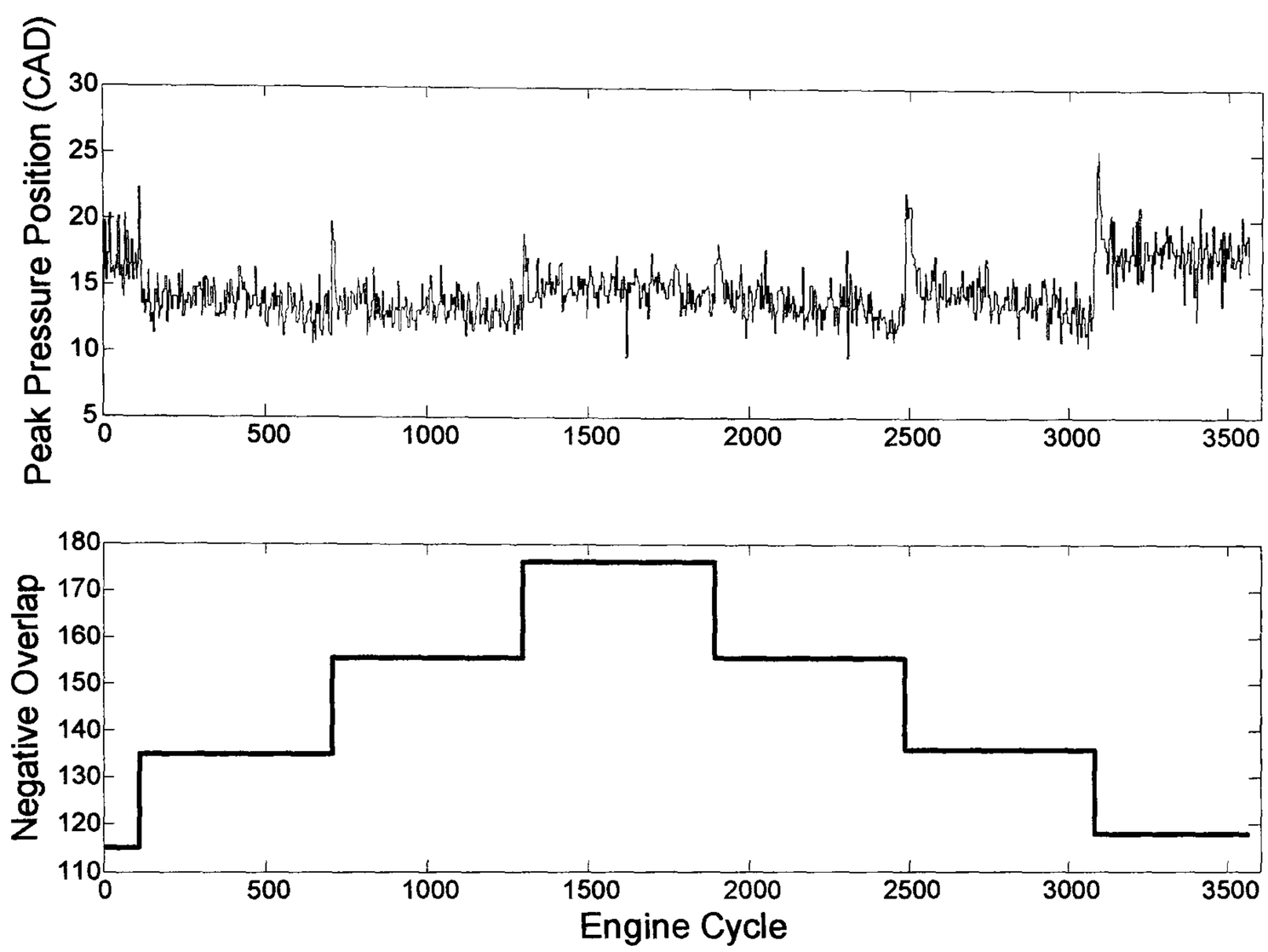

Figure 151: Cycle-to-cycle PPP values and associated NVO setting.

Figure 151, displays the NVO settings used (bottom) and the resulting PPP values (top). The corresponding TRG values are 20% to 50% in steps of 10% in both increasing and decreasing directions. The spark timing is constant in all cases at 20 CAD BTDC, while speed is kept constant at 2000 RPM.

Given that all other engine parameters are also kept constant, PPP response is related to changes in NVO only. The overall trend for *average* PPP is to occur earlier as NVO is increased. However, at the highest NVO setting, this trend is reversed and *average* PPP is retarded with respect to its previous values. This because on one hand increased TRG introduces higher amounts of heat, thus advancing combustion, while, on the other hand, increased dilution (at constant temperature) retards it. At very high NVO values, the latter effect starts overcoming the former.

Ion current signals associated with these tests are a useful tool for tracking PPP. Moreover, in these cases where transient operation is encountered, the use of ANNs in the

form presented for the steady state cases is not necessarily the best way to treat these measurements. Hence, a different approach has been employed, through the use of the *System Identification Toolbox* in MATLAB, using the difference equations based models ARX and ARMAX.

The main difference between these and the ADALINEs and GRNNs employed in the steady state cases, is that ARX/ARMAX are specifically designed to analyse dynamic behaviour, being time series models. What has to be noted here is that, conceptually, ion current as an engine variable is an effect, rather than a cause and hence it is not what would be normally considered an input to a *System Identification* model. Using ion current as an input in an ARX/ARMAX model, renders the model the equivalent of the ANNs in the steady state cases. This is because there is no prediction involved just an interpretation of ion current in terms of PPP. A similar design would be exercised in a real life implementation and has proved to yield good results in this case.

As seen on Figure 151, there are 3 increasing and 3 decreasing NVO "steps". The middle decreasing step (that is, from 155 to 135 NVO) has been set aside as validation, while the rest have been used for training. A close up of the validation step is shown on Figure 152, displaying PPP and Ion Current Peak Position as well as the NVO step.

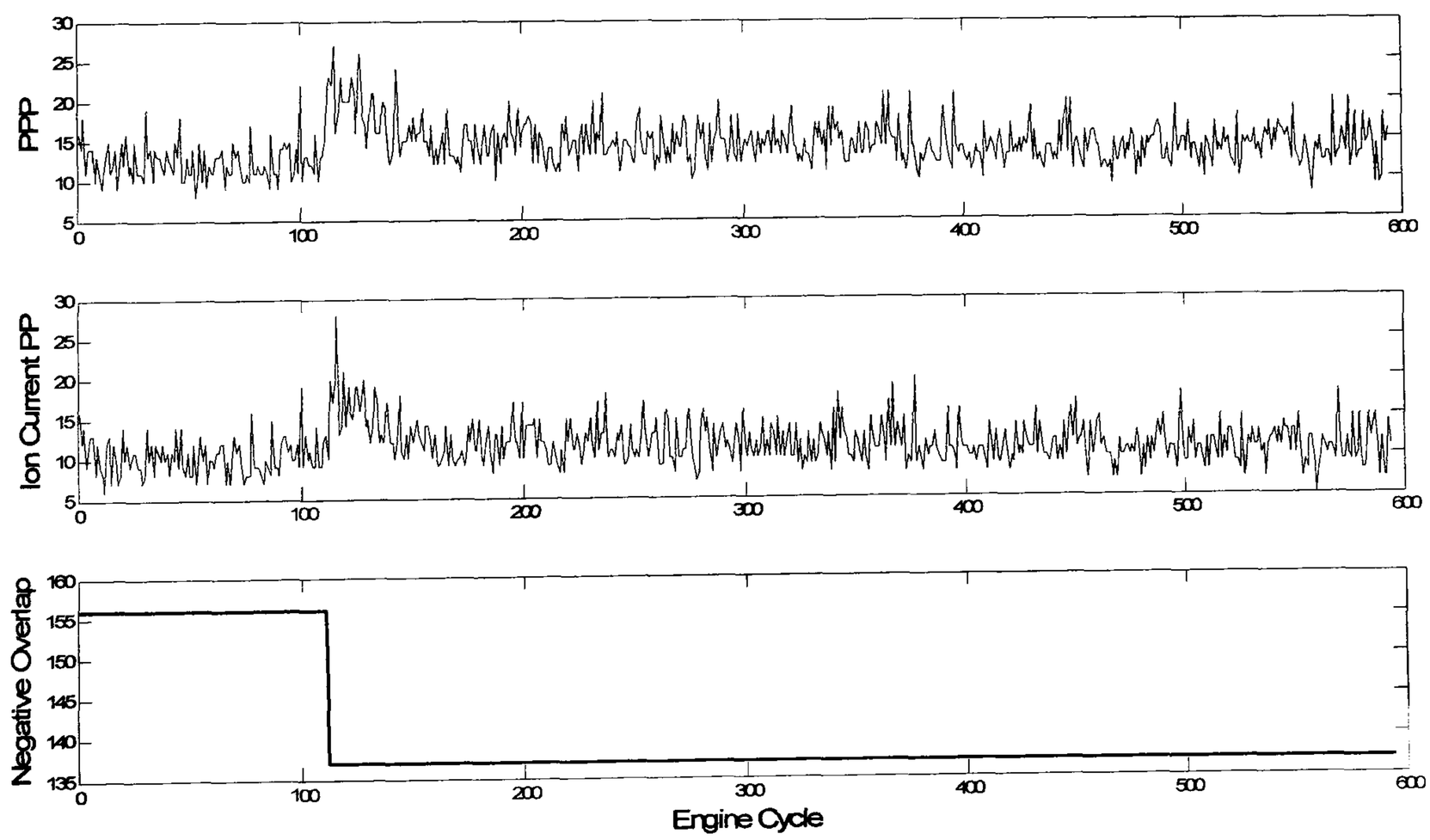

Figure 152: PPP and Ion Current Peak Position during a transient.

Results for the validation data are as summarized on Table 12.

Table 12: Validation data results

	ARMAX error	GRNN error
All 600 cycles	1.4 CAD	1.2 CAD
Pre NVO switch region	1.2 CAD	1.2 CAD
Switch region (~40 cycles)	1.9 CAD	1.8 CAD

The ARMAX and GRNN errors are shown for the total (600 cycles), the pre-NVO switch and the switch regions of the data.

The performance of both ARMAX and GRNN models give similar performance. It has to be noted however that the advantage, generally, of using an ARMAX model is that it can do a forward prediction of the future behaviour. Usually, the prediction is based on prior knowledge of the inputs which are normally externally controllable variables. However, in this formulation where the ion current (which is an effect not a cause) is among the inputs, the ARMAX model cannot have knowledge of its future value. Hence, it is reduced in effect to a linear predictor of the future state with information of previous states. In this light, its identical performance with that of the GRNN is expected. However, a low order ARMAX model is far faster than a GRNN (how much, depends on the order but running times are similar to ADALINEs).

The relative strength of the ARX/ARMAX models, when considering reduced inputs and prediction strength, was then examined. To that end, an ARX model has been trained on a reduced set of three NVO "steps" and both including and excluding ion current information. When excluding ion current information, prediction performance has been tested. The results are as follows:

With ion current information available, the switch region RMS error is 1.6 CAD. Removing this information, the error increases to 3.74 CAD. However, by introducing a prediction with 4 point horizon, the error remains essentially the same at 3.76 CAD. Increasing the horizon beyond 4 points doubles the error and the prediction becomes unacceptable. These results are demonstrated in Figure 153.

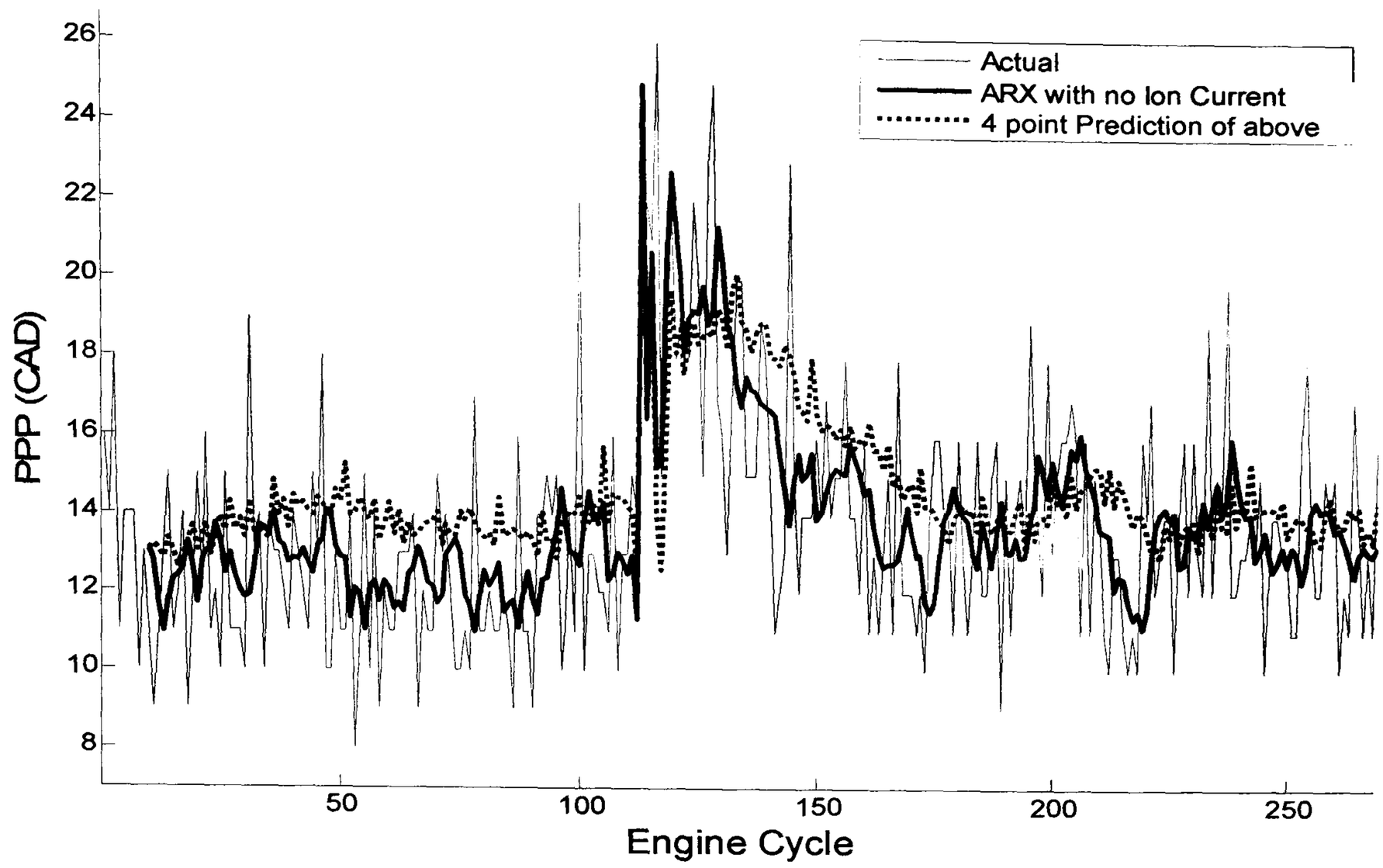

Figure 153: ARX output and 4 point prediction ARX output for reduced training and NVO as sole input.

7.5 Conclusion

In this chapter ion current has been evaluated under two main tactical approaches. The first is a simple signal analysis while the second is interpretation of the signal through the use of artificial neural networks. Also, a look at each performance during TRG level switching was taken.

When looking at basic approaches to analyzing ion current performance, it can be concluded that it can be used to monitor CAI combustion events. It has proven to produce a signal that can be processed with adequate accuracy and speed for real time feedback closed loop control.

Results of monitoring combustion under steady state operation, over a variety of speeds and trapped residual gas amounts were discussed. The results show that the ion signal is sufficiently high during CAI under all speeds and loads and that estimation of cylinder pressure parameters through the ion signal is possible.

Misfire detection, pre-ignition detection, and estimation of TRG% were shown possible with trivial mathematical approaches.

PPP, MFB50 and dQmax were all determined with RMS errors less than 2 deg CAD, with a simple linear relationship when a specific engine operating condition was examined.

When a linear relationship that would cover the whole CAI operating spectrum, from 0% TRG to maximum possible TRG, was derived, the maximum error rose to 2.64 deg CAD, remaining accurate enough for feedback purposes.

A straightforward monitoring of the effect of ITA on PPP is also possible through ion-current signal monitoring.

As far as advanced interpretation is concerned, two different approaches to ANN design have been described and evaluated. One is based upon extraction of relevant measurants from the ion current signal in order to present them to the ANN. The other relies upon the reduction in size which is achieved through wavelet decomposition in order to achieve a small and fast ANN.

The two approaches that have been tried were organized in two different ways. In the first instance, the data is presented in various groups and an ANN is trained specifically for each case. In the second instance, data is not classified according to speed but is presented to the ANN as a whole, with and without information on operating conditions as part of the input.

Two types of ANNs have been tested, ADALINEs and GRNNs.

The results from the trials within the same speed groups are as follows:

Both types of ANNs achieve an RMS error between 1.5 and 3 CAD, depending on RPM, for the ANNs whose input is based upon measurants extracted from the ion current signal (Table 9 and

Table 10).

Both types of ANN achieve an RMS error between 3 and 4 CAD when their input is the wavelet decomposed ion current signal itself (Table 11).

The results from the trials where testing is done across all data are as follows:

On ANNs whose input is based upon extracted ion current measurants, with no information on operating conditions as part of the input, GRNNs outperform ADALINEs by achieving an RMS error of around 2.2 CAD as opposed to around 3 CAD for ADALINEs. When information on operating conditions is added to the inputs, the error drops to under 3 CAD for ADALINEs and to around 1.7 CAD for GRNNs (Figure 148).

On ANNs whose input is the wavelet decomposed ion current signal, the error always remains between 3.5 and 4 CAD, largely independent of the type of ANN, the presence of operating conditions in the input, choice of wavelet, or removal of potentially problematic cycles from the data (Figure 150).

From the above, it follows that the ANNs whose inputs are based upon extracted ion current measurants by far outperform the ANNs whose input is the wavelet decomposed ion current signal. Hence, for the particular task at hand, it is preferable to expend the computational resources required to extract the measurants from the signal and not use wavelet decomposition, if the ANN of choice is the ADALINE or the GRNN. However, some more successful results by other researchers using wavelet decomposition as input have been obtained [172], but these were combined with other types of ANNs.

On the contrary, the performance of both these types of ANN using extracted measurant inputs is all the more noteworthy, considering that no averaging takes place and the results at their best performance are only 50% above the sampling rate (best performance around 1.5 CAD with a sampling rate of 1 CAD). Thus, either of these ANNs could potentially be a strong candidate as part of a control system for the steady state operation of a CAI engine.

Ion current for engine diagnostics during TRG level switching was also shown possible. It can be said that in a real life implementation the step changes in NVO should be kept as small as possible, without compromising driveability. Thus, a trade-off between responsiveness and combustion stability should be made.

If the steps are reasonably small, steady-state models could be used. If greater steps are needed, this might be gradually introduced. As these are applied ion current can be used as a feedback signal to examine the progression of the transition. Decisions on subsequent action can be taken just based on the signal, without need for predictive models.

It is obvious from the results presented, that it is possible to make up to at least 10% TRG step changes at once, if needed. Such conditions might require predictive models. It was shown that both RMAX and GRNNs are suited for this task.

One might argue that a thorough open-loop strategy might be adequate. However, lack of a feedback signal would deny the controller the potential to diagnose and adapt to unforeseen conditions.

Issues like fuel additive effects and carbon contamination of the sensor were not experimentally examined. However, other studies [164] have shown that fuel additives affect mainly the amplitude and not the shape of the signal curve. As such, they can be overcome through data normalization. Soot contamination, although not a major problem in gasoline engines, could be resolved through techniques like auto-calibration, by measuring the resistance of the ion sensor prior to combustion [173].

Overall, ion current was proven to be a cost effective and adequately informative feedback signal for both SI and CAI engine control, requiring only simple electronics to implement linear correlation for combustion properties estimation. With the addition of more complex signal interpretation techniques further diagnostic refinement was also proven possible.

8. Autoignition Timing Investigation and Ion Current as a Measure Avoidance Tool of Instability

8.1 Introduction

Homogeneous Charge Compression Ignition (HCCI) is thought to be largely or solely regulated by chemical kinetics [174,175,176,177,178]. In Controlled Auto Ignition, it is common practice to use a spark in order to ensure ignition or to strengthen combustion if it has already set off. Its timing, however, affects the combustion event slightly or not at all, during operating conditions that support pure autoignition, relying mainly upon it to orchestrate the heat release. For this reason, a workable model of the onset of autoignition is a valuable tool in understanding and controlling combustion.

Where pure autoignition was possible the spark was retarded to 0 CAD (i.e. at TDC). For combustion to be designated as autoignition the criterion used was that MFB5 had to be located before spark timing. In the data gathered, autoignition has been observed to be consistently occurring within a short Crank Angle Degree (CAD) window under varying engine states. Simplified modelling of chemically driven processes has proved insufficient to account for this behaviour. Hence, an alternative autoignition mechanism, based upon a joint thermochemical/geometrical approach is being proposed.

8.2 Observed Behavior of Experimental Data

While there are various detailed chemical kinetics methods for modelling the reactions leading to autoignition, a number of researchers have successfully employed variants of the integrated Arrhenius rate in the form of a knock integral in order to model autoignition in various forms of HCCI combustion. [179, 180, 181, 182, 183].

The Arrhenius rate formulation appears in many forms, typically as a function of temperature and time (or CAD), while pressure and species concentrations are sometimes included. For HCCI applications, it has been shown to provide a satisfactorily accurate indicator of when autoignition will occur.

For the data in both valve strategies used in this research, the integrated Arrhenius rate proved inadequate to accurately predict the autoignition of the fuel. Although a series of different formulations have been tried, no Arrhenius based equation can satisfactorily fit the data, even between individual cycles at a given operating condition.

Although, some researchers [182,181] have pointed out certain limitations of the Arrhenius rate fitting, the discrepancies between experiment and best fit are difficult to account for. The experimental data in this research exhibit a puzzling behaviour. That is, for operating conditions where the combustion mechanism is pure autoignition, combustion occurs within a very small CAD window regardless of a multitude of changing operating conditions. This might be partially due to the fact that the spark ignition, even though located after MFB5 has a regulating effect on combustion that in turn regulates EGT and thus the next cycle's autoignition timing. As mentioned in the Lotus test rig description section, the compression ratio was set to 10.5 and the fuel used was commercial gasoline 95 RON. With this CR and fuel combination, SI efficiency was retained while also the CAI operation window was found to be adequate. It was selected so that knocking, in this case meaning early ignition, at high TRG levels did not occur. The results are as follows:

For the fixed IVC – EVO valve strategy, where the highest amount of autoigniting operating conditions exist, combustion occurs within a window of 6 CAD, centered on 4 CAD BTDC, with a standard deviation of 1.5 CAD. This behaviour is maintained across an RPM span of 2000 – 4000, a TRG span of 37% – 76% (by volume) and a lambda span of 0.8 to 1.7. Shown in Figure 154 are averaged pure autoignition signals acquired through the operating condition envelope described above. Note that given the total volume is approximately 500cc the volume window is just under 0.5%. The pressure window size is approximately 14% of the average autoignition pressure (21bar) and the temperature window size is approximately 26% of the average autoignition temperature (1000K) with a standard deviation of 65K.

For the fixed duration valve strategy, the pure CAI operational region is much reduced due to the effect of reduced effective compression ratio as TRG increases. However, the observed behaviour hints at similar values of autoignition occurring within a window of 4 CAD, centered at 2 CAD ATDC with a standard deviation of 2 CAD. The RPM span is 2000-2500, TRG span is 28% to 38% by volume, all under stoichiometry.

The corresponding temperatures are centered at 890 K with a window of 25 K and standard deviation of 12 K. However, the scarcity of the pure CAI data points due to the limited operating region in this case makes such statistical metrics unreliable.

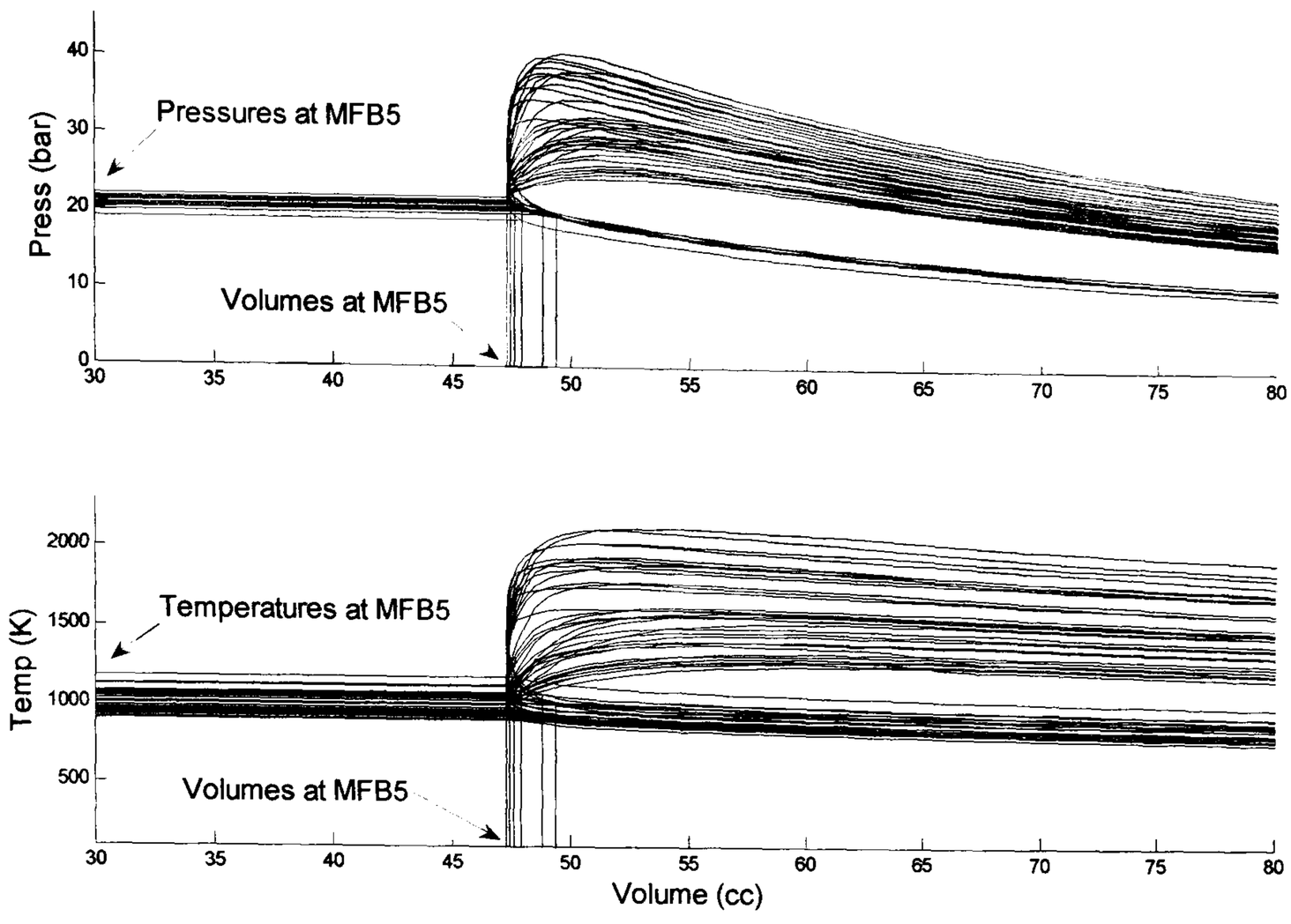

Figure 154 : Autoignition timing clustering as seen on PV and PT diagrams.

In both strategies, temperature based and integrated Arrhenius rate based predictions yield results whose scattering is far larger than the aforementioned clustering (worst case window of the order of 6 CAD) observed by the data. The best predictions based on variants of integrated Arrhenius rate formulation give results within a CAD window at least double the size of that observed in practice.

The failure of the Arrhenius rate models and data clustering seem to indicate that different mechanisms might be at work in initiating the combustion of the mixture. Hence, a more detailed analysis has to be performed in order to investigate the possible explanation for the satisfactory behaviour of the engine over so diverse operating conditions. Looking at it more spherically, it is like trying to infer a parameter based model, over an event that seems to occur at a very consistent CAD. I.e. it appears that cylinder volume is the governing parameter. It might be argued that volume is very closely related to pressure in a normally aspirated non-throttled CAI engine, but again Arrhenius and similar simplified chemistry models, usually exhibit more temperature than pressure sensitivity.

8.3 Data Analysis

Combustion is analyzed, as in the rest of this research, using methods described in section 3.3 and also in the author's relevant paper [184].

Two important points should be understood before proceeding. The first one is that, the species' amounts inside the cylinder are hard to calculate and verify. However, the impact on the heat calculation does not affect the *shape* of the heat flow curve, which contains the most important information regarding the distribution of heat changes within the cycle. Second, the number of moles does not alter much by combustion. The number of moles of a stoichiometric mixture will change less than 5% between being unburnt and fully burnt (and in CAI combustion not all of the in-cylinder gas is combustible mixture further reducing this percentage). The specific heat is similarly relatively insensitive. Hence, knowledge of the combustion timing, for non misfiring cycles, is by and large irrelevant in this calculation.

The traces normally exhibit a Gaussian-like curve of the short duration typically associated with the sudden nature of CAI combustion. It is of interest however, to compare the trace of normal combustion with that of a misfiring cycle as shown in Figure 155.

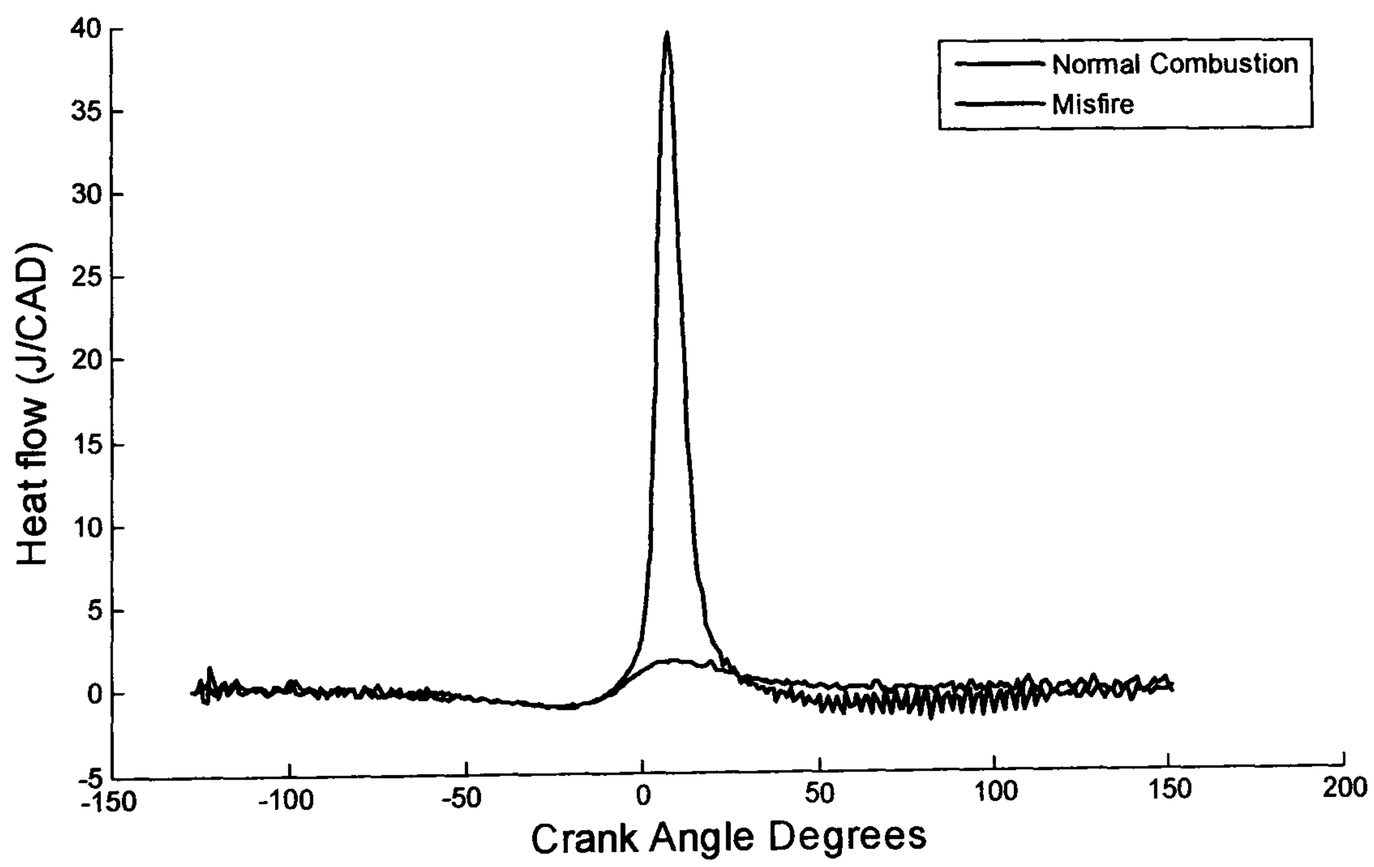

Figure 155: Heat profiles of a misfiring and a non misfiring CAI combustion cycle.

This figure shows the average of firing and misfiring cycles across a wide band of RPM / TRG values. The dip at the start of both traces can be explained by increasing heat transfer as the gases are warmed up through compression. Similarly, the discrepancy between the two traces in the region after the combustion can be attributed to the increased heat transfer of the firing case.

What is less easy to explain is the apparent small magnitude heat addition in the misfiring case. It can be argued that the cycles used to create it were not complete misfires. However, all individual misfiring cycles observed exhibit a similar heat profile.

To get a clearer understanding of the mechanisms involved in heat flow during misfires, the NVO region of each cycle needs to be investigated. This is in order to gauge the effect of compression and expansion on a theoretically completely inert mass of gases, as is the case of TRG during NVO.

Heat flow profiles across the TRG range are sampled and the results shown in Figure 156.

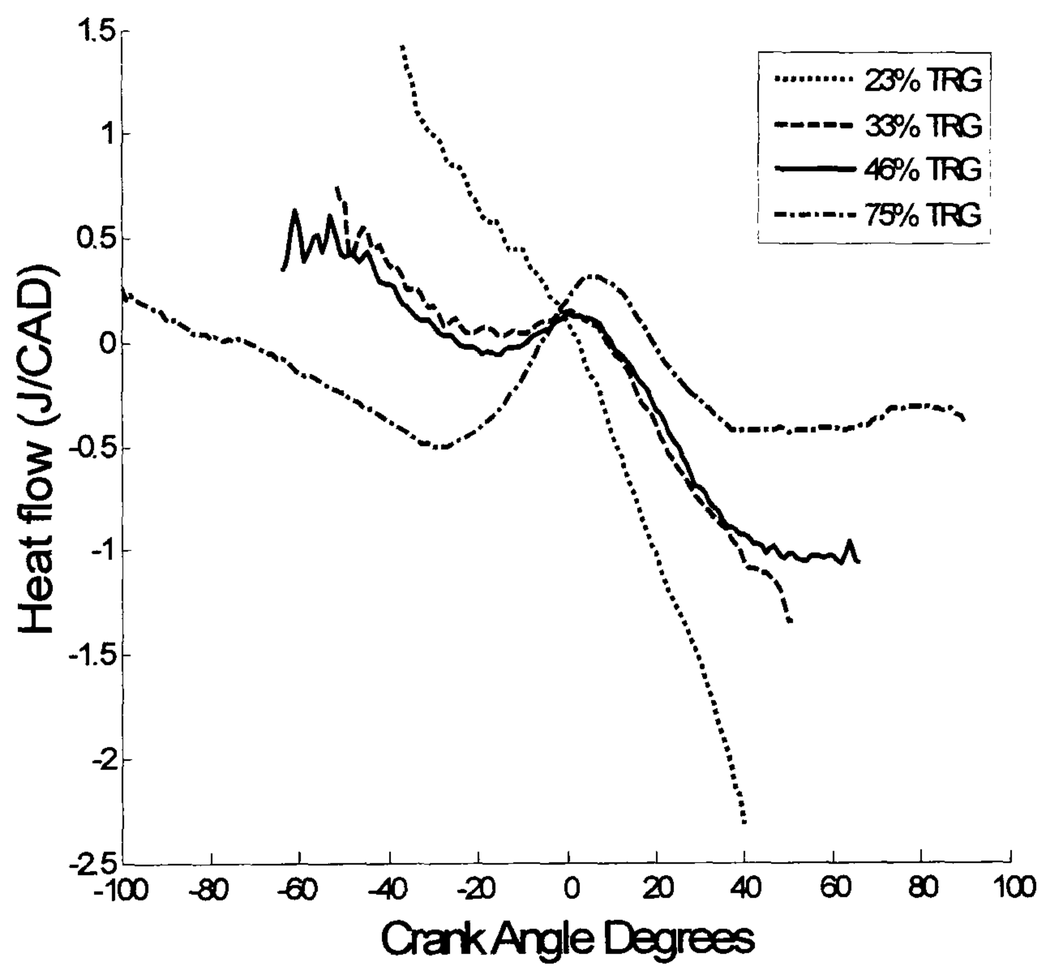

Figure 156: Heat flow profiles of NVO periods of cycles with varying TRG.

The curves presented in the figure indicate very clearly the connection between the amount of TRG and the different profiles of heat addition. Note that the higher TRG curves spread over a wider region of the x-axis. This is due to the fact that trapping higher amounts of TRG requires earlier closing of the exhaust valve (and subsequent later opening of the inlet valve).

The implication is that a source of heat, i.e. unburned mixture in the exhaust gas, is present in the case of high amounts of TRG which does not come into play when TRG is reduced. Other effects like differing blow-by are hard to quantify and the difference they would make between the two cases is unclear, however, it is unlikely to be the cause for such a big discrepancy in the overall shape of the curves involved, increasing the NVO period.

One more piece of information is the comparison of the relative magnitudes of different traces as shown in Figure 157. This gives an appreciation of the scale of heat profiles encountered in a typical misfire from unthrottled CAI, a typical trace at NVO of a high TRG CAI test and finally a misfire from throttled SI (normally, the two misfires are located around the TDC of the power stroke, whereas the NVO is located around the gas exchange TDC. In this figure, both these TDCs are overlaid at point 0 for comparison purposes).

One point that needs to be stressed here is that the SI tests in this case have zero overlap. Hence, although their TRG level is theoretically 0% by volume, they do retain a certain, amount of TRG. Also some heat addition due to the gases being surrounded mainly by the hot cylinder head and piston is possible, although at TDC the cylinder gases are already at around 600K, in SI. TRG presence, which is estimated around 20% for throttled operation at zero overlap, might be relevant to the behaviour exhibited in the figure since the presence of exhaust gases might play a role in initiating certain reactions in the inducted charge.

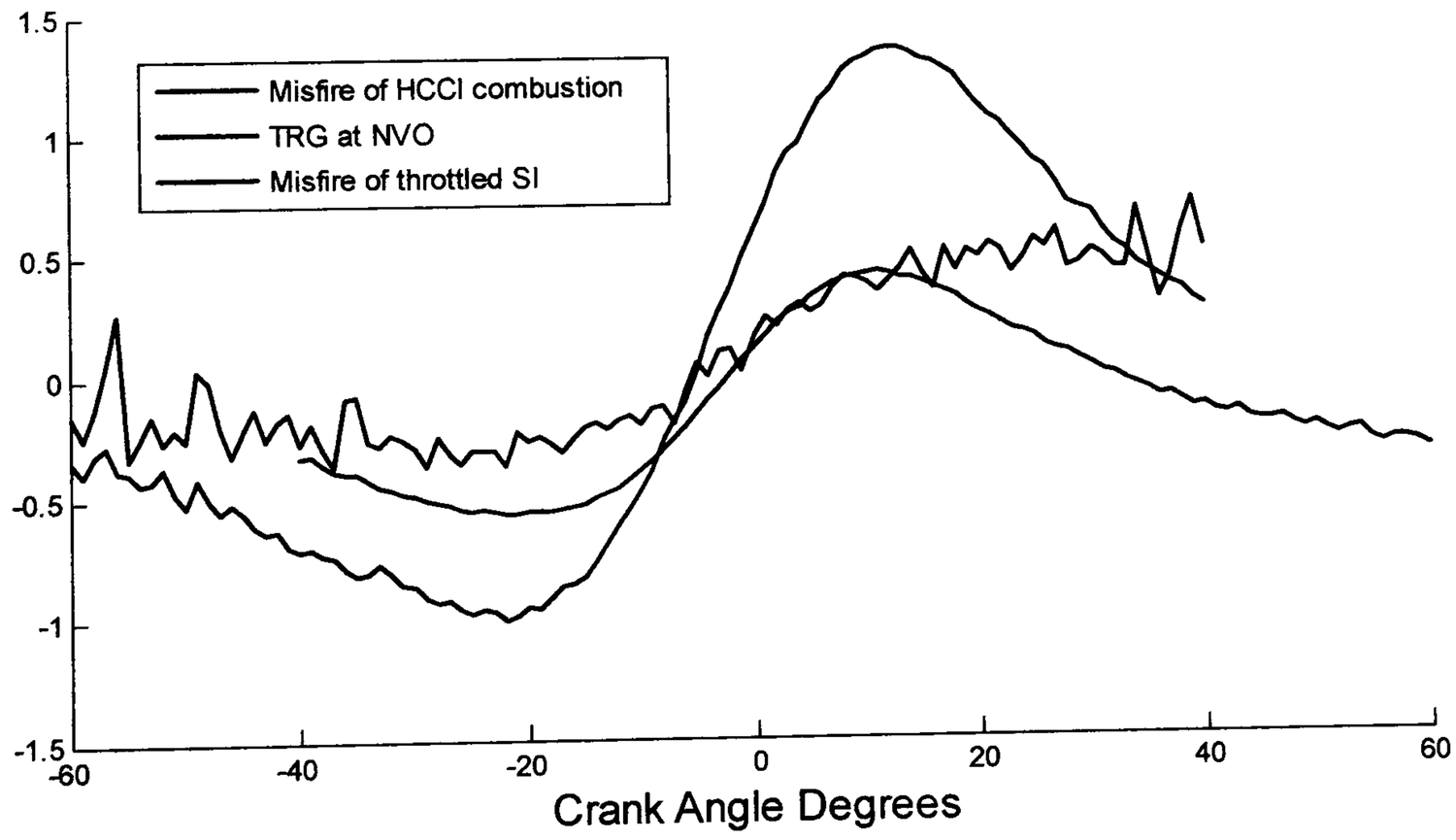

Figure 157: Heat profiles of SI and CAI misfires and TRG at NVO.

It is apparent here that the CAI misfire yields the most prominent heat flow profile, while the throttled SI and TRG at NVO are more or less on the same level. Also of note is that both the throttled SI and the TRG cycles reach lower pressures at every CAD than the

unthrottled CAI, though their starting temperatures are drastically different, the TRG being much hotter than the relatively cool gases of the SI.

Thus, the evidence presented so far seems to indicate the following:

1. Every misfiring combustion cycle (including SI) yields some amount of heat. This heat appears to be more prominent with increasing pressure.
2. Every TRG cycle above a certain level of TRG also yields some heat, the profile of which becomes more prominent with increasing TRG amounts.
3. TRG cycles below a certain level of TRG exhibit a different heat profile, being monotonically decreasing at the lower extreme of TRG.
4. These heat profiles, when prominent, are always well developed by TDC, peaking a short time *afterwards*.

In all of the above cases, the heat profiles are extremely low magnitude when compared to values of heat release expected at a normally combusting cycle. However, the persistence of their shapes, rather than their magnitudes which are almost negligible, indicates that there is a governing physical process, rather than random noise behind them.

8.3.1 Autoignition mechanism

8.3.1.1 Potential mechanisms involved

According to this evidence, it appears that some process of heat addition comes into play in all cases of compression. There are two possible ways in which energy could be added to the gases, externally, by heat transfer, or internally, by chemical reactions (or a combination of the two). Both these mechanisms have some advantages and disadvantages as far as explaining these data is concerned.

If chemical energy addition is assumed to be the mechanism, a number of questions arise:

1. Why autoignition onset appears insensitive to both time (RPM-valve timing) and composition (AFR, TRG) and
2. Why heat addition, which appears in every single case, will not always develop into proper combustion (Figure 155).

The evidence points to the fact that autoignition within the CAI operation window is more affected by piston position (i.e. CAD) than by temperature, pressure or time. These are not normally characteristics of a chemically driven process.

On the other hand, if an external heat transfer mechanism is assumed, similar questions arise:

1. Why is heat transfer, which is dependent upon the geometrical shape of the cylinder, as well as the gases' pressure and temperature, not symmetrical around TDC?

2. How can conduction from the wall to the gases occur, since especially close to TDC, the gases reach temperatures in the proximity of 1000 K by compression alone (in CAI) and similar temperatures are not to be found on the surrounding material?

8.3.1.2 Noteworthy Engine Characteristics

With both internal and external heat sources being unlikely to account alone for the observed heat profiles, a combination of the two might be able to help. Before proceeding, certain characteristics of the engine used in the experiments have to be pointed out.

The engine is equipped with hydraulically activated valves. In particular, the cylinder head is not lubricated, reaching higher temperatures than conventional cylinder heads where oil circulation helps with cooling.

The valve stems are longer than those of conventional engines, resulting in higher than normal temperatures of, in particular, the exhaust valves. Also, with combustion being very similar to a two-stroke, in that it compresses hot gases at every cycle while never inhaling purely fresh charge piston-top temperature is also higher.

Finally, the cylinder head has a squish zone. As the piston nears TDC, this zone can be expected to violently expel a volume of gas towards the centre of the combustion chamber, increasing turbulence at a certain CAD-dependent phase during compression.

8.3.1.3 Proposed mechanism

Based on the facts presented so far, it is the author's view that what is exhibited is a combination between both internal and external heat sources.

The main evidence for the chemical nature of the heat addition profile is the asymmetry around TDC. The main evidence for a strong effect by (external) heat transfer is the locality of the traces, which seems largely unaffected by changing engine speed.

Hence, what has to be appreciated is that, although temperature and pressure increase as the piston moves up, the ratio of the area of gases exposed to the cold cylinder wall to the area of gases exposed to the relatively hotter exhaust valves and piston-top decreases. Hence, although a *positive* heat flow, from the surroundings to the gases is unlikely, it is possible that the heat losses are reduced close to TDC, despite the gases at TDC presenting their greatest area to volume ratio. The reduced heat losses might have quite a significant effect on a slow, low magnitude chemical reaction that is always present, but not easily noticeable.

The squish zone might also play an important role by increasing turbulence. Turbulence is thought to play an important role in the autoignition mechanism [185,175,186,178,89]. The gases in close contact with the walls generally incur higher heat losses. The temperature dependent reactions taking place will, therefore be more prominent at the regions where fresh charge is in better contact with hot TRG, i.e. the mixing zone, and preferentially away from the cold walls. As the piston gets closer to TDC, the gases in the squish zone are expelled suddenly towards the centre of the cylinder, increasing turbulence just as peak compression approaches. Since this effect will always happen close to TDC, it is possible that it also plays a role in the observed clustering of the autoignition events.

One more thing to notice in the case of combustion cycles is the dependency of the heat profile upon the pressure. Highly throttled SI, exhibits a lower magnitude profile than CAI, which operates unthrottled. This dependency on pressure is a possible explanation for the observed delay in the combustion timing of the fixed duration valve strategy, where, due to late inlet valve closing, lower pressures dominate.

Moving to the TRG at NVO region, similar conclusions can be drawn. The very strong dependence of the heat profile on TRG has already been demonstrated on Figure 156. The different heat flow profiles of the low and high TRG cases indicate a very marked difference between the two.

It is generally the case that reactions are still occurring after the exhaust gases have been expelled from the cylinder. Heat is probably being added by the reaction of the residual gases trapped within the combustion chamber during the NVO period. The reaction

initiator is the pressure and temperature rise due to the compression of the TRG. At low TRG cases, the completeness of combustion is higher during the expansion stroke while the compression is lower during NVO leading to low, or zero, heat addition. As TRG is increased, lower combustion temperature leads to more unburnt mixture in the exhaust gases. In addition, the higher effective compression ratio during NVO at high TRG cases, due to the higher in-cylinder mass, increases the in-cylinder temperature thus helping at autoigniting these gases at that time.

It has to be pointed out that all these phenomena are very low magnitude and are unlikely to be obvious purely by inspection of the pressure trace. However, evidence can be derived by looking at the TDC region of averaged log(P) – log(V) diagram of TRG at NVO as in Figure 158.

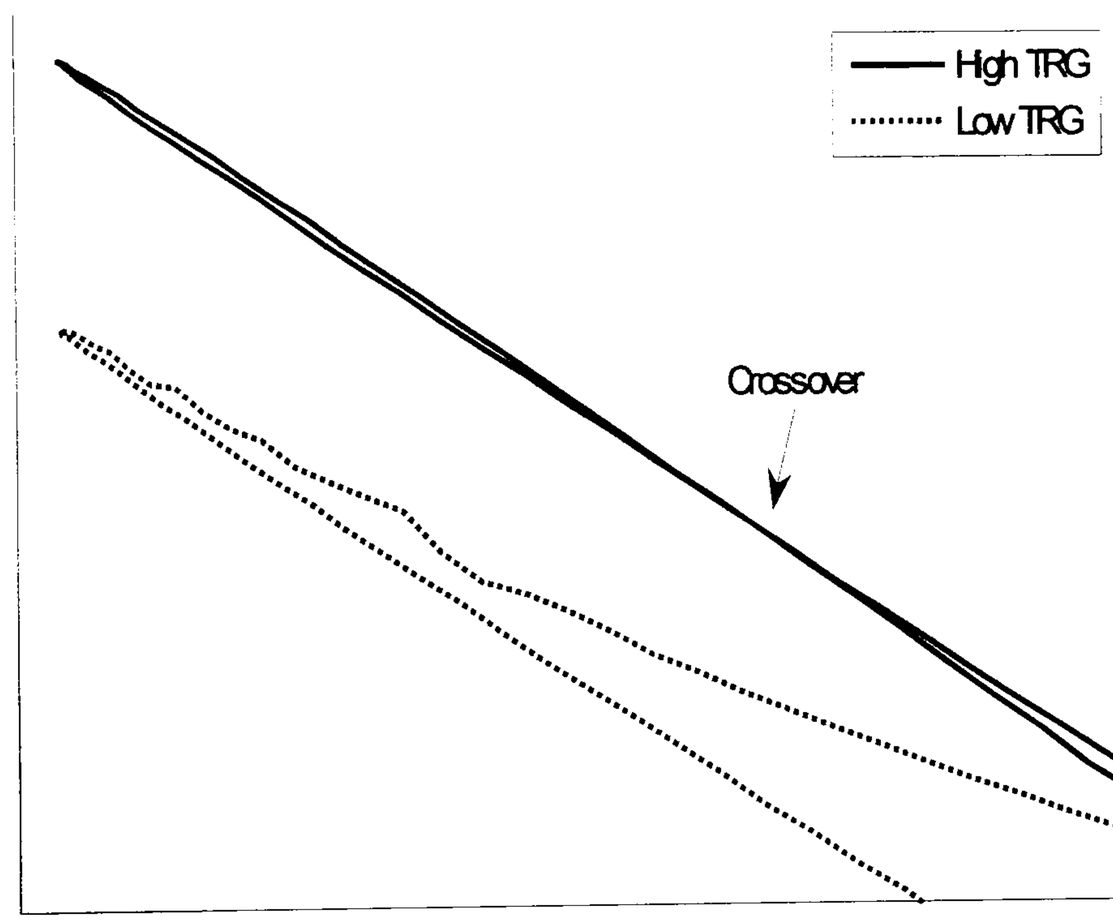

Figure 158: Detail of crossover at NVO region in high TRG case.

In this case, there is an obvious difference between the two traces. The lower one, with low TRG (4% by volume) is a conventional trace of TRG compression and expansion, with associated losses making the trace lower on the expansion side. On the contrary, the top one, with high TRG (76% by volume), exhibits almost identical traces in both compression and expansion. Closer examination reveals that there is in fact a crossover point before TDC, leading the end of the expansion segment to be *above* the compression segment. This is a first indication of heat release in the TRG at NVO region.

8.3.1.4 Instability

Having an understanding of the mechanisms involved in the autoignition of the charge, a question that arises is that of unstable combustion. While CAI combustion can exhibit very low cyclic variation this is not necessarily true at all operating points. Near the upper TRG boundary, combustion can become increasingly unstable, for one of the two valve strategies tested. The linking of cycles through the use of TRG is the key mechanism in this situation and an understanding of the effects at play is desirable in order to avoid unstable regions which can have detrimental effects on the engine's operation.

As has been described in the previous section, in general, combustion timing is a largely self regulating process in the engine tested, most likely dependent on thermochemical and geometric characteristics. However, this does not imply that it does not have certain limitations. As hinted by the shift in mean autoignition location between the two valve strategies (effectively switching compression ratios) as well as by the different heat flow profiles of throttled SI as opposed to unthrottled CAI misfires, the initial reaction leading the way to autoignition is dependent on at least pressure which, in turn, implies a certain temperature regime as well. The relevance of temperature is unclear seeing how SI, with greatly different temperatures to CAI, exhibits similar heat profiles to TRG at the NVO region of CAI).

Hence, the upper limits of CAI in the first valve strategy of fixed IVC seem not to be prone to instability due to the non varying compression and the fact that high TRG operates throttleless, ensuring a roughly similar pressure rise in all cases. Maximum recorded TRG at 76%, yields a remarkably stable combustion with no misfires as seen in Figure 159.

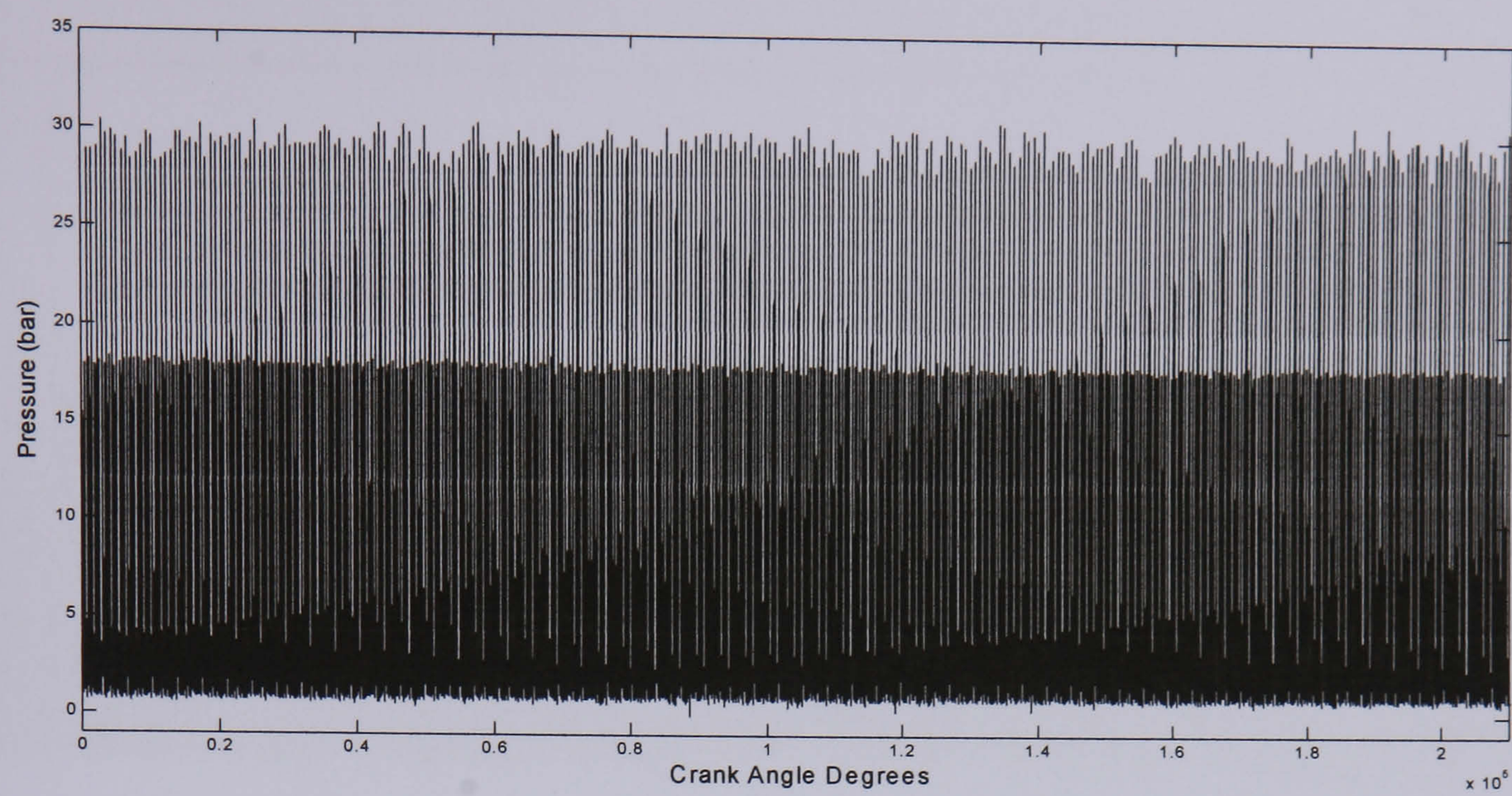

Figure 159: Example of stable combustion.

In the constant duration valve strategy, the maximum attainable TRG level is decreased to around 55% by volume, since the effect of reduced compression due to shifting IVC comes into play, particularly at high TRG. The high TRG operating points in this valve strategy are greatly prone to instability, resulting from pushing the autoignition point too late. Hence, random variations (potentially in non recordable quantities like for example homogeneity) among cycles can influence certain cycles while leaving others unaffected. This can have a cascading effect often leading to misfires.

Unstable CAI combustion exhibits great variations in maximum pressures, yielding some cycles with uncharacteristically large values for maximum pressure. Although the onset of instability is by and large unpredictable, a closer look at individual cycles reveals certain patterns that generally characterize unstable combustion.

The first and most obvious sign is the great overall variation in maximum pressure, an extreme case of which is demonstrated in Figure 160.

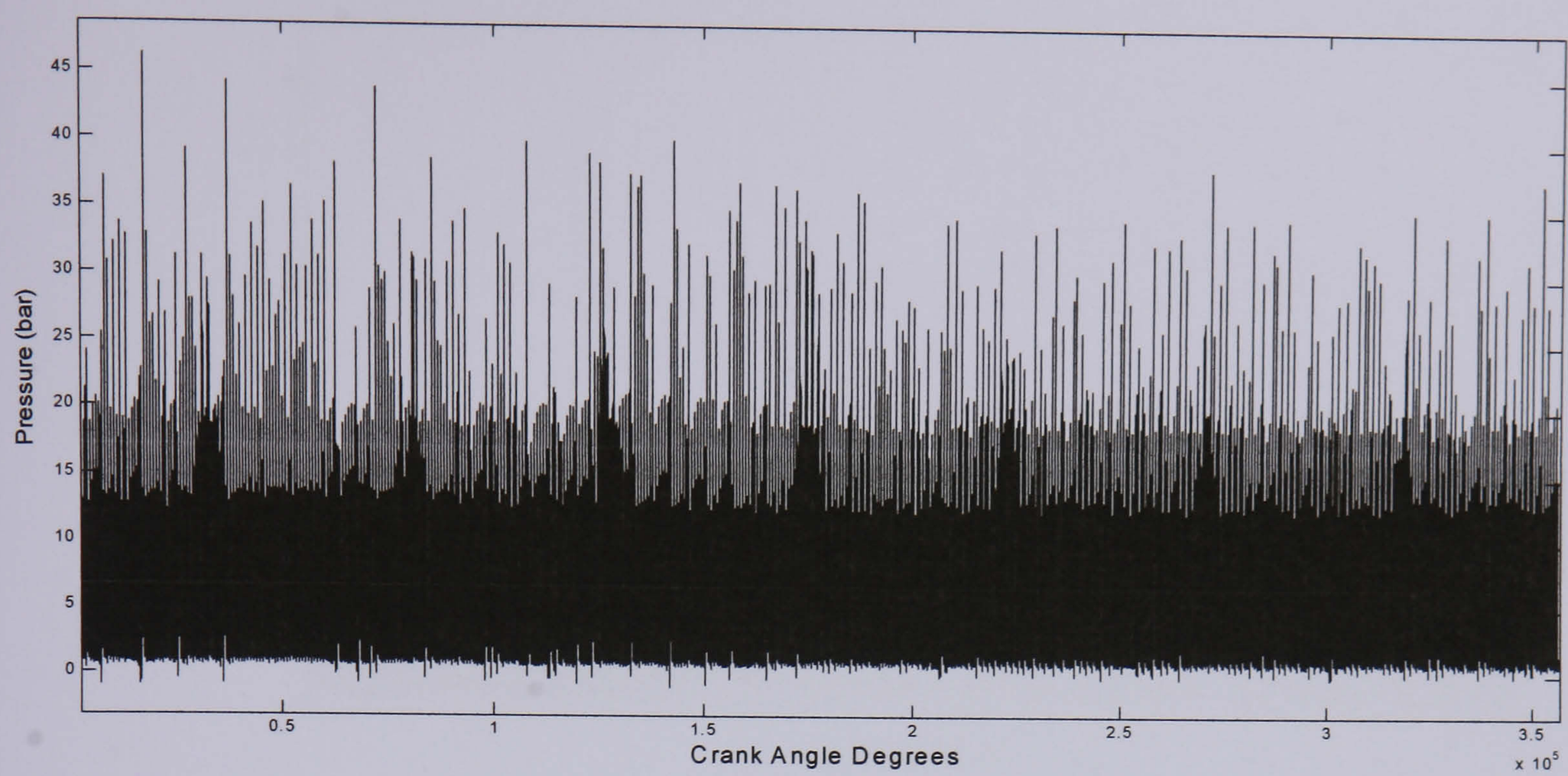

Figure 160: Example of extreme instability.

An important observation on this figure is the pressure drop to *negative* values in certain places. This is an example of the pressure transducer being heavily influenced by thermal shock, occurring after strongly knocking cycles. The short duration of CAI combustion, coupled with the violent rates of pressure rise of preignition, present in unstable regions, cause tremendous stress on the sensor (not to mention the engine) which greatly undershoots the subsequent low pressure regions of the trace (typically the valve opening events). A methodology for compensating for this kind of measurement error has been proposed by the author in chapter 3.3. However, the extremes of behaviour exhibited in unstable combustion cannot be accounted for without a host of extra sensor inputs correcting the major deviations of the in-cylinder transducer, leading mainly to uncertainty in individual cycle estimation of TRG amount, AFR and temperature.

The instability demonstrated in Figure 160 was deliberately caused in order to investigate this kind of behaviour. In practice, this kind of operation should never be encountered. Instead, instability will most likely arise through what initially appears as a normal, stable CAI, gradually deteriorating until the engine stalls. This is illustrated in the pressure trace of Figure 161 which is based on an experiment designed to test this gradual deterioration.

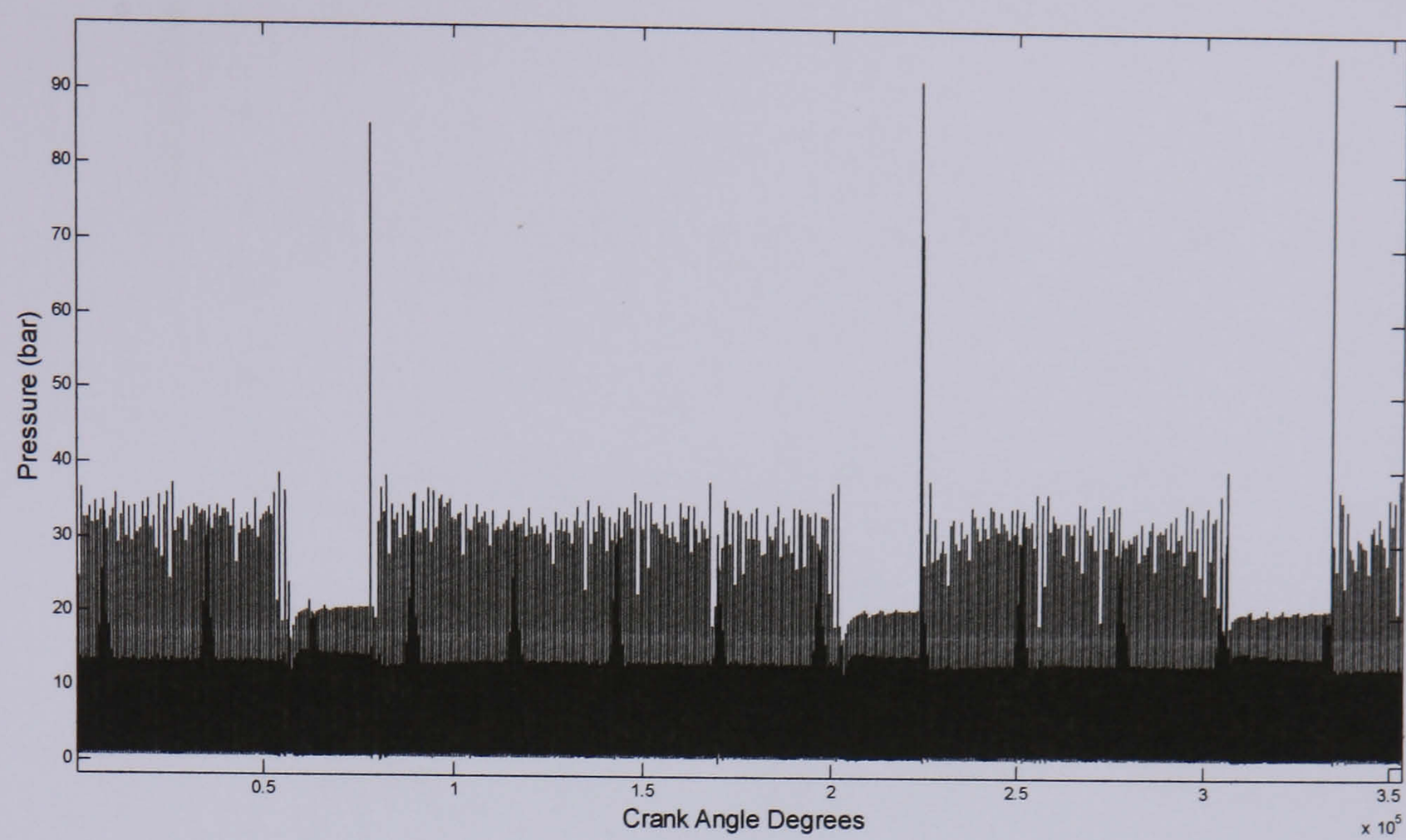

Figure 161: Test of repeated instability leading to misfires.

In this experiment, the spark is switched off three times. Each time, the engine runs in pure CAI mode, at 38% TRG by volume, 2500 RPM, until it stalls. After having stalled, the spark is reintroduced and then switched off again and so on.

A few things are noticeable initially just by looking at the overall pressure trace. The three regions where the engine has stalled are clearly visible. Also visible are three very high magnitude pressure peaks at the end of each stalled period. These correspond to the first cycle that ignites on spark reintroduction after the stalled period. These cycles have expelled all exhaust gases and are charged with fresh charge at WOT. Given a spark (at 30 degrees BTDC), they reach much higher pressures than the subsequent cycles, where the charge is diluted with TRG.

Looking closer, Figure 162, the first piece of information on misfires is given by these cycles, the three high magnitude combustions on each spark reintroduction. They have the earliest combustion timings, with Mass Fraction Burnt 5% (MFB5) values at 10, 12 and 14 degrees BTDC. However, what is more interesting is that all of them are followed either by misfires (in the case of the first one), or by much delayed, weak combustions (in the case of the second two).

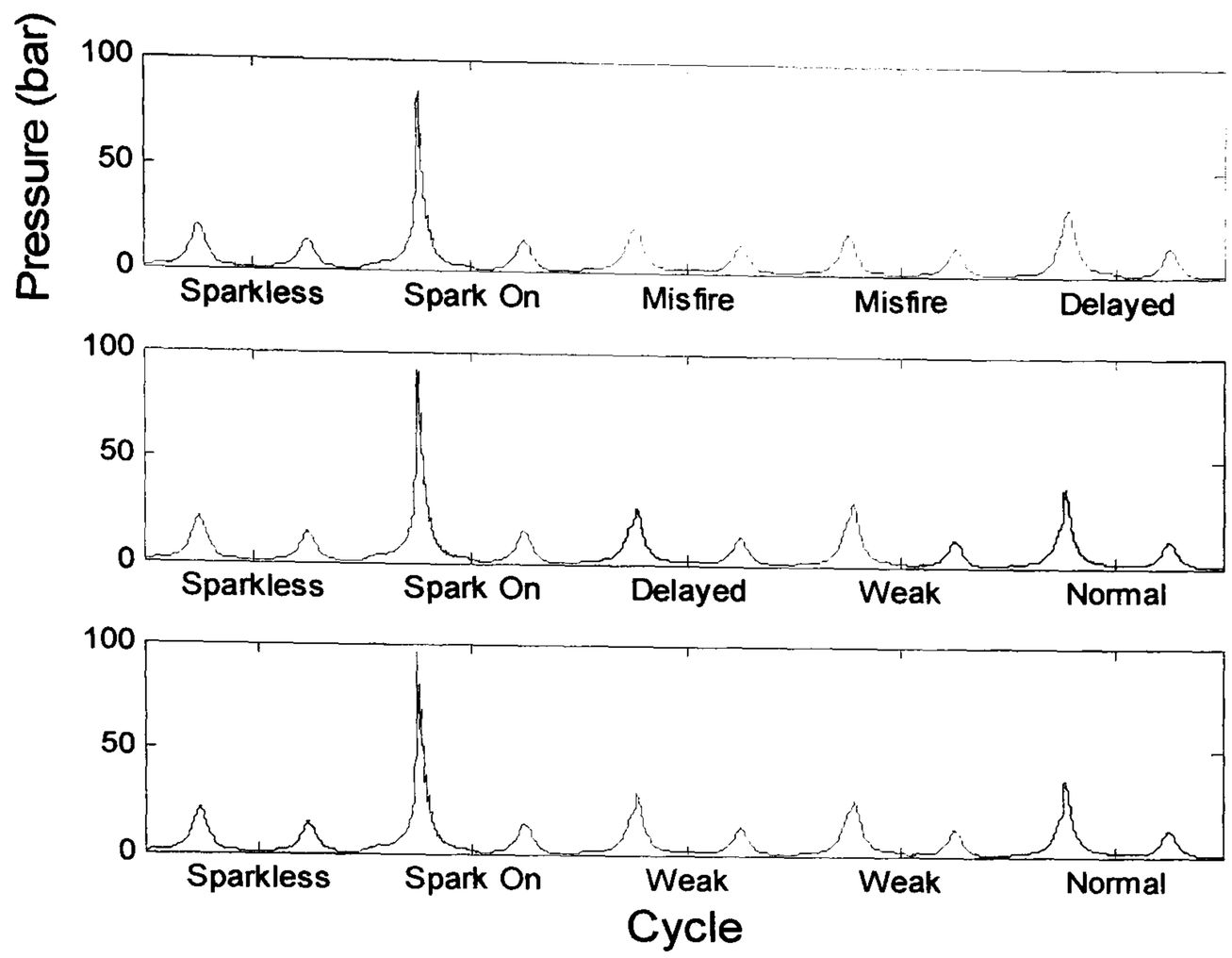

Figure 162: Close-up of spark reintroduction after misfires

This is the first piece of relevant information on the instability exhibited by this engine. The next step is to plot the MFB5 values for the cycles in the three regions. These are shown in Figure 163.

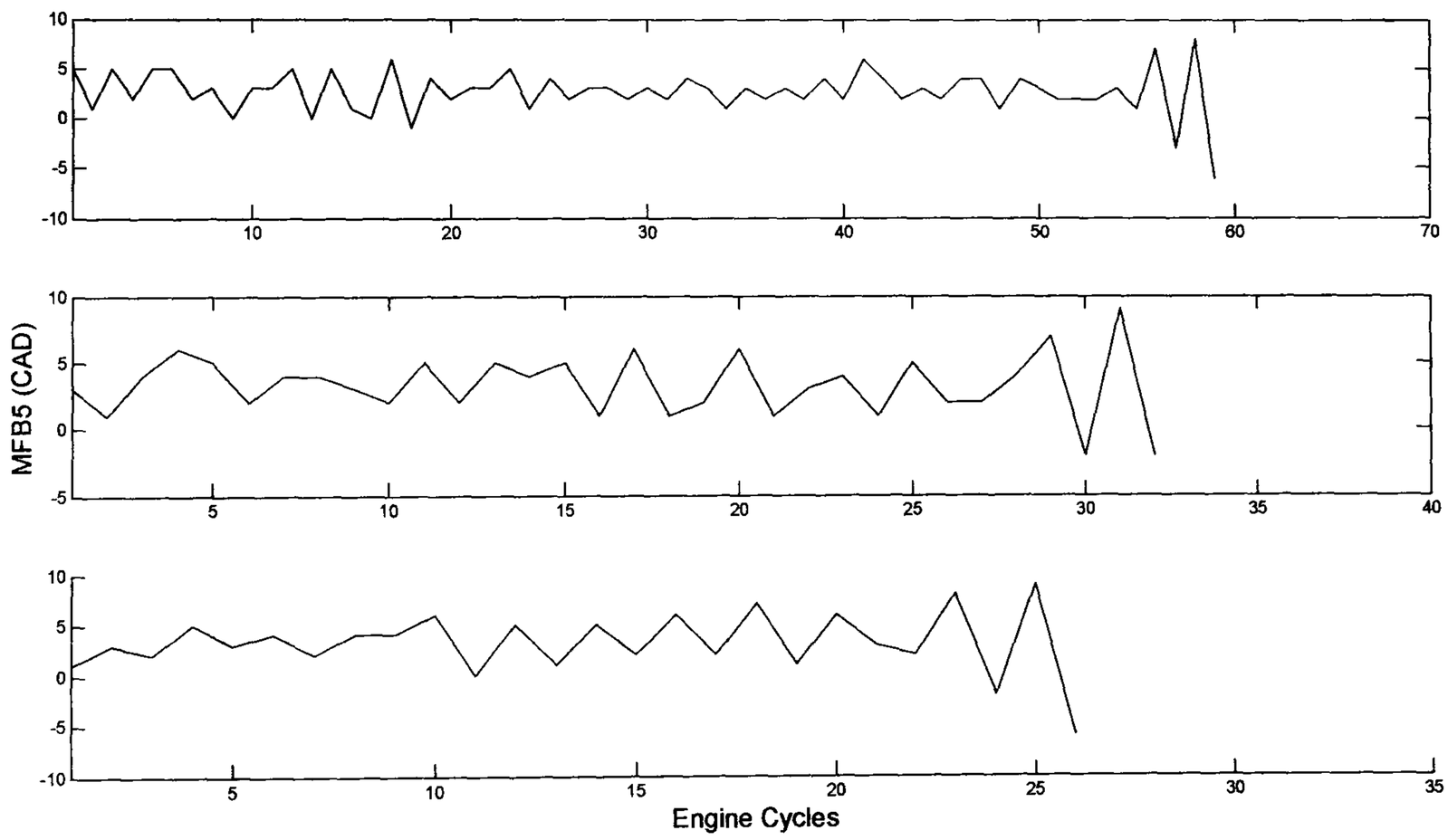

Figure 163: MFB5 values for regions prior to misfire.

On all three of these, the blank region on the right is where misfires start. An important thing to notice is that in all cases, before the misfires, a large oscillation has been established, the last firing cycle of which exhibits a very early MFB5 value.

The oscillations established in the above examples are visible, in general, across experiments of the second valve strategy (constant duration, low lift) at the upper limits of TRG. The explanation proposed for them is the following.

At the limit of CAI, the autoignition is constantly at the threshold of failure (in the experiment presented here, mean MFB5 for non misfiring cycles is 2 degrees ATDC). When, for any reason, autoignition almost fails, a very late combustion occurs. When that is the case, the exhaust gas temperature rises, both because combustion occurring later incurs fewer heat losses, or, in extreme cases, because combustion is still occurring strongly at EVO. Part of these hotter, than average, exhaust gases are then passed as TRG to the next cycle. Thus, at the intake stroke of that cycle, less than average mass of air is introduced to the cylinder since the energy of the hotter than average TRG expands the incoming air more. Since the injector pulse remains unchanged, the charge ends up slightly rich. This cycle now starts compression at higher than average temperature, richer than average and because of the increased temperature, it combusts early. This early ignition is not problematic from a knocking point of view, but it ends up lowering the exhaust gases temperature, since more time for heat transfer is allowed, coupled with the fact that the slightly rich mixture does not have the sufficient amount of oxygen to release all its available energy. Hence, low temperature TRG will be produced and the cycle following this one, will have a delayed ignition, leading to hotter gases, leading to an early ignition and so on, until eventually a misfire happens. In pure CAI mode with the spark off, a misfire is non recoverable, since it produces no TRG to ignite the subsequent cycles, hence the cascading misfires witnessed in this experiment.

Having this framework in mind, further evidence surfaces when considering the TRG compression and expansion cycles occurring at NVO. Using the ion current probe a trace that can be interrogated for possible hints of activity during the supposedly inert TRG compression and expansion cycles is available. The results are displayed in Figure 164.

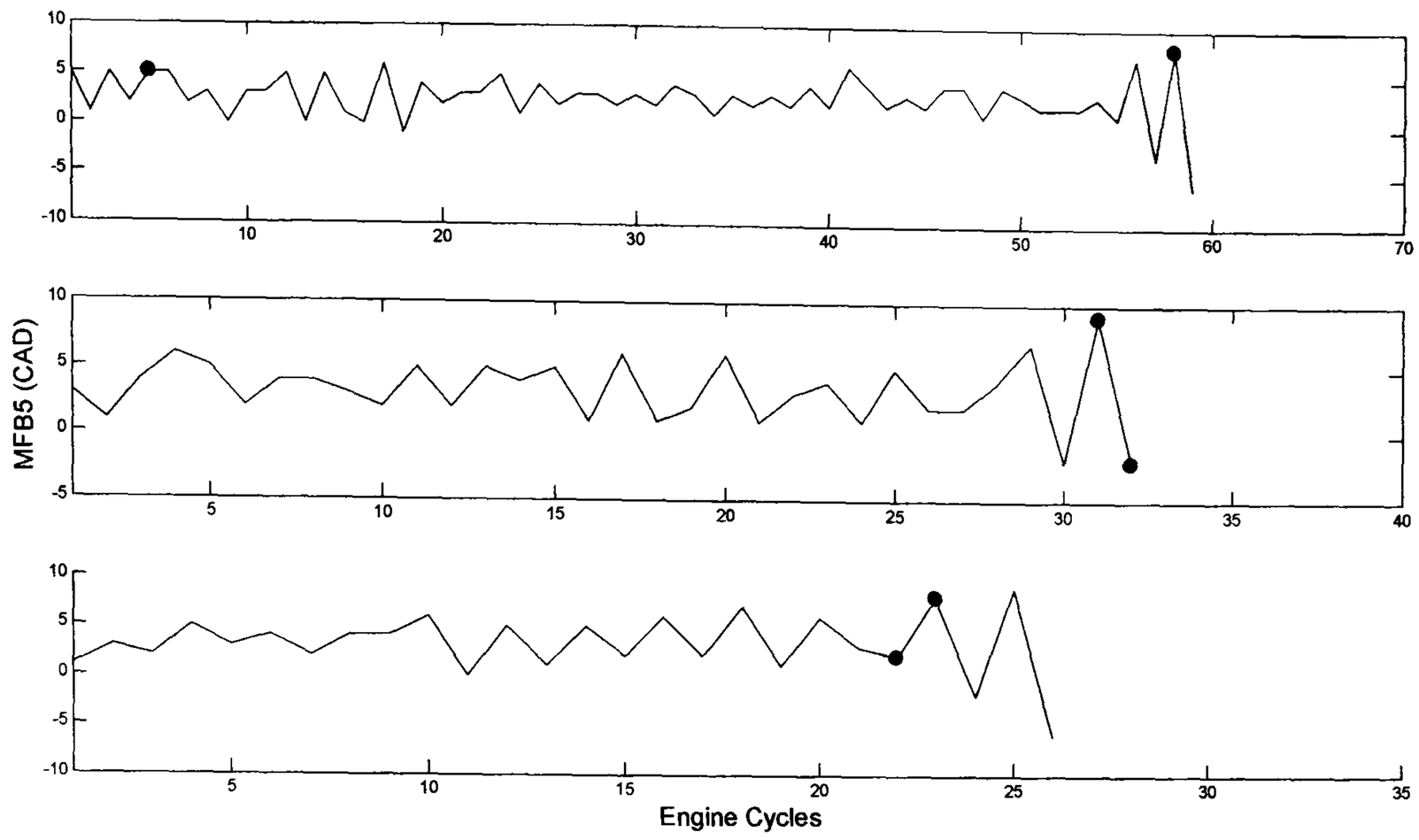

Figure 164: MFB5 values for regions prior to misfire with cycles of ion current activity in the NVO region distinguished by black circles.

This figure is the same as Figure 163, displaying the three regions leading to the misfires, but it has the cycles where ion current activity during NVO has been recorded marked with circles. Unfortunately, the results are not conclusive, the main reason being that the probe used in the collection of this data has been adequate for collecting a significant ion current signal during the combustion cycles but too small for the requirements of the much lower magnitude events of the TRG cycles. Still, it is evident that all three instability oscillations leading to the cascading misfires (the rightmost parts of all three traces) have exhibited ion current activity in their TRG at NVO. It is also evident that activity has been recorded at least once in other regions even if these did not lead to misfires.

The behaviour described above is clearly demonstrated in Figure 165 taken from a very similar unstable log at 30% TRG by volume, 2200 RPM (again spark switched off until cascading misfires recorded):

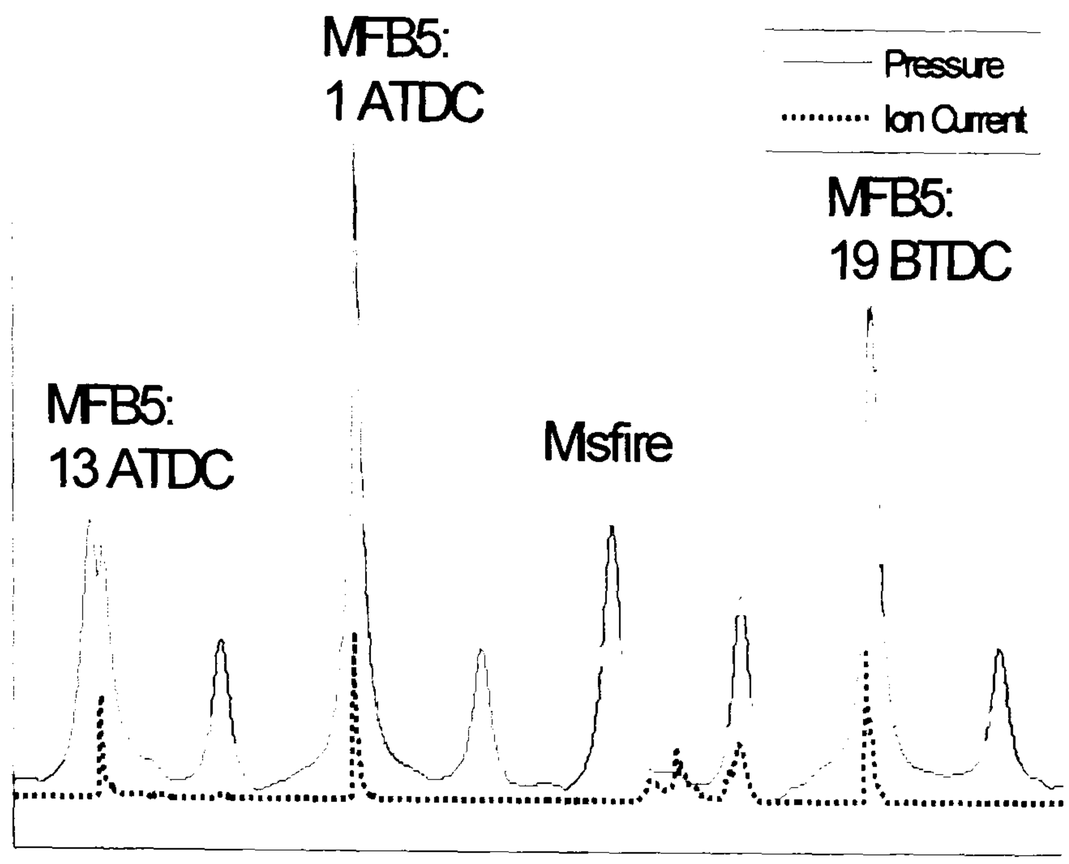

Figure 165: Ion Current evidence of TRG combustion in the NVO region of misfiring cycle.

The text above each cycle indicates the cycle's MFB5 value. Starting from the left, a very delayed ignition at 13 degrees ATDC results in the following cycle combusting relatively early at 1 degree ATDC, when the average value for non misfiring cycles for this experiment was 6 degrees ATDC.

The early combusting cycle is followed by a complete misfire. Looking at the ion current trace however, it is evident that the charge ignites at EVO, most possibly through contact with the exhaust gases. This combustion is carried into the NVO region where a highly prominent ion current signal is given throughout. The effects of the TRG combustion in the NVO region are obvious from the pressure trace by comparing its peak magnitude to that of the same feature of the neighbouring cycles.

In addition, the increased temperature of this region is being made evident by the noticeable pressure trace dip in the induction region just before the compression of the final cycle. Namely, notice how the start of pressure at the start of that final cycle touches the base level of the ion current signal (in fact it is slightly negative at –0.006 bar). This is most possibly evidence of thermal shock. This effect makes the pressure trace undershoot following heat release. In the pressure values usually encountered it is hardly noticeable, however, in the low pressure region of the induction, it can lead to suspiciously low values. In this case, the heat release in the NVO region has left no time for the transducer to recover, leading to this pronounced effect.

Hence, the final cycle in the figure gets mixed with very hot TRG, resulting in a lower amount of air in the fresh charge and an extremely early ignition with an MFB5 value of 19 degrees BTDC. The reduced amount of oxygen in the charge is most likely the reason why the combustion fails to yield very high maximum pressure. It has to be noted here that these cycles are at the end of an unstable region. After the final cycle in the graph, continuous misfires occur until the spark is reintroduced.

The test presented in this figure illuminates a few more things not covered by tests of Figure 163 and Figure 164. Unlike those, where the high TRG limit had been pushed too far, 38% by volume, which is a lot for this valve strategy at 2500 RPM, this test operated in a more sedate region of 30% by volume (at 2200 RPM). Thus, running times between switching off the spark and eventual misfires are much longer, allowing for a better study of the unstable pure CAI region.

The relation between combustion timing and ion current has been extensively researched [131,104,111,101]. In the context of this research here, the location of the peak of the ion current trace in the combustion region of a cycle would be the most obvious candidate, had MFB5 (whose estimation requires a pressure transducer) not been available. Figure 166 highlights their strong interrelation (correlation coefficient of 0.93). Of course, a misfire will produce no ion current but it is possible to avoid reaching misfires altogether by searching for instability in the peak ion current location and thus pre-empting possible misfires.

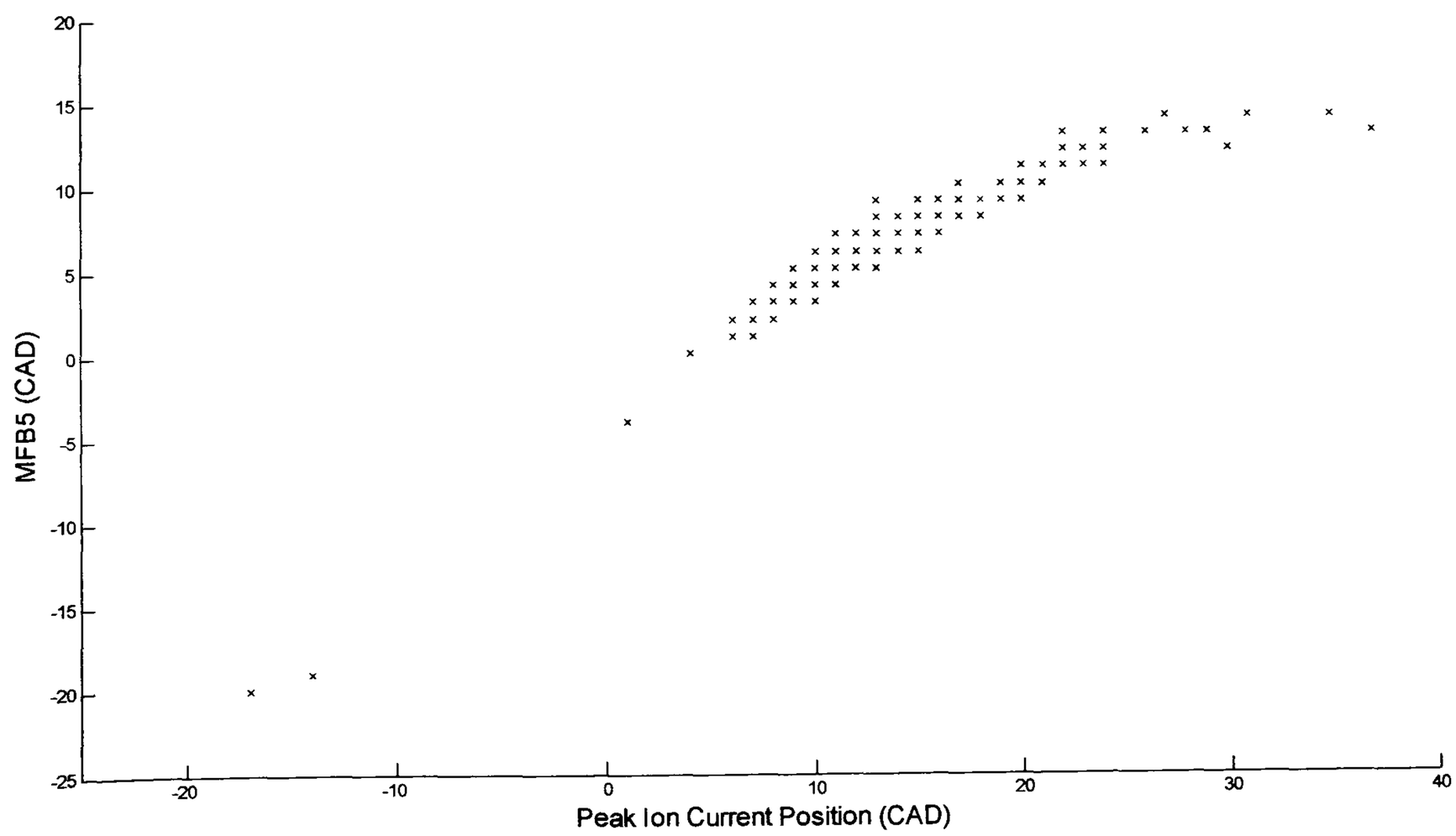

Figure 166: Example of relationship between MFB5 and peak ion current position.

8.3.2 Ignition Coil Ion Sensing

The secondary use of ion current, as a diagnostic for TRG heat release combustion in the NVO region has been proposed above. However, there is yet another signal lending itself to the same task, a simple processing of the trace of the (inactive in pure CAI) spark plug's low tension coil voltage. Although it is not claimed here that the exact mechanism behind this signal is known, it can be speculated that its source is the electron to positive ions imbalance in the ionized flame at the time of combustion [94,95]. As already stated in Calcote's model description, in the ion formation section, at U_s=0 (where U_s is the measurement voltage) as is the case when the plug is essentially "off", the electron current will dominate over the positive ion current due to the higher mobility and the higher temperature. This will then create a measurable voltage in our circuit, despite the fact that the "ion sensor" (i.e. the spark plug in this case) is not being driven by an external voltage source, as is the case in the results in this section.

Under normal operation, this signal describes the voltage in the primary ignition coil. In pure CAI, the inactive spark plug acts as a sensor, returning an information poor signal that shows a weak response to the combustion. Figure 167 shows average traces from pressure and coil for comparison.

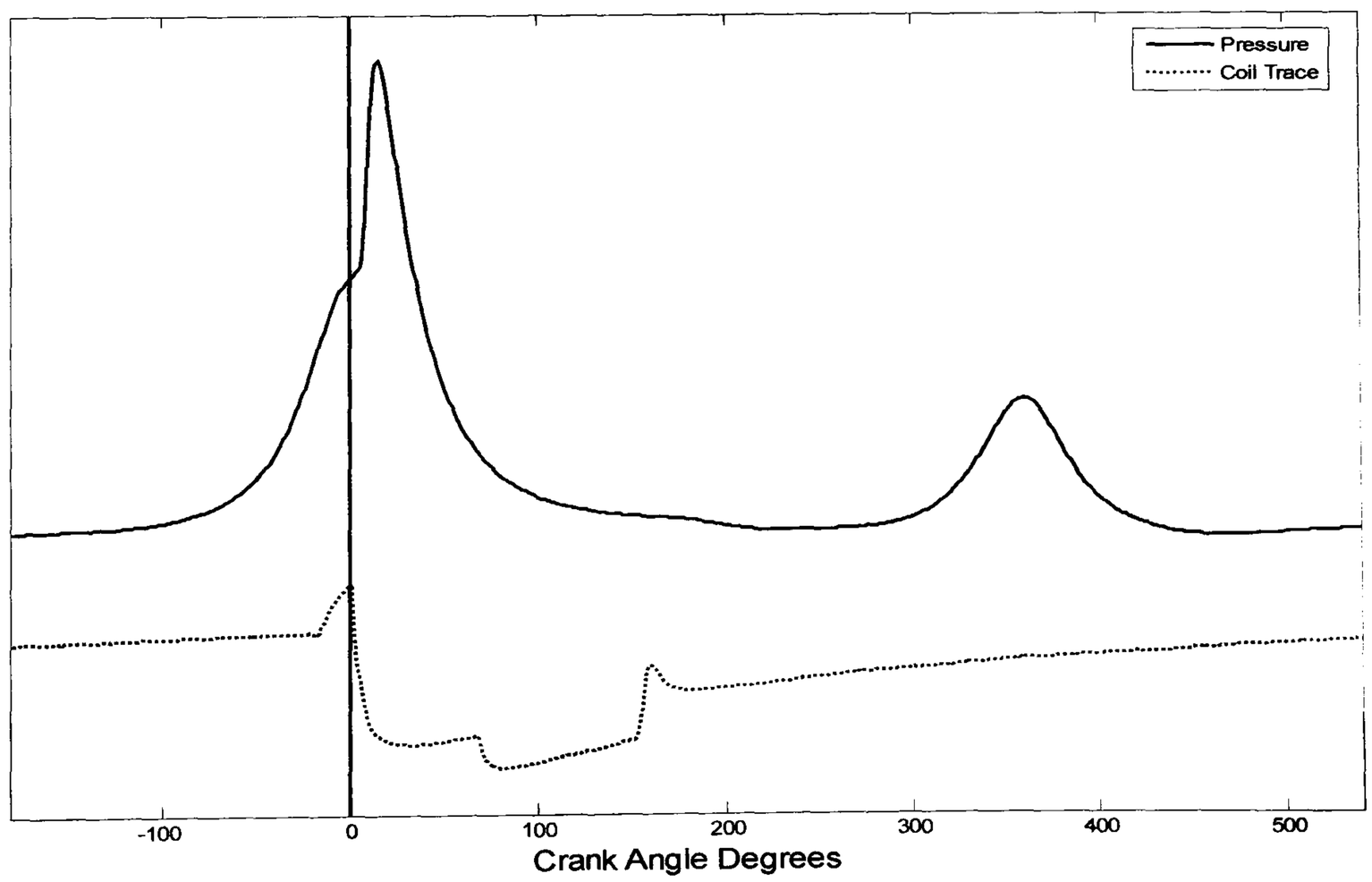

Figure 167: Pressure and coil signal traces.

Normally, the coil trace seems to initially respond to compression by deflecting upwards. After TDC, there is a drop, followed by another drop, the first one presumably related to the effects of combustion while the second one to the effects of EVO.

In late combustion, the second drop is less accentuated, making the first drop the most dominant as seen in Figure 168. While the exact mechanism behind this different behaviour between normal and late combustion timings is unclear, it is clearly a potentially useful diagnostic for detection of instability during CAI combustion and a promising candidate for further investigation using advanced signal processing techniques.

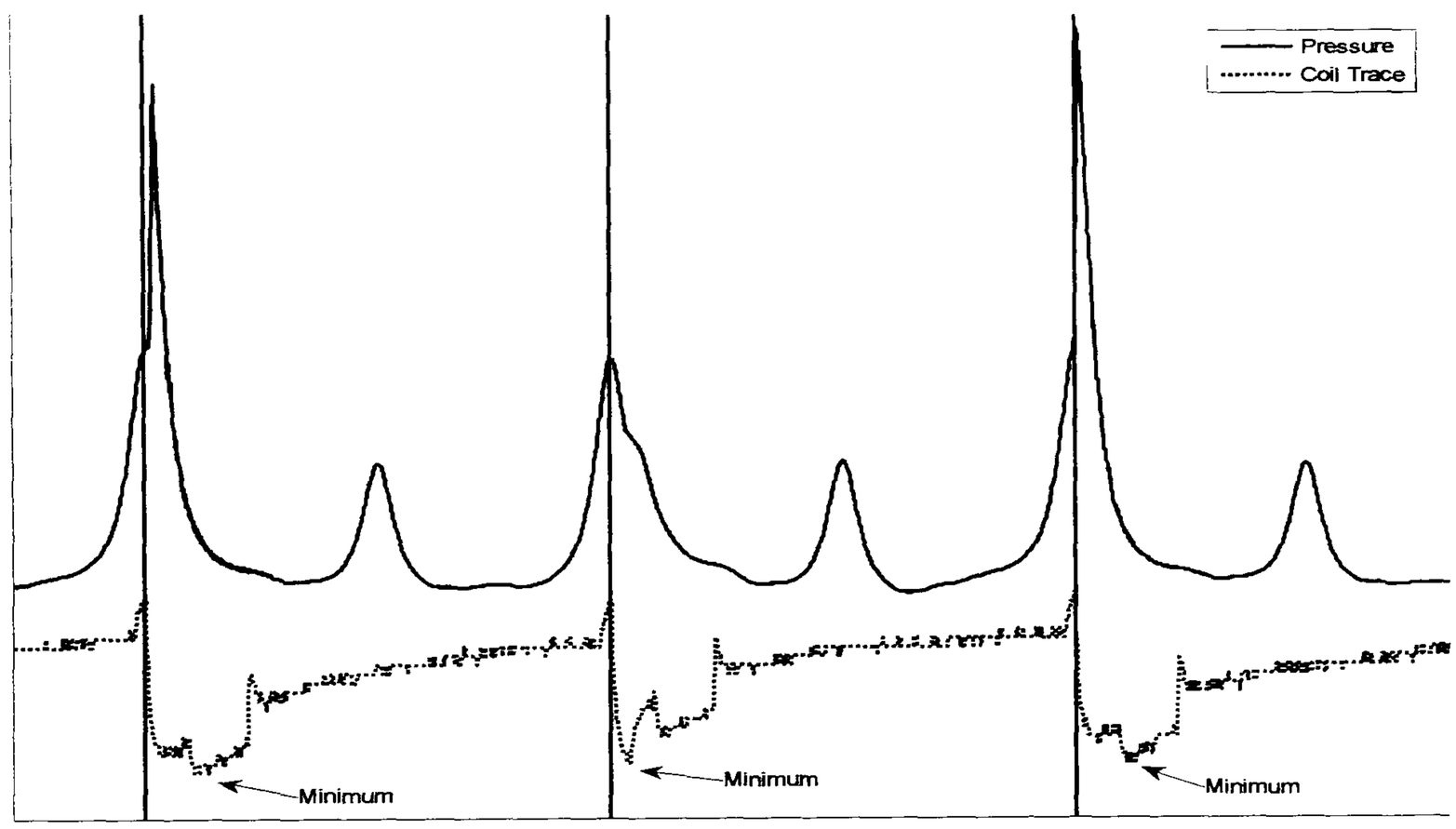

Figure 168: Detail of pressure and coil traces in normal and misfiring cycles.

The potential use of this signal becomes apparent when comparing the location of its minimum value within each cycle against the corresponding MFB5 values. The results are shown in Figure 169.

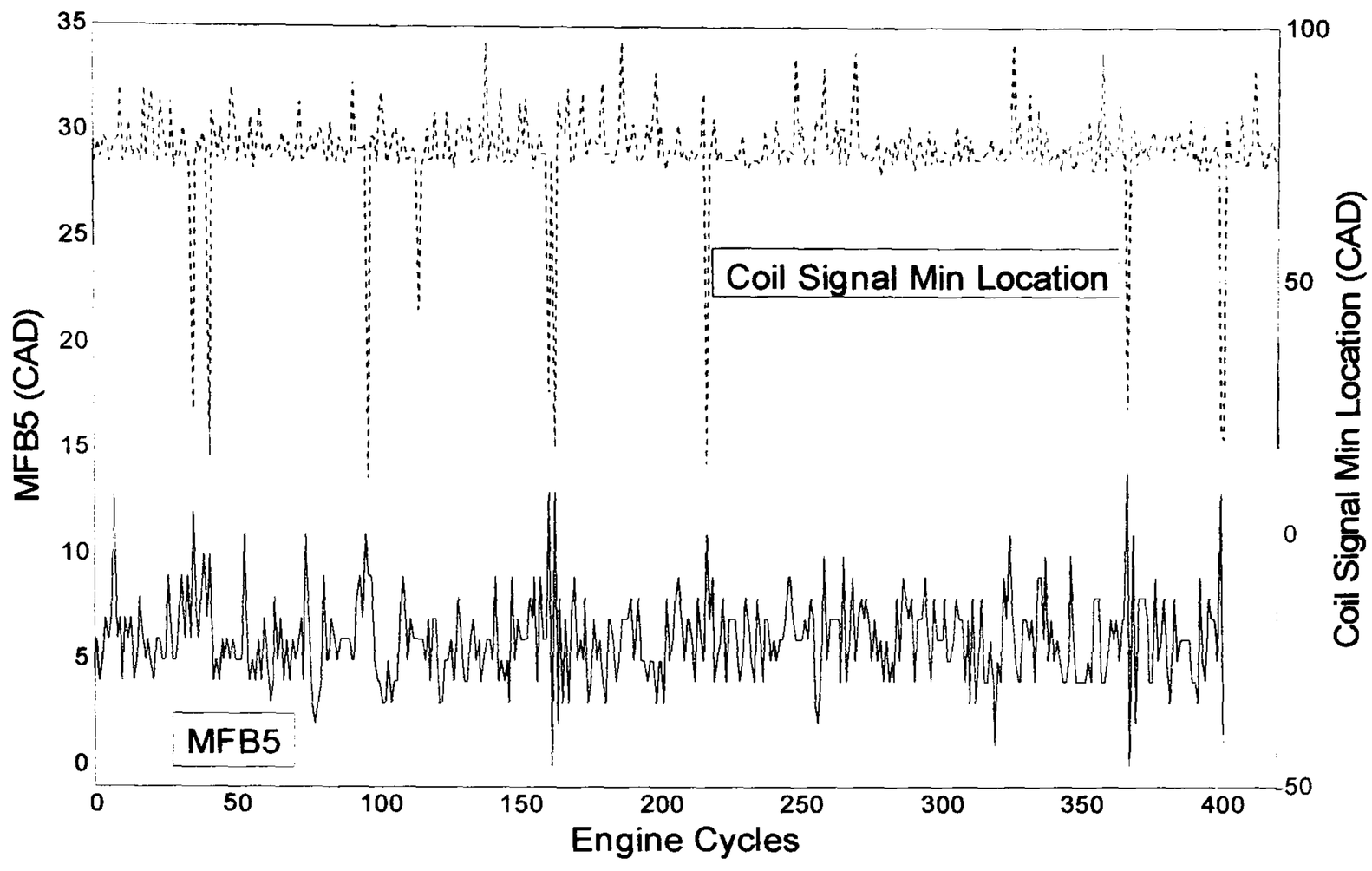

Figure 169: MFB5 and location of minimum coil signal values during sustained, unstable CAI combustion.

As shown in the figure, the location of the minimum of the coil trace presents a tendency to respond to the late combustions present at unstable regions.

The most intuitive way to visualise the effect described above is by considering the signal to be made of two descending segments. Instead of relying on how the location of the minimum will be shifted, it is straightforward to derive the ratio of the minimum points of these segments. When the results cross 1, a late combustion can be flagged and possibly the onset of unstable combustion (Figure 170).

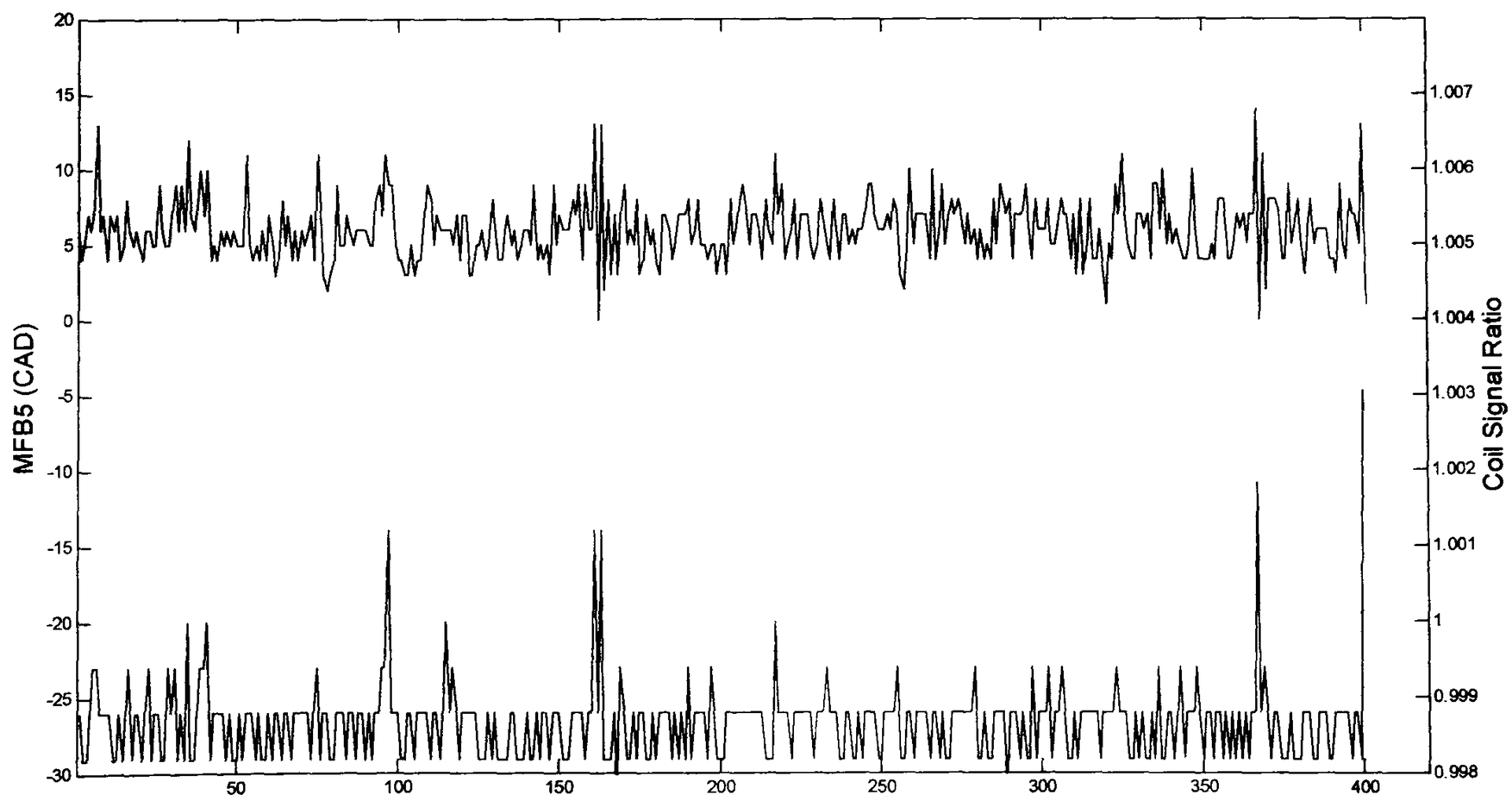

Figure 170: MFB5 and coil signal ratio values during sustained, unstable CAI combustion.

The ratio of the two segments appears to respond to delayed MFB5. Hence, it is potentially a cheap and very computationally efficient method for getting an early warning of the onset of an unstable region, even in the absence of pressure or ion current sensors.

8.3.3 Conclusion

A mechanism for the strong CAD dependency of autoignition of gasoline CAI has been proposed, based on experimental data gathered over a wide range of operating conditions. In the process, the effect on autoignition of two different valve strategies for retaining exhaust gases has been evaluated. The proposed autoignition mechanism aims to explain why "pure" CAI operation for this particular engine seems largely insensitive to operating conditions. To that end, a two effect process theory, combining a geometric and a chemical process has been put forward.

Further investigation has revealed possible mechanisms leading to instability in the case of high TRG for one of the two valve strategies. A linking of successive cycles through TRG at varying temperatures has been proposed to explain the oscillatory behaviour often seen leading to instability and, eventually, to misfires. Evidence of vigorous combustion in the TRG cycles is being backed up by ion current measurements as well as investigation of P-V diagrams.

In this type of engine, autoignition has been witnessed to be less responsive to AFR, TRG, and RPM than to effective compression ratio. In conclusion, it is the author's belief that an engine with a geometry similar to the one used for these experiments should operate reliably in CAI as long as the effective compression ratio is not reduced through throttling or unsuitable valve strategies.

9. Ending Conclusion & Future Issues

This thesis started by studying the work of other researchers in order to get a good understanding of how HCCI has been implemented in the past and what the relevant pros and cons of each strategy are. Also, a wider look at uses other than automotive, in the strict sense of the term, was taken so that the reader can acquire a spherical view of this relatively untried technology.

A decision then had to be made, on which technology would be the most promising, from a practicality but also novelty perspective. Gasoline Controlled Auto-Ignition on a Variable Valve Timing engine was decided to be pursued and experiment design had to be determined. Emissions, fuel consumption and pumping losses were all examined under different operating conditions, mostly governed by the valve timing controlling parameter.

With results mostly verifying previous research work, specific questions emerged that guided the follow-through experiments. Two valve timing strategies were used, one was chosen due to the ease with which it could be implemented with conventional camshafts, the other due to its superior performance. Regardless of the executing procedure however, control was always the underlying consideration, since it is by far the most demanding area. As such, in-cylinder pressure and ion current were evaluated as closed loop feedback signal candidates under diverse conditions covering the whole operating spectrum of the engine.

It was shown possible to control the engine under CAI over a considerable window of operation, with substantial improvements in fuel consumption and emissions. These owe to better tracking of the ideal Otto thermodynamic cycle, reduced pumping losses and reduced peak combustion temperatures. Despite the engine proving to be quite self-stabilizing under pure autoignition, most of the usable operating envelope was shown to be possible to control directly by spark timing, even at gas retention levels that would be considered impossible for SI. This is a principal advantage of SI over CI based, hybrid HCCI, since the spark plug's presence shifts control strategies to what closely resembles conventional SI.

It was also shown that ion current is a valuable and very reliable feedback signal that can diagnose and control engine operation under both regimes. Steady state operation both in SI and CAI, smooth transitions between them and also jumps in TRG level and between SI and CAI were covered, with successful results.

In essence, if the author was forced to give his verdict on immediate HCCI applicability to mass production engines, it would be a positive one. My suggestion would concentrate around a system with mechanical camshafts equipped with phasers, ideally on a multi-lobe camshaft. This should provide the necessary control over the negative valve overlap. AFR can be controlled on an oxygen sensor closed-loop basis, only relying on a map for fast SI-HCCI switching. Ignition timing would preferably be controlled with ion current based closed loop. However, if fast SI-HCCI switching, or jumps between TRG levels is not required, i.e. reduced coverage of the drive cycle under HCCI can be tolerated, map based spark advance would suffice for slow changes in overlap. Thus, HCCI and more specifically CAI emerges as a viable proposition for immediate utilization.

9.1 Future Work

Further research should of course be carried out, in order to take maximum advantage of this technology. The areas suggested would include thermal barriers, coolant management, direct fuel injection, faster and more accurate sensors, more sophisticated ion current implementations, water injection and variable geometry turbos or superchargers. In addition hybrid two-stroke four-stroke operation is also a possibility that needs to be examined.

More analytically, to solve the low speed operation limit, thermal barriers or coolant management can be used to diminish thermal losses, allowing operation at lower rpm. Two-stroke operation can be used to allow low speed operation too, but it might require complementary turbo/supercharging for breathing management. Given that a flexible VVT system is available the engine could switch between two and four strokes between cycles. Both of these techniques could reduce THC emissions. Thermal barriers will help by keeping the exhaust gases at higher temperatures for a longer time period and HCCI two-stroke operation since it has given promising experimental results in THC reduction.

To tackle uncertainties over AFR, fast response mass airflow and/or exhaust gas flow sensors or at least fast response exhaust gas thermocouples could prove beneficial. More complicated arrangements of ion current sensors, i.e. multiple collectors and advanced interpretation algorithms, with some of them located around the head gasket "ring" could serve as flame speed estimators, and also better AFR estimators. Also, the ion current signal that can be acquired from the low voltage side of the ignition coil, without connection to any voltage source, should be further examined and analysed.

For rapid SI-CAI switching, water injection can be used in order to avoid early autoignition, and can also serve as an autoignition suppressor, when a turbo/super charged engine is used.

To increase the high load/speed limit under HCCI turbo/super chargers can be used that would allow for high TRG to be used in conjunction with high mixture mass flows. Variable geometry turbos in particular appear as a cost effective, simple and efficient solution for this. Complementary water injection could further increase allowable effective compression ratios to be used, by allowing increased boost pressures, both in CAI and in normal SI.

Appendix 1 - Information on ceramic thermal barrier coatings

In the mid 1970's materials such as silicon carbide (SiC) and silicon nitride (Si3N4) were first used as materials in engine cylinder construction [187]. Silicon carbide in granular form possess good wear resistance, high temperature capabilities, low coefficient of friction, good corrosion resistance, half the density of steel. But they are more brittle and shrinking to about 18% during sintering. Even though it was successful in some high temperature engine application more advanced materials were developed then for Low Heat Rejection Engines. The other substances of interest include Silicon Nitride (Si3N4), Aluminium Titanate (Al203 TiO2), Aluminium Magnesium Silicate (AMS). Figure 17, shows a list of ceramic materials and their properties [188].

Zirconia, a ceramic material that has very low thermal conductivity values, good strength, thermal expansion coefficients similar to metals and is able to withstand much higher temperatures than metals. However one disadvantageous trait is its characteristic of changing phases with increase in temperature. Eliminating this phase change would ease the burdens of construction and use of the material in an engine [187]. Partially Stabilized Zirconia (PSZ) has been developed that decreases the magnitude of these changes. At present Partially Stabilized Zirconia has been found to be quite desirable for adiabatic engine application because of its excellent insulating characteristics, adequate strength characteristics and thermal expansion characteristics, which are relatively close to some metals. Investigation of M.Marmach et al [189] indicates that Toughened Partially Stabilized Zirconia (PSZ) ceramics possess a number of advantageous properties for advanced engine components, in particular for adiabatic engine system. It has also been stated that Magnesia Partially Stabilized Zirconia (Mg-PSZ) is suitable for LHR engine components. Magnesium and Nickel have been added to PSZ to improve strength and ductility characteristics respectively. Magnesia Partially Stabilized Zirconia (Mg PSZ) has a thermal expansion coefficient and elastic modulus close to that of Iron and Steel and is suitable for liners, valve guides and seats, hot plates, tappet inserts, and piston caps in the engine cylinder. Mg PSZ is made of 20 to 24% Magnesia. This has the highest fracture toughness of all the PSZ materials. Stabilization of Zirconia can be accomplished with the addition of CaO, MgO and Y2O3, but these formations tend to be coarse, lack strength and toughness and exhibit poor thermal shock resistances. Alloys with 20% Yttria or 5% Calcia create fully stabilized Zirconia and good thermal coefficients of

expansion [190]. Another way to improve PSZ characteristics is to impregnate the surface after forming of the part. Success has been shown with a Cr2O3 impregnation treatment [191]. This is also referred as densification treatment. A coating of plasma sprayed Zirconia densified with this treatment exhibits an 87% lower wear rate than a similar undensified coating. The Chromium Oxide fills the open pores between molecular structures and hardens the surface. Another promising material is Syalon (Si-Al-O-N) ceramics. Silicon Nitride mentioned above is one derivative of this classification. The major advantage of the material is the low creep characteristics at high temperatures. The material also has low density and low coefficient of friction. This will be good for reciprocating parts such valves and bearings. However, ceramic materials are not ductile in general and any small imperfection produces stress concentration, which develops crack. Other ceramic, composite and advanced materials are being developed for different engine applications. Research is continuing to obtain ceramics with greater ductility.

Appendix 2 - Photographs of engines for remote controlled vehicles

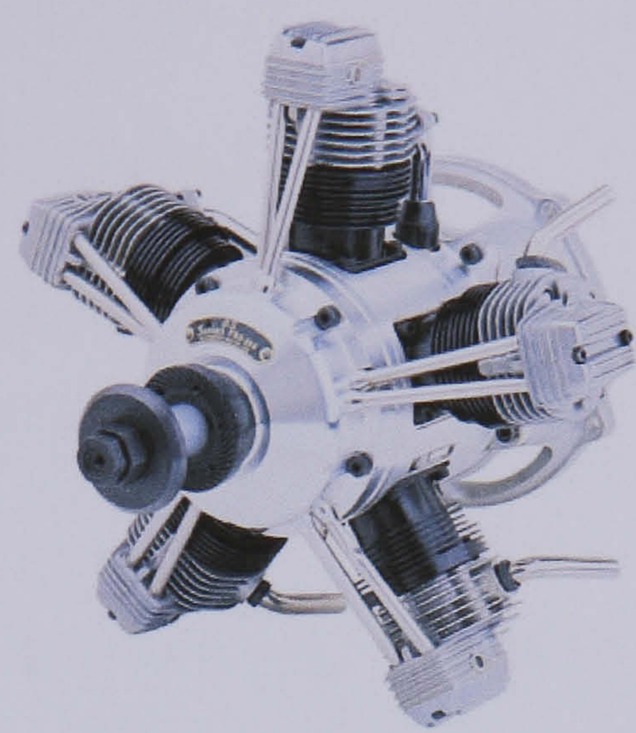

Figure 171: A big displacement radial engine (4-stroke, displacement 9.96cm^3, 4BHP@8000rpm).

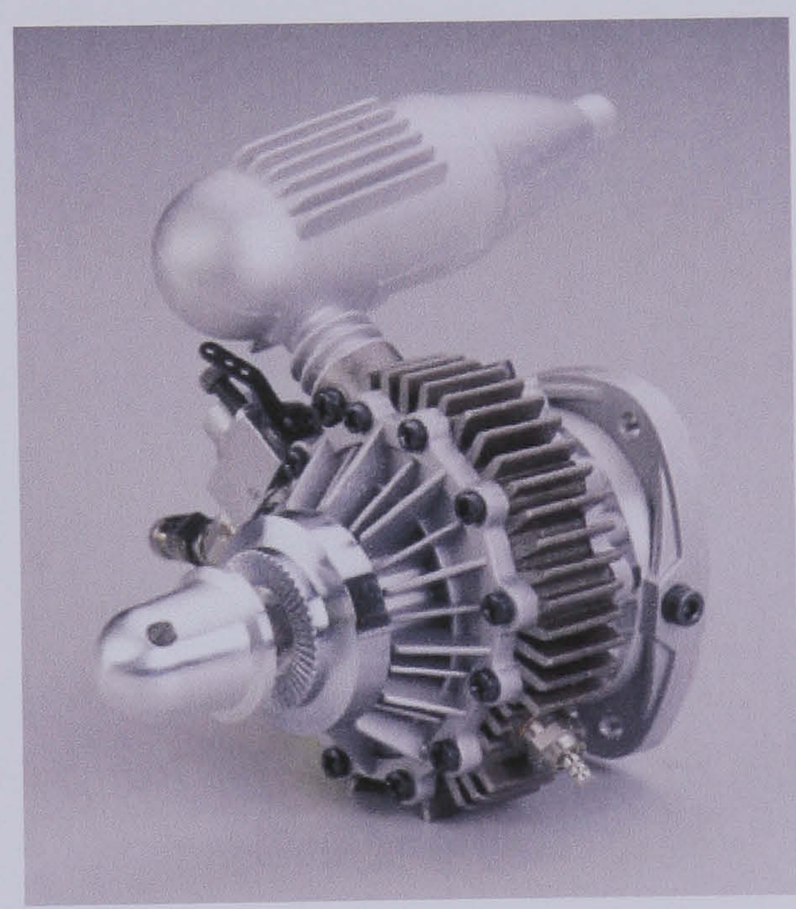

Figure 172: Wankel glow plug engine.

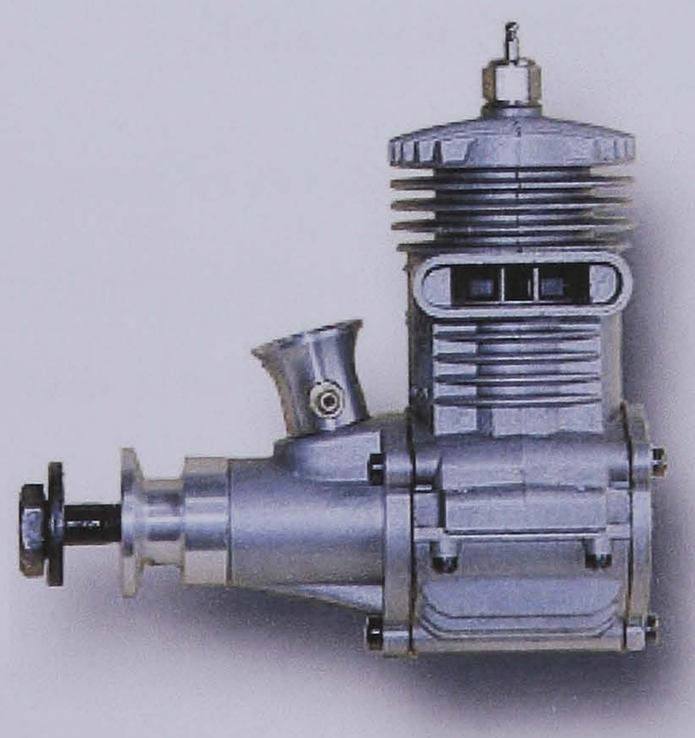

Figure 173: A 2-stroke medium sized glow plug engine. The glow plug can be seen at the top of the cylinder head.

Appendix 3 – Chemical Kinetics

The material presented here is mainly a summary of the literature review of [192], although other sources of literature were used where it was thought appropriate.

Low-temperature Paraffin Oxidation

In the low-temperature autoignition chemistry of paraffinic fuels an abstraction of a hydrogen atom by oxygen to form an alkyl radical (R•) and a hydroperoxy radical (HO_2•) happens first.

$$RH + O_2 \rightarrow R\bullet + HO_2\bullet \quad (1)$$

Due to the different molecular structure of the parent paraffin, the hydrogen abstraction results in a variety of alkyl radicals. The alkyl radicals are consumed in two parallel paths, one being the abstraction of another hydrogen atom by oxygen to form a conjugate olefin and a hydroperoxy radical.

$$R\bullet + O_2 \rightarrow \text{olefin} + HO_2\bullet \quad (2)$$

The other path is the addition of oxygen to the radical to form an alkylperoxy radical (RO_2•).

$$R\bullet + O_2 \leftrightarrow RO_2\bullet \quad (3)\ [80]$$

The RO_2• radical undergoes internal isomerisation by the oxygen abstraction of a hydrogen atom from a C-H bond elsewhere within the molecule to form a hydroperoxyalkyl radical (•ROOH).

$$RO_2\bullet \rightarrow \bullet ROOH \quad (4)$$

In turn the •ROOH radical reacts in two separate routes. In the first route an OH• radical is produces when the hydroperoxyalkyl radical either spontaneously decomposes in a lower molecular weight alkene or forms a cyclic ether and an OH•.

$$\bullet ROOH \rightarrow CARBONYL + R'\bullet + OH\bullet \quad (5)$$

The second route has the •ROOH radical undergoing a second oxygen addition to form a hydroperoxyalkylperoxy radical (•OOROOH), following an internal H atom abstraction to produce an alkylhydroperoxide (HOOROOH). The alkylhydroperoxide then decomposes into an aldehyde (RCHO) and two OH• radicals.

$$\bullet ROOH + O_2 \leftrightarrow \bullet OOROOH \rightarrow HOOROOH \ (6)$$

$$HOOROOH \rightarrow RCHO + R'O + OH\bullet + OH\bullet \ (7)$$

The production of alkylperoxy radicals (reaction 3) is faster than olefin formation (reaction 2) at all temperatures. However, as the temperature is increased above 500 K at atmospheric pressure (700 K at 10 atmospheres pressure) the reverse of reaction (3) is favoured, and olefin production increases. The fuel consumption rate decreases as the rate of olefin formation increases. It is the competition between reactions (2) and (3) that defines the transition between the low- and intermediate-temperature regimes.

Intermediate-Temperature Paraffin Oxidation

Olefin and hydroperoxy radical formation is increased through temperature increase and hydrogen peroxide (H_2O_2) production now becomes significant by HO_2 radicals abstracting a Hydrogen atom from the fuel.

$$RH + HO_2\bullet \leftrightarrow R\bullet + H_2O_2 \ (8)$$

The buildup of hydrogen peroxide in the system eventually decomposes with increasing temperature producing two hydroxyl radicals from each H_2O_2 molecule and the overall reaction rate begins to increase. This is why hydrogen peroxide is so important in the autoignition process.

$$H_2O_2 + M \rightarrow OH\bullet + OH\bullet + M \ (9)$$

Benson has termed this process 'hot-ignition' since there is a ready source for OH radicals for the system [193]. Note that it takes time for the H_2O_2 concentrations to build up before the reaction rate increases, which is parallel to the buildup of the ROOH radical in the low temperature regime.

Functionally, in the intermediate temperature regime the HO_2 radical replaces the RO_2 radical of the low temperature reaction and H_2O_2 replaces HOOROOH. The beginning of the intermediate temperature reactions occur at lower temperature as the pressure is increased thus the range of temperatures over which NTC behavior is exhibited becomes narrower at higher pressures and eventually disappears at very high pressures.

At atmospheric pressures and temperatures higher than roughly 800 K, the oxidation chemistry of most paraffins begins to change significantly. The alkyl radicals are

decomposed into smaller hydrocarbon radicals and olefins by a thermal decomposition process known as beta-scission [194]. Depending upon the structure of the alkyl radical, a wide range of species can be produced via β-scission.

High-Temperature Paraffin and Olefin Oxidation

The high-temperature oxidation of hydrocarbons can be described as a sequential three step process:

- After initiation the parent fuel is converted to lower molecular weight hydrocarbons and water with little energy release.
- The intermediate hydrocarbon species are further converted to produce CO and water.
- CO is oxidized into CO_2 and the large fraction of the energy is released from the combustion process.

Thermodynamics calculation show that roughly half of the energy released from C_7 and C_8 hydrocarbons results from CO oxidation. The reaction sequence can be conceptualized as,

$$RH + OH\bullet \rightarrow R'\bullet + R''\bullet + H_2O \rightarrow CO + H_2O \rightarrow CO_2 + \text{heat} \quad (10)$$

The final reaction in all hydrocarbon combustion systems is the oxidation of CO to CO_2. Because the radicals preferentially react with any hydrocarbons present in the mixture, CO oxidation is delayed until after the majority of the hydrocarbons are consumed.

The important chain-carrying radicals in the high-temperature regime are the OH•, H• and O•. These radicals are very reactive and correspondingly the hydrocarbon oxidation rates are extremely fast.

The important chain-branching reactions are shown below.

$$H\bullet + O_2 \rightarrow OH\bullet + O\bullet \quad (11)$$

$$O\bullet + H_2 \rightarrow OH\bullet + H\bullet \quad (12)$$

$$H_2O + O\bullet \rightarrow OH\bullet + OH\bullet$$

At the high pressures obtained in engines radical recombination reactions are also important. The dominant recombination reaction at these pressures is,

$$H\bullet + O_2 + M \rightarrow HO_2\bullet + M$$

where M represents a third body collision partner. The transition between intermediate- and high-temperature kinetic regimes is generally defined as the condition where the branching reaction (11) dominates over the recombination reaction (14) [194]. This transition is a function of not only pressure, but of the third body efficiencies of the other molecules in the system. At atmospheric pressure with nitrogen as a third body, the transition to high temperature kinetics occurs at roughly 950 K as previously stated while at 10 atmospheres the transition does not occur until 1400 K.

The final stage of the energy release at high temperature is CO oxidation, where 45 to 50% of the energy is released. The principal reactions consuming CO are,

$$CO + OH\bullet \rightarrow CO_2 + H\bullet \quad (15)$$

$$CO + HO_2\bullet \rightarrow CO_2 + OH\bullet \quad (16)$$

$$CO + O\bullet + M \rightarrow CO_2 + M \quad (17)$$

At high temperatures nearly all of the CO is consumed by OH• radicals via reaction (15) with only a small contribution from the other reactions. As already mentioned, CO oxidation is inhibited by the presence of hydrocarbons, since the OH• radicals preferentially react with those [195].

It should be added here that oxidation of aromatics, not analyzed at all here, is also important. Especially high-temperature aromatic oxidation is slightly problematic and thus these are used mainly for increasing gasoline octane rating.

10. REFERENCES

[1] Engine and Emission Control Technologies and Fuel Requirements, GM Public Policy Centre, 20th September 2001

[2] Andrew Waterman, "Automobile Emissions and Air Pollution", April 9, 1998

[3] IDC.Hunter, Expression of Interest, Maslen Engine, Commercial in Confidence, 2004

[4] http://www.yournextcar.org/YNCandenviron.html

[5] Ricardo, Emissions and Efficiency Targets: Advanced Technology Reciprocating Internal Combustion Engines, ARICE Workshop, 10th July 2001

[6] European Federation for Transport and Environment, Euro 5 Update, New Emission Standard for Passenger Cars, 1st October 2004

[7] www.mitsubishi-motors.com

[8] http://www.me.iastate.edu/biodiesel/Pages/bio14.html

[9] Guenthner, M., Sauter, W., Schwarz, F., Velji , A., and Spicher, U., "A Study of the Ignition and Combustion Process in a Gasoline HCCI Engine Using Port and Direct Fuel Injection", Institute of Reciprocating Engines, University of Karlsruhe, Germany

[10] Zhao, H., Peng, Z., and Ladommatos, N., "Understanding of Controlled Autoignition Combustion in a Four-Stroke Gasoline Engine", Proc Instn Mech Engrs Vol215 PartD, IMechE, 2001

[11] Christensen, M., Hultqvist, A., and Johansson, B., "Demonstrating the Multi-Fuel Capability of a Homogeneous Charge Compression Ignition Engine with Variable Compression Ratio", SAE Paper, No. 1999-01-3679, 1999

[12] Milovanovic, N., Chen, R., Dowen, R., and Turner, J., "An Investigation of Using Various Diesel-Type Fuels in Homogeneous Charge Compression Ignition Engines and Their effects on Operational and Controlling Issues", Int J Engine Research, Vol5, No4, Jer 03502, IMechE, 2004

[13] American Council for an Energy-Efficient Economy, Advanced Technology Showroom, http://www.aceee.org/transportation/showroom.htm

[14] Osborne, R.J., Li, G., Sapsford, S.M., Stokes, J., Lake, T.H., and Heikal, M.R., "Evaluation of HCCI for Future Gasoline Powertrains", SAE Paper, No. 2003-01-0750, 2003

[15] "Homogeneous Charge Compression Ignition (HCCI) Technology", A Report to the U.S. Congress, U.S. Department of Energy, Energy Efficiency and Renewable Energy, Office of Transportation Technologies, April 2001

[16] Alperstein, M., Swim, W. B., and Schweitzer, P. H., "Fumigation Kills Smoke – Improves Diesel Performance," SAE Transactions, vol. 66, pp.574 – 588, 1958

[17] Onishi S., Jo S. H., Shoda K., Jo P. D., and Kato S., "Active Thermo-Atmosphere Combustion (ATAC) – A New Combustion Process for Internal Combustion Engines", SAE 790501, 1979

[18] Noguchi M., Tanaka Y., Tanaka T., and Takeuchi Y., "A Study on Gasoline Engine Combustion by Observation of Intermediate Reactive Products during Combustion", SAE 790840, 1979

[19] Najt P. M., and Foster D. E., "Compression-Ignited Homogeneous Charge Combustion", SAE 830264, 1983

[20] Thring R. H., "Homogeneous-Charge Compression-Ignition (HCCI) Engines", SAE 892068, 1989

[21] Green, R.M., Gernansky, N.P., Pitz, W.J. and Westbrook, C.K., "The role of Low Temperature Chemistry in the Autoignition of n-Butane", SAE paper No. 872109, 1987

[22] Green, R.M., Gernansky, N.P., Pitz, W.J. and Westbrook, C.K., "Chemistry of oxidation Preceding End-gas Autoignition", Comb. Sci. Technol., 1986

[23] Held, T.J., Marchese, A.J. and Dryer, F.L., "Asemi-empirical reaction mechanism for n-eptane oxidation and pyrolysis", Combust. Sci. Technol., 1997

[24] Curran, H.J., Gaffuri, P., Pitz, W.J. and Westbrook, C.K., "Acomprehensive Modelling Study of n-Heptane Oxidation", Combust. Flame, 1998

[25] Zheng, J., Miller, D., and Cernasky, N., "The Effect of Active Species in Internal EGR on Preignition Reactivity and on Reducing UHC and CO Emissions in Homogeneous Charge Engines", SAE paper 2003-01-1831, 2003

[26] Easley, W.L., Agarwal, A., and Lavoie, G.A., "Modelling of HCCI Combustion and Emissions Using Detailed Chemistry", SAE paper 2001-01-1029, 2001

[27] Fuerhapter,A., Unger, E., Piock, W.F., and Fraidl, G.K., "The new AVL CSI Engine – HCCI Operation on a Multi Cylinder Gasoline Engine", SAE paper 2004-01-0551, 2004

[28] Green J. Jr, "Novel Combustion Regimes for Higher Efficiency and Lower Emissions", National Transportation Research Centre, Oak Ridge National Laboratory, 2002

[29] Murase E., Hanada K., Miyaura T., Ikeda J., and Konishi N., "Experimental Studies of HCCI Combustion", Kyushu University, Nobby Tech. Ltd., Japan

[30] Reitz R., "The Use of CFV Technology for Internal Combustion Engine Applications", University of Wisconsin-Madison, 2004

[31] Glassman, I., "Combustion", 2 ed: Academic Press, Inc., 1987

[32] Koopmans, L., "HCCI for Gasoline Engines Retaining Residuals – An Experimental Study", Department of Thermo and Fluid Dynamics, Chalmers University of Technology, Sweden 2002

[33] Heywood J., "Internal Combustion Engine Fundamentals", McGraw-Hill International, 1988

[34] Christensen, M., Johanson, B., Amneus, P., and Mauss, F., "Supercharged homogeneous charge compression ignition", SAE Paper 980787, 1998

[35] Urushihara, T., Hiraya, K., Kakuhou, A., and Itoh, T., "Parametric Study of Gasoline HCCI with Various Compression Ratios, Intake Pressures and Temperatures", Proceedings of the IFP International Congress, Paris, November 26-27, pp. 77-84, 2001

[36] Wolters, P., Salber, W., and Dilthey, J., "Radical Activates Combustion a New Approach for Gasoline Engines", Proceedings of the IFP International Congress, Paris, November 26-27, pp. 153-162m 2001

[37] Drangel, H., Olofsson, E., and Reinmann, R., "The Variable Compression (SVC) and the Combustion Control (SCC) – Two Ways to Improve Fuel Economy and Still Comply with World-Wide Emission Requirements", SAE Paper 2002-01-0996, 2002

[38] Erlandsson, O., Lundholm, G., Soderberg, F., Johansson, B., and Wong, V.W., "Demonstrating the Performance and Emission Characteristics of a Variable Compression Ratio Alvar-Cycle Engine", SAE Paper 982682, 1998

[39] Schwaderlapp, M., Habermann, K., and Yapici, K. I., "Variable Compression Ratio-A Design Solution for Fuel Economy Concepts", SAE Paper 2002-01-1103, 2002

[40] Sharke P., "Otto or Not, Here it Comes", Mechanical Engineering, Vol. 122, No. 6, June 2000, pp. 62-66

[41] Chen, Z., Konno, M., and Goto, S., "Study on homogenous premixed charge CI engine fuelled with LPG", JSAE Review, vol.22, pp.265-270, 2001

[42] Stanglmaier, R. H., Ryan, T. W., and Souder, J. S., "HCCI Operation of a Dual-Fuel Natural gas Engine for Improved Fuel Efficiency and Ultra-Low NOx Emissions at Low to Moderate Engine Loads", SAE paper 2001-01-1897, 2001

[43] Olsson, J. O., Tunestal, P., Haraldsson, G., and Johansson, B., "A Turbo Charged Dual Fuel HCCI Engine", SAE Paper 2001-01-1896, 2001

[44] Olsson, J. O., Tunestal, P., and Johansson, B., "Closed-Loop Control of an HCCI Engine", SAE Paper 2001-01-1031, 2001

[45] Zur, L., Akinyeni, O., Durrett, R., Flynn, P., Hunter, Gary., Moore, G., Mudd, J., Muntean, G., Wagner, J., and Wright, J., "Premixed Charge Compression Ignition Engine with Optimal Combustion Control", International Patent WO09942718, World Intellectual Property Organization

[46] Olsson, J.O., Tunesta, P., Johansson, B., Fiveland, S., Agama, R., Willi, M., and Assanis, D., "Compression Ratio Influence on Maximum Load of a Natural Gas Fuelled HCCI Engine", SAE 02P-147, 2002

[47] Denbratt, I., "Method of controlling the process of combustion in an internal combustion engine with means for controlling the engine valves", Volvo Car Corporation, Patent application No. WO0028197, 1998

[48] Law, D., Kemp, D., Allen, J., Kirkpatrick, G., and Copland, T., "Controlled Combustion in an IC-Engine with a Fully Variable Valve Train", SAE Paper 2000-01-0251, 2000

[49] Kontarakis, G., Collings, N., and Ma, T., "Demonstration of HCCI Using a Single Cylinder Four-stroke SI Engine with Modified Valve Timing", SAE Paper 2000-01-2870, 2000

[50] Koopmans, L., and Denbratt, I., "A Four Stroke Camless Engine, Operated in Homogeneous Charge Compression Ignition Mode with Commercial Gasoline", SAE 2001-01-3610, 2001

[51] Willand, J., Nieberding, R. G., Vent, G., and Enderle, C., "The knocking syndrome: its cure and potential", in Automotive Engineering International, pp. 64-68, 1999

[52] Sasaki, H., Sekiyama, S., and Nakashima, K., "A New Combustion System of a Heat-Insulated Natural Gas Engine with a Pre-Chamber Having a Throat Valve", Int J Engine Research, Vol3, No4, Jer 01602, IMechE, 2002

[53] Lassi, U., "Deactivation Correlations of Pd/Rh Three-way Catalysts Designed for Euro IV Emission Limits", Thesis, Department of Process and Environmental Engineering, University of Oulu

[54] Jaichandar, S. and Tamilporai, P,. "Low Heat Rejection Engines – An Overview", SAE 2003-01-0405, 2003

[55] Kamo, R. and Bryzic, W. "Uncooled, Unlubricated Diesel", Automotive Engineering, Vol. 87n6, 1979

[56] Curran, H.J., Gaffuri, P., Pitz, W.J. and Westbrook, C.K., "A Comprehensive Modelling Study of n-Heptane Oxidation", Combustion and Flame 114:149, 1998

[57] Peter Van Blarigan, "Hydrogen Program Review", Proceedings of the 2002 U.S. DOE, NREL/CP-610-32405, Sandia National Laboratories,Livermore, CA 94550

[58] Karim, G.A. and Watson, H.C., "Experimental and Computational Considerations of the Compression Ignition of Homogenous Fuel-Oxidant Mixtures", SAE paper 710133, 1971

[59] Underwood, A.F., "The GMR 4-4 'Hyprex' Engine – A Concept of the Free-Piston Engine for Automotive Use", SAE Paper 570032, 1957

[60] Klotsch, P., "Ford Free-Piston Engine Development," SAE Paper 590045,1959

[61] Achten, P. A. J., "A Review of Free Piston Engine Concepts," SAE Paper 941776, 1994

[62] http://www.sae.org/ohmag/techinnovations_04-00/02.htm

[63] http://www.icel.tkk.fi/research/Pulse_Two.html

[64] Braun, A. T. and Schweitzer, P. H., "The Braun Linear Engine," SAE Paper 730185, 1973

[65] Epstein, A.H., Senturia, S.D., Anathasuresh, G., Ayon, A., Breuer, K., Chen, K., Ehrich, F.E., Gauba, G., Ghodssi, R., Groshenry, C., Jacobson, S., Lang, J.H., Lin, C., Mehra, A., Miranda, J.M., Nagle, S., Orr, D.J., Piekos, E., Schmidt, M.A., Shirley, G., Spearing, M.S., Tan, C.S., Tzeng, Y., and Waitz, I. A., "Power MEMS and Microengines.", Transducers '97 Chicago : digest of technical papers, pp. 753, 1997

[66] Kapat, J. and Chow, L., "Scaling Laws in Miniature Heat Engines" ASME Advanced Energy, Systems Division Newsletter, 2001

[67] Waitz, I.A., Gauba, G. and Tzeng, Y., "Combustors for Micro-Gas Turbine Engines", Journal of Fluids Engineering, vol. 120, no. 1, pp. 109-117, 1998

[68] Disseau, M., Kirtas, M., Scarborough, D., Jagoda, J., and Menon, S., "Investigation of Combustion Processes in Small Aspect Ratio Combustors", Georgia Institute of Technology Internet Document (Last loaded August 2000)

[69] Fernandez-Pello, C., Liepmann, D., Pisano, A., et al., 2001. "MEMS Rotary Combustion Laboratories", University of California at Berkeley Internet Document, URL http://www.me.berkeley.edu/mrcl/, (Last loaded July 2001)

[70] Knobloch, A., "MEMS Rotary Combustion Laboratories", University of California at Berkeley Internet Document, URL http://euler.me.berkeley.edu/mrcl/, (Last loaded August 2000)

[71] Taylor, C.F., "The Internal Combustion Engine in Theory and Practice: Volume II: Combustion, Fuels, Materials, Design", The M.I.T. Press, Cambridge, MA, 1985b

[72] http://towerhobbies.com/listings/cat-cat-g.html

[73] Gierke, C.D., "Two-Stroke Glow Engines for R/C Aircraft", Air Age Inc., 251 Danbury Rd. Wilton, CT 06897, 1994

[74] www.dft.gov.uk/stellent/groups/dft_avsafety/documents/source/dft_avsafety_source_501515.doc - Aerostar SA Yak-52, G-BVMU, AAIB Bulletin No: 3/2002, Ref: EW/G2001/08/23

[75] Wintenberger, E. and Shepherd, J.E., Explosion Dynamics Laboratory, Graduate Aeronautical Laboratories, California Institute of Technology, Pasadena, CA 91125 Ae103, http://www.galcit.caltech.edu/EDL/projects/pde/Ae103-012704.pdf, January 2004

[76] Clutton, E., "Dr. Diesel's Diary: All You Wanted To Know About Model Diesels." Prepared Pamphlet. 913 Cedar Lane, Tullahoma, TN 37388 (931) 455-2256, 2000

[77] Richmond, S., "A Close Look at the Davis Diesel Converter Heads", Radio Control Modeler, vol. 33, no. 10, pp. 164-168, 1996

[78] Richmond, S., "Sunday Fun", Radio Control Modeler, vol. 36, no. 8, pp. 38,40, 1999

[79] Burns, V., Hochhauser, A., Reuter, R., Rapp, L., Knepper, J., Rippon, B., Koehl, W., Leppard, W., Rutherford, J., Benson, J., Painter, L., "Gasoline Reformulation and Vehicle Technology Effects on Emissions – Auto/Oil Air Quality Improvement Research Program", SAE Technical Paper. 952509,1995

[80] Halstead, M., Kirsch, L., and Quinn C., "The Autoignition of Hydrocarbon Fuels at High Temperatures and Pressures-Fitting of a Mathematical Model", Combustion and Flame 30, Pages 45-60, 1977

[81] Acaves, S., Flowers, D., Westbrook, C., and Pitz, W., "A multi-zone model for prediction of HCCI combustion and emissions", SAE paper 2000-01-0327, 2000

[82] Westbrook, C., Dryer, F., and Schug, K., "A comprehensive mechanism for the pyrolysis and oxidation of ethylene", In: Symposium (International) on Combustion. Pitsburg: The Combustion Institute, 1982. p. 153

[83] Westbrook, C., Pitz, W., and Leppard, W., "The autoignition chemistry of paraffinic fuels and pro-knock and anti-knock additives: a detailed chemical kinetic study", SAE paper 912314, 1991

[84] Tanaka, S., Ayala, F., Keck, J., and Heywood, J., "Two-Stage ignition in HCCI combustion and HCCI control by fuels and additives", Combust Flame 2003;132:219-39

[85] Richter, M., Engstrom, J., Franke, A., Alden, M., Hultqvist, A., and Johansson, B., "*The influence of charge inhomogeneity on the HCCI combustion process*", Division of Combustion Physics, Lund Institute of Technology, SAE paper 2000-01-2868

[86] Hultqvist, A., Christensen, M., Johansson, B., Franke, A., and Richter, M., "*A study of the Homogeneous Charge Compression Ignition combustion process by chemiluminescence imagin*", SAE Fall Fuel and Lubricants meeting and exposition 1999. SAE paper NR. 1999-01-3680

[87] Zhao, H., Li, J., Ma, T., and Ladommatos, N., "*Performance and Analysis of a 4-Stroke Multi-Cylinder Gasoline Engine with CAI Combustion*", SAE 2002-01-0420

[88] Peng, Z., Zhao H., Ladommatos, N., "Visualization of the Homogeneous Charge Compression Ignition/Controlled Autoignition Combustion Process Using Two-Dimensional Planar Laser-Indiced Fluoresence Imaging of Formaldehyde", Proc Instn Mech Engrs Vol217 PartD, D07803, IMechE, 2003

[89] Christensen, M., "HCCI Combustion - Engine Operation and Emission Characteristics", PhD thesis, Lund University

[90] Richter, M., Franke, A., Engstrom, J., Hultqvist, A., Johansson, B., and Alden, M., "The Influence of Charge Inhomogeneity on the HCCI Combustion Process", SAE paper 2000-01-2868, 2000

[91] Koopmans, L., Backlund, O., and Denbratt, I., "Cycle to cycle variations: their influence on cycle resolved gas temperature and unburned hydrocarbons from a camless gasoline compression ignition engine". SAE paper 2002-01-0110, 2002

[92] Koopmans, L., Ogink, R. and Denbratt, I., "Direct Gasoline Injection in the Negative Valve Overlap of a Homogeneous Charge Compression Ignition Engine", SAE 2003-01-1854

[93] Koopmans, L., Ogink, R. and Denbratt, I., "Visualization (PLIF) of Intermediates Generated in the Negative Valve Overlap of an HCCI operated engine", Presented at the Joint Meeting of the Scandinavian-Nordic and Italian Sections of the Combustion Institute, Italy,September 2003

[94] Calcote, H.F., "Ion production and recombination in flames", 8th Symposium on Combustion, 1962

[95] Calcote, H.F., "Ion and electron profiles in flames", 9th Symposium in Combustion, 1963

[96] Shuler, K., "Ionization in High-Temperature Gases", Academic Press, New York, London, 1963

[97] Shimasaki, Y., Kanehiro, M., Baba, S., Maruyama, S., Hisaki, T., and Miyata, S., "Spark plug voltage analysis for monitoring combustion in an internal combustion engine", (SAE paper No. 930461), 1993

[98] Saitzkoff, A., Reinmann, R., Berglind, T., and Glavmo, M., "An ionization equilibrium analysis of the spark plug as an ionization sensor", (SAE paper No. 960337), 1996

[99] Yoshiyama, S., Tomita, E., and Hamamoto, H., "Fundamental study on combustion diagnostics using a spark plug as ion probe", SAE 2000-01-2828, 2000

[100] Iinuma, K., "Ionization current in spark-ignition engines", Technical Report 3, Report of the Technical College, 1958

[101] Eriksson, L., Nielsen, L., and Glavenius, M., "Closed Loop Ignition Control by Ionization Current Interpretation", 970854, SAE Technical Paper Series

[102] Aithal, S., White, R., Subramaniam, V., Babu, V., and Rizzoni, G., "A Chemical Kinetics Model of Current Signatures in an Ionization Sensor", *AIAA Plasmadynamics and Lasers Conference*, (AIAA-1999-3606), 1999

[103] Eriksson, L., "Spark Advance Modelling and Control", PhD thesis, Linkoping University, May 1999

[104] Hellring, M., and Holmberg, U., "An Ion Current Based Peak-Finding Algorithm for Pressure Peak Position Estimation", 2000-01-2829, SAE Technical Paper Series

[105] Calcote, H.F., "Mechanisms for the formation of ions in flames", Combustion and Flames, Volume 1:385-403, 1957

[106] Reinmann, R., "Theoretical and Experimental Studies of the formation of Ionized gases in Spark Ignited Engines", PhD Thesis, Lund Institute of Technology, 1998

[107] Reinmann, R., Saitzkoff, A., Mauss, F. and Glavmo, M.: "Local Air-Fuel Ratio Measurements Using the Spark Plug as an Ionization Sensor", *SAE Technical Paper Series*, (970856), 1997

[108] Hellring, M., Rognvaldsson, T., Wickstrom, N., and Larsson, M., "Ion Current based Pressure Peak Detection Under Different Air Humidity Conditions", Technical Paper, Advanced Microsystems for Automotive Applications (AMAA), 2000

[109] Hellring, M., and Holmberg, U., "A Comparison of Ion Current Based Algorithms for Peak Pressure Position Control", 2001-01-1920, SAE Technical Paper Series, 2001

[110] Hellring, M., Munther, T., Rognvaldsson, T., Wickstrom, N., Carlsson, C., Larsson, M., and Nytomt, J., "Spark Advance Control Using the Ion Current and Neural Soft Sensors", 1999-01-1162, SAE Technical Paper Series, 1999

[111] Nielsen, L., and Ericsson, L., "An Ion-Sense Engine-Fine-Tuner", Vehicular Systems, Department of Electrical Engineering, IEEE Control Systems Magazine, Vol. 18, no.8, 1998

[112] Auzins, J., Johansson, H., and Nytomt, J., "Ion – Gap Sense in misfire detection, knock and engine control", SAE 950004, 1995

[113] Saitzkoff, A., Reinmann, R., Mauss, F., Glavmo, M., "In-Cylinder Pressure Measurements Using the Spark Plug as an Ionization Sensor", 970857, SAE Technical Paper Series

[114] Peron, L., Charlet, A., Higelin, P., Moreau, B., and Burq, J., "Limitations of Ionization Current Sensors and Comparison with Cylinder Pressure Sensors", SAE Technical Paper Series, (2000-01-2830), 2000

[115] Asano, M., Ito, A., Kuma, T., Kajitani, M., Takeuchi, M., Fukumura, Y., and Izumi, M., "Further Development of an Ion Current Combustion Control System", SAE Technical Paper Series, (2001-01-0266), 2001

[116] Russ, S., Peet, G., and Stockhausen, W., "Measurements of the Effect of In-Cylinder Motion on Flame Development and Cycle-to-Cycle Variations Using an Ionization Probe Head Gasket", SAE Technical Paper Series, (970507), 1997

[117] SMETEC GmbH, An Furthenrode 52, D-52511 Geilenkirchen, Fon: +49 (0) 2451/4900-900, Fax: -911, email:info@smetec.de, Webpage: http://www.smetec.de

[118] Anderson, I., "Cylinder pressure and Ionization Current Modelling for Spark Ignited Engines", Linkoping, 2002

[119] Saitzkoff, A., Reinmann, R., Bergling, T., and Glavmo, M., "An ionization equilibrium analysis of the spark plug as as an ionization sensor" SAE paper, No. 960337, 1996

[120] Wilstermann, H., "Wechselspannungszundung mit integrierter Ionenstrommessung als Sensor fur die Verbrennungs- und Motorregelung", PhD thesis, University Fridericiana of Karlsrube, April 1999

[121] Bruce, M., "Estimation of the EGR rate in a GDI engine working in stratified mode using the ionization current", PhD Thesis, December 12, 2000

[122] Kiencke, U., and Nielsen, L., "Automotive Control Systems", SAE International, 2000

[123] Catania, A.E. Misul, D., Mittica, A., and Spessa, E., " A refined two-zone heat release model for combustion analysis in SI engines", JSME International Journal Series B, 46(1), 2003

[124] Eriksson, L., and Andersson, I., "An analytical model for cylinder pressure in a four stroke SI engine", SAE 2002-01-0371, 2002-01-0371, 2002

[125] Gazis, A., Panousakis, D., Chen, R., Chen, W., "Computationally inexpensive methods of ion current signal manipulation for predicting characteristics of engine in-cylinder pressure", International Journal of Engine Research, EU_CA_143, 2006

[126] Panousakis, D., Gazis, A., Chen, R., "Analysis of SI combustion diagnostics methods using ion current sensing techniques", SAE, SAE 2006-01-1345, 2006

[127] Lapuerta, M., Armas, O., and Hernandez, J., "Diagnosis of DI diesel combustion from in-cylinder pressure signal by estimation of mean thermodynamic properties of the gas", Applied Thermal Engineering, 19:513-529, 1999

[128] Gazis A., "Algorithm development on the use of feedback signals in the context of gasoline HCCI combustion.", PhD Thesis, Loughborough University, November 2006

[129] U.S. National Bureau of Standards, JANAF Thermochemical Tables, 1971

[130] Stone. R., "Introduction to Internal Combustion Engines", Macmillan, 1999

[131] Tunestal, P.A., "The Use of Cylinder Pressure for Estimation of the In-Cylinder Air/Fuel Ratio of an Internal Combustion Engine", PhD thesis, Lund University, 1993

[132] Rai, S., Brunt, M., and Loader, C., "Quantification and reduction of IMEP errors resulting from pressure transducer thermal shock in an S.I. engine", SAE 1999-01-1329, 1999

[133] Edson, M., "The influence of compression ratio and dissociation on ideal Otto cycle engine thermal efficiency", Digital Calculations of Engine Cycles, SAE Prog. In Technology, vol. 7, pp. 49-64

[134] Caris, D., and Nelson, E., "A New Look at High Compression Engine," (SAE Paper 730185), 1973

[135] Overington, M., and Thring, R., "Gasoline Engine Combustion – Turbulence and the Combustion Chamber" (SAE Paper 810017), 1981

[136] Muranaka, R., Klein, R., Peters, N. and Konig, G., "Theoretical and Experimental Investigation of Knock Induced Surface Destruction", SAE Transactions, vol. 99, section 3, pp. 99-137, 1990

[137] Das, L., "Hydrogen Engines: A View of the Past and a Look Into the Future," International Journal of Hydrogen Energy, vol. 15, no. 6, pp. 425-443, 1990

[138] Van Blarigan, P., and Green, R., "NO Emission Data Verified in a Hydrogen Fueled Engine," Combustion Research Facility News", vol.17, no 4, January/February, 1995

[139] Braligan, P.V., "Proceedings of the 2002 U.S. DOE Hydrogen Program Review NREL/CP-610-32405: Advanced Internal Combustion Electrical Generator", Sandia National Laboratories, Livermore, CA 94550

[140] Shelby, M., Stein, A., and Warren, C., "A New Analysis Method for Accurate Accounting of IC Engine Pumping Work and Indicated Work", SAE Paper 2004-01-1262

[141] Forster, J., Gunther, A., Ketterer, M., and Wald, K., "Ion current sensing for spark ignition engines" , SAE 1999-01-2004,1999

[142] Ohashi, Y., Koiwa, M., Okammura, K., and Ueda, A., "The application of ionic current detection system for the combustion control", SAE 1999-01-0550, 1999

[143] Peron, L., Charlet, A., Higelin, P., Moreau, B., and Burq, J., "Limitations of Ionization Current Sensors and Comparison with Cylinder Pressure Sensors", SAE 2000-01-283, 2000

[144] Hellring, M., Munther, T., Rognvaldsson, T., Wickstrom, N., Carlsson, C., Larsson, M., Nytomt, J., "Robust AFR Estimation Using the Ion Current and Neural Networks", SAE 1999- 01-1161, 1999

[145] VanDyne, E., Burckmyer, L., and Wahl, A., "Misfire Detection from Ionization Feedback Utilizing The Smartfire Plasma Ignition Technology", SAE Technical Paper Series, (2000-01-1377), 2000

[146] Lunsdstrom, D., and Schagerberg, S., "Misfire Detection for Prechamber SI Engines Using Ion-Sensing and Rotational Speed Measurements", SAE Technical Paper Series, (2001-01-0993), 2001

[147] Raymond, R., Andre, S., and Fabian, M., "Local Air-Fuel Ratio Measurements Using the Spark Plug as an Ionization Sensor", SAE Technical Paper Series, (970856), 1997

[148] Devesh, U., and Giorgio, R., "AFR Control on a single Cylinder Engine Using the Ionization Current", SAE Technical Paper Series, (980203), 1998

[149] Balles, E., VanDyne, E., Wahl A., Ratton, K., and Lai, M., "In-Cylinder Air-Fuel Ratio Approximation Using Spark Gap Ionization Sensing", SAE Technical Paper Series, (980166), 1998

[150] Hellring, M., Munther, T., Rognvaldsson, T., Wickstrom, N., Carlsson, C., Larsson, M., and Nytomt, J., "Robust AFR Estimation Using the Ion Current and Neural Networks", SAE Technical Paper Series, (1999-01-1161), 1999

[151] Schneider, D., and Lai, M., "Real-Time Air/Fuel Ratio Control in a Small SI Engine Using the Ionic Current Signal", SAE Technical Paper Series, (1999-01-3323), 1999

[152] Klovmark, H., Rask, P., and Forssell, U., "Estimating the Air/Fuel Ratio from Gaussian Parametrizations of the Ionization Currents in Internal Combustion SI Engines", SAE Technical Paper Series, (2000-01-1245), 2000

[153] Ohashi, Y., Fukui, W., Tanabe, F., and Ueda, A., "The Application of Ionic Current Detection System for the Combustion Limit Control", SAE Technical Paper Series, (980171), 1998

[154] Bie, T., Ericsson, M., and Rask. P., "A Novel Start Algorithm for CNG Engines Using Ion Sense Technology", SAE Technical Paper Series, (2000-01-2800), 2000

[155] Asano, M., Kuma, T., Kajitani, M., and Takeuchi, M., "Development of New Ion Current Combustion Control System", SAE Technical Paper Series, (980162), 1998

[156] Franke, A., Einewall, P., Johansson, B., and Reinmann, R., "Employing an Ionization Sensor for Combustion Diagnostics in a Lean Burn Natural Gas Engine", SAE Technical Paper Series, (2001-01-0992), 2001

[157] Forster, J., Gunther, A., Ketterer, M., and Wald, K., "Ion Current Sensing for Spark Ignition Engines", SAE Technical Paper Series, (1999-01-0204), 1999

[158] Rognvaldsson, T., Carlsson, C., Hellring, M., Larsson, M., Munther, T., Wickstrom, N., "Spark advance control using the ion current and neural soft sensors", *SAE Technical Paper Series*, (1999-01-1162), 1999

[159] Daniels, C., "The comparison of mass fraction burned obtained from the cylinder pressure signal and spark plug ion signal", *SAE Technical Paper*, (980140), 1998

[160] Wickstrom, N., Taveniku, M., Linde, A., Larsson, M., and Svensson, B., "Estimating peak pressure position and air-fuel ratio using the ionization current and artificial neural networks", *Proceedings of IEEE Conference on Intelligent Transportation Systems*, 1997

[161] Rognvaldsson, T., Carlsson, C., Hellring, M., Larsson, M., Munther, T., Wickstrom, N., "Spark advance control using the ion current and neural soft sensors", *SAE*, (99P-78), 1998

[162] Hellring, M., Munther, T., Rognvaldsson, T., Wickstrom, N., Carlsson, C., Larsson, M., and Nytomt, J., "Robust AFR Estimation Using the Ion Current and Neural Networks", 1999-01-1161, SAE Technical Paper Series, 1999

[163] Daniels, C. F., "The Comparison of Mass Fraction Burned Obtained from the Cylinder Pressure Signal and Spark Plug Ion Signal", 980140, SAE Technical Paper Series

[164] Strandh, P., Christensen, M., Bengtsson, J., Johansson, R., Vressner, A., Tunestål, P., and Johansson, B., "Ion Current Sensing for HCCI Combustion Feedback", *SAE Paper 2003-01-3216*

[165] Schneider, D., and Lai, M., "Real-time air/fuel ratio control in a small SI engine using the ionic current signal", SAE Technical Paper Series, (1999-01-3323), 1999

[166] Ming, C. L., Ratton, K., Balles, E., Vandyne, E., Wahl, A., Darin, B., and Hirschlieb, G., "In-cylinder air-fuel ratio approximation using spark gap ionization sensing", SAE Technical Paper Series, (980166), 1998

[167] Strandh, P., Bengtsson, J., Johansson, R., Tunestål, P., and Johansson, B., "Cycle-to-cycle Control of a Dual-Fuel HCCI Engine", *SAE Technical paper 2004-01-0941,* 2004

[168] Corcione, F., Bianca, V., and Simona, M., "Evaluation of Knocking Combustion by an Ion Current System and Optical Diagnostics of Radical Species", The Sixth International Symposium on diagnostics and Modelling of Combustion in Internal Combustion Engines, COMODIA 2004

[169] Zhao, H., Li, J., Ma, T., and Ladommatos, N., "Performance and Analysis of a Four Stroke Multi-cylinder Gasoline Engine with CAI Combustion", SAE 2002-01-0420

[170] Hellring, M., and Holmberg, U., "An ion current based peak finding algorithm for pressure peak position estimation", SAE Technical Paper Series, (2000-01-2829), 2000

[171] Graps, A. L., "An introduction to wavelets", IEEE Computational Sciences and Engineering, 2(2):50-61, 1995

[172] Malaczynski, G., and Baker, M., "Real-time digital signal processing of ionization current for engine diagnostic and control", SAE Technical Paper Series, (2003-01-1119), 2003

[173] Glavmo, M., Spadafora, P., and Bosch, R., "Closed Loop Start of Combustion Control Utilizing Ionization Sensing in a Diesel Engine", Delphi Automotive Systems, SAE 1999-01-0549

[174] Bhave, A., Kraft, M., Montorsi, L., and Mauss, F., "Modelling a Dual-fuelled Multi-Cylinder HCCI Engine Using a PDF-based Engine Cycle Simulator", *SAE Paper* 2004-01-0561, 2004

[175] Maigaard, P., and Kraft, M., "Homogeneous Charge Compression Ignition Engine: A Simulation Study on the Effects of Inhomogeneities", Journal of Engineering for Gas Turbines and Power ,125, 466-471, 2003

[176] Flowers, D., Aceves, S., Westbrook, C., Smith, J., and Dibble, R., "Detailed Chemical Kinetic Simulation of Natural Gas HCCI Combustion: Gas Composition Effects and Investigation of Control Strategies", ASME Journal of Engineering for Gas Turbines and Power, 123, 433–439, 2001

[177] Tsotsis, T., Langille, A., Ren, J., Egolfopoulos, F., and Wang, H., "Chemical reactive control of HCCI engines", Los Angeles, CA 90089-1453

[178] Flowers, D., Aceves, S., Dibble, R., Hessel, R., and Babajimopolous, A., "Modelling of HCCI and PCCI Combustion Processes", U.S. Department of Energy by University of California, Lawrence Livermore National Laboratory under Contract W-7405-ENG-48

[179] Soylu, S., "Examination of Combustion Characteristics of an HCCI Engine", Sakarya University, Turkey

[180] Rausen, D., and Stefanopoulou, A., "A Mean-Value Model for Control of Homogeneous Charge Compression Ignition (HCCI) Engines", in Proceedings of the American Control Conference (2004), volume 1, 125-131

[181] Shaver, G., Gerdes, C., Jain, P., Caton, P., and Edwards, C., "Modelling for Control of HCCI Engines". Proceedings of the American Control Conference, 749-754, 2003

[182] Bengtsson, J., Gafvert, M., Strandh, S., "Modelling of HCCI Engine Combustion for Control Analysis", in Conference in Decision and Control (CDC), 2004

[183] Ogink, R., "Computer Modelling of HCCI Combustion", PhD Thesis, Chalmers University of Technology, Sweden, 2004

[184] Panousakis, D., and Gazis, A., "In-cylinder gas estimation and thermodynamic analysis of HCCI combustion", submitted for consideration in Experimental Heat Transfer Journal

[185] Flowers, D., Aceves, S., Martinez, J., Espinosa, F., and Dibble, R., "Detailed Modelling of HCCI and PCCI combustion and Multi-cylinder HCCI Engine Control", DEER Meeting, Newport, RI, 2003

[186] Zhang, Y., Kung, E., and Haworth, D., "A PDF Method for Multidimensional Modelling of HCCI Engine Combustion: Effects of Turbulence/Chemistry Interactions on Ignition Timing and Emissions", International multidimensional Engine Modelling User's Group Meeting, 2004

[187] Churchill, R., Smith, J., Clark, N., and Turton, R., "Low Heat Rejection Engines – A Concept Review", SAE paper No. 880014, 1988

[188] Kamo, R., and Bryzik, W., "Uncooled, Unlubricated Diesel?", Automotive Engineering, Vol87, n6, June 1979, pp. 59-61, 1979

[189] Marmach, M., Server, D., Hannink, R.H.J., Murray, M., and Swain, M., "Toughened PSZ Ceramics – Their Role as Advanced Engine Components", SAE paper No. 830316, 1983

[190] Moorhouse, P., and Johnson, M., "Development of Tribological Surfaces and Insulating Coatings for Diesel Engines", SAE paper No. 870161, SP-700, 1987

[191] Carr, J., and Jones, J., "Post Densified Cr2O3 Coatings for AdiabaticEngines", SAE Paper No.840432, SP-571

[192] Zhao, F., Asmus, T., Assanis, D., Dec, J., Eng, J., and Najt, P., "Homogeneous Charge Compression Ignition (HCCI) Engines" – Key Research and Development Issues, SAE 2003

[193] Benson, S., Combustion, "A Chemical and Kinetic View", 21st Symposium on Combustion, 1986

[194] Dryer, F., "The Phenomenology of Modelling Combustion Chemistry in Fossil Fuel Combustion: A Source Book", 1991

[195] Yetter, R., Dryer, F., "Inhibition of Moist Carbon Monoxide Oxidation by Trace Amounts of Hydrocarbons", 24th Symposium on Combustion, 1992

Appendix 1.

Information on ceramic thermal barrier coatings

In the mid 1970's materials such as silicon carbide (SiC) and silicon nitride (Si3N4) were first used as materials in engine cylinder construction [1]. Silicon carbide in granular form possess good wear resistance, high temperature capabilities, low coefficient of friction, good corrosion resistance, half the density of steel. But they are more brittle and shrinking to about 18% during sintering. Even though it was successful in some high temperature engine application more advanced materials were developed then for Low Heat Rejection Engines. The other substances of interest include Silicon Nitride (Si3N4), Aluminium Titanate (Al203 TiO2), Aluminium Magnesium Silicate (AMS). **Error! Reference source not found.**, shows a list of ceramic materials and their properties [2].

Zirconia, a ceramic material that has very low thermal conductivity values, good strength, thermal expansion coefficients similar to metals and is able to withstand much higher temperatures than metals. However one disadvantageous trait is its characteristic of changing phases with increase in temperature. Eliminating this phase change would ease the burdens of construction and use of the material in an engine [1]. Partially Stabilized Zirconia (PSZ) has been developed that decreases the magnitude of these changes. At present Partially Stabilized Zirconia has been found to be quite desirable for adiabatic engine application because of its excellent insulating characteristics, adequate strength characteristics and thermal expansion characteristics, which are relatively close to some metals. Investigation of M.Marmach et al [3] indicates that Toughened Partially Stabilized Zirconia (PSZ) ceramics possess a number of advantageous properties for advanced engine components, in particular for adiabatic engine system. It has also been stated that Magnesia Partially Stabilized Zirconia (Mg-PSZ) is suitable for LHR engine components. Magnesium and Nickel have been added to PSZ to improve strength and ductility characteristics respectively. Magnesia Partially Stabilized Zirconia (Mg PSZ) has a thermal expansion coefficient and elastic modulus close to that of Iron and Steel and is suitable for liners, valve guides and seats, hot plates, tappet inserts, and piston caps

in the engine cylinder. Mg PSZ is made of 20 to 24% Magnesia. This has the highest fracture toughness of all the PSZ materials. Stabilization of Zirconia can be accomplished with the addition of CaO, MgO and Y2O3, but these formations tend to be coarse, lack strength and toughness and exhibit poor thermal shock resistances. Alloys with 20% Yttria or 5% Calcia create fully stabilized Zirconia and good thermal coefficients of expansion [4]. Another way to improve PSZ characteristics is to impregnate the surface after forming of the part. Success has been shown with a Cr2O3 impregnation treatment [5]. This is also referred as densification treatment. A coating of plasma sprayed Zirconia densified with this treatment exhibits an 87% lower wear rate than a similar undensified coating. The Chromium Oxide fills the open pores between molecular structures and hardens the surface. Another promising material is Syalon (Si-Al-O-N) ceramics. Silicon Nitride mentioned above is one derivative of this classification. The major advantage of the material is the low creep characteristics at high temperatures. The material also has low density and low coefficient of friction. This will be good for reciprocating parts such valves and bearings. However, ceramic materials are not ductile in general and any small imperfection produces stress concentration, which develops crack. Other ceramic, composite and advanced materials are being developed for different engine applications. Research is continuing to obtain ceramics with greater ductility.

---

[1] Churchill, R. A., et all, "Low Heat Rejection Engines – A Concept Review", SAE paper No. 880014, 1988.
[2] Kamo, R., and Bryzik, W., "Uncooled, Unlubricated Diesel?", Automotive Engineering, Vol87, n6, June 1979, pp. 59-61, 1979.
[3] Marmach, M., Server, D., Hannink, R.H.J., Murray, M.J. and Swain, M.V., "Toughened PSZ Ceramics – Their Role as Advanced Engine Components", SAE paper No. 830316, 1983.
[4] Moorhouse, P., and Johnson, M., "Development of Tribological Surfaces and Insulating Coatings for Diesel Engines", SAE paper No. 870161, SP-700, 1987.
[5] Carr, J., and Jones, J., "Post Densified Cr2O3 Coatings for AdiabaticEngines", SAE Paper No.840432, SP-571

Appendix 2

Photographs of engines for remote controlled vehicles

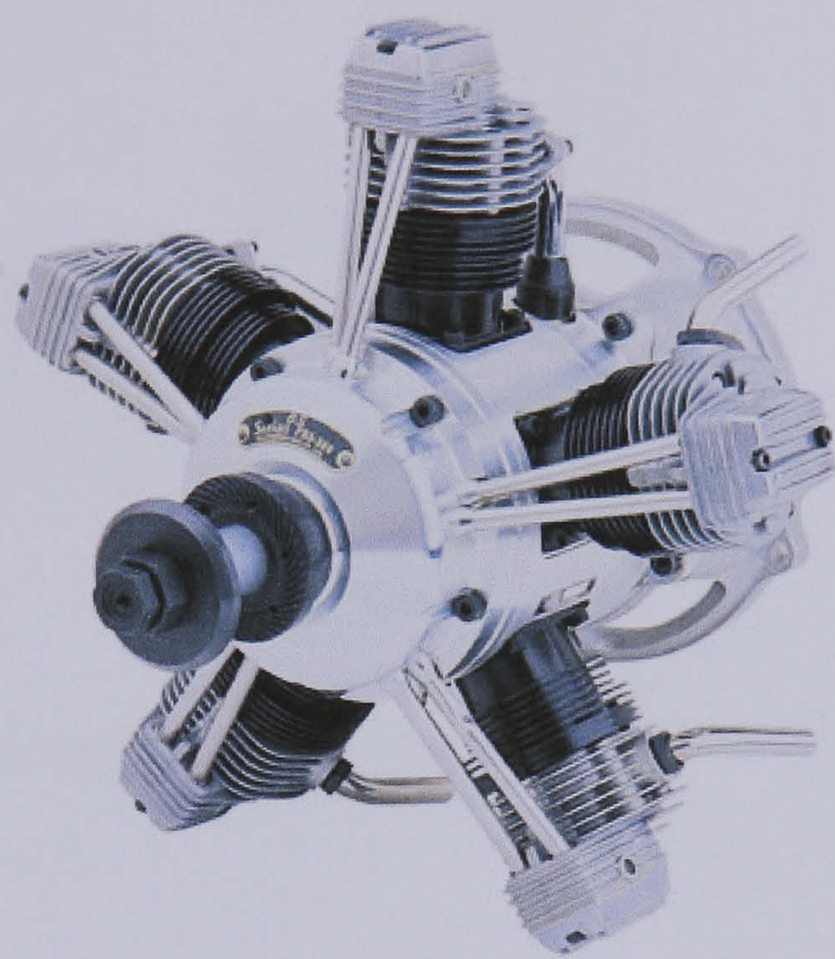

Figure 1: A big displacement radial engine (4-stroke, displacement 9.96cm^3, 4BHP@8000rpm).

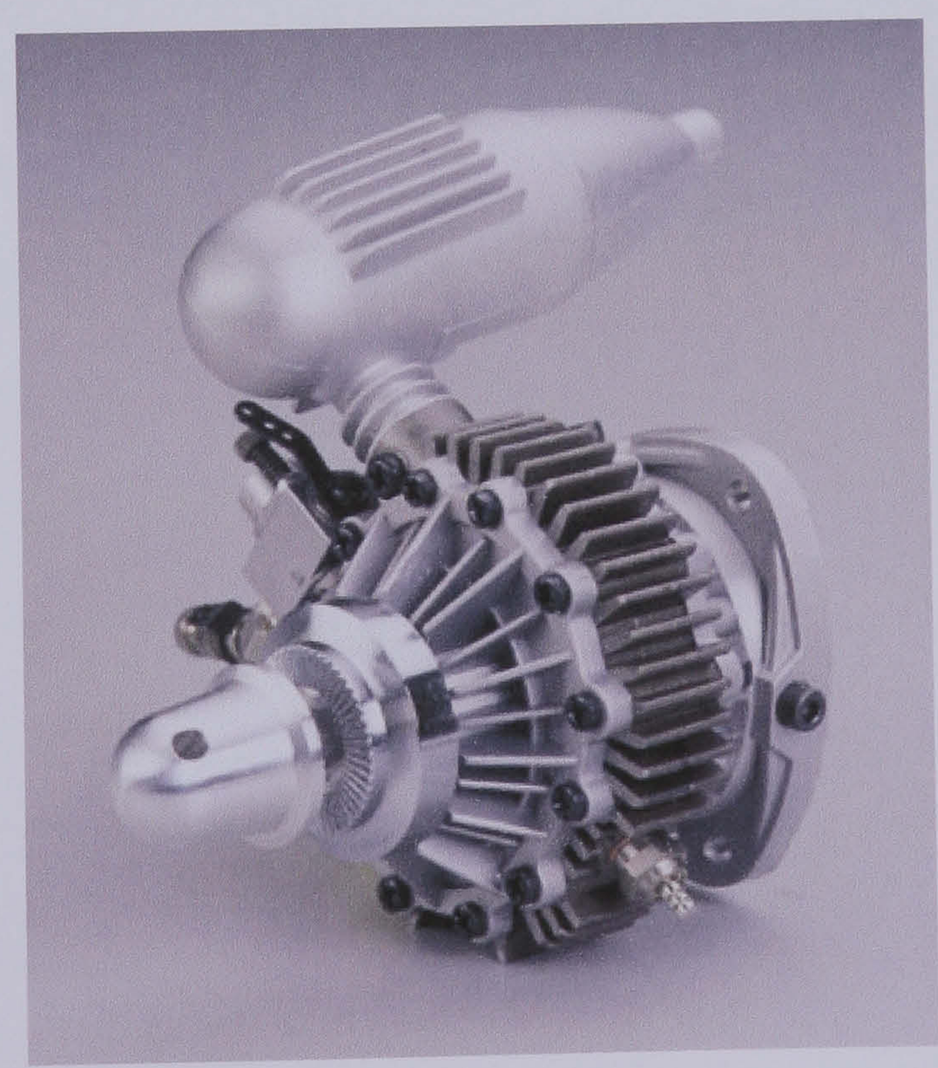

Figure 2: Wankel glow plug engine.

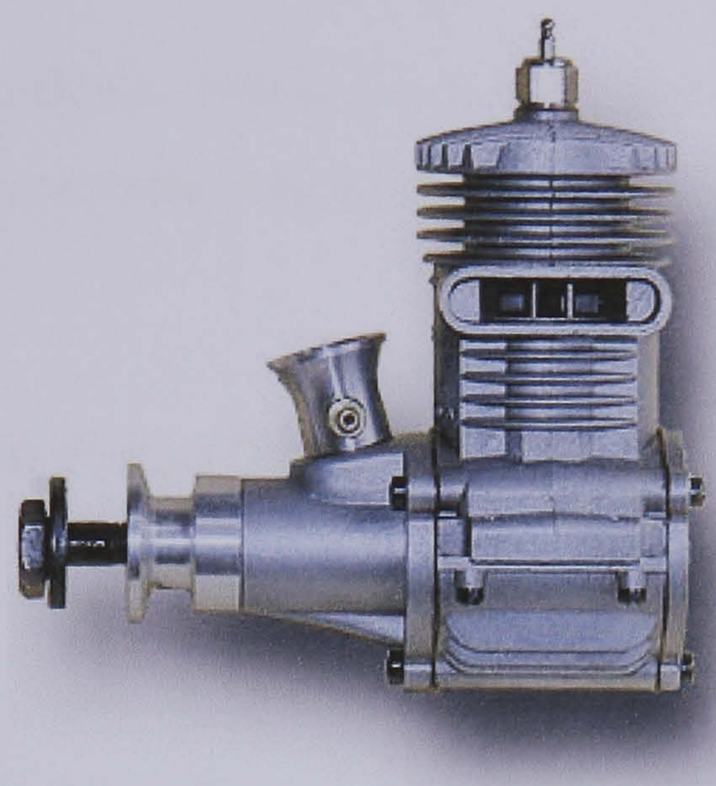

Figure 3: A 2-stroke medium sized glow plug engine. The glow plug can be seen at the top of the cylinder head.

Appendix 3.

The material in this section is mainly a summary of the literature review of [1], although other sources of literature were used where it was thought appropriate.

Low-temperature Paraffin Oxidation

In the low-temperature autoignition chemistry of paraffinic fuels an abstraction of a hydrogen atom by oxygen to form an alkyl radical (R•) and a hydroperoxy radical (HO_2•) happens first.

(1) $RH + O_2 \rightarrow R\bullet + HO_2\bullet$

Due to the different molecular structure of the parent paraffin, the hydrogen abstraction results in a variety of alkyl radicals. The alkyl radicals are consumed in two parallel paths, one being the abstraction of another hydrogen atom by oxygen to form a conjugate olefin and a hydroperoxy radical.

(2) $R\bullet + O_2 \rightarrow$olefin $+ HO_2\bullet$

The other path is the addition of oxygen to the radical to form an alkylperoxy radical (RO_2•).

(3) $R\bullet + O_2 \leftrightarrow RO_2\bullet$ [Error! Bookmark not defined.]

The RO_2• radical undergoes internal isomerisation by the oxygen abstraction of a hydrogen atom from a C-H bond elsewhere within the molecule to form a hydroperoxyalkyl radical (•ROOH).

(4) $RO_2\bullet \rightarrow \bullet ROOH$

In turn the •ROOH radical reacts in two separate routes. In the first route an OH• radical is produces when the hydroperoxyalkyl radical either spontaneously decomposes in a lower molecular weight alkene or forms a cyclic ether and an OH•.

(5) $\bullet ROOH \rightarrow CARBONYL + R'\bullet + OH\bullet$

The second route has the •ROOH radical undergoing a second oxygen addition to form a hydroperoxyalkylperoxy radical (•OOROOH), following an internal H atom abstraction to produce an alkylhydroperoxide (HOOROOH). The alkylhydroperoxide then decomposes into an aldehyde (RCHO) and two OH• radicals.

(6) $\bullet ROOH + O_2 \leftrightarrow \bullet OOROOH \rightarrow HOOROOH$

(7) $HOOROOH \rightarrow RCHO + R'O + OH\bullet + OH\bullet$

The production of alkylperoxy radicals (reaction 3) is faster than olefin formation (reaction 2) at all temperatures. However, as the temperature is increased above 500 K at atmospheric pressure (700 K at 10 atmospheres pressure) the reverse of reaction (3) is favored, and olefin production increases. The fuel consumption rate decreases as the rate of olefin formation increases. It is the competition between reactions (2) and (3) that defines the transition between the low- and intermediate-temperature regimes.

Intermediate-Temperature Paraffin Oxidation

Olefin and hydroperoxy radical formation is increased through temperature increase and hydrogen peroxide (H_2O_2) production now becomes significant by HO_2 radicals abstracting a Hydrogen atom from the fuel.

(8) $RH + HO_2\bullet \leftrightarrow R\bullet + H_2O_2$

The buildup of hydrogen peroxide in the system eventually decomposes with increasing temperature producing two hydroxyl radicals from each H_2O_2 molecule and the overall reaction rate begins to increase. This is why hydrogen peroxide is so important in the autoignition process.

(9) $H_2O_2 + M \rightarrow OH\bullet + OH\bullet + M$

Benson has termed this process 'hot-ignition' since there is a ready source for OH radicals for the system [2]. Note that it takes time for the H_2O_2 concentrations to build

up before the reaction rate increases, which is parallel to the buildup of the ROOH radical in the low temperature regime.

Functionally, in the intermediate temperature regime the HO_2 radical replaces the RO_2 radical of the low temperature reaction and H_2O_2 replaces HOOROOH. The beginning of the intermediate temperature reactions occur at lower temperature as the pressure is increased thus the range of temperatures over which NTC behavior is exhibited becomes narrower at higher pressures and eventually disappears at very high pressures.

At atmospheric pressures and temperatures higher than roughly 800 K, the oxidation chemistry of most paraffins begins to change significantly. The alkyl radicals are decomposed into smaller hydrocarbon radicals and olefins by a thermal decomposition process known as beta-scission [3]. Depending upon the structure of the alkyl radical, a wide range of species can be produced via β-scission.

High-Temperature Paraffin and Olefin Oxidation

The high-temperature oxidation of hydrocarbons can be described as a sequential three step process:

- After initiation the parent fuel is converted to lower molecular weight hydrocarbons and water with little energy release.
- The intermediate hydrocarbon species are further converted to produce CO and water.
- CO is oxidized into CO_2 and the large fraction of the energy is released from the combustion process.

Thermodynamics calculation show that roughly half of the energy released from C_7 and C_8 hydrocarbons results from CO oxidation. The reaction sequence can be conceptualized as,

(10) $RH + OH\bullet \rightarrow R'\bullet + R''\bullet + H_2O \rightarrow CO + H_2O \rightarrow CO_2 + \text{heat}$

The final reaction in all hydrocarbon combustion systems is the oxidation of CO to CO_2. Because the radicals preferentially react with any hydrocarbons present in the mixture, CO oxidation is delayed until after the majority of the hydrocarbons are consumed.

The important chain-carrying radicals in the high-temperature regime are the OH•, H• and O•. These radicals are very reactive and correspondingly the hydrocarbon oxidation rates are extremely fast.

The important chain-branching reactions are shown below.

(11) $H\bullet + O_2 \rightarrow OH\bullet + O\bullet$

(12) $O\bullet + H_2 \rightarrow OH\bullet + H\bullet$

$H_2O + O\bullet \rightarrow OH\bullet + OH\bullet$

At the high pressures obtained in engines radical recombination reactions are also important. The dominant recombination reaction at these pressures is,

$H\bullet + O_2 + M \rightarrow HO_2\bullet + M$

where M represents a third body collision partner. The transition between intermediate- and high-temperature kinetic regimes is generally defined as the condition where the branching reaction (11) dominates over the recombination reaction (14) [3]. This transition is a function of not only pressure, but of the third body efficiencies of the other molecules in the system. At atmospheric pressure with nitrogen as a third body, the transition to high temperature kinetics occurs at roughly 950 K as previously stated while at 10 atmospheres the transition does not occur until 1400 K.

The final stage of the energy release at high temperature is CO oxidation, where 45 to 50% of the energy is released. The principal reactions consuming CO are,

(15) $CO + OH\bullet \rightarrow CO_2 + H\bullet$

(16) $CO + HO_2\bullet \rightarrow CO_2 + OH\bullet$

(17) $CO + O\bullet + M \rightarrow CO_2 + M$

At high temperatures nearly all of the CO is consumed by OH• radicals via reaction (15) with only a small contribution from the other reactions. As already mentioned, CO oxidation is inhibited by the presence of hydrocarbons, since the OH• radicals preferentially react with those [4].

It should be added here that oxidation of aromatics, not analyzed at all here, is also important. Especially high-temperature aromatic oxidation is slightly problematic and thus these are used mainly for increasing gasoline octane rating.

This is too long for a thesis that is not about chemical kinetcs.

---

[1] Zhao F., Asmus T., Assanis D., Dec J., Eng J. and Najt P., "Homogeneous Charge Compression Ignition (HCCI) Engines" – Key Research and Development Issues, SAE 2003

[2] Benson S. W., Combustion, "A Chemical and Kinetic View", 21st Symposium on Combustion, 1986

[3] Dryer F. L., "The Phenomenology of Modeling Combustion Chemistry in Fossil Fuel Combustion: A Source Book", 1991

[4] Yetter R. A. et al., "Inhibition of Moist Carbon Monoxide Oxidation by Trace Amounts of Hydrocarbons", 24th Symposium on Combustion, 1992

Appendix 4.

Pressure Transducer Data Sheet

KISTLER

3.6123 7.97 1 ... 2

Quarz-Drucksensor
Capteur de pression à quartz
Quartz Presure Sensor

6123, 6123A1, 6123A2

Robuster Hochtemperatur-Drucksensor für Zylinderdruckmessung in Verbrennungsmotoren. Dank widerstandsfähiger Membran ist der Sensor auch für Messungen im klopfnahen Betrieb geeignet.
Für max. Lebensdauer des Steckers wird das Kabel Typ 1959A1 unbedingt empfohlen. Dieses passt ausschliesslich auf den Sensor Typ 6123.

A1: Ausführung mit M10 x 1-Montagenippel
A2: Ausführung mit 3/8"x24UNF-Montagenippel

Als Typ 6623... ist dieser Sensor auch in einer Version mit im Kabelstecker integriertem Impedanzwandler (Spannungsausgang) erhältlich. Nähere Information auf Datenblatt 12.5147.

Capteur de pression robuste pour températures élevées, pour mesurer la pression cylindre dans moteurs à combustion interne. Grâce au diaphragme résistant, le capteur est aussi employé pour faire des mesures proches du cliquetis.
Pour garantir une durée de service maximale de la fiche, le câble type 1959A1 est recommandé, qui est spécialement adapté au capteur type 6123.

A1: Construction avec écrou de montage M10 x 1
A2: Construction avec écrou de montage 3/8"x24UNF

Comme type 6623... ce capteur est disponible aussi comme version avec convertisseur d'impédance intégré dans la fiche du câble (sortie en tension). Voir notice technique 12.5147.

Robust high temperature pressure sensor for cylinder pressure measurements in internal combustion engines. Due to its resistant diaphragm the sensor is also suitable for measuring near the knocking limit.
In order to guarantee a maximum service life of the connector, the cable Type 1959A1 is recommended. This is especially adapted to the sensor Type 6123.

A1: Construction with M10 x 1 mounting nut
A2: Construction with 3/8"x24UNF mounting nut

As Type 6623... this sensor is also available in a version with impedance converter integrated in the cable Connector (voltage output). See data sheet 12.5147.

- Klopffest
  Résistant au cliquetis
  Resistant to knocking
- Neu mit verbessertem Kabel Typ 1959 erhältlich
  Nouveau avec câble type 1959 amélioré
  New with improved cable Type 1959
- Auch mit eingebautem Impedanzwandler erhältlich
  Disponible aussi avec convertisseur d'impédance incorporé
  Available with built-in impedance converter, too

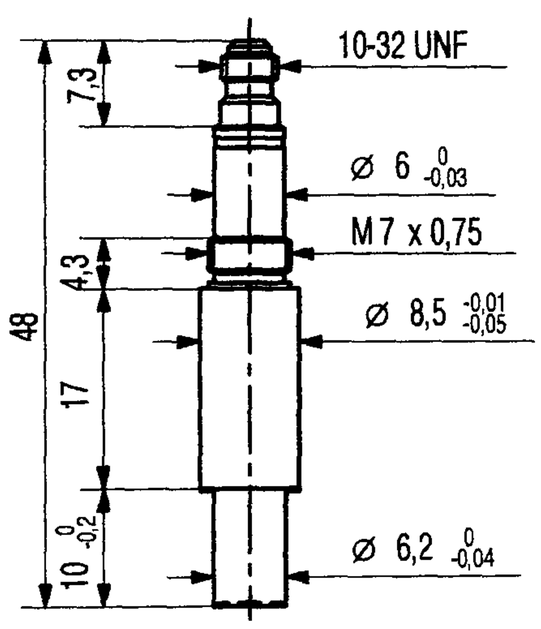

1 : 1

Technische Daten	Données techniques	Technical Data*		
Bereich	**Gamme**	**Range**	bar	0 ... 250
Kalibrierter Teilbereich	**Gamme partielle étalonnée**	**Calibrated partial range**	bar	0 ... 50
Überlast	**Surcharge**	**Overload**	bar	300
Empfindlichkeit	**Sensibilité**	**Sensitivity**	pC/bar	≈–16
Eigenfrequenz	**Fréquence propre**	**Natural frequency**	kHz	≈100
Linearität, alle Bereiche	**Linéarité,** toutes les gammes	**Linearity,** all ranges	%FSO	≤±0,5
Beschleunigungsempfindlichkeit	**Sensibilité aux accélérations**	**Acceleration sensitivity**	bar/*g*	<0,0015
Betriebstemperaturbereich	**Température d'utilisation**	**Operating temperature range**	°C	–50 ... 350
Empfindlichkeitsänderung	**Décalage de la sensibilité**	**Sensitivity shift**		
200± 150°C	200± 150°C	200± 150°C	%	<±3
200± 50°C	200± 50°C	200± 50°C	%	≈±1
Thermoschock	**Choc thermique**	**Thermal shock**		
Abweichung von der Referenz 7061B bei 1500 r/min, p_{mi} = 9 bar	Différence par rapport à la référence 7061B à 1500 r/min, p_{mi} = 9 bar	Difference from reference 7061B at 1500 r/min, IMEP = 9 bar		
Δp (Kurzzeitdrift)	Δp (dérive due au court temps)	Δp (short-time drift)	bar	<–1,5
Δp_{mi} bis zu	Δp_{mi} jusqu'à	ΔIMEP up to	%	<–10
$\Delta p_{max.}$ bis zu	$\Delta p_{max.}$ jusqu'à	$\Delta p_{max.}$ up to	%	<–3
Isolationswiderstand bei 20°C	**Résistance d'isolement** à 20°C	**Insulation resistance** at 20°C	TΩ	≥10
Anzugsmoment	**Couple de serrage**	**Tightening sensitivity**	Nm	10
Kapazität	**Capacité**	**Capacitance**	pF	8
Gewicht	**Poids**	**Weight**	g	10
Stecker, Keramik-Isolator	**Connecteur,** isolateur céramique	**Connector,** ceramic insulator	Type	10-32 UNF

1 bar = 10^5 Pa = 10^5 N · m^{-2} = 1,0197... at = 14,503... psi; 1 psi = 0,06894... bar; 1 *g* = 9,80665 m · s^{-2}; 1 Nm = 0,73756... lbft; 1 g = 0,03527... oz

* In all Kistler documents, the decimal sign is a comma on the line (ISO 31-0:1992).

Beschreibung

Durch den Einsatz von polystablen Quarzelementen wird selbst bei hohen mechanischen Beanspruchungen Sicherheit gegen Zwillingsbildung gewährleistet. Dadurch bleibt die Empfindlichkeit im Bereich von -50°C ... 350°C weitgehend konstant.
Herausragende Merkmale dieses Sensors sind seine robuste Membran und die hohe Ansprechempfindlichkeit auf Klopfen.

Anwendung

Der ungekühlte Sensor Typ 6123 eignet sich besonders für Klopferkennung in Benzinmotoren und für Langzeiteinsatz.

Montagebeispiele

Der Sensor kann direkt im Zylinderkopf eingebaut werden (als A1/A2 Version, Fig. 1) oder mittels einer Montagehülse Typ 6433A/34A durch den Wasserkanal (Fig. 2). Er soll möglichst brennraumbündig montiert werden, um Pfeifenschwingungen zu verhindern.

Zubehör	*Typ*
• Drehmomentschlüssel 5 ... 40 Nm	1371B
• Steckschlüssel SW8	1373
• Stufenbohrer	1337
• Gewindebohrer M10x1	1353
• Ausziehwerkzeug	1317
• Montagehülse M10x1 inkl. O-Ring	6433A...
• Montagehülse 3/8"x24 UNF inkl. O-Ring	6434A...
• Kühladapter M14x1.25	6521
• Cu-Dichtring	1102
• Ni-Dichtring	1102A
• Anschlusskabel BNC pos. Teflon	1631C...
• Anschlusskabel 10-32 UNF pos. Teflon	1635C...
• Anschlusskabel 10-32 UNF pos. Metall	1959A1
• Montagenippel M10x1	6431
• Montagenippel 3/8"x24 UNF	6432
• Klemmring für Nippel	1141
• O-Ring für Montagehülse	1169
• Adapter für Druckgenerator Typ 6905A	Z12779

Description

L'utilisation d'éléments à quartz polystables garantit la sécurité contre la formation de jumeaux (structure cristalline double) même à des sollicitations mécaniques élevées. Ainsi la sensibilité reste pratiquement constante dans la gamme de -50°C ... 350°C.
Les particularités importantes de ce capteur sont son diaphragme robuste et sa sensibilité au cliquetis.

Application

Le capteur non refroidi type 6123 est tout spécialement destiné à la détection du cliquetis dans moteurs à essence et pour l'utilisation à long terme.

Exemples de montage

Le capteur peut être installé directement dans la culasse du cylindre (version A1/A2, Fig. 1), ou à travers le conduit d'eau au moyen d'une douille de montage type 6433A/34A (Fig. 2). Il devrait être installé en affleurant la chambre de combustion pour éviter les sifflements.

Accesoires	*Type*
• Clé dynamométrique 5 ... 40 Nm	1371B
• Clé à douille à ouverturel OC8	1373
• Aléseuse progressive	1337
• Taraud age M10x1	1353
• Outil extracteur	1317
• Douille de montage M10x1 incl. joint torique	6433A...
• Douille de montage 3/8"x24 UNF incl. joint torique	6434A...
• Adaptateur refroidi M14x1.25	6521
• Joint en cuivre	1102
• Joint en nickel	1102A
• Câble de connexion BNC pos., téflon	1631C...
• Câble de connexion 10-32 UNF pos., téflon	1635C...
• Câble de connexion 10-32 UNF pos., métal	1959A1
• Ecrou de montage M10x1	6431
• Ecrou de montage 3/8"x24 UNF	6432
• Bague de fixation pour écrou	1141
• Joint torique pour douille de montage	1169
• Adaptateur pour générateur de pressions type 6905A	Z12779

Description

The use of polystable quartz elements assures safety against twinning even under high mechanical loads. This guarantees a practically constant sensitivity over the temperature range of -50°C ... 350°C.
Special features of the sensor are its robust diaphragm and the high sensitivity response to knocking.

Application

The uncooled sensor Type 6123 is especially suitable for knocking detection in gas engines and for long-time use.

Mounting examples

The sensor can directly be mounted in the cylinder head (A1/A2 version, Fig. 1) or across water ducts by means of a mounting sleeve Type 6433A/34A (Fig. 2). It should be installed flush with the combustion chamber in order to avoid pipe oscillations.

Accessories	*Type*
• Torque wrench 5 ... 40 Nm	1371B
• Tubular socket wrench WS8	1373
• Step drill	1337
• Screw tap M10x1	1353
• Extraction tool	1317
• Mounting sleeve M10x1 incl. O-ring	6433A...
• Mounting sleeve 3/8"x24 UNF incl. O-ring	6434A...
• Cooling adapter M14x1.25	6521
• Copper seal	1102
• Nickel seal	1102A
• Connecting cable BNC pos., teflon	1631C...
• connecting cable 10-32 UNF pos., teflon	1635C...
• Connecting cable 10-32 UNF pos., metal	1959A1
• Mounting nut M10x1	6431
• Mounting nut 3/8"x24 UNF	6432
• Clamping ring for nut	1141
• O-ring for mounting sleeve	1169
• Adapter for pressure generator Type 6905A	Z12779

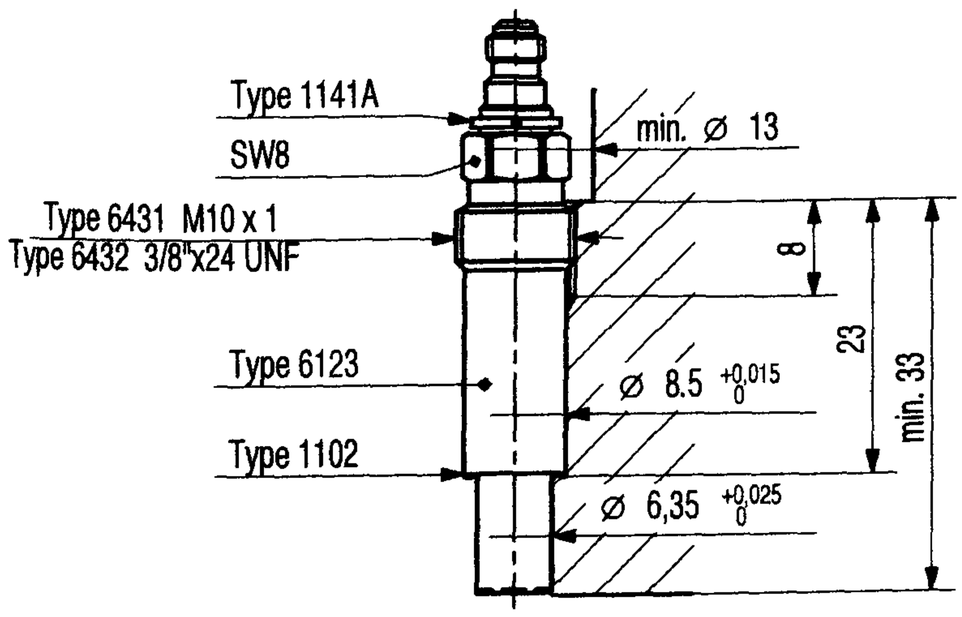

Fig. 1:

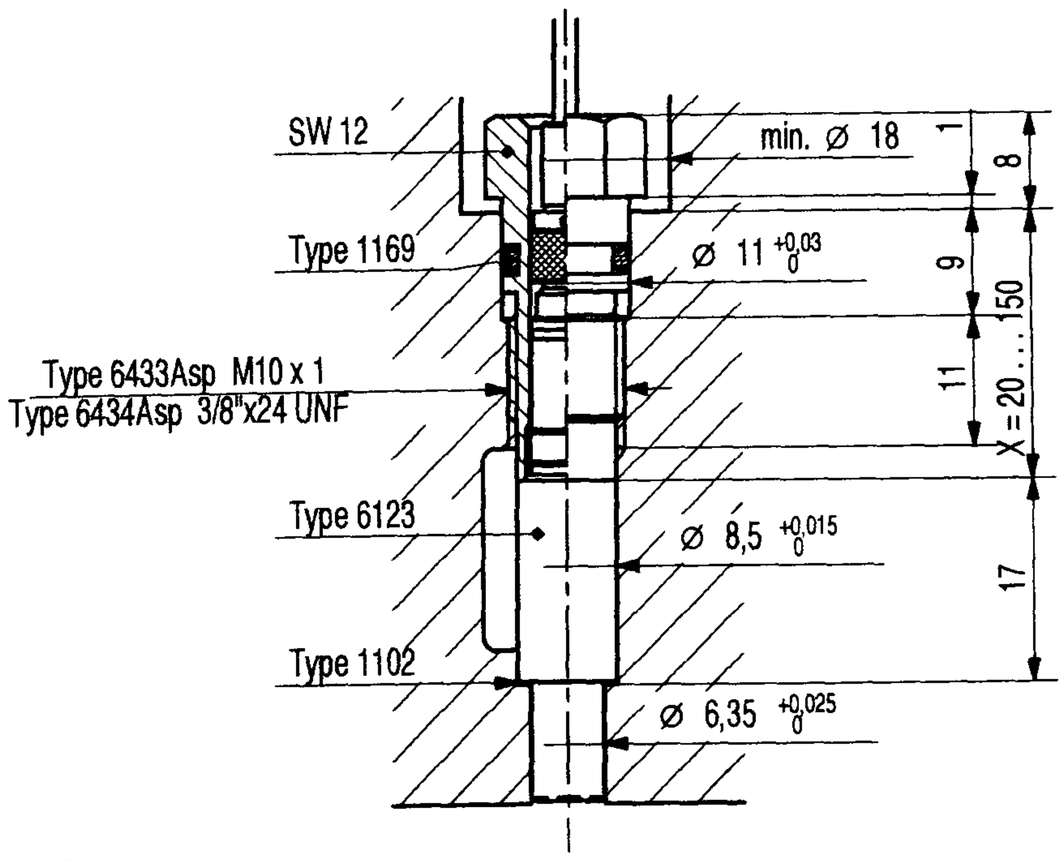

Fig. 2: